

# Development of sustainable protective Ultra-High Performance Fibre Reinforced Concrete (UHPFRC)

Design, assessment and modeling

Rui Yu

/ Department of the Built Environment

**bouwstenen 209**

DEVELOPMENT OF SUSTAINABLE  
PROTECTIVE ULTRA-HIGH  
PERFORMANCE FIBRE REINFORCED  
CONCRETE (UHPFRC)

*Design, assessment and modeling*

De promotiecommissie is als volgt samengesteld:

*Voorzitter:* Prof. dr. ir. B. De Vries  
*Promotor:* Prof. dr. ir. H.J.H. Brouwers  
*Co-promotor:* Dr. ir. P. Spiesz (ENCI HeidelbergCement Benelux)  
*Leden:* Prof. dr. Z.H. Shui (Wuhan University of Technology)  
Prof. ir. S.N.M. Wijte  
Prof. dr. ir. A.S.J. Suiker  
Prof. dr. ir. J.C. Walraven (Delft University of Technology)  
Prof. dr. dr. H. Pöllmann (Martin Luther University of Halle-Wittenberg)



CIP-DATA LIBRARY TECHNISCHE UNIVERSITEIT EINDHOVEN

Development of sustainable protective Ultra-High Performance Fibre Reinforced Concrete (UHPFRC) - Design, assessment and modeling / by Rui Yu

A catalogue record is available from the Eindhoven University of Technology Library  
ISBN: 978-90-386-3924-6

Bouwstenen 209

NUR 955

Copyright © 2015 by Rui Yu

Ph.D. Thesis, Eindhoven University of Technology, the Netherlands

Cover design: A.C.J. de Korte and R. Yu

Cover photographs supplied by the author.

Printed by: Proefschriftmaken.nl || Uitgeverij BOXPress

Published by: Uitgeverij BOXPress, 's-Hertogenbosch

All rights reserved. No part of this publication may be reproduced in any form or by any means without permission in writing form from the author.

DEVELOPMENT OF SUSTAINABLE PROTECTIVE  
ULTRA-HIGH PERFORMANCE FIBRE REINFORCED  
CONCRETE (UHPFRC)

*Design, assessment and modeling*

PROEFSCHRIFT

ter verkrijging van de graad van doctor  
aan de Technische Universiteit Eindhoven,  
op gezag van de rector magnificus, prof.dr.ir. F.P.T. Baaijens,  
voor een commissie aangewezen door het College voor Promoties,  
in het openbaar te verdedigen op dinsdag 13 oktober 2015 om 16:00 uur

door

Rui Yu

geboren te Hubei, China

Dit proefschrift van het proefontwerp is goedgekeurd door de promotoren en de samenstelling van de promotiecommissie is als volgt:

*Voorzitter:* Prof. dr. ir. B. De Vries  
*Promotor:* Prof. dr. ir. H.J.H. Brouwers  
*Co-promotor:* Dr. ir. P. Spiesz (ENCI HeidelbergCement Benelux)  
*Leden:* Prof. dr. Z.H. Shui (Wuhan University of Technology)  
Prof. ir. S.N.M. Wijte  
Prof. dr. ir. A.S.J. Suiker  
Prof. dr. ir. J.C. Walraven (Delft University of Technology)  
Prof. dr. dr. H. Pöllmann (Martin Luther University of Halle-Wittenberg)

*Dedicated to my grandfather Daoyuan Yu*  
*(1936-2005)*



## Preface

When I was writing the preface of this thesis, a series of classical prefaces from my friends' or colleagues' Ph.D. thesis came to my mind. Mostly, they announced that the Ph.D. study is a really challenging work, full of difficulties, frustrations and unhappiness. However, they still treat the Ph.D. research as one of the most unforgettable and fantastic periods of their lives. To be honest, before I started my Ph.D. research at Eindhoven University of Technology, I completely could not understand my friends' or colleagues' opinions mentioned above, since I really enjoy the feeling of challenge and I believe a Ph.D. study should be interesting and fascinating. Already when I was in the second year of my master's study, I decided to pursue a Ph.D. degree in a foreign country. Now, I still clearly remember the date (Oct. 10<sup>th</sup> 2011), the first exciting day when I arrived in the Netherlands. How time flies! After almost four years, I am already close to the end of this study. When looking back, I have to admit that all my friends' and colleagues' opinions on the Ph.D. study are definitely correct. During the past four years, I have experienced many difficulties, disappointments or even doubts about myself. I have never expected that pursuing a Ph.D. degree is such a time, energy and courage consuming process. Nevertheless, with the help and support that I received from so many people, I never thought of giving up. Without the support of my family, colleagues and friends, it would be impossible for me to complete and successfully finish my Ph.D. study. Consequently, I want to show my sincere acknowledgement to all of these people.

First of all, I want to express my gratitude to my supervisor and promoter prof.dr.ir. H.J.H. (Jos) Brouwers, who gave me the chance to join the Building Materials group at Eindhoven University of Technology for doing my Ph.D. study. I still clearly remember the first meeting and talk with Jos in 2010 in Wuhan. During the past four years, I obtained a lot of guidance, suggestions, comments and patience from Jos, and I want to say thank you very much for all your help and support. In addition, I want to thank my daily supervisor and co-promoter dr. ir. P. Spiesz for all his help, patience, and discussions during the development of this Ph.D. project. Przemek, in the past four years, we have experienced a lot: discussions, arguments or even a tense silence. But, now, I have to say all of these were beneficial for me in thinking, understanding and creating during my Ph.D. research. Thank you very much for treating me as I was your younger brother and teaching me so many interesting things about the Netherlands and Europe at the beginning of my arrival, particularly the names of various fruits.

I also appreciate the financial support of the Chinese Scholarship Council (CSC) and the sponsors of Building Materials group (chaired by prof.dr.ir. Jos Brouwers) at Eindhoven University of Technology.

Furthermore, my thanks go to Prof. dr. ir. Z.H. Shui (Wuhan University of Technology, China), Prof. dr. ir. J.C. Walraven (Delft University of Technology), Prof. dr. dr. H. Pöllmann (Martin-Luther University at Halle-Wittenberg, Germany), Prof. ir. S.N.M. Wijte (Eindhoven University of Technology) and Prof. dr. ir. A.S.J. Suiker (Eindhoven University of Technology) for reading and commenting on my thesis and forming my Ph.D. defence committee. Particularly, to Prof. dr. ir. Z.H. Shui, I want to thank you for your continuous trust and support during the past almost ten years, and it's my pleasure to join your group and work with you in the future.

During the four years' Ph.D. research, Ing. A.D. Verhagen gave a lot of professional help, guidance and suggestions. He provided the idea, design and part of the construction for the "Modified Pendulum Impact Device" (shown in Chapter 7). Beside scientific support, Ing. A.D. Verhagen also taught me an optimistic attitude to face difficulties in daily life. Hence, I want to show my great appreciation to Ing. A.D. Verhagen and wish him always good health. Thanks also go to Capt. L. Kaim (Dutch Army), Ing. J.P. Zeeman (Dutch Army) and Ing. D. Krabbenborg (Netherlands Defence Academy) for supporting the shooting experiments and many valuable suggestions.

Additionally, I want to thank G.A.H. Maas (Eindhoven University of Technology) for his patient and professional experimental support. Geert-Jan, I know that there are many Ph.D. students waiting for your help, but you always could help me timely and perfectly. It has been a great pleasure to work with you. I was impressed by your exhaustless energy and optimistic attitude. Thank you very much for all your help and support. Thanks also go to P.H. Cappon, Ing. A.C.A. Delsing and ir. H.M. Lamers (all from Eindhoven University of Technology) for their help in the laboratory.

Part of this thesis could not have been finished without the contribution of some master students: N. Kanavas, D. van Onna and L.J.P. van Beers. Thank you for your help in assisting my research. I hope my supervision was helpful for your professional careers in the future.

After spending almost four years in the Building Materials group at Eindhoven University of Technology, I have to admit that I really love the working atmosphere and colleagues here. The time we spent at the sports center, coffee corner, sky bar and conferences is really a precious memory for me. They are Alberto, Ariën, Azee, Bo, Chris, George, Guillaume, Katerina, Katrin, Miruna, Pei, Perry, Przemek, Qadeer, Qingliang, Rubina, Štěpán, Veronika, Xu and Yuri. My appreciations are also expressed to the BPS secretaries: Renée, Yeliz, Janet, Ginny, Léontine and Moniek. I am hoping to keep in touch with all of you in the future. Particularly, to Miruna, thank you for reading my thesis and help me to further improve its quality.

I would also like to express my appreciations to all my Chinese friends in the Netherlands. Due to the quite long list, I will not mention all the names, to all of you: thank you very much for helping and sharing all the fantastic times with me and my family.

Finally, but also most importantly, I need to sincerely thank my family. My grandfather, though you died 10 years ago, your personality and enthusiasm psychologically supported me on the road of striving after wisdom. This thesis contains all my outcomes and sweat in the past four years, and I want to dedicate it to you. For my parents, I know it has been tough for you to have a distance of about 8000 km between you and your only son for more than four years. Thank you for your continuous support and understanding. My thanks also go to all my aunts and uncles for taking care of my grandmother when I was not at home. At last, to the most important person of my life - my wife Shuo, it is definitely not enough to express my feelings in several thanks or appreciations. I owe you too much in the past four years. You sacrificed your promising career and came to the Netherlands with me four years ago. At that time, both of us were unsophisticated and immature. In the past four years, we have faced so many difficulties in work and daily life, but you always supported me to challenge them and finally to conquer them. After this four years' experience and toughening, I have grown a lot. On Sep. 22<sup>nd</sup> 2012 and Feb. 1<sup>st</sup> 2015, you gave me two invaluable presents of my life - our two sons (Kevin and Shawn). Thank God for giving them to us. The coming of Kevin and Shawn let me know more about responsibility, patience and persistence. I hope they can be always healthy and happy. I love you all forever, my wife and my sons.

*Rui Yu*

*June 2015*

*Eindhoven, the Netherlands*



# Contents

<b>Preface.....</b>	<b>iii</b>
<b>1 Introduction .....</b>	<b>1</b>
1.1 Scope of this research.....	1
1.2 Ultra-High Performance Fibre Reinforced Concrete (UHPFRC).....	5
1.2.1 Development .....	5
1.2.2 Available standard and specificity for UHPFRC .....	6
1.3 Research objectives and strategies .....	8
1.4 Outline of the thesis.....	9
<b>2 Materials characterization and experimental methodologies .....</b>	<b>13</b>
2.1 Introduction .....	13
2.2 Utilized materials .....	14
2.2.1 Powders characterization.....	14
2.2.2 Aggregates characterization .....	21
2.2.3 Fibres characterization .....	26
2.2.4 Superplasticizer .....	27
2.3 Experimental methodologies.....	27
2.3.1 Workability.....	27
2.3.2 Air content.....	28
2.3.3 Water-permeable porosity .....	30
2.3.4 Mechanical properties .....	30
2.3.5 Hydration kinetics .....	31
2.3.6 Thermal properties .....	31
2.4 Conclusions .....	32
<b>3 Optimized mix design approach for UHPFRC.....</b>	<b>35</b>
3.1 Introduction .....	35
3.2 Mix design of concrete based on the optimized particle packing .....	37
3.3 Experimental validation of the optimized particle packing model .....	39
3.3.1 Materials and mix design .....	39
3.3.2 Experimental methodologies.....	42
3.3.3 Results and discussions .....	44
3.3.4 Summary .....	56
3.4 Conclusions.....	57
<b>4 Efficient application of powders in UHPC.....</b>	<b>59</b>
4.1 Introduction .....	59
4.2 Effect of nanosilica on the properties of UHPC.....	60

4.2.1	Background .....	60
4.2.2	Materials and mix design of UHPC with nanosilica .....	61
4.2.3	Experimental methodologies .....	63
4.2.4	Results and discussions .....	64
4.2.5	Summary .....	76
4.3	Effect of mineral admixtures on the properties of UHPC .....	76
4.3.1	Background .....	76
4.3.2	Materials and mix design of UHPC with mineral admixtures .....	78
4.3.3	Experimental methodologies .....	81
4.3.4	Results and discussions .....	82
4.3.5	Environmental significance of using mineral materials in UHPFRC .....	94
4.3.6	Summary .....	95
4.4	Conclusions .....	96
<b>5</b>	<b>Efficient application of steel fibres in UHPFRC .....</b>	<b>97</b>
5.1	Introduction .....	97
5.2	UHPFRC with binary straight steel fibres.....	100
5.2.1	Materials and mix design .....	100
5.2.2	Experimental methodologies .....	101
5.2.3	Results and discussions .....	101
5.2.4	Summary .....	109
5.3	UHPFRC with hook ended fibres (ternary hybridization) .....	109
5.3.1	Materials and mix design .....	109
5.3.2	Experimental methodologies.....	110
5.3.3	Results and discussions .....	113
5.3.4	Summary .....	121
5.4	Conclusions .....	121
<b>6</b>	<b>Development of UHPFRC with waste bottom ash (WBA) .....</b>	<b>123</b>
6.1	Introduction .....	123
6.2	Materials and methodologies .....	125
6.2.1	Materials and mix design .....	125
6.2.2	Experimental methodologies.....	127
6.3	Results and discussions .....	129
6.3.1	Fresh behaviour of the UHPFRC with WBA.....	129
6.3.2	Water-permeable porosity of the UHPFRC with WBA .....	131
6.3.3	Flexural behaviour of the UHPFRC with WBA .....	132
6.3.4	Compressive strength of the UHPFRC with WBA.....	138
6.3.5	Hydration kinetics of cement in the UHPFRC with WBA .....	139
6.3.6	Microscopy analysis of the UHPFRC with WBA.....	140

6.4	Conclusions .....	143
<b>7</b>	<b>Performance of the sustainable UHPFRC under impact .....</b>	<b>145</b>
7.1	Introduction .....	145
7.2	Background of concrete under impact loadings .....	146
7.2.1	Effect of loading rates on the dynamic behaviour of concrete .....	146
7.2.2	Dynamic behaviour of internal structure of concrete .....	148
7.2.3	Improvement of energy dissipation capacity of concrete .....	149
7.3	Performance of the sustainable UHPFRC under impact loadings .....	153
7.3.1	Materials and mix design .....	154
7.3.2	Experimental methodologies .....	154
7.3.3	Energy dissipation capacity of UHPFRC with only straight steel fibres ....	162
7.3.4	Energy dissipation capacity of UHPFRC with hook ended steel fibres .....	169
7.3.5	Comparison of the results obtained from different pendulum impact tests	179
7.3.6	Summary .....	180
7.4	Conclusions .....	180
<b>8</b>	<b>Modeling of concrete target under projectile impact.....</b>	<b>183</b>
8.1	Introduction .....	183
8.2	The state of the art.....	185
8.2.1	Introduction of LS-DYNA .....	186
8.2.2	Material models for concrete in LS-DYNA .....	186
8.2.3	Macro-scale simulation based on LS-DYNA.....	187
8.2.4	Meso-scale simulation based on LS-DYNA .....	188
8.2.5	Summary .....	189
8.3	Modeling of the concrete target under projectile impact .....	189
8.3.1	Model of concrete plate under projectile impact.....	190
8.3.2	Model validation.....	192
8.3.3	Prediction of the sustainable UHPFRC dynamic performance .....	196
8.3.4	Summary .....	199
8.4	Conclusions .....	199
<b>9</b>	<b>Application of the sustainable UHPFRC in protective elements .....</b>	<b>201</b>
9.1	Introduction .....	201
9.2	Materials and methodologies .....	202
9.2.1	Materials, mix design and concrete production.....	202
9.2.2	Experimental methodologies .....	203
9.3	Experimental results and discussions.....	207
9.3.1	The sustainable UHPFRC under bullet (7.62 mm) impact .....	207
9.3.2	The sustainable UHPFRC under FSP (20 mm) impact.....	219
9.3.3	Summary .....	229

9.4	Modeling of the sustainable UHPFRC under projectile impact.....	229
9.4.1	Introduction .....	229
9.4.2	Model of UHPFRC slab under high velocity bullet impact .....	230
9.4.3	Validation of the model.....	232
9.4.4	Summary .....	235
9.5	Conclusions .....	235
<b>10</b>	<b>Conclusions and recommendations.....</b>	<b>239</b>
10.1	Conclusions .....	239
10.1.1	Optimized mix design of UHPFRC.....	240
10.1.2	Sustainable development of UHPFRC focus on ingredients point of view	240
10.1.3	Energy dissipation capacity of the developed UHPFRC.....	242
10.1.4	Modeling of UHPFRC under impact loadings .....	243
10.2	Recommendations for future research.....	244
	<b>Bibliography .....</b>	<b>247</b>
	<b>List of abbreviations and symbols.....</b>	<b>269</b>
	<b>Appendix 1.....</b>	<b>275</b>
	<b>Appendix 2.....</b>	<b>277</b>
	<b>Summary.....</b>	<b>278</b>
	<b>List of publications.....</b>	<b>279</b>
	<b>Curriculum vitae.....</b>	<b>283</b>

# Chapter 1

## Introduction

### 1.1 Scope of this research

Concrete is the most widely used manmade material, since its annual production exceeded 30 billion tons in 2013 (Amstrong, 2013; Quercia, 2014). Beside application of concrete in common buildings, it is also applied in sensitive objects which need to be resistant against incidental events. For example, to guarantee the safe and stable development of nuclear power, the nuclear power stations have to resist the impact load caused by incidents or attacks. Pillars of bridges having a large span have to resist the impact load of land or water vehicles. When impacts happen, if the building materials could deform and simultaneously absorb a large amount of energy without causing the structural collapse, then more trapped people could be rescued and less damage would be inflicted. These are only few examples of important infrastructural buildings that have to be protected against a possible collapse in the case of a critical incident. Nevertheless, not only important infrastructural buildings have to be protected against impact loads but also smaller technical facilities can cause serious damaging events when they fail. For instance, the protection of tanks used for storing liquefied petroleum gas (LPG) at gas stations in densely populated areas is an important aspect and demands the application of suitable materials. Moreover, not only accidental events can result in the collapse of infrastructural buildings and great loss of life but also intentional events, such as terrorist attacks, have to be considered nowadays seriously (Luccioni et al., 2004). In the latter case, the use of explosives is a commonly used practice to inflict damage on important infrastructural buildings. In this case, the generated pressure wave forms the destructive force on the concrete. Besides, the use of rockets and other ballistic weapons against civil or military targets is also increasing in conflict areas and is a serious problem for the protection of peacekeeping forces in these areas (Booker et al., 2009; Wu et al., 2015). Military rockets and mortar rounds, e.g. calibre 107 mm, become available for terrorist groups on the black market and allow them to attack targets over a large distance. The damaging effect of these projectiles is devastating as the projectile is penetrating unhindered ordinary concrete or steel and causes spalling of the material at the back side. The spalling of the concrete creates small pieces of concrete that act as further projectiles and contribute to the damaging effect of the original projectile. Therefore, it can be concluded that a strong demand for impact resistant materials exists in both civil and military fields.

The investigation of impact generated by hard projectiles started in the middle of the 1700s (Kennedy, 1976), considering the fact that the projectile impact is the most common impact type compared to other impact categories (high-rate impact, shock, blast loads and so on). Afterwards, to protect soldiers and important military constructions in battles, the military showed a great interest in designing high performance protective barriers and understanding the impact resistance capacity of different materials. Therefore, since the beginning of the last century, a series of small-scale lab tests and full-scale prototype tests were executed and used to study the performance of building materials against the projectile impact loadings (Li et al., 2005). In these tests, due to its relatively low price and good performance, concrete has attracted a lot of attention, which leads to various empirical formulae and analytical models to predict the dynamic performance of concrete under projectile impacts. Nevertheless, with the development of the concrete industry, a series of advanced concretes (e.g. self-compacting concrete, fibre reinforced concrete, reactive powder concrete, Ultra-High Performance Fibre Reinforced Concrete) have been developed nowadays, which have much better properties than the conventional concretes that were developed in the last century. Moreover, the destructive power of the modern bullets or missiles is continuously increasing. Hence, the empirical formulae proposed around 70 years ago are not suitable for predicting the impact resistance of these advanced concretes. Furthermore, there is also an urgent need to develop materials that can be used in the construction of protective structures nowadays.

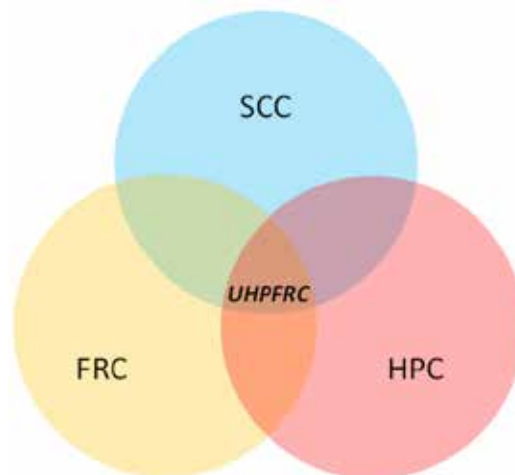


**Figure 1.1: Different types of special concretes (Camacho, 2013)**

From the available literature (Bindiganavile et al., 2002; Zhang et al., 2007; Parant et al., 2007; Habel and Gauvreau, 2008; Lai and Sun, 2009), it can be concluded that a strong concrete matrix and a high contents of steel fibres are beneficial for improving the impact resistance capacity of concrete, since the damage of the concrete matrix and pullout of steel fibres can absorb large quantity of energy released during the impact process. With the development of concrete technology and chemical admixtures, a series of new

materials (advance superplasticizer, nanosilica etc.) can be utilized to produce concrete with superior properties. Not only new materials but also new insights in particle packing and the influence of the particle packing on the mechanical properties allowed the design of concrete mixes that have higher strength and deformation capacity than normal strength (NSC). Based on the requirements of a strong concrete matrix and a high content of steel fibres, the Ultra-High Performance Fibre Reinforced Concrete (UHPFRC), developed initially in 1990s, can be a good candidate to be utilized in protective structures.

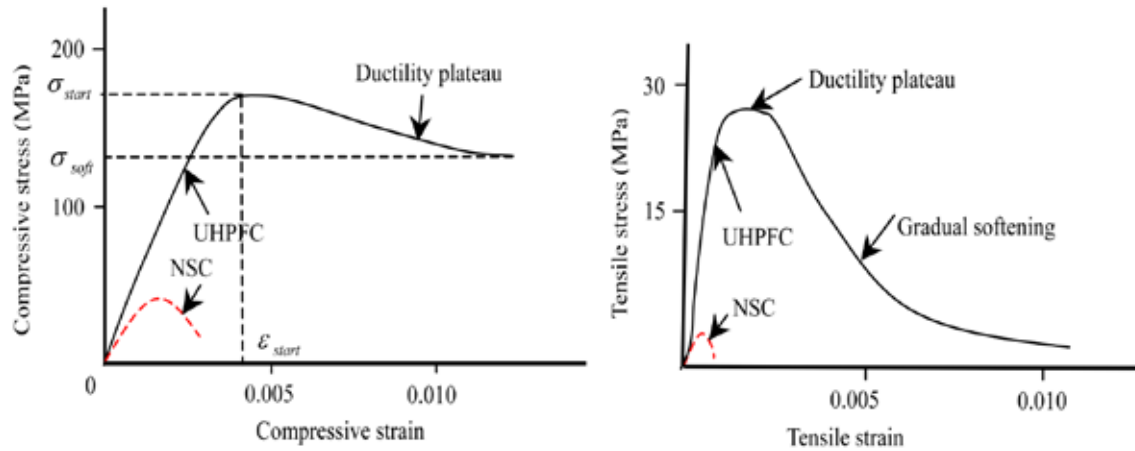


**Figure 1.2: Mechanical properties of conventional concrete and UHPFRC under compressive load (left) and tensile load (right) (Wu et al., 2009)**

Ultra-High Performance Fibre Reinforced Concrete (UHPFRC) is a relatively new construction material, which is a combination of high performance concrete matrix and fibre reinforcement (Richard and Cheyrezy, 1995). It can be treated as a combination of three concrete technologies to a greater extent (as shown in Figure 1.1): self-compacting concrete (SCC), fibre reinforced concrete (FRC) and high performance concrete (HPC) (Camacho, 2013). Due to the relatively high binder amount, low water to binder ratio and high fibre dosage, UHPFRC has superior mechanical properties and energy absorption capacity (El-Dieb, 2009; Tayeh et al., 2012; Hassan et al., 2012; Rossi, 2013). The stress-strain curves depicted in Figure 1.2 clearly show that the energy adsorbed by UHPFRC in straining is extensive. The consumed energy is represented by the area under the stress-strain curves. This high potential of energy absorption capacity makes UHPFRC suitable for applications where high energy release rates exist. This is the case for all the mechanical impact loads acting on structural members. These impact loads can be caused by e.g.: 1) vehicle impacts, 2) deflagration of inflammable chemicals, 3) detonation of explosives, 4) ballistic impacts. The latter two cases become more important nowadays as terrorist attacks are aiming at the collapse of complete buildings or the destruction of sensitive infrastructure. Here, UHPFRC can be used for strengthening and protection of already existing buildings or the design of new structural members. In fact, the use of

UHPFRC already showed good results in minimizing the damaging effects caused by intentional events, such as terrorist attacks (Bindiganavile et al., 2002; Parant et al., 2007). However, the detailed fracture mechanisms of UHPFRC under external impact are still not clear enough, which causes that the impact resistance capacity of such material also contains a great potential to be explored.

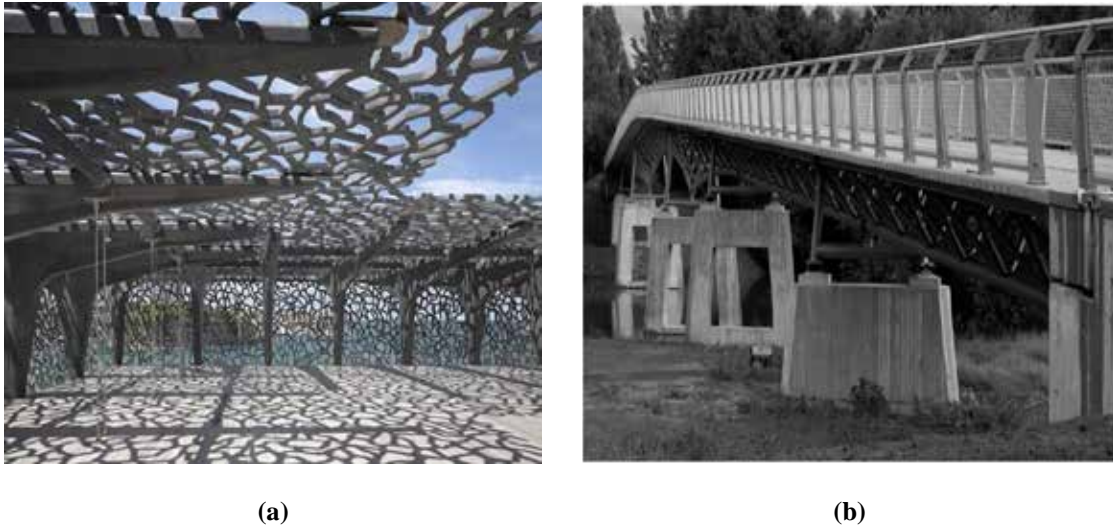


**Figure 1.3: Examples of the application of UHPFRC: (a) Mediterranean Culture Museum in Marseille, France; (b) UHPFRC bridge across the River Fulda in Kassel, Germany (Fehling et al., 2008; Kanavas, 2014)**

As commonly known, the building materials sector is the third-largest CO<sub>2</sub> emitting industrial sector world-wide, as well as in the European Union. The cement production is said to represent about 7% of the total anthropogenic CO<sub>2</sub> emissions (UNSTATS, 2010; Friedlingstein et al., 2010; Capros et al., 2001). Therefore, to promote a sustainable development also in the concrete industry, one of the promising approaches is to design and produce a type of concrete with less clinker, thus inducing lower CO<sub>2</sub> emissions than traditional ones while providing the same reliability, with a much better durability (Denarié and Brühwiler, 2011; Habert et al., 2013). Considering the successful application of UHPFRC in practice (e.g. Mediterranean Culture Museum in Marseille in France and UHPFRC bridge build in Kassel of Germany, as shown in Figure 1.3), UHPFRC seems to be a suitable candidate to reduce the global warming impact of construction materials. Due to its superior mechanical properties and durability, a structure made of UHPFRC can be much more slender compared to a normal concrete structure. One example is illustrated in Figure 1.4 here, where notable differences between conventional reinforced concrete and UHPFRC (used for the construction of an L-shaped wall meeting the same project requirements) can be observed (Voo et al., 2012). In this application, the UHPFRC solution requires 73% less material than the ordinary rebar-reinforced wall. Thus it weighs 260 kg/m, much less than the 1200 kg/m of the wall constructed with conventional reinforced concrete. However, as can be found in available

literature (El-Dieb, 2009; Park et al., 2012; Tayeh et al., 2012; Hassan et al., 2012; Rossi, 2013), when producing UHPFRC, the binder and fibre contents are always relatively high. Moreover, in most cases, the UHPFRC compositions are not optimized. Hence, it can be assumed that binders and fibres are not all efficiently utilized in the UHPFRC production, which can significantly increase the materials and energy cost. Nowadays, as the sustainable development is currently a crucial global issue, high material cost, high energy consumption and embedded CO<sub>2</sub> for UHPFRC are the typical disadvantages that restrict its wider application. Hence, to efficiently develop a sustainable UHPFRC still needs further investigation.

Based on the premises mentioned above, it can be summarized that the development of sustainable protective Ultra-High Performance Fibre Reinforced Concrete (UHPFRC) is challenging and important.



**Figure 1.4: Difference in sectional dimensions of an L-shaped wall, made of conventional and UHPFRC (Voo et al., 2012)**

## **1.2 Ultra-High Performance Fibre Reinforced Concrete (UHPFRC)**

### **1.2.1 Development**

Ultra-High Performance Fibre Reinforced Concrete (UHPFRC) is the outcome of a demand that began in the 1930s to seek for approaches to increase the mechanical properties of concrete, in particular its compressive strength. At the beginning of the 1950s, Graf produced a type of concrete with strength of 70 MPa (Bache, 1991). This did not change until 1966, when a special production method allowed the production of concrete with the strength of 140 MPa. After that, it was demonstrated that the addition of silica fume and water reducing agents/plasticizers is a simple way to produce a concrete with high strength and good workability. In this field, a significant innovation was the development of the material SIFCON (Slurry Infiltrated Fibre Concrete), in which the fibres are preplaced in the formwork moulds to its full capacity and the

resulting fibre network is infiltrated by a cement-based slurry (Naaman and Homrich, 1989). In 1994, a new mix named "Reactive Powder Concrete" was developed, which continues to exist today as "Ductal" (Richard and Cheyrezy, 1995). With further developments of the concrete technology, engineers realized that the advanced concrete, besides the high strength, should also have other excellent properties, which led to the term "Ultra-High Performance Concrete (UHPC)" and "Ultra-High Performance Fibre Reinforced Concrete (UHPFRC)" (Acker and Behloil, 2004). Then, the UHPC and UHPFRC attracted more and more attention (Yang et al., 2009; Tuan et al., 2011a; Tuan et al., 2011b; Hassan et al., 2012; Tayeh et al., 2012; Park et al., 2012; Rossi, 2013; Wang et al., 2014; Yu et al., 2014a; Yu et al., 2014c; Yu et al., 2015). In 2002, the first design rules for UHPFRC were published in France (French Interim Recommendations, 2002).

### 1.2.2 Available standard and specificity for UHPFRC

So far, there is no systematical standard for design and production of UHPFRC, other than one French Interim Recommendations (2002). These recommendations constitute a reference document serving as a basis for an appropriate use of this material in civil engineering. UHPFRC refers to a material with a cement matrix and a characteristic compressive strength of about 150 MPa, containing steel fibres in order to achieve ductile behaviour under tension and, if possible, to dispense of the need for passive (non-prestressed) reinforcement. Due to the use of admixtures such as plasticizers/water reducers and superplasticizers, UHPFRC mixes generally have a low water-binder ratio. Special attention should be paid to controlling the quantities of water added to the concrete by the different ingredients (mixing water, water in aggregate and admixtures). Generally speaking, the mix design of UHPFRC should obey the following procedure (Interim Recommendations, 2002):

- 1) Establish the nominal mix design on the basis of design studies;
- 2) Confirm the mix design by means of suitability tests;
- 3) Follow-up manufacture by means of routine checks.

The nominal mix design includes:

- 1) The designation and weight of each class of aggregates (dry ingredients);
- 2) Designation and weight of cement (indicating the quantity of silica fume in the case of a cement with premixed silica fume);
- 3) Designation and dry weight of each addition (silica fume, filler, fly ash, slag);
- 4) Total volume of water: volume of mix water and volume of water in each ingredient (aggregate, any additions, admixtures);
- 5) Designation and weight of dry extracts of any admixtures.

In the last 25 years, the outcome in concrete technology has allowed the production of UHPFRC with excellent rheological behaviour (workability, self-placing and self-

densifying properties), mechanical properties (very high compressive strength and non-brittle tensile behaviour) and durability performance (Jacques and Cete, 2004). The actual development of a UHPFRC starts with the design of the granular structure of the aggregates, for which the selection and characterization of suitable fines for optimum packing density are of key importance. Currently, to achieve excellent mechanical behaviour, some special techniques and raw materials must be adopted in the preparation of UHPFRC, which include (Wang et al., 2012):

- 1) Coarse aggregate is mostly removed to improve the homogeneity of concrete;
- 2) Steel fibre is introduced to improve ductility;
- 3) High quality superplasticizer and large quantities of fine microsilica and quartz are added, to achieve a low water/binder ratio, to reduce porosity and improve strength;
- 4) Pressure may be applied before and during the setting to increase the compactness of the concrete;
- 5) High activity microsilica and/or nanosilica may be mixed into cementitious materials to accelerate the hydration of cement and catalyse a strong pozzolanic reaction effect;
- 6) Steam curing may be applied to gain higher strengths.

In short, to gain the desired properties of a UHPFRC, well-chosen raw materials and sophisticated technical procedures are conventionally required. Several literature examples of the ingredient composition of UHPFRC mixtures are summarized in Table 1.1.

**Table 1.1: Ingredient composition of different UHPFRC mixtures**

Materials (kg/m <sup>3</sup> )	(Bornemann and Schmidt, 2002)	(Fröhlich and Schmidt, 2012)	(Deeb et al., 2012)	(Wang et al., 2012)
Water	166	183	188	162
Cement	832	775	543.5	810
Slag	-	-	311.5	0
Silica fume	135	164	214	90
Quartz (fine)	207	193	470	-
Quartz (Coarse)	-	-	470	616
Silica sand	975	946	-	-
Basalt (2-8)	-	-	-	923
Micro-fibres (vol.)	2.5%	2.5%		2%
Macro-fibres (vol.)	-	-	2.5%	-
Superplasticizer	10.6	10.3	41.33	18

From Table 1.1, it can be observed that, compared to normal concrete, a high binder amount is typically utilized in the production of UHPFRC. In addition, a large dosage of

superplasticizer (SP) is also added into UHPFRC, which causes the required water content is low and the workability of UHPFRC is still acceptable. Furthermore, the coarse aggregate ( $> 8$  mm) amount is normally limited.

In general, it can be noticed that, though UHPFRC has outstanding mechanical properties, its preparation method requires costly materials and relatively sophisticated technology. Hence, the limited available resources and the high cost constrain its application in modern construction industry, especially in the developing countries, which gives a motivation for a search of alternative materials with similar functions to substitute the expensive composites in UHPFRC.

### **1.3 Research objectives and strategies**

#### ***Research objectives***

Due to the strong demand for impact resistant building materials in both civil and military fields and the specificities of UHPFRC, it is logic to apply UHPFRC in the production of protective structures. From the available literature, the investigations regarding dynamic behaviour and energy dissipation capacity of UHPFRC are still insufficient. Moreover, in most cases, the produced UHPFRC is not sustainable or environmentally friendly, since the efficiencies of the utilized powders (e.g. cement) and fibres are relatively low (Yu et al., 2014a, Yu et al., 2014d). Hence, based on these premises, the objectives of this research can be summarized as:

- 1) Design and production of a sustainable UHPFRC;
- 2) Properties (static and dynamic) assessment of the developed UHPFRC;
- 3) Modeling of the developed sustainable UHPFRC under impact loadings.

#### ***Research strategies***

To develop a sustainable UHPFRC, four strategies are mainly employed in this research: 1) optimized design of UHPFRC matrix applying particle packing model; 2) efficient application of the powders in the UHPFRC production; 3) efficient utilization of fibres in the UHPFRC production; 4) appropriate application of waste/recycled materials in the UHPFRC production. Here, the design of UHPFRC is based on the aim to achieve a densely compacted cementitious matrix, employing the modified Andreasen & Andersen particle packing model. Moreover, industrial by-products (fly ash, ground granulated blast-furnace slag) and waste/recycled material (waste bottom ash) are appropriately utilized to replace cement and aggregates, respectively. Additionally, a hybridization design of utilized fibres is employed to improve the fibre efficiency. For the properties assessment of the developed UHPFRC, a series of methods are employed to evaluate its workability, air content, water-permeable porosity, mechanical properties, flexural toughness, microstructure development, hydration kinetics, thermal properties and impact

resistance capacity. For the impact resistance capacity, two types of pendulum impact set-ups and a high velocity projectile launcher are employed. Afterwards, based on the obtained experimental results, the modeling of dynamic behaviour of the sustainable UHPFRC under different impact loadings is performed. The modeling can be mainly divided into two sections: 1) energy absorption of UHPFRC under Charpy impact loading; 2) numerical modeling of UHPFRC under projectile impacts.

This research is performed based on a combination of theoretical and experimental investigations. A schematic description of the research objectives and strategies is shown in Figure 1.5.

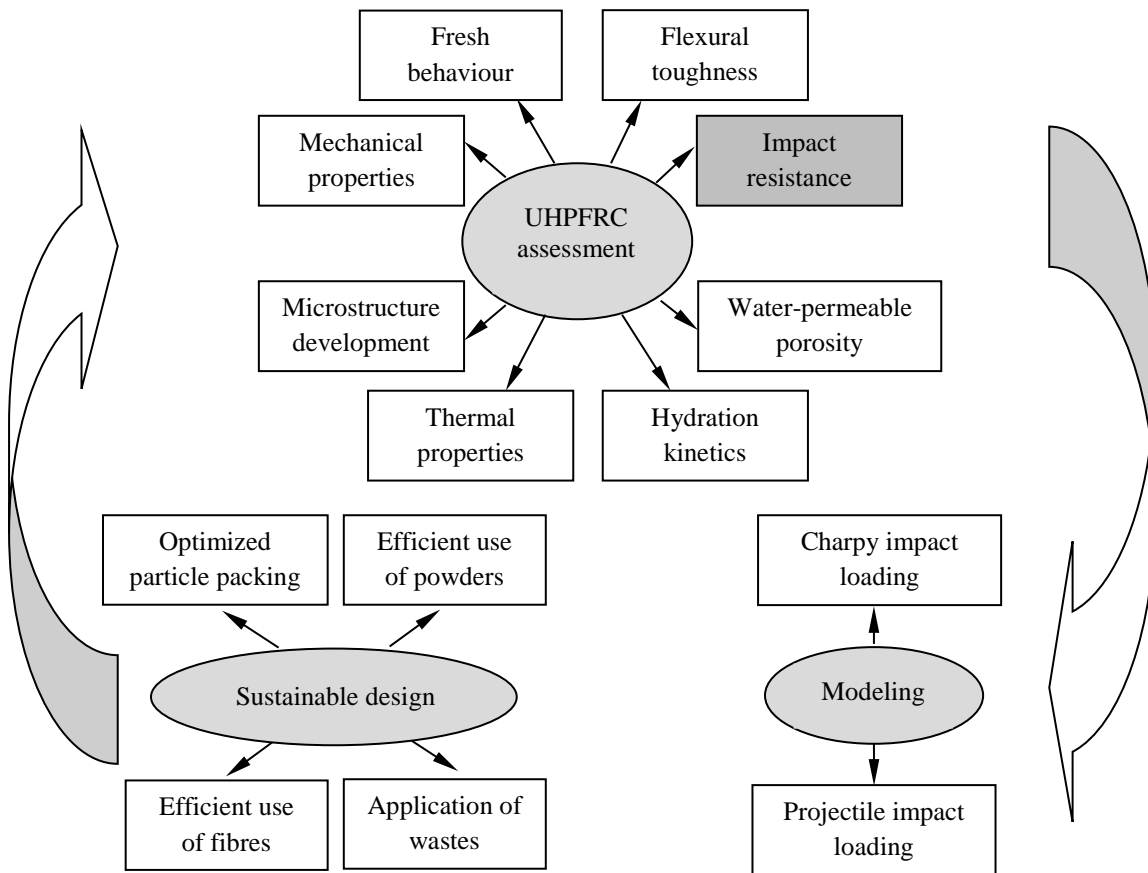
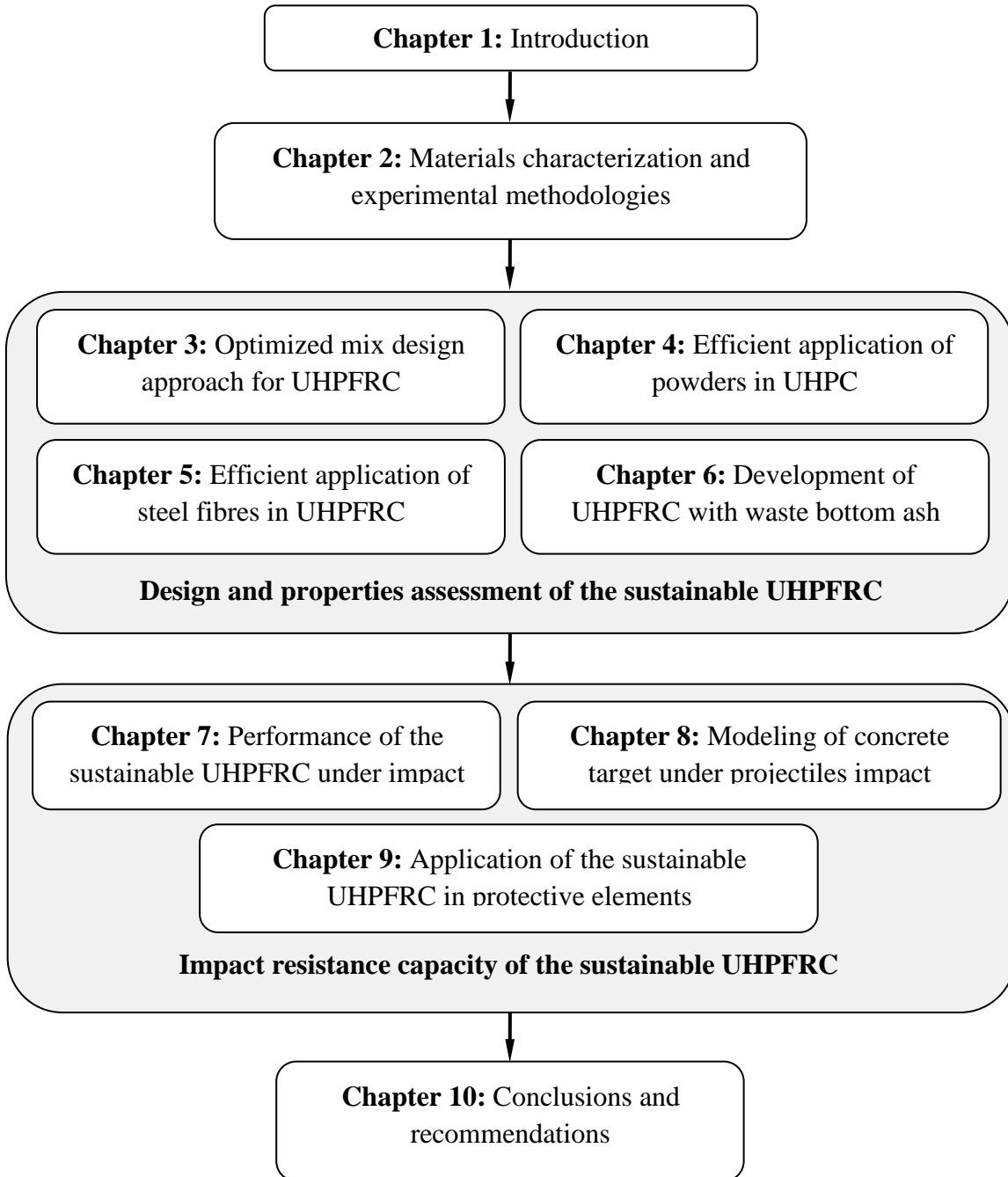


Figure 1.5: Schematic description of the research objectives and strategies

## 1.4 Outline of the thesis

To obtain a new product that contributes to a better and safer life for human beings, this research aims at the development of sustainable protective UHPFRC. Firstly, a series of methods and strategies are utilized to design a sustainable UHPFRC. Then, the properties of the developed UHPFRC are evaluated. Finally, based on the obtained experimental results, the modeling of dynamic performance of the developed sustainable UHPFRC

under different impacts is performed. The research framework of this thesis is shown in Figure 1.6, and the content of each chapter is explained in the following paragraphs.



**Figure 1.6: Outline of the thesis**

Chapter 2 focuses on the materials characterization and experimental methodologies. The raw materials can be mainly divided into three categories: 1) powders (particles smaller than 125  $\mu\text{m}$ ); 2) aggregates (granular materials except powders); 3) fibres. Then, all the used materials are characterized according to their physical and chemical properties,

including particle size distribution, specific density, water demand, chemical composition, microstructure and so on. Additionally, a series of test methods are employed to assess the properties (e.g. workability, air content, water-permeable porosity, mechanical properties, thermal properties and cement hydration kinetics) of the developed sustainable UHPFRC.

Chapter 3 provides a mix design method for UHPFRC. Due to the fact that normally a large amount of cement or binders is utilized to produce UHPFRC and the hydration degree of the cement in UHPFRC is relatively low, fillers such as limestone and quartz powders are used to partly replace cement, based on the modified Andreasen & Andersen particle packing model. Then, the properties of the optimized UHPFRC are evaluated and compared with those of other UHPFRCs. The aim of this chapter is to develop a UHPFRC with lower binder amount without sacrificing the mechanical properties.

Chapter 4 addresses the investigations regarding an efficient application of powders in UHPC (matrix of UHPFRC). This chapter can be mainly divided into two parts: 1) effect of nanosilica on the properties of UHPC; 2) effect of different mineral admixtures (fly ash, ground granulated blast slag and limestone powder) on the properties of UHPC. All the concrete mixtures are designed based on the modified A&A model. Then, the fresh and hardened behaviour, hydration kinetics, thermal properties and microstructures of the developed UHPC are evaluated. The aim of this chapter is to use all the powder materials efficiently and produce a sustainable UHPFRC matrix.

Chapter 5 shows the effect of different steel fibres (with various geometries) on the properties of UHPFRC. This chapter can also be divided into two parts: 1) UHPFRC with binary fibres; 2) UHPFRC with ternary fibres. The concrete matrix is designed based on the modified A&A model and fibre hybridization theory. The effect of hybrid fibres on the workability, mechanical properties and flexural toughness of UHPFRC is presented. The aim of this chapter is to clarify the contribution of different steel fibres on the properties of UHPFRC and to efficiently use the steel fibres based on the different requirements in practice.

In Chapter 6, to further reduce the materials cost and environmental impact of UHPFRC, waste bottom ash (WBA) originating from municipal solid waste incineration (MSWI) is included in the UHPFRC production. Due to the fact that the particle size distribution of the selected fraction of WBA is similar to that of sand (0-2), the WBA is used to partly replace the sand (0-2). Then, the effect of nanosilica and hybrid fibres on the properties of the UHPFRC with WBA is assessed, and the intrinsic mechanisms are investigated.

Chapter 7 firstly gives a brief review of the dynamic performance of concrete under impact loadings and the available methods to improve the impact resistance of concrete. Then, based on the results obtained in previous chapters, the sustainable UHPFRC is

produced and its dynamic performance under impact loadings is evaluated, by employing the “Charpy Impact Device” and “Modified Pendulum Impact Device”. Moreover, the dominant factors to improve the impact resistance capacity of the sustainable UHPFRC are analysed. Finally, based on the obtained experimental results, the modeling of energy absorption capacity of the sustainable UHPFRC under Charpy impact test is performed. The aim of this chapter is to evaluate the energy dissipation capacity of the sustainable UHPFRC under pendulum impact loadings and clarify the dominant factors in the production of protective structures.

Chapter 8 presents numerical modeling results of concrete targets under projectile impact, since the impact from hard projectile is the most common impact among all the impact categories (high-rate impact, shock, blast loads and so on). A brief review of classical and up-to-date investigations is firstly presented. Then, a finite elements model of concrete under projectile impact loading is created in a commercial hydrocode - LS-DYNA. Afterwards, the literature experimental results are used to validate the proposed model. Finally, the energy dissipation capacity of the developed sustainable UHPFRC in dynamic mode is assessed and predicted by using the validated model in LS-DYNA. The aim of this chapter is to investigate the energy dissipation capacity of the developed sustainable UHPFRC under hard projectile impact based on numerical approaches.

Chapter 9 continues the investigation of dynamic performance of the sustainable UHPFRC under projectile impact loading. In this chapter, the sustainable UHPFRC is applied in the production of protective elements, and the impact resistance of these protective elements is evaluated by executing high velocity projectile impact tests (in cooperation with the Dutch army). Based on the obtained experimental results, the numerical modeling of the sustainable UHPFRC under high velocity projectile impact is performed in LS-DYNA. The aim of this chapter is to apply the developed sustainable UHPFRC in practice (as protective elements), and create a suitable model to represent its dynamic performance under high velocity projectile impact.

Finally, in Chapter 10, the conclusions of the present thesis are drawn and some recommendations for further research in continuation of this work are presented.

## Chapter 2

### **Materials characterization and experimental methodologies**

#### **2.1 Introduction**

As commonly known, the properties of concrete are closely related to the compositions and characteristics of the utilized materials. Hence, to appropriately design and produce a concrete with superior properties (e.g. Ultra-High Performance Concrete (UHPC) or Ultra-High Performance Fibre Reinforced Concrete (UHPFRC)), a comprehensive understanding of the basic characteristics of raw materials is essential. In this research, a variety of raw materials is applied, which can be mainly divided into three categories: 1) powders, considered as granular materials with particle size smaller than 125  $\mu\text{m}$ ; 2) aggregates (granular materials with particles  $> 125 \mu\text{m}$ ); 3) fibres.

Powders can be generally divided into reactive and non-reactive types. Due to its chemical composition, the reactive powder has reactivity, which means in the presence of water they form on their own or with the help of accelerators (e.g. cement clinker crystalline reaction products), and contribute to the strength development (Hunger, 2010). The reaction mechanisms of different powders can be summarized as (Taylor, 1997): 1) hydraulic (dominant reaction type for the curing of Portland cement); 2) latent-hydraulic (in principle react like cement clinker but need calcium hydroxide or sulphate, respectively both as accelerator for their hydration); 3) pozzolanic (dissolved silicates coming along with the pozzolan react with calcium hydroxide under formation of C-S-H phases). In addition, for the non-reactive powder, they can provide a physical filler effect to concrete mixture, since the fine particles can fill the voids between coarser particles. The literature in this field shows that the void fraction in concrete can be significantly minimized by including fine non-reactive powders with appropriate particle sizes, which can lead to a substantial improvement of workability for the fresh concrete, as well as improved durability and mechanical properties in hardened state (Hunger and Brouwers, 2009; Hunger, 2010; Quercia et al., 2012; Spiesz, 2013).

Ultra-High Performance Fibre Reinforced Concrete (UHPFRC) is a relatively new building material, in which the coarse aggregates ( $> 4 \text{ mm}$ ) application is limited and a large amount of powders is normally utilized. From the available literature (El-Dieb, 2009; Park et al., 2012; Tayeh et al., 2012; Hassan et al., 2012; Rossi, 2013), it can be noticed that reactive powders are the main ingredients in the production of UHPFRC, since UHPFRC has strict requirements on the mechanical properties. Nevertheless, it is unclear that whether all of these reactive powders are effectively used, and whether it is possible to partially replace the reactive powders by cheaper and less energy-intensive

non-reactive powders. Hence, to clearly understand the efficiency of these powder materials and their effect on the properties of UHPFRC, their properties such as particle size distribution, specific density, water demand, chemical composition and microstructure are firstly evaluated in this study.

The importance of densified granular system is known since the early days of concrete production (Féret, 1892). However, at that time, only the aggregate fractions were included in this consideration, which can be attributed to the fact that the volumetric amount of aggregates (fine and coarse aggregates) in concrete is commonly around 70%. As described before, the coarse aggregates amount ( $> 4$  mm) is normally limited in the production of UHPFRC, since the aggregates with relatively large sizes may disturb the homogeneity of UHPFRC matrix. Hence, in this research, two types of fine aggregates ( $< 2$  mm) are mainly utilized. Moreover, to further reduce the environmental impact of UHPFRC, one type of waste materials (waste bottom ash - WBA) is utilized to partially replace the normal aggregates in this study. A detailed comparison of the WBA and normal aggregates are shown in the following part.

Compared to normal strength concrete (NSC), high strength concrete (HSC) and normal fibre reinforced concrete (NFRC), UHPFRC has much better mechanical properties, which should be mainly attributed to the relatively high amount of additional fibres. In fact, the concept of using fibres to improve the mechanical attributes of construction materials can be traced back to thousands years ago. For instance, straws were added into mud bricks; horse hair was utilized to reinforce plaster, and asbestos was used to reinforce pottery. The modern development of fibre-reinforced concrete (FRC) was initiated in the early sixties (Wafa, 1990), while a more efficient material (compared to rebar) was searched to optimize the plasticity of the plain concrete. Nowadays, with the development of steel and polymer industries, there are a number of different fibres available (e.g. steel fibres, polymer fibres, natural fibres, glass fibres, carbon fibres and others) ranging from a few millimetres to several centimetres length. In this research, three types of steel fibres and one type of polypropylene fibres are utilized in the UHPFRC production, and their basic characteristics are presented in the following part.

Additionally, some test procedures mainly employed to assess the properties (workability, air content, water-permeable porosity, mechanical properties and cement hydration kinetics) of the developed UHPFRC are also explained in this chapter.

## **2.2 Utilized materials**

### **2.2.1 Powders characterization**

In this research, various powders of different types are utilized. These powder materials can be mainly divided into two categories: 1) reactive materials (cement, microsilica, nanosilica, fly ash, and ground granulated blast furnace slag); 2) non-reactive materials

(limestone powder, quartz powder). Due to the fact that the physical and chemical properties of powder materials have very close relationship with the later developed concrete, the utilized powder materials are systematically analysed, including their particle size, specific density, water demand, chemical composition and microstructure.

· *Particle size distribution*

The particle size distribution (PSD) of all the solid ingredients is important for the mix design of concrete, since the fresh state behaviour and hardened properties of concrete mixtures are influenced by the particle packing of all the utilized granular materials. There are numerous approaches suitable for determining the PSDs. Besides sieving and microscopy-techniques, most of the existing methods are based on either sedimentation of particles in suitable liquids or diffraction of light (Hunger, 2010). In this study, considering the relatively small particle size of powders ( $< 125 \mu\text{m}$ ), a laser light scattering (LLS) technique (Malvern Mastersizer 2000<sup>®</sup> PSD analyzer) is employed to determine the PSDs of all the powder materials. This method is using the feature that the diffraction angle of laser beam on the particle surfaces is inversely proportional to the particle size. A projection of this diffracted light waves is analysed and the particle size is computed (Quercia, 2014). In the calculation, the spherical particle shape is assumed, as explained in (Hunger, 2010). Based on the ISO standard 13320-1 (2009), the powders are measured in liquid dispersion using the Mie scattering model. Due to the fact that some reactive materials can react with water, propan-2-ol is utilized as the dispersion liquid.

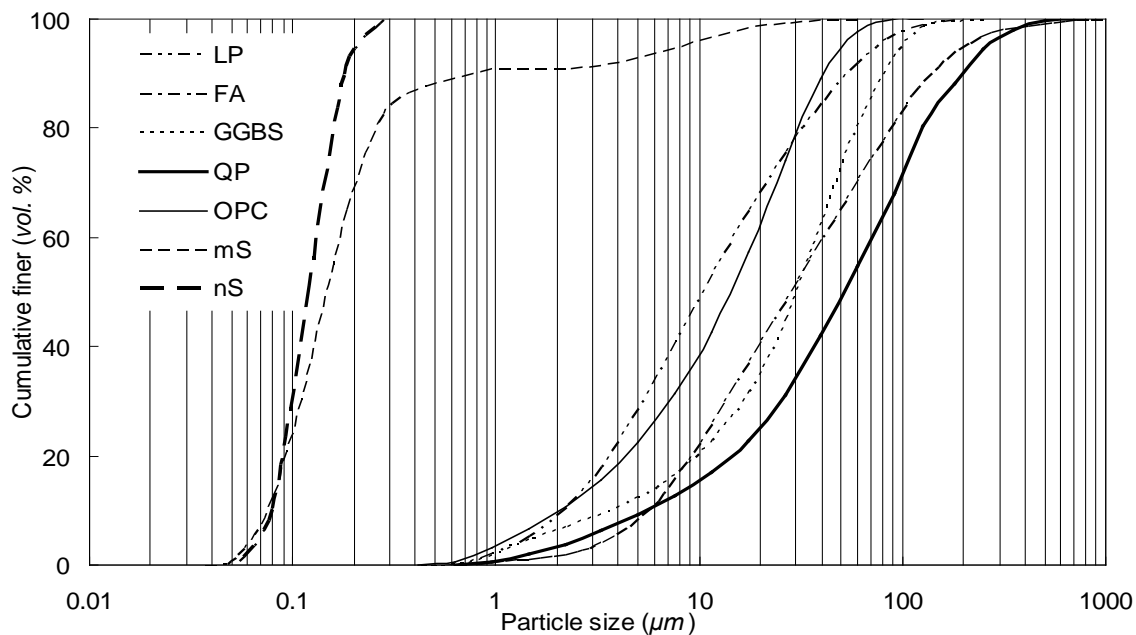


**Figure 2.1: Cumulative particle size distributions of the used powders (LP: limestone powder, FA: fly ash, GGBS: ground granulated blast slag, QP: quartz powder, OPC: Ordinary Portland Cement (CEM I 52.5 R), mS: microsilica; nS: nanosilica)**

The PSDs of all the powders utilized in this study are shown in Figures 2.1 and 2.2. It can be noticed that the PSD of cement is very similar to that of limestone powder, which implies that the limestone powder can be utilized to replace cement without significantly altering the particle packing of concrete skeleton. Moreover, the particles of quartz powder, fly ash and ground granulated blast slag are coarser than cement, while the utilized microsilica and nanosilica are much finer. Additionally, compared to microsilica, nanosilica is richer in small particles distributing in the range of 30 - 100 nm. Due to the fact that the ultra-fine silica particles are vital for the mechanical properties, the effect of nanosilica amount on the properties of UHPFRC will be investigated in the pertaining chapters.

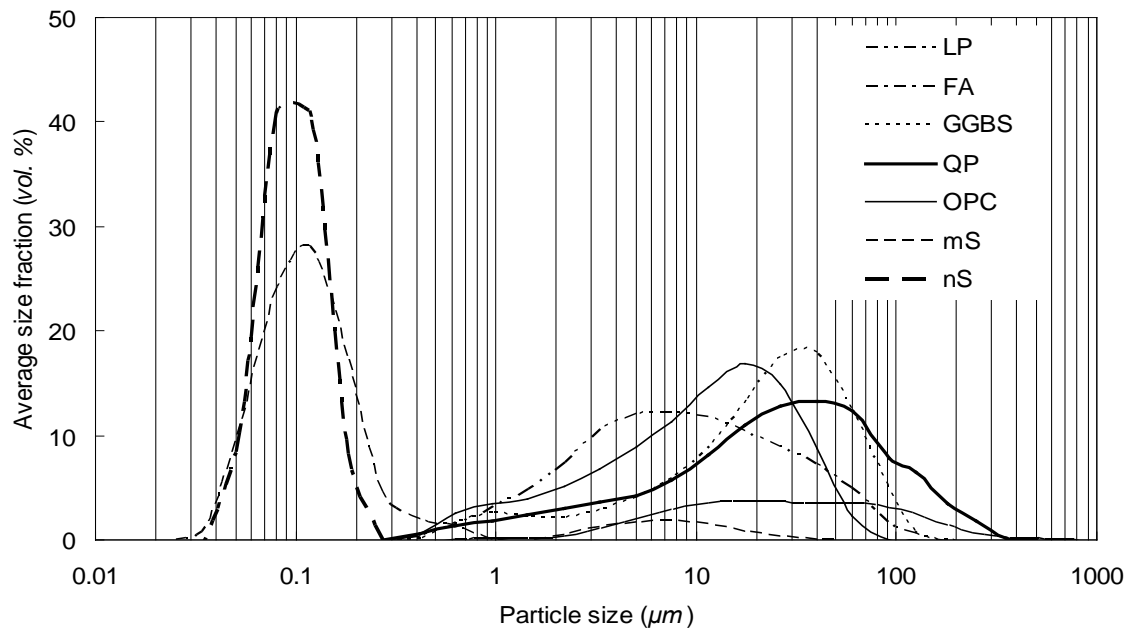


**Figure 2.2: Average sieve fractions by volume of the used powders (LP: limestone powder, FA: fly ash, GGBS: ground granulated blast slag, QP: quartz powder, OPC: Ordinary Portland Cement (CEM I 52.5 R), mS: microsilica; nS: nanosilica)**

#### • *Specific density*

According to EN 1097-7 (1999), the true volume of the materials can be measured by using water (for nonreactive materials) or ethanol (for reactive materials) liquid pycnometer. However, as described in (Yu, 2012), surface tension of the powders and entrapped gases can affect the filling of very small pores. Hence, in this study, a gas pycnometer method (AccuPyc 1340 II Pycnometer) is employed to test the true volume of powders. Compared to the liquid pycnometer, this gas pycnometer method is easier and faster. Here, the helium gas is utilized as a medium. Due to the fact that the size of a helium molecule is very small, it can rapidly fill the voids between the particles and tiny

pores on the surface of the sample. Then, the true volume of the powders can be computed by comparing the change of gas pressure and gas amount. Then, the specific density of the material can be calculated by the following equation:

$$\rho_{specific} = \frac{m}{V_{true}} \quad (2.1)$$

where  $\rho_{specific}$  is the specific density ( $\text{g/cm}^3$ ),  $m$  is the mass of the material (g) and  $V_{true}$  is the true volume of the material ( $\text{cm}^3$ ).

**Table 2.1: Specific densities of powders measured by AccuPyc 1340 II Pycnometer**

Materials	Specific density ( $\text{g/cm}^3$ )			
	Sample 1	Sample 2	Sample 3	Average
OPC	3.154	3.151	3.158	3.154
LP	2.728	2.724	2.722	2.725
FA	2.294	2.295	2.292	2.294
GGBS	2.891	2.895	2.894	2.893
QP	2.665	2.664	2.662	2.664
mS	2.232	2.232	2.235	2.233
nS	2.221	2.219	2.223	2.221

(OPC: Ordinary Portland Cement (CEM I 52.5 R), LP: limestone powder, FA: fly ash, GGBS: ground granulated blast furnace slag, QP: quartz powder, mS: microsilica, nS: nanosilica)

Prior to the true volume determination, all the powders have been dried in oven at temperature of 105 °C for 24 hours. Then, the dry materials are stored in a desiccator for cooling down to a room temperature. To minimize the errors, the measurement of one powder is performed at least three times. The obtained specific densities of the powders are presented in Table 2.1. It can be seen that the specific density of cement is the highest ( $3.15 \text{ g/cm}^3$ ), while the specific density of limestone powder, quartz powder and ground granulated blast slag are similar to each other and fluctuate around  $2.7 \text{ g/cm}^3$ . The density of fly ash, microsilica and nanosilica fluctuate about  $2.2 \text{ g/cm}^3$ .

Based on the obtained specific densities and particle size distributions of powders, it can be concluded that limestone powder is suitable to be utilized to partially replace cement without significantly affecting the particle packing skeleton in concrete.

#### • **Water demand**

The water demand of powders, particularly of the fine particles, is a crucial parameter for the properties of concrete. The total water demand is strongly influenced by a layer of adsorbed water molecules around the particles and an additional amount needed to fill the inter-granular voids of the powder system (Hunger, 2010). Due to the fact that the fine particles always have a high specific surface area, they can significantly affect the total

water demand and fresh behaviour of concrete. As commonly known, to achieve superior mechanical properties, a very limited water amount is normally utilized in the cementitious system of UHPFRC. Therefore, it is very important to carefully evaluate the water demand amount of all the utilized powder materials.

In this study, the water demands of cement, limestone powder, fly ash, ground granulated blast slag are evaluated by employing the Puntke test. As described in (Hunger, 2010), the water demand from Puntke test shows the water absorption capacity of the tested powder at the point of saturation, which depicts the transition from a coherent packing to a suspension. Therefore, a fine, cohesion-free granular skeleton cannot be self-compacted to a specific packing density until the water content is sufficient for the saturation of the dense granular structure. The first sign of bleeding is a glimmering surface of the water-powder mixture, which also is the evaluation target criterion of the addressed test. The test results are shown in Table 2.2.

**Table 2.2: Particle information of Ordinary Portland Cement (OPC), limestone powder (LP), fly ash (FA) and ground granulated blast slag (GGBS)**

Materials	Water demand (Puntke test) $m_{w-p}$ (g)	Computed void fraction $\psi$ (%)	Particle shape factor $\zeta_{Reschke}$ (-) (Hunger, 2010)
OPC (CEM I 52.5 R)	13.2	45.4	1.68
LP	10.8	37.0	1.26
FA	11.2	33.9	1.20
GGBS	13.2	43.3	1.58

Additionally, Puntke test assumes that for the point of saturation, the granular blend becomes free of air (the void fraction is completely filled with water), which derives a relation between the void fraction and the involved volumes of water and powder represented by their masses. Hence, void fraction of the saturated powder material can be computed as follows (Puntke, 2002):

$$\psi = \frac{V_w}{V_p + V_w} \quad (2.2)$$

where  $\psi$  is the void fraction of the saturated powder material (%),  $V_w$  is the volumetric water demand of the powder material for saturation ( $\text{cm}^3$ ),  $V_p$  is the volume of the tested powder material ( $\text{cm}^3$ ).

#### • *Chemical composition*

As commonly known, there is a strong connection between the chemical composition of a powder and its physical and chemical properties. Moreover, the chemical composition of

reactive powders can significantly influence the properties of concrete. Hence, in this study, the chemical compositions of all the utilized powders are analysed by using X-ray Fluorescence (XRF) (PANalytical - Epsilon 3), and the results are presented in Table 2.3.

**Table 2.3: Chemical composition of Ordinary Portland Cement (OPC), limestone powder (LP), fly ash (FA), ground granulated blast slag (GGBS), microsilica (mS) and nanosilica (nS)**

Substance	OPC (mass %)	FA (mass %)	GGBS (mass %)	LP (mass %)	mS (mass %)	nS (mass %)
CaO	64.60	4.46	38.89	89.56	0.28	0.08
SiO <sub>2</sub>	20.08	55.32	34.18	4.36	97.82	98.68
Al <sub>2</sub> O <sub>3</sub>	4.98	22.45	13.63	1.00	0.29	0.37
Fe <sub>2</sub> O <sub>3</sub>	3.24	8.52	0.51	1.60	0.61	-
K <sub>2</sub> O	0.53	2.26	0.43	0.34	0.51	0.35
Na <sub>2</sub> O	0.27	1.65	0.33	0.21	0.02	0.32
SO <sub>3</sub>	3.13	1.39	1.41	-	0.15	-
MgO	1.98	1.89	10.62	1.01	0.26	-
TiO <sub>2</sub>	0.30	1.17	-	0.06	-	0.01
Mn <sub>3</sub> O <sub>4</sub>	0.10	0.11	-	1.605	-	-
P <sub>2</sub> O <sub>5</sub>	0.74	0.76	-	0.241	-	0.15
Cl <sup>-</sup>	0.05	0.02	-	-	0.06	0.04

#### · *Microstructure*

In concrete, the particle shape and surface roughness (texture) of powders can directly affect its water absorption capacity, flowability, bonding behaviour and so on. Here, to further clarify the micro-morphology of the utilized powders, the microstructure of the investigated powders is determined by employing the scanning electron microscopy (SEM) (Quanta 650 FEG, FEI), and the results are illustrated in Figure 2.3.

As can be seen, a number of spherical particles can be observed in fly ash, while the particles in the other powders have rather irregular particle shape. Therefore, it can be predicted that when the spherical fly ash particles are added to replace cement, the flowability of UHPFRC may be improved. Moreover, the irregular particle shape of ground granulated blast slag is beneficial for improving the bonding and interlocking strength between materials in the matrix, which in turn leads to a better mechanical properties of UHPFRC. Additionally, the SEM picture of microsilica shows that a number of microsilica particles agglomerate to form some big particle clusters, which can be attributed to the drying process of the material before the SEM test. In this study, the utilized nanosilica is a slurry material. Considering that the water evaporation and drying process may cause serious agglomeration of the nanosilica particles, the microstructure of nanosilica is not analysed.

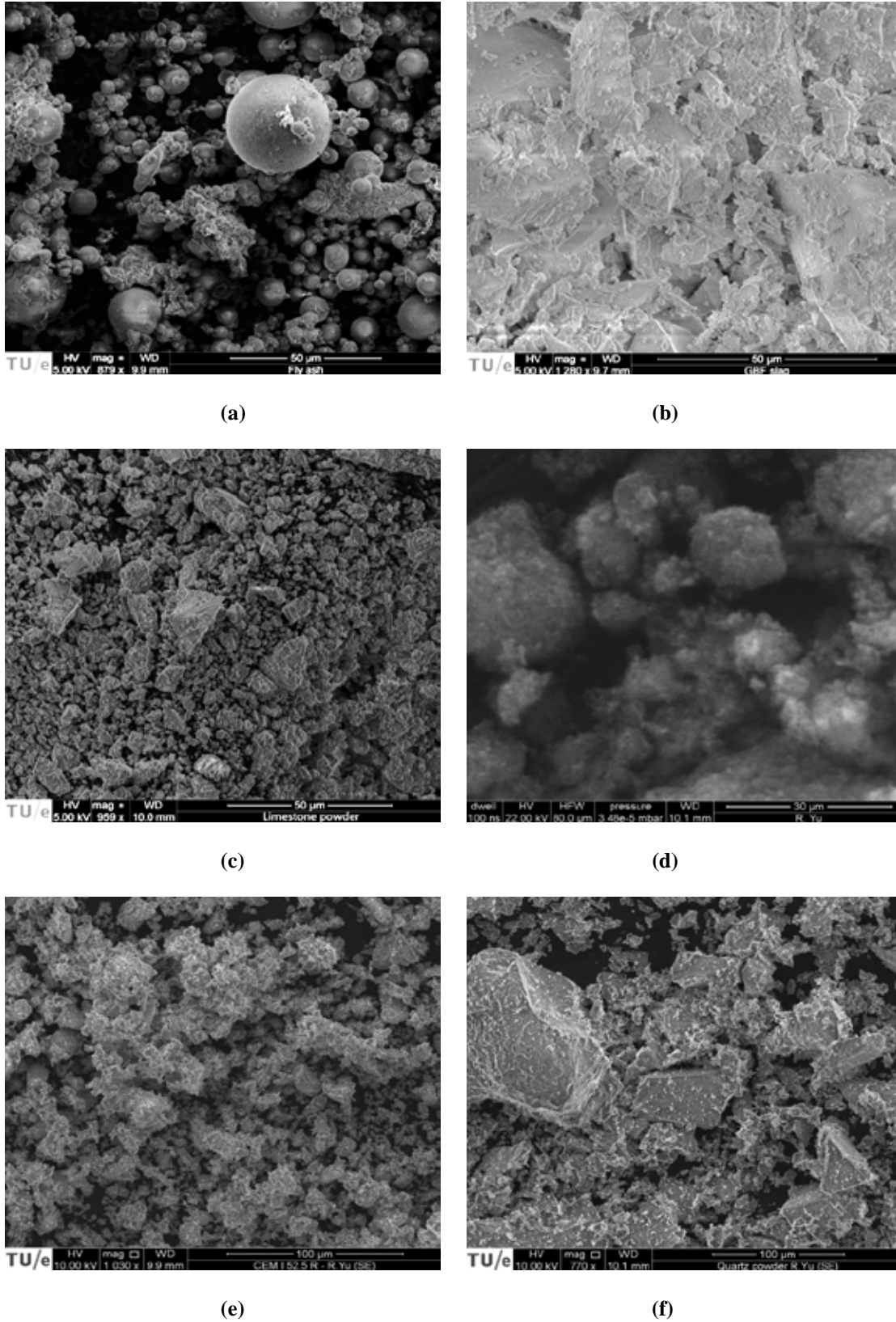


**Figure 2.3: Scanning electron microscopy (SEM) pictures of used fly ash (a), ground granulated blast slag (b), limestone powder (c), microsilica (d), cement (e) and quartz powder (f)**

### 2.2.2 Aggregates characterization

In this research, two types of normal fine aggregates are mainly utilized: one is normal sand with the fraction 0-2 mm and the other one is microsand with the fraction 0-1 mm (Graniet-Import Benelux, the Netherlands). In addition, to further reduce the materials cost and produce a sustainable UHPFRC, one type of waste bottom ash (WBA) is utilized to replace sand (0-2) in the UHPFRC production. The WBA used in this study is obtained from a local municipal solid waste incineration (MSWI) plant (provided by Attero, the Netherlands), which can be described as heterogeneous particles consisting of glass, magnetic and paramagnetic metals, minerals, synthetic and natural ceramics, and unburned matter (Chimenos et al., 1999). According to the European Landfill Directive, the weathered WBA is considered suitable for land filling or reuse. The most widespread practice is the reuse of WBA as an aggregate substitute for road base (Izquierdo et al., 2001, Forteza et al., 2004), which is subject to strict requirements that are defined by each European country. Another important way of applying WBA is as an aggregate for concrete (Lee et al., 2010; Kim and Lee, 2011b; Kim et al., 2012). Hence, to successfully utilize the WBA in the UHPFRC production, its basic characteristics need to be deeply understood. In this part, the particle size distribution, specific density, chemical composition, phase composition and morphology of the used aggregates are assessed.

- *Particle size distribution*

Differently from the method employed to evaluate the particle size distribution of powders, the PSDs of the utilized aggregates are measured by sieve analysis based on EN-933-1 (1997). The aggregates pass through a series of sieves that are arranged in the order of increasing sieve openings from bottom to top. Then, the mass of materials retaining on each sieve is weighted and used to calculate the proportion of the total mass. However, for the microsand used in this study, due to the fact that it contains a large amount of fine particles, its PSD is determined by a combination of both sieve and laser diffraction analyses. The obtained PSDs results of all the aggregates are presented in Figure 2.4. It is noteworthy that the cumulative particle size distributions of the used sand (0-2) and the WBA are similar to each other. Moreover, compared to the sand (0-2) and WBA, the utilized microsand has much more smaller particles, which is beneficial for filling the gaps between powders and aggregates and further improving the properties of UHPFRC.

- *Specific density*

Similarly to the method employed to evaluate the specific density of powders, the helium pycnometer (AccuPyc 1340 II Pycnometer) is utilized to measure the specific density of all the used aggregates. The results are shown in Table 2.4. It can be found that the specific density of all the utilized aggregates fluctuates around  $2.7 \text{ g/cm}^3$ . Hence, based

on the obtained particle size distribution and specific density results, it can be summarized that the particle packing of the solid skeleton in concrete would be only slightly affected when the sand (0-2) is partly replaced by WBA.

**Table 2.4: Specific densities of powders measured by AccuPyc 1340 II Pycnometer**

Materials	Specific density ( $g/cm^3$ )			
	Sample 1	Sample 2	Sample 3	Average
Microsand	2.721	2.726	2.722	2.723
Sand (0-2)	2.648	2.644	2.639	2.644
WBA	2.734	2.729	2.728	2.730

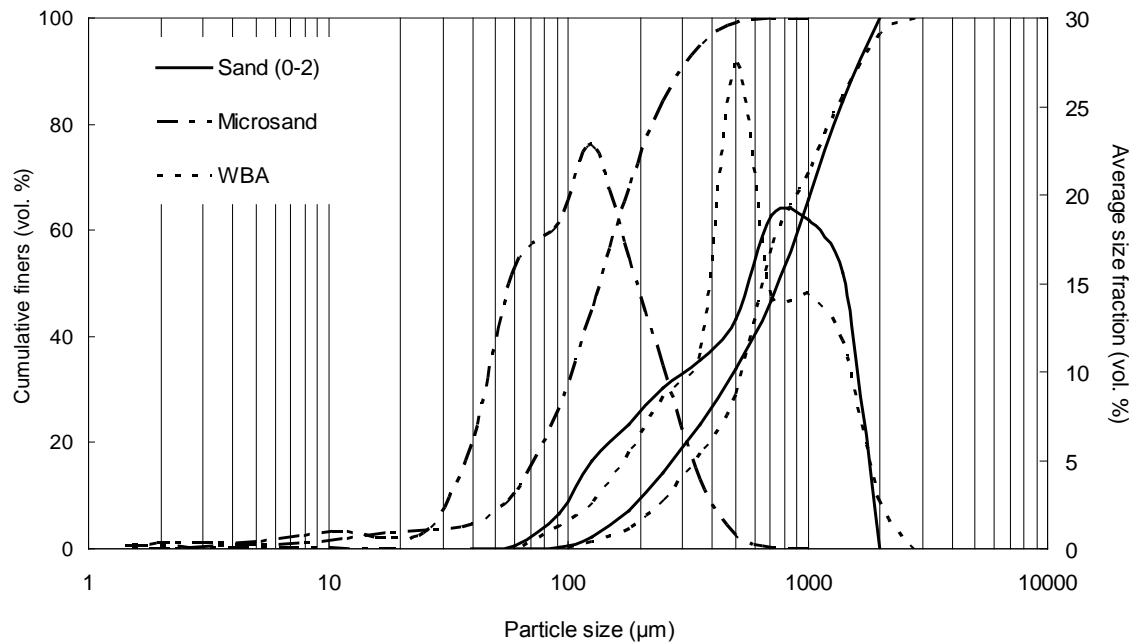


**Figure 2.4: Particle size distributions of the used aggregates (WBA: waste bottom ash)**

#### • *Chemical composition*

To further clarify the difference between the WBA and sand (0-2), their chemical compositions are evaluated by X-ray Fluorescence (XRF) (PANalytical - Epsilon 3). The results are presented in Table 2.5. It can be noticed that the sand (0-2) is mainly composed of  $SiO_2$ , while the WBA has more complicated composition. The  $SiO_2$  (59.11%) is still the main component in WBA, which is followed by  $CaO$  (14.06%) and  $Fe_2O_3$  (11.64%). Furthermore, it is important to see that the WBA has a higher  $Al_2O_3$  content than that of sand (0-2). As commonly known (Pera et al., 1997; Müller and Rübner, 2006), the metallic aluminium particles in WBA can react with alkaline substances in concrete and release hydrogen, which may seriously affect the microstructure development of cement hydration products and produce cracks in concrete.

Hence, to confirm the existence of metallic aluminium, some other test devices or procedures are needed.

**Table 2.5: Chemical composition of sand (0-2) and the WBA**

Substance	Sand (0-2) (mass %)	WBA (mass %)
CaO	0.12	14.85
SiO <sub>2</sub>	92.61	59.11
Al <sub>2</sub> O <sub>3</sub>	6.21	8.13
Fe <sub>2</sub> O <sub>3</sub>	0.04	12.29
K <sub>2</sub> O	0.54	0.93
Na <sub>2</sub> O	0.02	1.96
SO <sub>3</sub>	0.15	0.78
MgO	0.26	1.13
P <sub>2</sub> O <sub>5</sub>	0.03	0.78
Cl <sup>-</sup>	0.02	0.04

• *Phase compositions*

The phase compositions of the WBA are obtained by using X-ray diffraction analysis (XRD, Cu tube, 40 kV, 30 mA, 10-90°, 0.02°/step, 2°/min). The results are illustrated in Figure 2.5. The main peaks are marked according to the crystalline diffractogram specification, which are SiO<sub>2</sub>, CaCO<sub>3</sub>, CaSO<sub>4</sub> and Fe<sub>2</sub>O<sub>3</sub>. In addition, the peak representing SiO<sub>2</sub> is very obvious. This is similar to that of normal sand. However, the peak representing metallic aluminium cannot be clearly observed.

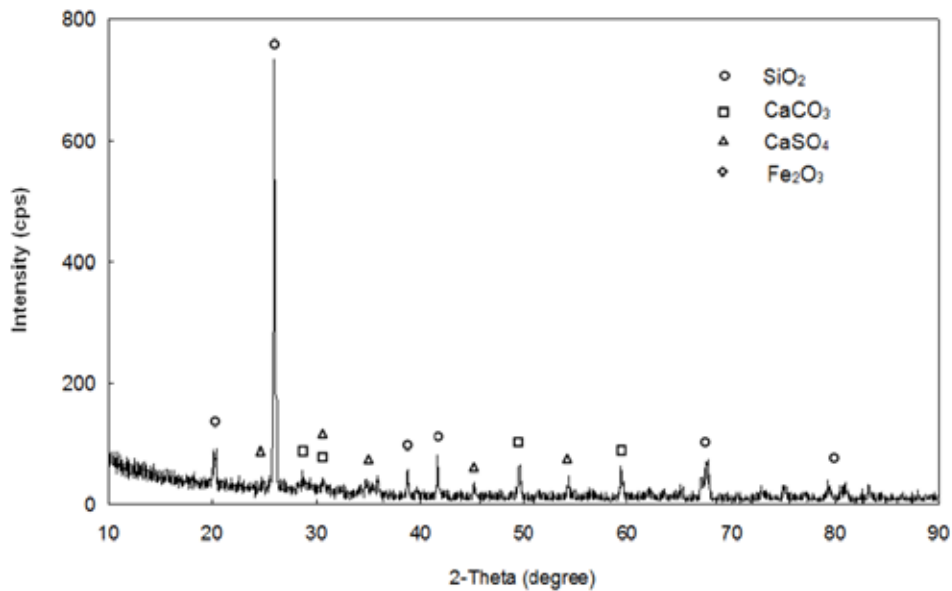
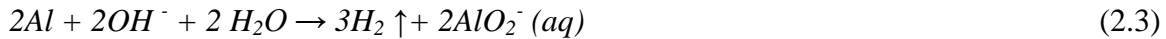


**Figure 2.5: XRD analysis of the used waste bottom ash (WBA)**

### · *Hydrogen release*

To clarify the existence of metallic aluminum in the utilized WBA, the hydrogen release of WBA is evaluated, following the method shown in (Qiao et al., 2008). As has been widely reported that metallic aluminum in WBA can react with hydroxyl ions under high pH conditions to produce hydrogen gas as (Müller and Rübner, 2006; Qiao et al., 2008):



Therefore, in this study, the volume of the gas released from WBA samples during alkaline solution curing is determined using the experimental setup shown in Figure 2.6. WBA is mixed with NaOH solution (1 mol/L), and the experiment finishes when no further gas can be collected. Then, the total released hydrogen amount is recorded. At least three samples are measured to calculate the average value. Based on the collected hydrogen amount, the calculated metallic aluminium proportion in the utilized WBA is around 0.43% by the mass of the WBA.

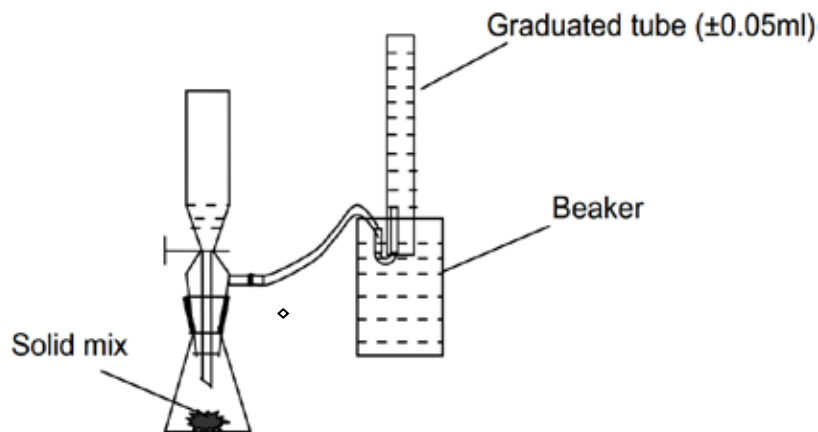


Figure 2.6: Schematic diagram of the experimental set-up to determine gas released from the utilized WBA (Qiao et al., 2008)

### · *Morphology comparison*

In this study, to compare the morphologies difference between the WBA and sand (0-2), two microscopes are utilized: one is an optical microscope (maximum magnification of 80 ×), while the other one is a scanning electron microscope (SEM) (Quanta 650 FEG, FEI). The results are presented in Figure 2.7. As can be seen, the appearance of the WBA and sand (0-2) is relatively similar to each other. Nevertheless, compared to the sand (0-2), the surface of the WBA is much rougher and contains many fine pores. In addition, some waste threadlike stuff can be often observed at the WBA particles surface, which may act as fibres when applied in concrete and improve its flexural strength.

Based on the analysis shown above, it can be summarized that the utilized WBA has similar density and particle size distribution as that of sand (0-2). However, due to the influence of heating treatment (waste burning process), the WBA has a much rougher surface than the sand (0-2), and the metallic aluminium in WBA may cause negative effect on the properties of concrete.

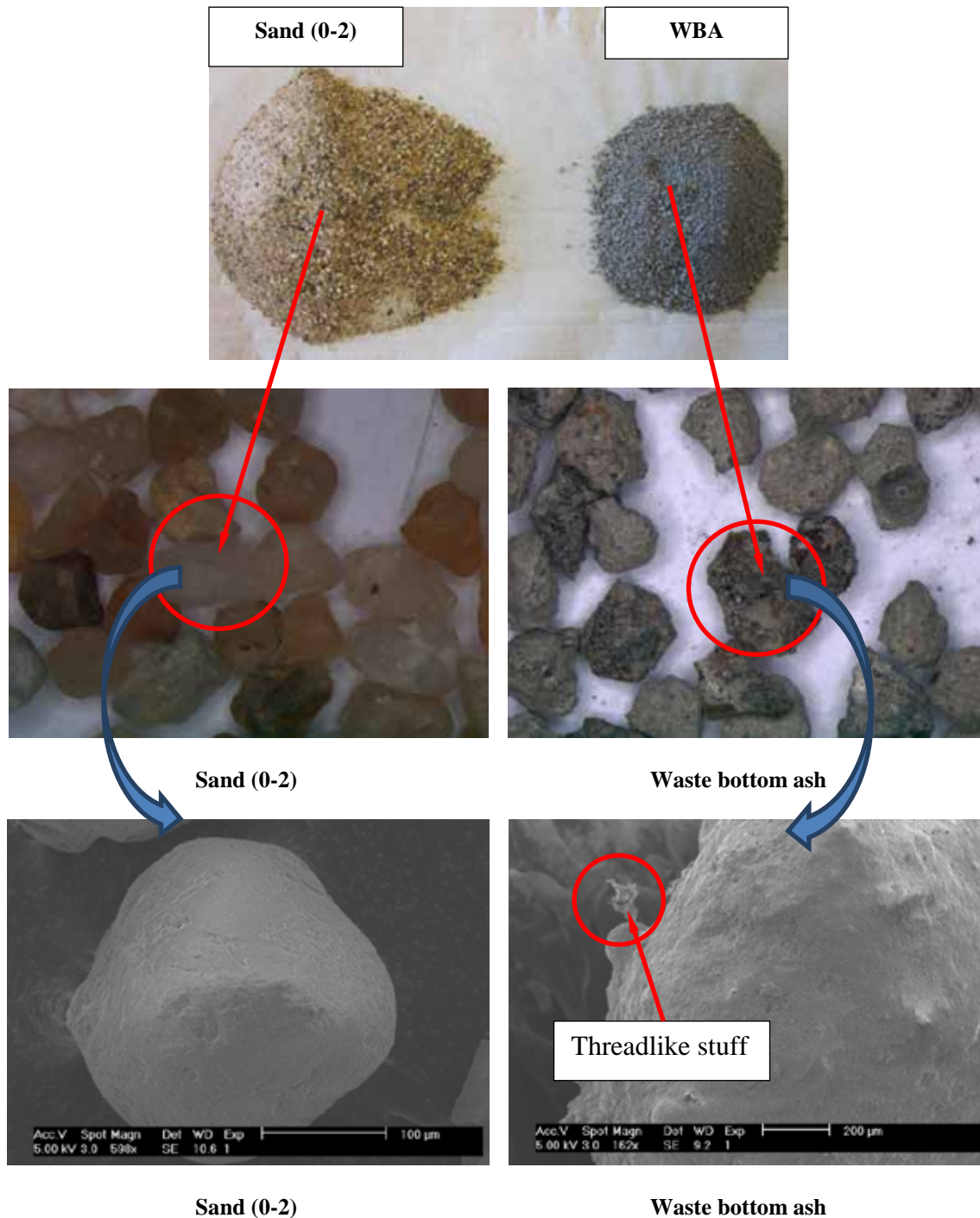


Figure 2.7: Morphology comparison of sand (0-2) (left) and waste bottom ash (WBA) (right)

### 2.2.3 Fibres characterization

There are a large amount of fibres available on the market that can be used to reinforce concrete. They can be roughly divided into three categories: 1) steel fibres; 2) synthetic fibres; 3) natural fibres. In most cases, the steel fibres can significantly improve the mechanical properties of concrete, while the natural fibres are relatively weak. Nevertheless, with the development of chemical industry, some of the synthetic fibres have even larger tensile strength than the steel fibres and simultaneously can effectively enhance the mechanical properties of concrete. Moreover, some of the synthetic fibres can be produced in very small dimensions ( $\mu\text{m}$  scale in diameter), which can be utilized to restrain the growth of micro-cracks in the matrix of concrete.

Due to the fact that the aim of this study is to produce a sustainable UHPFRC with low environmental impact, the steel fibres are still mainly utilized, since the synthetic fibres are normally more expensive than the steel fibres. In general, three types of steel fibres are used in this research. Additionally, as mentioned before, to limit the growth of micro-crack, one type of polypropylene fibres is used together with steel fibres in Chapter 6. All the used fibres are shown in Figure 2.8, and their characteristics are presented in Table 2.6.

**Table 2.6: Characteristics of utilized steel fibres**

Fibre type	Length (mm)	Diameter (mm)	Aspect ratio	Density ( $\text{g}/\text{cm}^3$ )	Tensile strength (MPa)
Hook ended steel fibre	35	0.55	64	7.8	1200
Long straight steel fibre	13	0.2	65	7.8	1100
Short straight steel fibre	6	0.16	38	7.8	1100
Polypropylene fibre	8	0.015	533	0.91	400



Polypropylene fibres

Short straight steel fibres

Long straight steel fibres

Hook ended steel fibres

**Figure 2.8: Fibres used in this study**

### 2.2.4 Superplasticizer

In the development of UHPFRC, except the powders, aggregates and fibres (mentioned above), superplasticizer (SP) is also very important, since very limited amount of water and relatively high content of SP are normally utilized in the concrete design. From the available literature (Houst et al., 2008; Plank et al., 2009), it can be concluded that SP can significantly improves the flow of cement pastes by changing the degree of flocculation in the system. This can be attributed to that fact that SP polymers are adsorbed at the solid-liquid interface and alter the degree of flocculation in three different ways (Nelson and Guillot, 2006; Schmidt, 2014): 1) by increasing the zeta potential of the material; 2) by increasing the solid-liquid affinity; 3) by steric hindrance as a result of physical barriers to flocculation. Moreover, the type of SP based on polycarboxylic ether (PCE) has been demonstrated to be effective in the production of HPC with a high content of fine particles (Houst et al., 2008; Artelt and Garcia, 2008). Therefore, in this research, the used SP is an innovative admixture based on modified polycarboxylic ether (PCE) polymers. This product is primarily developed for the use in the concrete industry where the highest durability and performance are required. The detailed information on the used SP is shown in Table 2.7.

**Table 2.7: Characteristics of utilized superplasticizer**

Appearance	Brown liquid
Specific gravity (20 °C)	1.095 ± 0.02 g/cm <sup>3</sup>
pH-value	7.0 ± 1
Alkali content (%)	≤ 5.0
Chloride content (%)	≤ 0.10

## 2.3 Experimental methodologies

### 2.3.1 Workability

In this research, two standards are employed to evaluate the workability of UHPFRC: EN-1015-3 (2007) and EN-12350-8 (2010). Following the EN-1015-3 (2007), fresh UHPFRC is filled in a conical mould in the form of a frustum (Hägermann cone), as shown in Figure 2.9. Then, the cone is lifted straight upwards in order to allow a free flow for the paste/concrete without any jolting. Eventually, two diameters ( $d_1$  and  $d_2$ , perpendicular to each other) of the spread flow are measured. Their mean is recorded as the slump flow value of UHPFRC. As originally introduced by Okamura and Ozawa (1995), the average spread flow value can be utilized to calculate the relative slump ( $\Gamma$ ) via:

$$\Gamma = \frac{\frac{d_1 + d_2}{2}}{d_0} - 1 \quad (2.4)$$

where  $d_0$  represents the base diameter of the used cone (mm), 100 mm in case of the Hägermann cone. The relative slump  $\Gamma$  is a measure for the deformability of the mixture.

Additionally, considering the effect of hook ended long steel fibres, the flowability of fresh mixtures of UHPFRC with these fibres is tested following EN-12350-8 (2010). The Abrams cone (as shown in Figure 2.10) with the internal upper/lower diameter equal to 100/200 mm and height equal to 300 mm is utilized without any jolting. Two diameters ( $d_1$  and  $d_2$ ) perpendicular to each other are recorded and their mean is recorded as the slump flow value of UHPFRC.

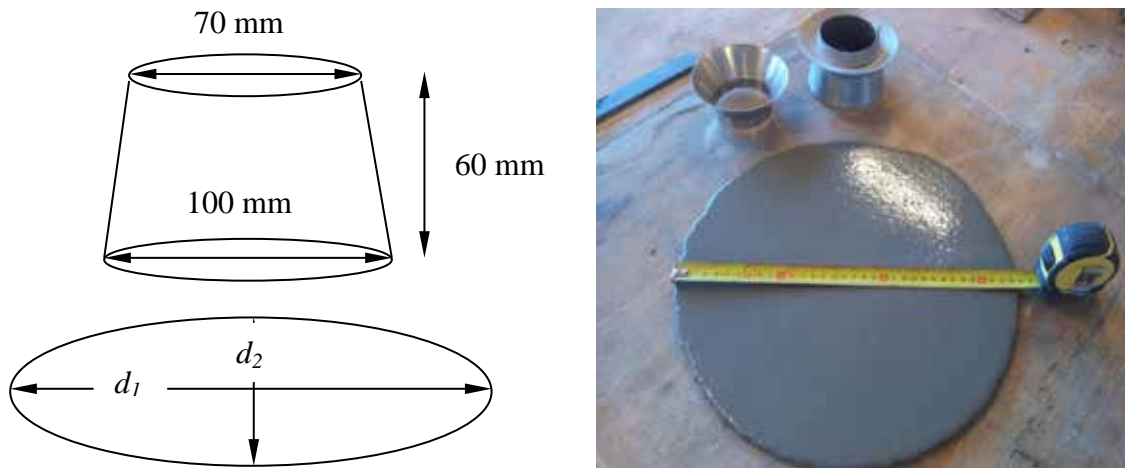


Figure 2.9 Geometry of Hägermann cone (left), an example of an executed spread flow test (right)



Figure 2.10 Abrams cone (left), workability test of UHPFRC with hook ended fibres (right)

### 2.3.2 Air content

The air content in fresh UHPFRC is experimentally determined following the subsequent procedure. The fresh concrete is filled in cylindrical container of known volume and vibrated for 30 seconds. The exact volume of the container is determined beforehand

using demineralized water of at °C. In order to avoid the generation of menisci at the water surface, the completely filled contained is covered with a glass plate, whose mass is determined before. Hence, based on the assumption that the fresh concrete is a homogeneous system, the air content of concrete can be derived from the following equation:

$$\varphi_{air} = \frac{V_{container} - V_{solid} - V_{liquid}}{V_{container}} g100 \quad (2.5)$$

where  $\varphi_{air}$  is the air content (%) of UHPFRC,  $V_{container}$  is the volume of the cylindrical container that mentioned before ( $\text{cm}^3$ ),  $V_{solid}$  and  $V_{liquid}$  are the volumes of solid particles and liquid in the container ( $\text{cm}^3$ ), respectively.

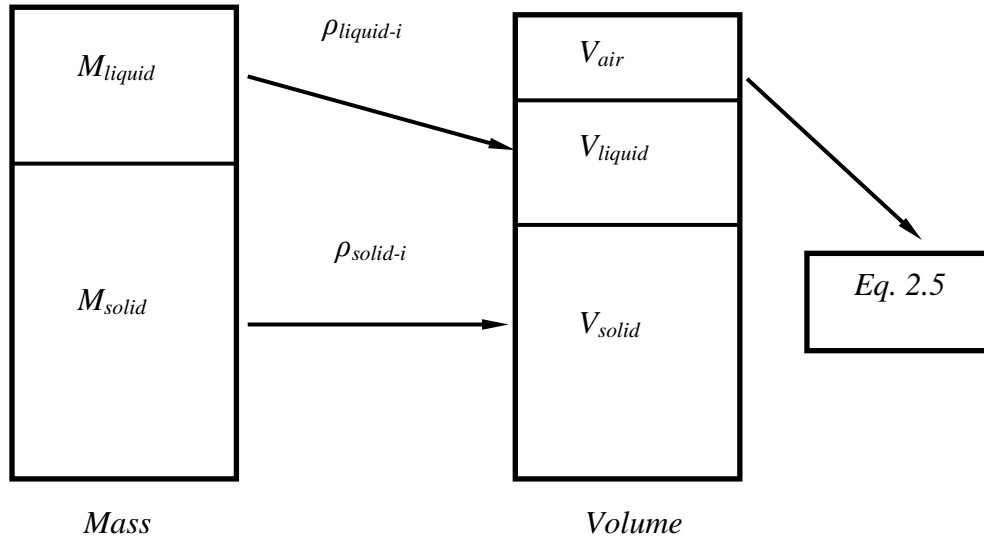


**Figure 2.11: Scheme of the method to estimate the air content in fresh UHPFRC**

As the composition of the tested mixture is known, the mass percentage of each ingredient can be computed. After measuring the total mass of concrete in the container, the individual masses of all materials in the container can be obtained. Applying the density of the respective ingredients, the volume percentages of each mix constituent can be computed. Hence,

$$V_{solid} = \sum_i \frac{M_i}{r_i} \quad (2.6)$$

and

$$V_{liquid} = \sum_j \frac{M_j}{r_j} \quad (2.7)$$

where  $M_i$  and  $\rho_i$  are the mass (g) and density ( $\text{g/cm}^3$ ) of the fraction  $i$  in solid materials,  $M_j$  and  $\rho_j$  are the mass (g) and density ( $\text{g/cm}^3$ ) of the fraction  $j$  in liquid materials, respectively. The schematic diagram for calculating the air content in concrete is shown in Figure 2.11.

### 2.3.3 Water-permeable porosity

The water-permeable porosity of the developed UHPFRC is measured applying the vacuum-saturation technique, which is referred to as the most efficient saturation method (Safiuddin and Hearn, 2005). Samples with a format of a square (with a height of 10 - 15 mm, and an edge size of 100 mm) are extracted from the 100 mm cubes for each prepared UHPFRC composite. The test is carried out on at least 3 samples for each mix, following the vacuum-saturation description given in NT Build 492 (1999) and ASTM C1202 (2005):

- 1) Place the samples in a dessicator and apply a pressure of 40 mbar for three hours;
- 2) Fill in slowly the dessicator with water (with the pump still connected and running) until approximately 10 mm more than the top surface of the samples;
- 3) Maintain the pressure for an additional hour, then turn the pump off;
- 4) Let the samples soak in water for 18 hours;
- 5) Measure the mass of the surface dry samples in air;
- 6) Measure the hydrostatic mass of the samples (in water);
- 7) Dry the sample in an oven at 105 °C until a constant mass is reached, then measure the mass.

The water-permeable porosity is calculated from the following equation:

$$j_{v,water} = \frac{m_s - m_d}{m_s - m_w} \times 100 \quad (2.8)$$

where  $\phi_{v,water}$  is the water-permeable porosity (%),  $m_s$  is the mass of the saturated sample in surface-dry condition measured in air (g),  $m_w$  is the hydrostatic mass of the water-saturated sample (g) and  $m_d$  is the mass of oven dried sample (g).

### 2.3.4 Mechanical properties

After performing the workability test, fresh UHPFRC is cast in moulds with different sizes (40 mm × 40 mm × 160 mm, 100 mm × 100 mm × 100 mm and 100 mm × 100 mm × 500 mm). All the samples are demolded approximately 24 h after casting and then cured in water at about 21 °C. Afterwards, the mechanical properties of UHPFRC are tested based on different standards. For compressive strength, the samples are tested based on EN-196-1 (2005) and EN-12390-3 (2009), while that the flexural behaviour of UHPFRC are tested following EN-196-1 (2005) and EN-12390-5 (2009).

### 2.3.5 Hydration kinetics

As commonly known, the hydration of Portland cement involves the reaction of anhydrous calcium silicate ( $C_3S$  and  $C_2S$ ) and aluminate phases ( $C_3A$  and  $C_4AF$ ) with water to form hydrated phases. Both  $C_3S$  and  $C_2S$  react with water to produce an amorphous calcium silicate hydrate known as C–S–H gel which is the main product that binds the sand and aggregate particles together in cement mortars and concrete (Taylor, 1997). The hydration process of  $C_3S$  and  $C_2S$  can be shown as:



The reactions of  $C_3A$  and  $C_4AF$  with water are relatively complex. In general, with the addition of soluble calcium sulphate,  $C_3A$  can quickly react with water to form the  $C_2AH_8$  and  $C_4AH_{19}$  phases, which subsequently convert to  $C_3AH_6$  (Taylor, 1997). In this process, normally a large amount of heat is released. The reaction can be shown as:



Then, when the available sulphate has been consumed, the ettringite will react with  $C_3A$  to form mono-sulphate, which can be summarized as (Taylor, 1997):



Nevertheless, due to the fact that the cementitious system of UHPFRC normally has a large cement (or binder) amount, low water content and high superplasticizer addition, the cement hydration may be significantly affected and is different from that occurring in normal strength concrete. Therefore, to efficiently use the cement or binders in UHPFRC and eventually produce a sustainable UHPFRC, it is very important to clarify the hydration kinetics of cement in UHPFRC.

In this study, the heat flow calorimetry test is employed to investigate the hydration kinetics of cement. Before the testing, the samples are mixed for two minutes and transferred into a sealed glass ampoule, which is then placed into the isothermal calorimeter (TAM Air, Thermometric). The instrument is set to a temperature of 20 °C. After 7 days, the measurement is stopped and the obtained data is analysed. All results are ensured by double measurements (two-fold samples).

### 2.3.6 Thermal properties

In the research on the cement hydration, TG/DSC is one of the mostly used techniques, which can effectively identify the phases, clarify the chemical reactions and study the effect of mineral admixtures (Ramachandran et al., 2002). In this research, a Netzsch simultaneous analyser, model STA 449 C, is used to obtain the Thermo-gravimetric (TG)

and Differential Scanning Calorimetry (DSC) curves of UHPFRC paste. The pastes are produced without any aggregates. Analyses are conducted at a heating rate of 10 °C/min, from 20 °C to 1000 °C under flowing nitrogen.

Based on the TG test results, the hydration degree of the cement in each UHPFRC paste is calculated. Here, the loss-on-ignition (LOI) measurements of non-evaporable water content for hydrated UHPFRC paste are employed to estimate the hydration degree of cement (Bentz et al., 2000). Assuming that the UHPFRC paste is a homogeneous system, non-evaporable water content is determined according to the following equation:

$$M'_{Water} = M_{105} - M_{1000} - M_{CaCO_3} \quad (2.13)$$

where the  $M'_{water}$  is the mass of non-evaporable water (g),  $M_{105}$  is the mass of UHPFRC paste after heat treatment at 105 °C for 2 hours (g),  $M_{1000}$  is the mass of UHPFRC paste after heat treatment at 1000 °C for 2 hours (g) and  $M_{CaCO_3}$  is the mass change of UHPFRC paste caused by the decomposition of  $CaCO_3$  during the heating process (g). Then, the hydration degree of the cement in the UHPFRC paste is calculated as:

$$\beta_t = \frac{M'_{Water}}{M_{Water-Full}} g 100 \quad (2.14)$$

where  $\beta_t$  is the cement hydration degree at hydration time  $t$  (%) and  $M_{water-Full}$  is the water required for the full hydration of cement (g). According to the investigations shown in (Pane and Hansen, 2005), the maximum amount of non-evaporable water is 0.228 (g  $H_2O$ /g OPC) for a pure OPC system and 0.256 (g  $H_2O$ /g blended cement) for 90% OPC + 10% SF system.

## 2.4 Conclusions

In this chapter, the characterization of the utilized materials and the experimental procedures employed in this thesis are presented. The used materials are mainly divided into three categories: powders, aggregates and fibres. The materials analysis mainly focuses on the particle size distribution, specific density, water demand, chemical composition and microstructure analysis. The following conclusions are drawn:

- 1) A high content of powders is utilized in the production of UHPFRC. Hence, it is very important to understand the water demand of powders, since very limited amount of water is normally used in the design of UHPFRC. From the obtained experimental results, the water demand of the tested powders follows the order: limestone powder (LP) < fly ash (FA) < ground granulated blast slag (GGBS) < Ordinary Portland Cement (OPC, CEM I 52.5 R), which implies that when the cement is partially replaced by LP in UHPFRC, its workability can be improved.

- 2) The utilized limestone powder (LP) has a very similar particle size distribution to that of cement, which implies that the LP can be utilized to partially replace cement without significantly altering the particle packing of the solid matrix.
- 3) To secure the homogeneity of the UHPFRC micro-structure, two types of normal fine aggregates are mainly utilized: normal sand with the fraction 0-2 mm and microsand with the fraction 0-1 mm. Additionally, one type of waste material (bottom ash) is also included in the production of sustainable UHPFRC. The experimental results show that the utilized waste bottom ash (WBA) has a similar density and particle size distribution to that of sand (0-2) (as shown in Table 2.4 and Figure 2.4). However, due to the influence of heat treatment, the WBA has a much rougher surface than sand (0-2), and the metallic aluminium present in the WBA may cause negative effects on the properties of UHPFRC.
- 4) Considering the high performance and convenience, steel fibres (straight and hook ended) are mainly used in the UHPFRC production in this study. Moreover, to further restrict the growth of micro-cracks in the concrete matrix, one type of polypropylene fibres is used, which is much thinner compared to the steel fibres.
- 5) A type of superplasticizer (SP) based on polycarboxylic ether (PCE) has been demonstrated to be effective for the use in HPC with a large amount of fine particles. Therefore, in this research, the used SP is an innovative admixture based on modified polycarboxylic ether (PCE) polymers. This product is primarily developed for the use in the concrete industry where the highest durability and performance are required.
- 6) A series of test methods are employed to evaluate the properties of the developed UHPFRC, focusing on workability, air content, water-permeable porosity, mechanical properties, cement hydration kinetics and thermal properties. To develop a sustainable UHPFRC with a low cement content, good workability and high mechanical properties, the cement hydration kinetics should be deeply investigated. In most cases, a high cement content is utilized in the production of UHPFRC, and many of these cement particles are not hydrated even after curing for 91 days. Hence, it is very important to evaluate the cement hydration degree in UHPFRC. Based on the TG/DSC results, the cement hydration degree of the developed sustainable UHPFRC can be assessed.



# Chapter 3

## Optimized mix design approach for UHPFRC

### 3.1 Introduction

Ultra-High Performance Fibre Reinforced Concrete (UHPFRC) is a combination of high strength concrete matrix and fibres reinforcement. In particular, it is a super plasticized concrete, reinforced with fibres, with improved homogeneity because traditional large aggregates are most often replaced with fine sand (Richard and Cheyrezy, 1995). According to Richard and Cheyrezy (1995), UHPFRC represents the highest development of High Performance Concrete (HPC) and its ultimate compressive strength depends on the curing conditions (either standard curing, steam curing or autoclave curing), possible thermal treatments as well as on the adopted manufacturing technique, and its value could rise up to 800 MPa in the case of compressive molding.

In the last 25 years, advances in concrete technology have allowed the designing of UHPFRCs that show excellent rheological behaviour (workability and self-placing capability), mechanical properties (very high compressive strength and non-brittle tensile behaviour) and durability performance (Kooiman, 2000; Grünewald, 2004; Markovic, 2006; Schumacher, 2006; Lappa, 2007; Hassan et al., 2012; Tayeh et al., 2012; Park et al., 2012; Rossi, 2013; Wang et al., 2014). As mentioned in Chapter 1, to gain the desired strength of a UHPFRC, well-chosen raw materials and sophisticated technical procedures are conventionally required. Moreover, a large amount of cement or binders are normally used in the production of UHPFRC. For instance, Rossi (2013) presented an experimental study of the mechanical behaviour of an UHPFRC with 1050 kg/m<sup>3</sup> cement. Park et al. (2012) investigated the effects of hybrid fibres on the tensile behaviour of Ultra-High Performance Hybrid Fibre Reinforced Concrete, in which about 1000 kg/m<sup>3</sup> of binder was used. Considering that the high cost of UHPFRC is a disadvantage that restricts its wider usage, some industrial by-products such as ground granulated blast-furnace slag (GGBS) or silica fume (SF) have been used as partial cement replacements. For example, El-Dieb (2009) produced UHPFRC with about 900 kg/m<sup>3</sup> cement and 135 kg/m<sup>3</sup> silica fume. Tayeh et al. (2012) utilized about 770 kg/m<sup>3</sup> cement and 200 kg/m<sup>3</sup> silica fume to produce a UHPFRC as a repair material. Hassan et al. (2012) show some mechanical investigation on a UHPFRC with around 650 kg/m<sup>3</sup> cement, 420 kg/m<sup>3</sup> GGBS and 120 kg/m<sup>3</sup> silica fume. Additionally, some waste materials are also included in the UHPFRC production to reduce its cost. Tuan et al. (2011a and 2011b) investigated the possibility of using rice husk ash (RHA) to replace silica fume (SF) in producing Ultra-High

Performance Concrete (UHPC). The experimental results show that the compressive strength of UHPC incorporating RHA reaches more than 150 MPa. Yang et al. (2009) utilized recycled glass cullet and two types of local natural sand to replace the more expensive silica sand in UHPFRC. Nevertheless, the experimental results show that the use of recycled glass cullet (RGC) gives approximately 15% lower performance, i.e. flexural strength, compressive strength and fracture energy.

As commonly known, the sector of building materials is the third-largest CO<sub>2</sub> emitting industrial sector world-wide, as well as in the European Union. The cement production is said to represent 7% of the total anthropogenic CO<sub>2</sub> emissions (Capros et al., 2001; UNSTATS, 2010; Friedlingstein et al., 2010). Hence, one of the key sustainability challenges for the next decades is to design and produce a type of concrete with less clinker and inducing lower CO<sub>2</sub> emissions than traditional ones, while providing the same reliability, with a much better durability (Denarié and Brühwiler, 2011; Habert et al., 2013). Considering the successful achievement on the application of UHPFRC for rehabilitation of bridges since 1999 (Brühwiler and Denarié, 2008), UHPFRC seems to be one of the candidates to reduce the global warming impact of construction materials. However, as shown before, when producing UHPC or UHPCRC, the cement or binder content is always relatively high (normally more than 1000 kg/m<sup>3</sup>). Although some investigations show that it is possible to replace significant amounts of the cement in UHPC mixes by limestone powder or fine quartz sand of comparable size and distribution, while keeping the absolute water added constant, without significantly decreasing the compressive strength (Bornemann and Schmidt, 2002; Habert et al., 2013), how to find a reasonable balance point between the binder amount and the mechanical properties of UHPC or UHPFRC still remains an open question.

As already been accepted, an optimum packing of the granular ingredients of concrete is the key for a good and durable concrete (Brouwers and Radix, 2005; Hüsken, 2010; Hunger, 2010). Nevertheless, from the available literature, it can be found that the investigation of design or production of UHPFRC with an optimized particle packing is not sufficient (De Larrard and Sedran, 1994; De Larrard and Sedran, 2002; Toledo Filho et al., 2012). In most cases, the recipes of UHPC or UHPFRC are given directly, without any detailed explanation or theoretical support for the given concrete proportions. Hence, it can be predicted that a large amount of binders or other particles are not optimally used in UHPFRC.

Consequently, the objective of this chapter is to figure out how to effectively design and produce a UHPFRC with a low cement amount. The design of the concrete mixtures is based on the aim to achieve a densely compacted cementitious matrix, employing the modified Andreasen & Andersen particle packing model (A&A model) (Funk and Dinger, 1994). Fillers (limestone and quartz powders) are used to replace cement in the concrete.

### 3.2 Mix design of concrete based on the optimized particle packing

For the design of mortars and concretes, several mix design tools are in use. Based on the properties of multimodal, discretely sized particles, De Larrard and Sedran (1994, 2002) postulated different approaches to design concrete: the Linear Packing Density Model (LPDM), Solid Suspension Model (SSM) and Compressive Packing Model (CPM). Based on the model for multimodal suspensions, De Larrard and Sedran (1994) developed the Linear Packing Density Model composing multimodal particle mixtures. The functions of the LPDM are describing the interaction between the sizes classes of the materials used. Due to the linear character of the LPDM, the model was improved by De Larrard and Sedran (1994) by introducing the concept of virtual packing density. The virtual packing density is the maximum packing density which is only attainable if the particles are placed one by one. The improvements of the LPDM resulted in the Solid Suspension Model (SSM). In the further development of their model, De Larrard and Sedran (2002) introduced the compaction index to the so-called Compressive Packing Model (CPM). The compaction index considers the difference between the actual packing density and virtual packing density and characterizes therefore the placing process. However, also the CPM still uses the packing of monosized classes to predict the packing of the composed mixture made up of different size classes. Fennis et al. (2009) have developed a concrete mix design method (cyclic design method) based on the concepts of De Larrard and Sedran (1994, 2002). However, all these design methods are based on the packing fraction of individual components (cement, sand etc.) and their combinations, and therefore it is complicated to include very fine particles in these mix design tools, as it is difficult to determine the packing fraction of such fine materials or their combinations. As mentioned before, due to the fact that a large amount of fines are normally utilized in the production of UHPFRC, the design methods shown above are inefficient for the design of UHPC or UHPFRC.

Another possibility for the mix design is offered by an integral particle size distribution approach of continuously graded mixes, in which also the very fine particles can be integrated with considerably lower effort. First attempts describing an aimed composition of concrete mixtures, which generally consists of continuously graded ingredients, can be traced already back to 100 years ago. The fundamental work of Fuller and Thompson (1907) showed that the packing of concrete aggregates is affecting the properties of the produced concrete. They concluded that a geometric continuous grading of the aggregates in the composed concrete mixture can help to improve the concrete properties. Based on the investigation of Fuller and Thompson (1907) and Andreasen and Andersen (1930), a minimal porosity can be theoretically achieved by an optimal particle size distribution (PSD) of all the applied particle materials in the mix, as shown in Eq. (3.1).

$$P(D) = \frac{D^q}{D_{max}^q} \quad (3.1)$$

where  $P(D)$  is a fraction of the total solids being smaller than size  $D$ ,  $D$  is the particle size ( $\mu\text{m}$ ),  $D_{max}$  is the maximum particle size ( $\mu\text{m}$ ), and  $q$  is the distribution modulus.

However, in Eq. (3.1), the minimum particle size is not incorporated, while in the reality there must be a finite lower size limit. Hence, Funk and Dinger (1994) proposed a modified model based on the Andreasen and Andersen Equation. In this study, all the concrete mixtures are designed based on this so-called modified A&A model, which is shown as follows (Funk and Dinger, 1994):

$$P(D) = \frac{D^q - D_{min}^q}{D_{max}^q - D_{min}^q} \quad (3.2)$$

where  $D_{min}$  is the minimum particle size ( $\mu\text{m}$ ).

The modified A&A model has already been successfully employed in the optimization algorithms for the design of self-compacting concrete (Hunger, 2010), zero-slump concrete (Hüsken, 2010), lightweight concrete (Yu et al., 2013; Spiesz et al., 2013) and concrete with nanosilica (Quercia, 2014). Different types of concrete can be designed using Eq. (3.2) by applying different values of the distribution modulus  $q$ , as it determines the proportion between the fine and coarse particles in the mixture. Higher values of the distribution modulus ( $q > 0.5$ ) lead to coarse mixtures, while lower values ( $q < 0.25$ ) result in concrete mixes which are rich in fine particles (Hüsken and Brouwers, 2008). Brouwers (2006) demonstrated that theoretically a  $q$  value range of 0 - 0.28 would result in an optimal packing. Hunger (2010) recommended using  $q$  in the range of 0.22 - 0.25 in the design of self-compacting concrete.

In the design of concrete performed in this study, the modified A&A model (Eq. (3.2)) acts as a target function for the optimization of the composition of mixture of granular materials. The proportions of each individual material in the mix are adjusted until an optimum fit between the composed mix and the target curve is reached, using an optimization algorithm based on the Least Squares Method (LSM), as presented in Eq. (3.3). When the deviation between the target curve and the composed mix, expressed by the sum of the squares of the residuals (RSS) at defined particle sizes, is minimized, the composition of the concrete is treated as the optimum.

$$RSS = \frac{\sum_{i=1}^n (P_{mix}(D_i^{i+1}) - P_{tar}(D_i^{i+1}))^2}{n} \quad (3.3)$$

where  $P_{mix}$  is the composed mix, and the  $P_{tar}$  is the target grading calculated from Eq. (3.2),  $n$  is the number of the chosen points between  $D_{min}$  and  $D_{max}$ .

As commonly known, the quality of the curve fit is assessed by the coefficient of determination ( $R^2$ ), since it gives a value for the correlation between the grading of the target curve and the composed mix. Therefore, the coefficient of determination ( $R^2$ ) is calculated in this study as follows:

$$R^2 = 1 - \frac{\sum_{i=1}^n (P_{mix}(D_i^{i+1}) - P_{tar}(D_i^{i+1}))^2}{\sum_{i=1}^n (P_{mix}(D_i^{i+1}) - \overline{P_{mix}})^2} \quad (3.4)$$

Where  $\overline{P_{mix}} = \frac{1}{n} \sum_{i=1}^n P_{mix}(D_i^{i+1})$ , which represents the mean of the entire distribution of the particles.

### 3.3 Experimental validation of the optimized particle packing model

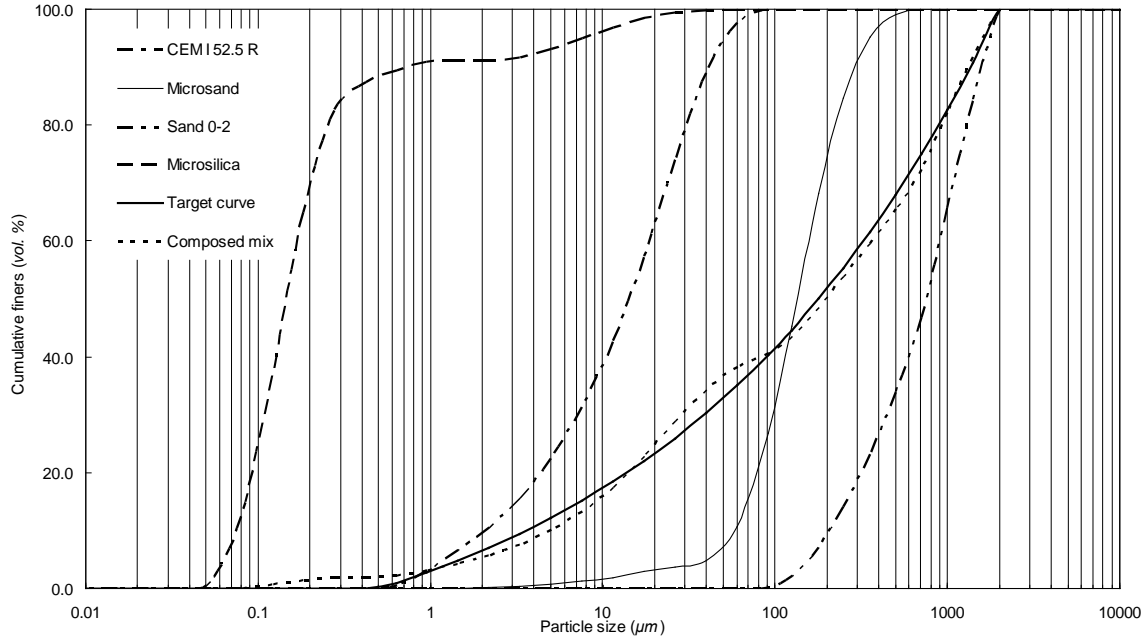
To demonstrate whether the modified A&A model is suitable to be used in the design of UHPFRC, an experimental validation is shown in this paragraph. The strategy is to develop a UHPFRC with low cement or binders amount without sacrificing its mechanical properties.

#### 3.3.1 Materials and mix design

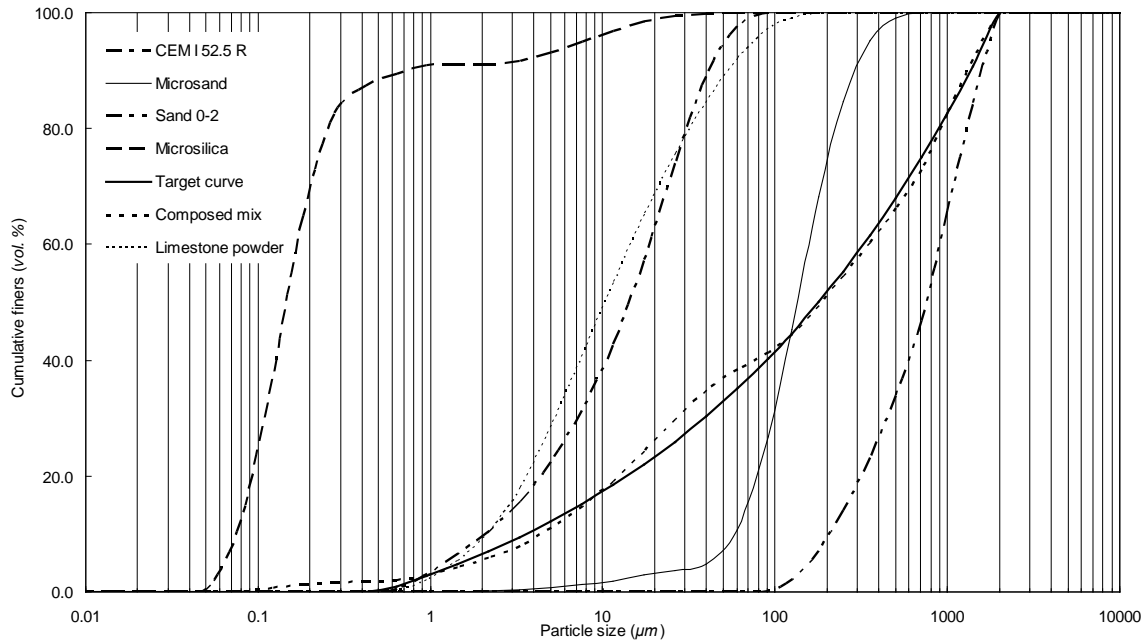
The cement used in this study is Ordinary Portland Cement (OPC, CEM I 52.5 R), provided by ENCI (the Netherlands). A polycarboxylic ether based superplasticizer is used to adjust the workability of concrete. The limestone and quartz powder are used as fillers to replace the cement. Two types of sand are used, one is normal sand with the fractions of 0-2 mm and the other one is microsand with the fraction 0-1 mm (Graniet-Import Benelux, the Netherlands). One type of commercial microsilica (powder) is selected as pozzolanic material. Long straight steel fibres (length of 13 mm and diameter of 0.2 mm) are employed to produce UHPFRC. All the detailed information and characteristics of the utilized raw materials can be found in Chapter 2.

Based on the modified A&A model shown above, the developed UHPFRC matrices are listed in Table 3.1. In this study, considering that a large amount of fine particles are utilized to produce the UHPFRC, the value of  $q$  is fixed at 0.23. In total, three different types of UHPC composites are designed. The reference concrete mixture (UHPC1) has a high cement content (about 875 kg/m<sup>3</sup>). In UHPC2 and UHPC3, about 30% and 20% of cement is replaced by limestone and quartz powder, respectively. Although the raw material contents are different in each mixture, the particle packing of the UHPC1, UHPC2 and UHPC3 are very similar, which follows from the target grading curves and

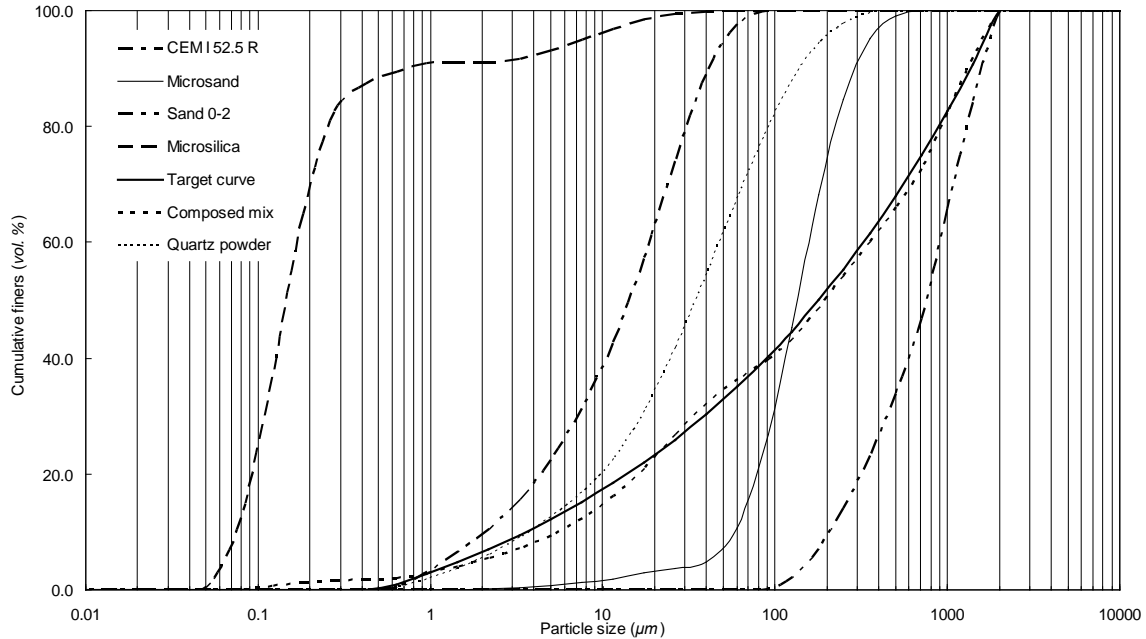
the resulting integral grading curves (Figure 3.1). Hence, based on the properties comparison among UHPC1, UHPC2 and UHPC3, it is possible to evaluate the efficiency of binders and try to produce a dense UHPC matrix with a low binder content.



(a) UHPC1



(b) UHPC2



(c) UHPC3

**Figure 3.1: PSDs of the involved ingredients, the target and optimized grading curves of the mixtures: UHPC1 (a), UHPC2 (b) and UHPC3 (c)**

**Table 3.1: Recipes of developed UHPFRC matrixes**

Materials	UHPC1 (kg/m <sup>3</sup> )	UHPC2 (kg/m <sup>3</sup> )	UHPC3 (kg/m <sup>3</sup> )
OPC	874.9	612.4	699.9
LP	0	262.5	0
QP	0	0	175.0
MS	218.7	218.7	218.7
S	1054.7	1054.7	1054.7
mS	43.7	43.7	43.7
W	202.1	202.1	202.1
SP	45.9	45.9	45.9
W/C	0.23	0.33	0.29

(OPC: Ordinary Portland Cement (CEM I 52.5 R), LP: limestone powders, QP: quartz powders, MS: microsand, S: sand (0-2), mS: microsilica, W: water, SP: superplasticizer, W/C: water to cement ratio)

Here, it is important to notice that the finest microsilica particle (about 0.05  $\mu\text{m}$ ) is not used as the  $D_{min}$  of the modified A&A model, and the additional microsilica amount is about 5% (bwoc). When the fine particles in microsilica would be included into the modified A&A model, then the distribution modulus ( $q$ ) would increase to about 0.29 to obtain the optimal concrete mixture (similar as that shown in Table 3.1). One example of

the modified target and optimized grading curves (with  $D_{min} = 0.05 \mu\text{m}$  and  $q = 0.29$ ) of the UHPC mixture is presented in Figure 3.2. This phenomenon is in line with that presented in (Quercia, 2014). As concluded by Quercia (2014), the modified A&A model is suitable to design concrete with very fine particles (e.g. nano particles). However, to achieve a densely compacted cementitious matrix, the mixture with nano particles should have a smaller  $D_{min}$  and a larger  $q$  value in the application of the modified A&A model, compared to the normal optimized concrete mixes without very fine particles.

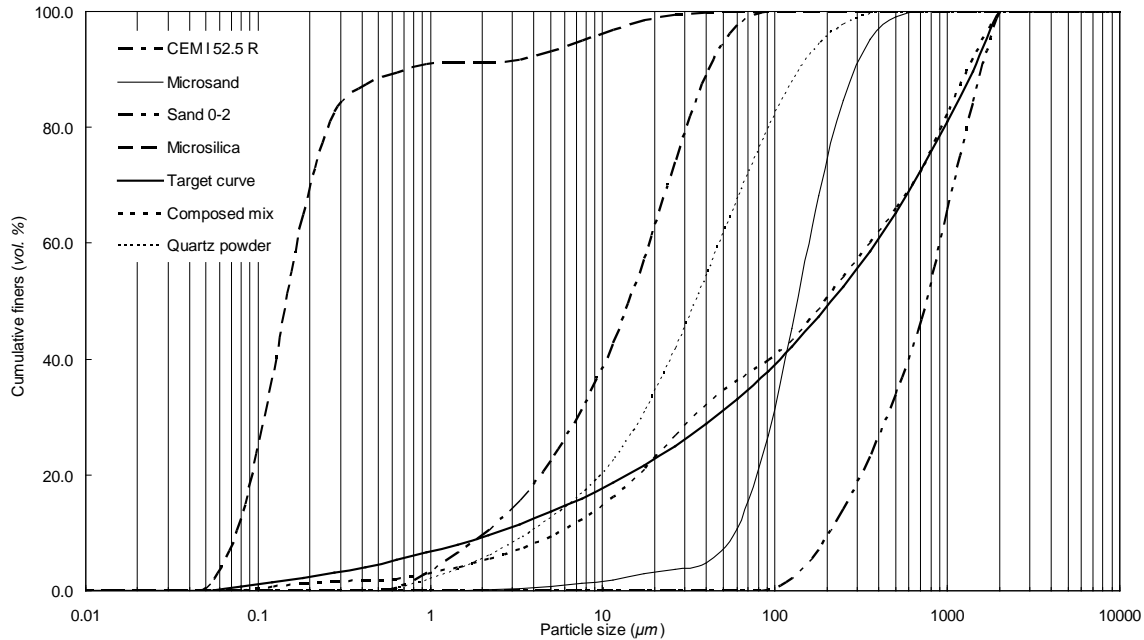


**Figure 3.2: One example of optimized concrete mixture (UHPC3) with smaller  $D_{min}$  ( $0.05 \mu\text{m}$ ) and larger  $q$  ( $0.29$ ) value**

Additionally, for normal fibre reinforced concrete (FRC), the fibre content is about 1-2% by volume of concrete (Grünwald, 2004). However, in UHPFRC, this value often increases to more than 2%, and sometime reaches even 5% (Park et al., 2012). Hence, in this study, to investigate the effect of fibres on the properties of UHPFRC, the steel fibres (straight long, as shown in Table 2.6 and Figure 2.8) are added into each UHPC mixes in the amount of 0.5%, 1.0%, 1.5%, 2.0% and 2.5% (vol.), respectively.

### 3.3.2 Experimental methodologies

#### · *Employed mixing procedures*

In this study, a simple and fast method is utilized to produce all the UHPFRC samples. The detailed information of the mixing procedures is shown in Figure 3.3. In total, 7 minutes and 30 seconds are required to finish the UHPFRC production, which is much shorter than other mixing procedures for UHPFRC (Yang et al., 2009; Yang et al., 2010).

Moreover, mixing is always executed under laboratory conditions with dried and tempered aggregates and powder materials. The room temperature while mixing, testing and casting is constant at around 21 °C.

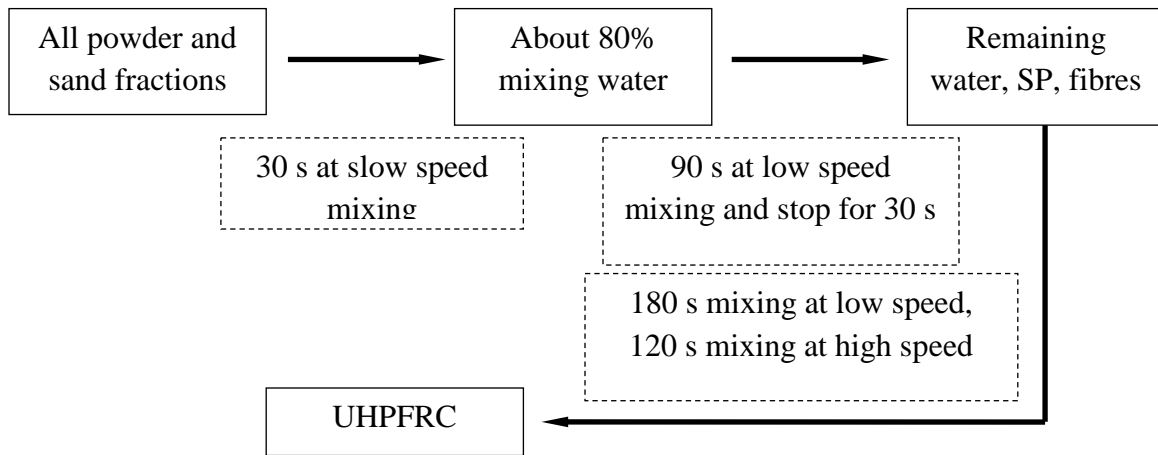


**Figure 3.3: Detailed information on the mixing procedure for producing UHPFRC**

- ***Fresh behaviour***

The fresh behaviour of the developed UHPFRC is measured following the method shown in Section 2.3.1. The Hägermann cone is utilized and the relative slump ( $I$ ) is calculated.

- ***Air content***

The air content of the developed UHPFRC in fresh state is measured following the method shown in Section 2.3.2.

- ***Water-permeable porosity***

The water-permeable porosity of the developed UHPFRC in hardened state is measured following the method shown in Section 2.3.3.

- ***Mechanical properties***

After performing the workability test, fresh UHPFRC is cast in moulds with the size of 40 mm × 40 mm × 160 mm and compacted on a vibrating table. The prisms are demolded approximately 24 h after casting and then cured in water at about 21 °C. After curing for 7 and 28 days, the flexural and compressive strengths of the specimens are tested according to EN-196-1 (2005). At least three specimens are tested at each age to compute the average strength.

- ***Thermal properties***

The thermal analysis and cement hydration degree are determined by the method presented in Section 2.3.6.

- ***SEM analysis***

Scanning electron microscopy (SEM) is employed to study the morphology of UHPFRC microstructure. After curing, the specimens are cut into small fragments and soaked in ethanol for more than 7 days in order to stop the hydration of cement. Subsequently, the samples are dried and stored in a sealed container before the SEM imaging.

### **3.3.3 Results and discussions**

- ***Relative slump***

The relative slump of the fresh UHPFRC mixes, calculated as described in Eq. (2.4), versus the volumetric content of steel fibres is depicted in Figure 3.4. The data illustrates a direct relation between the steel fibres content and workability of the fresh UHPFRC. It is important to notice that with the addition of steel fibres, the relative slump of all the UHPFRC decreases linearly. Particularly for the group of UHPC2, its relative slump sharply drops from 4.29 to 1.10, when the steel fibre content grows from 0.5% to 2.5% by volume of concrete. Moreover, with the same content of steel fibres, the relative slump of UHPC2 is always the largest, which is followed by UHPC3 and UHPC1, respectively. This difference between the mixtures is quite obvious at a low fibre amount and gradually declines when additional fibres are included. Furthermore, based on the linear equations shown in Figure 3.4, it can be noticed that the slope of the line for the UHPC2 is the largest, which means the addition of fibres can cause more notable workability loss for UHPC2.

As commonly known, the effect of steel fibres on the workability of concrete is mainly due to the following reasons (Grünwald, 2004): 1) the shape of the fibres is much more elongated compared with aggregates and the surface area at the same volume is higher, which can increase the cohesive forces between the fibres and matrix; 2) stiff fibres change the structure of the granular skeleton and stiff fibres push apart particles that are relatively large compared with the fibre length; 3) steel fibres often are deformed (e.g. have hooked ends or are wave shaped) to improve the anchorage between fibre and the surrounding matrix. The friction between the hook ended steel fibres and aggregates is higher compared with straight steel fibres. In this chapter, only short and straight steel fibres are used, which means the workability loss of concrete with the addition of fibres can be attributed to the increase in the internal surface area that produces higher cohesive forces between the fibres and concrete matrix. As presented by Edgington et al. (1978), with an increase of the fibre content, the workability of the normal concrete decreases sharply. Hence, it can be concluded that when more fibres are added, the cohesive forces are higher, and the relative slump flow of the UHPFRC will decrease. Furthermore, the

difference of cement content in each UHPFRC should also be considered. The cement content of UHPC1, UHPC2 and UHPC3 is  $875 \text{ kg/m}^3$ ,  $612 \text{ kg/m}^3$  and  $699 \text{ kg/m}^3$ , respectively. Hence, with the same water and superplasticizer amount, utilizing fillers to replace cement can significantly improve the workability of concrete, similarly to the results shown in (Violeta, 2003; Madani et al., 2011; Mehmet et al., 2012).

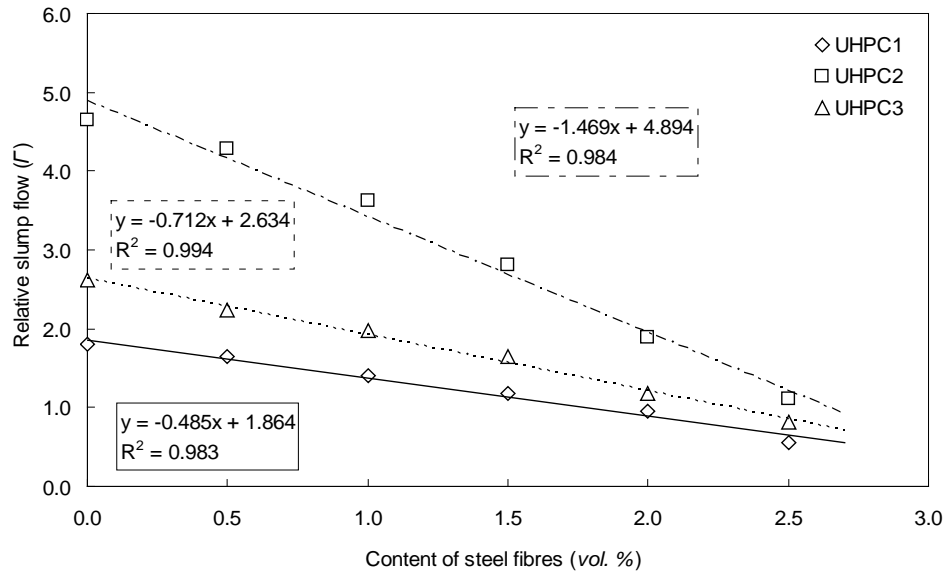


**Figure 3.4: Variation of the relative slump of UHPFRC with different cement content as function of the steel fibre content**

To summarize, due to the high cohesive forces between the fibres and concrete matrix, the addition of steel fibres will decrease the workability of UHPFRC. A linear decrease of the relative slump of UHPFRC with the increase of steel fibre content can be observed in this research. However, similarly to the normal concrete, appropriate utilization of fillers to replace the cement could also be treated as an effective method to improve the workability of UHPFRC.

• ***Air content and water-permeable porosity***

The determined air content of UHPFRC in fresh state and the water-permeable porosity of UHPFRC in hardened state are presented in Figures 3.5 and 3.6. As can be seen in Figure 3.5, all the curves are very similar to each other, which implies that the particle packing and void fraction of the developed UHPFRC are close to each other. Especially when the content of steel fibres increases to 2.5%, the difference in the air content among UHPC1, UHPC2 and UHPC3 is difficult to distinguish. Moreover, with an increase of the steel fibres content, the air content of each UHPFRC increases linearly, which means the more steel fibres are added, the more air will be entrained into UHPFRC.

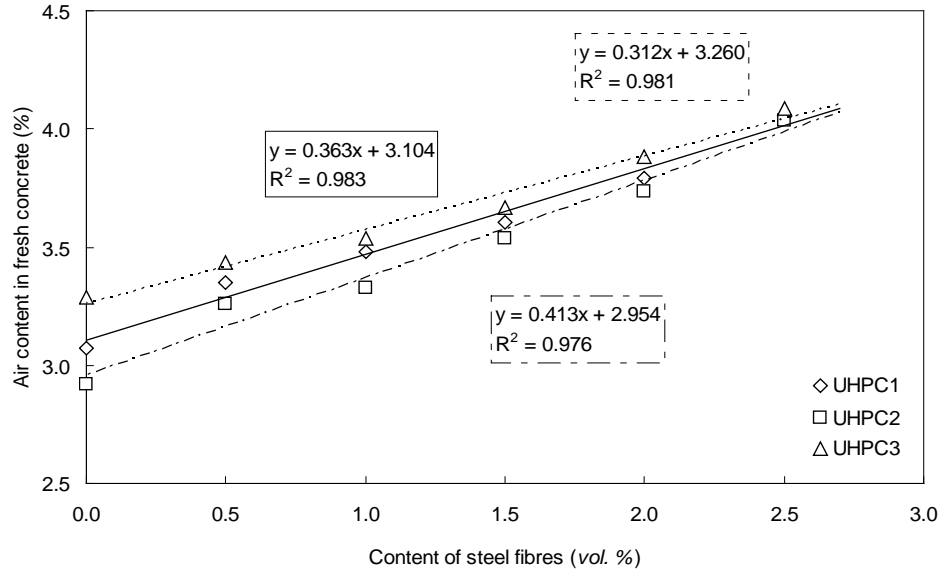


**Figure 3.5: Variation of the air content in fresh UHPFRC with different cement content as function of steel fibre content**

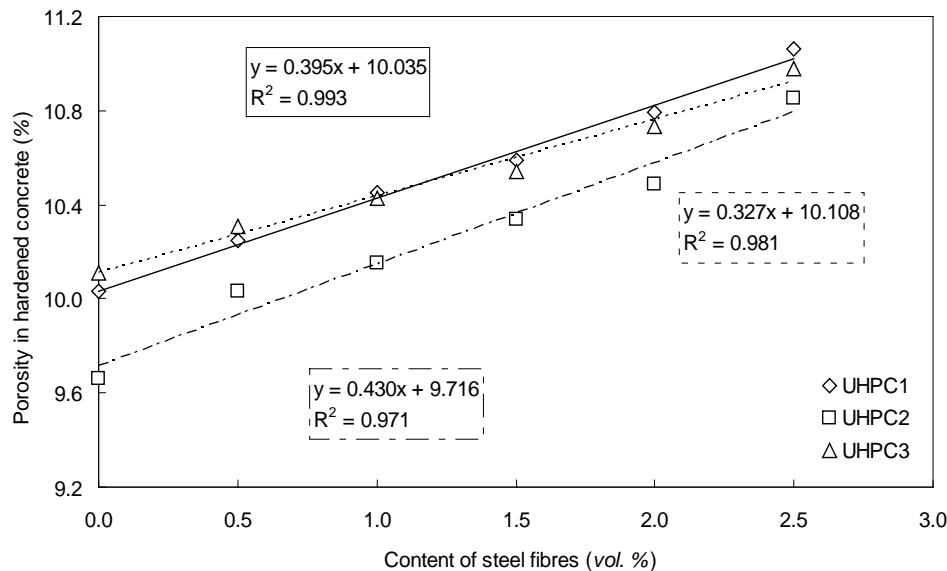


**Figure 3.6: Total water-permeable porosity of UHPFRC with different cement content as function of steel fibre content**

The influence of additional steel fibres on the air content of UHPFRC could be explained by the effect of fibres on the particle packing of concrete ingredients. As shown in (Grünwald, 2004), due to the internal force between the fibres and aggregate (and/or fibres themselves), the packing density of concrete will significantly decrease with the addition of steel fibres. Hence, in this study, with the increase of the fibre content, a clear increase of air content in UHPFRC can be observed.

In Figure 3.6, it can be noticed that the effect of steel fibres on water-permeable porosity of concrete is similar to the effect of the steel fibres on the air content in fresh concrete (as shown in Figure 3.5). With an increase of the content of steel fibres, the water-permeable porosity of each developed UHPFRC linearly grows. Moreover, the water-permeable porosity values obtained in this study are smaller compared to conventional concrete. For instance, Safiuddin and Hearn (2005) reported a water-permeable porosity of 20.5% for concrete produced with a water/cement ratio of 0.60, employing the same measurement method (vacuum-saturation technique). Furthermore, with the same content of steel fibres, the water-permeable porosity of UHPC2 is the smallest among the three investigated mixtures.

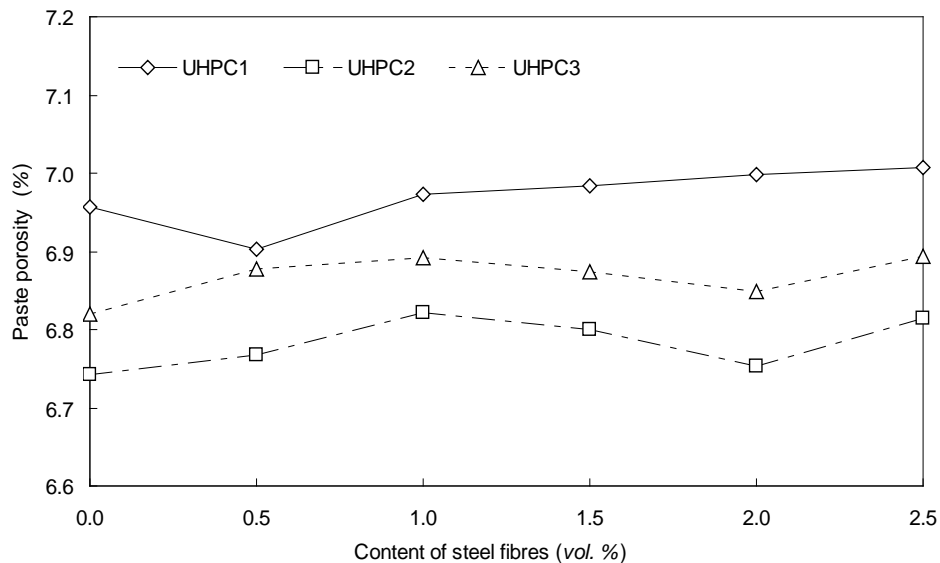


**Figure 3.7: Paste porosity results of UHPFRC with different cement and fibre content**

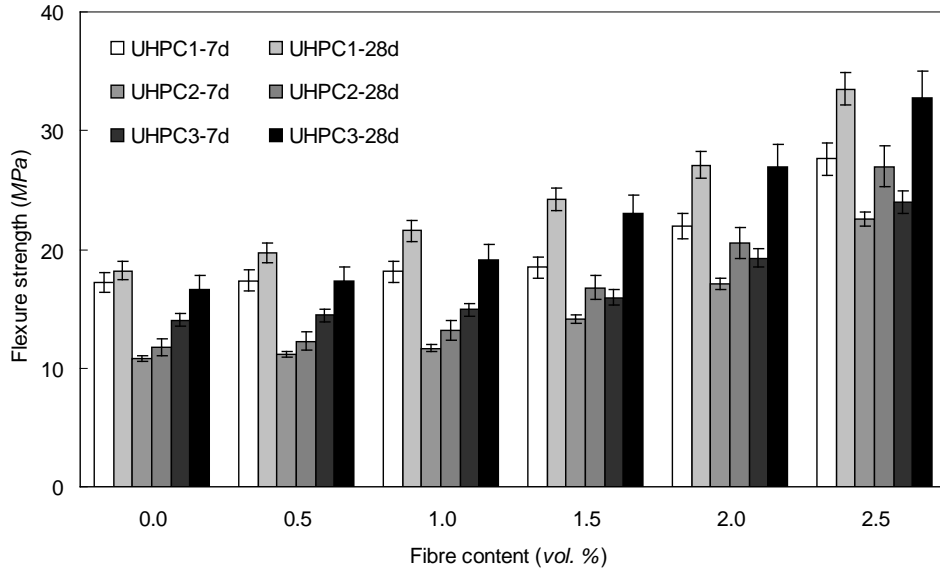
Here, it is assumed that the water-permeable porosity of UHPFRC is composed of the air voids (entrapped in fresh concrete) and the paste porosity (generated during the hydration of cement). Hence, based on the results shown in Figures 3.5 and 3.6, the paste porosity of UHPC mixes versus the volumetric steel fibres content is revealed in Figure 3.7. It is apparent that with an increase of the steel fibre content, the paste porosity remains relatively constant. For instance, in UHPC2, the paste porosity is in the range of 6.7-6.8%, while it increases to 6.8-6.9% and 6.9-7.0% for UHPC3 and UHPC1, respectively. According to the investigation of Tazawa and Miyazawa (1999), with the same water content, the more cement there is, the higher chemical shrinkage porosity of the hardened cement matrix will be generated. Hence, the small difference of paste porosity between UHPC should also be owed to the different cement contents.

To sum up, as supported by the experimental results, due to the optimized particle packing of concrete mixtures and low water/ binder ratio, the developed UHPFRC has a low water-permeable porosity and dense internal structure.

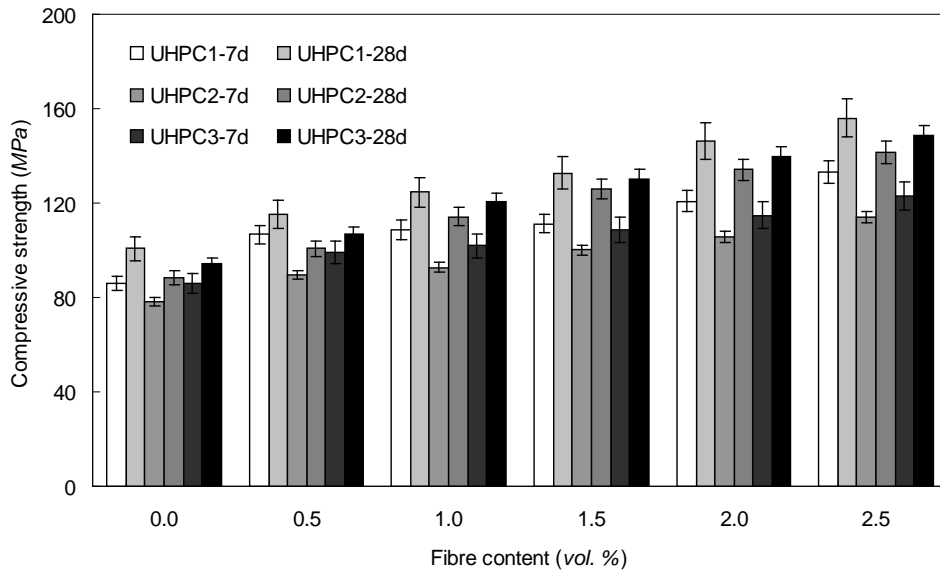
· ***Mechanical properties***

The flexural and compressive strengths of UHPFRC at 7 days and 28 days versus the volumetric steel fibres contents are shown in Figure 3.8. It is important to notice that with the addition of steel fibres, the flexural and compressive strengths of UHPFRC can be significantly enhanced, similarly to the results shown in the literature (Romualdi et al., 1964; Rossi et al., 1987; Zhang et al., 2008). Taking UHPC3 as an example, with the addition of steel fibres, the flexural strength at 28 days increases from 16.7 MPa to 32.7 MPa, and the compressive strength increases from 94.2 MPa to 148.6 MPa. Moreover, with the same fibre content and curing time, the flexural and compressive strengths of UHPC1 are always larger than those of UHPC2 and UHPC3. For instance, with the addition of 2.5% (by volume of concrete) steel fibres, the flexural and compressive strengths of UHPC1 at 28 days are 33.5 MPa and 156 MPa, while that of UHPC2 are 27.0 MPa and 141.5 MPa, respectively. Additionally, the comparison of the binder amount and compressive strength (28 days) between the optimized and the non-optimized UHPFRC is shown in Table 3. It is clear that with lower binder amount, the compressive strength of the optimized UHPFRC is still comparable to the non-optimized UHPFRC (which have a large amount of binder). For instance, as the results shown by Hassan et al. (2012), about 1200 kg/m<sup>3</sup> of binder is utilized in producing UHPFRC, and its compressive strength at 28 days is about 150 MPa. However, in this study, there is only about 650 kg/m<sup>3</sup> of binders in UHPC2, but its compressive strength can also reach around 142 MPa. Hence, it can be concluded that, based on the modified A&A model, it is possible to produce a UHPFRC with low binder amount.

Fibres in concrete can bridge cracks and retard their propagation, which directly results in the increase of strength (especially the flexural strength) of concrete. Additionally, the cement content also has a close relationship with the strength of concrete. As the investigation of Sun et al. (1986) shows, with a reduction of water/cement ratio, the interface between the matrix and aggregates or matrix and fibres will become denser. Hence, in this study, the UHPC1 (the one with the highest cement content) has the largest flexural and compressive strength, compared to that of UHPC2 and UHPC3. However, it should also be noticed that the strength difference between UHPC1 and UHPC3 is not so obvious anymore after 28 days, although there is 175 kg/m<sup>3</sup> difference in the content of cement between them. Consequently, the influence of steel fibres and cement content on the strength of UHPFRC should be considered separately.



(a) Flexural strength



(b) Compressive strength

**Figure 3.8: Flexural (a) and compressive (b) strengths of the developed UHPFRC after curing for 7 and 28 days**

To clarify the effect of the additional steel fibres on the flexural and compressive strengths of UHPFRC, the strength improvement ratio is utilized and shown as follows (Pu, 2004):

$$K_t = \frac{S_i - S_0}{S_0} \quad (i = 0.5, 1.0, 1.5, 2.0, 2.5) \quad (3.5)$$

where the  $K_t$  is the strength improvement ratio (%),  $S_i$  is the strength of concrete with fibres (MPa) ( $i$  represents the addition of fibres, by volume) and  $S_0$  is the strength of concrete without fibres (MPa).

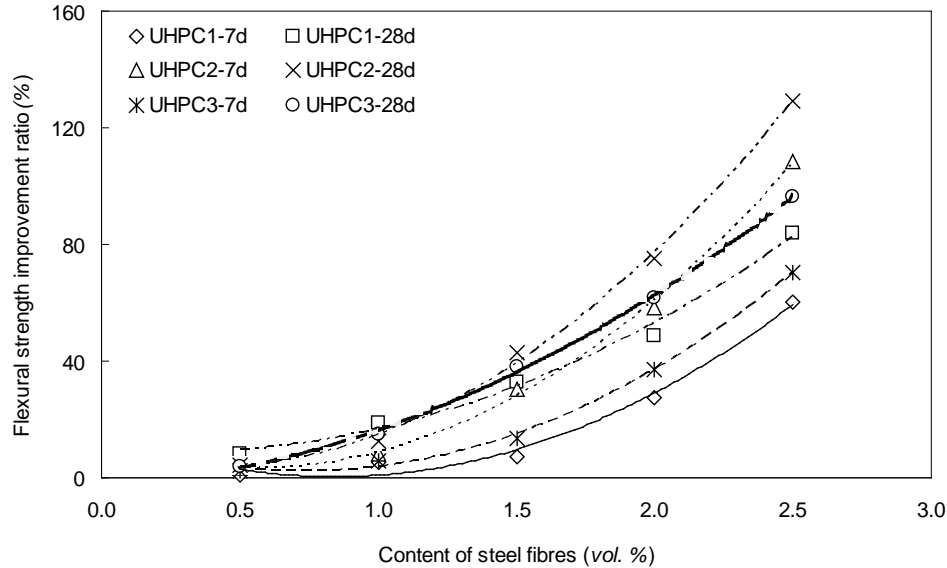
**Table 3.2: Comparison of the binder amount and compressive strength (28 days) of optimized and non-optimized UHPFRC**

Mixtures	Binders (kg/m <sup>3</sup> )			Water/binder ratio	Steel fibre amount (vol. %)	Compressive strength at 28 days (MPa)
	Cement	GGBS	Silica fume			
a	950	0	238	0.2	2	190
b	860	0	215	0.2	2	198
c	657	418	119	0.17	2	150
d	657	430	119	0.15	2	120
e	1011	0	58	0.15	2	160
f	960	0	240	0.16	2.5	155
g	1050	0	275	0.14	6	160
UHPC1	875	0	44 (micro)	0.19	2.5	156
UHPC2	612	0	44 (micro)	0.19	2.5	142
UHPC3	700	0	44 (micro)	0.19	2.5	149

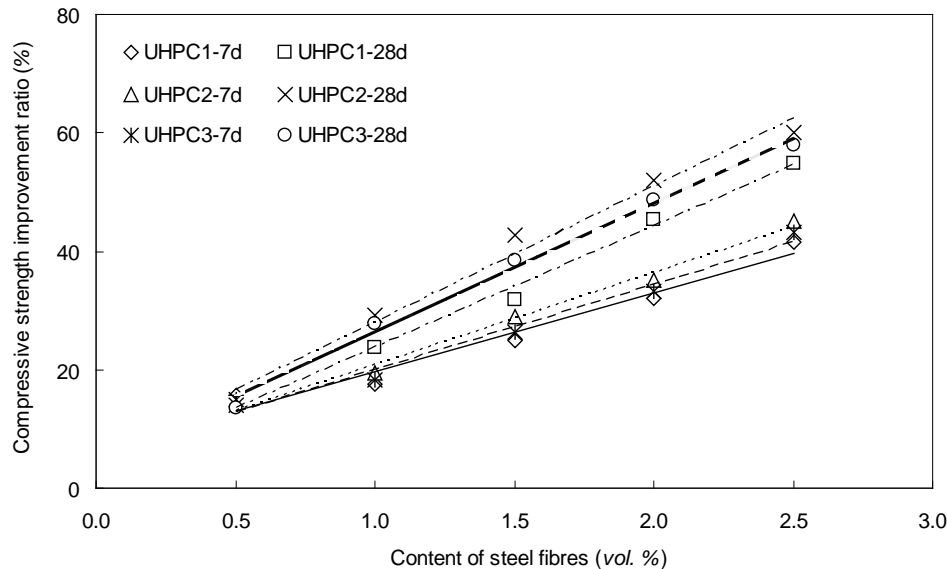
(a: (Yang et al., 2010), b: (Kang et al., 2011), c: (Hassan et al., 2012), d: (Yang et al., 2009), e: (Toledo Filho et al., 2012), f: (Corinaldesi and Moriconi, 2012), g: (Habel et al., 2006))

The flexural and compressive strength improvement ratios of the UHPC mixes versus the volumetric steel fibres contents are illustrated in Figure 3.9. As indicated in Figure 3.9(a), with an increase of the steel fibres content, a parabolic increase tendency of the flexural strength improvement ratio can be observed. The increase of the additional fibres amount can significantly improve the flexural strength improvement ratio. Moreover, the difference in the flexural strength improvement ratio between the UHPFRCs is small when only 0.5% of steel fibres are added. Nevertheless, with a further increase of the steel fibre content, its influence on the flexural strength improvement ratio of UHPC2 is more significant than that of UHPC1 and UHPC3. For instance, with only 0.5% of steel fibres, the flexural strength improvement ratios of UHPC1, UHPC2 and UHPC3 at 28 days are 8.2%, 4.4% and 3.8, which then increase to 84.0%, 129.3% and 96.3%, respectively, when 2.5% of steel fibres are included. As can be seen in Figure 3.9(b), with an increase of the steel fibres content, there is a linear increase tendency of the compressive strength improvement ratio in each mixture. Similarly to the results shown in Figure 3.9(a), the difference of compressive strength improvement ratios between the UHPC is not obvious when small amount of steel fibres (around 0.5%) are added. When more steel fibres are included (more than 2%), the increase rate of such values for UHPC2 is much higher than that of UHPC3 and UHPC1.

Hence, it can be summarized that the inclusion of steel fibres can bring a considerable enhancement to the strengths of UHPC, especially to the flexural strength. Additionally, the efficiency of additional fibres in UHPC2 is higher and more notable compared to the other mixtures. This may be due to the low cement content and the inclusion of large quantity of filler materials in UHPC2.



(a) Flexural strength improvement ratio



(b) Compressive strength improvement ratio

Figure 3.9: Flexural (a) and compressive (b) strengths improvement ratios of UHPFRC at 7 and 28 days as function of steel fibre content

However, it can be noticed that the porosities and the compressive strengths of the developed UHPCs follow the same order: UHPC1 > UHPC3 > UHPC2, which is not in line with the commonly approved trend that a higher water-permeable porosity corresponds to a lower compressive strength. Here, this phenomenon may be attributed to the variation of the cement content in each developed UHPCs. It can be noticed that, based on the modified A&A model, the porosities of all the developed UHPCs are low and similar to each other (as shown in Figures 3.5 and 3.6). Furthermore, the cement amount in UHPC1 is obviously higher than that in UHPC2 and UHPC3, which may cause that more cement particles can hydrate. However, to clearly explain this question and accurately calculate the hydrated cement amount in the developed UHPCs, the cement hydration degree of each sample should be firstly determined, which will be shown in the following part.

Consequently, it can be concluded that based on the modified A&A model, it is possible to develop a UHPFRC with a low binder amount without sacrificing mechanical properties. When utilizing quartz powder to replace about 20% cement, the decrease of flexural and compressive strengths is not significant. On the other hand, using limestone powder to replace around 30% cement in preparing UHPFRC, the strengths will decrease about 10%, but the efficiencies of steel fibres and cement can be significantly enhanced.

#### · *Thermal analysis*

The DSC and TG curves of the UHPC pastes after hydrating for 7 and 28 days are presented in Figures 3.10 and 3.11. From the DSC curves, it is apparent that there main peaks exist in the vicinity of 120 °C, 450 °C and 820 °C for all the samples, which can be attributed to the evaporation of free water, decomposition of Ca(OH)<sub>2</sub> and decomposition of CaCO<sub>3</sub>, respectively (Grattan-Bellew, 1996; Handoo et al., 2002; Alonso and Fernandez, 2004; Castellote et al., 2004; Alarcon-Ruiz et al., 2005). Normally, there is also a peak at about 576 °C, which occurs due to the conversion of quartz (SiO<sub>2</sub>) from  $\alpha$ -SiO<sub>2</sub> to  $\beta$ -SiO<sub>2</sub>. However, in this study, this peak has not been found, which may be attributed to the absence of aggregates (i.e. sand) in the tested sample and the low content of quartz powder.

Based on the test results shown in Figure 3.10, the samples for TG analysis are subjected to isothermal treatment during the test, which is set at 105 °C, 450 °C, 570 °C and 800 °C for 2 h. As can be seen in Figure 3.11, the TG curves of all the UHPC pastes show a similar tendency of losing their mass. However, their weight loss rate at each temperature range is different, which means that the amount of the reacted substances in each treatment stage is different. Taking the UHPC2 paste as an example, there is an obvious weight loss at 800 °C, which is caused by the decomposition of CaCO<sub>3</sub>. In addition, with an increase of the curing time, the weight loss at 800 °C simultaneously increases, which means the hydration of cement is still ongoing, and more Ca(OH)<sub>2</sub> is generated and

carbonated. Hence, to calculate the cement hydration degree in UHPC paste, the decomposition of  $\text{CaCO}_3$  (both from limestone powder and from carbonation of  $\text{Ca}(\text{OH})_2$ ) cannot be ignored.

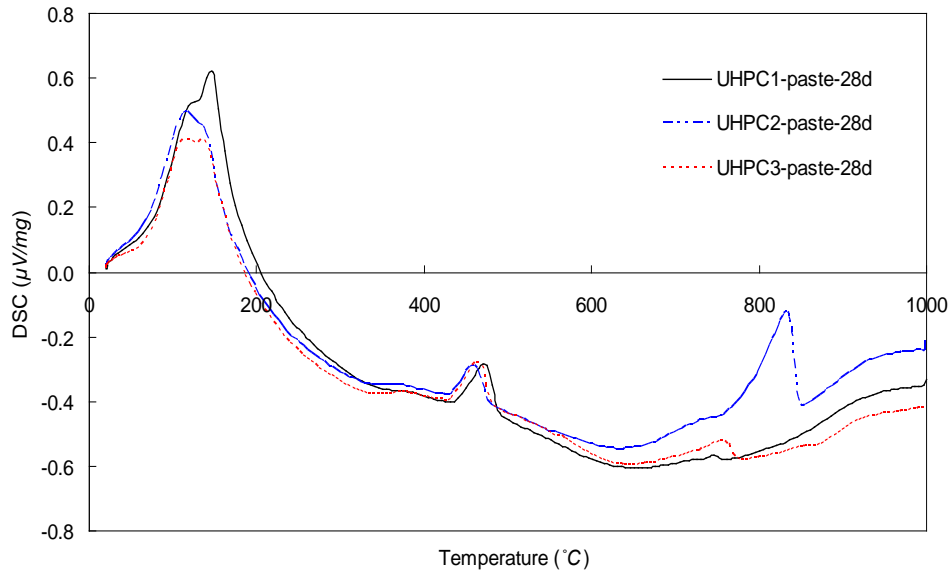


**Figure 3.10: DSC curves of UHPC pastes after hydrating for 28 days**

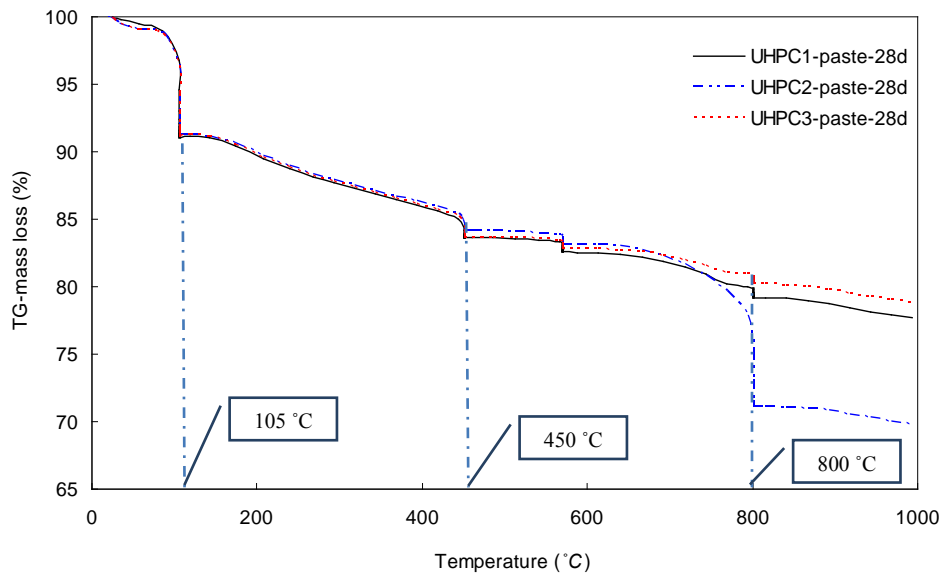


**Figure 3.11: TG curves (mass loss - %) of UHPC1, UHPC2 and UHPC3 pastes after hydrating for 28 days**

Here, the hydration degree of the cement in UHPFRC paste after hydrating for 1, 3, 7 and 28 days is computed based on the TG results and Eqs. (2.13) and (2.14). As indicated in Figure 3.12, the shapes of the three curves are similar to each other. This shape can be characterized with a sharp increase before 3 days, followed by a gradual slowing down

between 3 and 7 days and a region of a very low increase later. This indicates that the hydration speed of cement in UHPC paste is fast during the first 3 days, then gradually becomes slower and very slow after 7 days. For instance, after curing for 7 days, the hydration degree of cement in UHPC1 is 50.3%, which increases only to 52.4% at 28 days. Furthermore, the cement hydration degree in UHPC2 paste is always the highest, which is followed by UHPC3 and UHPC1, respectively. This phenomenon can be explained by the following two reasons: on the one hand, the water/cement ratios of UHPC1, UHPC2 and UHPC3 are 0.23, 0.33 and 0.29, respectively. Hence, after the same curing time, a larger water/cement ratio corresponds to a higher degree of the cement hydration. On the other hand, due to the addition of limestone and quartz powder, the nucleation effect originating from the fine particles may also promote the hydration of cement. As shown in Figure 3.12, the cement hydration degrees of UHPC1, UHPC2 and UHPC3 at 28 days are 52.4%, 67.6% and 61.1%, respectively. Based on the cement amount in each mixes (in Table 3.1), it can be calculated that the reacted cement amount (after 28 days) of the developed UHPCs are  $458.5 \text{ kg/m}^3$ ,  $413.8 \text{ kg/m}^3$  and  $427.9 \text{ kg/m}^3$ , respectively. Hence, it is clear that the absolute cement hydrated amount in UHPC1 is higher than that in UHPC2 and UHPC3. This can also explain the phenomenon that the compressive strengths of the developed UHPCs follow the same order:  $\text{UHPC1} > \text{UHPC3} > \text{UHPC2}$ .

In summary, for the development of UHPFRC, an appropriate utilization of filler materials (such as limestone powder and quartz powder in this study) to replace the cement can significantly enhance the cement hydration degree (as shown in Figure 3.12) and the cement service efficiency, which is beneficial for the production of sustainable UHPFRC.

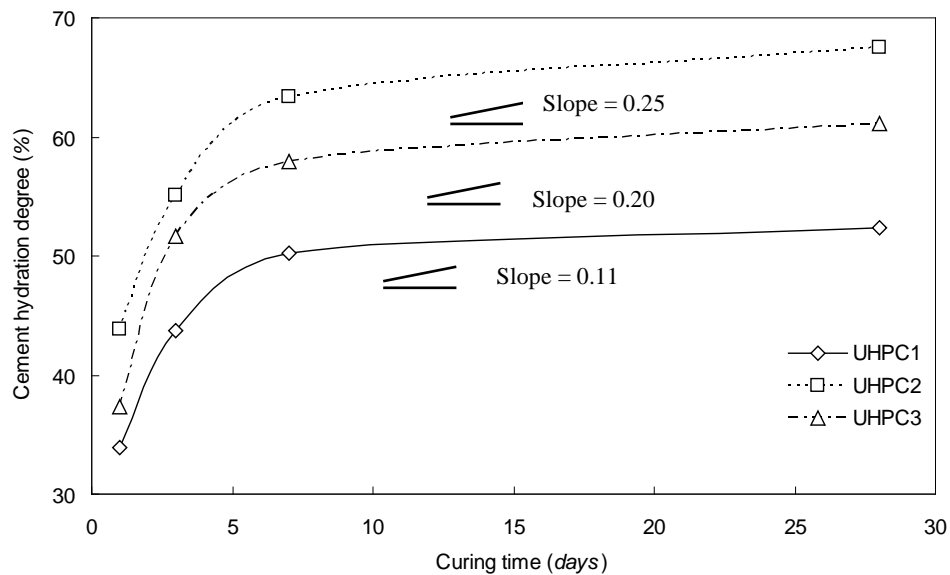


**Figure 3.12: Cement hydration degrees in each UHPC paste after hydrating for 1, 3, 7 and 28 days**

• *SEM analysis*

To explain the superior mechanical properties of UHPFRC, the scanning electron microscopy (SEM) is employed to study its morphology and microstructure. The samples are chosen from UHPC2 with 2.5% of fibres by volume and without fibres after curing in water for 28 days. The SEM images of the hardened cement matrix and the ITZ (interface transition zone) in the developed UHPFRC are presented in Figure 3.13.

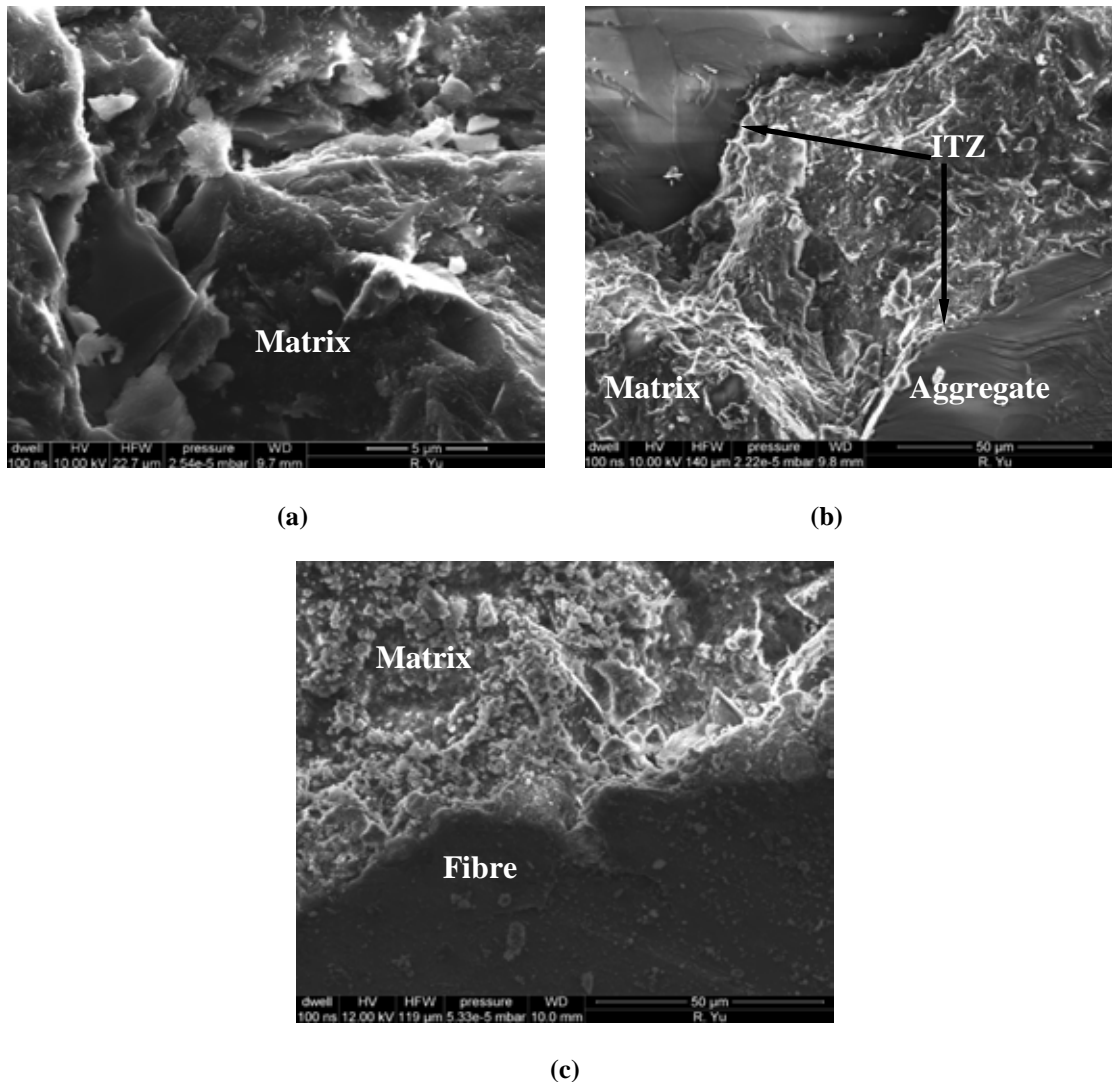


**Figure 3.13: SEM micrographs of UHPFRC mixtures: (a) matrix of UHPFRC, (b) matrix / aggregate interface of UHPFRC (ITZ-interface transition zone), (c) matrix / fibre interface of UHPFRC**

As can be seen in Figure 3.13(a), one can observe a very dense structure in the hardened matrix with only a few air pores. In addition, the main hydration product of the cement matrix is the foil-like C-S-H gel, and no  $\text{Ca}(\text{OH})_2$  or ettringite can be easily found. From Figure 3.13(b), a very compact ITZ can be observed. The dense matrix closely catches the surrounding aggregates, and no distinct air bubbles or other inclusions are presented

in the micrograph. Figure 3.13(c) shows that the interface zone between the fibre and the cement matrix is also dense and homogenous (no air bubbles or other inclusions present). Due to the dense and homogeneous microstructure of UHPFRC, its mechanical properties are superior compared to the normal concrete.

The phenomena observed in the SEM pictures could be mainly attributed to two factors. On the one hand, low water/binder ratio and the incorporation of microsilica result in a dense and homogeneous microstructure of concrete. As shown in Figure 2.2, it can be noticed that the particles of utilized microsilica are very small, and their large amount (about 25%) is smaller than 100 nm. Hence, after the hydration begins, the hydration products diffuse and envelop nanoparticles as kernels, which can promote the hydration of cement and make the cement matrix more homogeneous and compact (Björnström et al., 2004; Land and Stephan, 2012). Furthermore, the crystallization and growth of  $\text{Ca}(\text{OH})_2$  will be restricted with the addition of fine microsilica particles (Li et al., 2007). These also explain why no  $\text{Ca}(\text{OH})_2$  could be easily found in the ITZ between matrix and aggregates or fibres. Hence, by eliminating  $\text{Ca}(\text{OH})_2$  from the ITZ of UHPFRC, its mechanical properties can be significantly improved. On the other hand, the superior particle packing of UHPC can also densify its microstructure. Based on the modified A&A model, the particle packing of UHPC is optimized and its water-permeable porosity is low, leading to a dense and homogenous skeleton and close-grained microstructure of hardened concrete.

To conclude, due to the low water/binder ratio, inclusion of microsilica and appropriate mix design of the concrete skeleton, the matrix and the ITZ of UHPFRC is dense and homogeneous, which results in superior mechanical properties of UHPFRC as shown in Figure 3.8.

### 3.3.4 Summary

In this section, a series of experiments are performed to validate the possibility of using modified A&A model to develop Ultra-High Performance Fibre Reinforced Concrete (UHPFRC), without scarifying mechanical properties. From the obtained experimental results, the following conclusions can be drawn:

- 1) Using the modified A&A model, it is possible to develop a dense and homogeneous skeleton of UHPC with a relatively low binder amount (about  $650 \text{ kg/m}^3$ ). In this study, the maximum compressive and flexural strengths at 28 days of the developed UHPFRC (with steel fibre 2.5% vol.) are about 150 MPa and 30 MPa, respectively.
- 2) Due to the low water/binder ratio and relatively high cement content, the cement hydration degree is small. Hence, it is reasonable to replace these unreacted

- cement particles with some alternative filler materials (such as limestone or quartz powder) to enhance the efficiency of the used cement.
- 3) Using fillers (such as limestone and quartz powder) as a cement replacement to produce UHPFRC can significantly improve its workability and enhance the efficiency of steel fibres and binder. Additionally, the utilization of fillers can also reduce the required amount of micro silica, which is significant for UHPFRC both in economic and environmental aspects.
  - 4) The addition of steel fibres can decrease the relative slump of UHPFRC, and increase the air content in the fresh state and water-permeable porosity in the hardened state. Nevertheless, an appropriate particle packing and low cement content should be treated as the effective methods to reduce the negative influence of the additional steel fibres.

### 3.4 Conclusions

Concrete is a material composed of a number of granular materials. As has been demonstrated here, an optimum packing of the granular ingredients of concrete is the key for a good and durable concrete. However, from the available literature, the design and production of Ultra-High Performance Fibre Reinforced Concrete (UHPFRC) based on the optimized particle packing model is insufficient. In this study, the modified A&A model is utilized to design UHPFRC, and a series of experiments are performed to demonstrate that the optimized UHPFRC can be produced with a relatively low binder amount, without sacrificing its superior mechanical properties. From the obtained experimental results, a UHPFRC can be produced with around  $650 \text{ kg/m}^3$  binders and 2.5% (vol.) steel fibres, with flexural and compressive strengths of 27 MPa and 142 MPa, respectively. Consequently, the modified A&A model is an effective tool to develop sustainable UHPFRC with reduced cost and environmental impact.



## Chapter 4

### Efficient application of powders in UHPC

#### 4.1 Introduction

During the recent years, with the development of new plasticizing concrete admixtures and fine pozzolanic materials, it has become possible to produce high performance concrete (HPC) or even Ultra-High Performance Concrete (UHPC). In the production of UHPC the pozzolanic materials (silica fume, fly ash and ground granulated blast-furnace slag) are widely utilized (Madani et al., 2012; Berra et al., 2012; Hou et al., 2013). Due to its high purity and high specific surface area, the pozzolanic reaction of silica fume is fast and compared to other pozzolanic materials could more effectively promote the strength development of concrete (Schmidt et al., 2013). Additionally, the recent developments of nano-technology guarantee that various forms of nano-sized amorphous silica can be produced, which have higher activities compared to conventional silica fume (Björnström et al., 2004; Land and Stephan, 2011). Hence, a considerable investigation effort has been paid to the clarification of the nanosilica effect on the properties of concrete (Qing et al., 2007; Lin et al., 2008; Senff et al., 2009; Senff et al., 2010). However, based on the available literature, it can be noticed that the investigation of the effect of nanosilica on the cement hydration and microstructure development of UHPC is insufficient (Oertel et al., 2013). This should be owed to the fact that the nanosilica is still a relatively new material for the application in concrete, and its price is much higher compared to that of silica fume or other pozzolanic materials (Kong et al., 2012).

However, with the development of chemical industry, nowadays it become possible to produce a type of “green” nanosilica at low temperatures, from the dissolution of olivine (Lazaro et al., 2012; Lazaro, 2014), which implies that the nanosilica will be more available for the production of UHPC. Moreover, due to the fact that the water/binder ratio is relatively low and a high amount of superplasticizer is commonly used in UHPC, it is not reliable to predict the effect of nanosilica in UHPC based on the experimental results that are obtained for normal strength concrete. Hence, the goals of this chapter are also to clarify the effect of nanosilica on the properties of UHPC and to use nanosilica effectively.

Additionally, as mentioned in the previous chapters, sustainable development is currently a pressing global issue and various industries have strived to achieve energy savings. Nevertheless, the high material cost, high energy consumption and embedded CO<sub>2</sub>

emission for UHPC are the typical disadvantages that restrict its wider application (Friedlingstein et al., 2010; Habert et al., 2013). By far, the measures pursued to reduce the economic and environmental disadvantages of UHPC are limited in most cases to the application of industrial by-products or even waste materials, without sacrificing the UHPC performance (El-Dieb, 2009; Yang et al., 2009; Tuan et al., 2011a; Tuan et al., 2011b; Hassan et al., 2012).

Nevertheless, in most cases, for the mix design of UHPC, the amounts of mineral admixtures (e.g. fly ash, ground granulated blast-furnace slag, limestone powder and silica fume) are given directly, without any detailed explanations or theoretical support. Moreover, due to the complex cementitious system of UHPC (very low water amount and relatively high SP content), the influence of different mineral admixtures on the hydration kinetics and properties of UHPC still needs further investigation.

In general, based on the premises mentioned above, the objective of this chapter is to investigate the effect of the powders (nanosilica, fly ash, ground granulated blast-furnace slag and limestone powder) on the properties of UHPC, so that they could be efficiently used. The concrete matrix is designed based on the modified A&A model, as presented in Chapter 3. Then, the fresh and hardened behaviours, hydration kinetics and thermal properties of the developed UHPC are investigated.

## **4.2 Effect of nanosilica on the properties of UHPC**

### **4.2.1 Background**

From the available literature, it can be found that with the addition of nanosilica in cement or concrete, even at small dosages, nanosilica can significantly improve the mechanical properties of cementitious materials (Shih et al., 2006). For instance, Nazari and Riahi (2011) showed that a 70% compressive strength improvement of concrete can be achieved with an addition of 4% (by mass of cement) of nanosilica. Li et al. (2004) found that when 3% and 5% nanosilica were added to plain cement mortar, the compressive strength increased by 13.8% and 17.5% at 28 days, respectively. However, some contradictory experimental results can also be found in the literature. For example, Senff et al. (2012) found that the contribution of nano-SiO<sub>2</sub>, nano-TiO<sub>2</sub>, and nano-SiO<sub>2</sub> together with nano-TiO<sub>2</sub> defined by factorial design, did not lead to a significant effect on the compressive strength. Moreover, they also found that the values of torque, yield stress and plastic viscosity of mortars with nano-additives increased significantly. According to the experimental results of Ltfi et al. (2011), even a lower compressive strength of samples with 3% nanosilica was observed, compared to the plain specimens. The difference of these experimental results can be attributed to the basic characteristics of the nanosilica (e.g. pozzolanic activity, specific surface area). To interpret the influence of nanosilica on the cement hydration, some theoretical mechanisms were suggested in

the available literature. Land and Stephan (2011) observed that the hydration heat of Ordinary Portland Cement blended with nanosilica in the main hydration period increases significantly with an increasing surface area of silica. Thomas et al. (2009) showed that the hydration of tri-calcium silicate ( $C_3S$ ) can be accelerated by addition of nano-scaled silica or C–S–H-particles. Björnström et al. (2004) monitored the hydration process of  $C_3S$  pastes and the accelerating effects of a 5 nm colloidal silica additive on the rate of  $C_3S$  phase dissolution, calcium-silicate-hydrate C–S–H gel formation and removal of non-hydrogen bound OH groups. Quercia (2014) systematically investigated the characteristics of nanosilicas and their effect on the properties of concrete. It was found that the promotion of cement hydration and concrete properties (mechanical properties and durability) has close relationship with the specific area of the utilized nanosilica.

As summarized by Quercia (2014), the nanosilicas currently available on the market have one very clear drawback - a relatively high price. Thus, despite its positive influence on the properties of concrete, the economic factor strongly limits its use in concrete mass products. Hence, at present, nanosilica is mainly used in the so-called high performance concretes, eco-concretes and self-compacting concretes (Sari et al., 1999; Sobolev and Ferrara., 2005a; Sobolev and Ferrara, 2005b; Sobolev et al., 2006; Quercia et al., 2014; Quercia, 2014), because of the high requirements on these advanced concretes. When applied in high performance concrete and self-compacting concrete, the addition of nanosilica can increase the cohesiveness of concrete and reduce the segregation tendency, which is beneficial for improving the properties of concrete (Sari et al., 1999; Sobolev and Ferrara, 2005b; Green, 2006). However, by far, nanosilica is seldom used in the production of UHPC, and the influence of nanosilica on the properties of UHPC still needs further attention.

Consequently, the aim of this section is to investigate the effect of nanosilica on the hydration and microstructure development of UHPC with a relatively low binder amount. The design of the concrete mixtures is based on the aim to achieve a densely compacted composite, employing the modified A&A model, following the description provided in Chapter 3. The fresh and hardened behaviour of UHPC are evaluated. Techniques such as isothermal calorimetry, thermal analysis and scanning electron microscopy are employed to analyse the cement hydration and microstructure development of UHPC.

#### **4.2.2 Materials and mix design of UHPC with nanosilica**

The cement used in this study is Ordinary Portland Cement (OPC) CEM I 52.5 R, provided by ENCI (the Netherlands). A polycarboxylic ether based superplasticizer is used to adjust the workability of UHPC. The limestone and quartz powders are used as fine fillers. Due to the relatively high fineness of the utilized limestone and quartz powder, their cementitious activity is not considered in this study. Two types of sand are used, one is normal sand with the fractions of 0-2 mm and the other one is microsand

with the fraction 0-1 mm (Graniet-Import Benelux, the Netherlands). One type of commercially available nanosilica slurry is used. Some detailed information on this nanosilica is shown in Table 4.1.

**Table 4.1: Characterization of the used nanosilica (Data obtained from the supplier)**

Type	Slurry
Stabilizing agent	Ammonia
Specific density (g/cm <sup>3</sup> )	2.2
pH (at 20 °C)	9.0-10.0
Solid content (% w/w)	50
Viscosity (mPa s)	≤100
BET (m <sup>2</sup> /g)	22.7
PSD by LLS (μm)	0.05-0.3
Mean particle size (μm)	0.12

The UHPC mixtures, designed using the modified A&A model ( $q = 0.29$ ), are listed in Table 4.2. The  $q$  value is in line with the recommendation by Quercia (2014). It can be noticed that the OPC amount in UHPC is relatively low, around 440 kg/m<sup>3</sup>. Moreover, the nanosilica is added in the amount of 1%, 2%, 3%, 4% and 5% to replace the cement. Hence, based on the results of the fresh and hardened properties of the developed UHPC, it would be possible to evaluate the influence of nanosilica on its properties. An example of the target curve and the resulting integral grading curve of UHPC is shown in Figure 4.1.

**Table 4.2: Mix recipe of the UHPC with nanosilica**

	OPC (kg/m <sup>3</sup> )	LP (kg/m <sup>3</sup> )	QP (kg/m <sup>3</sup> )	MS (kg/m <sup>3</sup> )	S (kg/m <sup>3</sup> )	nS (kg/m <sup>3</sup> )	W (kg/m <sup>3</sup> )	SP (kg/m <sup>3</sup> )
Ref.	439.5	263.7	175.9	218.7	1054.7	0	175.8	43.9
UHPC-1%	435.1	263.7	175.9	218.7	1054.7	4.4	175.8	43.9
UHPC-2%	430.7	263.7	175.9	218.7	1054.7	8.8	175.8	43.9
UHPC-3%	426.3	263.7	175.9	218.7	1054.7	13.2	175.8	43.9
UHPC-4%	421.9	263.7	175.9	218.7	1054.7	17.6	175.8	43.9
UHPC-5%	417.5	263.7	175.9	218.7	1054.7	22.0	175.8	43.9

(OPC: Ordinary Portland Cement (CEM I 52.5 R), LP: limestone powder, QP: quartz powder, MS: microsand, S: sand (0-2), nS: nanosilica, W: water, SP: superplasticizer)

Additionally, Table 4.3 presents the characteristics of each recipe listed in Table 4.2, which includes the water/cement ratio, water/binder ratio, water/powder ratio, SP content by the weight of cement and SP content by the weight of powders. Due to the fact that a large amount of cement has already been replaced by limestone and quartz powder, the water to cement ratio is relatively high (about 0.4). However, the water/powder ratios of all the batches are still comparatively low (around 0.18). Considering the fact that the

used water can be significantly absorbed by the powder materials, the SP amount by the weight of powder is fixed to about 4.5%.

**Table 4.3: Characteristics of the developed concrete recipes**

	W/C	W/B	W/P	SP content (% bwoc)	SP content (% bwop)
Ref.	0.400	0.400	0.180	9.987	4.486
UHPC-1%	0.404	0.400	0.180	10.090	4.486
UHPC-2%	0.408	0.400	0.180	10.193	4.486
UHPC-3%	0.412	0.400	0.180	10.298	4.486
UHPC-4%	0.417	0.400	0.180	10.405	4.486
UHPC-5%	0.421	0.400	0.180	10.515	4.486

(W: water, C: cement, B: binder, P: powder (particle size < 125 $\mu$ m), bwoc: by the weight of cement, bwop: by the weight of powder)

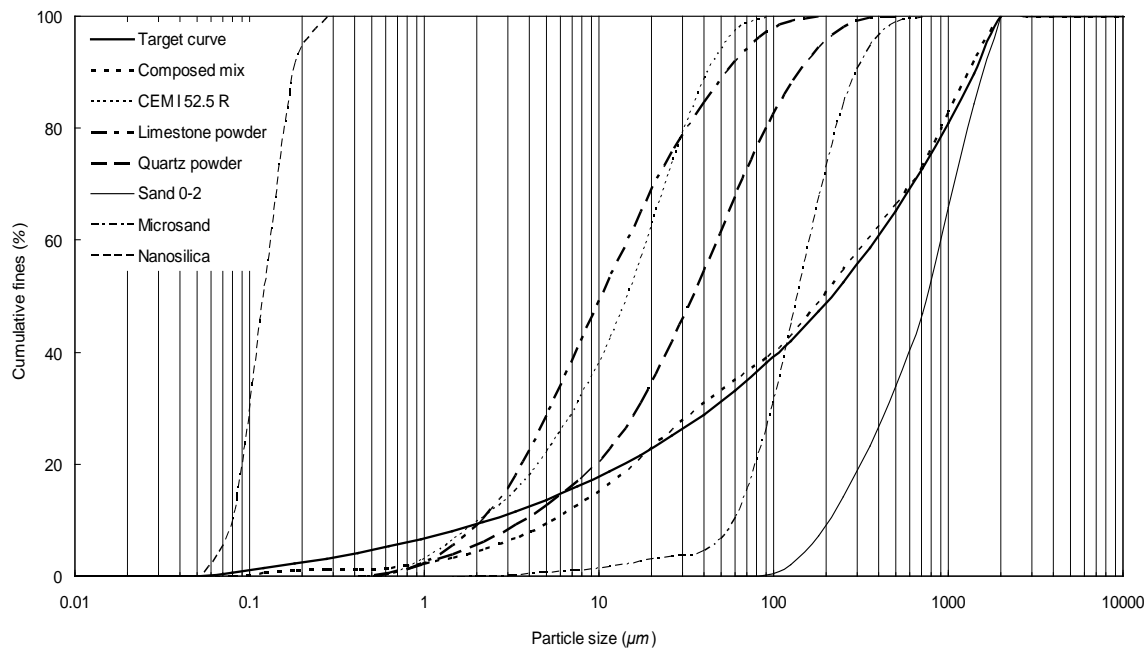


**Figure 4.1: PSDs of the involved ingredients, the target and optimized grading curves of the developed UHPC mixture (one example: UHPC-4%)**

### 4.2.3 Experimental methodologies

- *Employed mixing procedures*

Following the mix procedures shown in Figure 3.2, about 7 minutes and 30 seconds is required to finish the UHPC mixing.

- *Fresh behaviour*

The fresh behaviour of UHPC is measured following the method shown in Section 2.3.1. The Hägermann cone is utilized.

- ***Air content and water-permeable porosity***

The air content in fresh concrete and water-permeable porosity of hardened concrete are measured following the method shown in Sections 2.3.2 and 2.3.3, respectively.

- ***Mechanical properties***

The concrete samples are cast in moulds with the size of 40 mm × 40 mm × 160 mm. The prisms are demolded approximately 24 h after casting and then cured in water at about 20 ± 1 °C. After curing for 3, 7 and 28 days, the flexural and compressive strengths of the specimens are tested according to EN-196-1 (2005). At least three specimens are tested at each age to compute the average strength.

- ***Hydration kinetics***

Based on the method shown in Section 2.3.6, cement, limestone and quartz powder are mixed with silica slurry, superplasticizer and water. Here, nanosilica/binder mass ratios from 1% to 5% are investigated. Moreover, another reference sample (Reference - 2) with only cement and water (water/cement = 0.4) is simultaneously prepared. All the pastes are mixed for two minutes and then injected into a sealed glass ampoule, which is then placed into the isothermal calorimeter (TAM Air, Thermometric). The instrument is set to a temperature of 20 °C. After 7 days, the measurement is stopped and the obtained data is analysed. All results are ensured by double measurements (two-fold samples).

- ***Thermal properties***

The thermal analysis and cement hydration degree are determined by the method presented in Section 2.3.6.

- ***SEM analysis***

Scanning electron microscopy (SEM) is employed to study the microstructure of UHPC. After curing for 28 days, the specimens are cut into small fragments and soaked in ethanol for over 7 days, in order to stop the cement hydration. Subsequently, the samples are dried and stored in a sealed container before the SEM imaging.

#### **4.2.4 Results and discussions**

- ***Fresh behaviour***

The slump flow of fresh UHPC mixes versus the amount of added nanosilica is depicted in Figure 4.2. The data illustrates the direct relation between the nanosilica amount and

the workability of fresh UHPC. It is important to notice that with the addition of nanosilica, the slump flow of fresh UHPC decreases linearly. For the UHPC developed here, the slump flow value of the reference sample is 33.75 cm, which drops to about 22.5 cm when 5% of nanosilica is added. This behaviour is in line with the results shown in Senff et al. (2012), which indicates that the addition of nanosilica strongly increases the water demand of cementitious mixes. A hypothesis explaining this is that the presence of nanosilica decreases the amount of lubricating water available within the interparticle voids, which causes an increase of the yield stress and plastic viscosity of concrete (Senff et al., 2012).

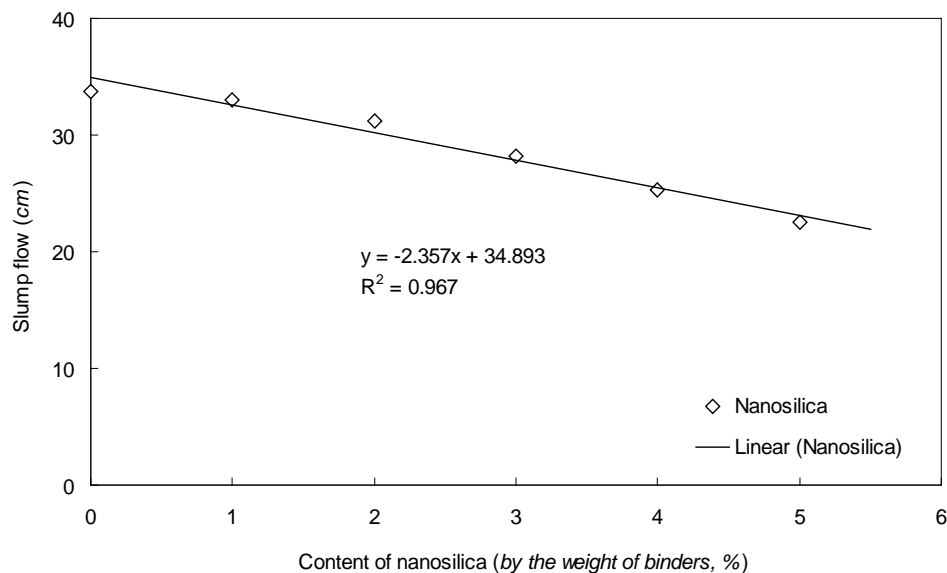


**Figure 4.2: Variation of the slump flow of UHPC as function of nanosilica amount**

- ***Air content and water-permeable porosity***

The air content of UHPC in fresh state and the water-permeable porosity of UHPC in hardened state are presented in Figure 4.3. As can be observed, the air content of the reference sample (without nanosilica) is relatively low (2.01%), which can be attributed to the dense particle packing and good self-compaction of the developed UHPC. However, with an increasing amount of nanosilica, the air content of UHPC clearly increases. When the additional nanosilica amount is 5%, the air content in fresh UHPC increases to about 3.5%. To interpret this phenomenon, the effect of nanosilica on the viscosity of UHPC should be considered. With an increasing amount of nanosilica, the viscosity of UHPC significantly increases (Senff et al., 2012), which causes that the entrapped air cannot easily escape from the fresh concrete. Hence, the air content of the fresh concrete with high content of nanosilica is relatively higher.

Compared to the air content results, the water-permeable porosity of hardened UHPC show very different development tendency. With an addition of nanosilica, the water-permeable porosity of UHPC firstly decreases, and then slightly increases after reaching a critical value. In this study, the water-permeable porosity of reference sample is about 10.5%, and decreases to about 9.5% when 4% of nanosilica is added. However, the water-permeable porosity of the sample with 5% of nanosilica increases to about 9.8% again. This phenomenon can be attributed to the positive effect of nanosilica on the cement hydration. As commonly known, due to the nucleation effect of nanosilica, the formation of C–S–H phase is no longer restricted on the grain surface alone, which cause that the hydration degree of cement is higher and more pores can be filled by the newly generated C–S–H (Thomas et al., 2009). For this reason, the water-permeable porosity of UHPC firstly decreases with the addition of nanosilica. However, due to the fact that the air content of UHPC increases with the addition of nanosilica, the water-permeable porosity of UHPC will increase again when the newly generated C–S–H is insufficient to compensate for the entrapped air in fresh concrete. Consequently, considering these two opposite processes, there is an optimal nanosilica amount (around 4%), at which the lowest water-permeable porosity of UHPC can be obtained.

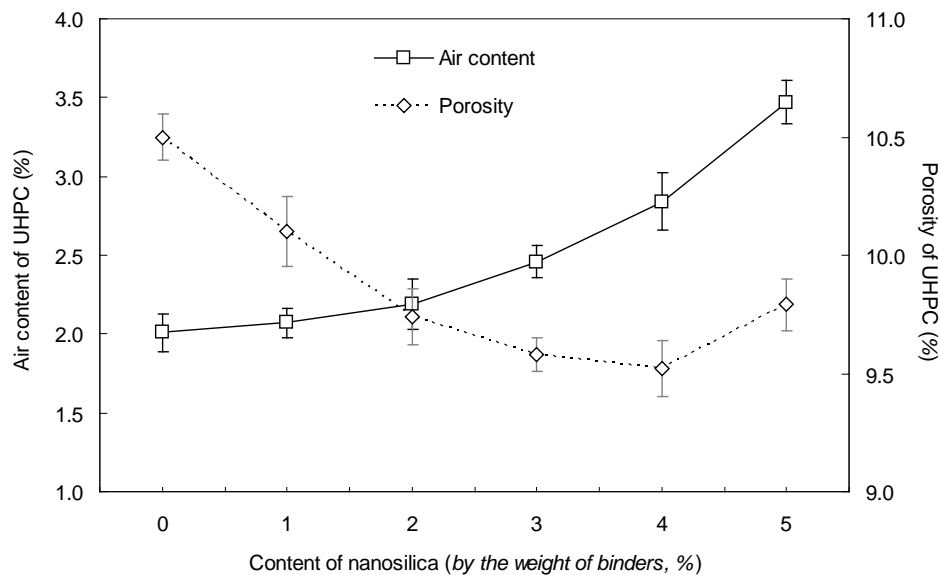
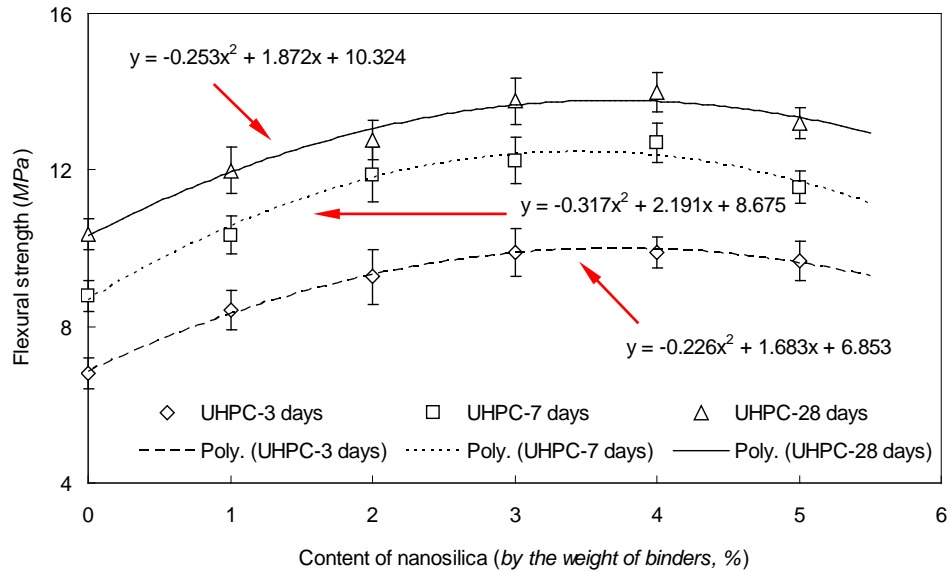


**Figure 4.3: Air content and water-permeable porosity of UHPC with different amounts of nanosilica**

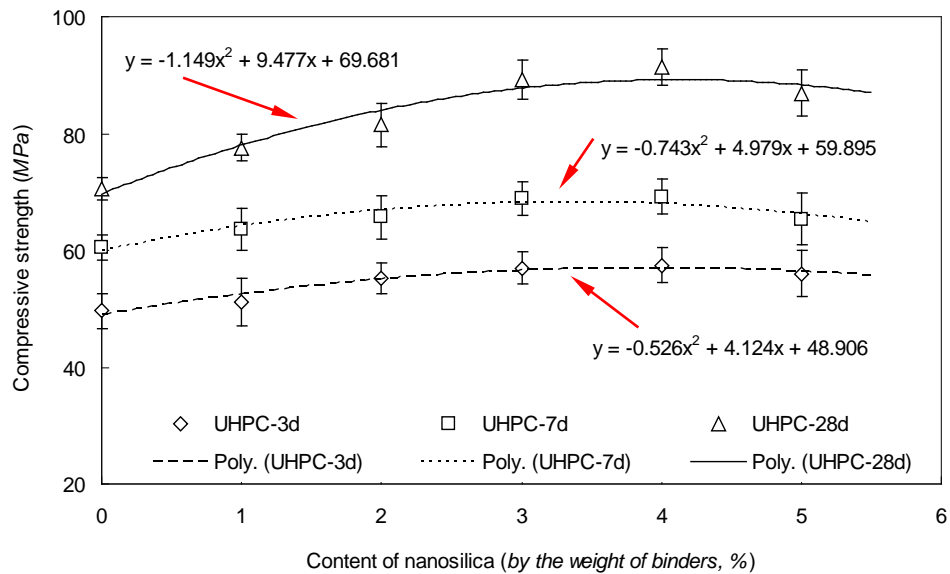
#### • *Mechanical properties*

The flexural and compressive strengths of UHPC at 3, 7 and 28 days versus the added nanosilica amounts are shown in Figure 4.4. With the addition of nanosilica, a parabolic growth tendency of the flexural and compressive strength of UHPC can be observed. For example, the flexural strength of the reference sample at 28 days is about 10.4 MPa, which gradually increases to about 14.0 MPa when 4% of nanosilica is added. Yet, this

value slightly decreases to about 13.2 MPa when 5% of nanosilica is included. Hence, there should be an optimal amount of nanosilica, at which the flexural and compressive strengths of UHPC can be theoretically highest.



(a) Flexural strength



(b) Compressive strength

**Figure 4.4: Variation of the strengths of UHPC after curing for 3, 7 and 28 days as a function of nanosilica amount: (a): flexural strength, (b): compressive strength**

According to the regression equation of each parabola shown in Figure 4.4, it is easy to understand that when the differential coefficient ( $y'$ ) of each function equals zero, the

value of  $x$  represent the optimal nanosilica amount to obtain the best mechanical properties. Hence, the optimal nanosilica amount and the computed maximum flexural and compressive strengths at 3, 7 and 28 days are shown in Table 4.4. As can be seen, the optimal nanosilica amount for the flexural strength at 3, 7 and 28 days are 3.72%, 3.46% and 3.70%, respectively, and 3.92%, 3.90% and 4.29% for the compressive strength. Based on these optimal nanosilica amounts, the computed maximum strengths are 10.0 MPa, 12.5 MPa and 13.8 MPa for flexural strength and 57.0 MPa, 69.6 MPa and 88.9 MPa for the compressive strength. Moreover, it is important to notice that computed maximum compressive strength at 28 days is 88.9 MPa, which is even smaller than the one with 4% of nanosilica (91.29 MPa). This can be attributed to the deviation of the regression equation. As can be noticed that the coefficient of determination ( $R^2$ ) of the one representing the compressive strength at 28 days is only 0.862. Hence, to accurately obtain the optimal nanosilica amount in this study, only 3.72%, 3.46%, 3.70%, 3.92% and 3.90% are selected to calculate the average value (3.74%), which represents the optimal amount for this nanosilica in UHPC to theoretically get the best mechanical properties. The calculated optimal nanosilica amount is similar as that shown in (Quercia, 2014).

**Table 4.4: Optimal nanosilica amount for flexural and compressive strength at 3, 7 and 28 days**

Calculated results	Flexural			Compressive		
	3 d	7 d	28 d	3 d	7 d	28 d
Optimal nanosilica amount (%)	3.72	3.46	3.70	3.92	3.90	4.29
Theoretical maximum strength (MPa)	10.0	12.5	13.8	57.0	69.6	88.9
Coefficient of determination ( $R^2$ )	0.996	0.980	0.982	0.948	0.969	0.862

In this study, to clearly demonstrate the advantages of the modified A&A model for the design of UHPC, the concept of the binder efficiency is utilized and shown as follows:

$$X_{binder} = \frac{f_c}{m_{binder}} \quad (4.1)$$

where  $X_{binder}$  is the binder efficiency,  $f_c$  is the compressive strength of UHPC at 28 d (MPa) and  $m_{binder}$  is the total mass of the used binders (kg).

A comparison of the binder efficiencies between the available literature and results obtained in this study is shown in Table 4.5. As can be seen, the binder efficiency of the mixtures designed in this study is significantly higher than that presented in the literature. Hence, it can be concluded that by the utilization of modified A&A model, a dense and homogeneous skeleton of UHPC can be obtained with a relatively low binder amount (about 440 kg/m<sup>3</sup>), and the binders can be well utilized.

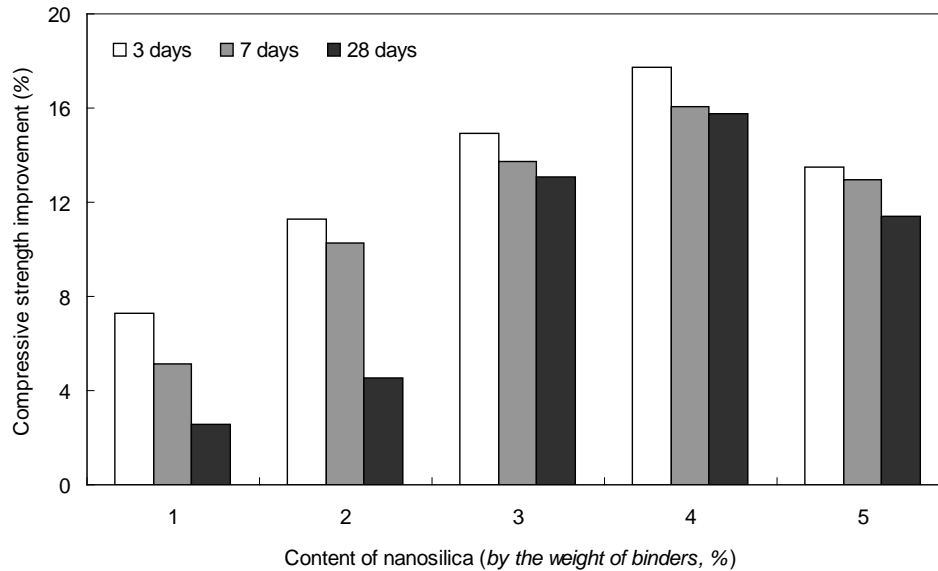


**Figure 4.5: Compressive strength improvement of UHPC with different nanosilica amount at 3, 7 and 28 days**

**Table 4.5: Comparison of the binder efficiency of the UHPCs**

Reference	Binders (kg/m <sup>3</sup> )				Water (kg/m <sup>3</sup> )	28 days compressive strength (MPa)	Binder efficiency (N/mm <sup>2</sup> )/(kg/m <sup>3</sup> )
	OPC	GGBS	Fly ash	Silica (micro/nano)			
a	825.0	0.0	0.0	175.0	175.0	140.0	0.14
b	500.0	0.0	350.0	150.0	160.0	92.0	0.09
c <sub>1</sub>	810.0	0.0	0.0	90.0	162.0	138.0	0.15
c <sub>2</sub>	630.0	180.0	0.0	90.0	162.0	123.0	0.14
c <sub>3</sub>	450.0	360.0	0.0	90.0	162.0	110.0	0.12
d	500.0	0.0	0.0	72.0	166.0	80.0	0.14
e	850.0	0.0	0.0	260.0	170.0	115.0	0.10
Ref.	439.5	0.0	0.0	0.0	175.8	78.0	0.18
UHPC-1%	435.1	0.0	0.0	4.4	175.8	79.9	0.18
UHPC-2%	430.7	0.0	0.0	8.8	175.8	81.5	0.19
UHPC-3%	426.3	0.0	0.0	13.2	175.8	89.2	0.20
UHPC-4%	421.9	0.0	0.0	17.6	175.8	91.3	0.21
UHPC-5%	417.5	0.0	0.0	22.0	175.8	86.9	0.20

(Ref., UHPC-1%, UHPC-2%, UHPC-3%, UHPC-4% and UHPC-5% are the mixtures designed in this study, in which the 1% -5% means the nanosilica amount by the total mass of binders, a: (Oertel et al., 2013), b: (Zhao et al., 2014), c<sub>1-3</sub>: (Wang et al., 2012), d: (Deeb et al., 2012), e: (Yazici, 2007))

Additionally, to evaluate the promotive effect of the employed nanosilica on the mechanical properties of UHPC, Eq. (3.4) (Pu, 2004) is utilized. The compressive

strengths improvement ratios of UHPC mixtures versus the nanosilica amount are illustrated in Figure 4.5. It can be seen that, similarly to the flexural and compressive strengths results, the compressive strength improvement firstly increases with the increase of the nanosilica amount, and then decreases. Moreover, the effect of the nanosilica on the improvement of UHPC compressive strength is more efficient at 3 days, compared to that at 7 and 28 days. This phenomenon also implies that nanosilica can significantly promote the early hydration process of cement in UHPC.

#### • Hydration kinetics

The influence of the nanosilica additions on the cement hydration of UHPC is analysed based on the calorimetry test results. From Figure 4.6, it is apparent that with an increase of the nanosilica amount, the height of the early rate peak is increased and the time required to reach the maximum rate is simultaneously reduced, compared to the reference paste. This is in good agreement with the results presented in (Madani et al., 2012). After the hydration begins, hydrate products diffuse and envelop nanoparticles as kernels, which can promote the cement hydration and make the cement matrix more homogeneous and compact (Jalal et al., 2012). Additionally, the time of reaching the main rate peak varies significantly with a change of the reactivity of the silicas, with more reactive pozzolans giving an earlier peak. Therefore, in this study, with an increase of the nanosilica amount, more reactive kernels will be generated during the hydration, and the time to reach the main rate peak will correspondingly shorten.

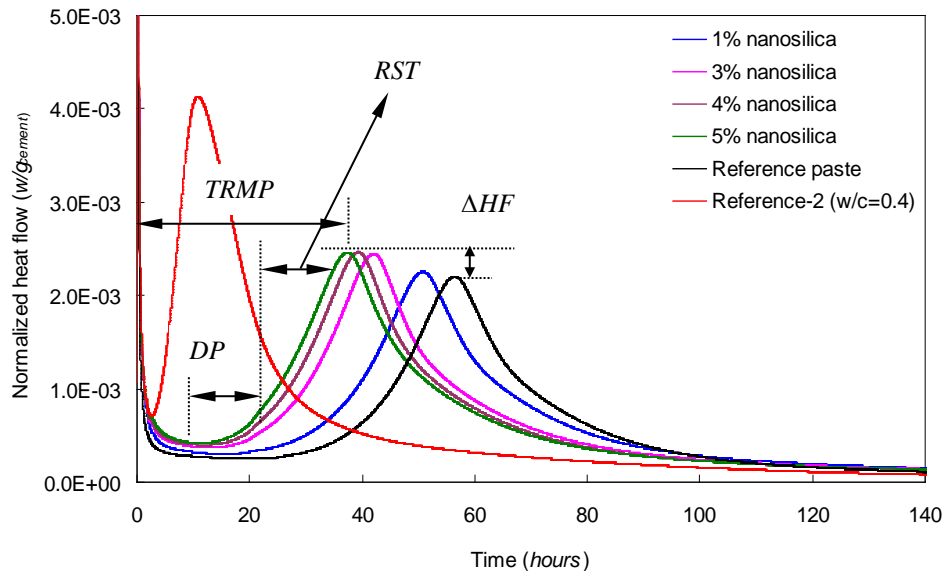


**Figure 4.6: Calorimetry test results of UHPC pastes with different amount of nanosilica (Reference-2: sample with only cement and water, w/c = 0.4, TRMP: Time to reach the maximum peak; DP: Dormant period; ΔHF: Change in heat flow RST: Relative setting time)**

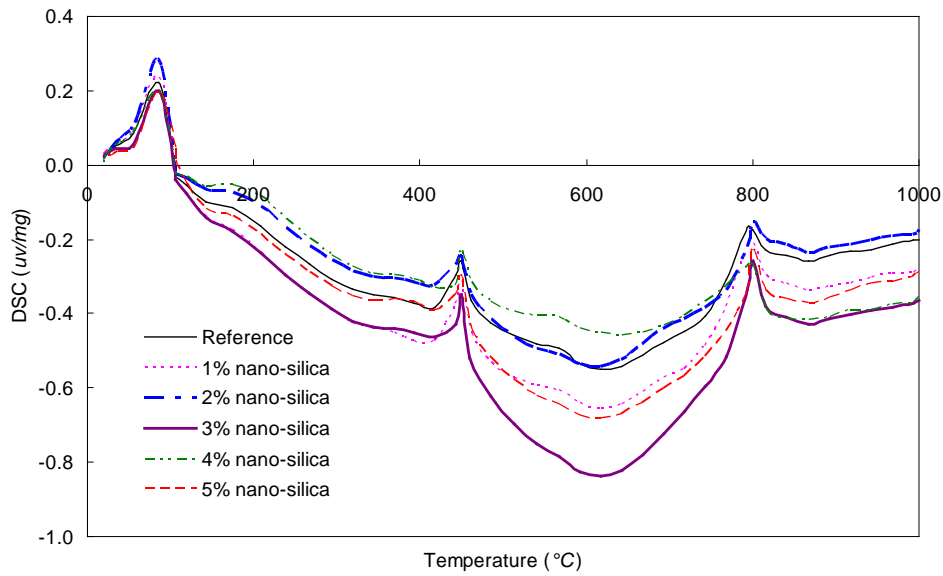
Additionally, it can be clearly noticed that the dormant period for cement hydration in the reference sample is relatively long, which is about 30 h. Normally, in the cement hydration process (only cement and water) the dormant period lasts only about 1-2 h, as shown in Figure 4.6 (Reference-2). The phenomenon observed in this study can be attributed to the retardation by the superplasticizer. According to the investigation of Jansen et al. (2012), a complexation of  $\text{Ca}^{2+}$  ions (from pore solution) and polymers (from the superplasticizer) is as considerable as the absorbed polymer on the nuclei or the anhydrous grain, which in turn might lead to the prevention of the growth of the nuclei or the dissolution of the anhydrous grains. Hence, due to a large amount of superplasticizer utilized to produce UHPC in this study, the cement hydration is significantly retarded, which also causes that the mechanical properties of reference UHPC are relatively poor at early ages. Nevertheless, with the addition of nanosilica, the retardation effect from superplasticizer can be largely compensated. As shown in Figure 4.6, with around 5% of nanosilica, the dormant period of cement hydration can be reduced to about 10 h.

#### · *Thermal analysis*

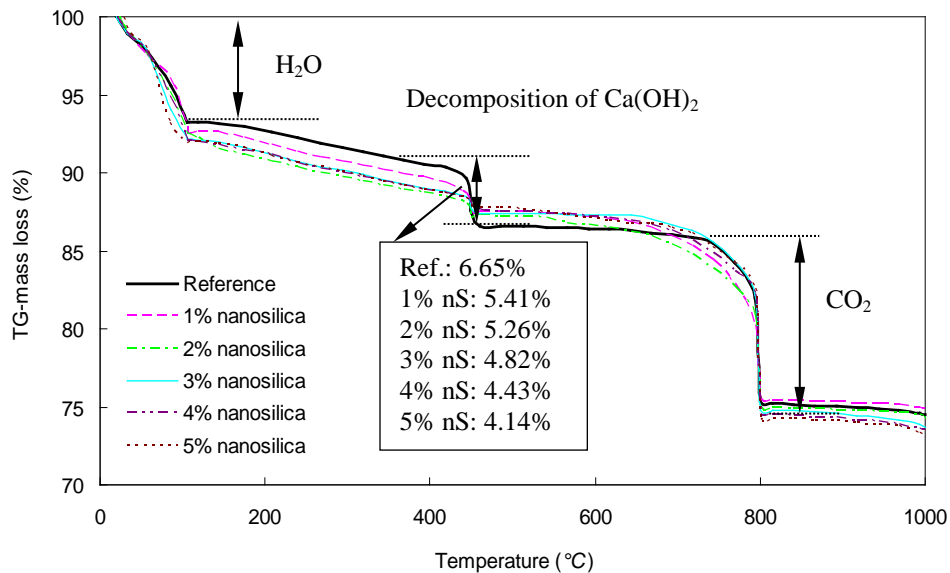
The TG/DSC curves for the UHPC with different amounts of nanosilica are presented in Figure 4.7. From Figure 4.7(a), it is apparent that three main peaks exist in the vicinity of 105 °C, 450 °C and 800 °C for all the samples. As commonly known, the hydrated cement paste subjected to an elevated temperature loses the free water, dehydrates and the hydrated products are transformed (Grattan-Bellew, 1996; Handoo et al., 2002; Alonso and Fernandez, 2004; Castellote et al., 2004; Alarcon-Ruiz et al., 2005). Hence, the three peaks shown in Figure 4.7(a) can be attributed to the evaporation of free water, decomposition of  $\text{Ca}(\text{OH})_2$  and decomposition of  $\text{CaCO}_3$ , respectively. Figure 4.7(b) shows the mass losses of the UHPC samples due to temperature effects. It can be found that the mass loss of free water and ettringite in the reference sample is the lowest, and slightly increases with additions of nanosilica. Moreover, the mass loss of  $\text{Ca}(\text{OH})_2$  in the reference sample is the largest, which gradually reduces with an increasing nanosilica amount. These can be attributed to the following two reasons: 1) nanosilica can promote the hydration of cement and more hydration products (such as ettringite and C-S-H) can be produced; 2) nanosilica can react with  $\text{Ca}(\text{OH})_2$  to generate more C-S-H gel.

Additionally, the hydration degree of the cement in UHPC paste after hydrating for 28 days is computed based on the TG results and Eq. (2.18). As indicated in Figure 4.8, with an increasing amount of the added nanosilica, the cement hydration degree linearly increases. As observed here, the cement hydration degree of the reference UHPC is about 57.1%, and increases to about 66.7% when a 5% addition of nanosilica is included. Moreover, it can be noticed that the hydration degrees of the sample with 3%, 4% or 5% of nanosilica are similar to each other, which implies that promotion effect of nanosilica on cement hydration is ineffective for a nanosilica addition over 3%. This phenomenon is in agreement with the results shown in Figure 4.6. Furthermore, it can also be found that

the cement hydration degrees of all the developed UHPCs are larger than for other UHPCs found in the literature (Tuan et al., 2011a; Tuan et al., 2011b). Normally, for the production of the UHPC, the water to binder ratio is low (less than 0.2), which causes that a large amount of cement particles is still unhydrated after 28 days. However, in this study, due to the relatively low binder amount, the water to binder ratio is about 0.4, and the cement hydration degree is enhanced.



(a) DCS curves



(b) TG curves

**Figure 4.7: TG curves for UHPC with different nanosilica amount, (a) DSC (differential scanning calorimetry), (b) TG (sample mass loss in percentage)**

Combining the results of the calorimetry test and thermal analysis, it can be concluded that, in the UHPC cementitious system, the addition of superplasticizer can obviously extend the dormant period of cement hydration. However, due to the fact that the nanosilica can significantly promote the hydration of cement, the retardation effect from superplasticizer can be largely compensated and the cement hydration degree at later age (e.g. 28 days) is less affected.

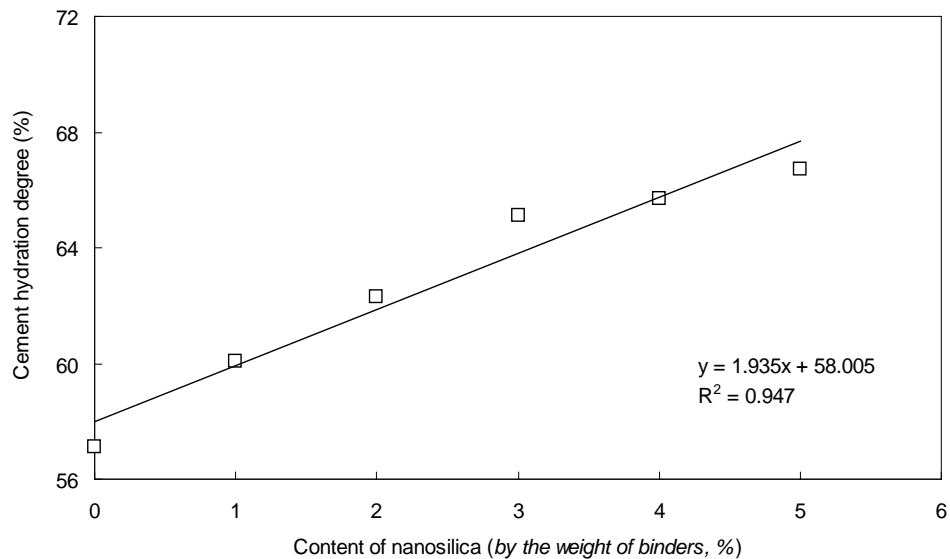


**Figure 4.8: Cement hydration degree (after 28 days) of UHPC with different nanosilica amount**

· *Hydration and microstructure development mechanism analysis*

For normal cement grains, the initial hydration is limited to take place on the grain surface alone. With an ongoing hydration, the cement grain will be consumed and the hydration products that are deposited on the cement grain surface will grow thicker. With an increasing curing time, due to the packed hydration products, the ionic transfer between the unhydrated cement particle and the surrounding solution is restricted, which limits further cement hydration and generation of a dense C–S–H structure. In the present study, the hydration of the reference sample should be similar to such a process. Its water-permeable porosity in hardened state is relatively high and the mechanical properties are comparatively low. When nanosilica is included into the cement hydration system, an early pozzolanic reaction will take place on the silica surface to form C–S–H seeds (Land and Stephan, 2011; Madani et al., 2012) (as shown in Figure 4.9(a)). Consequently, the formation of C–S–H phase is no longer limited to occur on the grain surface alone, and more C–S–H gel can be generated. Here, due to the complexation of  $\text{Ca}^{2+}$  ions from the pore solution and polymer from the superplasticizer (SP), the dormant period of cement hydration in UHPC can be significantly retarded (Jansen et al., 2012). Yet, the added nanosilica can efficiently compensate the retardation effect of SP.

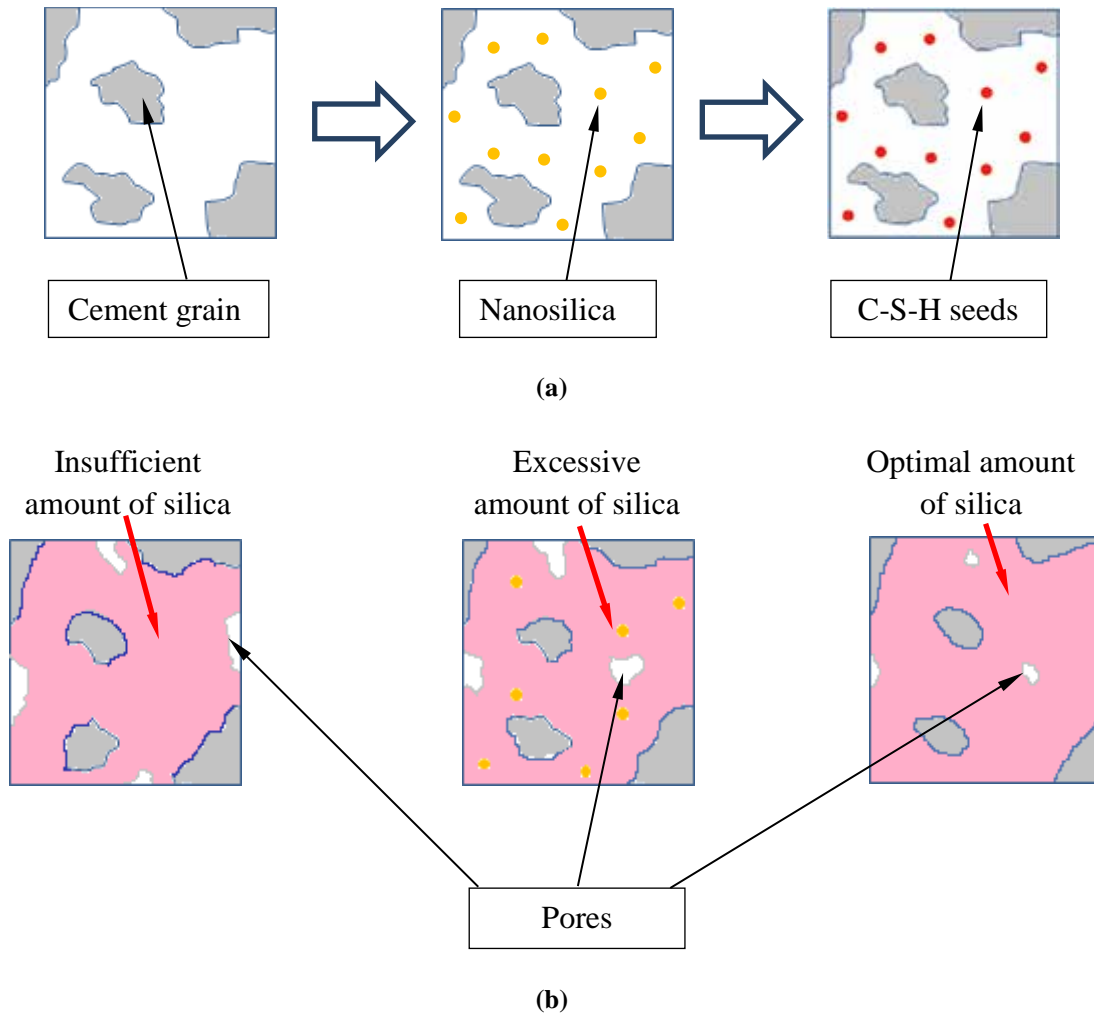


**Figure 4.9: Schematic diagram of the nucleation effect of nanosilica on UHPC: (a) mechanism of the generation of C–S–H seeds, (b) effect of the nanosilica amount on the microstructure development and water-permeable porosity of UHPC**

Based on the obtained results, it can be found that the nanosilica amount is important for hydration and microstructure development of UHPC. As shown in Figure 4.9(b), when the amount of nanosilica is low (e.g. less than 2%), the amount of the newly generated C–S–H seeds is low, which means that, to a large extent, most hydration still takes place on the surface of the cement particles. Hence, the water-permeable porosity of the hardened cement matrix is still relatively large. When the amount of nanosilica is too high (e.g. 5% by the weight of binders), the sufficient amount of the generated C–S–H seeds can enable that the hydration products grow on their surfaces and result in a dense C–S–H gel. However, because the addition of nanosilica greatly increases the viscosity of cementitious mixes, a large amount of air can be entrapped into the cementitious system, which in turn increases the water-permeable porosity of hardened concrete (as shown in Figure 4.3). When the nanosilica amount is optimal, the positive effect of the nucleation and the negative influence of the entrapped air can be well balanced. Therefore, there is

an optimal nanosilica amount, at which the water-permeable porosity of UHPC can be the lowest.

- SEM analysis

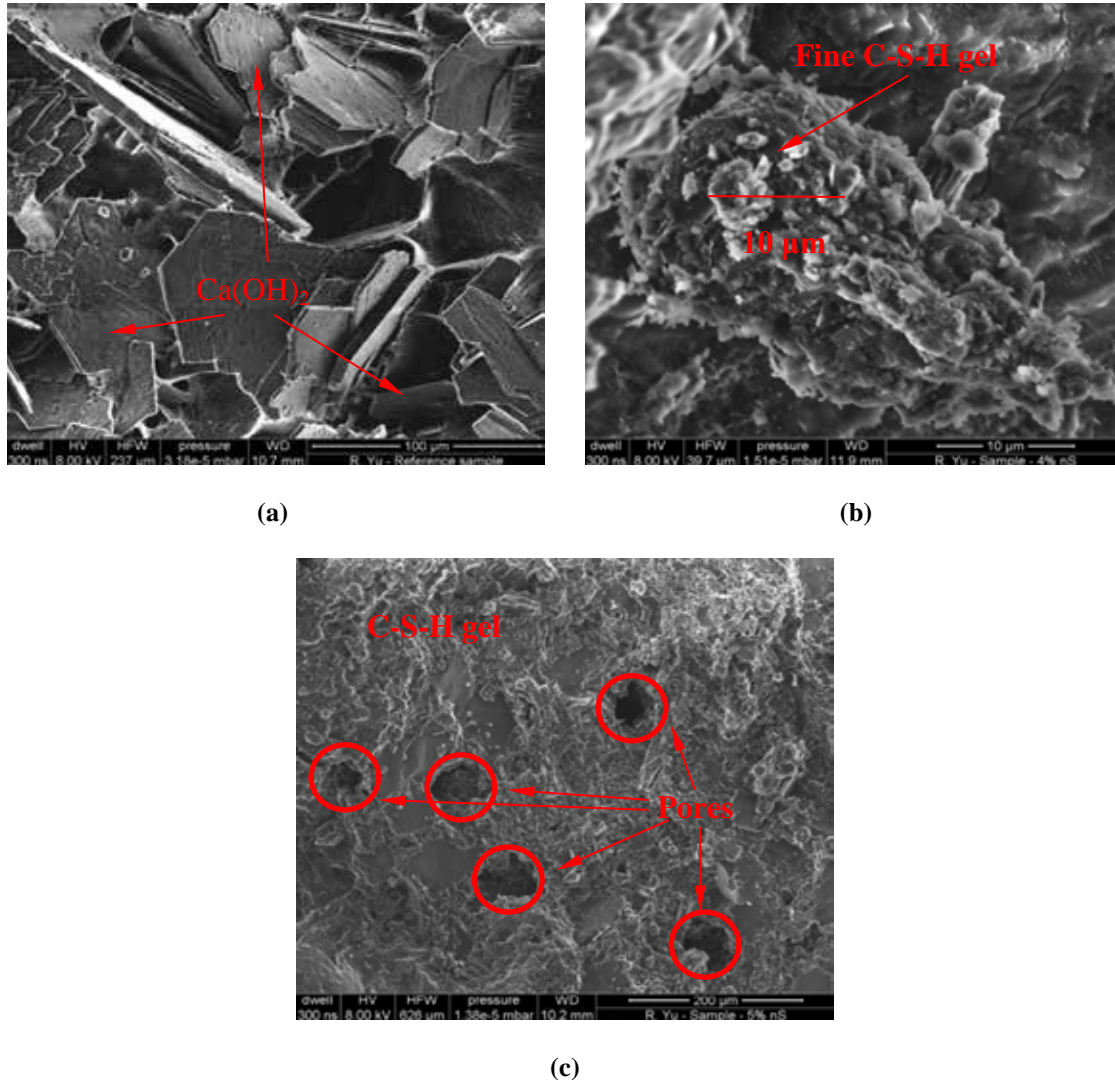


**Figure 4.10: SEM images: (a) reference sample, (b) UHPC with 4% of nanosilica, (c) UHPC with 5% of nanosilica**

Scanning electron microscopy (SEM) is employed to study the morphology and microstructure of the reference sample and the samples with nanosilica additions. In Figure 4.10(a) (reference sample), a large amount of well-developed  $\text{Ca}(\text{OH})_2$  plates can be observed, which implies that without nanosilica, the water-permeable porosity of the hardened concrete is relatively high and the  $\text{Ca}(\text{OH})_2$  has enough space to grow. In Figure 4.10(b) (UHPC with 4% of nanosilica), one can observe a dense structure in the hardened matrix with only a few air pores. The main hydration product of the cement matrix is the foil-like C-S-H gel, and no  $\text{Ca}(\text{OH})_2$  crystal can be easily found.

Furthermore, fine C–S–H gel can be found, which is probably generated from the pozzolanic reaction of nanosilica with  $\text{Ca}(\text{OH})_2$ . The microstructure of the specimen with 5% addition of nanosilica is presented in Figure 4.10(c), in which a number of pores can be observed. As explained previously, because the addition of nanosilica greatly increases the viscosity of cementitious mixtures, a large amount of air can be entrapped in the cementitious system, which in turn increases the water-permeable porosity of hardened concrete.

#### 4.2.5 Summary

This section presents the effect of nanosilica on the hydration and microstructure development of Ultra-High Performance Concrete (UHPC) with a low binder amount. From the results addressed in this section the following conclusions can be drawn:

- 1) Using the modified A&A model, a dense and homogeneous skeleton of UHPC can be obtained with a relatively low binder amount (about  $440 \text{ kg/m}^3$ ). The used  $q$  value is 0.29, which is in line with the recommendation by Quercia (2014).
- 2) An optimal amount of the utilized nanosilica (3.74% by the mass of the binder amount found here) corresponds to the highest mechanical properties of UHPC, which is also in line with the conclusions of Quercia (2014).
- 3) In this study, due to a large amount of superplasticizer utilized to produce UHPC, the hydration of cement is obviously retarded. However, the addition of nanosilica can significantly compensate this retardation effect.
- 4) With the addition of nanosilica, the viscosity of UHPC significantly increases, which causes that more air voids are entrapped in the fresh mixtures and the water-permeable porosity of the hardened concrete correspondingly increase. However, in contrary, due to the nucleation effect of nanosilica, the cement hydration can be promoted and more C–S–H gel can be generated. Hence, there is an optimal nanosilica amount for the production of UHPC, at which the positive effect of the nucleation and the negative influence of the entrapped air can be well balanced.

### 4.3 Effect of mineral admixtures on the properties of UHPC

#### 4.3.1 Background

Nowadays, mineral admixtures are widely used in concrete either in blended cements or added separately. For instance, the ground granulated blast furnace slag (GGBS) or fly ash (FA) from coal combustion currently represents a viable solution to partially substitute the Portland cement clinker, which leads to a significant reduction in  $\text{CO}_2$  emissions per ton of cementitious materials (grinding, mixing and transport of concrete

use very little energy compared to the clinkering process) (Lothenbach, 2011). These mineral admixtures undergo chemical reactions and improve the properties of concrete, and part of them act as filler material to improve the particle packing in the micro-scale (Hüsken, 2010).

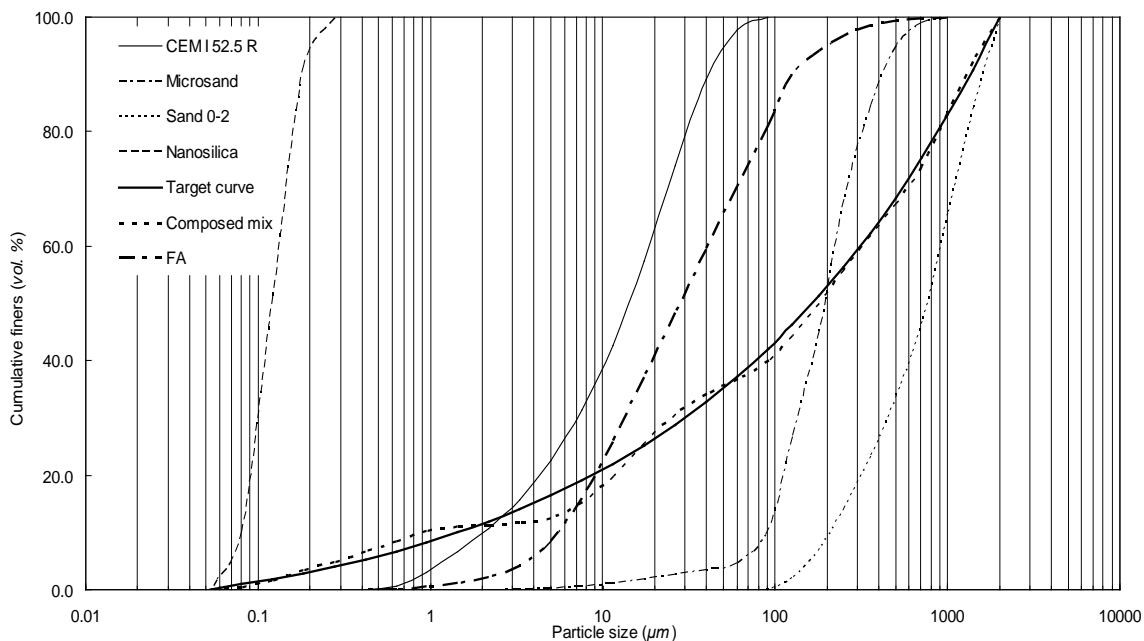
As commonly known, GGBS has hydraulic properties although the rate of the reaction with water is low (Regourd et al., 1983). The reaction can be activated by several methods, but the main hydration product is always C–S–H. In blended cements, GGBS is chemically activated by  $\text{Ca(OH)}_2$  and gypsum (Thomassin et al., 1977; Regourd, 1980; Chen and Brouwers, 2007a; Chen and Brouwers, 2007b). In most cases, GGBS reacts with water or alkaline solution relatively quickly, which causes that the enhancement of mechanical properties of mortar or concrete with GGBS can be observed already at the early age (Wu et al., 1983; Wu et al., 1990; Hwang and Shen, 1991). On the contrary, the pozzolanic reaction of FA is relatively slow, and the addition of FA can retard the hydration of cement (Kovács, 1975; He et al., 1984; Wei et al., 1985). The retardation phenomenon is related to the presence and condition of the FA surfaces. It is suggested that the FA surface acts somewhat like a calcium-sink, and calcium in solution is removed by the abundant aluminium associated with FA, as an AFt phase preferentially forms on the surface of the FA (He et al., 1984; Wei et al., 1985). This depresses the  $\text{Ca}^{2+}$  concentration in the pore solution during the first 6 hours of hydration, and the formation of a Ca-rich surface layer on the clinker minerals is also postponed (He et al., 1984; Wei et al., 1985). Therefore, the  $\text{Ca(OH)}_2$  and C–S–H nucleation and crystallization are delayed and the cement hydration is simultaneously retarded (Wei et al., 1985). Nevertheless, with a slow increase of the  $\text{Ca(OH)}_2$  concentration, the pozzolanic reaction of FA can be further proceeded and the mechanical properties of concrete at 91 days can be further enhanced (Berry et al., 1990; Feldman et al., 1990; Neville, 1995). Additionally, the activity of limestone powders (LP) in the cementitious system is still under a debate. Many researches treat LP as filler and experimentally demonstrated that the principal properties of cement are not negatively affected if small quantities of LP (5–6%) are added during the cement grinding (Soroka and Setter, 1977; Kevin and Kenneth, 1991; Bentz, 2006; Valcuende et al., 2012). On the other hand, some investigations (Bessey, 1938; Carlson and Berman, 1960; Lea, 1971) showed that, during the hydration process of cement with LP, tri-calcium aluminate ( $\text{C}_3\text{A}$ ) can react with calcium carbonate to form both high- and low carbonate forms of calcium carboaluminate in much the same manner as  $\text{C}_3\text{A}$  reacts with calcium sulphate to form high- and low-sulphate forms of calcium sulpoaluminate. Furthermore, the reaction of LP largely depends on its fineness, which can be demonstrated by the phenomenon that the LP with  $d_{50}$  (Mass-median-diameter (MMD)) around  $0.7 \mu\text{m}$  could effectively enhance the heat flow of cement during the hydration process (Kumar et al., 2013). Although a significant part of investigations regarding the effect of mineral admixtures on the physical and chemical characteristics of mortar or concrete can be easily found, they focus only on normal

strength concrete (NSC), in which the water to binder ratio is relatively high and very limited SP is utilized. However, the cementitious system of UHPC is very different from that of NSC, which causes that it is difficult to evaluate the influence of mineral admixtures on the cement hydration and properties development of UHPC, based on the knowledge obtained on NSC system only. Therefore, to efficiently develop a sustainable UHPFRC, it is important to understand the effect of different mineral admixtures on the properties and hydration process of UHPC.

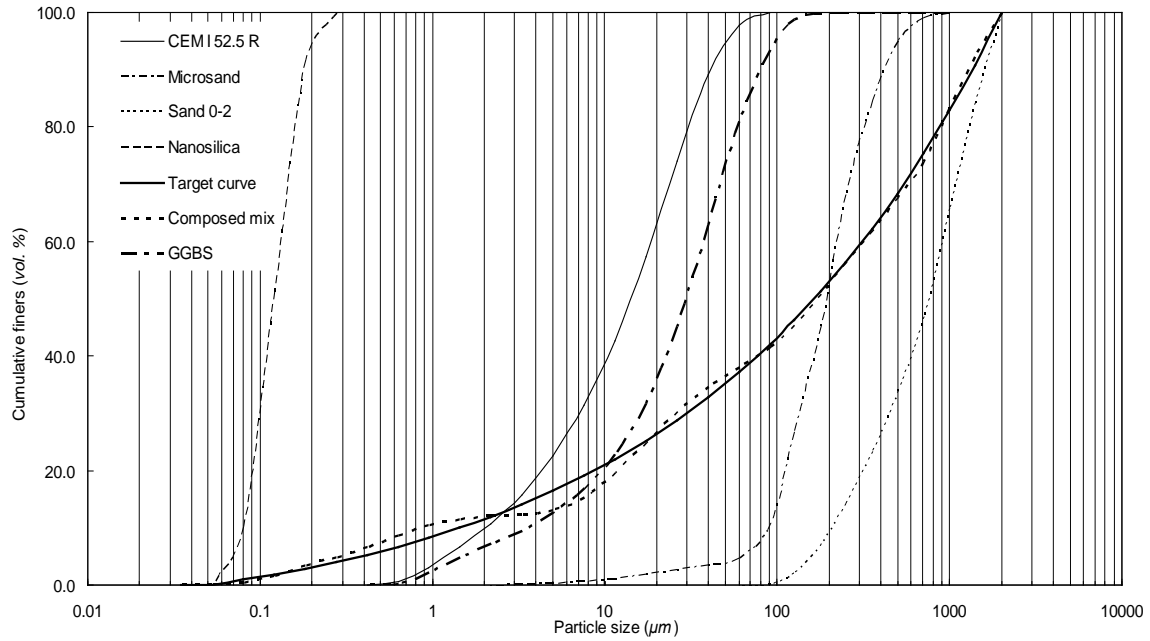
In general, based on these premises, the objective of this section is to evaluate the influence of different mineral admixtures on the fresh and hardened behaviour, hydration kinetics and thermal properties of the developed UHPC. Techniques such as isothermal calorimetry, thermal analysis and scanning electron microscopy are employed to investigate the hydration and microstructure development mechanisms of the concrete. Additionally, to evaluate the environmental impacts of the developed UHPC, its embedded CO<sub>2</sub> emission is evaluated.

#### 4.3.2 Materials and mix design of UHPC with mineral admixtures

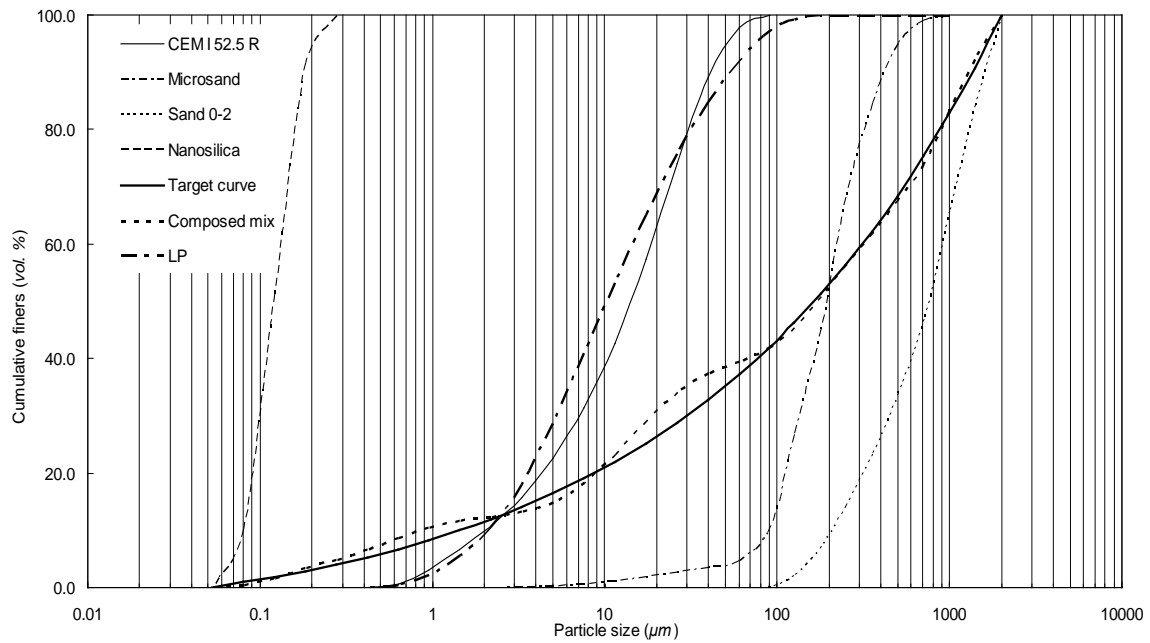
The cement, nanosilica, aggregates and superplasticizer used in this part are the same as that described in Section 4.2.2. In addition, The FA, GGBS and LP are used to replace cement. The detailed information of FA, GGBS and LP can be found in Section 2.2.1. It can be noticed that the density and particle size distributions of the used FA, GGBS and LP are comparable to that of cement. Therefore, when the cement is replaced by FA, GGBS or LP, the particle packing of the whole solid skeleton is only slightly affected.



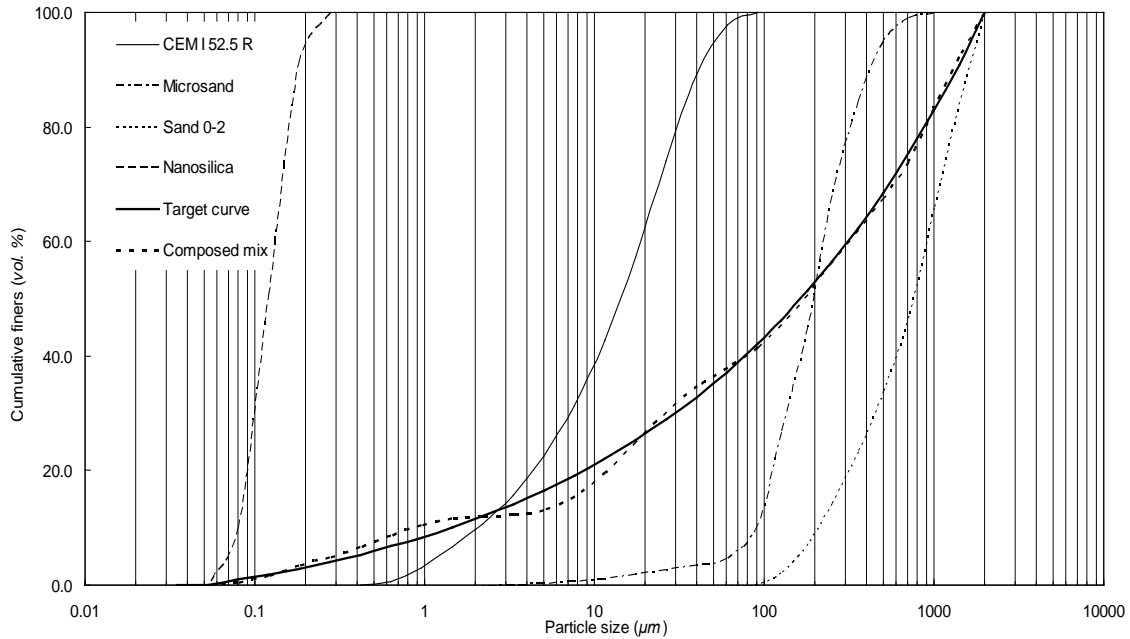
(a) Mixture with FA



(b) Mixture with GGBS



(c) Mixture with LP



(d) Reference mixture (without mineral admixtures)

**Figure 4.11: PSDs of the involved ingredients, the target and optimized grading curves of the developed UHPCs: (a) with FA, (b) with GGBS, (c) with LP and (d) reference mixture**

**Table 4.6: Mix recipes of the developed concretes**

NO.	OPC	FA	GGBS	LP <sup>#</sup>	S	MS	nS	W	SP	W/B	SP/C
1	582	260	0	0	1040	217	24.3	173	43.3	0.2	0.07
2	592	264	0	0	1057	220	24.7	159	44.0	0.18	0.07
3	600	268	0	0	1071	223	25.0	148	44.6	0.165	0.07
4	596	0	266	0	1065	222	24.8	177	44.4	0.2	0.07
5	606	0	271	0	1083	226	25.3	163	45.1	0.18	0.07
6	615	0	275	0	1098	229	25.6	152	45.8	0.165	0.07
7	593	0	0	265	1058	221	24.7	176	44.1	0.2 <sup>#</sup>	0.07
8	603	0	0	269	1077	224	25.1	162	44.9	0.18 <sup>#</sup>	0.07
9	611	0	0	273	1091	227	25.5	151	45.5	0.165 <sup>#</sup>	0.07
Ref. 1	869	0	0	0	1073	223	25.0	179	44.7	0.2	0.05
Ref. 2	884	0	0	0	1091	227	25.5	164	45.5	0.18	0.05
Ref. 3	896	0	0	0	1107	231	25.8	153	46.1	0.165	0.05

(OPC: Ordinary Portland Cement (CEM I 52.5 R), FA: fly ash, GGBS: ground granulated blast-furnace slag, LP: limestone powder, S: sand (0-2), MS: microsand, nS: nanosilica, W: water, SP: superplasticizer, W/B: water to binder ratio, SP/C: superplasticizer to cement ratio, Ref.: reference samples, #: LP is considered as a binder in the calculation, the units of OPC, FA, GGBS, LP, S, MS, nS, W and SP are kg/m<sup>3</sup>)

The UHPC mixtures designed using the modified A&A model are listed in Table 4.5. In total, three different types of UHPC and one reference are designed, and three different water to binder ratios are chosen. Compared to the reference sample, about 30% of Portland cement is replaced (by mass) by FA, GGBS or LP in the UHPC mixtures. It can be noticed from Figure 4.11, that the resulting integral grading curves of all the developed concretes are rather comparable to each other.

### 4.3.3 Experimental methodologies

- *Employed mixing procedure*

Following the mixing procedures shown in Figure 3.2, about 7 minutes and 30 seconds is required to finish the UHPC mixing.

- *Fresh behaviour*

The fresh behaviour of the developed UHPC is measured following the method shown in Section 2.3.1. The Hägermann cone is utilized and relative slump of the developed UHPC is calculated.

- *Water-permeable porosity*

The water-permeable porosity of UHPC in hardened state is measured following the method shown in Section 2.3.3.

- *Mechanical properties*

After performing the flowability tests, the fresh concrete is cast in moulds with the dimensions of 40 mm × 40 mm × 160 mm. The prisms are demolded approximately 24 h after casting and then cured in water at about 21 °C. After curing for 28 and 91 days, the flexural and compressive strength of the specimens are tested according to EN-196-1 (2005). At least three specimens are tested at each age to compute the average strength.

- *Hydration kinetics*

Based on the method shown in Section 2.3.6, cement and mineral admixtures, are mixed with silica slurry, superplasticizer and water. The water to binder ratio is fixed at 0.18 (based on the mechanical properties that will be shown later). All the pastes are mixed for two minutes and then injected into a sealed glass ampoule, which is then placed into the isothermal calorimeter (TAM Air, Thermometric). The instrument is set to a temperature of 20 °C. After 7 days, the measurement is stopped and the obtained data is analysed. All results are ensured by double measurements (two-fold samples).

- *Thermal properties*

The thermal properties of the developed UHPC are determined by the method presented in Section 2.3.6.

#### 4.3.4 Results and discussions

##### • *Fresh behaviour*

The relative slump of fresh UHPC mixtures calculated from Eq. (2.4) versus the volumetric water to powder (particle size  $< 125 \mu\text{m}$ ) ratio is presented in Figure 4.12. As can be seen, with an increase of the water amount, the relative slump of all the concrete mixtures increases linearly. The intersection of these linear functions with the axis of ordinates at  $\Gamma = 0$  depicts the retained water ratio where no slump takes place (Okamura and Ozawa, 1995). In other words, this denotes the maximum amount of water which can be retained by the particles. Exceeding this water content will turn the coherent bulk into a concentrated suspension (Hunger, 2010). In this study, it can be noticed that the water demand of each mixture follows the order: FA (0.306)  $<$  LP (0.315)  $<$  GGBS (0.359)  $<$  reference sample (0.384). Nevertheless, these results are not in accordance with the results obtained from Puntke test (as shown in Table 2.2). This can be attributed to the following two reasons: 1) the used mineral admixtures are different from each other, which can also affect the workability of the concrete mixture. As presented in Figure 2.3, a large amount of angular particles can be observed in GGBS, while that the FA particles are more spherical. The particle shape factors (shown in Table 2.2) of the used mineral admixtures are 1.20, 1.58 and 1.28 for FA, GGBS and LP, respectively (Hunger, 2010). When the shape factor is close to 1, the shape of the particle is spherical, which can further help to improve the flowability of the concrete mixture; 2) the utilized superplasticizer has different effect on the slump flow value of various powders. As described in (Schmidt, 2014), the efficiency of superplasticizer largely depends on the zeta potential along the entire surface of the tested powder particles. The experiments shown in (Schmidt, 2014) demonstrate that, in most cases, cement needs more superplasticizer to reach a certain slump flow value compared to that of FA, GGBS and LP. Hence, based on the two reasons mentioned above, the mixture with FA has the lowest demand water amount among all the analysed concrete mixtures.

The slope of each line shown in Figure 4.12, called the deformation coefficient, represent the sensitivity of the mixture to the water amount needed to attain a certain flowability (Okamura and Ozawa, 1995). When the value of deformation coefficient is relatively small, a big change in the deformability can be observed (to a certain change in water dosage), which means the mixture tends to bleed or segregate sooner than the mixtures with larger deformation coefficients (Hunger, 2010; Quercia et al., 2012). In this study, the obtained deformation coefficient values are small and similar to each other, which implies that all the developed mixtures are sensitive to the water amount. This can be attributed to the specific characteristics of UHPC, which has a large amount of

superplasticizer and low water content. Hence, to achieve a flowable UHPC mixture, the water dosage should be precisely controlled.

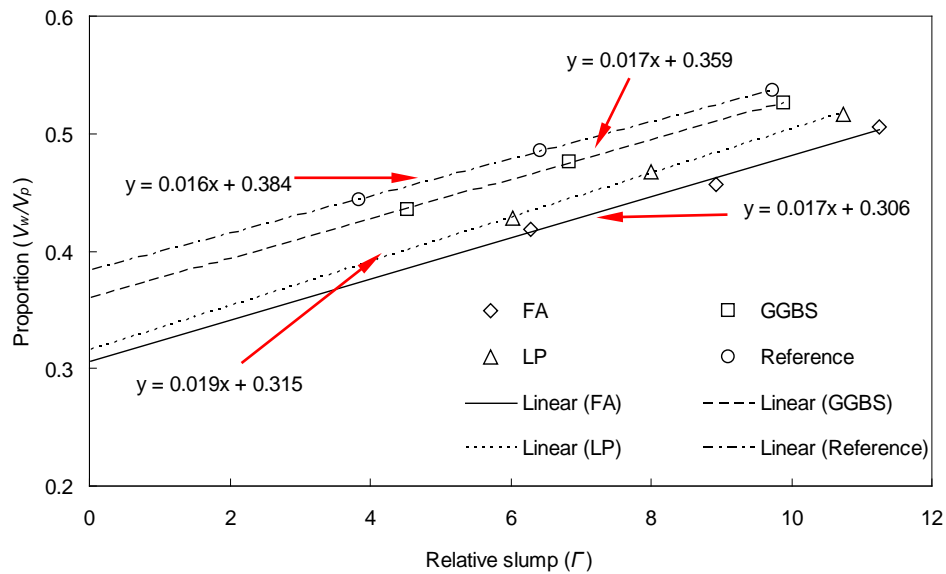
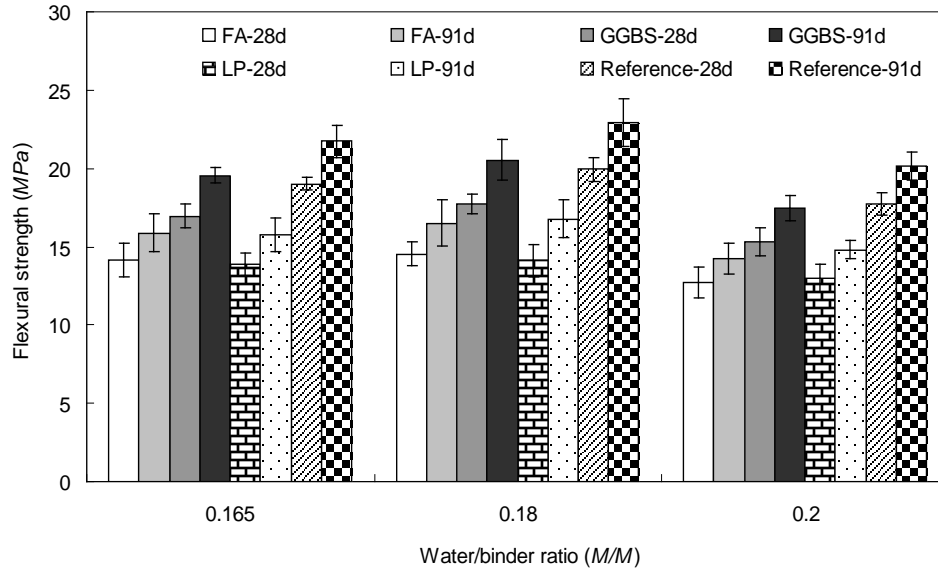


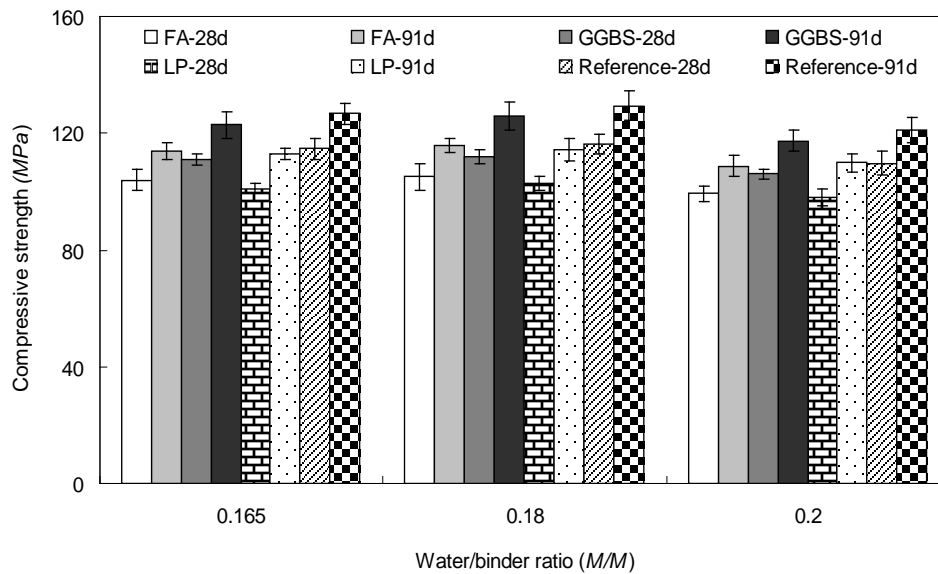
**Figure 4.12: Volumetric water/powder ratio ( $V_w/V_p$ ) versus relative slump ( $\Gamma$ )**

- **Mechanical properties**

The flexural and compressive strengths of UHPC at 28 and 91 days are shown in Figure 4.13. A very slight increase of the strengths can be observed when the water/binder ratio increases from 0.165 to 0.18. Nevertheless, with a further increase of the water/binder ratio (from 0.18 to 0.20), the mechanical properties of the produced UHPC decrease. This phenomenon is different from that shown in (Neville, 1995). In most cases, due to the fact that the excessive water can enhance the porosity of concrete, the strengths of concrete gradually decrease with an increase of the water amount. The difference between the obtained results and the results presented in the literature can be attributed to the fact that a large amount of powder and limited water are utilized to produce the UHPC. When the water to binder ratio is relatively small, the added water is more significantly absorbed by the powders (cement, FA, GGBS or LP in this study), and cannot react with cement, which causes that the amount of cement hydration products is limited and the strength development of UHPC is restricted. Hence, in this study, the strengths difference between the mixtures with lowest and medium water amount is not obvious. There is an optimal value of water/binder ratio, at which the strengths of the UHPC can be highest.



(a) Flexural strength



(b) Compressive strength

**Figure 4.13: Flexural (a) and compressive (b) strengths of the developed UHPC mixtures with different mineral admixtures and water amount**

Furthermore, it can be found here that the mixture with GGBS has superior mechanical properties at both 28 and 91 days, while that the strengths of the mixtures with FA or LP are similar to each other. The observed trend is conflicting with the results obtained for normal strength concrete (Kovács, 1975; Thomassin et al., 1977; Regourd, 1980; Regourd et al., 1983; Wu et al., 1983; He et al., 1984; Wei et al., 1985; Wu et al., 1990; Berry et al., 1990; Feldman et al., 1990; Hwang and Shen, 1991; Neville, 1995).

Normally, the pozzolanic reaction of FA begins at the age of 3 days after blending with cement and water (Papadakis, 1999; Hanehara et al., 2001; Zeng et al., 2012). Nevertheless, this pozzolanic reaction is much slower than the Portland cement hydration (Papadakis, 1999; Hanehara et al., 2001; Zeng et al., 2012). The main hydrate of cement and fly-ash, calcium silicate hydrate (C–S–H), adopts two distinct morphologies: a low density C–S–H at the surface of cement and FA particles and a high density C–S–H deeper into the cement and FA particles (Constantinides and Ulm, 2007; Li et al., 2010). After curing for 28 days, a limited amount of C–S–H gel can be generated, and the microstructure of the concrete is less dense than the one with GGBS. With an ongoing cement hydration, more portlandite can be generated and the pozzolanic reaction of FA can therefore be accelerated, which causes that the already formed pore structure in concrete is filled by the newly generated C–S–H and the mechanical properties of concrete are improved after curing for 91 days (Kovács, 1975; He et al., 1984; Wei et al., 1985; Berry et al., 1990; Feldman et al., 1990; Neville, 1995). Nevertheless, in this study, the strengths of the mixture with FA are similar to that of the mixture with LP after curing for 91 days, which implies that the pozzolanic reaction of FA cannot proceed well in the cementitious system of UHPC (assuming limestone is a non-reactive material).

From the results obtained in this study, it can be summarized that the specific system of UHPC (very low water amount and high SP content) can significantly affect the pozzolanic reaction of FA, which cause that the mechanical properties of UHPC with FA slowly increase. However, the mechanical properties of the UHPC with GGBS are less influenced by the low water amount and high SP content, while its strengths are still superior and comparable to the reference sample (with 50% more cement). To further investigate the pozzolanic reaction of FA/GGBS or their effect on cement hydration at early age, some other techniques (isothermal calorimetry, thermal analysis) are employed and presented later.

- ***Water-permeable porosity***

Figure 4.14 illustrates the variation of the total water-permeable porosity (after curing for 28 or 91 days) of UHPC at different water to binder ratios. In accordance with the mechanical properties results, the water-permeable porosity of UHPC firstly remains stable and then increases with an increase of the water to binder ratio. This can be attributed to the fact that a large amount of powder and limited water are utilized to produce the UHPC. When the water amount is relatively low, the added water is more significantly absorbed by the powders (cement, FA, GGBS or LP in this study), and cannot react with cement, which cause that the amount of cement hydration products is limited and the water-permeable porosity is relatively high. On the other hand, when the water content is higher, the excessive water can obviously enhance the porosity of concrete, as described in (Neville, 1995). Hence, there is an optimal water to binder ratio, at which the water-permeable porosity of UHPC can be minimized. Moreover, it can also

be found that the water-permeable porosity of the mixtures with FA or LP is relatively higher than that with GGBS and the reference mixture, which implies that the mechanical properties of the mixtures with FA and LP are lower than that of the mixture with GGBS.

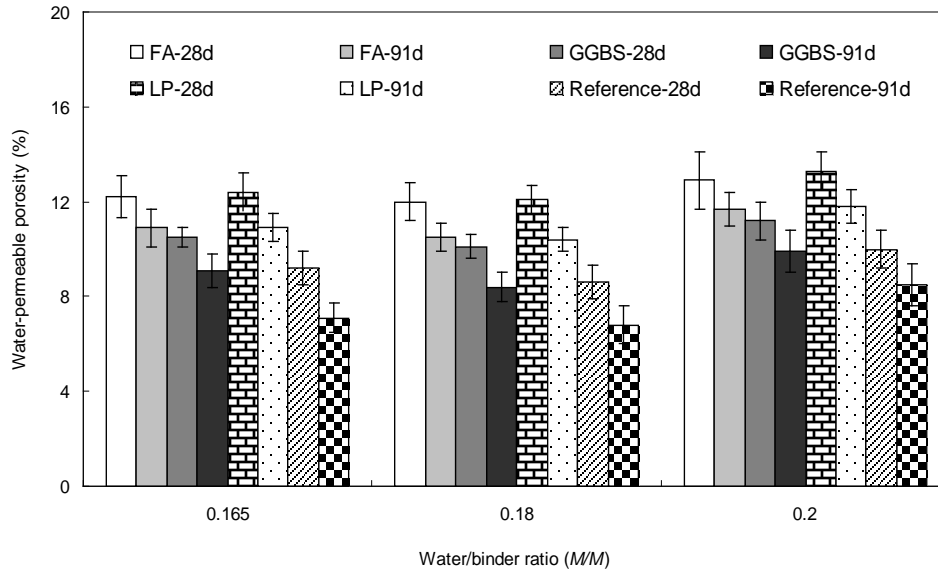


**Figure 4.14: Total water-permeable porosity of the developed UHPC with different mineral admixtures and water amount**

To clearly determine the relationships between the water-permeable porosity and mechanical properties of UHPC, the results obtained here are compared with the existing models (as shown in Figure 4.15). Historically, several general types of models, have been developed for cement-based materials, representing the strengths development versus the variation of material porosity. From a study of the compressive strength of  $\text{Al}_2\text{O}_3$  and  $\text{ZrO}_2$ , Ryshkewitch (1953) proposed the following relationship:

$$\sigma = \sigma_0 \times \exp(-k \times p) \quad (4.2)$$

where  $\sigma$  is the strength (MPa),  $\sigma_0$  is the strength at zero porosity (MPa),  $p$  is the porosity of the tested material (%) and  $k$  is an empirical constant.

Balshin (1949) suggested the following relationship:

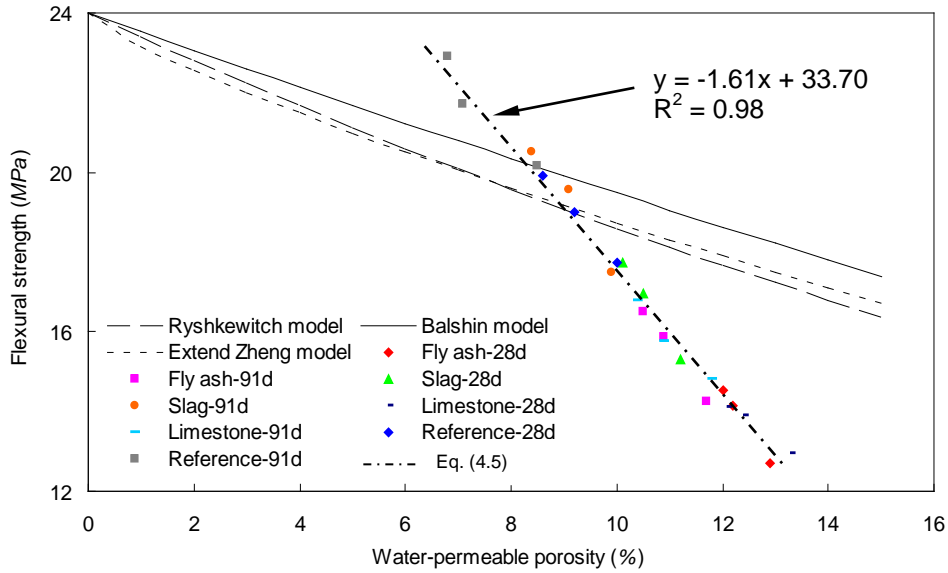
$$\sigma = \sigma_0 \times (1 - p)^b \quad (4.3)$$

where  $b$  is the empirical constant.

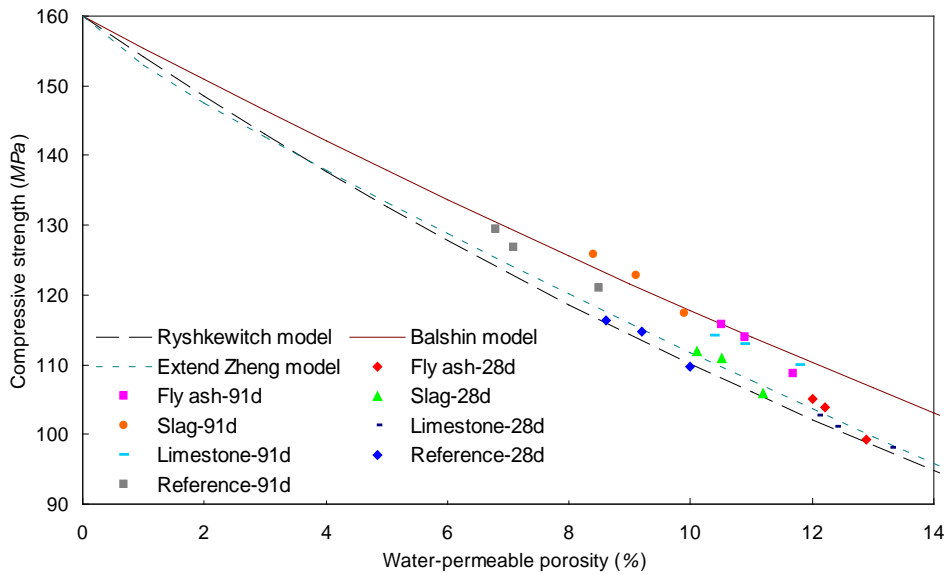
Chen et al. (2013) proposed the extended Zheng's model:

$$\sigma = \sigma_0 \times \frac{p_c - p}{p_c} \times \left(1 - p^{2/3}\right)^{1/2} \quad (4.4)$$

where  $p_c$  is the percolation porosity at failure threshold (%).



(a) Flexural strength



(b) Compressive strength

Figure 4.15: Relationship between water-permeable porosity and strengths of the developed UHPC: (a) flexural strength, (b) compressive strength

In the present study, all the empirical constants for the models mentioned above are chosen as recommended in Chen et al. (2013). Based on the empirical fitting of the experimental data to the presented models, the maximum flexural and compressive strengths ( $\sigma_0$ ) of the UHPC are 24 and 160 MPa, respectively.

From Figure 4.15, it can be found that all the presented models can well represent the relationships between the water-permeable porosity and the compressive strength of the developed UHPC. However, these models are inaccurate in predicting the relationship between the water-permeable porosity and the flexural strength. The existing models obviously underestimate the flexural strength of UHPC when its water-permeable porosity is lower than about 8%. Additionally, these models also overestimate the flexural strength of UHPC when its water-permeable porosity is higher than 10%. These phenomena may be attributed to the relatively low water-permeable porosity and high strengths of UHPC. For normal concrete, the water-permeable porosity is relatively high, which is the reason for lower mechanical properties (especially the flexural strength). For instance, Safiuddin and Hearn (2005) reported a water-permeable porosity of 20.5% for concrete produced with a water/cement ratio of 0.60. Most of these empirical formulas are derived for normal strength concrete (NSC). However, for UHPC, its water-permeable porosity is very low and its flexural strength is about 3 to 4 times of that of NSC. Therefore, these empirical equations are less precise to represent the relationships between the water-permeable porosity and the flexural strength of UHPC.

Based on the obtained results, a new relationship between the water-permeable porosity and the flexural strength of the UHPC is shown as follows:

$$\sigma = \frac{\alpha p_c - p_0}{\beta p_c} \sigma_0 \quad (4.5)$$

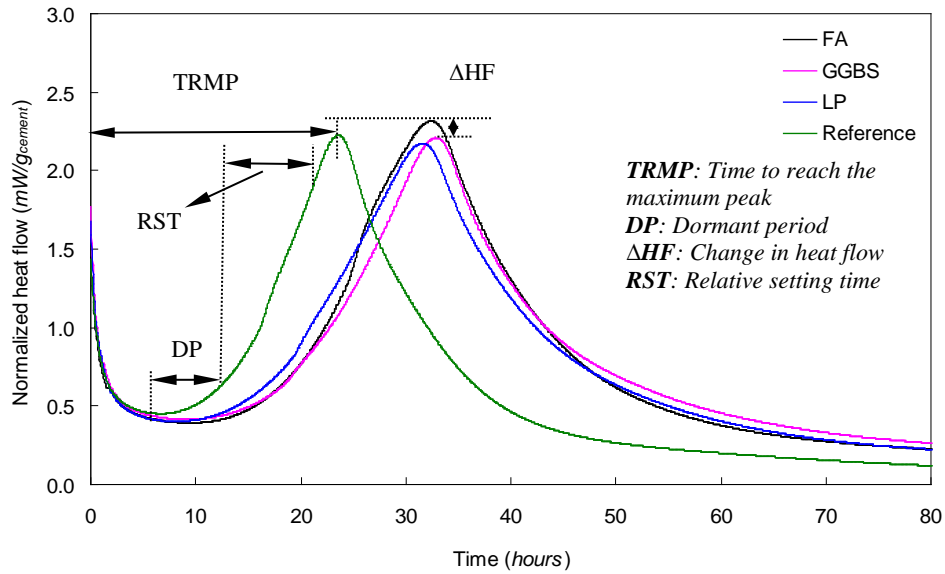
in which the  $\sigma_0$  is about 33.7 MPa, and the  $p_c$  is around 0.21.

It can be noticed that the derived  $p_c$  value is much smaller than that recommended in Chen et al. (2013), namely 0.78, which could be the reason that the existing models cannot well represent the relationships between the water-permeable porosity and the flexural strength of the developed UHPC. As mentioned before, compared to the NSC, the UHPC has a much lower water-permeable porosity and higher flexural strength. Therefore, to precisely establish the relationships between the water-permeable porosity and the flexural strength of UHPC, the crucial parameters should be reasonably adjusted.

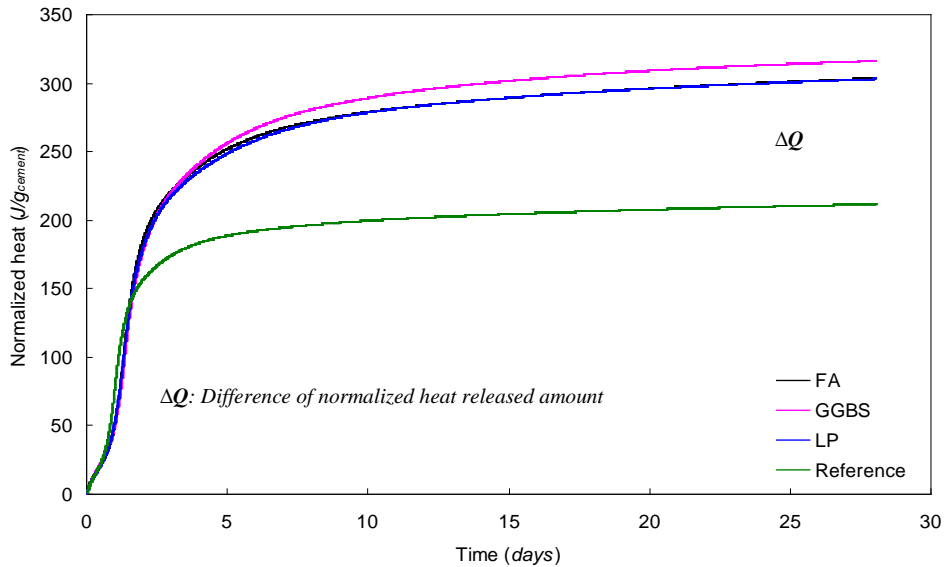
#### • *Hydration kinetics*

Based on the calorimetry test results, the influence of the different mineral admixtures on the cement hydration of UHPC is investigated and presented in Figure 4.16. It is apparent

that the influence of FA, GGBS or LP on the early hydration kinetics of the developed UHPC is very similar, which can be demonstrated by that the relatively small difference between the observed dormant period (calculated as the time between the lower point of the heat flow curve and the first inflection point in the main peak), relative setting time (calculated as the time between the first and the second inflection points in the heat flow curve), as well as the time to reach the maximum hydration peak.



(a) Normalized heat flow



(b) Normalized total heat

**Figure 4.16: Calorimetry test results of UHPC pastes with different mineral admixtures: (a) normalized heat flow, (b) normalized total heat**

The phenomenon observed above is not in accordance with the results shown in (Wu et al., 1983; He et al., 1984; Wei et al., 1985; Hwang and Shen, 1991; Schutter, 1999). In most cases, GGBS can relatively quickly react with  $\text{Ca}(\text{OH})_2$  and generate the C–S–H gel, while the reaction between FA and portlandite is relatively slower. It is suggested that the fly ash surface acts as a  $\text{Ca}^{2+}$  sink, which is caused by the reaction of the aluminate in the fly ash with the  $\text{Ca}^{2+}$  from the solution and/or chemisorption of  $\text{Ca}^{2+}$  ions on the fly ash surface (Ogawa et al., 1980; Wei et al., 1985). This would retard the formation of C–S–H nuclei and thereby delay the end of the induction period. Hence, with similar fineness, the activity of GGBS should be much higher than that of FA and LP in concrete at early age.

To better explain these phenomena, the following reasons should be considered: 1) a large amount of superplasticizer is utilized in the production of the UHPC. According to the investigation of Jansen et al. (2012), a complexation of  $\text{Ca}^{2+}$  ions (from pore solution) and polymers (from the superplasticizer) is as thinkable as the absorbed polymer on the nuclei or the anhydrous grain, which in turn might lead to the prevention of the growth of the nuclei or the dissolution of the anhydrous grains.. Hence, the early hydration of the cement is significantly retarded and the generation of  $\text{Ca}(\text{OH})_2$  is restrained. Due to the insufficient amount of portlandite in the mixtures, the pozzolanic reaction cannot well progress, which causes that the difference of the pozzolanic activity between FA and GGBS is not easy to be observed in the calorimetry tests; 2) low water content is used in the UHPC mixtures. To achieve good mechanical properties, high powder amount and low water content are normally used to produce UHPC, which causes that much water is absorbed by the powder materials and there is little free water in the cementitious system. Hence, the diffusion of  $\text{Ca}^{2+}$  and  $\text{OH}^-$  is restricted, and pozzolanic reaction of FA or GGBS is postponed.

The normalized (by 1 g of cement) total heat of the developed UHPC mixtures is illustrated in Figure 4.16(b). The total heat is the contribution of the heat produced by the cement particles themselves and by the pozzolanic reaction between the active mineral admixtures and the precipitated  $\text{Ca}(\text{OH})_2$  (Hewlett, 1988). The total heat can be related to the hydration degree of the paste, and this hydration degree is related to the compressive strength of the mixture, if the parameters of the microstructure are similar. Thus, a higher compressive strength is expected with the progressive increase of the total heat released. In this study, after 28 days, it can be noticed that the normalized heat of the mixture with GGBS is the highest, which is followed by the one with FA and LP. As described before, due to effect of the large amount of superplasticizer and low water content in the UHPC, the pozzolanic reaction of GGBS cannot well progress during the initial 5 days. However, afterwards, with an increasing concentration of  $\text{Ca}(\text{OH})_2$ , the pozzolanic reaction of GGBS is promoted, which simultaneously causes that more heat can be released and the mechanical properties of the concrete can be enhanced. Moreover, it can be observed that the normalized heat of the mixture with FA is similar to that with LP, which implies that

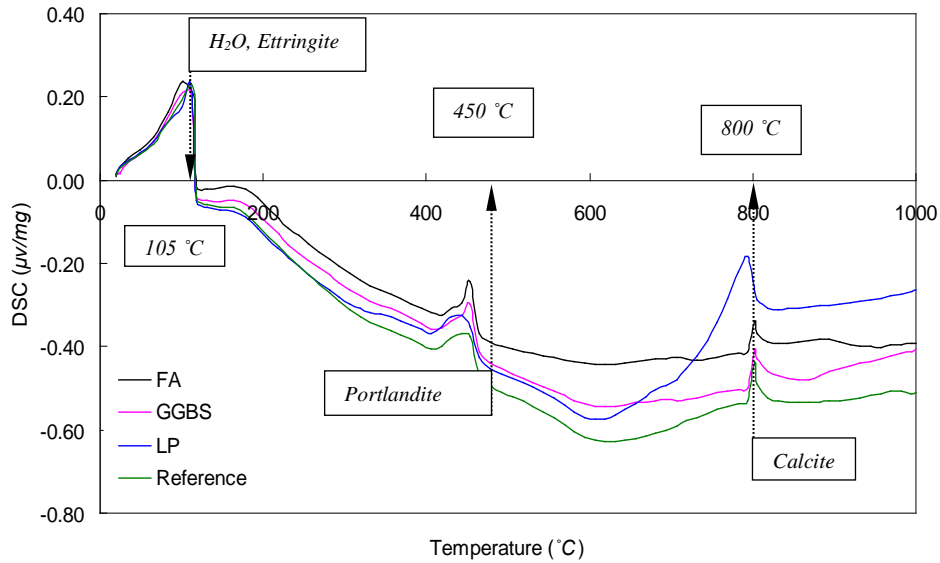
the FA and LP have similar contributions to the cement hydration after 28 days. Additionally, it can be found that the normalized heat of the reference sample is significantly lower than the mixtures with mineral admixtures. This can be attributed to the fact that the calculation of normalized heat is based on the released heat per gram cement, and in the mixtures with mineral admixtures the used cement amount is much lower than that of reference sample.

Consequently, according to the results obtained in this section, it can be found that the hydration kinetics of UHPC is different from that of conventional concrete. Due to the effects related to the superplasticizer and water dosages, the cement hydration and pozzolanic reaction of mineral admixtures are significantly retarded.

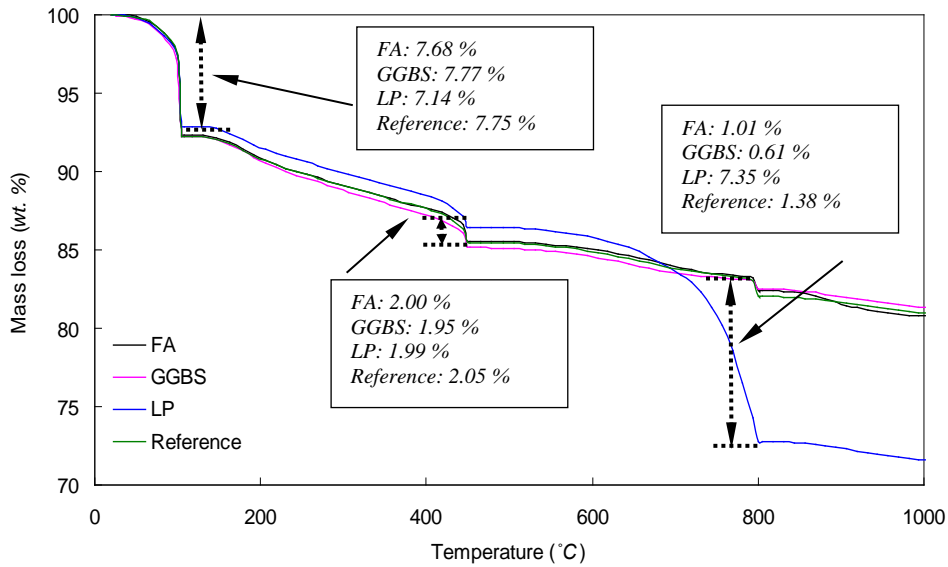
- Thermal properties

The DSC and TG curves of the UHPC pastes after hydrating for 28 and 91 days are presented in Figures 4.17 and 4.18, respectively. From the DSC curves, it is apparent that three main peaks exist in the vicinity of 105 °C, 450 °C and 800 °C for all the samples, which can be attributed to the evaporation of free water, decomposition of  $\text{Ca}(\text{OH})_2$  and decomposition of  $\text{CaCO}_3$ , respectively (Grattan-Bellew, 1996; Handoo et al., 2002; Alonso and Fernandez, 2004; Castellote et al., 2004; Alarcon-Ruiz et al., 2005). Based on the test results shown in Figures 4.17(a) and 4.18(a), the samples for TG analysis were subjected to isothermal treatment during the test, which was set at 105 °C, 450 °C and 800 °C for 2 h. From the obtained TG curves, it can be noticed that all the tested samples show a similar tendency of losing their weight. However, their weight loss rates at each temperature range are different, which means that the amounts of the substances reacting at each treatment stage are different. It is important to note that the mass loss of portlandite of the mixture with GGBS is the smallest at 28 days, which implies that the pozzolanic activity of GGBS is relatively higher so that more portlandite has already been consumed. Figure 4.16 confirms this phenomenon. However, after curing for 91 days, the mass loss of portlandite still follows the order: GGBS < FA < LP < reference concrete, while the differences between the mixtures with FA and LP are relatively small. Hence, it can be concluded that the specific cementitious system of UHPC significantly restricts the pozzolanic reaction of FA, which causes that very limited amount FA can react with  $\text{Ca}(\text{OH})_2$  even after 91 days. Therefore, it explains why the mechanical properties of the mixture with FA are lower than that with GGBS at both 28 and 91 days. The observed phenomenon is not in accordance with the results obtained in normal concrete system. As mentioned before, with the increase of the portlandite amount, the pozzolanic reaction of FA can be promoted, and the already-formed pore structure in concrete is filled by the newly generated C-S-H (Thomassin et al., 1977; Regourd, 1980; Regourd et al., 1983; Wu et al., 1983; Wu et al., 1990; Hwang and Shen, 1991). Consequently, it is not reliable to predict the effect of FA on the properties of UHPC, based on the results obtained on traditional concrete. Additionally, it can be noticed that

the difference between the  $\text{Ca(OH)}_2$  amounts in mixtures with different mineral admixtures is relatively small. This phenomenon may be attributed to the reaction between nanosilica and  $\text{Ca(OH)}_2$ , which cause that very limited  $\text{Ca(OH)}_2$  is available to react with FA or GGBS.

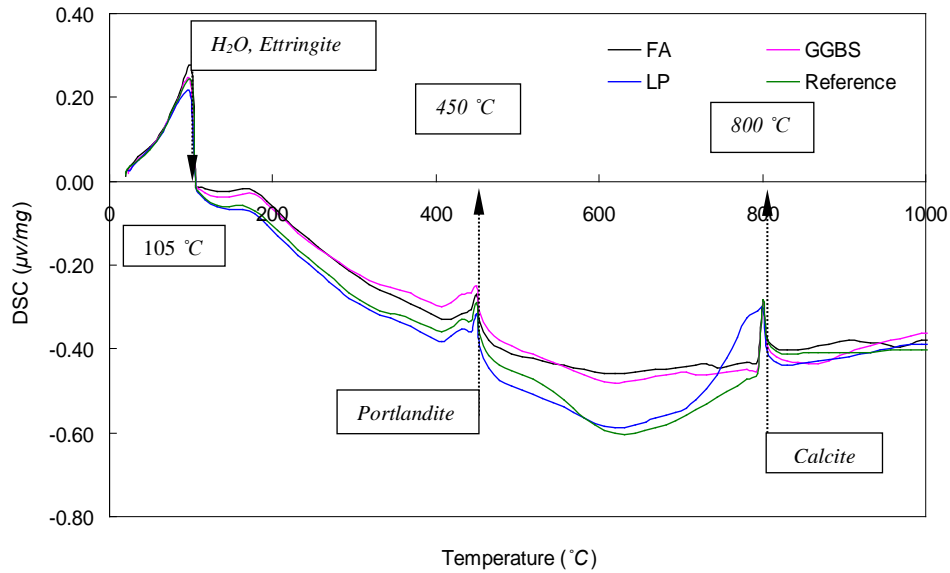


(a) DCS curves

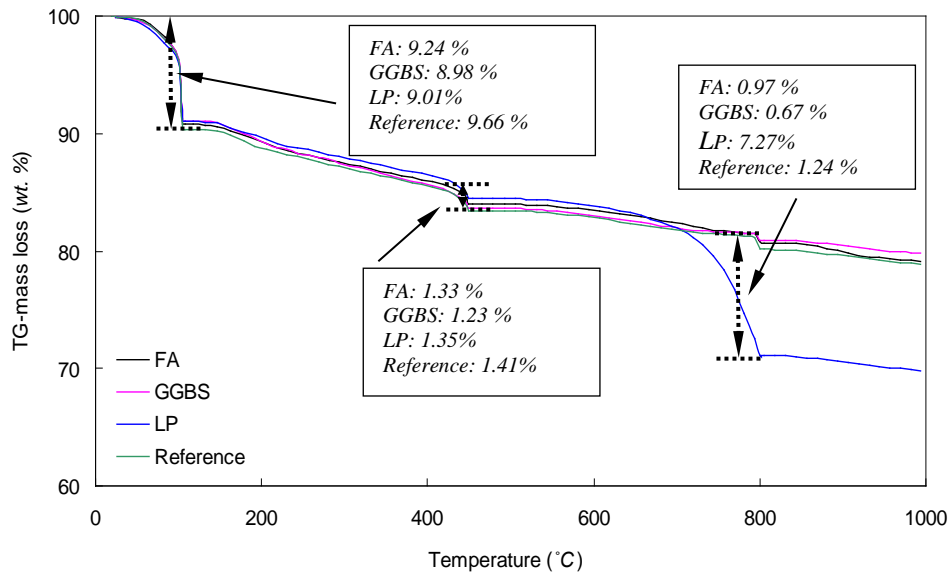


(b) TG curves

**Figure 4.17: Thermal analysis results of UHPC pastes with different mineral admixtures (after hydrating for 28 days): (a) DCS curves (differential scanning calorimetry), (b) TG curves (sample mass loss in percentage)**



(a) DCS curves



(b) TG curves

**Figure 4.18: Thermal analysis results of UHPC pastes with different mineral admixtures (after hydrating for 91 days): (a) DCS curves (differential scanning calorimetry), (b) TG curves (sample mass loss in percentage)**

According to the thermal analyses results, it is clear that there is more portlandite in the concrete with larger amount of cement (e.g. the reference sample) than in the pastes with mineral admixtures. The portlandite normally plays a negative role in improving the mechanical properties of concrete, especially when the portlandite hexagonal plates form around the ITZ. When cement is appropriately replaced by GGBS, the portlandite amount

can be reduced and the already-formed pore structure in concrete can be filled by the newly generated C–S–H.

#### 4.3.5 Environmental significance of using mineral materials in UHPFRC

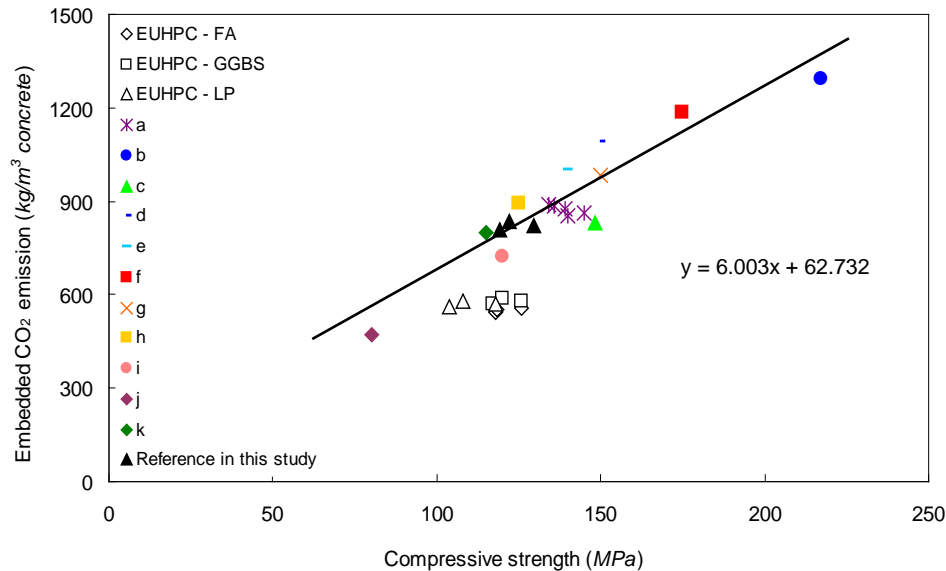


**Figure 4.19:** Comparison of embedded CO<sub>2</sub> emission of the developed UHPC and other UHPCs or UHPFRCs (EUHPC: the eco-UHPC developed in this study; a: (Ghafari et al., 2014); b: (Makita et al., 2014); c: (Máca et al., 2014); d: (Habel and Gauvreau, 2008); e: (Wang et al., 2014); f: (Habel et al., 2006); g: (Corinaldesi and Moriconi, 2012); h: (Millard et al., 2010); i: (Yang et al., 2009); j: (Deeb et al., 2012); k: (Yazici, 2007))

To demonstrate that the developed UHPC is eco-friendly, its embedded CO<sub>2</sub> emission is evaluated in this section, focusing on the amount of materials required for 1 m<sup>3</sup> of the compacted concrete. Based on the embedded CO<sub>2</sub> values for each component of concrete (King, 2012; Randl et al., 2014), the relationship between the CO<sub>2</sub> emission and the compressive strength of UHPCs is illustrated in Figure 4.19. It can be noticed that the enhancement of the compressive strength of all the analysed UHPCs corresponds to the increase of the embedded CO<sub>2</sub> emission, thus to a greater environmental impact. Some of the presented UHPCs have superior mechanical properties (more than 200 MPa), but simultaneously, their embedded CO<sub>2</sub> emissions are also high (more than 1200 kg/m<sup>3</sup> concrete). However, it is important to notice that the data points representing UHPC developed in this study are all below of the trend line, which means the UHPC developed here has a lower environmental impact than the other UHPCs. This is significant especially for the mixture with GGBS, as its compressive strength is larger than that with FA and LP, with a comparable embedded CO<sub>2</sub> emission at the same age. Additionally, it can be also found that the data points representing the reference UHPC developed here are on the trend line, which means the reference UHPC has relatively high environmental impact than the developed UHPC with mineral admixtures. This phenomenon can be

attributed to the fact that when the cement amount is relatively high, the cement hydration degree is smaller and the cement efficiency is lower, compared to the concrete with low cement amount (Yu et al., 2014a; Yu et al., 2014b). Hence, to efficiently produce an eco-friendly UHPC with a reduced environmental impact, the mineral admixtures should be utilized to replace cement and the concrete design should be based on the optimized particle packing model.

#### 4.3.6 Summary

This section addresses the effect of mineral admixtures (FA, GGBS, LP) on the properties of Ultra-High Performance Concrete (UHPC). Based on the obtained results, the following conclusions can be drawn:

- 1) Based on the modified A&A model, UHPC with different mineral admixtures (FA, GGBA, and LP) is produced. After comparing the embedded CO<sub>2</sub> emissions of the developed UHPC and other UHPCs, it is demonstrated that the proposed methodology allows for a production of an eco-friendly concrete with a relatively low environmental impact.
- 2) The fresh behaviour of the developed UHPC is evaluated. It is found that the water demand of UHPC mixtures with FA, GGBS, LP and reference concrete follows the order: FA < LP < GGBS < reference. Moreover, the deformation coefficient values of UHPCs are small and close to each other, which implies that all the developed mixtures are sensitive to the water amount.
- 3) The mechanical properties of UHPC with GGBS are obviously higher than that with FA or LP at both 28 and 91 days. Furthermore, very slight increase of the strengths can be observed when the water/binder ratio increases from 0.165 to 0.18. Nevertheless, with a further increase of the water/binder ratio (from 0.18 to 0.20), the mechanical properties of the produced UHPC decrease.
- 4) The existing models used to correlate the porosity and mechanical properties of concrete obviously underestimate the flexural strength of UHPC when its water-permeable porosity is less than about 8%, and overestimate the flexural strength when its water-permeable porosity is larger than 10%. However, all the presented models can well represent the relationships between the water-permeable porosity and the compressive strength of the developed UHPC.
- 5) The hydration heat development curves of the UHPC mixtures with FA, GGBS and LP are similar to each other during the initial five days. Afterwards, the hydration rate of the mixture with GGBS is obviously accelerated. Due to the specific cementitious system of UHPC (very small water/binder ratio and relatively high SP amount), it is observed that the pozzolanic reaction of FA is

significantly retarded, which causes that a very limited amount of FA can react with  $\text{Ca}(\text{OH})_2$  after curing for 91 days.

#### **4.4 Conclusions**

In this chapter, the effect of powders (nanosilica and mineral admixtures, such as FA, GGBS and LP) on the properties of UHPC is evaluated. Nanosilica is a relatively new material, which has ultra-small particle size and higher activity than that of microsilica. From the obtained experimental results, a relatively small amount of nanosilica can significantly promote the microstructure development and mechanical properties improvement of UHPC. The optimal amount of the utilized nanosilica is about 3.74% by the mass of the binder amount as found in this study. In addition, it is found that the hydration process of UHPC mixtures with almost the same amount of FA, GGBS and LP are similar to each other during the initial five days. Afterwards, the hydration of the mixture with GGBS is more accelerated. Due to the specific cementitious system of UHPC (very small water/binder ratio and relatively high SP amount), it is observed that the pozzolanic reaction of FA is significantly retarded, which causes that a very limited amount of FA can react with  $\text{Ca}(\text{OH})_2$  after curing for 91 days. Additionally, it is demonstrated that the developed UHPC has lower environmental impact than the other UHPCs. Hence, based on the different requirements (workability, mechanical properties, or environmental impact) from the practice, different mineral admixtures should be appropriately chosen in the production of UHPC.

## Chapter 5

### Efficient application of steel fibres in UHPFRC

#### 5.1 Introduction

As mentioned before, the concept of using fibres in building materials can be traced back to thousands years ago, since the addition of fibres can improve the mechanical properties of construction materials. The modern development of fibre-reinforced concrete (FRC) was initiated in the early sixties (Wafa, 1990), when a more efficient material (compared to rebar) was searched to optimize the plasticity of the plain concrete. In fact, not only the mechanical properties, many other properties (e.g. workability, durability, and energy absorption capacity) of concrete are also be influenced by the additional fibres.

Fibres are produced from a wide variety of materials, and in various dimensions and shapes, while the steel fibre is the most common fibre type in the building industry. Steel fibre reinforced concrete (SFRC) appears stiffer (lower slump) compared to conventional concrete without fibres (Johnston, 2001). The effect of steel fibres on the fresh behaviour of concrete can be mainly attributed to the following reasons (Grünewald, 2004): 1) the shape of fibres is more elongated compared with aggregates; 2) stiff fibres change the structure of the granular skeleton; 3) steel fibres often are deformed (e.g. have hooked ends or are wave shaped) to improve the anchorage between a fibre and the surrounding matrix. The friction between the hook ended steel fibres and aggregates is higher compared with straight steel fibres. The size of the fibres relative to that of the aggregates determines their distribution (as shown in Figure 5.1). Theoretically, with an increasing difference between the fibre length and the aggregate diameters, the influence of the fibres on the aggregates' packing simultaneously reduces (cases 2 and 4 in Figure 5.2) (Markovic, 2006). It is clear that the fine particles can efficiently pack around long stiff fibres (case 2), and also the packing of very large grains will not be much disturbed by the presence of very short thin fibres between them (case 4). In contrary, when the length of fibres and the diameter of the grains are in the same order of magnitude (cases 1 and 3), the granular skeleton may significantly disturbed by the additional fibres, since the stiff fibres can push the surrounding aggregates away and more voids are generated in the concrete. These voids can obviously increase the porosity of concrete and decrease its mechanical properties simultaneously. Hence, in practice, to minimize the effect of steel fibres on the structure of the granular skeleton, it is recommended to choose fibres not shorter than the maximum aggregates size (Vandewalle, 1993; Johnston, 1996). In most

cases, the fibre length is about 2-4 times of that of the maximum aggregate size (Grünewald, 2004).

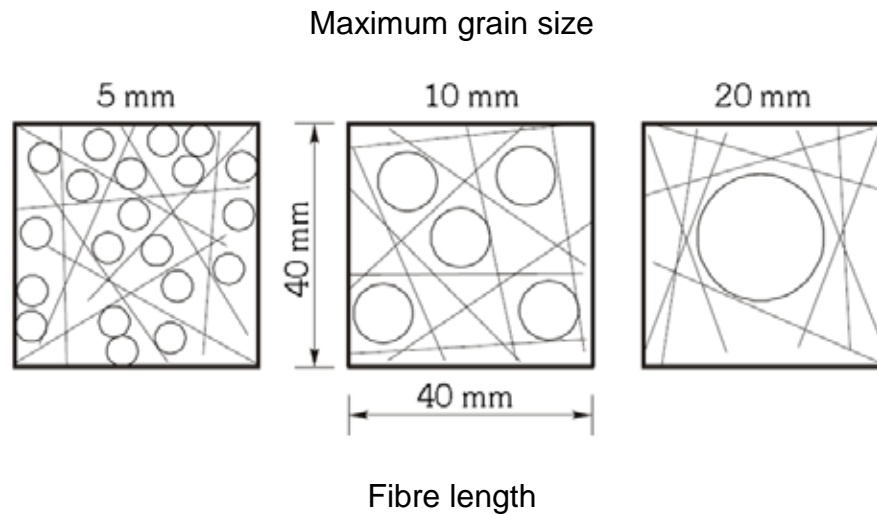


**Figure 5.1: Effect of steel fibres on the structure of the granular skeleton in concrete (Johnston, 1996; Grünewald, 2004)**

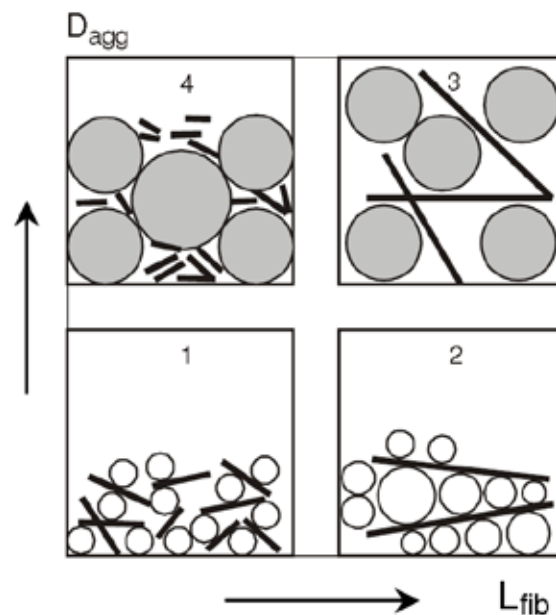


**Figure 5.2: Interaction between fibres of different lengths ( $L_{fib}$ ) and aggregate grains of different diameters ( $D_{agg}$ ) (Markovic, 2006)**

In the design and production of UHPFRC, due the fact that the large aggregates are normally excluded ( $d > 4$  mm) and the used fibre length is much longer compared to the aggregate diameters (Habel et al., 2006; Hassan et al., 2012; Mahmud et al., 2013; Yoo et al., 2014; Sovják et al., 2015), the effect of steel fibres on the particles packing was not

considered in this study. Moreover, from the literature mentioned above, it can be noticed that the utilized steel fibres in the production of UHPFRC are of various types (e.g. shape: straight, hook ended, wave shape, length: 6 - 40 mm) and the steel fibres dosage is normally arbitrarily selected without considering the efficiency of these used fibres. Sometimes, the added fibres amount is relatively high, e.g. more than 5% vol. (Habel et al., 2006). As mentioned in the previous chapter, to continue the theme of sustainable development, the disadvantages of UHPFRC (high material cost, high energy consumption and high embedded CO<sub>2</sub> emission) should be well minimized. Except for the optimized matrix approaches (appropriate reduction of cement amount and inclusion of industrial by-products) (Yang et al., 2009; Tuan et al., 2011a; Tuan et al., 2011b; Hassan et al., 2012; Yu et al., 2014a; Yu et al., 2014c; Yu et al. 2015), the efficient application of steel fibres is also vital in reducing the materials' cost, energy consumption and embedded CO<sub>2</sub>, since the cost of 1% volume content of steel fibre applied in UHPFRC is generally higher than that of the matrix (Kim et al., 2011a). Consequently, the improvement of the steel fibre efficiency is very important for developing a sustainable UHPFRC.

To efficiently utilize fibres in UHPFRC, one of the promising methods is to appropriately blend several different types of fibres in one concrete matrix (Banthia et al., 2014; Ganesan et al., 2014). As commonly known, in most cases, the hybrid fibres reinforced concretes show better hardened properties than the concretes with only single sized fibres (Banthia and Nandakumar 2003; Yao et al., 2003; Banthia and Gupta, 2004; Markovic, 2006; Park et al., 2012; Banthia et al., 2014; Ganesan et al., 2014; Yap et al., 2014; Rambo et al., 2014). The application of different types of fibres combined in one concrete mixture was firstly proposed by Rossi (1987), as the so-called multi-modal fibre reinforced concrete (MMFRC). Due to the fact that the short fibres can bridge the micro-cracks while the long fibres are more efficient in preventing the development of macro-cracks, the stress in the hybrid fibres reinforced concrete can be well distributed and its mechanical properties can be improved (Markovic, 2006). From a mechanical point of view, the combination of fibres with different geometry seems to be an optimal solution to increase both the mechanical properties and the ductility (Markovic, 2006).

In general, based on the premises mentioned above, the aim of this chapter is to understand the contribution of different steel fibres to the properties of UHPFRC, in order to use the fibres more efficiently. The modified A&A model is again employed to design the UHPFRC matrix with low cement amount. Following the fibres hybridization concept, binary and ternary steel fibres reinforced UHPC are designed and produced. Afterwards, fresh and hardened behaviour of the developed UHPFRC is evaluated.

## 5.2 UHPFRC with binary straight steel fibres

### 5.2.1 Materials and mix design

The cement, limestone powder, nanosilica, aggregates and superplasticizer used in this part are the same as that shown in Section 4.2.2. Additionally, two types of straight steel fibres are utilized (as shown in Figure 2.8): 1) fibre length = 13 mm, fibre diameter = 0.2 mm; 2) fibre length = 6 mm, fibre diameter = 0.16 mm.

**Table 5.1: Recipes of the developed UHPFRC**

No.	OPC kg/m <sup>3</sup>	LP kg/m <sup>3</sup>	MS kg/m <sup>3</sup>	S kg/m <sup>3</sup>	nS kg/m <sup>3</sup>	W kg/m <sup>3</sup>	SP kg/m <sup>3</sup>	LSF vol. %	SSF vol. %
1	594.2	265.3	221.1	1061.2	24.8	176.9	44.2	0	0
2	594.2	265.3	221.1	1061.2	24.8	176.9	44.2	2.0	0
3	594.2	265.3	221.1	1061.2	24.8	176.9	44.2	1.5	0.5
4	594.2	265.3	221.1	1061.2	24.8	176.9	44.2	1.0	1.0
5	594.2	265.3	221.1	1061.2	24.8	176.9	44.2	0.5	1.5
6	594.2	265.3	221.1	1061.2	24.8	176.9	44.2	0	2.0

(OPC: Ordinary Portland Cement (CEM I 52.5 R), LP: limestone powder, MS: microsand, S: sand (0-2), nS: nanosilica, W: water, SP: superplasticizer, LSF: long straight fibres, SSF: short straight fibres)

The UHPFRC mixtures developed applying the optimized particle packing model (Eq. (3.2)) are listed in Table 5.1. The resulting integral grading curve of the composed mixture is shown in Figure 4.11(c). As commonly known, for normal fibre reinforced concrete, the fibre content is often about 1% by the volume of concrete (Grünwald, 2004). However, in UHPFRC, this value often increases to around 2% vol., and sometime reaches up to 5% vol. (Grünwald, 2004). Hence, in this research, to investigate the effect of binary steel fibres on the properties of UHPFRC, the steel fibres are added into the mixes in the total amount of 2% vol., and the proportions of long and short straight fibres are shown in Table 5.1. Here, a concept named “short fibre volume fractions ( $X_s$ )” is utilized (Eq. (5.1)), representing the fraction of short straight fibres in the total fibre amount.

$$X_s = \frac{V_s}{V_s + V_l} \quad (5.1)$$

where  $V_s$  means the volumetric amount of short straight fibres (SSF) in the concrete mixture (%), and  $V_l$  represents the volumetric amount of long straight fibres (LSF) in concrete (%).

## 5.2.2 Experimental methodologies

- *Employed mixing procedure*

In this study, the hybrid fibres are mixed together beforehand. Subsequently, following the method presented in Figure 3.2, the concrete matrix is mixed with the hybrid steel fibres, for which around 7 minutes and 30 seconds is needed.

- *Fresh behaviour*

The flowability of the developed UHPFRC is measured following the method shown in Section 2.3.1. The Hägermann cone is again utilized.

- *Mechanical properties*

After performing the workability test, fresh UHPFRC is cast in moulds with the size of 40 mm × 40 mm × 160 mm. The prisms are demolded approximately 24 h after casting and subsequently cured in water at about 21 °C. After curing for 7 and 28 days, the prism specimens are tested under three-point loading. During the test, the set-up is running in a displacement control mode, which is set at 0.1 mm/min. The span of the two supported points under the samples is 100 mm. Afterwards, the compressive strength on samples is executed according to EN-196-1 (2005). During the testing, at least three specimens are tested for each batch.

## 5.2.3 Results and discussions

- *Fresh behaviour*

The slump flow of fresh UHPFRC mixes versus the short fibre volume fraction ( $X_s$ ) is depicted in Figure 5.3. The data illustrates the relationship between the proportions of long and short straight fibres and the workability of fresh UHPFRC. It is important to notice that with an increase of the short fibre volume fraction, the slump flow ability of UHPFRC first linearly increases, and then significantly decreases. For example, when the short fibre volume fraction is zero (2% vol. long straight fibres (LSF)), the slump flow is 28.8 cm, which slightly increases to around 30.0 cm when the short fibre volume fraction grows to 0.75 (0.5% vol. long straight fibres (LSF) and 1.5% vol. short straight fibres (SSF)). This phenomenon implies that the addition of short straight fibres (increasing  $X_s$ ) improves the workability of UHPFRC. However, when all the LSF are replaced by SSF, the flowability of UHPFRC sharply reduces. As shown in Figure 5.3, when the short fibre volume fraction is 1 (2% vol. SSF), the slump flow of UHPFRC is only about 28.3 cm, which is even lower than that of concrete with 2% (vol.) LSF.

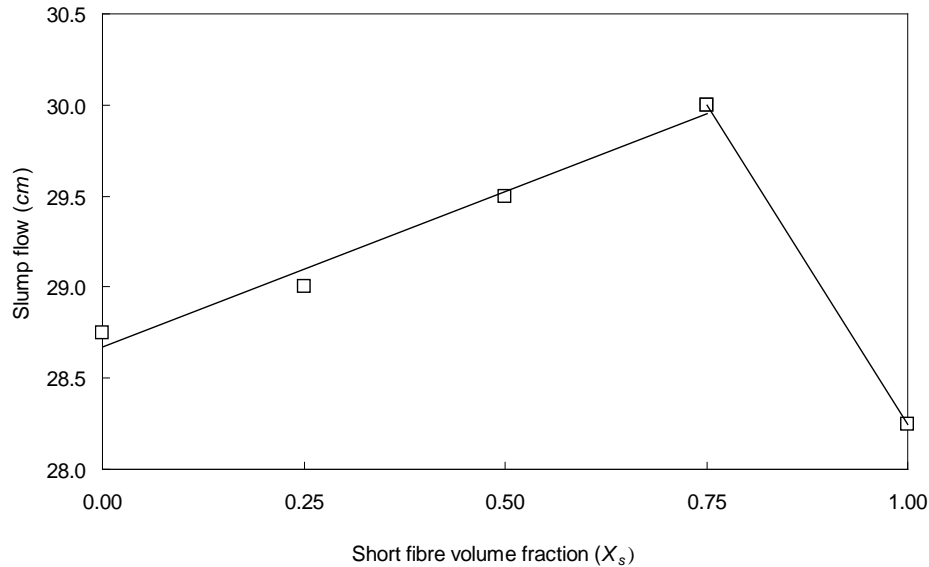


**Figure 5.3: Variation of the spread flow of the developed UHPFRC as function of the short fibre volume fraction ( $X_s$ )**

As mentioned before, the negative effect of steel fibres on the workability of concrete is mainly due to three reasons (Grünewald, 2004): 1) Compared to aggregates, the fibres' shape is much more elongated and the surface area is higher; 2) Stiff fibres can push apart particles and change the structure of the granular skeleton; 3) Steel fibres are often deformed (e.g. hook ended or wave shaped) to improve the anchorage between the fibre and surrounding matrix. The friction between the hook ended steel fibres and aggregates is higher compared with straight steel fibres. Moreover, in this study, the hybrid fibres are utilized to produce the concrete, which means not only the above mentioned reasons, but also the mutual effects between the fibres should be considered. Based on the investigation by Boulekbache et al. (2010), it is known that flow velocities affect the fibres and may cause them to rotate in such a way that the fibres reorient perpendicularly to the flow direction (Figure 5.4). In the presence of different relative velocities in translation and rotation, the fluid exerts forces and momentums on the fibres. Hence, for the fresh concrete with single sized fibres, the entire fibre orientation tends to be perpendicular to the flow direction in the fountain flowing mode, which can generate the largest resistant force and reduce the slump flow of the fresh concrete. Nevertheless, when hybrid fibres are added into the fresh concrete, the fountain flowing mode may be relatively disturbed. When casting concrete in moulds, the fibres close to the walls of the moulds tend to be parallel to the borders, which is named the "wall-effect" (Grünewald, 2004; Markovic, 2006). Hence, in this study, when hybrid fibres are added into the fresh concrete, the long straight fibres can be treated as "imaginary borders" to the short straight fibres, and can relatively resist the rotation of the short fibres and reduce the resistance force in the fountain flow (Figure 5.5). Furthermore, the short straight fibres

can also conversely restrict the rotation of the long straight fibres and further improve the “wall-effect” of long straight fibres. Therefore, the flowability of the hybrid fibres reinforced concrete is higher than that with only one type of steel fibres.

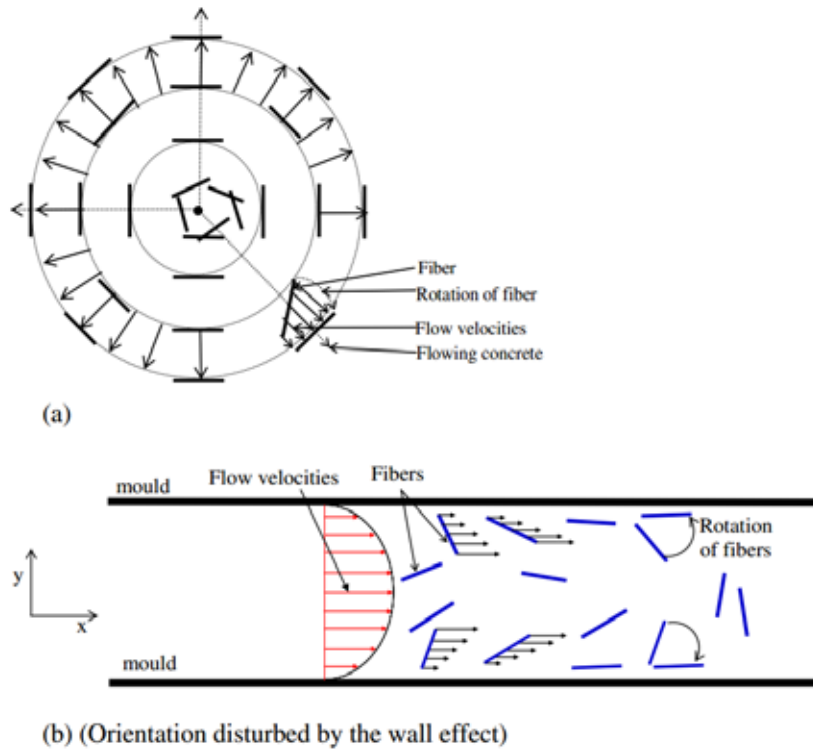


Figure 5.4: Single sized steel fibre orientations in (a) fountain flowing, (b) canal channel flowing (Boulekbache et al., 2010)

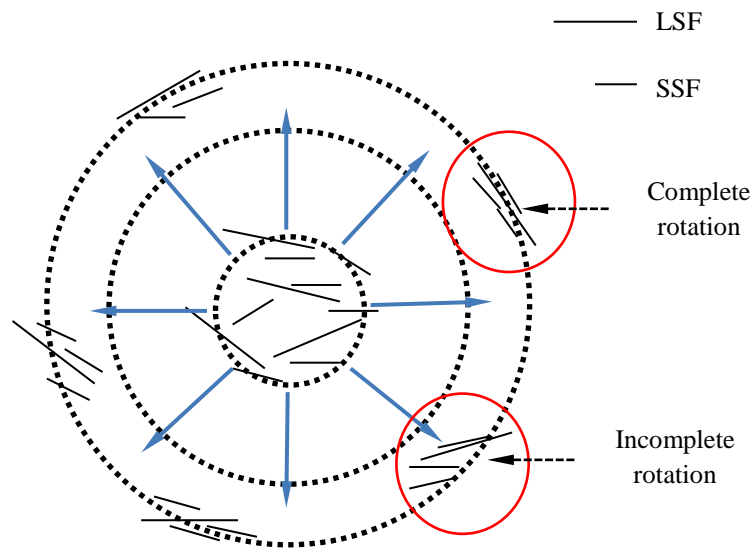


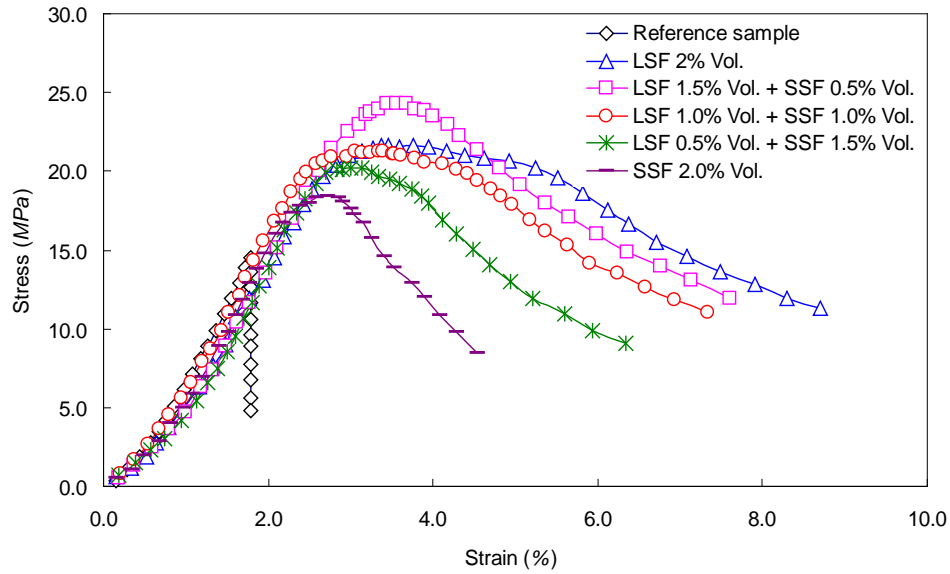
Figure 5.5: Scheme of the influence from the imaginary “wall-effect” between the long and short straight fibres in this study

### • *Flexural behaviour*

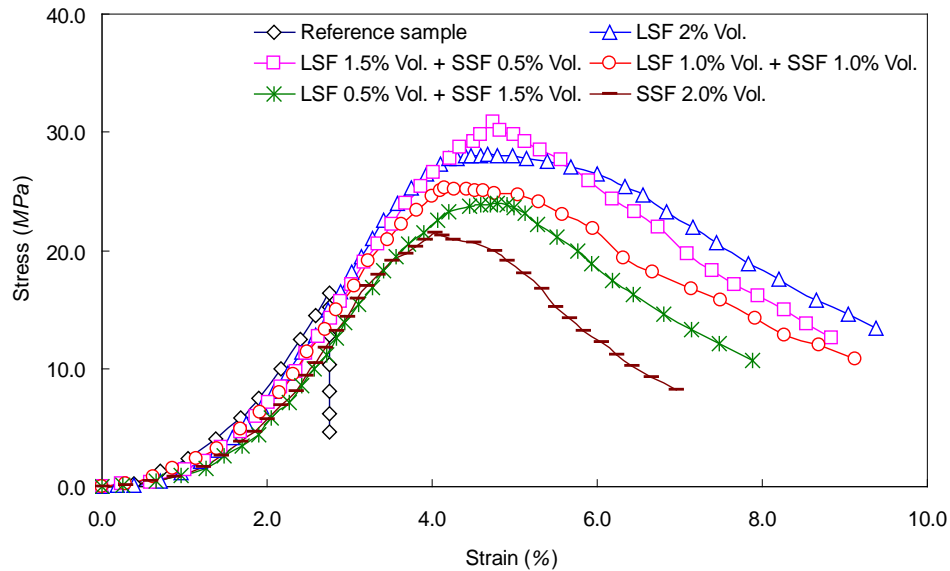
The stress–strain curves of UHPFRC during the flexural test at 7 and 28 days are shown in Figure 5.6. Similarly to the results shown in the literature (Hassan et al., 2012; Mahmud et al., 2013; Sovják et al., 2015), the addition of steel fibres cannot only enhance the ultimate flexural strength, but also improve the energy absorption capacity of the developed UHPFRC. This can be attributed to the fact that the additional steel fibres can bridge cracks and retard their propagation, which could change the fracture behaviour of concrete from brittle to plastic and significantly increase the ultimate flexural strength of concrete (Grünwald, 2004). Moreover, it is important to notice that the flexural properties of the specimen strongly depend on the fractions of the long and short straight fibres in the total fibre amount. As can be seen in Figure 5.6, the ultimate flexural strengths of the concrete with LSF (1.5% vol.) and SSF (0.5% vol.) at 7 and 28 days are always the highest, which are 24.3 MPa and 30.9 MPa, respectively. When only SSF are utilized (2% vol.), the ultimate flexural strengths at 7 and 28 days reduce to around 18.4 MPa and 21.5 MPa, respectively. This can be explained by the following two reasons: 1) SSF can bridge micro-cracks more efficiently, because they are very thin and their number in concrete is much higher than that of the LSF, for the same fibre volume. Hence, when the micro-cracks are just generated in the concrete specimen, the SSF can effectively bridge the micro-cracks. As the micro-cracks grow and merge into larger macro-cracks, the LSF become more and more active in crack bridging. In this way, primarily the ductility can be improved, and partly also the flexural strength. LSF can therefore provide a stable post-peak response. SSF will then become less and less active, because they are being more and more pulled out, as the crack width increases (Markovic, 2006); 2) LSF are always well oriented between the two imaginary borders, if casting the concrete performed in layers (these borders may also be the walls of the moulds). With such positions, the LSF form a kind of a barrier for SSF, and limit their space for rotation. The SSF will therefore be somewhat better oriented when combined together with LSF, than on their own (Figure 5.7) (Markovic, 2006). Hence, more fibres will distribute in the direction parallel to the applied force direction in the flexural test, and the mechanical properties can be significantly improved.

Additionally, for the sample with the highest ultimate flexural strength, it is important to notice that the stress relatively quickly drops after reaching the stress peak. This can be attributed to the fact that the short straight fibres are less effective in bridging the macro-cracks and cannot provide a stable post-peak response. After calculating the area under the curves shown in Figure 5.6, it is demonstrated that the energy absorption capacity (at 28 days) of the batch with the highest flexural strength is not the largest, compared to the other mixtures presented in Figure 5.6 (161.4 units for the sample with 2% (vol.) LSF and 139.8 units for the mixture containing 1.5% vol. LSF and 0.5% vol. SSF).

In summary, the flexural properties of UHPFRC largely depend on the proportions between the long and short straight fibres. In this study, although the sample with LSF (1.5% vol.) and SSF (0.5% vol.) shows the largest ultimate flexural strength, its post-peak response is not the highest observed.



(a) after curing for 7 days



(b) after curing for 28 days

Figure 5.6: Stress - strain curve of UHPFRC under 3-point bending test after cuing for: (a) 7 day and (b) 28 days

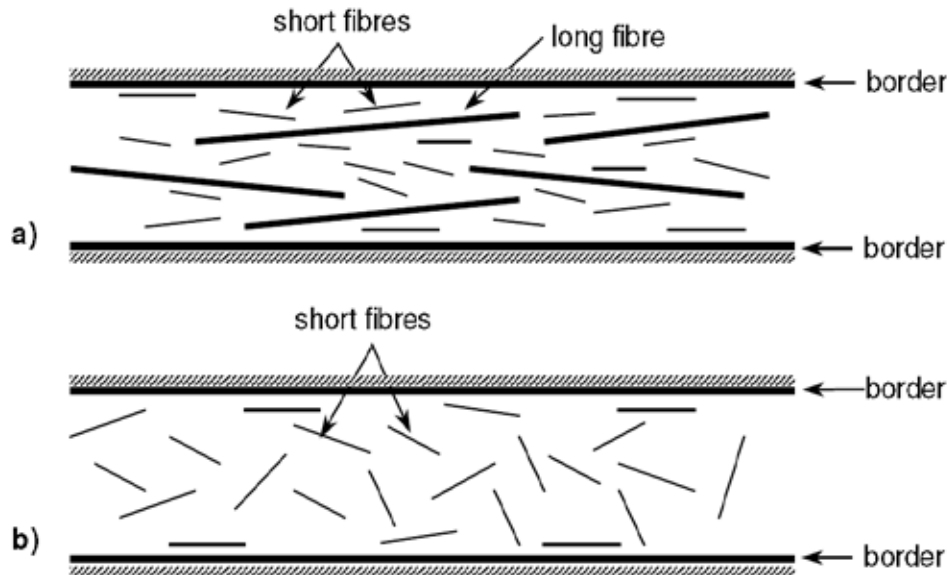


**Figure 5.7:** Orientation of short fibres between the walls of the mould (or any other borders in general), in combination with long fibres (a), and when they are alone on their own (b) (Markovic, 2006)

• *Compressive behaviour*

The compressive strengths of the developed UHPFRC with different short fibre volume fraction are presented in Figure 5.8. As can be seen, compared to the reference sample, the additional steel fibres significantly increase the compressive strength of UHPFRC. For instance, the compressive strengths of the reference sample (without the fibres) at 7 and 28 days are 86.0 MPa and 99.0 MPa, respectively. When LFS are added (2% vol.) into the concrete, its compressive strengths increase to about 114.3 MPa and 139.3 MPa after curing for 7 and 28 days, respectively. Moreover, similarly to the results shown in Figure 5.6, the sample with LSF (1.5% vol.) and SSF (0.5% vol.) shows the highest compressive strengths, which are 117.1 MPa and 141.5 MPa after curing for 7 and 28 days, respectively. This can also be attributed to the combined effect of hybrid fibres in restricting the cracks development. Although the used steel fibres are efficient in improving the properties of concrete under tensile or flexural loads, they can also bridge the cracks that are generated in the compressive test and enhance the ultimate compressive strength of the concrete. However, it is important to notice that, when only short straight fibres are added into the concrete, the compressive strength slightly increases to 111.4 MPa and 120.8 MPa after 7 and 28 days, respectively. This can be attributed to the dimensions and aspect ratio of the short straight fibres. As shown in Figure 2.8, the length of the SSF used in this study is 6 mm, which is less efficient in restricting the growth of macro-cracks. Hence, the addition of only SSF (2% vol.) is not as efficient as only LSF (2% vol.) in improving the compressive strength of UHPFRC.

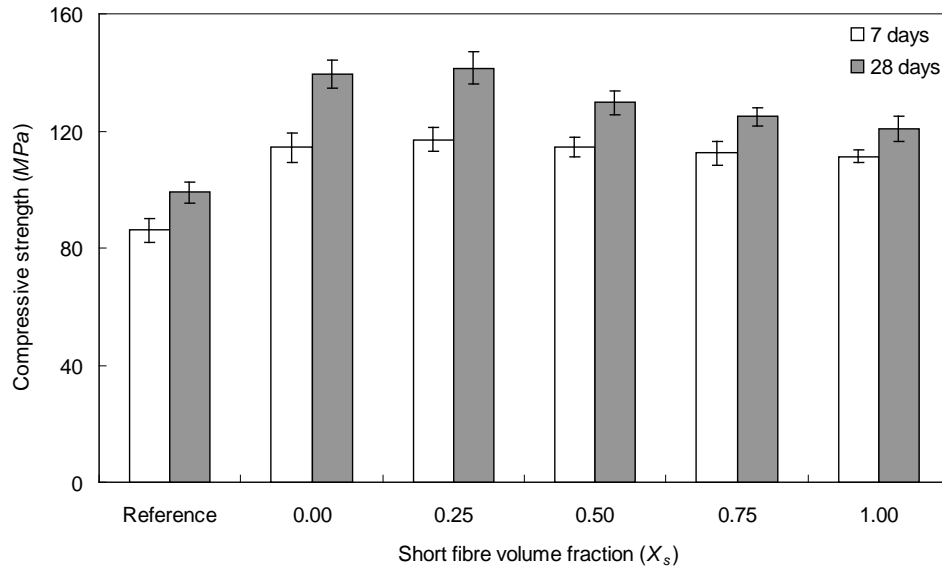


**Figure 5.8: Compressive strength of UHPFRC with different short fibre volume fraction ( $X_s$ )**

**Table 5.2 Comparison of the binder amount and compressive strength (28 days) of optimized and non-optimized UHPFRC**

References	Binders ( $\text{kg/m}^3$ )			Water/binder ratio	Steel fibre amount (vol. %)	Compressive strength at 28 days (MPa)
	Cement	GGBS	Silica			
a	950	0	238	0.20	2.0	125
b	860	0	215	0.20	2.0	198
c	657	418	119	0.17	2.0	150
d	657	430	119	0.15	2.0	120
e	1011	0	58	0.15	2.0	160
f	960	0	240	0.16	2.5	155
g	1050	0	275	0.14	6.0	160
Optimized UHPFRC	594.2	0	24.8	0.2	2.0	142

(a: (Yang et al., 2009), b: (Kang et al., 2011), c: (Hassan et al., 2012), d: (Yang et al., 2010), e: (Toledo Filho et al., 2012), f: (Corinaldesi and Moriconi, 2012), g: (Habel et al., 2006))

The compressive strength results demonstrate that, based on the modified A&A model and optimized fibre hybridization design, it is possible to produce UHPFRC with a relatively low cement or binder amount. The comparison of the binder amounts and compressive strengths (28 days) between the optimized and non-optimized UHPFRC is shown in Table 5.2. It is clear that, with a lower binder amount, the compressive strength of the optimized UHPFRC is still comparable to the non-optimized UHPFRCs, which have a much higher amount of binder. For instance, in the results shown by Hassan et al.

(2012), about  $1200 \text{ kg/m}^3$  of binder is utilized to produce UHPFRC, and its compressive strength at 28 days is about 150 MPa. In this study, only about  $620 \text{ kg/m}^3$  of binder is utilized in UHPFRC, to reach a comparable compressive strength. Additionally, according to Hunger (2010), the cement efficiency of the developed UHPFRC can be calculated, which is about  $0.17 \text{ MPa}/(\text{kg/m}^3)$ . Although this value is smaller than some of the Eco-concretes (Hunger and Brouwers, 2009; Hunger 2010; Hüsken and Brouwers, 2008; Hüsken, 2010), it is much higher than that of other UHPCs (Habel et al., 2006; Deeb et al., 2012; Wang et al., 2012; Zhao et al., 2014; Yazici, 2007). Hence, it is confirmed here that the optimized UHPFRC matrix can have significantly reduced binder amount without sacrificing the mechanical properties and be more ‘‘green’’ in the terms of cement amount and embedded  $\text{CO}_2$  emissions.

· ***Improvement of the mechanical properties***

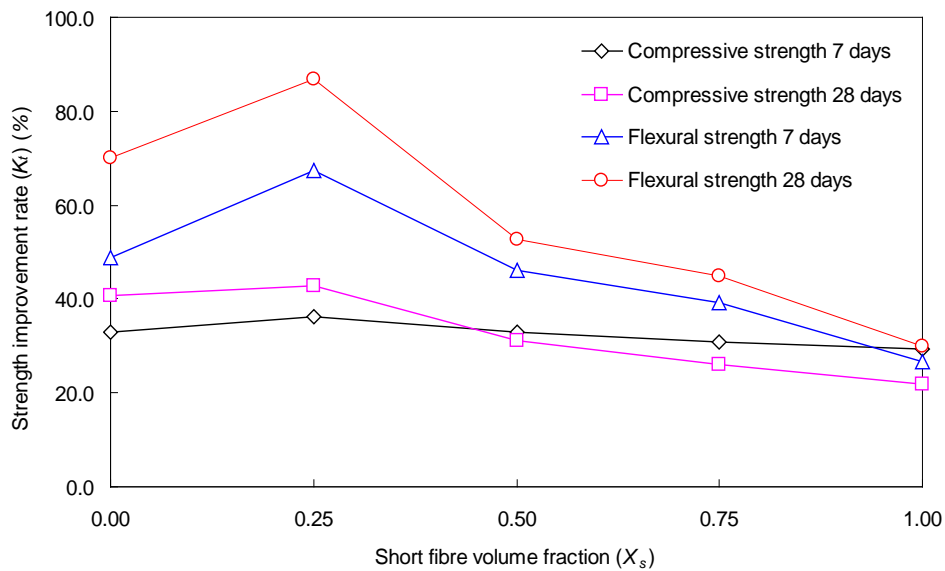


**Figure 5.9: Variation of the strength improvement rate ( $K_f$ ) of UHPFRC with different short fibre volume fraction ( $X_s$ )**

To better explain the effect of the additional steel fibres on the UHPFRC flexural and compressive strengths improvement, the strength improvement ratio is computed applying Eq. (3.4). The flexural and compressive strength improvement ratios of UHPFRC versus the short fibre volume fraction ( $X_s$ ) are illustrated in Figure 5.9. It can be noticed that with an increasing value of the short fibre volume fraction ( $X_s$ ), the flexural strength improvement ratio firstly increases and then decreases. For instance, when  $X_s$  equals to 0.25, the flexural strength improvement ratios are 48.9% and 70.1% at 7 and 28 days, which both drop about 30% when the short fibre volume fraction increases to 1. Moreover, the influence of the short fibre volume fraction on the compressive strength improvement ratio is relatively smaller, and fluctuates in the range of 35 – 40%.

This phenomenon also proves that the additional steel fibres are more efficient in improving the flexural properties. However, to enhance the efficiency of the utilized steel fibres, the hybrid design is preferable. In this study, the UHPFRC with LSF (1.5% vol.) and SSF (0.5% vol.) shows the best fibre efficiency and best mechanical properties. This can be also attributed to the mutual effect of long and short straight fibres on the fibre distribution, which has already been explained in the previous part.

#### 5.2.4 Summary

This section presents the properties of UHPFRC with binary straight steel fibres. The design of the concrete mixtures is based on the aim to achieve a densely compacted cementitious matrix, employing the modified A&A model. Based on the obtained results, the following conclusions are drawn:

- 1) By using the A & A model and optimized fibre hybridization design, it is possible to produce a UHPFRC with relatively low binder amount (about  $620 \text{ kg/m}^3$ ) and low fibres content (2% vol.), which is beneficial for developing an eco-friendly and sustainable UHPFRC.
- 2) At the same total steel fibre amount, the hybrid fibre reinforced UHPC shows better workability than the one with single sized fibres. This may be attributed to the fact that the long straight fibres can be treated as imaginary borders to the short straight fibres, which can relatively well restrict the rotation of the short fibres and reduce the resistance force in the fountain flow. Furthermore, the short straight fibres can also conversely restrict the rotation of the long straight fibres and further improve the “wall-effect” of the long straight fibres.
- 3) Based on the mechanical test results, it is found that the UHPC with LSF (1.5% vol.) and SSF (0.5% vol.) shows the highest flexural and compressive strengths after curing for 28 days, which are 30.9 and 141.5 MPa, respectively. However, its flexural stress–strain curve more quickly decreases (compared to the mixture with 2% vol. LSF) after reaching the peak stress, which implies that the addition of SSF is unbeneficial for improving the energy absorption capacity of UHPFRC during the post-peak process.

### 5.3 UHPFRC with hook ended fibres (ternary hybridization)

#### 5.3.1 Materials and mix design

The ingredients used in this section for the production of UHPFRC matrix are the same as that shown in Section 5.2.1. Additionally, three types of steel fibres are utilized here: 1) long straight fibres (LSF), length = 13 mm, diameter = 0.2 mm; 2) short straight fibres (SSF), length = 6 mm, fibre diameter = 0.16 mm; 3) hook ended fibre (HF) length = 35 mm, diameter = 0.55 mm. More detailed information on these fibres can be found in Figure 2.8 and Table 2.6.

The UHPFRC mixtures developed in this part applying the optimized particle packing model are listed in Table 5.3. The concrete mixture proportions (except the fibres) are the same as those shown in Table 5.1 and the resulting integral grading curve of the composed mixture is the same as that presented in Figure 4.11(c). The steel fibres are added into the developed concrete matrix with different hybridizations and proportions (as shown in Table 5.3). As shown in Figures 5.6 and 5.8, due to the fact that the developed UHPFRC mixture with LSF (1.5% vol.) and SSF (0.5% vol.) at 7 and 28 days shows the best mechanical properties, the designed volumetric ratio of HF/LSF or HF/SSF are all fixed to 3/1. In addition, in the mixture with ternary hybrid fibres, the volumetric ratio of HF/LSF/SSF is fixed to 12:3:1 (thus, the volumetric ratio of hook ended fibres (long) to straight fibres (short) is still 3:1). In all the mixtures, the total fibre amount is 2% (vol.).

**Table 5.3: Recipes of the developed UHPFRC**

No.	OPC kg/m <sup>3</sup>	LP kg/m <sup>3</sup>	MS kg/m <sup>3</sup>	S kg/m <sup>3</sup>	nS kg/m <sup>3</sup>	W kg/m <sup>3</sup>	SP kg/m <sup>3</sup>	LSF vol. %	SSF vol. %	HF vol. %
1	594.2	265.3	221.1	1061.2	24.8	176.9	44.2	0	0	2
2	594.2	265.3	221.1	1061.2	24.8	176.9	44.2	0.125	0.375	1.5
3	594.2	265.3	221.1	1061.2	24.8	176.9	44.2	0.5	0	1.5
4	594.2	265.3	221.1	1061.2	24.8	176.9	44.2	0	0.5	1.5

(OPC: Ordinary Portland Cement (CEM I 52.5 R), LP: limestone powder, MS: microsand, S: sand (0-2), nS: nanosilica, W: water, SP: superplasticizer, LSF: long straight fibres, SSF: short straight fibres, HF: hook ended fibre)

### 5.3.2 Experimental methodologies

- *Employed mixing procedure*

Here, the hybrid fibres are mixed together beforehand. Subsequently, following the method presented in Figure 3.2, the concrete matrix is mixed with the hybrid steel fibres.

- *Fresh behaviour*

Considering the length of the utilized hook ended steel fibres, the workability of the developed fresh UHPFRC mixtures are tested following EN-12350-8 (2010). The Abrams cone with the internal upper/lower diameter equal to 100/200 mm and height equal to 300 mm is utilized without any jolting. Two diameters ( $d_1$  and  $d_2$ ) perpendicular to each other are recorded and their mean is recorded as the slump flow value of UHPFRC.

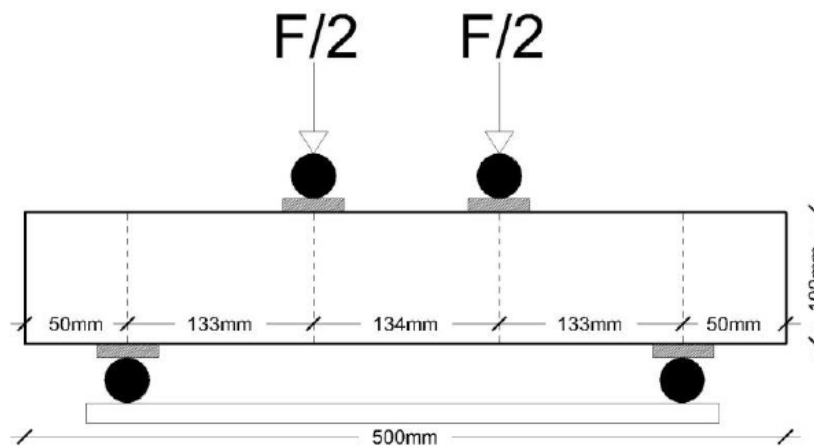
- *Mechanical properties*

Considering the restriction of the long hook ended fibres on the size of the mould, the produced fresh UHPFRC mixtures are cast in moulds with the size of 100 mm × 100 mm

$\times 500$  mm and  $100$  mm  $\times 100$  mm  $\times 100$  mm. The beams and cubes are demoulded approximately 24 h after casting and subsequently cured in water at about  $21$  °C. After curing for 28 days, the compressive strengths of the cubes are determined according to EN-12390-3 (2009), and the beams are subjected to the 4-point bending test. For the 4-point bending test, the span between the two supported points at the bottom side is  $400$  mm. To obtain flexural load over the middle deflection curve, a Linear Variable Differential Transformer (LVDT) mounted on the surface of the tested samples is utilized to record the mid-deflection. During the test, the set-up is running in a displacement control mode, which is set at  $0.1$  mm/min. The test device and a scheme of the sample during the test are illustrated in Figure 5.10. Before the test, the calibration of the used LVDT is done (as shown in Figure 5.11).



(a)



(b)

**Figure 5.10:** Employed 4-point bending test device (a) and scheme a sample during the test (b)



**Figure 5.11: Calibration of the Linear Variable Differential Transformer (LVDT)**

· ***Flexural toughness***

Based on the materials point of view, toughness means the capacity of a material to absorb energy and plastically deform without fracturing. From the available literature, two standards are mainly used to evaluate the flexural toughness of fibre reinforced concrete, which are ASTM C1018-97 (1998) and JSCE SF-4 (1984). In this study, both of these standards are utilized to calculate the flexural toughness of UHPFRC.

In ASTM C1018-97, the flexural toughness is calculated at four specified deflections ( $\delta$ ,  $3\delta$ ,  $5.5\delta$  and  $10.5\delta$ ). The  $\delta$  represents the deflection when the first crack appears, as presented in Figure 5.12. The flexural toughness is calculated at the deflection  $\delta$ , which is considered the elastic or pre-peak flexural toughness (first-crack flexural toughness), while the other three ( $3\delta$ ,  $5.5\delta$  and  $10.5\delta$ ) are considered as the post-peak flexural toughnesses. Furthermore, the flexural toughness indices  $I_5$ ,  $I_{10}$  and  $I_{20}$  are also defined, which are the ratios between the post-peak flexural toughness and the pre-peak (elastic) flexural toughness. Based on Figure 5.12, the flexural toughness indices can be calculated as:

$$I_5 = \frac{\text{AreaOACD}}{\text{AreaOAB}} \quad (5.2)$$

$$I_{10} = \frac{\text{AreaOAEF}}{\text{AreaOAB}} \quad (5.3)$$

$$I_{20} = \frac{\text{AreaOAGH}}{\text{AreaOAB}} \quad (5.4)$$

Differently from the ASTM C1018-97, the JSCE SF-4 defines the area under the load-deflection plot up to a deflection of span/150 as the flexural toughness. From this measurement, a flexural toughness factor ( $TF$ ) can be calculated as follows:

$$TF = \frac{A_{(L/150)} \times L}{(L/150) B \phi H^2} \quad (5.5)$$

where  $TF$  represents the flexural toughness factor,  $L$  is the span (mm),  $A_{(L/150)}$  is the flexural toughness (Nžm) at the deflection ( $L/150$ ) (calculated in this study using Matlab),  $B'$  is the specimen's width (mm) and  $H$  is the specimen's height (mm).

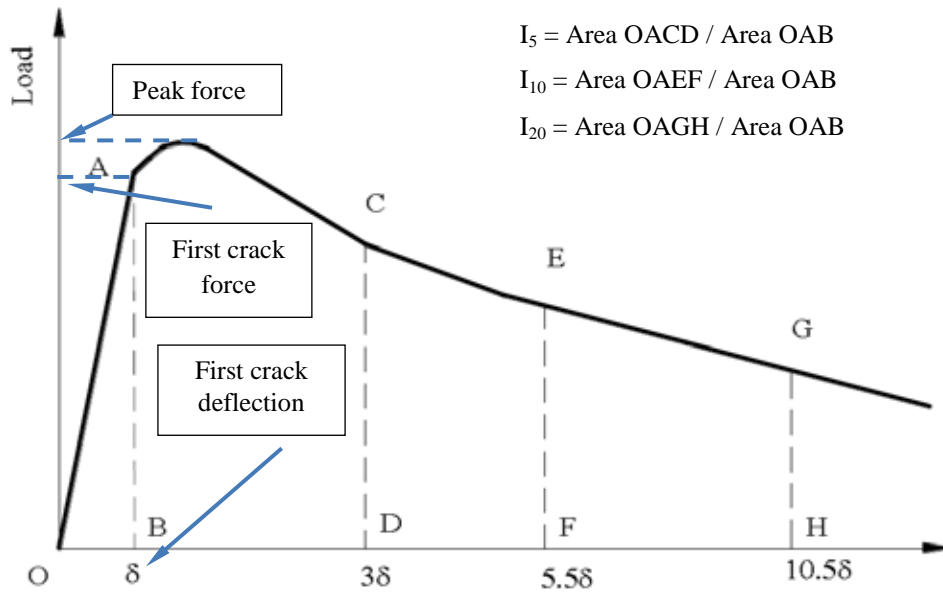


Figure 5.12: Typical load-deflection curve of fibre reinforced concrete and fracture toughness indices based on ASTM C 1018-97

### 5.3.3 Results and discussions

#### • Fresh behaviour

Figure 5.13 illustrates the slump flow of UHPFRC with hook ended fibres (HF). The data presents the variation of slump flow of UHPFRC with different fibres hybridization. The HF, HF+LSF+SSF, HF+LSF and HF+SSF represent the mixtures from No. 1 to No. 4, respectively (see Table 5.3). As can be noticed, the slump flow of all the developed UHPFRC with HF fluctuates around 85 cm, which is much more than that shown in Figure 5.3, because different cones and concrete volumes are used in these two flowability tests. The mixture with HF and SSF has the highest slump flow value (88.5 cm), which is followed by the one with ternary fibres. The UHPFRC with only HF shows the smallest slump flow value, around 83.5 cm. According to the European Guidelines for Self-Compacting Concrete (2005), the slump flow of concrete is divided into three

classes: 1) SF 1: 55 - 65 cm; 2) SF 2: 66 - 75 cm; 3) SF 3: 76 - 85 cm. The slump flows of the UHPFRCs developed here with HF are even higher than the SF 3 class. Moreover, it can be observed that, compared to the other mixtures with fibres, when the SSF is utilized, the flowability of UHPFRC can be further improved.

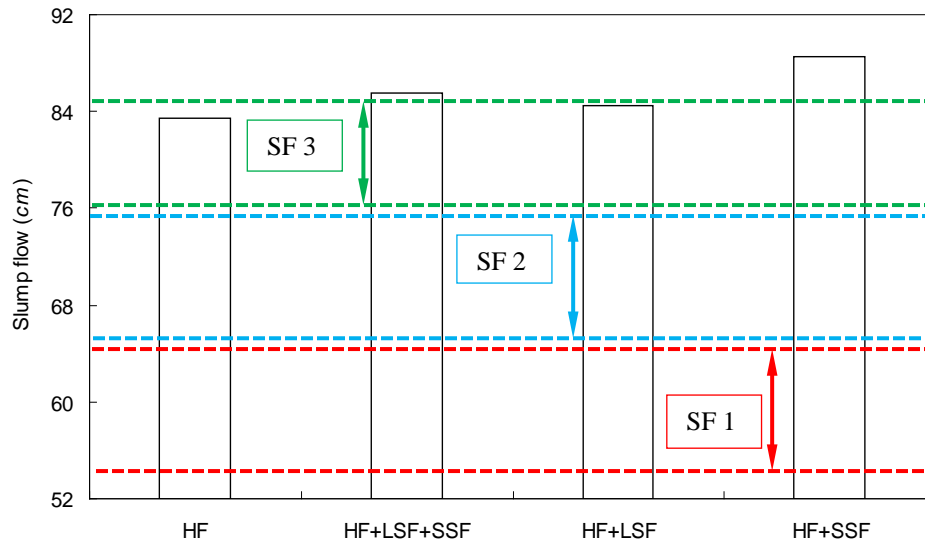


**Figure 5.13: Slump flow of the developed UHPFRC with hook ended fibres**

As mentioned before, the effect of steel fibres on the workability of concrete is mainly due to their elongated shape, relatively high surface area, influence on the granular skeleton, mutual effects between the hybrid fibres and anchorage between deformed fibres and concrete matrix (Grünwald, 2004; Yu et al., 2014d). Moreover, it is known that different flow velocities affect the fibres and may cause them to rotate in such a way that the fibres reorient perpendicularly to the flow direction. Hence, for the fresh concrete with single sized fibres, the fibres orientation tends to be perpendicular to the flow direction in the fountain flowing mode, which can generate the largest resistance force and reduce the slump flow of the fresh concrete (Boulekbache et al., 2010). Nevertheless, when hybrid fibres are added into the concrete, the fountain flowing mode may be disturbed. Due to the difference in geometry, the rotation of fibres can be restricted by each other, which causes that the resistance force in the fountain flow can be reduced and the slump flow value of the concrete mixture could be higher. Hence, as observed in this study, the hybrid fibre reinforced concretes have a higher slump flow ability than the mixtures with only single sized fibres.

#### • *Flexural behaviour*

Figure 5.14 presents the 4-point bending test results of the UHPFRC with HF. The load/mid-deflection curves can be mainly divided into three parts: elastic section, strain

hardening section and strain softening section, as shown in Figure 5.15. From the beginning of the test until the moment when the first crack appears, the linear section part of the curve can be observed. Due to the fact that the tested UHPFRC is very stiff, very small mid-deflections of the samples can be noticed. In this study, the first crack deflections of all the samples fluctuate around 0.01 mm, and the first crack forces follow the order: HF+LSF+SSF (30.9 kN) > HF+SSF (30.3 kN) > HF+LSF (30.1 kN) > HF (28.1 kN). It can be observed that the first crack forces of the concretes with hybrid fibres are rather similar to each other, and are obviously larger than the one with HF only. After the first crack appears, the strain hardening section begins, and a number of small cracks appear on the tested beam, as shown in Figure 5.14. In this process, the fibres in concrete will mainly endure the load and limit the growth of the generated cracks, until the peak force appears. In this study, the peak forces of all the tested UHPFRC follow the order: HF+LSF+SSF (43.1 kN) > HF+SSF (39.9 kN) > HF+LSF (38.2 kN) > HF (34.8 kN), and this trend is similar to that of the first crack force. When the fibres in concrete cannot restrain the further growth of the small cracks, they will be pulled out and the endurable force of the test beam will decrease, which reflects the initiation of the strain softening section. Nevertheless, due to the different characteristics of the fibres and the binding force between the fibres and concrete matrix, the strain softening behaviour of reinforced concrete can be very different. In this study, it is important to notice that the endurable force of the mixtures with SSF (e.g. HF+LSF+SSF and HF+LSF) decreases after reaching the peak force, while for concrete with only HF or HF+LSF a relatively slowly decreasing trends are observed. The residual load decreasing rates of the tested samples follow the order: HF < HF+LSF < HF+LSF+SSF < HF+SSF, which further implies that the addition of SSF is ineffective in improving the flexural toughness of UHPFRC.

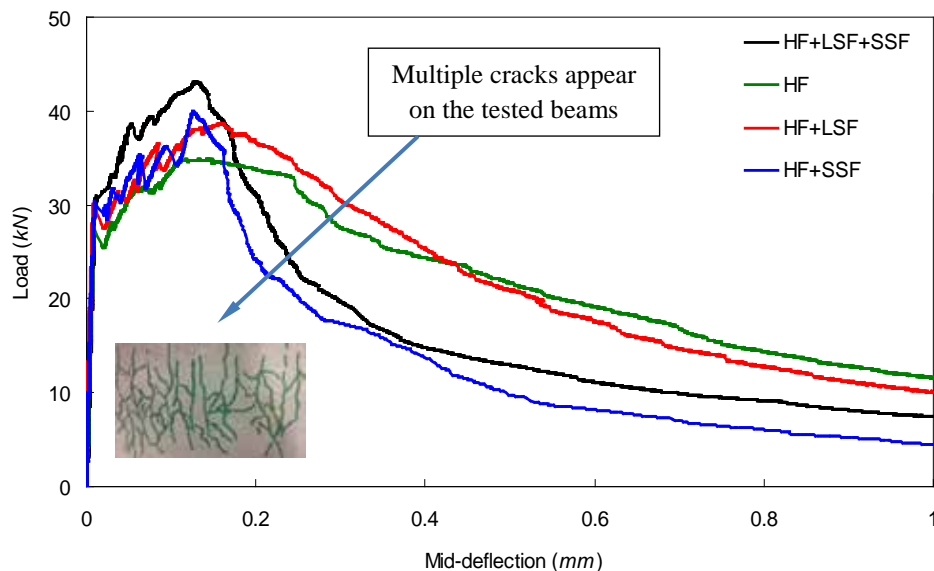
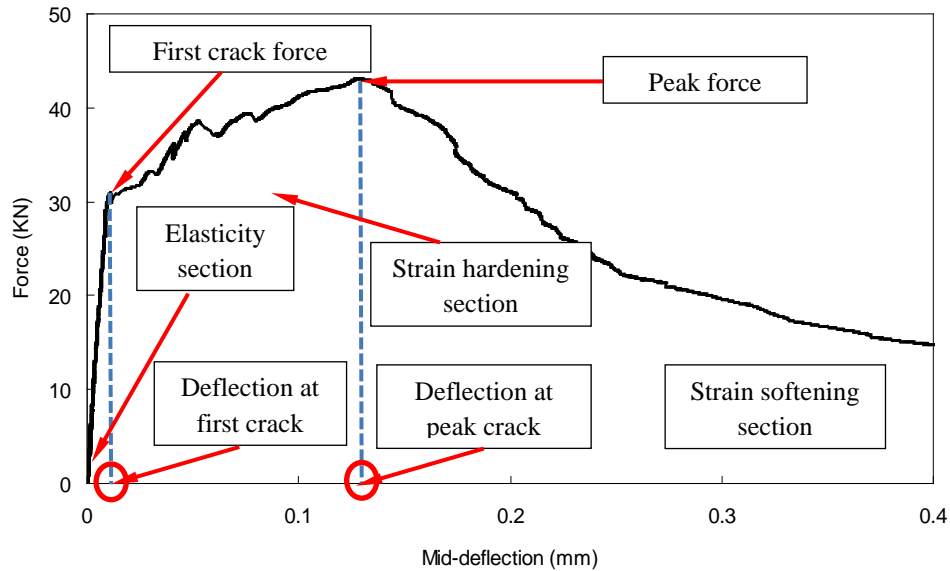


Figure 5.14: 4-point bending test results of the developed UHPFRC with hook ended fibres



**Figure 5.15: Key parameters of UHPFRC subjected to 4-point bending test**

The above observed phenomenon can be attributed to the following reasons: 1) during the 4-point bending test, the hybrid fibres can well disperse the loading force. For instance, the straight fibres can well bridge the micro-cracks, while the long hook ended fibres are more efficient in resisting the macro-cracks development. Hence, when ternary fibres are used in UHPFRC, the cracks generated at different length-scales can be better bridged compared to the mixture with only one or two types of fibres, which causes that the endurable force can be simultaneously larger; 2) due to the multiple effect among different fibres, more fibres in the ternary fibres reinforced mixture distribute in the direction perpendicular to the force direction during the 4-point bending test, which can further improve the first crack force and peak force; 3) although SSF works well in restraining the growth of micro-cracks, it is less efficient during the strain softening process, which can be attributed to its specific geometry. Due to the relatively short length and the corresponding lower binding force with the concrete matrix, many SSF can be pulled out after reaching the peak force, and the load endurable capacity of the tested beam decreases. In contrary to the characteristic of SSF, HF shows a greater ability in restraining the development of macro-cracks. As commonly known, the hooks at the ends of HF can improve the coupling force between the fibres and concrete matrix, which causes that a higher force is needed to pull this fibre type out (compared to SSF). Hence, during the strain softening process, HF can still bridge the macro-cracks, and the endurable force with only HF reduces slower with an increase of the mid-deflection.

#### • *Compressive behaviour*

Figure 5.16 illustrates the compressive strength of UHPFRC with hook ended steel fibres (HF) and the reference sample (without fibres). It can be found that the addition of steel

fibres can significantly improve the compressive strength of the developed concrete matrix. Moreover, the 28 days compressive strength of all the developed UHPFRC mixtures fluctuates around 135 MPa, and the difference between the mixtures with HF is relatively small. The mixture with HF and SSF shows the highest compressive strength at 28 days (136.5 MPa), while the mixture with only HF is the lowest - 129.2 MPa. Moreover, in the mixtures HF+LSF+SSF, HF+LSF and HF+SSF, the HF amount is the same (1.5% vol.), and their compressive strengths follow the order: HF+SSF > HF+LSF+SSF > HF+LSF. Hence, it can be concluded that: 1) when the total fibre amount is the same, the mixture with hybrid fibres shows a higher compressive strength than the one with HF only; 2) in the hybrid fibres system, when the total fibre and the HF amounts are the same, the SSF is more efficient in improving the compressive strength than the LSF. These phenomena should be also attributed to the combined effect of hybrid fibres in restricting the cracks development. The homogeneity of the tested sample is very important to improve its compressive strength. As can be easily understood, with the same volumetric amount, the SSF has the largest fibre number compared to the other used fibres. Hence, as observed in this study, the UHPFRC mixture with HF+SSF is more homogeneous and its compressive strength can be higher, compared to the sample with HF+LSF or HF only.

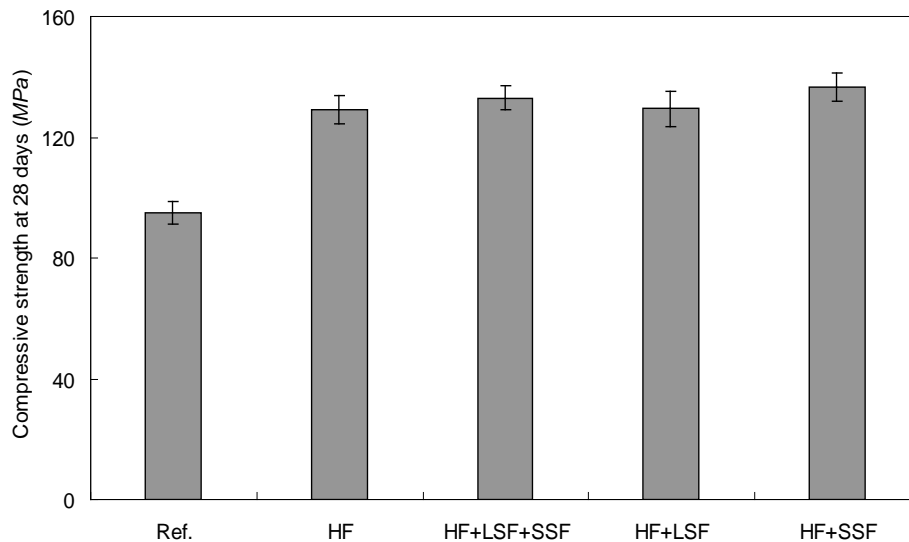


**Figure 5.16: Compressive strength test results of the developed UHPFRC with hook ended fibres**

• ***Flexural toughness***

To evaluate the effect of different fibres on the flexural toughness of UHPFRC, the procedures described in ASTM C1018-97 (1998) and JSCE SF-4 (1984) are employed for the flexural toughness determination.

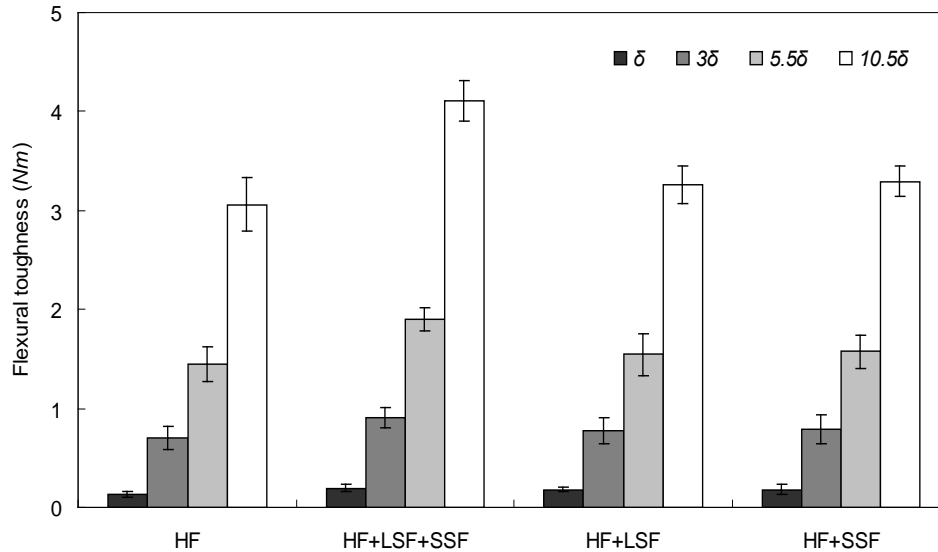


**Figure 5.17: Flexural toughness of the developed UHPFRC based on ASTM C1018-97**

Figure 5.17 shows the flexural toughness of UHPFRC calculated based on ASTM C1018-97. It can be noticed that the first crack flexural toughness of the tested UHPFRC are very small and similar to each other, and fluctuate around 0.2 Nžm. After that, with an increase of deflection, a difference of the post-crack flexural toughnesses between the UHPFRC with different fibres can be observed. Especially at the deflection of 10.5  $\delta$ , the mixture with ternary fibres has the largest post-crack flexural toughness (4.1 Nžm), which is followed by the HF+SSF (3.3 Nžm), HF+LSF (3.2 Nžm) and HF (3.1 Nžm), respectively. Hence, based on the ASTM C1018-97, the flexural toughness of the mixture with ternary fibres is the highest, while the flexural toughness of the mixture with only HF is the lowest. In addition, the flexural toughness indices of all the mixtures are calculated based on ASTM C1018-97, and are presented in Figure 5.18. It can be noticed that the  $I_5$  for all the mixtures are similar to each other. Moreover, the indices  $I_{10}$  and  $I_{20}$  show that the toughness indexes of the tested concretes with different fibres follow the order: HF > HF+LSF+SSF > HF+LSF > HF +SSF. Hence, it can be summarized that the concrete mixture with only HF has the largest flexural toughness, which is closely followed by the mixture with ternary fibres. However, it is important to notice that the calculated flexural toughness and flexural toughness indices are not in line with each other, which implies that the standard ASTM C1018-97 is not very suitable to evaluate the flexural toughness of UHPFRC.

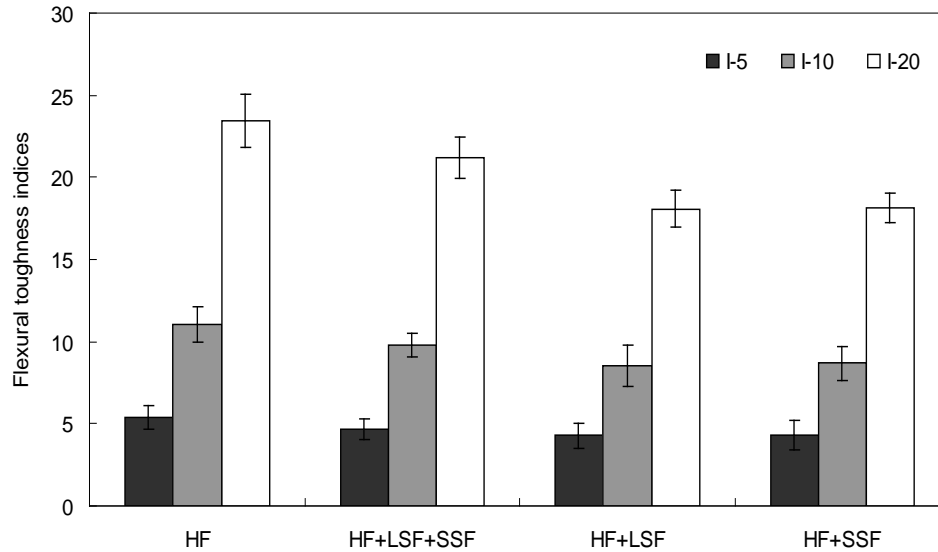


**Figure 5.18: Flexural toughness indices of the developed UHPFRC based on ASTM C1018-97**

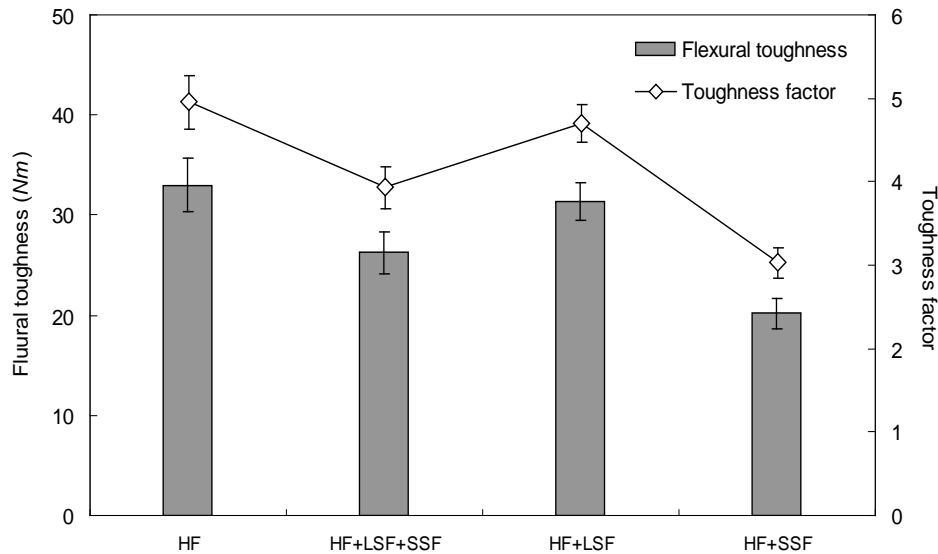


**Figure 5.19: Calculated flexural toughness and flexural toughness factor of the developed UHPFRC based on JSCE SF-4**

To clarify the conflicting results of flexural toughness based on ASTM C1018-97, the JSCE SF-4 is employed to further evaluate the flexural toughness of UHPFRC. The flexural toughness and flexural toughness factors of UHPFRC calculated based on JSCE SF-4 are shown in Figure 5.19. The calculated flexural toughnesses, presented in Figure 5.19, are all in the range from 25 to 35 N $\cdot$ m, and are much larger than those calculated based on ASTM C1018-97 (shown in Figure 5.17). In addition, the flexural toughness of UHPFRC calculated here based on JSCE SF-4 is similar to the results of other fibre

reinforced concrete found in the literature (Nataraja et al., 2000; Sukontasukkul, 2004). The calculated flexural toughnesses and flexural toughness factors shown in Figure 5.19 follow the order: HF > HF+LSF > HF+LSF+SSF > HF+SSF, which is in line with the obtained 4-point bending test results (Figure 5.14). Hence, it is demonstrated that the HF can significantly increase the flexural toughness of UHPFRC, while that the additional SSF is less effective in improving the flexural toughness of UHPFRC.

· ***Comparison of ASTM C1018-97 and JSCE SF-4***

This study demonstrates that the UHPFRC flexural toughness calculated based on ASTM C1018-97 and JSCE SF-4 show very different results. In the literature it can be noticed that these two standards are the most widely used standards to determine the flexural toughness of concrete or fibre reinforced concrete. Some comparisons and evaluations between these standards can be easily found. For instance, Nataraja et al. (2000) stated that the characterization of flexural toughness based on the JSCE SF-4 approach was very simple and was independent of the type of the deflection measuring technique. No sophisticated instrumentation was required to determine the flexural toughness factor. Moreover, Sukontasukkul (2004) found that a single value flexural toughness determined using JSCE SF-4 method can easily reflect the flexural toughness property of steel fibre reinforced concretes (SFRC). However, in the case of polypropylene fibres reinforced concrete (PFRC), JSCE SF-4 does not seem to be sufficient to reflect the true flexural toughness. On the other hand, the flexural toughness calculated by ASTM C1018-97 at different deflections seems to work well in terms of capturing and reflecting the true flexural toughness properties of both SFRC and PFRC (Sukontasukkul, 2004).

However, in this study, after comparing the obtained 4-point bending test results and the calculated flexural toughness, it can be found that the ASTM C1018-97 cannot correctly reflect the flexural toughness property of the tested UHPFRC, which conflicts with the conclusion presented in Sukontasukkul (2004). This can be attributed to the difference of the first crack deflection between the normal strength concrete and UHPFRC. As can be seen, the flexural toughness described in ASTM C1018-97 largely depends on the value of the deflection of the first crack (e.g.  $\delta$ ,  $3\delta$ ,  $5.5\delta$  and  $10.5\delta$ ). In the 4-point bending test of UHPFRC, due to the fact that the developed UHPFRC is very stiff, its deflection at the first crack appearance is much smaller than for the normal fibre reinforced concrete. In this study, the  $\delta$  of all the tested mixtures fluctuates around 0.01 mm, which causes that the calculated  $3\delta$ ,  $5.5\delta$  and  $10.5\delta$  are also relatively small. Hence, in the calculation of the flexural toughness following ASTM C 1018-97 (1998), only small part of the area under the load-deflection curve is considered. As shown in Figure 5.14, the deflection of  $10.5\delta$  (around 0.11 mm) is still in the strain hardening section. Hence, the flexural toughness calculated based on ASTM C1018-97 cannot truly represent the flexural toughness property of UHPFRC. In contrary, in the standard JSCE SF-4, the area under the load-deflection plot up to a deflection of span/150 (about 2.67 mm in this study) is calculated,

which guarantees that the section of elasticity, strain hardening and strain softening are all taken into account in the flexural toughness calculation. Consequently, it can be summarized that the JSCE SF-4 is more suitable to evaluate the flexural toughness property of UHPFRC than ASTM C1018-97.

#### 5.3.4 Summary

This section presents the development and properties evaluation of the developed UHPFRC with hook ended steel fibres, including ternary hybridization design. Based on the obtained experimental results of the UHPFRC with binary fibre (shown in Section 5.2), three types of steel fibres are incorporated into UHPFRC matrix. According to the obtained results, the following conclusions can be drawn:

- 1) Both the straight and the hook ended fibres can be used to produce UHPFRC with relatively good workability. Moreover, with the same steel fibre amount, the hybrid fibre reinforced concrete shows better workability than the one with single sized fibres.
- 2) The UHPFRC mixtures with hybrid fibres reach higher strengths than those with single sized fibres. The macro-fibres (hook ended steel fibres) can also be utilized to produce UHPFRC, with good mechanical properties. The addition of short straight fibres (SSF) can significantly improve the homogeneity of the concrete mixture and simultaneously enhance its compressive strength, while the ternary hybrid fibres are more beneficial in increasing the peak force of UHPFRC in the 4-point bending test. Hence, based on different requirements on the mechanical properties of UHPFRC, various hybridization designs of the fibres can be executed, which can significantly improve the fibre efficiency.
- 3) The flexural toughness of UHPFRC is evaluated following the most commonly used standards (ASTM C1018-97 and JSCE SF-4). The results show that, with the same fibre amount, the hook ended fibres (HF) can significantly increase the flexural toughness of UHPFRC, while that the additional short straight fibres (SSF) are less effective in improving the flexural toughness of UHPFRC. Moreover, due to the specific characteristics of UHPFRC, it is found that the JSCE SF-4 guideline is more suitable to be used to evaluate the flexural toughness property of UHPFRC than ASTM C1018-97.

#### 5.4 Conclusions

In this chapter, toward to efficiently utilize the steel fibres in UHPFRC, the effect of binary and ternary fibres on the properties of UHPFRC is investigated. From the obtained experimental results it can be noticed that different fibres can provide different contribution to the properties of UHPFRC. For instance, binary fibres are beneficial in

improving the workability (about 90 cm, based on EN-12350-8 (2010)) and mechanical properties (about 30 and 140 MPa for flexural and compressive strengths) of UHPFRC. Hook ended steel fibres (HF) can significantly increase the toughness of UHPFRC to about 35  $N\dot{m}$ , based on JSCE SF-4. Therefore, based on the different requirements (good workability, high mechanical properties or large toughness) from the practice, different fibre types and hybridization design should be well chosen, which could ensure the efficient use of the fibres and make UHPFRC more sustainable. In this research, to design a protective UHPFRC with relatively high energy absorption capacity, the hook ended fibres (HF) should be a good candidate.

In general, based on the obtained experimental results presented in Chapters 3-5, it is possible to produce a sustainable UHPFRC with low binder amount and efficient steel fibres use.

## Chapter 6

### Development of UHPFRC with waste bottom ash (WBA)

#### 6.1 Introduction

As described in the previous chapters, the sustainability of UHPFRC is important to widen its application in practice, since the cement production is said to represent 7% of the total anthropogenic CO<sub>2</sub> emissions (Capros et al., 2001; UNSTATS, 2010; Friedlingstein et al., 2010) and a large amount of cement is normally used in the production of UHPFRC. Although, compared to traditional concrete structures, the constructions made with UHPFRC can be much more slender, which means the total concrete amount can be reduced so the overall CO<sub>2</sub> footprint of the structure can be lower, UHPFRC is still a type of building material with high materials consumption, high energy consumption and high CO<sub>2</sub> emissions. To achieve the goal of sustainable development for UHPFRC, Chapters 3-5 provide some suitable methods: 1) reduction of the binder amount based on optimized particle packing; 2) efficient utilization of powders; 3) efficient utilization of steel fibres. The obtained experimental results show that based on the modified A&A model, appropriate addition of mineral admixtures and efficient hybridization design of steel fibres, it is possible to produce a UHPFRC with low binder amount and low CO<sub>2</sub> emissions. Nevertheless, it is still a fact that the production of UHPFRC requires costly materials. The limited available resource and the high cost constrain its application in modern construction industry, especially in developing countries, which give a motivation of searching for alternative materials or even suitable waste materials to substitute expensive UHPFRC ingredients with similar functions.

In the available literature, some waste/recycled materials have already been used in the production of UHPFRC. For example, Tuan et al. (2011a and 2011b) developed an Ultra-High Performance Concrete (UHPC) incorporating rice husk ash (RHA). Due to the fact that the RHA and silica fume have a similar chemical composition and a very high specific surface, the RHA can be used to replace silica fume, without sacrificing mechanical properties. From the investigation of Yang et al. (2009), recycled glass cullet and two types of local natural sand are examined as replacement materials for the more expensive silica sand normally used to produce UHPFRC. The experimental results show that the use of recycled glass cullet gives approximately 15% lowers performance, i.e. flexural strength, compressive strength and fracture energy. Moreover, the ultrafine palm oil fuel ash is also included in the design of UHPFRC (Aldahdooh et al., 2013). The results show that the ultrafine palm oil fuel ash is an efficient pozzolanic mineral

admixture, and the compressive strength, bending tensile strength and direct tensile strength of the developed UHPFRC are 158.3 MPa, 46.7 MPa and 13.8 MPa, respectively. In general, it is important and possible to include some suitable waste/recycled materials in the production of UHPFRC.

Waste bottom ash (WBA) is one of the by-products of municipal solid waste incineration (MSWI), which can be described as heterogeneous particles consisting of glass, magnetic and paramagnetic metals, minerals, synthetic and natural ceramics, and unburned matter (Chimenos et al., 1999). According to the European Landfill Directive (1999), the weathered WBA is considered suitable for land filling or reuse. However, considering the high amount of MSWI residue produced all over the world, European governments encourage the reuse of WBA as a secondary building material ingredient both to prevent the use of non-renewable natural gravels and to avoid excessive land filling (Forteza et al., 2004). The most widespread practice is the reuse of WBA as an aggregate substitute for road base (Izquierdo et al., 2001; Forteza et al., 2004), which is subject to strict requirements that are defined by each country individually, for example, the Spanish specifications for road construction (Ministerial Order PG-3, 2004). Another important way of application of WBA is as an aggregate for concrete (Lee et al., 2010; Kim and Lee, 2011b; Kim et al., 2012). Nevertheless, due to the fact that there is metallic aluminium in WBA, which can react in alkaline solution and generate hydrogen (Pera et al., 1997; Müller and Rübner, 2006; Qiao et al., 2008), many cracks can be generated in the concrete and its mechanical properties could be reduced. To solve this problem, one of the promising methods is inclusion of fibres, which may effectively restrict the growth of cracks and improve the properties of concrete.

Based on the available literature, the fibres can effectively bridge the cracks generated in concrete (Grünewald, 2004; Markovic, 2006). Especially in the hybrid fibres system, short fibres can bridge the micro-cracks while the long fibres are more efficient in preventing the development of macro-cracks (Markovic, 2006). Additionally, in the UHPFRC system, the active pozzolanic materials are commonly utilized, which can effectively improve the interface transition zone between the concrete matrix and fibres and enhance the properties of concrete (Li et al., 2004; Pan et al., 2008; Nazari and Riahi, 2011). Hence, it may be a good proposal to apply the WBA in sustainable UHPFRC production.

Taking into account the previously described advantages and disadvantages related to the use of WBA in concrete, the aim of this chapter is to assess the viability of the application of WBA in UHPFRC. The design of the concrete mixtures is based on the aim to achieve a densely compacted cementitious matrix, employing the modified A&A model. The nanosilica (nS), long straight fibres (LSF) and polypropylene fibres (PPF) are included in the concrete design, and their multiple effects on the properties (especially the mechanical characteristics) of the UHPFRC with WBA are investigated. Techniques, like

SEM and isothermal calorimetry, are further employed to evaluate the micro-morphology of WBA and the hydration process of binders with WBA.

## 6.2 Materials and methodologies

### 6.2.1 Materials and mix design

The cement, nanosilica, limestone powder and superplasticizer used here are the same as that described in Section 4.2.2. In addition, three types of aggregates are utilized in this chapter: 1) normal sand with the fractions of 0-2 mm; 2) microsand with the fraction 0-1 mm and 3) waste bottom ash (0-2 mm) (WBA). The waste bottom ash (WBA) used here is obtained from a local municipal solid waste incineration (MSWI) plant. The detailed information of the used ingredients for the production of UHPFRC can be found in Section 2.2. Additionally, two types of fibres are utilized (as shown in Figure 2.8): one is long straight fibres (LSF) and the other one is a short polypropylene fibres (PPF).

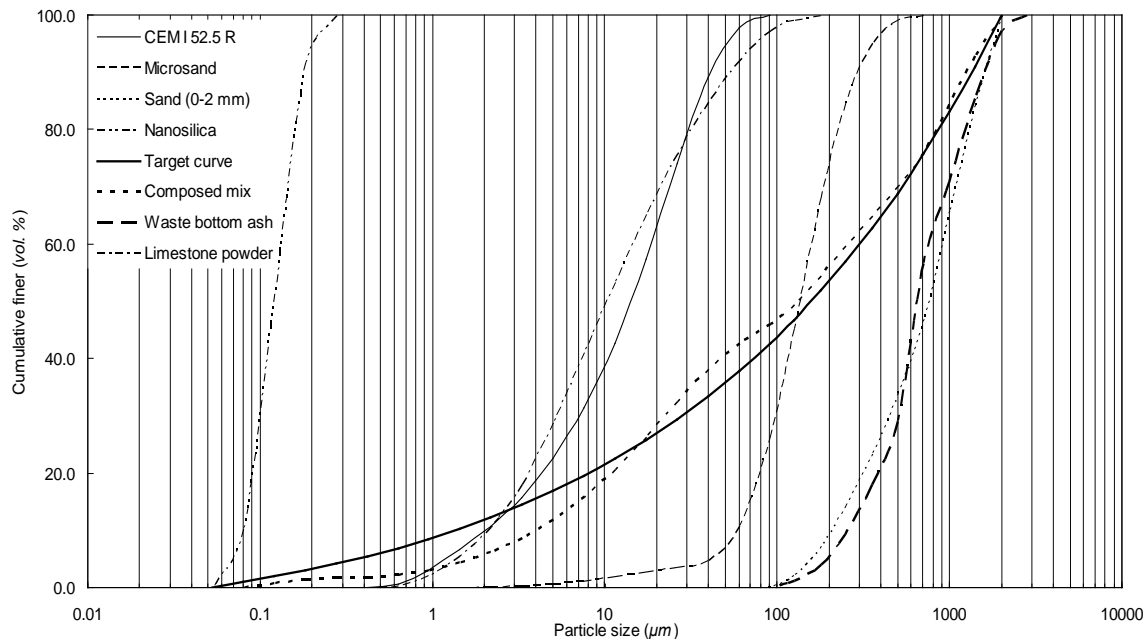


**Figure 6.1: PSDs of the involved ingredients, the target and optimized grading curves of the developed UHPFRC with WBA**

After comparing the used WBA and sand (0-2) (shown in Section 2.2.2), it can be summarized that the utilized WBA has similar density and particle size distribution as that of sand (0-2), which implies that the particle packing of the granular skeleton could be only slightly influenced when the sand (0-2 mm) is partially replaced by WBA. Therefore, in this study, the WBA is included in the design of UHPFRC by partially replacing sand (0-2 mm). However, due to the influence of heat treatment, the WBA has

a much rougher surface than sand (0-2), and the metallic aluminium in WBA may cause negative effect on the properties of concrete with WBA.

**Table 6.1: Recipes of the developed UHPFRC with waste bottom ash (WBA)**

No.	OPC kg/m <sup>3</sup>	LP kg/m <sup>3</sup>	MS kg/m <sup>3</sup>	S kg/m <sup>3</sup>	WBA kg/m <sup>3</sup>	nS kg/m <sup>3</sup>	W kg/m <sup>3</sup>	SP kg/m <sup>3</sup>	LSF vol. %	PPF vol. %
1	612.4	262.5	218.7	843.8	210.9	0	201.2	45.9	0	0
2	612.4	262.5	218.7	843.8	210.9	0	201.2	45.9	0	0.1
3	612.4	262.5	218.7	843.8	210.9	0	201.2	45.9	0	0.2
4	612.4	262.5	218.7	843.8	210.9	0	201.2	45.9	0	0.3
5	612.4	262.5	218.7	843.8	210.9	0	201.2	45.9	0	0.4
6	600.2	262.5	218.7	843.8	210.9	12.2	201.2	45.9	0	0
7	600.2	262.5	218.7	843.8	210.9	12.2	201.2	45.9	0	0.1
8	600.2	262.5	218.7	843.8	210.9	12.2	201.2	45.9	0	0.2
9	600.2	262.5	218.7	843.8	210.9	12.2	201.2	45.9	0	0.3
10	600.2	262.5	218.7	843.8	210.9	12.2	201.2	45.9	0	0.4
11	588.0	262.5	218.7	843.8	210.9	24.4	201.2	45.9	0	0
12	588.0	262.5	218.7	843.8	210.9	24.4	201.2	45.9	0	0.1
13	588.0	262.5	218.7	843.8	210.9	24.4	201.2	45.9	0	0.2
14	588.0	262.5	218.7	843.8	210.9	24.4	201.2	45.9	0	0.3
15	588.0	262.5	218.7	843.8	210.9	24.4	201.2	45.9	0	0.4
16	612.4	262.5	218.7	843.8	210.9	0	201.2	45.9	2	0
17	612.4	262.5	218.7	843.8	210.9	0	201.2	45.9	2	0.1
18	612.4	262.5	218.7	843.8	210.9	0	201.2	45.9	2	0.2
19	612.4	262.5	218.7	843.8	210.9	0	201.2	45.9	2	0.3
20	612.4	262.5	218.7	843.8	210.9	0	201.2	45.9	2	0.4
21	600.2	262.5	218.7	843.8	210.9	12.2	201.2	45.9	2	0
22	600.2	262.5	218.7	843.8	210.9	12.2	201.2	45.9	2	0.1
23	600.2	262.5	218.7	843.8	210.9	12.2	201.2	45.9	2	0.2
24	600.2	262.5	218.7	843.8	210.9	12.2	201.2	45.9	2	0.3
25	600.2	262.5	218.7	843.8	210.9	12.2	201.2	45.9	2	0.4
26	588.0	262.5	218.7	843.8	210.9	24.4	201.2	45.9	2	0
27	588.0	262.5	218.7	843.8	210.9	24.4	201.2	45.9	2	0.1
28	588.0	262.5	218.7	843.8	210.9	24.4	201.2	45.9	2	0.2
29	588.0	262.5	218.7	843.8	210.9	24.4	201.2	45.9	2	0.3
30	588.0	262.5	218.7	843.8	210.9	24.4	201.2	45.9	2	0.4
Ref	588.0	262.5	218.7	1054.7	0	0	201.2	45.9	0	0

(OPC: Ordinary Portland Cement (CEM I 52.5 R), LP: limestone powder, MS: microsand, S: sand (0-2), WBA: waste bottom ash, nS: nanosilica, W: water, SP: superplasticizer, LSF: long straight fibres, PPF: polypropylene fibres, Ref: reference sample)

The UHPFRC mixtures developed based on the optimized particle packing model are listed in Table 6.1. In total, 30 compositions of UHPFRC are designed in this study. Due to the fact that at about 30% normal aggregates (0–2 mm) replacement with WBA, the

workability of the developed concrete is very poor, the WBA is utilized to replace about 20% of the normal aggregate in this study. Moreover, the nanosilica is added in the amount of 0-4% of the total binder amount. One example of the resulting integral grading curve of the composed mix is shown in Figure 6.1. Additionally, according to the literature (Grünewald, 2004; Markovic, 2006; Yang et al., 2009; Toledo Filho et al., 2012; Tayeh et al., 2012), the content of steel fibre in fibre reinforced concrete often amounts to around 2% (by volume of the concrete), and the polymer fibre content is less than 0.5% (by volume of the concrete). Hence, in this study, the steel and polypropylene fibres amount is 2% and 0.1–0.4% (vol.), respectively. Therefore, by analysing the properties of the developed UHPFRCs, it is possible to evaluate the multiple effects of nanosilica and hybrid fibres on the properties of the UHPFRC with WBA.

## 6.2.2 Experimental methodologies

### · *Employed mixing procedure*

The detailed information on the adopted procedures for the production of UHPFRC with WBA is shown in Figure 6.2. Due to the inclusion of the WBA and the low water / binder ratio, the mixing time for UHPFRC is relatively long (about 12 mins), which is different from that shown in Figure 3.2. Moreover, mixing is always executed under laboratory conditions with dried and tempered aggregates and powder materials. The room temperature while mixing and testing is constant at around 21 °C.

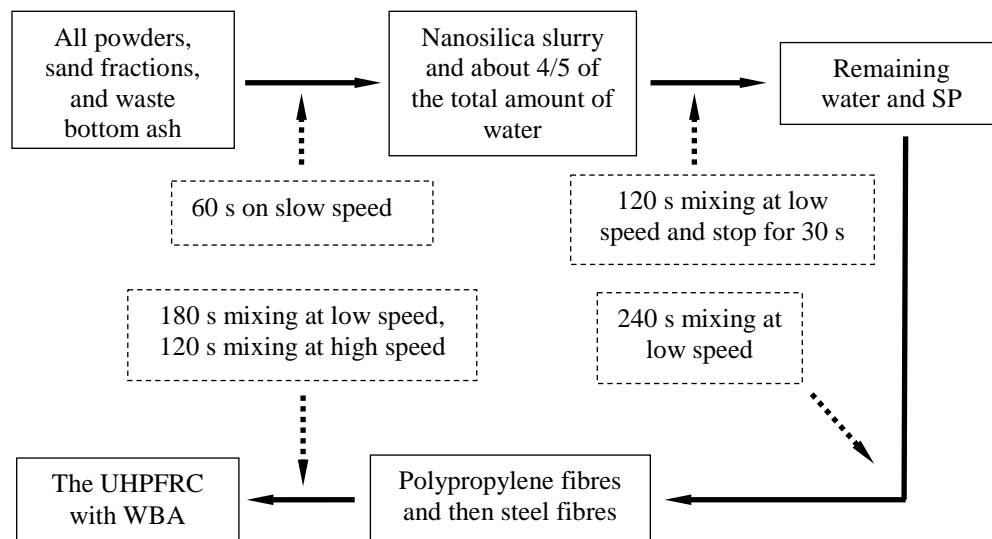


**Figure 6.2: Detailed information of the mixing procedure adopted for the production of UHPFRC with waste bottom ash (WBA)**

### · *Fresh behaviour of the UHPFRC with WBA*

The fresh state behaviour of the UHPFRC with WBA is evaluated following the method shown in Section 2.3.1. The Hägermann cone is again utilized in the tests.

- **Water-permeable porosity**

The water-permeable porosity of the UHPFRC with WBA in hardened state is measured following the method shown in Section 2.3.3.

- **Mechanical properties**

After performing the workability test, the fresh UHPFRC is cast in moulds with the size of 40 mm × 40 mm × 160 mm and compacted on a vibrating table. The prisms are demolded approximately 24 h after casting and subsequently cured in water at about 21 °C. After curing for 28 days, the samples are tested under three-point loading using displacement control and using a testing machine controlled by an external displacement transducer, such that the mid-span deflection rate of the prism specimen is held constant throughout the test. The specimen mid-span deflection rate is 0.10 mm/min, with a span of 100 mm. Afterwards, the compressive strength of UHPFRC samples is tested according to EN-196-1 (2005). During the testing, at least three samples are tested for each batch.

- **Hydration kinetics**

To clarify the effect of WBA and nanosilica on the hydration of cement, the heat flow calorimetry test is employed in this study. The recipes of the test samples are shown in Table 6.2. Before the testing, the samples are mixed for two minutes and then transferred into a sealed glass ampoule, which is then placed into the isothermal calorimeter (TAM Air, Thermometric). The instrument is set to a temperature of 20 °C. After 7 days, the measurement is stopped and the obtained data is analysed. All results are ensured by double measurements (two-fold samples).

**Table 6.2: Recipes of the samples for the isothermal calorimetry analysis**

No.	OPC kg/m <sup>3</sup>	LP kg/m <sup>3</sup>	MS kg/m <sup>3</sup>	S kg/m <sup>3</sup>	WBA kg/m <sup>3</sup>	nS kg/m <sup>3</sup>	W kg/m <sup>3</sup>	SP kg/m <sup>3</sup>
1	612.4	262.5	218.7	1054.7	0	0	201.2	45.9
2	612.4	262.5	218.7	843.8	210.9	0	201.2	45.9
3	600.2	262.5	218.7	843.8	210.9	12.2	201.2	45.9
4	588.0	262.5	218.7	843.8	210.9	24.4	201.2	45.9

(OPC: Ordinary Portland Cement (CEM I 52.5 R), LP: limestone powder, MS: microsand, S: sand (0-2), WBA: waste bottom ash, nS: nanosilica, W: water, SP: superplasticizer)

- **Microscopy analysis**

In this study, the optical microscopy is used to analyse the effect of hybrid fibres on the cracks developments. After curing for 28 days, the UHPFRC specimens are cut into small fragments with the dimensions of 40 mm × 40 mm × 15 mm. The details of the sampling

procedure are illustrated in Figure 6.3. Subsequently, the samples are stored in a sealed container before the imaging.

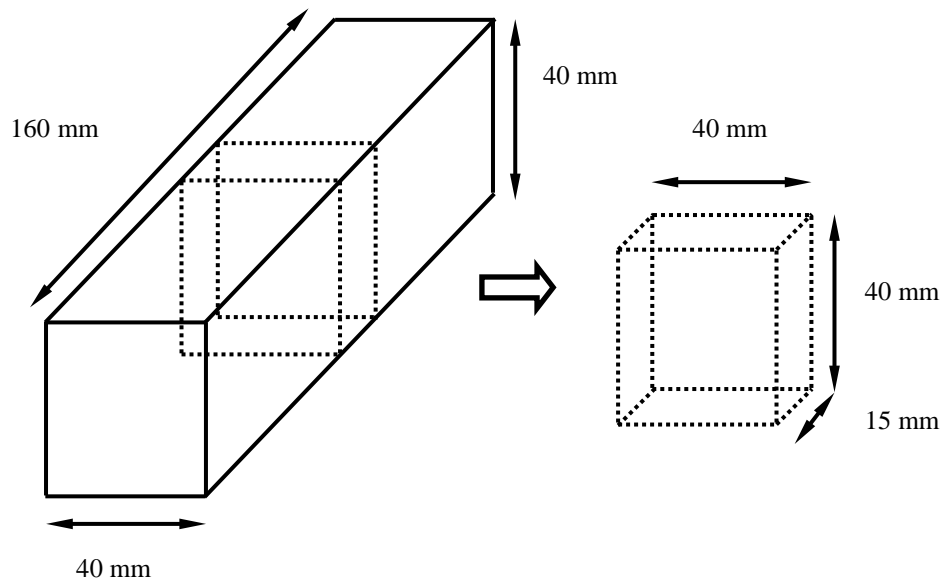


Figure 6.3: Details of the sampling for the microscopy analysis

## 6.3 Results and discussions

### 6.3.1 Fresh behaviour of the UHPFRC with WBA

In the preliminary experiments it has been found that the addition of WBA can decrease the workability of concrete. After about 20% sand is replaced by WBA, the slump flow of concrete drops from 34.5 cm to around 30.0 cm. This phenomenon can be attributed to the rough and porous surface of the WBA (as shown in Figure 2.7), which can absorb plenty of water. Furthermore, the effect of nanosilica and hybrid fibres addition on the slump flow ability of the fresh UHPFRC mixes incorporating WBA is depicted in Figure 6.4. The data illustrates the relationship between the nanosilica and hybrid fibres content and the flowability of the fresh UHPFRC. It is important to notice that with the addition of polypropylene fibres, the flowability of all the UHPFRC mixtures decreases linearly. As shown in Figure 6.4, the coefficients of determination ( $R^2$ ) of all the regression lines are all close to 1, which represent a linear trend between the polypropylene fibres amount and the slump flow of the developed UHPFRC. Moreover, the addition of nanosilica or steel fibres also reduces the workability of the UHPFRC. For instance, in the reference sample (without nanosilica and fibres), the slump flow value is about 30 cm, which drops to around 26.8 and 23.5 cm when nanosilica (2%) or steel fibre (2% vol.) are added, respectively. Eventually, the slump flow further reduces to about 22.3 cm when the nanosilica (2%) and steel fibre (2% vol.) are simultaneously added into the UHPFRC.

Additionally, when nanosilica (2%), steel fibre (2% vol.) and polypropylene fibres (0.4% vol.) are added into the UHPFRC together, the slump flow is the lowest, being about 14.8 cm.

As commonly known, the effect of fibres on the workability of concrete can be simply due to the elongated shape, influence on the particle packing and surface characteristics (Grünwald, 2004). In this study, LSF and PPF are used, which can produce higher cohesive forces between the fibres and concrete matrix and reduce the workability. Additionally, the effect of nanosilica on the flowability of concrete can be attributed to the increase of the viscosity of cement paste. Berra et al. (2012) explained that the significant water retention capacity of cement paste with nanosilica can be attributed to instantaneous interactions between nanosilica slurry and the liquid phase of cement pastes. One hypothesis proposed is that the presence of nanosilica decreases the amount of lubricating water available within the interparticle voids, which causes an increase of yield stress and plastic viscosity of concrete (Senff et al., 2009). In the present study, due to the multiple effects from nanosilica and hybrid fibres on the workability of the UHPFRC with WBA, the flowability of the sample simultaneously containing nanosilica (4%), steel fibres (2% vol.) and polypropylene fibre (0.3 or 0.4% vol.) can reduce to zero.

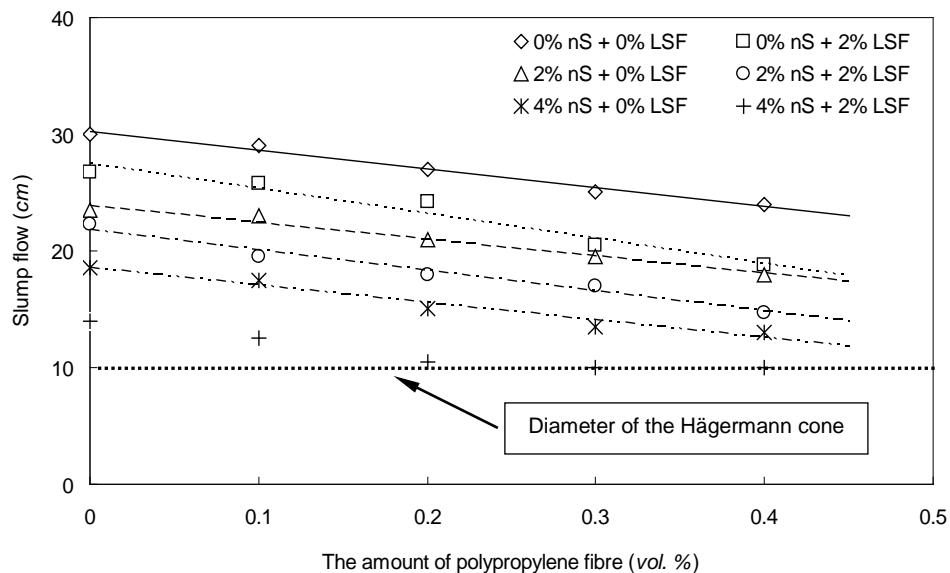


**Figure 6.4: Effect of nanosilica and hybrid fibres on the workability of the UHPFRC with waste bottom ash (WBA) (nS: nanosilica, LSF: long straight fibres)**

To summarize, in this study, after utilizing WBA to replace about 20% aggregates, the workability of the developed UHPFRC obviously decreases, compared to the one without WBA. Moreover, the addition of nanosilica, steel and polypropylene fibres can further reduce the flowability of UHPFRC with WBA. Hence, it is important to properly adjust the water and superplasticizer amounts to obtain a flowable UHPFRC with WBA.

### 6.3.2 Water-permeable porosity of the UHPFRC with WBA

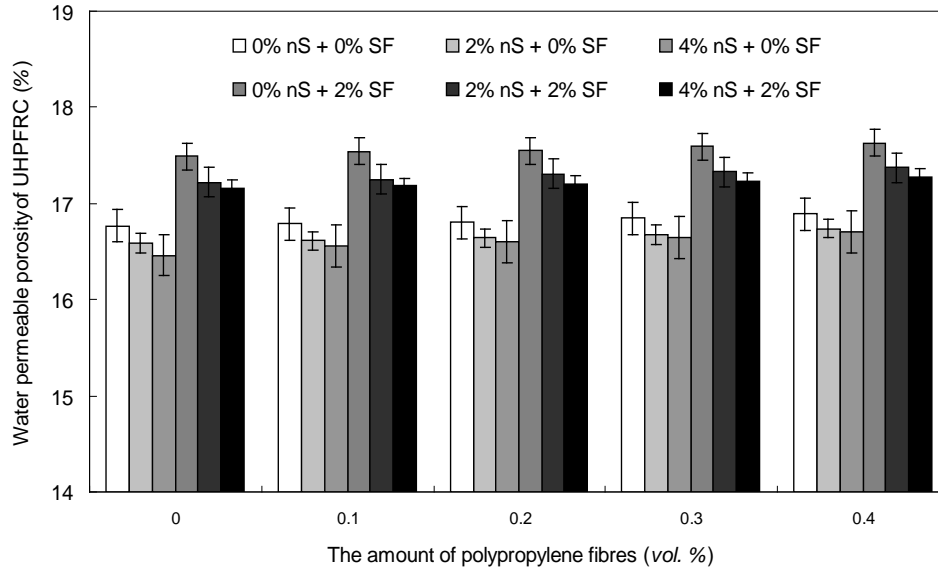


**Figure 6.5:** Effect of nanosilica and hybrid fibres on the water-permeable porosity of the UHPFRC with waste bottom ash (WBA) (nS: nanosilica, LSF: long straight fibres)

Figure 6.5 presents the effect of nanosilica and hybrid fibres on the water-permeable porosity of the UHPFRC with WBA. The water-permeable porosity of the developed UHPFRC is relatively high, with around 17% (vol.). From the preliminary experiments, it was found that the water-permeable porosity of the UHPFRC without WBA is about 10%, which means that about 7% of the water-permeable porosity can be attributed to the addition of WBA. As can be found in the literature (Pera et al., 1997; Müller and Rübner, 2006; Qiao et al., 2008), the metallic aluminium particles in WBA react in the alkaline environment in concrete and release hydrogen, which influences the microstructure development and generates cracks. Hence, in this study, due to the presence of metallic aluminium (as shown in Section 2.2.2), the water-permeable porosities of the UHPFRC are relatively high. Moreover, it can be noticed that the addition of steel fibres can significantly further increase the water-permeable porosity of the UHPFRC, while the polypropylene fibres only slightly increase the water-permeable porosity of the UHPFRC. These phenomena can be attributed to the fact that the steel fibre could change the structure of the granular skeleton, while flexible fibres fill the space between the large particles. Nevertheless, it is important to notice that the water-permeable porosity of the UHPFRC slightly decreases with the addition of nanosilica. For instance, in the samples without fibres, the addition of about 4% nanosilica can slightly reduce the water-permeable porosity of the UHPFRC from about 16.8% to 16.5%. This can be attributed to the nucleation and pozzolanic effect of nanosilica during the cement hydration. As commonly known, due to the nucleation effect, the formation of C-S-H-phase is no longer restricted on the cement grain surface alone, which causes that the hydration

degree of cement is higher and more pores can be filled by the newly generated C–S–H (Thomas et al., 2009). Therefore, the newly generated C–S–H gel can effectively fill the pores of the concrete and simultaneously decrease its water-permeable porosity.

In a short summary, the inclusion of WBA causes that the water-permeable porosity of the developed UHPFRC is relatively high. Additionally, the addition of steel and polypropylene fibres could both increase the water-permeable porosity of the concrete. However, appropriate addition of nanosilica can slightly reduce the water-permeable porosity of the concrete.

### 6.3.3 Flexural behaviour of the UHPFRC with WBA

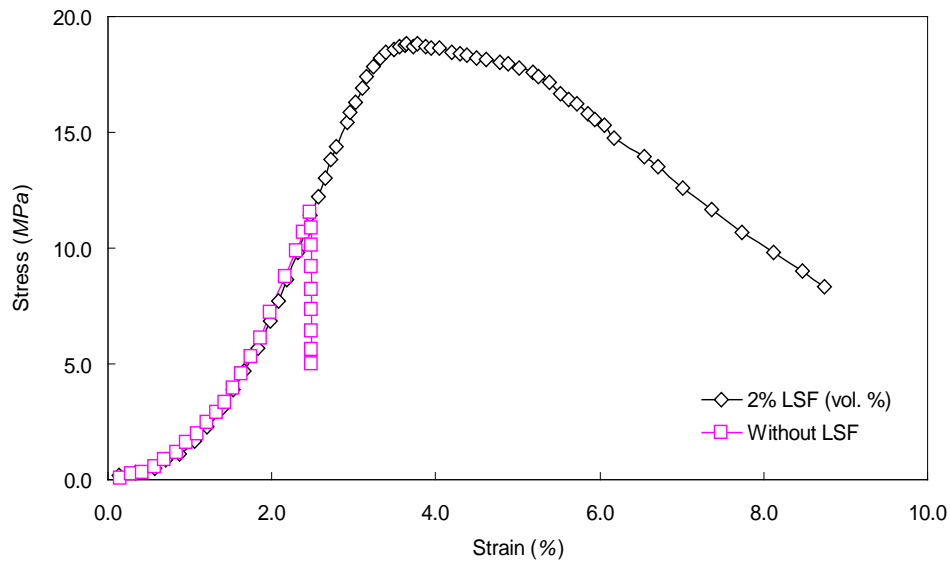
In this study, to better understand the effect of nanosilica, steel fibres and polypropylene fibres on the flexural behaviour of the UHPFRC with WBA, the 3-point flexural test is executed, and the results are compared in different groups, which are “single factor effect (single variable parameter)”, “dual factors effect (dual variable parameters)” and “triple factors effect (triple variable parameters)”, as presented in the following part.

#### · *Single factor effect*

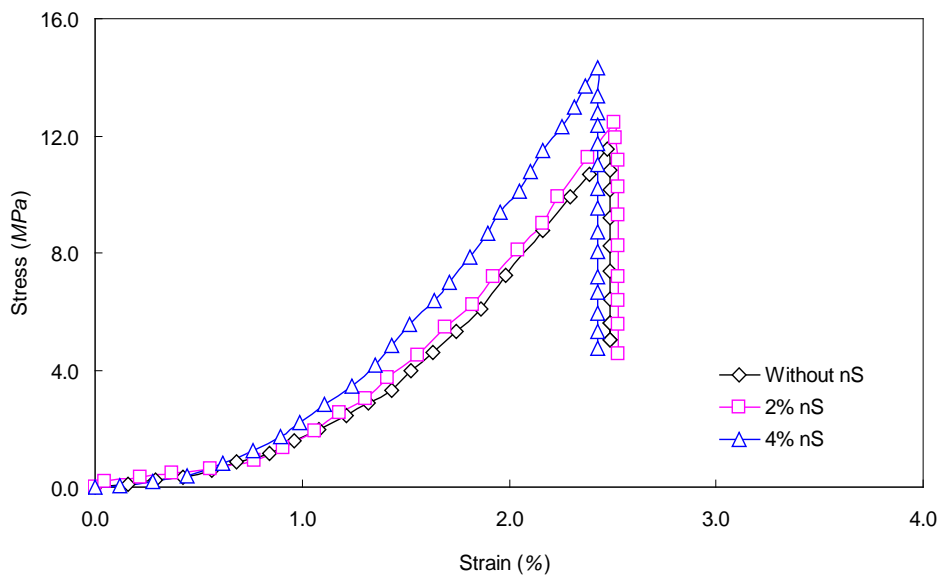
The single factor effect of steel fibres on the flexural strength of the UHPFRC with WBA is shown in Figure 6.6. Similarly to the results shown in other studies, the addition of steel fibres (2% vol.) does not only enhance the ultimate flexural strength, but also improves the energy absorption capacity of the developed UHPFRC. This can be attributed to the fact that the additional steel fibres can bridge cracks and retard their propagation, which could change the fracture mode of concrete from brittle fracture to plastic fracture and significantly increase the ultimate flexural strength of concrete (Grünwald, 2004). However, compared to the results available in the literature (El-Dieb, 2009; Tayeh et al., 2012; Hassan et al., 2012), it can also be noticed that the ultimate flexural strength of the UHPFRC (shown in Figure 6.6) is relatively smaller, which amounts to 11.6 MPa without steel fibre and 18.8 MPa with 2% steel fibre, respectively. This can be attributed to the negative influence of the additional WBA. The metallic aluminium in WBA react in the alkaline environment in concrete and release hydrogen, which may influence the microstructure development, generate cracks and increase the porosity. Though the steel fibres can retard the propagation of the macro-cracks, the development of the micro-cracks may also significantly reduce the mechanical properties.

Figure 6.7 presents the single factor effect of nanosilica on the flexural strength of the UHPFRC with WBA. It is clear that the addition of nanosilica can improve the ultimate flexural strength of the developed UHPFRC with WBA. For instance, the ultimate flexural strength of the sample with 4% nanosilica is 14.3 MPa, which is obviously larger than the one without nanosilica (11.6 MPa). This can be attributed to the nucleation and pozzolanic effect of nanosilica, as already explained in Section 6.4.2. Hence, the interface

between the matrix and aggregate could become much stronger, and the concrete strength could be simultaneously higher.



**Figure 6.6: Effect of the steel fibre (LSF) on the flexural strength of the UHPFRC with waste bottom ash (WBA)**



**Figure 6.7: Effect of the nanosilica (nS) on the flexural strength of the UHPFRC with waste bottom ash (WBA)**

The single factor effect of polypropylene fibres on the flexural strength of the UHPFRC with WBA is illustrated in Figure 6.8. Differently from the effect of steel fibre, the fracture mode of the samples with polypropylene fibres only is still a brittle fracture, as for the reference sample. Moreover, the addition of polypropylene fibres can slightly

increase the ultimate flexural strength and energy absorption capacity of the UHPFRC, which can be attributed to the fact that the polypropylene fibres have good ductility, fineness and dispersion, so they can restrain the plastic cracks (Saeid et al., 2012). Nevertheless, the elastic modulus and stiffness of polypropylene fibres are much lower than that of steel fibre, which cause that the improvement of the ultimate flexural strength and energy absorption capacity are not so obvious.

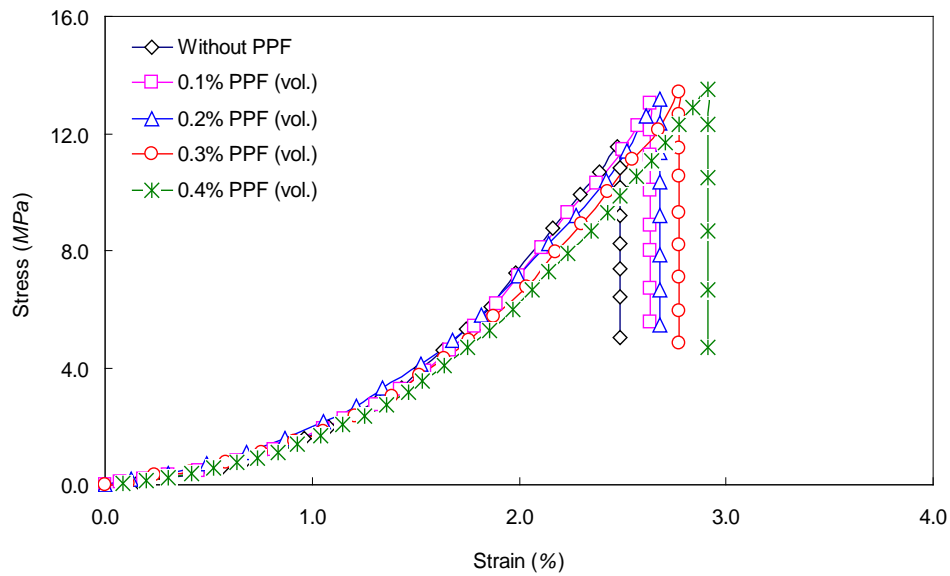


**Figure 6.8: Effect of the polypropylene fibres (PPF) on the flexural strength of the UHPFRC with waste bottom ash (WBA)**

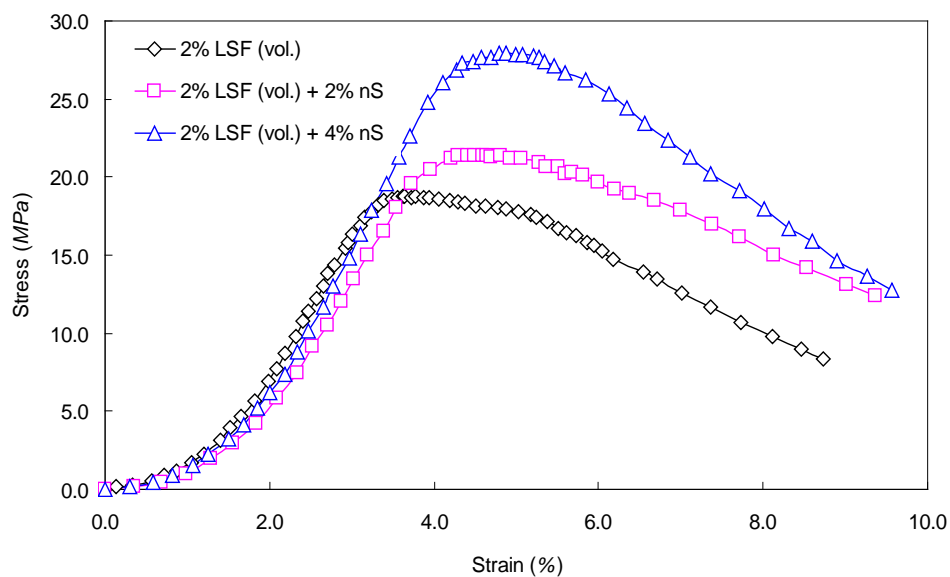


**Figure 6.9: Dual factors effect of the steel fibre (LSF) and nanosilica (nS) on the flexural strength of the UHPFRC with waste bottom ash (WBA)**

· *Dual factors effect*

Figure 6.9 shows the dual factors effect from steel fibres and nanosilica on the flexural strength of the UHPFRC with WBA. It is important to notice that the ultimate flexural strength and energy absorption capacity of the sample with both steel fibres and nanosilica are much larger than that of the reference sample. Especially for the one with steel fibre (2% vol.) and nanosilica (4%), the ultimate flexural strength is about 28 MPa. This can be attributed to the multiple effects of steel fibres and nanosilica. The nucleation effect of nanosilica in concrete can cause that the steel fibres are tightly caught by the matrix, which means more energy is needed to break the UHPFRC, and its energy absorption capacity is significantly enhanced.

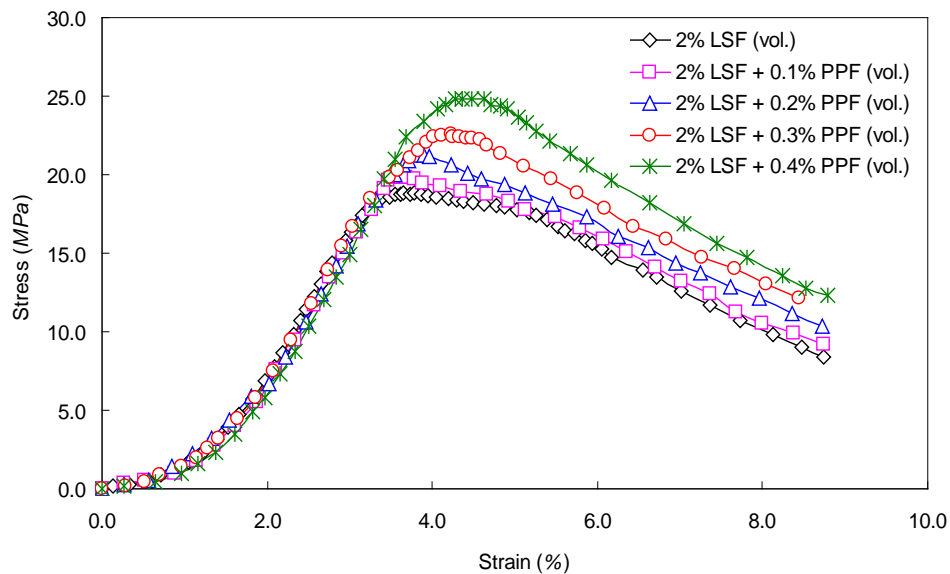
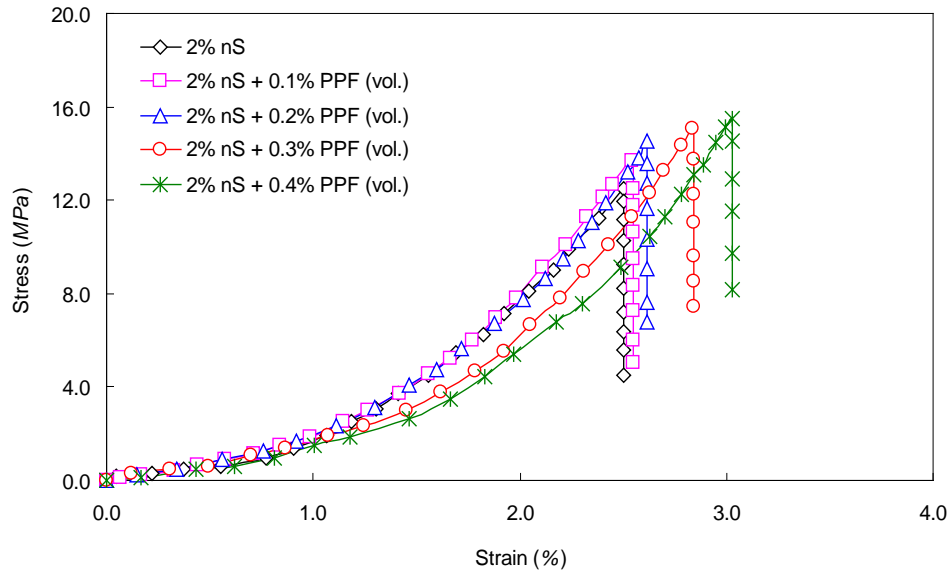


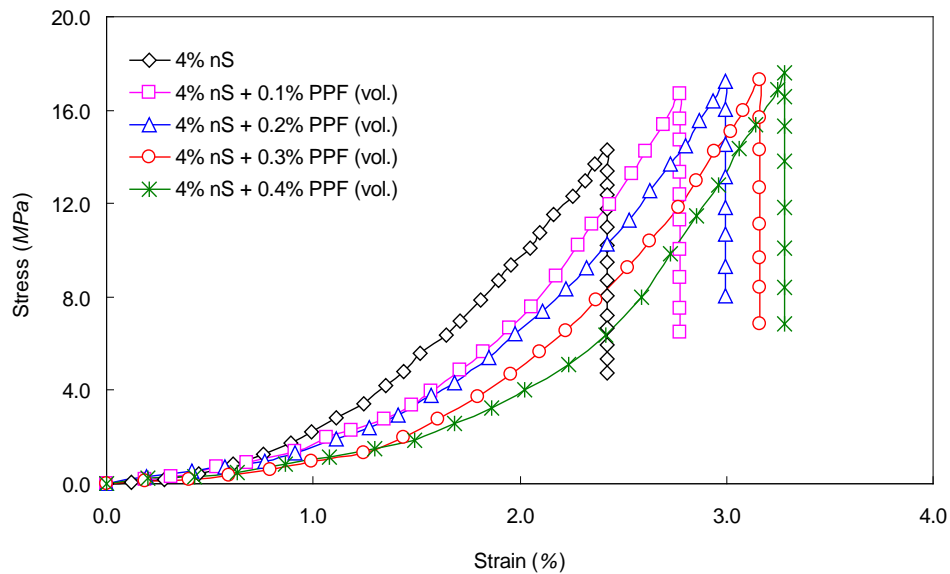
**Figure 6.10: Dual factors effect of the steel fibre (LSF) and polypropylene fibres (PPF) on the flexural strength of the UHPFRC with waste bottom ash (WBA)**

The multiple effects of steel fibres and polypropylene fibres on the flexural strength of the UHPFRC with WBA are presented in Figure 6.10. Note that the addition of polypropylene fibres can further improve the ultimate flexural strength and the energy absorption capacity of the steel fibre reinforced samples. For instance, the ultimate flexural strength of the sample with steel fibres (2% vol.) and polypropylene fibres (0.4% vol.) is about 25 MPa, which is clearly larger than the one with steel fibres only (about 19 MPa). As shown in (Grünewald, 2004; Markovic, 2006), short fibres can bridge micro-cracks more efficiently, because they are very thin and their number in concrete is much larger than that of long fibres (with the same fibre volume). Hence, when the micro-cracks are just generated in the concrete specimen, the short polypropylene fibres can effectively bridge them. As the micro-cracks grow and join into larger macro-cracks, the long straight fibres become more active in crack bridging. In this way, primarily the

ductility can be improved, and partly also the flexural strength. Long fibres can therefore provide a stable post-peak response. Short fibres will then become less active, because they are being pulled out, as the crack width increases.



(a) 2% nS addition



(b) 4% nS addition

**Figure 6.11: Dual factors effect of the nanosilica (nS) and polypropylene fibres (PPF) on the flexural strength of the UHPFRC with waste bottom ash (WBA)**

However, a simultaneous inclusion of nanosilica and polypropylene fibres in the UHPFRC with WBA cannot effectively enhance its flexural strength, which is illustrated

in Figure 6.11. The fracture mode of all the tested samples is the brittle fracture mode, and the enhancement of the ultimate flexural strength is also limited. For example, the ultimate flexural strength of the sample with nanosilica (4%) and polypropylene fibres (0.4% vol.) is about 18 MPa, which is relatively low. This can be attributed to the fact that although the interface between the matrix and fibres is improved by the addition of nanosilica, the polypropylene fibres are still less effective in bridging the macro-cracks. Hence, it can be predicted that to obtain the UHPFRC with superior flexural strength, the steel fibres, polypropylene fibres and nanosilica should be simultaneously used.

· *Triple factors effect*

The triple factors effect from nanosilica and hybrid fibres on the flexural strength of the developed UHPFRC is depicted in Figure 6.12. Here, only four typical curves are selected and compared. It is important to notice that the ultimate flexural strength of the sample with nanosilica (4%), steel fibre (2% vol.) and polypropylene fibres (0.4% vol.) is around 32 MPa, which is comparable to that of normal UHPFRCs without any waste materials (El-Dieb, 2009; Tayeh et al., 2012; Hassan et al., 2012). This can be attributed to the multiple effects of nanosilica and hybrid fibres. The polypropylene fibres bridge the micro-cracks and the steel fibres restrict the development of the macro-cracks. Moreover, the additional nanosilica can strengthen the interface between the fibres and matrix, so more energy can be absorbed by the samples.

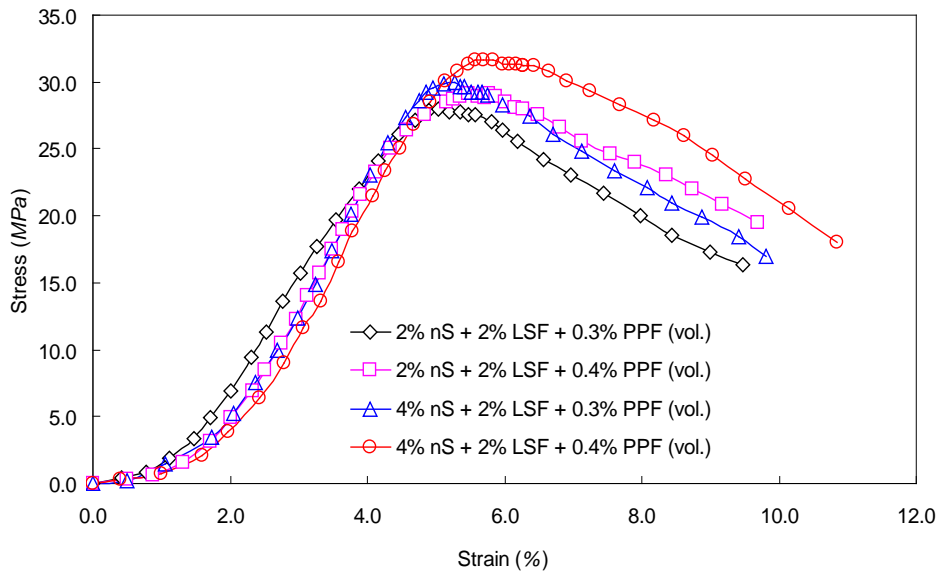


**Figure 6.12: Triple factors effect of the nanosilica (nS), steel fibres (SF) and polypropylene fibres (PPF) on the flexural strength of the UHPFRC with waste bottom ash (WBA)**

### 6.3.4 Compressive strength of the UHPFRC with WBA

The compressive strength of the developed UHPFRC with WBA is shown in Figure 6.13. As can be seen, the additional steel fibre could significantly increase the compressive strength of UHPFRC. For instance, the compressive strength of the samples without steel fibres fluctuates around 70 MPa, while the compressive strength of the steel fibre reinforced sample sharply increases to about 115 MPa. Furthermore, with an increase of the nanosilica amount, the compressive strength of the concrete slightly increases. Additionally, it can be observed that the effect of polypropylene fibres on the compressive strength is not significant. Nevertheless, it still can be noticed that the compressive strength of the developed UHPFRC is relatively lower than that of other UHPFRCs (El-Dieb, 2009; Tayeh et al., 2012; Hassan et al., 2012). This can be attributed to the following reasons: 1) the used WBA can generate hydrogen and affect the microstructure development of the concrete, which can increase the porosity and decrease the compressive strength of the concrete; 2) the quality of the used WBA is relatively poor, as it contains some impurities that have no contribution or even negative contribution to the compressive strength development.

**Table 6.3 Effect of the nanosilica (nS), steel fibre (LSF) and polypropylene fibres (PPF) on the mechanical properties of the concrete with WBA**

	WBA (%, mass)	nS (%, mass)	LSF (%, vol.)	PPF (%, vol.)	C-S (MPa)	F-S (MPa)
Ref.	0	0	0	0	75.8	10.8
1	20	0	0	0	63.3	11.6
2	20	4	0	0	69.6	14.3
3	20	0	2	0	102.9	18.8
4	20	0	0	0.4	62.9	13.5
5	20	4	2	0	113.9	27.9
6	20	4	0	0.4	67.8	17.6
7	20	0	2	0.4	101.9	24.9
8	20	4	2	0.4	112.4	31.7

(C-S: compressive strength (28 days), F-S: flexural strength (28 days), Ref.: reference sample, mass: mass fraction, vol.: volume fraction, by the volume of concrete)

A summary of the effect of nanosilica, steel fibres and polypropylene fibres on the mechanical properties of the concrete is shown in Table 6.3. It is clear that with the inclusion of the WBA in concrete, the compressive strength decreases, while the flexural strength is relatively comparable. However, a simultaneous inclusion of nanosilica, steel fibres and polypropylene fibres can significantly improve the mechanical properties of the concrete (particularly the flexural strength). Hence, the UHPFRC with WBA can be produced and utilized in applications with high flexural strength requirements.

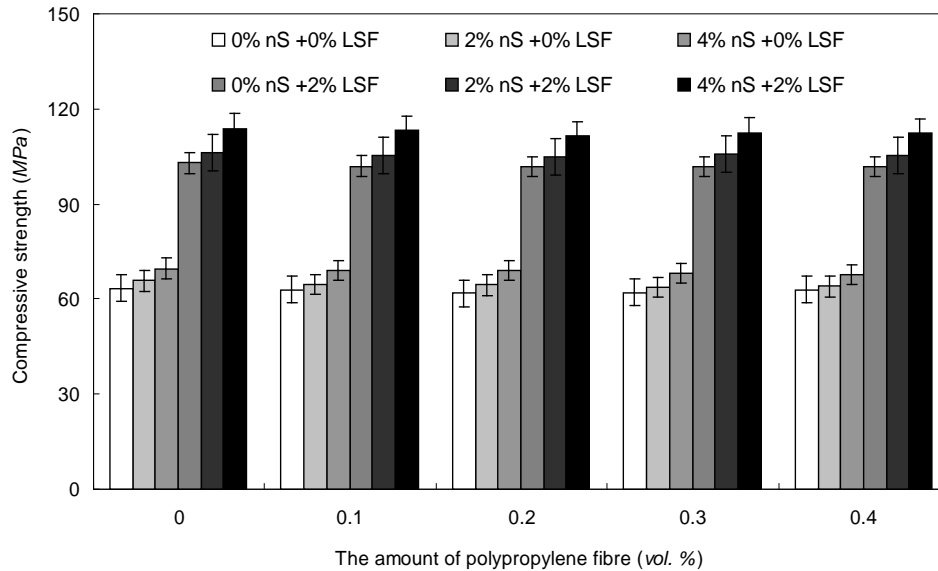


**Figure 6.13: Effect of nanosilica (nS), steel fibres (LSF) and polypropylene fibres on the compressive strength of UHPFRC with waste bottom ash (WBA) after curing for 28 days**

### 6.3.5 Hydration kinetics of cement in the UHPFRC with WBA

To clearly understand the effect of nanosilica on the properties of UHPFRC with WBA, the isothermal calorimetry is utilized to analyse its hydration process, and the results of these analyses are shown in Figure 6.14. It is apparent that with the addition of WBA, the height of the early rate peak is reduced, and the time required to reach the maximum rate is simultaneously extended. These imply that the hydration of cement is slightly retarded by the WBA, which is in line with the results presented in Giampaolo et al. (2002) and Li et al. (2012). From Table 2.5 and Figure 2.5, it can be noticed that there are many impurities in the utilized WBA, which may affect the hydration of cement. Moreover, the addition of nanosilica can significantly accelerate the cement hydration, and with the increased amount of nanosilica, the cement hydration rate simultaneously rises. Eventually, in this study, the additional nanosilica could compensate the negative influence of WBA on the hydration of cement. This phenomenon can be attributed to the nucleation and pozzolanic effect from nanosilica. After mixing, the nanoparticles are uniformly dispersed in concrete. When the hydration begins, the hydration products diffuse and envelop nanoparticles as kernels, which can promote the cement hydration and makes the cement matrix more homogeneous and compact (Jalal et al., 2012). Therefore, in this study, with the increase of nanosilica amount, more reactive kernels will be generated during the hydration, so in turn the hydration rate of cement is accelerated.

The hydration process of cement can be classified into four principle stages (Land and Stephan, 2012): 1) initial phases of dissolved substances; 2) induction period where the

C–S–H and portlandite-nucleation begins; 3) the acceleration period begins about one hour after mixing the cement with water; 4) After about three hours the reaction becomes controlled by the diffusion and the heat evolution rate starts to decrease. However, in this study, the induction and acceleration period of cement hydration are obviously longer than that for normal cement. For instance, in the sample without WBA, the induction and acceleration period are about 10 h and 15 h, respectively (see Figure 6.14). This can be attributed to the retardation influence of the superplasticizer. According to the investigation of Jansen et al. (2012), a complexation of  $\text{Ca}^{2+}$  ions (from pore solution) and polymers (from the superplasticizer) is as considerable as the absorbed polymer on the nuclei or the anhydrous grain, which in turn might lead to the prevention of the growth of the nuclei or the dissolution of the anhydrous grains. Hence, in this study, due to the fact that high amount of superplasticizer is utilized to produce the UHPFRC, the cement hydration is significantly retarded.

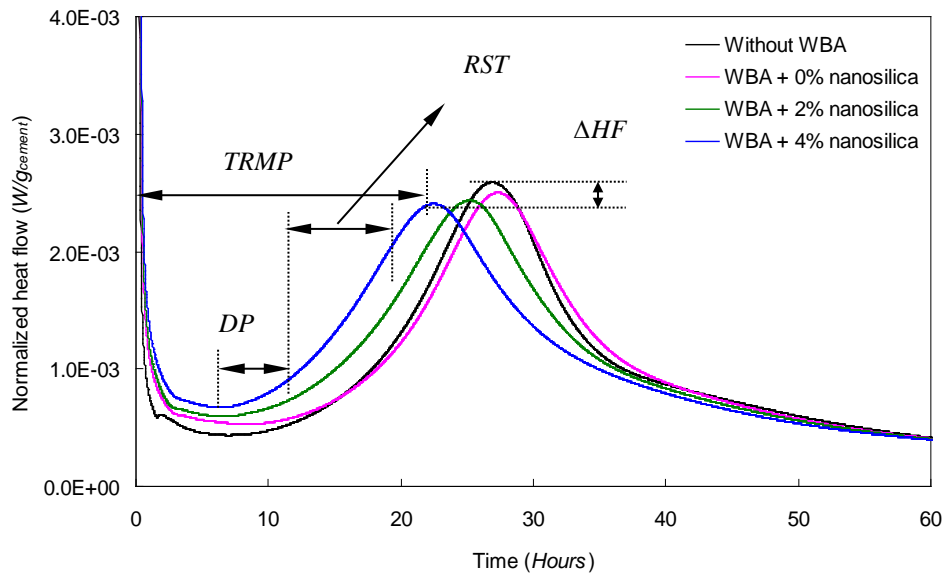


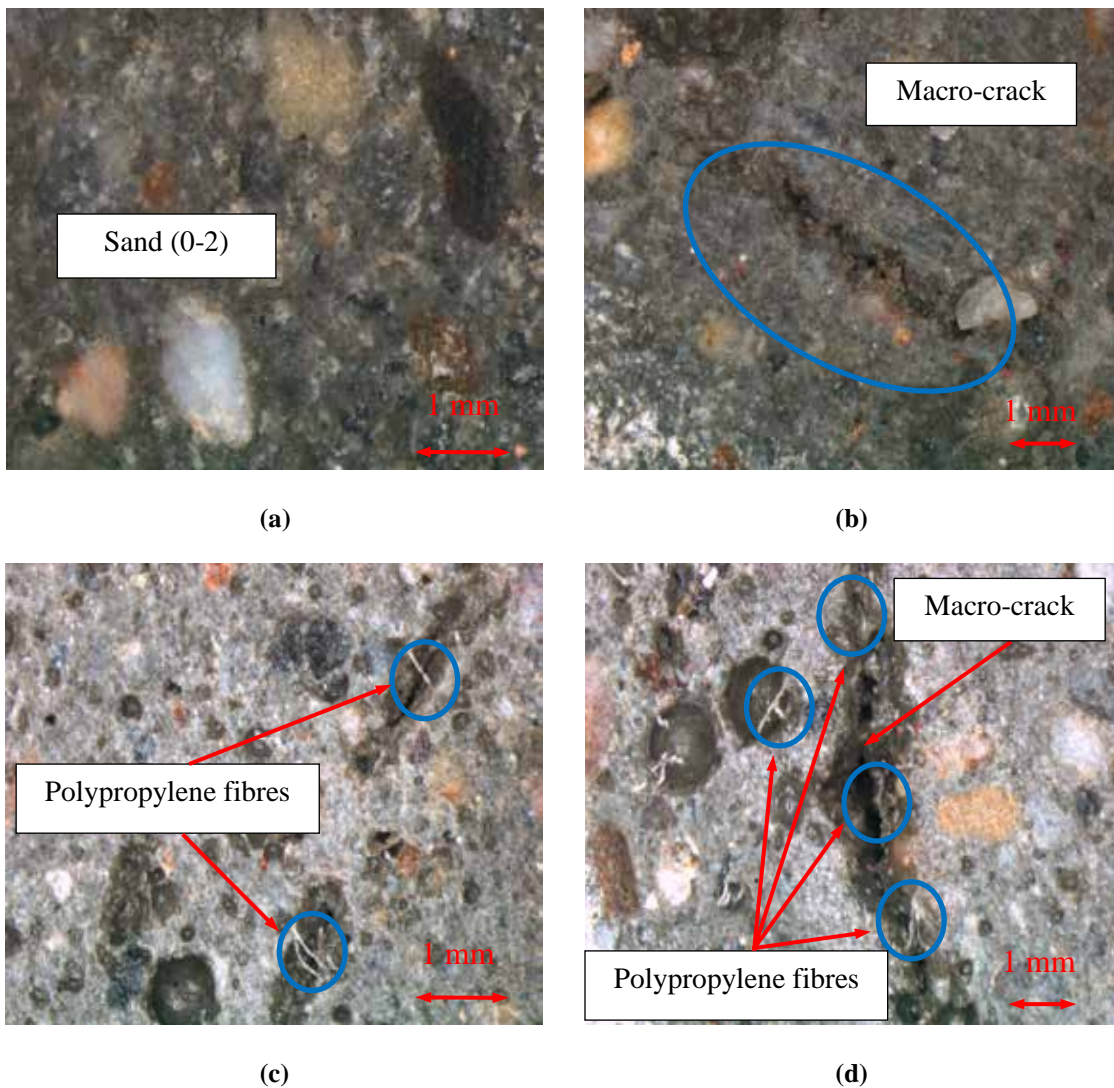
**Figure 6.14:** Calorimetry test results of the developed UHPFRC (incorporating WBA) with different amount of nanosilica (TRMP: Time to reach the maximum peak; DP: Dormant period;  $\Delta HF$ : Change in heat flow RST: Relative setting time)

### 6.3.6 Microscopy analysis of the UHPFRC with WBA

To clarify the effect of hybrid fibres on the mechanical properties of the UHPFRC with WBA, the microscopy images of the different samples are compared, which is shown in Figure 6.15.

As can be seen in Figure 6.15(a), the microstructure of the developed UHPFRC is dense and homogeneous, which can be attributed to the low water to cement ratio and the optimized particle packing. In this study, the design of UHPFRC is based on the aim to achieve a densely compacted cementitious matrix, employing the modified A&A model.

Hence, this also demonstrates that it is possible to utilize particle packing model to design UHPFRC incorporating waste materials. However, from Figure 6.15(b), a relatively long and narrow macro-crack can be observed. The length of the crack is about 4.75 mm, which is more than two times the diameter of the maximum aggregate in concrete. The generation of the macro-cracks can be attributed to the chemical reaction of the metallic aluminium particles in WBA with the alkaline solution in concrete, which generates hydrogen. Supposing that the generated hydrogen cannot timely escape from the concrete in fresh state, it will gradually produce a series of micro-cracks in the hardened concrete. With the increase and the interconnections of the micro-cracks, the visible macro-cracks could be created. Moreover, due to the fact that the distribution of the metallic aluminium particles is heterogeneous, the distribution of the visible macro-cracks is also heterogeneous. Hence, during the mechanical tests, the stresses may concentrate around the cracks and eventually reduce the mechanical properties of the UHPFRC.



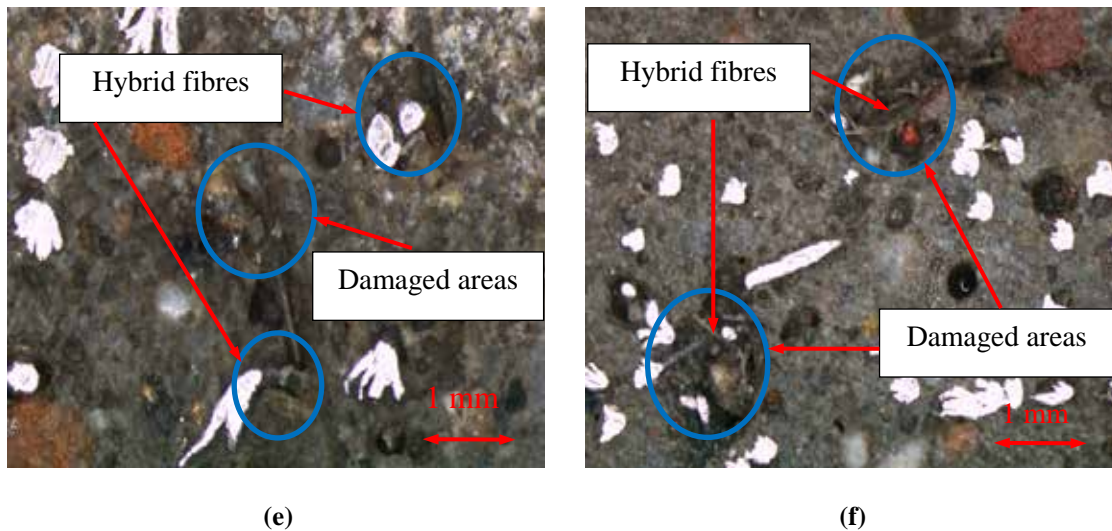


**Figure 6.15: Microscopy images of the developed UHPFRC with waste bottom ash (WBA)**

Figures 6.15(c) and (d) illustrate the microscopy images of the samples with only polypropylene fibres. As shown in Figure 6.15(d), some visible macro-cracks can still be found, and the length of the indicated crack is about 4.4 mm. Moreover, around the cracks, many polypropylene fibres can be observed, some of which even bridge the cracks. From the literature (Noumowe, 2005; Song et al., 2005a; Ramezani-pour et al., 2013), it can be stated that the polypropylene fibres can contribute to the concrete performance subjected to crack opening and slippage. Nevertheless, here, the addition of polypropylene fibres is less efficient in restricting the generation of the macro-cracks (compared to the steel fibres), which causes that the mechanical properties of the sample with only polypropylene fibres are relatively poor (Figure 6.8). This may be attributed to the following reasons: 1) the macro-cracks are created before the hardening of concrete, which means the interface between the polypropylene fibres, and the matrix is still quite weak and the fibres could not effectively bridge the cracks; 2) the size of the used polypropylene fibres in some cases is even smaller than the length of the macro-cracks, which causes that the fibres are useless in restricting the development of this type macro-cracks.

The microscopy images of the sample containing simultaneously nanosilica (4%), steel fibres (2% vol.) and polypropylene fibres (0.4% vol.) are shown in Figures 6.15(e) and (f). It is important to notice that although the mechanical properties of this sample are superior, a damaged microstructure can still be observed. Nevertheless, the damage area is much smaller than that shown in Figures 6.15(b) - (d). Furthermore, close to the damage area, many hybrid fibres can be found, and the interface between these fibres and concrete matrix is still compact and tight. As shown in Markovic (2006), in hybrid-fibre concrete, the short fibres can ‘help’ the long fibres to generate high tensile stresses. Therefore, the combining of different types of fibres in the same concrete results in better

mechanical behaviour compared to the concrete with only single sized fibres. In this study, due to the addition of hybrid fibres into the UHPFRC, the short polypropylene fibres can restrict the development of the micro-cracks and the long straight fibres could hinder the generation of the macro-cracks. Hence, the damage caused by the generated hydrogen can be minimized, and the mechanical properties of the developed UHPFRC are improved.

Consequently, based on the microscopy analysis and calorimetry test results, the multiple effect of nanosilica and hybrid fibres on the mechanical properties of the UHPFRC should be summarized as following: 1) the addition of hybrid fibres can effectively minimize the damage originating from the generated hydrogen and reduce the stress concentration under the external loading; 2) the additional nanosilica could promote the hydration of cement and improve the bond between matrix, aggregate and fibres.

## 6.4 Conclusions

This chapter presents the multiple effects of nanosilica and hybrid fibres on the properties of an Ultra-High Performance Fibre Reinforced Concrete (UHPFRC) incorporating waste bottom ash (WBA). From the results addressed in this paper the following conclusions are drawn:

- 1) By employing the modified A&A model, it is possible to utilize waste bottom ash to produce UHPFRC with a relatively low binder amount (about  $650 \text{ kg/m}^3$ ). The obtained maximum compressive and flexural strengths of the developed UHPFRC are about 115 and 32 MPa, respectively.
- 2) When using WBA to replace about 20% of conventional aggregates, the workability of the developed UHPFRC decreases. Moreover, the addition of nanosilica, steel fibres and polypropylene fibres can further reduce its flowability. Hence, it is important to properly adjust the water and superplasticizer amounts to obtain a flowable UHPFRC with WBA.
- 3) Due to the application of WBA, the water-permeable porosity of the developed UHPFRC is relatively high (about 17%). Moreover, the addition of steel and polypropylene fibres could both increase the water-permeable porosity of concrete. Nevertheless, an appropriate addition of nanosilica (around 4% by the mass of the binder) can slightly reduce the water-permeable porosity (to about 16.5 %).
- 4) The addition of WBA reduces the compressive strength of the developed concrete. However, due to the coarse surface of WBA and the threadlike stuff on its surface, the flexural strength of the developed concrete can be slightly enhanced. After the nanosilica and hybrid fibres are added into the concrete, its mechanical properties

- (particularly the flexural strength) can be significantly improved. Hence, the UHPFRC with WBA can be produced and utilized in concretes with high flexural strength requirements.
- 5) The addition of WBA can slightly retard the cement hydration. However, the small dosage of the additional nanosilica could compensate this retarding influence of WBA on the hydration rate of cement, which is attributed the nucleation effect of nanosilica.
  - 6) The microstructure development of concrete is influenced and some macro-cracks could be generated due to the addition of WBA. However, the simultaneous addition of nanosilica and hybrid fibres into the UHPFRC can effectively restrict and minimize the cracks, which causes that the mechanical properties of the developed UHPFRC with WBA could be significantly improved.

Applying WBA in UHPFRC can not only reduce the cost and environmental impact of UHPFRC, but also benefit for disposing the waste WBA, which are in line with the sustainable development of nowadays. However, due to the negative influence of the metallic aluminium in WBA, the compressive strength of the produced UHPFRC can be decreased. Therefore, the developed UHPFRC with WBA is unsuitable to be applied in the place with quite high requirements of compressive behaviour. In this research, the aim is to develop a sustainable protective UHPFRC, which implies that the produced material should be sustainable and simultaneously has great impact resistance capacity. Due to the fact that the material is under great compressive, flexural and tensile stresses during the impact process, the UHPFRC with WBA is unsuitable to be utilized to produce a protective structure. Hence, in the following chapters (Chapters 7-9), all the sustainable UHPFRC is produced based on optimized particle packing model, efficient application of powders and steel fibres.

## Chapter 7

### Performance of the sustainable UHPFRC under impact

#### 7.1 Introduction

As already mentioned in Chapter 1, high potential of energy absorption makes UHPFRC suitable for applications where high energy release rates exist. From the available literature, the blast-resistant characteristics and mechanical properties of UHPFRC under high strain rate loadings can be found. For example, Bindiganavile et al. (2002) demonstrated that UHPFRC has higher impact resistance than other types of concretes. Their impact tests were carried out with a 60 kg drop-mass, hitting a variable span beam specimen from heights of up to 2.5 m. To cover a large range of loading rates, Parant et al. (2007) employed two dynamic/impact tests using the four-point bending set-up on thin UHPFRC slabs with three quasi-static loading rates ( $3.3 \times 10^{-6}$ ,  $3.3 \times 10^{-4}$  and  $3.3 \times 10^{-3}$  s<sup>-1</sup>) and a block-bar device with a bar velocity of 5.55 m/s. Their results showed that with an increase in the strain rate, the modulus of rupture and the uniaxial tensile strength increase. Habel and Gauvreau (2008) presented an experimental and analytical study of load rate-dependent characteristics of UHPFRC. The results of this study showed a significantly increased strength and fracture energy of the dynamically loaded plates when compared to quasi-static loading. Lai and Sun (2009) studied the dynamic behaviour of UHPFRC with different steel fibre volume fractions under impact using the split Hopkinson pressure bar device. It was proven that, at high strain rates, the unreinforced specimens fracture into small parts while the fibre reinforced ones only have fine cracks on the edges. Máca et al. (2014) and Sovják et al. (2015) investigated the impact resistance of UHPFRC against bullets fired. It was experimentally verified that the optimal fibre content in the UHPFRC mixture is 2% by volume. No improvement in all damage parameters was observed when the fibre volume fraction was increased from 2% to 2.5% or 3%. Similarly to that, Wu et al. (2015) investigated the impact resistance of UHPFRC under projectile impact with the velocity of 510–1320 m/s. The experimental results confirmed that UHPFRC has excellent projectile impact resistance, such as reducing the depth of penetration and the crater dimensions of the rigid projectile, as well as defeating the structure and deviating the terminal ballistic trajectory of the abrasive projectile. Nevertheless, to the author's knowledge, the research focusing on dynamic performance of the sustainable UHPFRC is scarce, since the energy dissipation capacity results obtained from the literature are derived from the UHPFRC produced with a large amount of cement or binders. Therefore, it remains unclear whether the developed sustainable UHPFRC would be suitable for utilization in protective structures.

Consequently, based on these premises mentioned above, the main objective of this chapter is to evaluate the performance of the developed sustainable UHPFRC under impact loadings, including experimental studies and modeling analysis. In addition, to efficiently apply the steel fibres in the construction of protective structures, the effect of different fibres on the impact resistance of the sustainable UHPFRC is also investigated. According to the results obtained in previous chapters, the design of the sustainable UHPFRC matrix is based on the modified A&A model.

## 7.2 Background of concrete under impact loadings

### 7.2.1 Effect of loading rates on the dynamic behaviour of concrete

In the available literature it can be found that numerous tests have been conducted over the past century to explore the dynamic compressive behaviour of concrete-like materials (Bischoff and Perry, 1991; Cotsovos and Pavlovic, 2008). During impact loadings (the strain rate at about  $10\text{s}^{-1}$ ), the dynamic compressive strength of concrete has been found to be as much as 85-100% greater than its static strength. However, there is a wide variation in the test results of the dynamic strength, which becomes even greater as the strain rate increases. Today, it is generally accepted that the “dynamic increase factor” (*DIF*), defined by the ratio of the dynamic strength to the quasi-static strength in uniaxial compression, has an apparent increasing trend with the increase of the strain rate. Based on experimental results, some typical empirical formulae were proposed. The most comprehensive model for predicting the strain rate enhancement of concrete-like materials is presented by CEB Model Code (2010):

$$DIF = \frac{f_{cd}}{f_{cs}} = \frac{\dot{\epsilon}\epsilon' \dot{\epsilon}' \dot{\epsilon}'^{1.026\alpha_s}}{\dot{\epsilon}\epsilon_s \dot{\epsilon}' \dot{\epsilon}'^{1.026\alpha_s}} \quad (\epsilon' < 30\text{s}^{-1}) \quad (7.1)$$

and

$$DIF = \gamma_s \frac{\dot{\epsilon}\epsilon' \dot{\epsilon}'^{1/3}}{\dot{\epsilon}\epsilon_s \dot{\epsilon}' \dot{\epsilon}'^{1/3}} \quad (\epsilon' > 30\text{s}^{-1}) \quad (7.2)$$

where  $f_{cs}$  and  $f_{cd}$  are the unconfined uniaxial compressive strength in quasi-static and dynamic loading (MPa), respectively.  $\epsilon'$  and  $\epsilon'_s$  are the dynamic strain rate and quasi-static strain rate ( $\text{s}^{-1}$ ), respectively. Additionally,  $\gamma_s = 10^{(6.156 \alpha_s - 2.0)}$ ,  $\alpha_s = 1/(5+9f_{cs}/f_{co})$ ,  $f_{co} = 10$  MPa and  $\epsilon'_s = 30 \times 10^{-6} \text{s}^{-1}$ .

A series of tests have been conducted by Ross et al. (1989; 1995; 1996) and Tedesco and Ross (1998) using Split Hopkinson Pressure Bar (SHPB) test for different concrete strengths, moistures and strain rates. Based on the obtained experimental results, a *DIF* regression equation was suggested as follows (Tedesco and Ross, 1998):

$$DIF = 0.00965 \log \varepsilon' + 1.058 \varepsilon'^3 - 1.0 \quad (\varepsilon' < 63.1 \text{ s}^{-1}) \quad (7.3)$$

and

$$DIF = 0.758 \log \varepsilon' + 1.058 \varepsilon'^2 - 2.5 \quad (\varepsilon' > 63.1 \text{ s}^{-1}) \quad (7.4)$$

in which the transition point from a low strain rate sensitivity to a high sensitivity occurs at  $63.1 \text{ s}^{-1}$ .

More recently, Grote et al. (2001) tested mortar using the SHPB with the range of strain rates from 250 to 1700  $\text{s}^{-1}$ . A sharp increase in *DIF* was observed at strain rates around  $10^2 \text{ s}^{-1}$ . The following formulae were suggested to define the dependence of *DIF* on strain rate (Grote et al., 2001):

$$DIF = 0.0235 \log \varepsilon' + 1.07 \quad (\varepsilon' < 266.0 \text{ s}^{-1}) \quad (7.5)$$

and

$$DIF = 0.882 (\log \varepsilon')^3 - 4.4 (\log \varepsilon')^2 + 7.22 (\log \varepsilon') - 2.64 \quad (\varepsilon' > 266.0 \text{ s}^{-1}) \quad (7.6)$$

Besides the dynamic compressive strength loading, the dynamic tensile loading case is also very common in the service life of concrete-like materials. In the analysis of concrete structures subjected to impact loading, both concrete and steel are subjected to very high strain rates in the range of  $10 \text{ s}^{-1}$  to  $1000 \text{ s}^{-1}$ . At these high strain rates the apparent strength of these materials can increase significantly, by more than 600 percent for concrete in tension (Mellinger and Birkimer, 1966; Birkimer, 1968; Birkimer and Lindemann, 1971; Mcvay, 1988). Several sets of data are available for the strain rates in the range of  $1 \text{ s}^{-1}$  to  $200 \text{ s}^{-1}$  in tension (Malvar and Ross, 1998). At present, the most comprehensive model for strain rate enhancement of concrete in tension is also presented by the CEB Model Code (2010). The dynamic increase factor (*DIF*) of the tensile strength, is given by:

$$DIF = \frac{f_t}{f_{ts}} = \frac{\dot{\varepsilon}_{\varepsilon'} \dot{\varepsilon}'^{1.016\delta}}{\dot{\varepsilon}_{\varepsilon_s} \dot{\varepsilon}'_s} \quad (\varepsilon' < 30 \text{ s}^{-1}) \quad (7.7)$$

and

$$DIF = \frac{f_t}{f_{ts}} = \beta \frac{\dot{\varepsilon}_{\varepsilon'} \dot{\varepsilon}'^{1/3}}{\dot{\varepsilon}_{\varepsilon_s} \dot{\varepsilon}'_s} \quad (\varepsilon' > 30 \text{ s}^{-1}) \quad (7.8)$$

where  $f_t$  is the dynamic tensile strength (MPa) at  $\varepsilon'$  ( $\text{s}^{-1}$ ),  $f_{ts}$  is static tensile strength (MPa) at  $\varepsilon'_s$  ( $\text{s}^{-1}$ ),  $\varepsilon'$  is the strain rate in the range of  $3 \times 10^{-6}$  to  $300 \text{ s}^{-1}$ ,  $\varepsilon'_s$  is static strain rate ( $3 \times 10^{-6} \text{ s}^{-1}$ ),  $\log \beta = 7.11\delta - 2.33$ ,  $\delta = 1/(10 + 6f_{cs}/f_{co})$  and  $f_{co}' = 10 \text{ MPa}$ .

Although a large number of experiments have been done to investigate the *DIF* and some empirical formulae (Eqs. 7.1-7.8) are proposed to represent the *DIF* of concrete, the physical mechanisms controlling the strain rate effect on *DIF* of concrete are not yet fully understood. It is still unclear whether the tensile strength enhancement of concrete with increasing strain rate is intrinsic (only attributed to the strain rate effect) or it involves “structural” influences (e.g. inertia and stress).

### 7.2.2 Dynamic behaviour of internal structure of concrete

During the last decades, the development of advanced and effective investigation techniques has already demonstrated that the atomic level (nano and micro) properties of concrete have a profound effect upon its macro-level properties (Monteiro et al., 2009). Therefore, it is important to investigate the dynamic behaviour of concrete internal structure during the impact process, which may be helpful for clarifying the intrinsic effect of strain rate on concrete. However, the influence of external impact on the internal structure of concrete, and the mechanisms which cause different crack and failure patterns when varying the loading rate, remain open questions (Georgin and Reynouard, 2003). It is still an essential and challenging task for the concrete technologist to establish the relationship between the micro structure and macro properties of concrete under impact loadings.

As announced in the available literature, the presence of aggregates at the target impact face would enhance its penetration resistance. For example, Dancygier and Yankelevsky (1999) studied the effect of adding a layer of basalt aggregates, consisting of two different nominal aggregate sizes, 10 mm and 20 mm, respectively at the impact face. These concrete targets were impacted upon by sharp-nosed projectile with velocities ranging between 100 m/s and 250 m/s. At similar impact velocities, the specimens with larger sized basalt aggregates had smaller rear face damage compared to those with smaller sized basalt aggregates. This observation indicated that the use of hard and properly-sized aggregates plays a significant role in absorbing part of the projectile's kinetic energy at the beginning of the penetration process and altering its path. Similar research can also be found in Bludau et al. (2006), in which the influence of concrete composition on the impact resistance of high strength concrete (HSC) panels was investigated. The targets with thickness varying from 40 mm to 150 mm were subjected to 7.62 mm diameter ogive-nosed projectile impact at a velocity of 800 m/s. The results showed that the target impact resistance depended on the toughness and hardness of the aggregates. Specimens fabricated with harder and more ductile aggregates demonstrated better results compared to those fabricated with weaker aggregates. In addition, specimens with larger maximum aggregate sizes and those with higher fraction of large sized aggregates were observed to produce lower residual velocities of the projectile after perforation, indicating a higher energy absorption capacity. It was concluded that the maximum aggregate size and the aggregates grading curve should be designed to allow a

higher probability of the penetrating projectile striking a large aggregate particle, so as to ensure good absorption of the projectile's energy. From the investigation of Erdem et al. (2012a), the relationship between the nature of micro damage under impact loading and changes in mechanical behaviour associated with different microstructures was studied for concretes made with two different coarse aggregates. The results showed that the concrete prepared with lightweight aggregates was stronger in compression than the gravel aggregate concrete due to enhanced hydration as a result of internal curing. In addition, it was deduced that an inhomogeneous micro-structure in concrete led to strain incompatibilities and consequent localized stress concentrations in the mixture, leading to an accelerated failure. The pore structure, compressibility, and surface texture of the aggregates are of paramount importance for the micro-cracking growth. Moreover, the influence of the micro scale local mechanical properties of the interfacial transition zone (ITZ) on macro level mechanical response and impact behaviour was studied for concretes made with copper slag and gravel aggregates (Erdem et al., 2012b). It was deduced that a stronger and denser ITZ in the copper slag specimen would reduce its vulnerability to stiffness loss and contribute to its elastic and more ductile response under impact loading. The analysis also indicated that a significant degeneration in the pore structure of the gravel specimen associated with a relatively weaker and non-homogeneous ITZ occurred under impact. Finally, it was also concluded that increased roughness of ITZ may contribute to the load-carrying capacity of concrete under impact by improving contact point interactions and energy dissipation.

Nevertheless, after summarizing the findings presented in the literature, it can be noticed that some of the conclusions are contradicting to each other. For instance, some investigations suggested that large aggregates can enhance the impact resistance capacity of concrete, while other researchers demonstrated that the homogeneous microstructure of concrete is the most important factor in designing impact resistant concrete, in which the content of large aggregates should be limited. Hence, a fundamental investigation regarding appropriate improvement of concrete energy dissipation capacity is still needed.

### **7.2.3 Improvement of energy dissipation capacity of concrete**

As commonly known, both normal and high strength concretes are brittle, where the degree of brittleness increases as their strength increases. The conventional method to strengthen concrete against impact loading is by using continuous steel reinforcement bars (re-bars). The steel re-bars are effective in preventing the mass separation of the concrete target, keeping it intact and maintaining the structural integrity (Clifton, 1982). However, with the development in industry, this approach was demonstrated to be ineffective in reducing penetration depth under projectile impact (Dancygier and Yankelevsky, 1996; Luo et al., 2000). Therefore, some other methods were proposed to improve the energy dissipation capacity of concrete in recent decades.

- *Inclusion of fibres*

As commonly known, the ductility of concrete can be improved by introducing various types of fibres, especially steel fibres, into the concrete mixtures. The fibres can effectively restrict the crack opening and growth, and simultaneously enhance the energy dissipation capacity of concrete (Lu and Hsu, 2006; Lau and Anson, 2006; Camps et al., 2008; Afrough, 2008; Sharma et al., 2009). It is demonstrated that the added fibres could effectively reduce the possibility of spalling and scabbing failures, prevent crack propagation and extend the softening region in the concrete matrix (Farnam et al., 2010).

Compared to synthetic or natural fibres, steel fibres are the most commonly used to reinforce concrete. Steel fibre-reinforced concrete (SFRC) has gained acceptance for a variety of applications, including industrial floors, hydraulic structures, bridge deck overlays, pavement and overlays, explosive and penetration resistant structures, etc. (ACI Committee 544, 1993). In the available literature a large number of experimental results of SFRC under impact loadings can be found. For instance, the testing method from ACI Committee 544 was utilized to determine the impact resistance of structural lightweight concrete reinforced with steel fibres (Swamy and Jojagha, 1982). The results show that with a fibre volume of 1%, substantial increases in the impact strength and energy absorption can be achieved over those of plain concrete. Naaman and Gopalaratnam (1983) studied the effects of strain rate of loading on the bending properties of steel fibre reinforced mortar (SFRM) using an instrumented drop-weight impact machine. The parameters investigated in the experimental programme include three volume fractions of fibres (1%, 2% and 3%), three fibre aspect ratios (47, 62 and 100), two mortar mixes and four strain rates of loading ranging from  $0.5 \times 10^{-5}$  to 1.2 strains per second. It is found that depending on the fibre reinforcement parameters, the energy absorbed by the composite at static loading rates can be one to two orders of magnitude higher than that of the unreinforced matrix. Almansa and Cánovas (1999) described the main factors affecting the impact of small projectiles on steel fibre reinforced concrete (SFRC) targets. It can be found that fibre additions reduce by only a little the thickness needed to avoid perforation, but the thickness necessary to avoid scabbing is much smaller than that for plain concrete. Whereas for plain concrete a penetration equal to 45-50% of the thickness is sufficient to cause scabbing, and this ratio must grow up to 60% when fibres are added at the content of  $80 \text{ kg/m}^3$ . Nataraja et al. (1999) reported the variation in impact resistance of SFRC and plain concrete as determined from a drop weight test. It can be found that the impact strength results as determined from the drop weight test have large standard deviations, both for SFRC as well as plain concrete. The observed coefficients of variation are about 57 and 46% for first-crack resistance and the ultimate resistance in the case of fibre concrete and the corresponding values for plain concrete are 54 and 51%, respectively. Similar investigation results can also be found in Song et al. (2005b), which only focused on the statistical variations in impact resistance of high-strength concrete

(HSC) and high-strength steel fibre-reinforced concrete (HSSFRC). The effect of the steel fibre type and amount on the energy dissipation capacity of concrete was investigated in Mohammadi et al. (2009). The specimen incorporated three different volume fractions i.e. 1.0%, 1.5% and 2.0% of corrugated steel fibres. The results show that concrete containing 100% long fibres at 2.0% volume fraction gave the best performance under impact loading. Considering the fact that an increase of the additional fibres amount is beneficial for improving the energy dissipation capacity of concrete, about 8-11% (vol.) of steel fibres were added into concrete matrix maximally, e.g. the case of slurry infiltrated fibre concrete (SIFCON). A comparison of dynamic performance between conventional concrete and SIFCON under high velocity small projectile impact (860 m/s) was done by Anderson et al. (1992). The obtained experimental results showed that the damages on both front and rear faces of SIFCON were significantly reduced as compared to the conventional concrete. Nevertheless, despite its excellent performance against projectile impact, SIFCON is not widely used in the practice, mainly due to its high volume fraction of fibres and labour-intensive casting process.

In recent decades, with the development of the chemical industry products, various synthetic fibres with high mechanical properties are developed, which are mainly made from synthesized polymers. Normally, these synthetic fibres are polymerized into a long, linear chemical substance that bonds two adjacent carbon atoms, while different chemical compounds are used to produce different types of fibres. Although there are several different synthetic fibres, they generally have similar properties (Bhat and Kandagor, 2014).

Utilizing synthetic fibres to produce impact resistance concrete was very popular about 20 years ago. For instance, Mindess (1988) tested concrete beams containing fibrillated polypropylene fibres (0.1-0.5%, vol.) under impact loading. The results showed that the addition of the fibrillated polypropylene fibres increased both the fracture energy and the impact strength of the concrete. In addition, Mindess et al. (1993, 1998) also found that 0.5% by volume polypropylene fibres had little effect on the peak loads, but increased somewhat the energy required to perforate the plates. However, 1.0% by volume steel fibres led to a significant increase in both peak loads and fracture (perforation) energy. With a fibre addition of 1.5% by volume, the polyolefin fibre reinforced units were able to display essentially the same behaviour as the steel reinforced units, in terms of both the fracture energy and the maximum impact load. Due to the comparable properties between synthetic and steel fibres, some comparative investigations of them on the energy dissipation capacity of concrete can be found. For example, an investigation on fibre reinforced concrete slabs subjected to low velocity projectile impact was carried out to assess the impact resistance (Ong et al., 1999). The used fibres were polyolefin, polyvinyl alcohol and steel. The volume fractions of fibres examined were 0%, 1% and 2%. Test

results indicated that hook ended steel fibre reinforced concrete slabs have better crack resistance and energy absorption characteristics than slabs reinforced with other fibre types. Slabs reinforced with polyvinyl alcohol fibres exhibited higher fracture energy values compared to slabs reinforced with polyolefin fibres. Similar conclusions are also drawn in Wang et al. (1996) and Nia et al. (2012). Hence, it can be briefly summarized that steel fibre is more efficient than synthetic fibre in improving the energy dissipation capacity of concrete. Additionally, due to the fact that the steel fibres are cheaper and easier to be produced compared to the synthetic fibres, it is more practical to include steel fibres in the production of concrete with enhanced energy dissipation capacity.

Except the most commonly used fibres (steel fibres and synthetic fibres), natural fibres, fabrics and hybrid fibres were also utilized to improve the energy dissipation capacity of concrete (Al-Oraimi and Seibi, 1995; Banthia et al., 1998; Ramakrishna and Sundararajan, 2005; Vossoughi et al., 2007; Ohkubo et al., 2008; Li and Xu, 2009; Silva et al., 2011; Dawood and Ramli, 2012). The experimental results showed that almost all the additional fibres or fabric can improve the energy dissipation capacity of concrete. However, the steel fibres are still the most suitable fibres to be utilized in the production of concrete with relatively high impact resistance, which can be attributed to their relatively low price and simplicity.

- ***Strong concrete matrix***

Besides the addition of fibres, the basic properties of concrete matrix (e.g. porosity, bond strength of aggregate and mortar matrix) are also very important to improve its energy dissipation capacity, since the solid concrete matrix can strongly grip the fibres so that energy will be consumed in the fibre pullout process. For example, Zhang et al. (2005) presented the results of an experimental study on the impact resistance of concrete with compressive strengths of 45-235 MPa when subjected to impact by 12.6mm ogive-nosed projectiles at velocities ranging from 620 to 700 m/s. The results indicated that the penetration depth and crater diameter in target specimens exhibit an overall reduction with an increase in the compressive strength of the concrete. However, the trend is not linear. A further increase in the compressive strength requires a reduction in the water/binder ratio and the elimination of coarse aggregates. Dancygier et al. (2007) studied the influence of the concrete mix ingredients and amount and type of reinforcement on the performance of high strength concrete (HSC) under this type of loading. The main findings showed that the development of HPC barriers to withstand impact loads involves several aspects. These are aimed at achieving enhanced properties of the structural element, where only one of which is the concrete's compressive strength. Additionally, Tai (1999), Yan et al. (2009), Nili and Afroughsabet (2010a, 2010b) all demonstrated that the concrete matrix with relatively high strength can effectively improve the interface zone between fibres and concrete, reduce the number and size of cracks, and enhanced the ability of concrete to resist impact loadings.

- ***Multilayer protective structures***

Until now, there is no consensus regarding the effect of multiple layers design on the energy dissipation capacity of protective concrete, although this topic has attracted considerable interest among the researchers for a long time. For instance, Kojima (1991) performed impact experiments on monolithic concrete shield with the thickness of 18 cm and double layer concrete shields (the same concrete quality), 9 cm + 9 cm and 6 cm + 12 cm. The conclusion was that the impact resistance of a double-layer shield is inferior to that of a monolithic shield. Similar results can also be found in the investigation of Amde et al. (1997). They concluded that: 1) composite barriers manufactured from different materials are more efficient than layered barriers manufactured from the same material; 2) multiple barriers are less efficient than single layer panels having the same thickness. Nevertheless, some contradicting results can also be found in the literature. For example, Shirai et al. (1997) investigated experimentally and numerically the impact resistance of reinforced concrete plates against flat-nosed projectiles with an impact velocity of about 170 m/s. They compared the protective effectivities of the monolithic shield with the thickness of 9 cm and double-layer shields having same concrete but different structure, 4.5 cm + 4.5 cm and 3 cm + 6 cm. It was found that double-layer shields had a higher impact resistance than the monolithic shield. Moreover, Booker et al. (2009) presented an experimental investigation on the dynamic performance of segmented concrete targets under projectile impact. This work showed that segmented targets may produce reasonable projectile deceleration profiles if the interfaces between target segments can be mitigated with grout or similar materials. In general, to clearly clarify the influence of multilayers design on the energy dissipation capacity of concrete, further studies are still needed.

Based on all the literature results mentioned above, it can be concluded that a strong concrete matrix and appropriate inclusion of fibres (particularly steel fibres) are the most crucial factors in the production of concrete with relatively high energy dissipation capacity. As described before, UHPFRC is a type of concrete with a large amount of steel fibres and superior mechanical properties, which exactly meets the requirements of producing impact resistant concrete. Hence, it is logic to use UHPFRC in the application where a large amount of energy may be absorbed.

### **7.3 Performance of the sustainable UHPFRC under impact loadings**

As described in the previous chapters, a sustainable UHPFRC can be produced with relatively low binders' amount and efficient fibres application, based on the modified A&A model and fibre hybridization design. However, it is unclear whether this sustainable UHPFRC also has relatively high impact resistance capacity and how to improve its energy dissipation ability. Hence, in this section, the performance of the

developed sustainable UHPFRC under impact loadings is investigated. In general, the study can be divided into two parts: 1) energy dissipation of the sustainable UHPFRC with only straight steel fibres; 2) energy dissipation of the sustainable UHPFRC with hook ended steel fibres. Due to the restriction of different steel fibres on the sample dimensions, two pendulum impact set-ups are employed for the experimental investigation. More detailed information is presented in the following part.

### 7.3.1 Materials and mix design

The ingredients used in this section for the production of the sustainable UHPFRC matrix are the same as that shown in Section 4.2.2. Additionally, three types of steel fibres are utilized: 1) long straight fibres (LSF), length = 13 mm, diameter = 0.2 mm; 2) short straight fibres (SSF), length = 6 mm, fibre diameter = 0.16 mm; 3) hook ended fibre (HF) length = 35 mm, diameter = 0.55 mm. Some detailed information on these fibres can be found in Figure 2.8 and Table 2.6.

The sustainable UHPFRC's recipe, developed using the modified A&A model, is shown in Table 7.1. The resulting integral grading curve of the composite mixes is the same as that shown in Figure 4.11(c). In this study, the utilized steel fibre amount is fixed at 2% (vol.). In general, the developed concrete can be divided into three categories: 1) reference sample (without fibres, No. 1); 2) with only straight fibres (No. 2-6); 3) with hook ended steel fibres (No. 7 and 8).

**Table 7.1: Recipes of the developed UHPFRC**

No.	OPC kg/m <sup>3</sup>	LP kg/m <sup>3</sup>	MS kg/m <sup>3</sup>	S kg/m <sup>3</sup>	nS kg/m <sup>3</sup>	W kg/m <sup>3</sup>	SP kg/m <sup>3</sup>	LSF vol. %	SSF vol. %	HF vol. %
1	594.2	265.3	221.1	1061.2	24.8	176.9	44.2	0	0	0
2	594.2	265.3	221.1	1061.2	24.8	176.9	44.2	2.0	0	0
3	594.2	265.3	221.1	1061.2	24.8	176.9	44.2	1.5	0.5	0
4	594.2	265.3	221.1	1061.2	24.8	176.9	44.2	1.0	1.0	0
5	594.2	265.3	221.1	1061.2	24.8	176.9	44.2	0.5	1.5	0
6	594.2	265.3	221.1	1061.2	24.8	176.9	44.2	0	2.0	0
7	594.2	265.3	221.1	1061.2	24.8	176.9	44.2	0.5	0	1.5
8	594.2	265.3	221.1	1061.2	24.8	176.9	44.2	0	0	2

(OPC: Ordinary Portland Cement (CEM I 52.5 R), LP: limestone powder, MS: microsand, S: sand (0-2), nS: nanosilica, W: water, SP: superplasticizer, LSF: long straight fibres, SSF: short straight fibres, HF: hook ended fibres)

### 7.3.2 Experimental methodologies

Considering the effect of different fibres on the sample dimensions, two pendulum impact set-ups are employed here: one is “Charpy Impact Device” (Figures 7.1-7.3), and the other one is “Modified Pendulum Impact Device” (Figures 7.4 and 7.5).

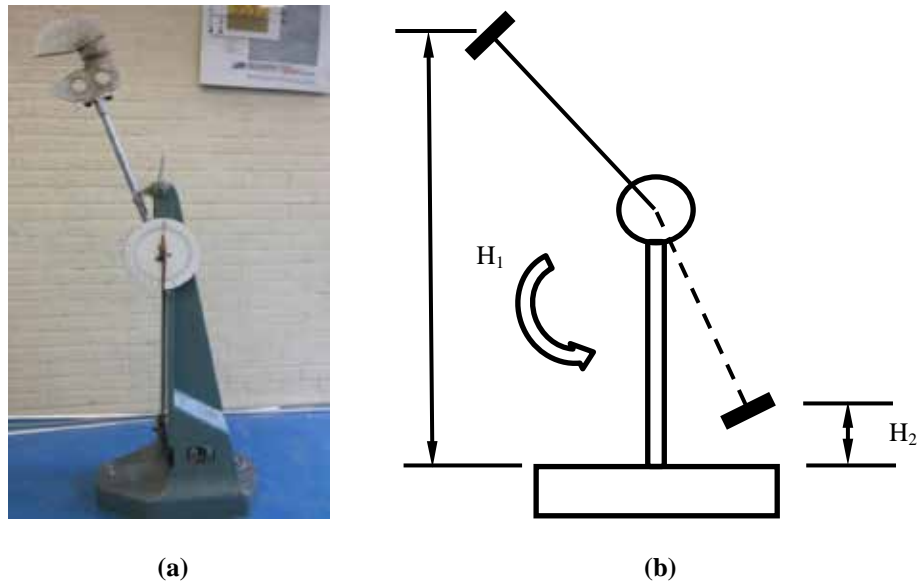


**Figure 7.1:** The “Charpy Impact Device” (a) used in this study and its working scheme (b)

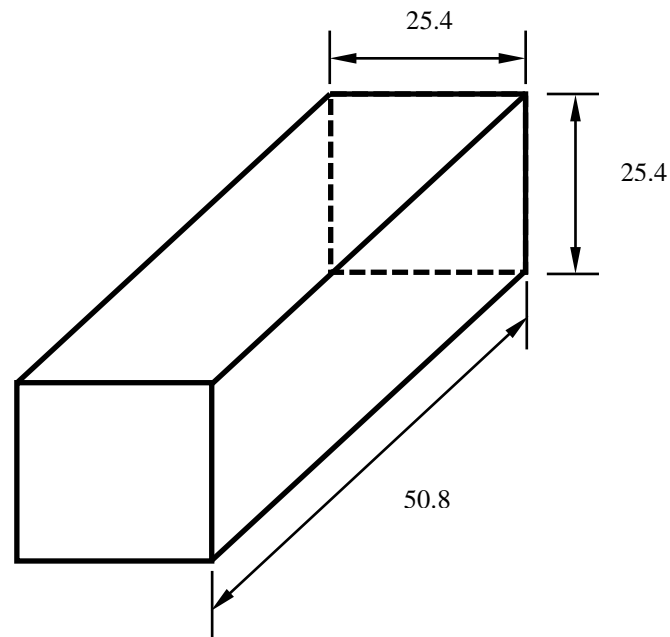


**Figure 7.2:** Dimensions of sample for Charpy impact test (units: mm)

The “Charpy Impact Device” is employed to test the energy dissipation capacity of the sustainable UHPFRC with only straight steel fibres (No. 2-6 in Table 7.1), referencing the ASTM E23 (1992). The “Charpy Impact Device” is shown in Figure 7.1, in which the maximum kinetic energy output is 147.1 J. According to Xu et al. (2010), the dimension of specimen and the configurations of the loading for the Charpy impact test are presented in Figures 7.2 and 7.3, respectively.

After curing in the water for 28 days, the hardened samples are prepared for the impact test. After embedding the specimen, the pendulum is released from a height  $H_1$  and swing through the specimen to a height  $H_2$ , as shown in Figure 7.1(b). Assuming negligible friction and aerodynamic drag (about 1% of the total impact energy), the energy absorbed by the specimen was equal to the height difference multiplied by the weight of the pendulum. During the testing, at least five specimens are tested for each batch.

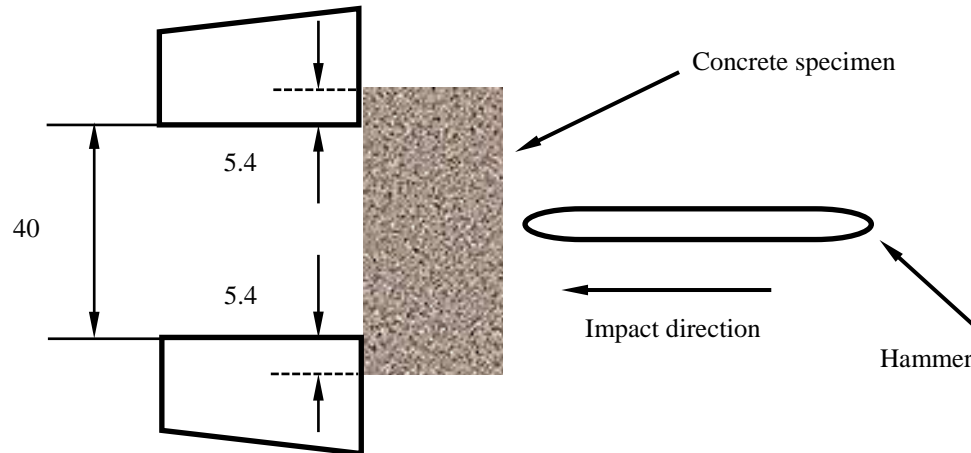


**Figure 7.3: Configuration of impact loading process of “Charpy Impact Device” (units: mm)**

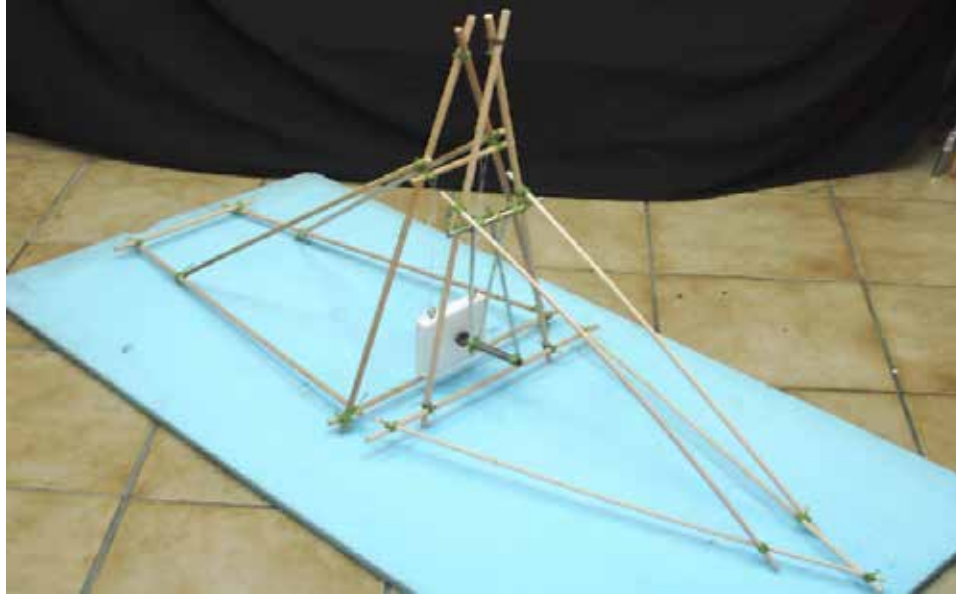


**Figure 7.4: Model of the “Modified Pendulum Impact Device” employed in this study (Verhagen, 2013)**

Figure 7.4 illustrates a down-scaled model of the “Modified Pendulum Impact Device” designed by Verhagen (2013). In this study, this device is employed to evaluate the energy dissipation capacity of the sustainable UHPFRC with hook ended fibres (mixtures

No. 7 and 8 in Table 7.1). The “Modified Pendulum Impact Device” can be treated as two main parts, assembled together: the sample part (“A” shown in Figure 7.5) and the hammer part (“B” shown in Figure 7.5). As can be noticed, this set-up is different from the normal pendulum impact device, in which the sample is commonly fixed on the frame. When the sample is fixed on the frame, a large amount of energy may be consumed for the oscillation of concrete slab and the test set-up during the impact process, which is not beneficial for a clear clarification of the energy dissipation capacity of the sustainable UHPFRC. Hence, in this study, the concrete sample is freely hung on the frame, as suggested by Verhagen (2013).

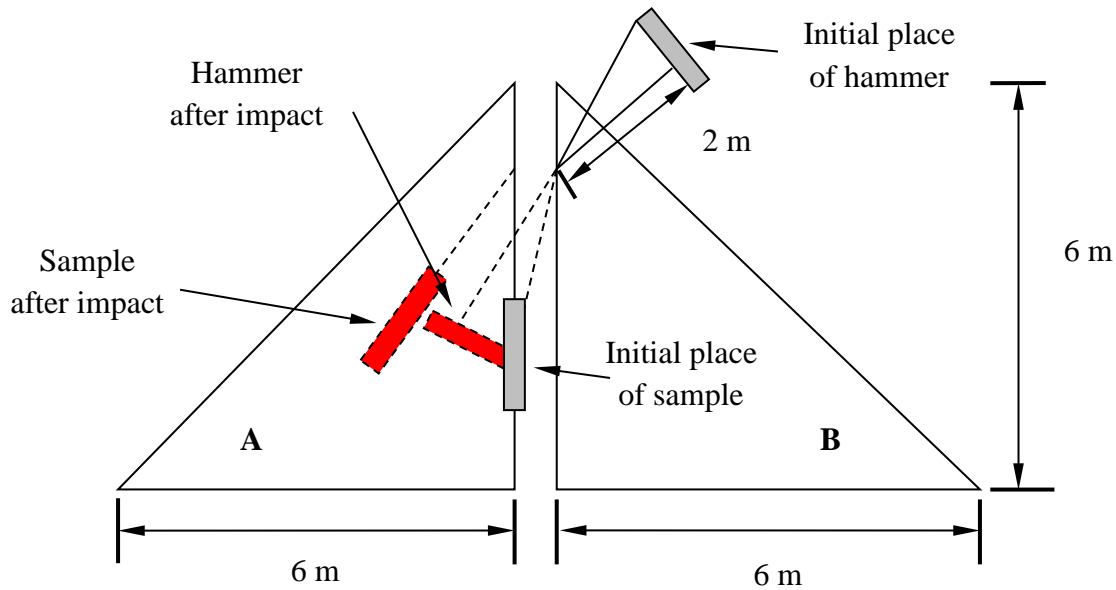


**Figure 7.5: Working scheme of the “Modified Pendulum Impact Device” employed in this study**

As shown in Figure 7.5, before the impact test, the hammer is lifted to a maximum height (about 3.2 meter). Then, it is released from the original height and follows the swing direction to the concrete slab centre. When the hammer swings to the lowest point, it has the largest impact velocity ( $V_{hammer}$ ). When the impact happens, the concrete slab will swing away with a velocity of  $V_{slab}$  and the hammer still has a residual velocity ( $V_{hammer-residual}$ ). Therefore, the energy absorbed by the UHPFRC slab during this impact can be calculated as follows:

$$E_{absorbed} = \frac{1}{2} M_{hammer} V_{hammer}^2 - \frac{1}{2} M_{slab} V_{slab}^2 - \frac{1}{2} M_{hammer} V_{hammer-residual}^2 \quad (7.9)$$

where the  $E_{absorbed}$  is the absorbed energy by the sustainable UHPFRC slab (J);  $M_{hammer}$  and  $M_{slab}$  are the masses of impact hammer and concrete slab (kg), respectively;  $V_{hammer}$  is the initial impact velocity of the hammer (m/s);  $V_{slab}$  is the slab velocity after impact (m/s);  $V_{hammer-residual}$  is the residual velocity of hammer after the impact (m/s).

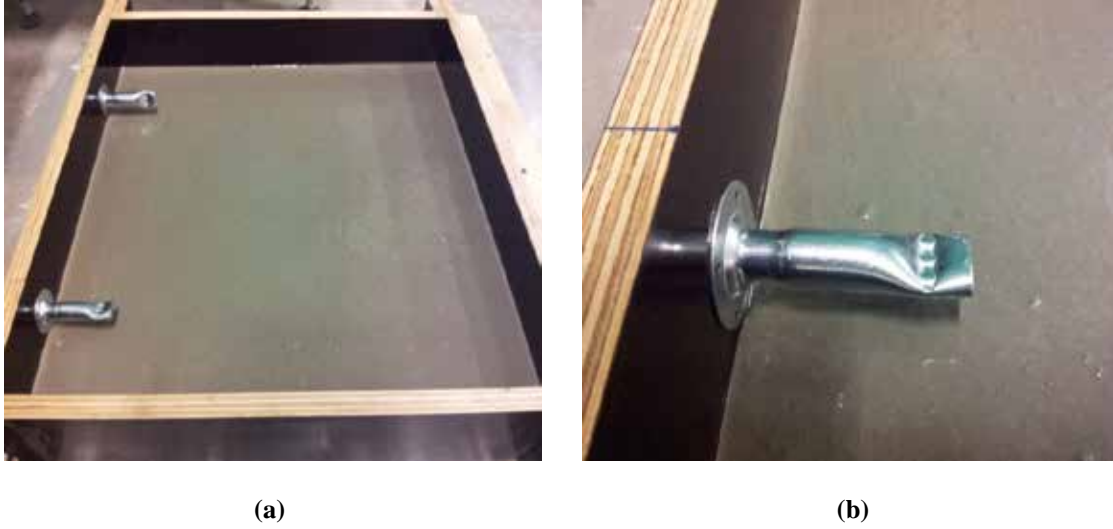


**Figure 7.6: Fresh sustainable UHPFRC in wooden mould (a) and prepositioned metal inserts in the UHPFRC slabs (b)**



**Figure 7.7: Constructed hammer, (a): hammer head; (b): hammer arm in the set-up**

During the impact process, all the velocities are recorded by a camera. The repeating strikes between hammer and sample during one impact are avoided in this study. If the UHPFRC slab is not damaged after one impact, then the hammer will be released from the original height again, triggering another impact. Until the concrete slab is entirely damaged, the total energy absorbed by the concrete slab can be roughly calculated as the summation of the absorbed energy in each impact:

$$E_{total- absorbed} = \sum_1^{n-1} E_{absorbed} \quad (7.10)$$

where  $n$  means the shock numbers when entire damage happens. Due to the fact that the last applied impact can cause the damage of the concrete sample and the velocities of the

fragments are difficult to be measured, the absorbed energy from the last impact is not possible to be quantified.

In this study, the fresh concrete is cast in the mould with the size of 500 mm × 500 mm × 100 mm. Two metal inserts are installed on the side of the mould (as shown in Figure 7.6), which can help to lift the concrete slab later. The distance between these two metal inserts is 300 mm.



**Figure 7.8: Constructed frames for hanging the hammer and concrete samples (a) and the simple tool utilized to control the distance between these two frames (b)**

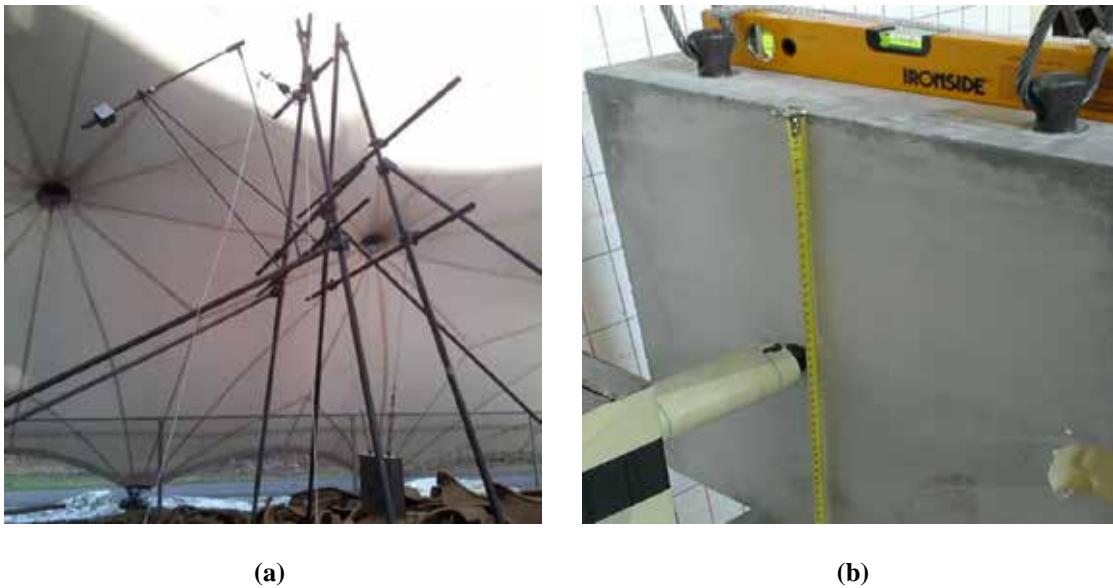


**Figure 7.9: Maximum height of the hammer (a) and the concrete slab central point impacted by the hammer (b)**

To improve the accuracy of the results obtained from the “Modified Pendulum Impact Device” and minimize some potential experimental errors, a series of technical issues should be addressed here. For instance, to flexibly adjust the impact energy, the mass of the hammer should be freely modified (Figure 7.7a). In addition, considering the fact that it is very important to keep the hammer impacting horizontally on the centre of the target, the location of the added weight can be flexibly adjustable (Figure 7.7b). Moreover, during the impact experiments, the distance between the two frames (for hammer and sample hanging) should be constant. Hence, a simple adapter (as shown in Figure 7.8b) is utilized in this study. For each impact, the hammer is lifted to the maximum height (about 3.2 m), as shown in Figure 7.9a, and the hammer always impacts at the centre of the concrete slab (as shown in Figure 7.9b). The velocities of the hammer and the samples are recorded by a camera and calculated with the help of a meshed board (as shown in Figure 7.10).



**Figure 7.10:** Meshed board used to calculate all the velocities of hammer and samples

At the beginning of the tests, the hammer impact velocity is calibrated. As shown in Figure 7.11, the time gap between these two pictures is 0.02 s, and the movement of the hammer is about 18 cm. Nevertheless, due to the fact that the used camera cannot be always perpendicular to the impact hammer and there is a gap between the hammer and meshed board, the real movement of the hammer during this 0.02 s should be less than 19 cm. As the mechanism presented in Figure 7.12, the hammer movement recorded by the camera is the distance between A and B. Actually, the real movement of the hammer should be the distance between C and D. Therefore, based on homothetic triangle theory, it is easy to calculate the real movement of the hammer, which is shown as follows:

$$\frac{D_{CD}}{D_{AB}} = \frac{D_{camera-hammer}}{D_{camera-board}} \quad (7.11)$$

where  $D_{AB}$  is the distance between A and B (as shown in Figure 7.12) (cm),  $D_{CD}$  is the distance between C and D (as shown in Figure 7.12) (cm),  $D_{camera-hammer}$  is the distance between camera and hammer (cm),  $D_{camera-board}$  is the distance between the camera and the mesh board (cm).

In this study, the  $D_{AB}$ ,  $D_{camera-hammer}$ , and  $D_{camera-board}$  are 19 cm, 151 cm and 185 cm, respectively. Hence, the real movement of the hammer ( $D_{CD}$ ) during the 0.02 s is about 15.5 cm, which means the impact velocity (maximum velocity) of the hammer yields about 7.75 m/s.

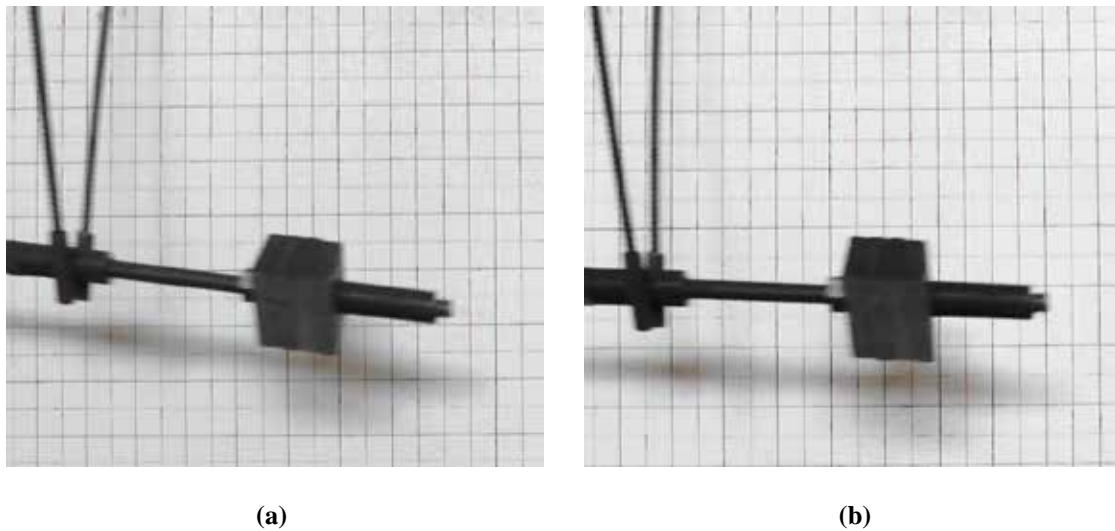


Figure 7.11: Recorded hammer movement during 0.02 s by the used camera

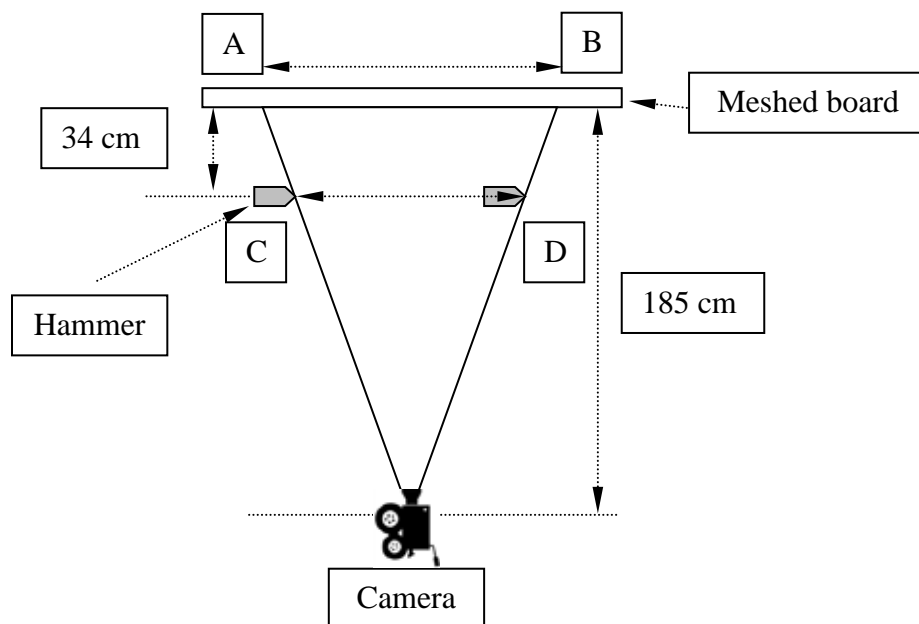


Figure 7.12: Relevant mechanisms to calculate the real impact velocity of the hammer

As mentioned before, the maximum height of the hammer is about 3.2 m and the mass of the hammer is about 40 kg. Hence, assuming that there is no energy consumed in the hammer swing process, the theoretical impact velocity of the hammer can be calculated as:

$$V_{theoretical} = \sqrt{2gh_{hammer}} \quad (7.12)$$

where  $V_{theoretical}$  is the hammer theoretical impact velocity (m/s),  $g$  is the gravity of earth constant ( $9.81 \text{ m/s}^2$ ) and  $h_{hammer}$  is the maximum height of the hammer (about 3.2m).

Here, the calculated theoretical hammer impact velocity is about 7.92 m/s. Hence, the energy loss during the hammer impact process can be calculated as follows:

$$E_{loss} = \frac{1}{2} m_{hammer} (V_{theoretical}^2 - V_{tested}^2) \quad (7.13)$$

where  $E_{loss}$  is the energy loss amount during the hammer swing process (J),  $m_{hammer}$  is the hammer mass (kg),  $V_{tested}$  is the tested hammer impact velocity (m/s).

In this research, the energy loss can be attributed to friction, air resistance and frame damping. Based on the equations listed above, the total energy loss amount is estimated at 53.3 J, which is about 4.4% of the hammer impact energy. Consequently, it can be stated that the created “Modified Pendulum Impact Device” has relatively low energy loss during the impact process and is suitable to be utilized to test the sustainable UHPFRC sample with relatively large dimensions.

### 7.3.3 Energy dissipation capacity of UHPFRC with only straight steel fibres

In this section, the dynamic performance of the sustainable UHPFRC produced with only straight fibres (LSF and SSF) is presented, including experimental results and modeling studies. Based on the obtained experimental results, a model is proposed to evaluate the energy dissipation capacity of the sustainable UHPFRC under Charpy impact loadings.

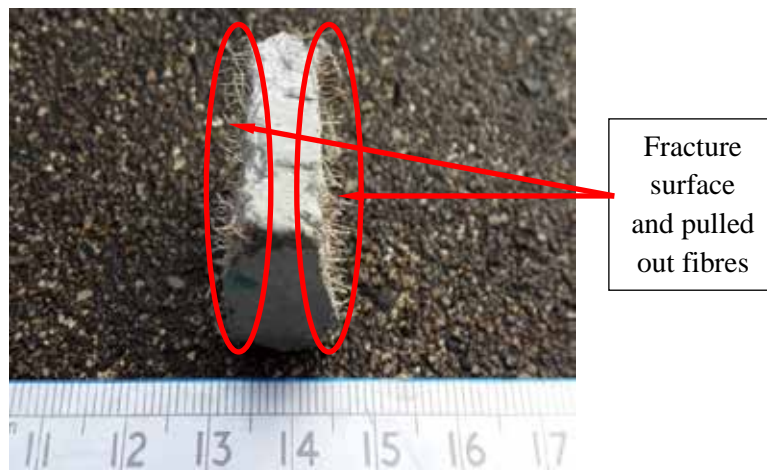
#### • *Experimental results*

Figure 7.13 shows the fractions of the sustainable UHPFRC and reference samples after the Charpy impact test. It can be noticed that the broken sustainable UHPFRC samples are always mainly composed of three cuboid-like fractions, while the fractions of reference samples are smaller and more irregular, as shown in Figure 7.13(a). Moreover, after the impact loading, not only the concrete matrix of the sustainable UHPFRC sample is destroyed, but also all the embedded steel fibres are pulled out (Figure 7.13(b)). Therefore, it can be summarized that the impact energy absorption of the sustainable UHPFRC specimen should mainly include two parts: the energy consumed in breaking

the concrete matrix and the energy spent to pull out the fibres embedded in the broken cross sections.



(a)



(b)

**Figure 7.13: Fractions of the samples after Charpy impact test: (a) Comparison of the reinforced and non-reinforced sample after impact loading; (b) Fractured surface of the reinforced sample after impact loading and the pulled out fibres**

As commonly known, the fracture mechanism of concrete under high strain rate or external impact loadings can be attributed to cracking, shearing and compaction, as shown in Figure 7.14 (Burlion, 1997). Hence, it can be predicted that concrete will be broken along the forces direction, such as compaction, tension or confining pressures. However, the final cracks development in the whole concrete element depends on the basic properties of the concrete, the addition of fibres or steel reinforcement. The numerical and experimental investigations of Süper (1980) on thick concrete plates show that when the first diagonal crack occurs, still a very high portion of the initial kinetic energy is transferred from the concrete to the reinforced steel, stirrups as well as

longitudinal reinforcement. When the first crack occurs, the fibres can still bridge the crack and disperse the energy to other places in the concrete. Once the fibres cannot restrict the development of cracks, they will be pulled out, and the concrete will be damaged following the stress distribution on concrete during the impact (Figure 7.14). Nevertheless, for non-reinforced concrete, due to the fact that no fibres or reinforcements can restrict the cracks development, the cracks always grow along the weakest interface in the concrete, which causes that the broken fractions of the reference sample are small and irregular (as shown in Figure 7.13(a)).

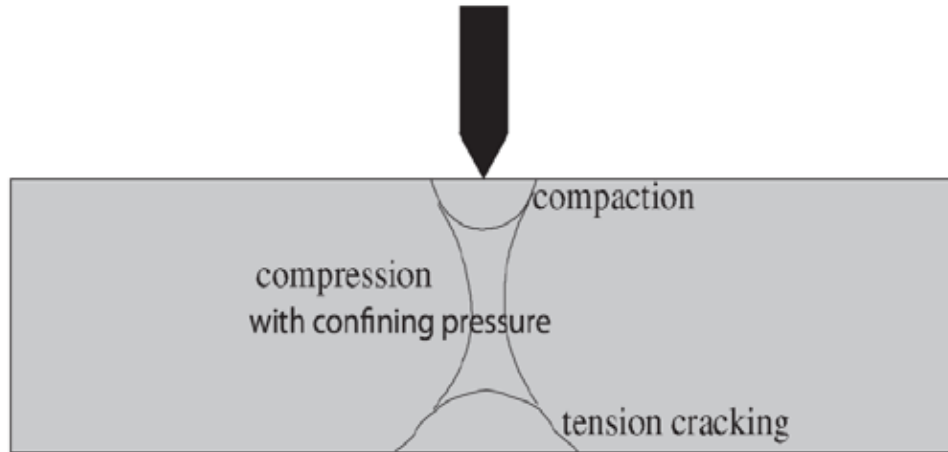


**Figure 7.14: Schematic description of the mechanisms activated in concrete under impact loading (Burlion, 1997)**

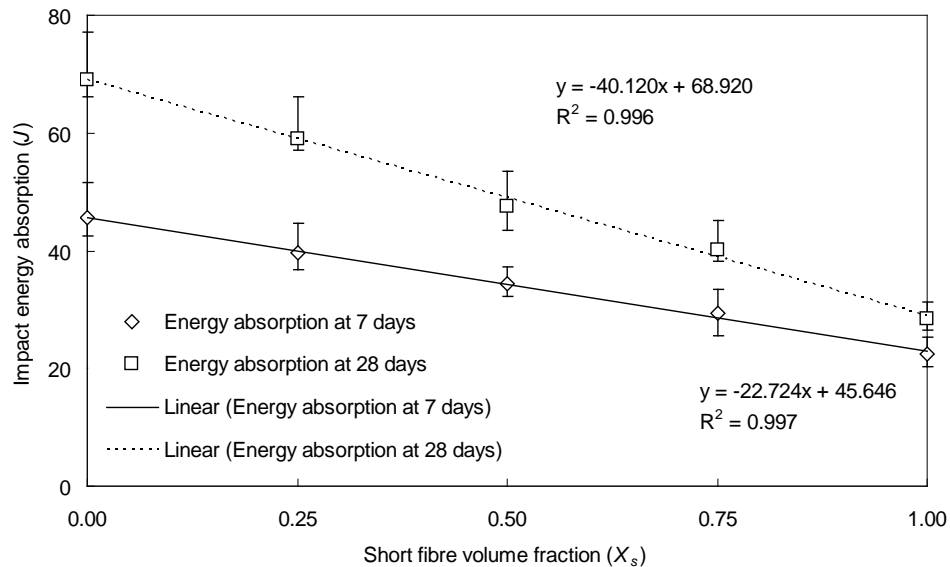


**Figure 7.15: Variation of the absorbed impact energy of the sustainable UHPFRC with different short fibre volume fractions ( $X_s$ ), total fibres amount is 2% (vol.)**

To quantify the energy dissipation capacity of concrete, the variation of the impact energy absorption of the sustainable UHPFRC with different short fibre volume fractions ( $X_s$ , as presented in Eq. (5.1)) is investigated, and is shown in Figure 7.15. As can be noticed, with an increase of the short fibre volume fraction the absorbed impact energy by the sustainable UHPFRC at 7 and 28 days decreases linearly. For instance, when the short fibre volume fraction increases from 0 to 1, the impact energy absorption of the sustainable UHPFRC reduces from about 45.6 J and 69.1 J to about 22.3 J and 28.4 J at 7 and 28 days, respectively. Furthermore, the slope of the decreasing line at 28 days is even higher than that at 7 days, which reflects that the addition of short straight fibres (SSF) has a significant effect on the sustainable UHPFRC with relatively high impact energy absorption capacity. Hence, based on the obtained experimental results, it can be concluded that the long straight fibres play a dominant role in improving the energy dissipation capacity of the sustainable UHPFRC. With a constant total steel fibre amount, the increase of short straight fibres content can cause a significant decrease of the energy absorption capacity of the sustainable UHPFRC. This phenomenon is in accordance with the results presented in Figure 5.6, in which the sample with long straight fibres (1.5% vol.) and short straight fibres (0.5% vol.) shows the highest ultimate flexural strength but an instable post-peak response.

In general, it can be concluded that the long straight fibres are more important than the short straight fibres in improving the energy dissipation capacity of the sustainable UHPFRC. However, to clearly understand the mechanism of energy absorption process of the sustainable UHPFRC under impact loadings, the theoretical analysis and modeling are needed, which are presented in the following part.

· ***Modeling studies***

As mentioned before, to evaluate the impact energy absorption of the sustainable UHPFRC, two parts should be mainly considered: the energy consumed in breaking the concrete matrix and the energy spent to pull out the fibres embedded in the broken cross sections. According to the available literature (Favre et al., 1997; Kanda and Li, 1998), the fibre pullout process usually consists of three processes: 1) fibre/matrix working together; 2) fibre/matrix debonding; 3) fibre/matrix sliding. In this study, the fibre/matrix interfacial shear strength is assumed equal to the equivalent shear bond strength. Hence, the total energy absorption of the sample during the impact testing can be simply expressed as (Xu et al., 2010):

$$U = U_m V_m + N_f U_f \quad (7.14)$$

where  $U$  is the total energy absorbed by the sustainable UHPFRC sample during the impact process (J),  $U_m$  is the crack energy absorbed by the reference sample without fibres (J),  $V_m$  is the volume fraction of the matrix (%),  $N_f$  is the number of fibres

embedded in the broken cross section and  $U_f$  is the energy per fibre needed to pull it out (J).

In this study, due to the fact that both the long and the short straight fibres are pulled out during the impact process, the energy consumed in pulling out long and short straight fibres should be considered individually. Assuming that the energies consumed in pulling long and short straight fibres are independent, Eq. (7.14) should be rewritten as follows:

$$U = U_m V_m + N_{f1} U_{f1} + N_{f2} U_{f2} \quad (7.15)$$

where  $N_{f1}$  and  $N_{f2}$  are the number of long and short fibres embedded in the broken cross section, respectively;  $U_{f1}$  and  $U_{f2}$  represent the energy per long and short fibre that is needed to pull them out (J), respectively.

The fibre number can be computed as:

$$N_f = \frac{S_a V_f}{\pi r^2} = \frac{4 S_a V_f}{\pi d \phi} \quad (7.16)$$

where  $S_a$  is the area of the broken cross section of the tested sustainable UHPFRC samples ( $\text{mm}^2$ ),  $V_f$  is the volumetric amount of the fibres in concrete (%),  $r$  and  $d'$  are the radius and diameter of the used fibres (mm), respectively.

Additionally, in the available literature, the investigation focusing on the estimation of the energy consumption in pulling out the embedded fibres can be found (Leung and Geng, 1995; Soetens et al., 2013; Alwan et al., 1991). Chawla (1997) assumed that the fibre with a diameter  $d'$  is pulled out through a distance  $x'$  against an interfacial frictional shear stress ( $\tau_i$ ), then the total force at that instant on the debonded fibre surface opposing the pullout is  $\tau_i \pi d' (k' - x')$ , where  $k'$  is the fibre embedded length. When the fibre is further pulled out a distance  $dx'$ , the work done by this force is  $\tau_i \pi d' (k' - x') dx'$ . The total work  $U_f$  done in pulling out the fibre over the distance  $k'$  can be obtained by integration as follows (Xu et al., 2010):

$$U_f = \int_0^{k'} \tau_i \pi d \phi (k \phi - x \phi) dx \phi = \frac{\tau_i \pi d \phi^2}{2} \quad (7.17)$$

Here, assuming that the steel fibre cannot be broken during the pulling out process, its pullout length can vary between a minimum of 0 and a maximum of  $l/2$ , where  $l$  is the fibre length. Hence, integrating  $dk'$  yields an average work of pullout per fibre, as follows (Xu et al., 2010):

$$U_f = W_{fp} = \frac{1}{l/2} \int_0^{l/2} \frac{\tau_i \pi d \phi^2}{2} dk \phi = \frac{\tau_i \pi d \phi^2}{24} \quad (7.18)$$

where  $W_{fp}$  is the average work (J) of pulling out per fibre.

Now, these equations from (Xu et al., 2010) are applied to the hybrid fibre reinforced concrete developed in this study. Substituting Eq. (7.16) and Eq. (7.18) into Eq. (7.15) gives:

$$U = U_m V_m + \frac{\tau_{i1} l_1^2 S_a V_{f1}}{6 d_1 \phi} + \frac{\tau_{i2} l_2^2 S_a V_{f2}}{6 d_2 \phi} \tag{7.19}$$

In order to calculate the total impact energy absorbed by the sustainable UHPFRC from Eq. (7.19), it is necessary to obtain the interfacial bond strength between the concrete matrix and long or short straight fibres ( $\tau_{i1}$  and  $\tau_{i2}$ ), which is defined as the friction between the fibre and the matrix (Xu et al., 2010). The ultimate flexural stress in the mid span can be expressed as the sum of the flexural stresses of the matrix and the fibres. Hence, the interfacial bond strength can be obtained as follows (Xu et al., 2010; Kanda and Li, 2006):

$$\sigma' \phi = \frac{1}{2} V_f g' \tau_i \frac{\sigma_m}{\phi} + \sigma_m (1 - V_f) \tag{7.20}$$

Where  $\sigma'$  is the flexural stress of the sustainable UHPFRC (MPa),  $\sigma_m$  is the flexural stress of the reference sample without fibres (MPa),  $g' = 1.5$  (Kanda and Li, 2006).

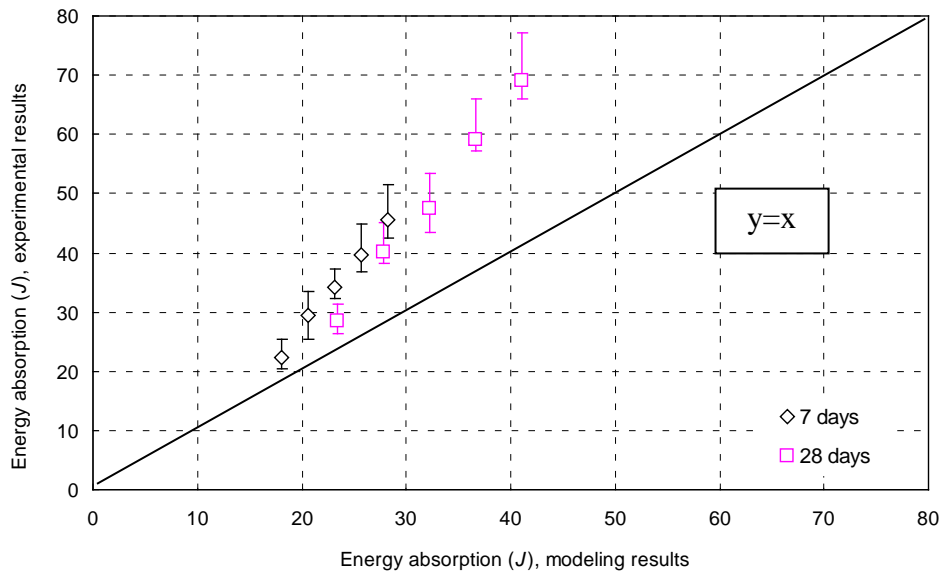


**Figure 7.16: Comparison of the experimental and modeling results (based on the model shown in Eq. (7.19)) of the energy absorption amount of the developed sustainable UHPFRC during the Charpy impact loading**

Hence, based on the results shown in Figure 5.6 and Eqs. (7.19 and 7.20), the energy absorbed by the sustainable UHPFRC during the impact can be computed. A comparison between the experimental and modeling results is presented in Figure 7.16.

It can be noticed that all the modeling results shown in Figure 7.16 underestimate the experimentally measured energy absorption capacity of the sustainable UHPFRC. Especially for the concrete mixtures having higher energy dissipation ability, the deviation between the experimental and modeling results is significant. Hence, to better match with the experimental results, the proposed model needs further consideration.

As mentioned before, in this study, the impact energy absorption of the sustainable UHPFRC is mainly composed of two parts: the energy consumed in breaking the concrete matrix and the energy spent to pull out the fibres embedded in the broken cross sections. Nevertheless, in Eq. (7.19), only a single broken cross section is considered per sample. In fact, as can be seen in Figure 7.13, after the impact loading, the sustainable UHPFRC is typically broken into three pieces, which means there are two broken cross sections and more energy is consumed in pulling out fibres. Consequently, assuming that the hybrid steel fibres are homogeneously distributed within the specimen, a new equation is proposed to give the impact energy dissipation of a hybrid fibre reinforced concrete in the Charpy test, which is shown as follows:

$$U_D = U_m V_m + 2 \times \frac{\alpha_{i1} l_1^2 S_a V_{f1}}{6 d_1 \phi} + \frac{\tau_{i2} l_2^2 S_a V_{f2}}{6 d_2 \phi} \quad (7.21)$$

where  $U_\Delta$  is the modified total energy absorbed by the sustainable UHPFRC samples (J),  $l_1$  and  $l_2$  are the lengths of long and short straight fibres (mm),  $d_1$  and  $d_2$  are the diameters of long and short straight fibres (mm),  $V_{f1}$  and  $V_{f2}$  are the volumetric amounts of the long and steel fibres in concrete (%), respectively.

Based on the experimental results shown in Figure 5.6 and Eqs. (7.20 and 7.21), the modified impact energy absorption of the sustainable UHPFRC can be calculated. The comparison between the experimental and modified modeling results is illustrated in Figure 7.17. It is important to find that the modified modeling results are in good agreement with the experimental results, especially for the samples with lower energy absorption capacities. However, when the impact resistance ability of the UHPFRC is relatively high, the modeling results slightly underestimate the experimental results. This could be attributed to the fact that the energy absorbed in the test device vibration or the friction between the sample and the device is neglected in the modeling. Actually, when the impact resistance capacity of the concrete is relatively high, small vibrations of the ‘‘Charpy Impact Device’’ could be observed indeed, which means that part of the impact energy is dissipated in the equipment.

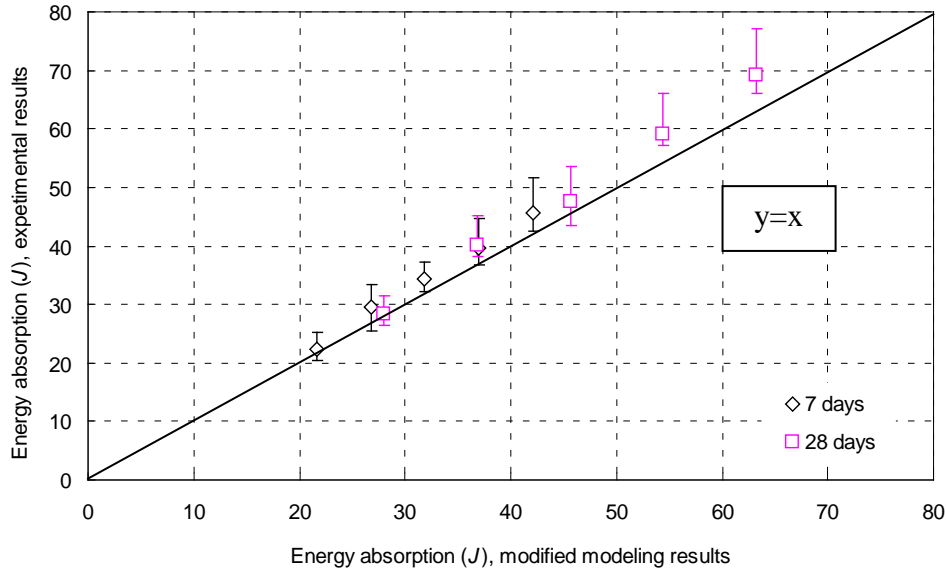


**Figure 7.17: Comparison of the experimental and modeling results (based on the model shown in Eq. (7.21)) of the energy absorption amount of the developed sustainable UHPFRC during the Charpy impact loading**

### 7.3.4 Energy dissipation capacity of UHPFRC with hook ended steel fibres

In this section, the energy dissipation capacity of the sustainable UHPFRC with hook ended steel fibres is evaluated by employing the “Modified Pendulum Impact Device”. In general, four types of different concrete sample are cast: 1) sustainable UHPFRC matrix without fibres (mixture No. 1 shown in Table 7.1); 2) sustainable UHPFRC with hybrid steel fibres (mixture No. 7 shown in Table 7.1); 3) sustainable UHPFRC with only hook ended steel fibres (mixture No. 8 shown in Table 7.1); 4) normal strength concrete without fibres (following the recipe presented in (Yu et al., 2012) and compressive strength at 28 days of about 67 MPa). Therefore, according to the dynamic performance of these concrete samples under pendulum impact loadings, it would be possible to assess the effect of steel fibres on the energy dissipation capacity of the sustainable UHPFRC and clearly understand the difference of impact resistance among UHPFRC, high strength concrete and normal strength concrete. Here, the dynamic performances of concrete are mainly focused on the cracks development, absorbed impact energy and fracture morphology of concrete samples.

#### • *Cracks development*

As shown in the previous sections, the impact energy of the used hammer is about 1200 J. After the first impact, both the normal strength concrete (NSC) and sustainable UHPFRC matrix (without fibres) have already been seriously damaged (as shown in Figures 7.18 and 7.19), which should be attributed to the fact that these concretes are relatively brittle and the growth of cracks cannot be well restricted. The cracks are created at the central

part of the concrete target and then develop towards the four corners. Nevertheless, different from the damage process of NSC, a clear circular scabbing at the rear surface of the sustainable UHPFRC matrix (UHPC) can be observed (as shown in Figure 7.19b), which cause that more fragments are created.

According to the obtained experimental results, it can be concluded that the energy dissipation capacity of a plain concrete target (without steel fibres) is relatively low. An increase of compressive strength from 67 MPa (NSC) to about 100 MPa (sustainable UHPFRC matrix) cannot significantly improve the impact resistance of concrete. Due to the fact that it is difficult to measure the velocities of all the fragments during the impact process, the absorbed energy by NSC or sustainable UHPFRC matrix is difficult to be quantified based on these tests.

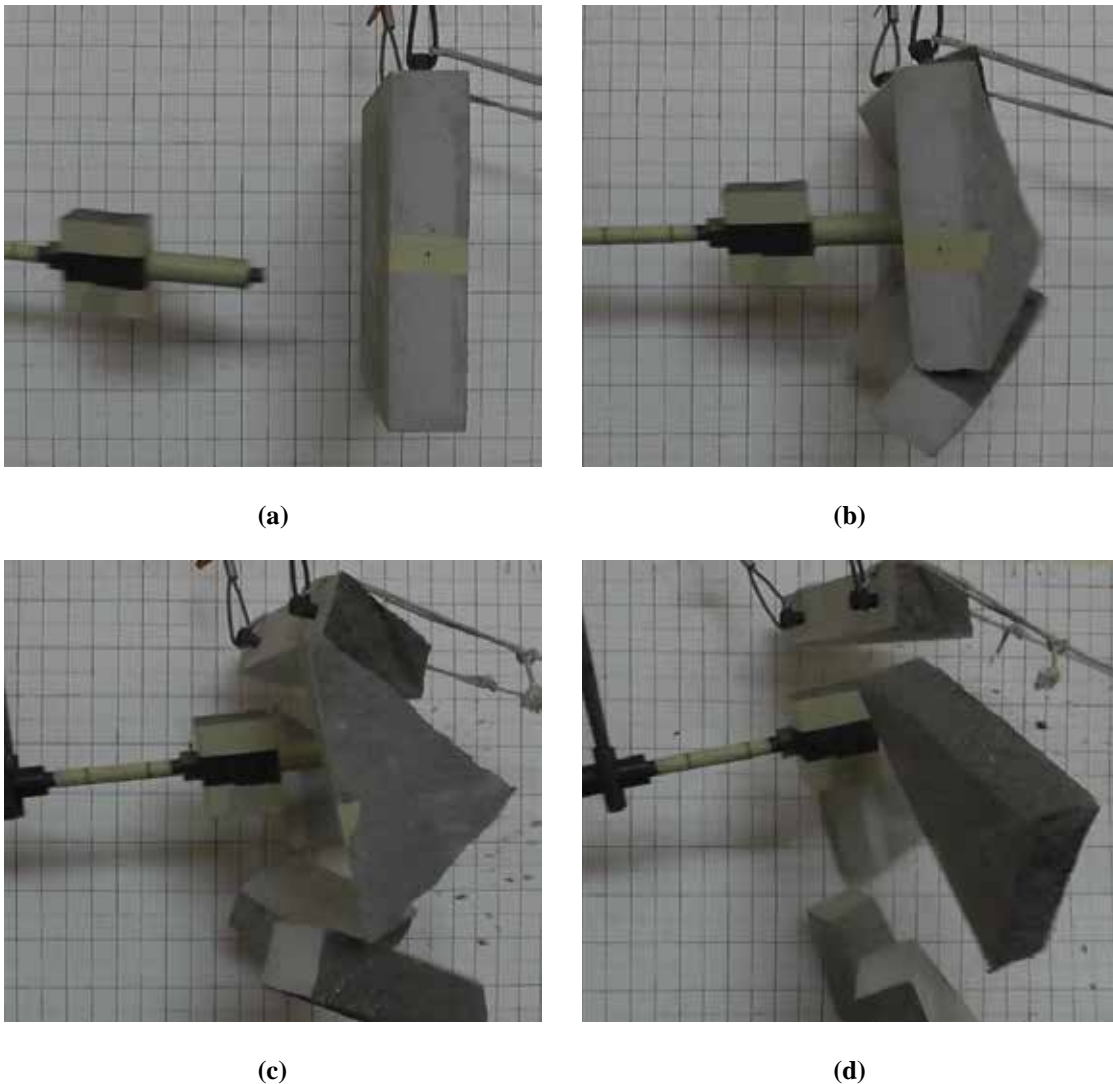


**Figure 7.18: Dynamic behaviour of normal strength concrete (NSC) during the first impact**

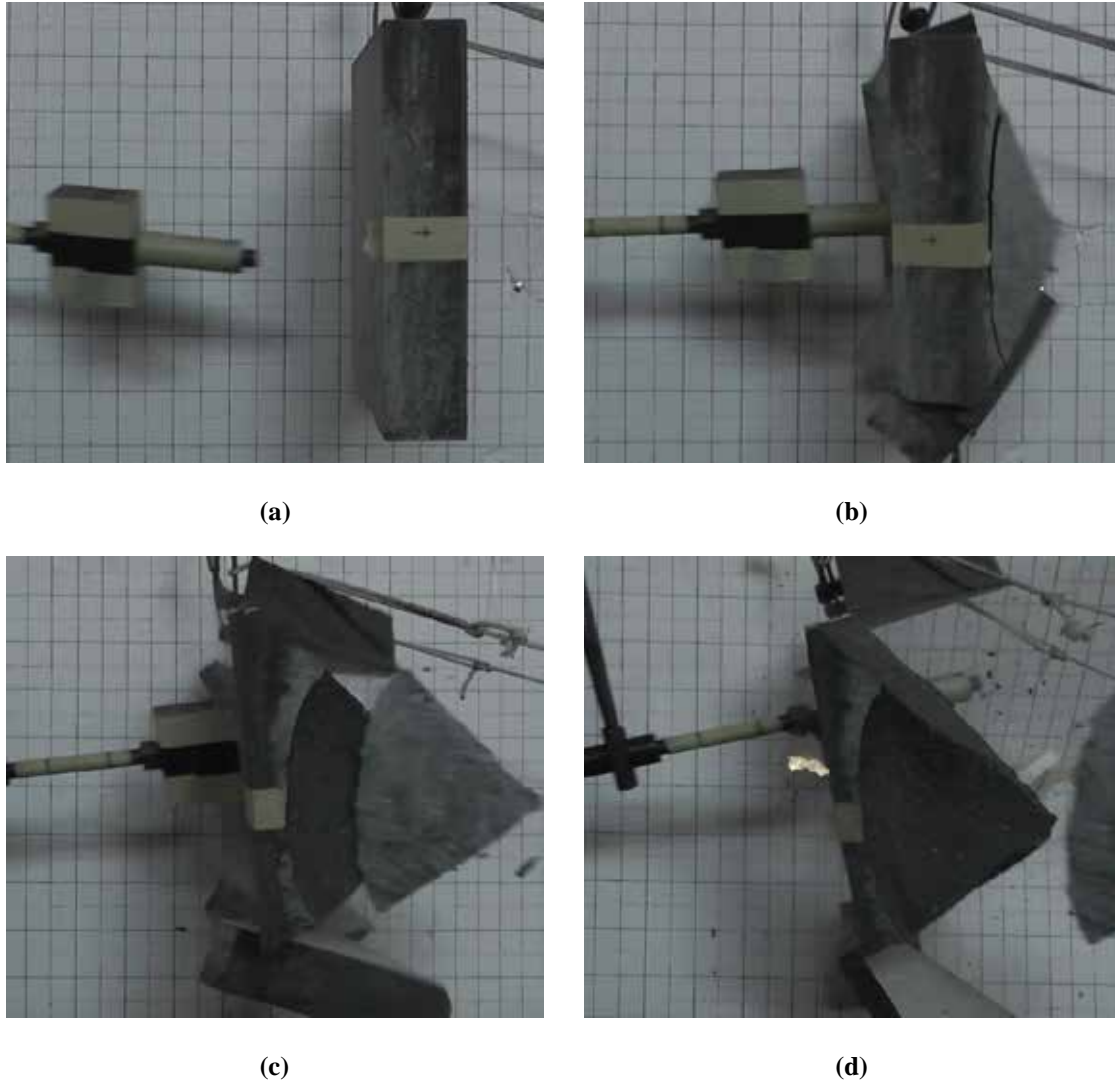


**Figure 7.19: Dynamic behaviour of UHPFRC matrix (UHPC without fibres) during the first impact**

Compared to the plain concrete (without fibres), the developed sustainable UHPFRC with single sized fibres and hybrid fibres shows much better energy dissipation capacity during the pendulum impact tests. Particularly the mixture with hybrid steel fibres, which is damaged after 8 times full impact (as described in Section 7.3.2), while the one with only hook ended steel fibres (HF) needs 5 times full impact to be damaged. At the front surface of these two types of concrete, the created crater area is relatively small, and the generated cracks are not easy to be observed after the impact. Nevertheless, at the rear surface of the concrete target, with the increase of shock numbers, the cracks number and size simultaneously increase. When the embedded steel fibres cannot resist the growth of cracks and hold the concrete slab together, the sustainable UHPFRC target is broken into two pieces. In Figures 7.20 and 7.21, the creation and development of cracks at front and rear surface of the sustainable UHPFRC with different fibres during each impact are illustrated.



(a) after the first impact



(b) after the first impact



(c) after the second impact



(d) after the second impact



(e) after the third impact



(f) after the third impact



(g) after the fourth impact



(h) after the fourth impact

**Figure 7.20: Cracks development in the sustainable UHPFRC with single sized steel fibres (HF) after each impact: (a), (c), (e) and (g) are front surfaces, (b), (d), (f) and (h) are rear surfaces**

As can be observed, after the first impact, a very small damage area can be found on the front surface of the sustainable UHPFRC with single sized fibres, while some crossed cracks can be noticed at its rear surface. After the subsequent 3 times impacts, no big difference can be noticed in the damage area on the front surface of the concrete target. Yet, at the rear surface of the concrete slab, the growth of the created cracks can be clearly observed. After 4 times impact, the concrete slab has already seriously bended, but the main concrete parts are still connected by the steel fibres. Similar results can also be noticed in the case of the sustainable UHPFRC with hybrid steel fibres, in which the damage area on the front surface is still relatively small after 7 times impact and clear cracks can be found on the concrete rear surface. However, compared to the sustainable UHPFRC with single sized fibres, more cracks can be observed in the mixture with hybrid steel fibres (as shown in Figure 7.21f), which is beneficial for improving the energy dissipation capacity of the sustainable UHPFRC.

The phenomena described above can be attributed to the reasons as follows: 1) compared to plain concrete, the addition of steel fibres can well hold the concrete matrix and restrict the growth of cracks; 2) the short fibres can bridge the micro-cracks while the long fibres are more efficient in preventing the development of macro-cracks, which cause that the stress in the hybrid fibres reinforced concrete can be better distributed; 3) compared to the sustainable UHPFRC with single sized fibres, more cracks can be created in the mixture with hybrid fibres, which means more energy is needed for the growth of cracks. Hence, to well resist the pendulum impact (as shown in this study), the sustainable UHPFRC with hybrid steel fibres is a good choice.



(a) after the first impact



(b) after the first impact



(c) after the second impact



(d) after the second impact



(e) after the third impact



(f) after the third impact



(g) after the fourth impact



(h) after the fourth impact



(i) after the fifth impact



(j) after the fifth impact



(k) after the sixth impact



(l) after the sixth impact



(m) after the seventh impact



(n) after the seventh impact

**Figure 7.21: Cracks development of the sustainable UHPFRC with hybrid steel fibres during each impact: (a), (c), (e), (g), (i), (k) and (m) are front surfaces, (b), (d), (f), (h), (j), (l) and (n) are rear surfaces**

· ***Absorbed impact energy***

Based on the results shown in the previous section, it can be concluded that the sustainable UHPFRC with hybrid steel fibres has better energy dissipation capacity than the one with only single sized fibres under the pendulum impact. To quantify the absorbed impact energy during the impact process, related calculations are executed and presented in this section.

As shown in Section 7.3.2, to calculate the energy absorbed by concrete slab, the hammer impact velocity, hammer residual velocity and the concrete target velocity should be measured. With the help of a camera and the meshed board, all these velocities can be obtained. One example is shown in Figure 7.22. During the 0.02 s time gap, the movement of the hammer after the impact is about 6 cm, and the movement of the concrete slab is about 10 cm. Yet, due to the effect of the gap between the hammer and the meshed board (as shown in Figure 7.12), the real movements during the 0.02 s of the hammer and concrete slab are about 4.9 cm and 8.2 cm, respectively. Therefore, the calculated hammer residual velocity and the concrete slab velocity after the impact are about 2.45 m/s and 4.10 m/s, respectively. Based on Eq. (7.9), during this impact, the absorbed energy by the concrete target is about 565.3 J, which is about 47% of the total impact energy (1201.3 J).

Afterwards, according to the method shown above and Eq. (7.10), it is possible to calculate the total energy absorbed amount ( $E_{total-absorbed}$ ) of the developed sustainable UHPFRC. Nevertheless, due to the fact that it is impossible to calculate the absorbed impact energy of the last impact (when concrete slab is broken into pieces), the obtained

$E_{total-absorbed}$  is the minimum energy absorption capacity of the developed concrete before being seriously damaged. In this study, the calculated  $E_{total-absorbed}$  values for the sustainable UHPFRC with single sized fibres and hybrid steel fibres are 2248.5 J and 3951.8 J, respectively. These results quantitatively demonstrate that the addition of hybrid steel fibres is beneficial for improving the impact resistance and energy absorption capacity of the developed sustainable UHPFRC.

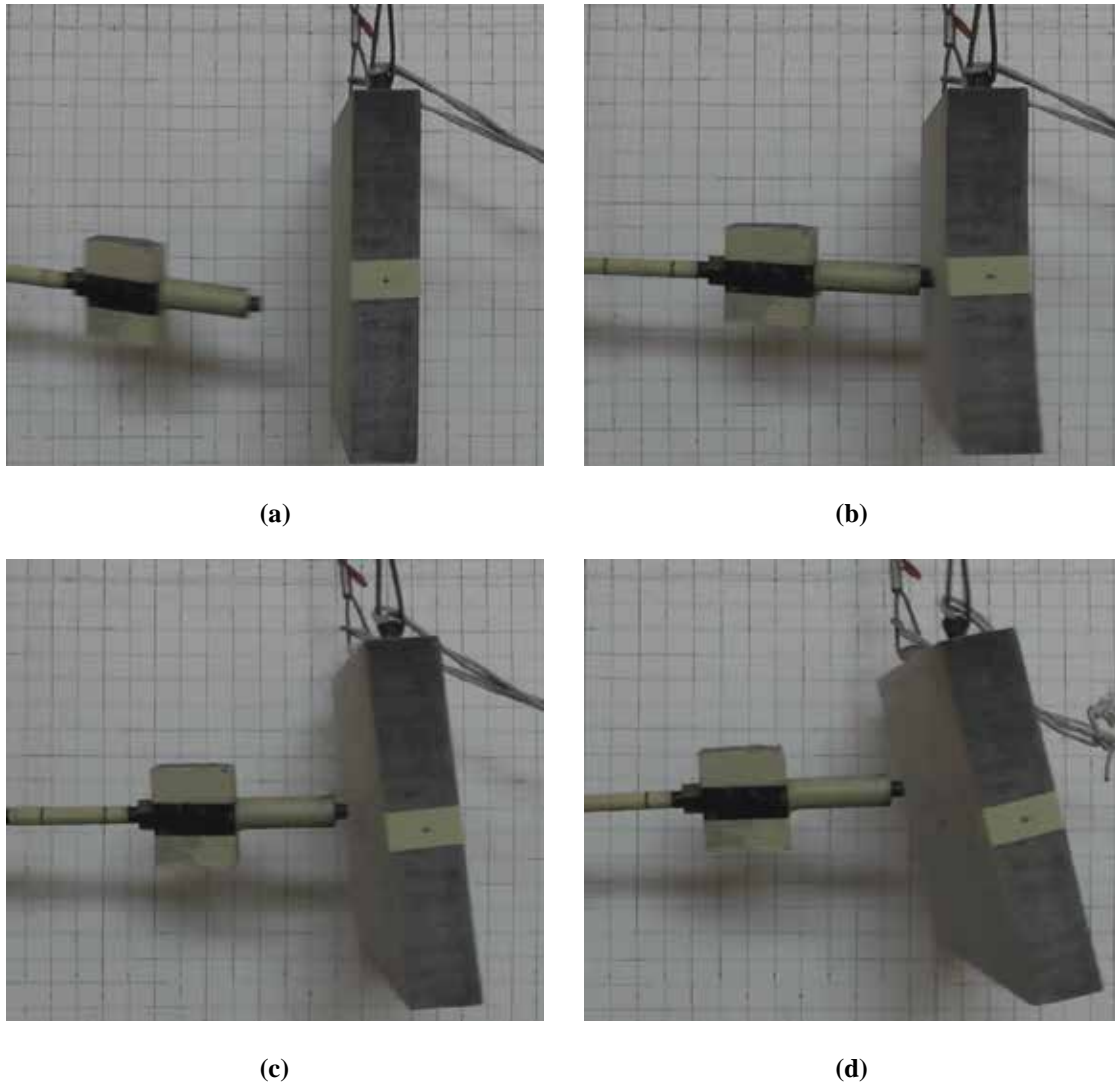


**Figure 7.22: One example of the impact process recorded by camera**

• ***Fracture morphology***

The fracture morphologies of the designed concrete samples after impact tests are presented in Figure 7.23. It can be noticed that the plain concretes (without fibres) are always broken into many pieces, while the sustainable UHPFRCs are normally broken into two pieces. This difference can be attributed to the fact that the added steel fibres can

well bridge the created cracks during the impact process. Moreover, for the plain concrete, it can be noticed that the one with high compressive strength (UHPC) is broken into more small pieces, which implies that more impact energy is absorbed than the one with lower compressive strength. However, the improvement of compressive strength is a relatively inefficient method to enhance the impact resistance of concrete. When steel fibres are added into the UHPC, the cracks growth can be significantly resisted and a large amount of energy is needed to pull the fibres out during the impact process. Particularly when the hybrid steel fibres are included, the stress can be homogeneously distributed and many small cracks are created (as shown in Figure 7.23d) under impact loadings, which is positive for improving the energy dissipation capacity of the developed sustainable UHPFRC.

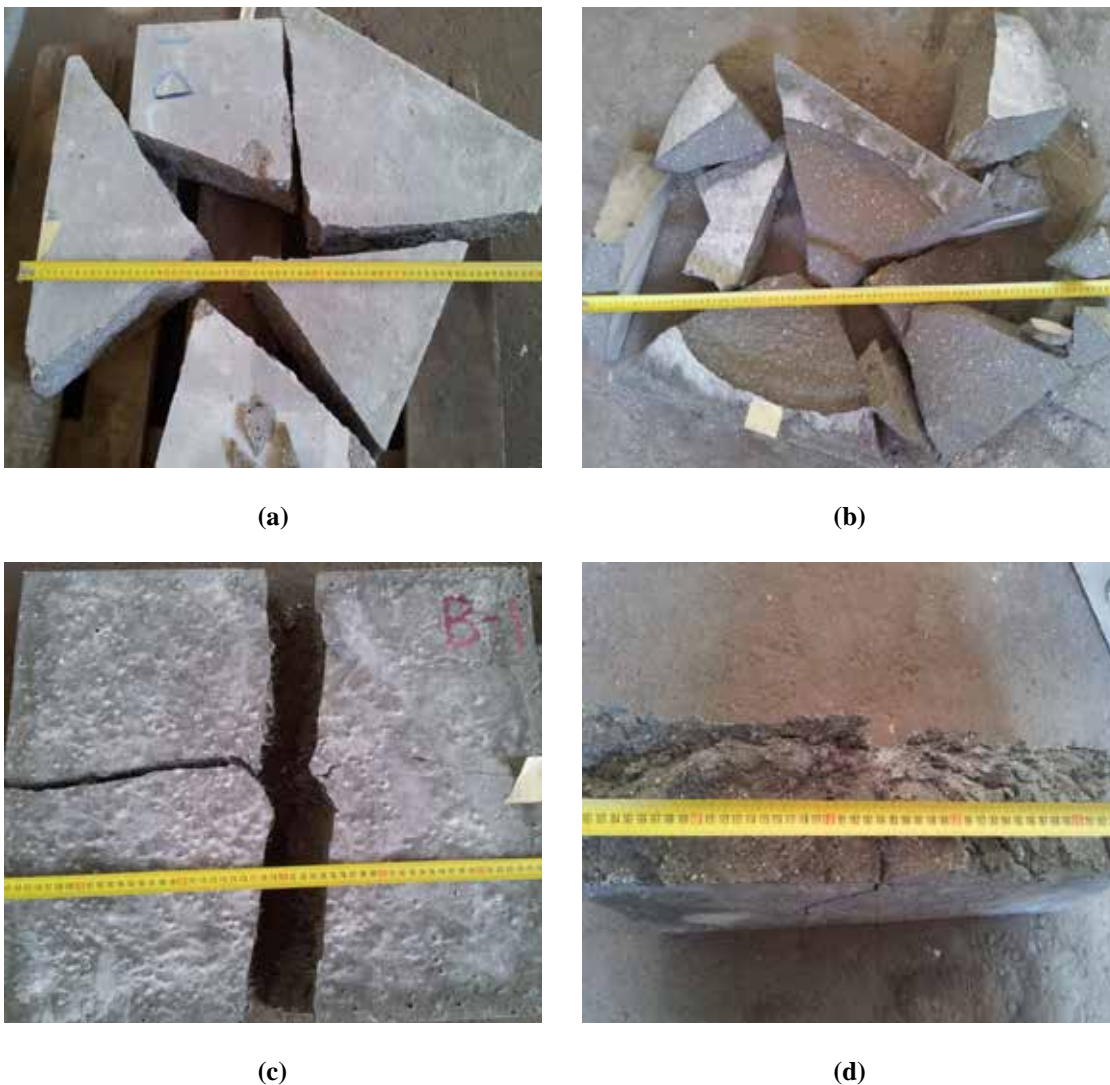


**Figure 7.23: Fracture morphologies of the designed concrete samples after impact tests: (a) normal strength concrete; (b) sustainable UHPC matrix (without fibres); (c) sustainable UHPFRC with single sized fibres; (d) sustainable UHPFRC with hybrid fibres**

### 7.3.5 Comparison of the results obtained from different pendulum impact tests

In this chapter, two different pendulum impact set-ups have been utilized in the experiments. The dynamic impact test results obtained from “Charpy Impact Device” show that the fibre length plays a dominating role in improving the energy dissipation capacity of the sustainable UHPFRC. With a constant total steel fibre amount, the addition of short fibres can cause a decrease of the energy absorption capacity of the concrete target. However, from the results obtained from the “Modified Pendulum Impact Device”, it is demonstrated that the addition of hybrid steel fibres is more efficient than single sized fibres in increasing the energy dissipation capacity of the sustainable UHPFRC.

The difference between the obtained results should be mainly attributed to the fibre categories and sample dimensions. As mentioned before, the impact energy absorbed by the sustainable UHPFRC is mainly composed of two parts: the energy used to break the concrete matrix and the energy used to pull out the fibres embedded in the broken cross sections. For the Charpy impact test, due to the fact that the used concrete sample is relatively small and the impact energy is relatively large, all the targets are broken after one time impact (as shown in Figure 7.13). Hence, the cracks can be created immediately, and more energy is consumed in pulling fibres out, which causes that the advantages of hybrid steel fibres (LSF + SSF) in stress distribution and micro-cracks resistance are not well utilized. Considering the fact that the used SSF is relatively short and easy to be debonded from the concrete matrix, the addition of short fibres (SSF) can cause a decrease of the energy absorption capacity of the concrete target.

On the contrary, in the case of the tests executed by the “Modified Pendulum Impact Device”, the employed sample dimensions are relatively large, which cause that the concrete target cannot be broken after the first impact (as shown in Figure 7.21). Therefore, the creation of cracks plays an important role in resisting the impact loadings. Due to the fact the stress in the hybrid fibres reinforced concrete can be better distributed than that in single sized fibres reinforced concrete, more small cracks are created in the sustainable UHPFRC with hybrid steel fibres, which simultaneously means more energy is consumed in the creation of cracks and also growth of these cracks. This can be demonstrated by the results shown in Figure 7.21, in which the first four times impact mainly causes the creation of cracks and increases the crack numbers.

Consequently, based on the experimental results obtained here, to effectively apply the sustainable UHPFRC in the production of protective structure, the one with hybrid steel fibres (HF+LSF) is a good choice.

### 7.3.6 Summary

This section investigates the energy dissipation capacity of the developed sustainable UHPFRC. Based on the results presented in the previous chapters, the modified A&A model is employed for the concrete matrix design. Two pendulum impact set-ups are utilized in the experiments: “Charpy Impact Device” and “Modified Pendulum Impact Device”. Based on the obtained results the following conclusions can be drawn:

- 1) For the Charpy impact test, the fibre length plays a dominating role in improving the energy dissipation capacity of the sustainable UHPFRC. With a constant total steel fibre amount, the addition of short fibres (SSF) decreases the energy absorption capacity of the concrete target.
- 2) An equation is proposed to compute the energy dissipated in the sustainable UHPFRC (with only straight steel fibres) under the Charpy impact test. This new model features a good correlation with the experimental results, especially for the samples with lower energy absorption capacity. When the impact resistance ability of the UHPFRC is relatively high, the modeling results slightly underestimate the experimental results (about 9.3%), which could be attributed to the energy dissipated into the test device.
- 3) The results obtained from the “Modified Pendulum Impact Device” demonstrate that the developed sustainable UHPFRC has much better energy dissipation capacity than normal strength concrete (NSC) and ultra-high performance concrete (UHPC). The increase of the compressive strength is ineffective in improving the impact resistance of concrete under the pendulum impact loadings.
- 4) Compared to the concrete with single sized fibres (HF), the addition of hybrid steel fibres (HF+LSF) is more beneficial for improving the energy dissipation capacity of the sustainable UHPFRC under the impact loadings from the “Modified Pendulum Impact Device”.
- 5) The different experimental results obtained from “Charpy Impact Device” and “Modified Pendulum Impact Device” can be attributed to the sample sizes and impact energies. Due to the fact that the dimensions of protective structure applied in practice are normally relatively large, the sustainable UHPFRC with hybrid steel fibres is a suitable selection.

## 7.4 Conclusions

To have a stable concrete structure and protect the human inside civil and military buildings, it is very important to clarify the dynamic performance of concrete under impact loadings. Based on the available literature, it is demonstrated that a strong concrete matrix and appropriate inclusion of fibres (particularly steel fibres) are the most crucial factors in the production of concrete with relatively high energy dissipation capacity. This implies that the UHPFRC is suitable to be utilized in structures where a

large amount of energy may be released suddenly. Nevertheless, the investigation regarding the energy dissipation capacity of UHPFRC is insufficient and it is unclear whether the developed sustainable UHPFRC would be suitable to be utilized in the construction of protective structures. Therefore, in this chapter, the dynamic performance of the developed sustainable UHPFRC under impact loadings is evaluated. Two types of pendulum impact set-ups are utilized in the experiments: “Charpy Impact Device” and “Modified Pendulum Impact Device”. The obtained experimental results demonstrate that the developed sustainable UHPFRC has much better energy dissipation capacity than normal strength concrete (NSC) and ultra-high performance concrete (UHPC). Moreover, for the production of protective structure with relatively large dimensions, the developed sustainable UHPFRC with hybrid steel fibres (hook ended steel fibres and long straight steel fibres) is a good choice.

In Chapter 5, it is demonstrated that the application of only hook ended steel fibres is beneficial for improving the toughness of concrete. However, according to the results obtained in this chapter, to design a sustainable UHPFRC with relatively high energy dissipation capacity under impact loadings, the addition of hybrid steel fibres is better. Consequently, based on the different requirements in practice, different fibre type and hybridization should be appropriately chosen, which is also beneficial for increasing the fibre efficiency and produce a more sustainable UHPFRC.



## Chapter 8

### Modeling of concrete target under projectile impact

#### 8.1 Introduction

Among all the impact categories (high-rate impact, shock, blast loads and so on), the impact from hard projectiles is the most common one, which have already been studied since the middle of 1700s (Kennedy, 1976). During those period, due to the continuous military interest in designing high destructive weapons and high performance protective barriers, more attention has been paid on the penetration and perforation of hard projectiles into concrete targets. Meanwhile, over the last several decades, a number of relative studies are performed experimentally, analytically and numerically to describe various penetration processes and the different reaction of concrete under impact loadings (Kennedy, 1976; Berriaud et al., 1978; Bangash, 1993; Williams, 1994; Corbett et al., 1996; Forrestal and Hanchak, 2002; Li et al., 2005; Vossoughi et al., 2007; Wang et al., 2007; Werner et al., 2013; Mohamed and Ahmed, 2014). A review of the progress in concrete design aimed at resisting missile impact can be found in (Kennedy, 1976), in which the terminology used when describing local projectile impact effects was clarified and the empirical formulae, commonly used to predict the local missile impact effects, were summarized. In general, there are seven phenomena associated with projectile impact effects on concrete targets, as shown in Figure 8.1.

Due to the difference in the fundamental characteristics between the projectiles and concrete plates, the performance of concrete targets can be totally different. Based on a number of experimental investigations (Bangash, 1993; Williams, 1994; Corbett et al., 1996), some empirical formulae were proposed to predict the penetration depth, scabbing limit and perforation limit (the scabbing and perforation limits means the minimum thickness of the target to prevent the corresponding failure for a given impact velocity, and the ballistic limit for perforation is defined here as the minimum impact velocity to perforate a target of a given thickness). For instance, Modified Petry formula, Ballistic Research Laboratory (BRL) formula for penetration and scabbing, Army corps of engineers (ACE) formula, Modified NDRC formula, Ammann and Whitney formula, Whiffen formula, Kar formula, CEA–EDF perforation formula, UKAEA formula, Bechtel formula, Stone and Webster formula, Degen perforation formula, Chang formula, Haldar–Hamieh formula, Adeli–Amin formula, Hughes formula, Healey and Weissman formula and the IRS formulae for penetration and complete protection (Li et al., 2005).

Among all the proposed empirical formulae, the Modified NDRC formula is the most accepted, which is described in the following content.

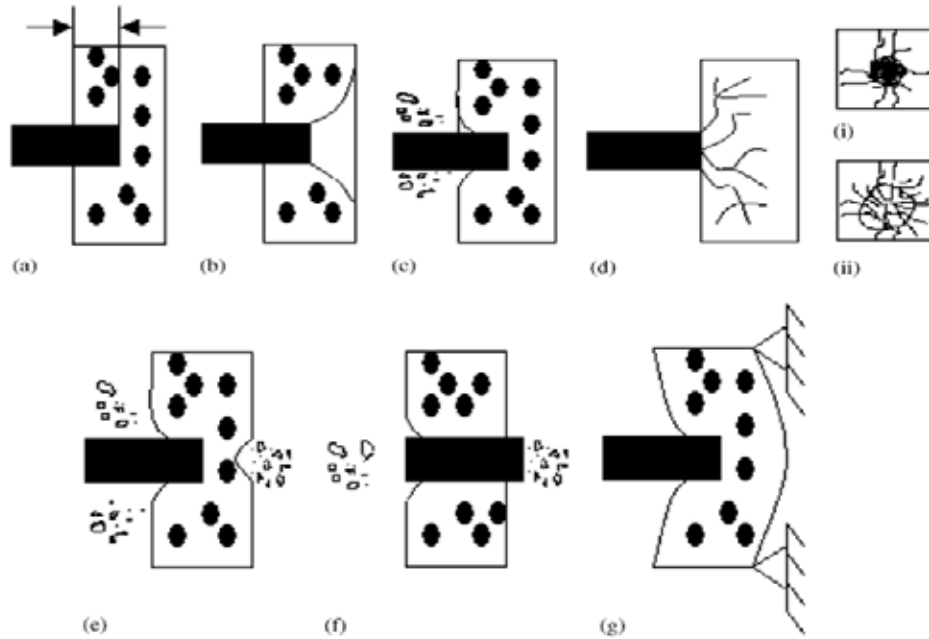


**Figure 8.1: Projectile impact effects on concrete target, (a) Penetration, (b) Cone cracking, (c) Spalling, (d) Cracks on (i) proximal face and (ii) distal face, (e) Scabbing, (f) Perforation, and (g) Overall target response (Kennedy, 1976).**

The Modified NDRC formula was put forward in 1946 by the US National Defence Research Committee based on the ACE formulae, further testing data and a penetration model for a rigid projectile penetrating a massive concrete target, where it was assumed that the contact force increased linearly to a constant maximum value when the penetration depth is small (NDRC, 1946; Kennedy, 1976). The Modified NDRC penetration formula defined by a G-function is shown as follows:

$$G = 3.8 \cdot 10^{-5} \frac{N^* M \frac{\sigma}{C} V_0^{1.8}}{d \sqrt{f_c} \frac{e}{d} \phi} \quad (8.1)$$

where  $N^*$  is the nose shape factor (equal to 0.72, 0.84, 1.0 and 1.14 for flat, hemispherical, blunt, and very sharp noses),  $M$  is the mass of the projectile (kg),  $d$  is diameter of the projectile (m),  $V_0$  is projectile impacting velocity (m/s),  $f_c$  is compressive strength of concrete target (MPa). The  $G$  value is subsequently used in the following equations:

$$\frac{x}{d} = 2G^{0.5} \quad (G > 1) \quad (8.2)$$

and

$$\frac{x}{d} = G + 1 \quad (G < 1) \quad (8.3)$$

where  $x$  is penetration depth of projectile (m).

Perforation and scabbing limits  $e$  and  $h_s$ , respectively, can be predicted by:

$$\frac{e}{d} = 3.19 \frac{\sigma_c}{\rho d v} - 0.718 \frac{\sigma_c}{\rho d v^2} \quad (x/d < 1.35 \text{ or } e/d < 3) \quad (8.4)$$

$$\frac{e}{d} = 1.32 + 1.24 \frac{\sigma_c}{\rho d v} \quad (1.35 < x/d < 13.5 \text{ or } 3 < e/d < 18) \quad (8.5)$$

and

$$\frac{h_s}{d} = 7.91 \frac{\sigma_c}{\rho d v} - 5.06 \frac{\sigma_c}{\rho d v^2} \quad (x/d < 0.65 \text{ or } h_s/d < 3) \quad (8.6)$$

$$\frac{h_s}{d} = 2.12 + 1.36 \frac{\sigma_c}{\rho d v} \quad (0.65 < x/d < 11.75 \text{ or } 3 < h_s/d < 18) \quad (8.7)$$

Although all of these proposed empirical formulae can be used to support the design of protective structure and contribute to the efficient application of raw materials, they are derived from a large amount of resources and labour cost, which is not in line with the sustainable development. Moreover, many of these empirical formulae were proposed around 70 years ago, which means they are only suitable to be used to predict the dynamic performance of concrete used at that time. With the development of concrete industry, powder technology and chemical industry, a series of advanced concretes (e.g. SCC, HSC, UHPC and UHPFRC) can be produced today. Due to the properties difference between the advance concretes and the “old” concrete used around 70 years ago, a new and reliable method to evaluate the impact resistance of the advanced concretes is needed. One of the promising approaches is the application of numerical modeling tools. From the available literature, it can be noticed that the modeling of concrete performance under impact loadings becomes very popular in recent years. Hence, in this chapter, one of a commercial hydrocode (LS-DYNA) is utilized to investigate the energy dissipation capacity of the developed sustainable UHPFRC.

## 8.2 The state of the art

As commonly known, concrete has very complicated nonlinear behaviour, which is difficult to be fully described for general stress conditions by a simple constitutive model. When concrete is subjected to extreme loads such as high velocity impact of missiles and

fragments, the modeling of concrete can be further complicated due to rate effects, overloading and large deformations (Tu and Lu, 2009). With the advancement in the computing power, it is now possible to perform numerical modeling for the response of concrete structures subjected to severe shock and impact loads, including the modeling of the loading sources if necessary. A number of commercial hydrocodes such as ABAQUS (2004), AUTODYN (2001) and LS-DYNA (2003) are available for the general simulation of structural nonlinear dynamic responses. In this study, LS-DYNA is employed to investigate the energy dissipation capacity of the sustainable UHPFRC.

### **8.2.1 Introduction of LS-DYNA**

LS-DYNA originated from the 3D FEA program DYNA3D, developed by Hallquist at Lawrence Livermore National Laboratory (LLNL) in 1976 (LSTC, 2009; Benson, 2009). DYNA3D used explicit time integration to study nonlinear dynamic problems, with the original applications being mostly stress analysis of structures undergoing various types of impacts (LSTC, 2009; Benson, 2009). The program was initially very simple, since the lack of adequate computational resources at the time. In 1979 a new version of DYNA3D was released. Improvements in 1982 further boosted the execution speed by about 10%. In 1986, many capabilities were added, including beams, shells, rigid bodies, single surface contact, interface friction, discrete springs and dampers, optional hourglass treatments, optional exact volume integration and so on. Metal forming simulation and composite analysis capabilities were added to DYNA3D in 1987. The final release of DYNA3D in 1988 included several more elements and capabilities (LSTC, 2009; Benson, 2009).

### **8.2.2 Material models for concrete in LS-DYNA**

In the modeling of projectile impact on concrete targets, a valid material model is crucial for the accuracy of simulation. In LS-DYNA, there are already some available models that could be used to represent concrete under dynamic impact loadings. For instance, to handle the problems where foams or soil-like materials are confined within an enclosure or when geometric boundaries are present, the “Soil foam model” can be utilized appropriately (Krieg, 1972). However, the various softening behaviour of concrete under different loading conditions cannot be captured anymore in this model. The “Isotropic elastic-plastic with oriented cracks model” is suitable for modeling brittle materials that fail primarily due to a large tension or significant shear loading. However, this model does not consider several factors which are important for concrete under extreme loading, including the pressure hardening, third stress invariant-dependent deviatoric section, rate dependency, and post-peak softening. Therefore, the application of such a model is rather limited (Shugar et al., 1992). The “Kinematic hardening cap model” can describe the plastic flow of material (Simo et al., 1988; Sandler and Rubin, 1979). However, the formulation of the failure surfaces generates a circular deviatoric cross section, due to

which the cap model cannot predict well the softening behaviour of concrete and also cannot represent satisfactorily the suppressing effect of the confining pressure on the dilatancy of concrete material (Koiter, 1953). Some common points can be found between the “Concrete damage model” and “Kinematic hardening cap model”. However, Yonten et al. (2005) demonstrated that the “Concrete damage model” does not give a smooth transition from the softening to the residual region of the stress-strain curve, and this is attributable to the abrupt variation of the scalar factor. The “Brittle damage model” is an anisotropic and smeared crack material model, which is formulated primarily for the evaluation of damage in concrete and also can be applied to other brittle materials (Govindjee et al., 1994; Govindjee et al., 1995). This model has been tailored for cases where the tensile cracking is the primary failure mode in concrete. The “Holmquist Johnson Cook Concrete model” can be used for concrete subjected to large strains, high strain rates and high pressures (Holmquist et al., 1993). The equivalent strength is expressed as a function of the pressure, strain rate, and damage. The pressure is expressed as a function of the volumetric strain and includes the effect of permanent crushing. The damage is accumulated as a function of the plastic volumetric strain, equivalent plastic strain and pressure. In this study, considering the fact that the concrete is subjected to projectile impact and large strains, high strain rates and high pressures will be generated, the Holmquist Johnson Cook Concrete model is employed. Some detailed mechanisms of this material model are shown in Appendix 1.

### **8.2.3 Macro-scale simulation based on LS-DYNA**

Macro-scale is one of the most common scales of simulating concrete under dynamic loadings, in which the concrete element and projectile are all treated as homogeneous parts. For instance, Sawamoto et al. (1998) proposed an analytical approach for assessing local damage to reinforced concrete structures subjected to impact load, applying the discrete element method. Johnson (2011) presented the investigation results of numerical algorithms and computational material models for high-velocity impact and other intense impulsive loading conditions. Agardh and Laine (1999) presented the simulations using LS-DYNA for the projectile perforation of a 60 mm thick fibre-reinforced concrete slab with a velocity of 1500 m/s. The material model used was Type 78 “Soil/Concrete” with erosion. The results were in fairly good agreement with the test results, but more studies are necessary to assess the sensitivity of certain material parameters. Teng et al. (2008) employed LS-DYNA to study the dynamic response of steel fibre reinforced concrete (SFRC) subject to impact loading. The elastic-plastic hydrodynamic material model was employed to model the non-linear softening behaviour of SFRC. The results show that the proposed model is useful and can be further developed for designing the protection of military structures, nuclear power plants and other facilities against high velocity projectiles. Beppu et al. (2008) described the evaluation of the local damage of concrete plates by the impact of high-velocity rigid projectiles. The damage or failure behaviour

was discussed on the basis of the failure process captured by a high speed video camera and the strain histories obtained by strain gauges on the concrete plate. The mechanism of the local damage of concrete plates was investigated by numerical tools. To determine an appropriate material model for engineered cementitious composite (ECC) materials under dynamic loading, Li and Zhang (2012) investigated several widely used material models for plain concrete under dynamic loading, especially the Concrete Damage model and the Elastic-Plastic Hydrodynamic model. In general, the macro-scale simulation of concrete under impact loading of projectiles is quite common, in which the concrete targets and projectiles are all treated as homogeneous parts. Due to the simplification of concrete and projectiles, the computation space and time can be obviously reduced.

#### **8.2.4 Meso-scale simulation based on LS-DYNA**

As commonly known, concrete is a heterogeneous material made of cement, water, and about 80% of aggregates including gravel, sand, fine fillers and chemical additives. Although all the ingredients influence the final mechanical behaviour, it seems that every ingredient has an influence according to its basic characteristics. Therefore, meso-scale should be the suitable working scale for material scientists in concrete research. Nevertheless, due to the relatively low calculating capacity of computer, very limited meso-scale simulations regarding concrete under impact loadings can be found in the open literature. For example, Xu et al. (2012a; 2012b) developed an axisymmetric mesoscale steel fibre reinforced concrete (SFRC) model to investigate the dynamic failure behaviour of SFRC material under impact loading at different strain rates. Based on the obtained numerical results, the influences of steel fibres on dynamic material properties, in particular the dynamic increase factor (DIF), and on dynamic failure mechanism of SFRC are analysed. In the investigation of Kim et al. (2011c), concrete is considered as a 3-phase composite material; mortar matrix, aggregates, and interfacial transmission zone (ITZ). The aggregates are modelled as a linear-elastic material, whereas the mortar matrix and ITZ are modelled using a coupled plasticity-damage model with different tensile and compressive mechanical behaviour. Aggregate shape, distribution, and volume fraction are considered as simulated variables. Snozzi et al. (2011) investigated the dynamic behaviour of concrete in relation to its composition within a computational framework. Concrete is modelled using a meso-mechanical approach in which aggregates and mortar are represented explicitly. Both continuum phases are considered to behave elastically, while nucleation, coalescence and propagation of cracks are modelled using the cohesive-element approach. However, a phenomenological rate-dependent cohesive law is needed to obtain a better agreement with experiments. Qin et al. (2011) developed a meso-scale dynamic model for numerical study of the dynamic failure behaviour of three-phase concrete (e.g. aggregate, mortar, and interface). The numerical modeling shows that the higher the strain rates, the more reticular mesocracks occur, the kinetic and frictional energies become more important,

which implies that the fracture process at high strain rates requires more energy to reach failure. To clarify the influence of free water on the performance of concrete under high strain rates impact loadings, Erzar and Forquin (2011) used a mesoscopic approach, in which the matrix and the aggregates are differentiated. Based on the references listed above, it can be noticed that concrete is mostly treated as a composition of at least three phases during the meso-scale simulation, and the effect of each phase on the performance of concrete is considered. Nevertheless, due to the complexity of the concrete under high strain rates impact loadings, the computation time is normally long and the accuracy of the simulation still needs further improvements.

### **8.2.5 Summary**

In summary, due to the development of the computation ability of computer and large amounts of experimental results for concrete under impact loadings, the modeling investigation of concrete dynamic performance has become very popular in recent years. Compared to the experimental research, modeling investigation can effectively save costs, resource and labour. From the available literature, some studies about the dynamic performance of concrete under impact employing LS-DYNA can be found, which can generally be divided into two categories: macro-scale simulation and meso-scale simulation. Due to the fact that concrete is a complex composite, which causes that the meso-scale simulation of concrete under impact loadings is relatively difficult.

However, in all these available modeling research, the numerical investigation of the impact resistance of UHPFRC is insufficient, which may be attributed to the fact that the UHPFRC is still a relatively new building material, and the investigation focus for UHPFRC is mainly the mix design and the performance under quasi-static circumstance. Hence, in this chapter, the macro-scale simulation method will be employed to investigate the energy dissipation capacity of the developed sustainable UHPFRC under projectile impact, which is shown in the following part.

## **8.3 Modeling of the concrete target under projectile impact**

As mentioned in previous parts, to simulate the dynamic performance of the developed sustainable UHPFRC, a commercial hydrocode (LS-DYNA) is employed here. In this study, a finite elements model is firstly created in LS-DYNA to evaluate the energy dissipation capacity of concrete slab under the impact of projectile with different velocities. Then, this model is validated by the experimental results obtained from the literature. Afterwards, the validated model is utilized to predict the performance of the sustainable UHPFRC under the projectile impact.

### 8.3.1 Model of concrete plate under projectile impact

Following the experiments described in Hanchak's test (1992), a finite elements model of concrete plate under projectile impact is created in LS-DYNA. The dimension of concrete target is  $610 \times 610 \times 178$  mm. The length of projectile is 143.7 mm, and its diameter is 25.4 mm. As can be found in Hanchak et al. (1992), to minimize the effects of steel reinforcement, the impact direction of projectile is carefully controlled to avoid that the projectile impact directly on the reinforcements. Moreover, Huang et al. (2005) demonstrated that rebar reinforced concrete and plain concrete have almost the same penetration resistance as the projectile typically possesses diameters much smaller than the grid size of slab reinforcement. Therefore, in this study, the concrete slab is regarded as a plain concrete for simplifying the modeling. In addition, in Hanchak et al. (1992), the calibre-radius-head (CRH) ratio of the used ogive-nose projectile is 3, which means the head of the used projectile is very sharp. The CRH means the radius of a circle with the curve of the shell's nose on its circumference, expressed in terms of the shell's calibre (as shown in Figure 8.2). Although the CRH ratio of the ogive-nose projectile is an important factor influencing the performance of concrete during the impact process, Wang et al. (2007) presented that the CRH ratio of the ogive-nose projectile only has close relationship with the crater area after the impact. Considering that the crater area of concrete slab after impact is not a focus in Hanchak's test and the detailed crater area values are not presented in Hanchak et al. (1992), the finite elements model of projectile is simplified in this study, as shown in Figure 8.3. In addition, Figure 8.3 also shows the finite element mesh for the concrete slab and projectile, in which the mesh used in the computation has 32960 elements and 36582 nodes. The contact types are "surface to surface" and "eroding". The boundary of the tested sample is fixed. However, the influence of the mesh size, mesh bias and friction effects are not included in this work. These issues will be focused in a future study.

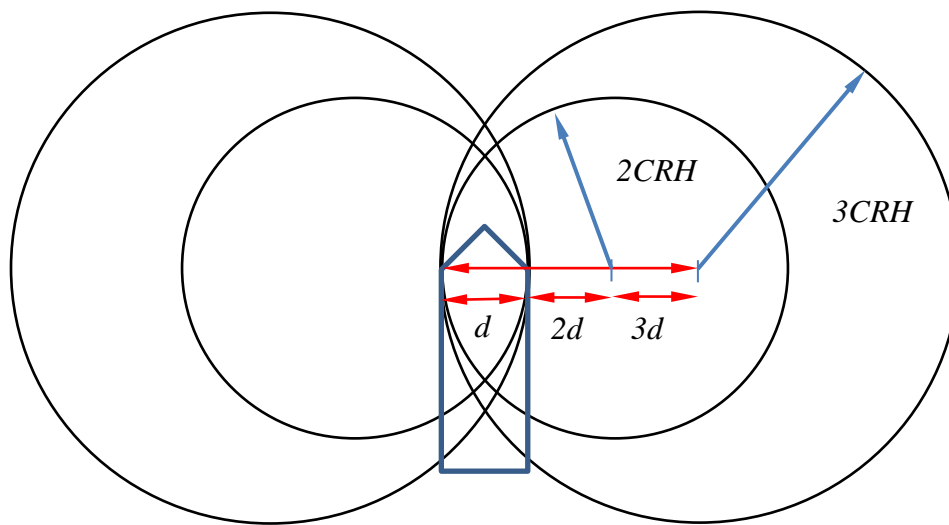
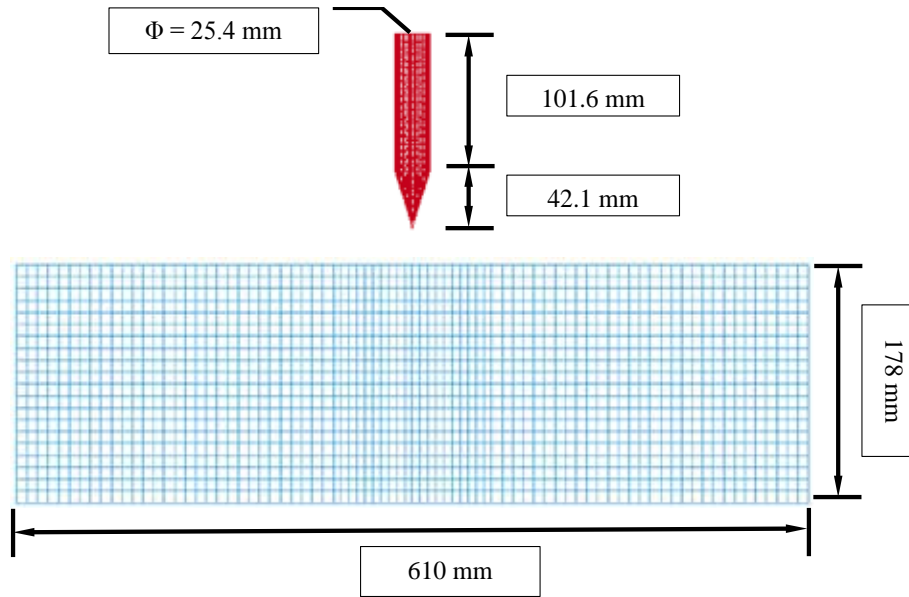


Figure 8.2: Schema of the calibre-radius-head (CRH) ratio calculation method



**Figure 8.3: Dimensions of the model created in LS-DYNA and the generated finite element grids in this study**

In this modeling, similarly to the experimental results shown in Hanchak et al. (1992), two concrete slabs with different compressive strength (one is 48 MPa and the other one is 140 MPa) are utilized. To fully describe the concrete's dynamic response within an impact force, the Holmquist Johnson Cook Concrete model (Holmquist et al., 1993) is chosen to describe the reaction of concrete under the high velocity impact. A detailed description of this model is shown in Appendix 1, and the parameters of material model for the used concrete are presented in Tables 8.1 and 8.2. In addition, during the impact process, the projectile is assumed to be a no-deformable part (rigid material), with velocities of 301 m/s, 360 m/s, 381 m/s, 434 m/s, 606 m/s, 746 m/s, 749 m/s and 1058 m/s for the low strength concrete (48 MPa), and 376 m/s, 382 m/s, 443 m/s, 522 m/s, 587 m/s, 743 m/s and 998 m/s for the high strength concrete (140 MPa). A detailed description of the used rigid material model is shown in Appendix 2.

**Table 8.1: Material parameters of concrete (48 MPa) for impact analysis**

<i>Density</i>	<i>Shear modulus</i>	<i>Strength constants</i>						
$\rho$ (kg/m <sup>3</sup> )	G (MPa)	A	B	N	C	$f'_c$ (MPa)	$S_{max}$ (MPa)	$\epsilon'_0$
2240	14860	0.79	1.60	0.61	0.07	48	7.0	1.0
<i>Damage constants</i>								
$D_1$			$D_2$			$(\epsilon_p^f + \mu_p^f)_{min}$		
0.04			1.0			0.01		
<i>Equation of state, EOS constants</i>								
$P_{crush}$ (MPa)	$\mu_{crush}$	$K_1$ (GPa)	$K_2$ (GPa)	$K_3$ (GPa)	$P_{lock}$ (GPa)	$\mu_{lock}$		
16.0	0.01	8.5	17.1	20.8	1.05	0.1		

Table 8.2: Material parameters of concrete (140 MPa) for impact analysis

<i>Density</i>		<i>Shear modulus</i>		<i>Strength constants</i>				
$\rho$ (kg/m <sup>3</sup> )	G (MPa)	A	B	N	C	$f'_c$ (MPa)	$S_{max}$ (MPa)	$\epsilon'_0$
2400	16400	0.75	1.65	0.76	0.07	140	11.7	1.0
<i>Damage constants</i>								
$D_1$			$D_2$		$(\epsilon'_p + \mu'_p)_{min}$			
0.04			1.0		0.01			
<i>Equation of state, EOS constants</i>								
$P_{crush}$ (MPa)	$\mu_{crush}$	$K_1$ (GPa)	$K_2$ (GPa)	$K_3$ (GPa)	$P_{lock}$ (GPa)	$\mu_{lock}$		
26.0	0.01	12.5	17.1	20.8	1.05	0.1		

### 8.3.2 Model validation

During the impact process, the concrete slab typically experiences brittle tensile fracture firstly, which is followed by compression-shear failure, since the compressive strength of concrete is much higher than its tensile strength (Katrin and Paul, 2008; Hassan et al., 2012; Park et al., 2012; Rossi, 2013). In this study, with the movement of projectile, both the compressive and tensile damage begin to accumulate, and the spalling of concrete can be observed. When the impact velocity of projectile is relatively high, then the scabbing appears on the rear side of concrete slab (as shown in Figure 8.4). Moreover, for both the normal strength concrete (NSC) (48 MPa) and high strength concrete (HSC) (140 MPa), the perforation phenomenon (from modeling results) can always be observed, when the impact velocity higher than a critical value (about 300 m/s for NSC and about 400 m/s for HSC). These obtained modeling results are similar as that shown in Wang et al. (2007).

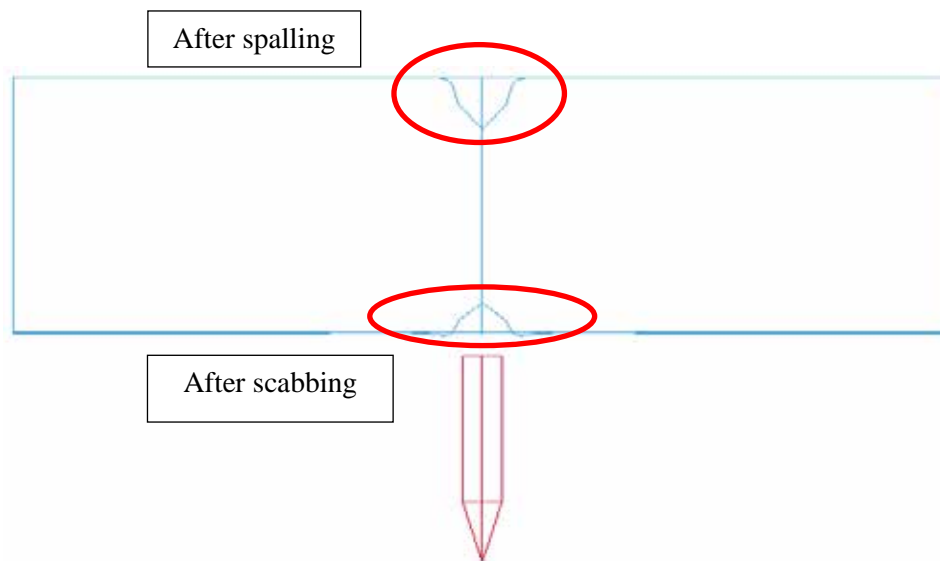
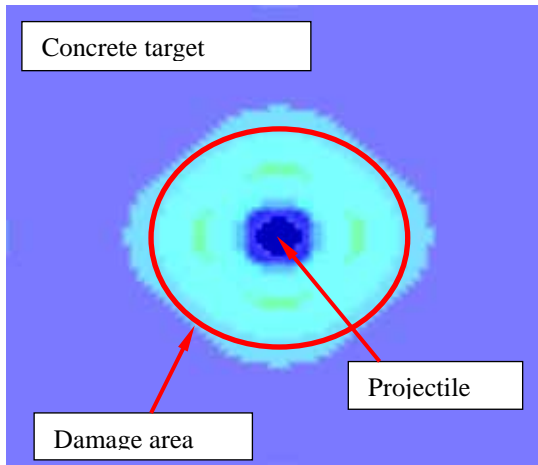
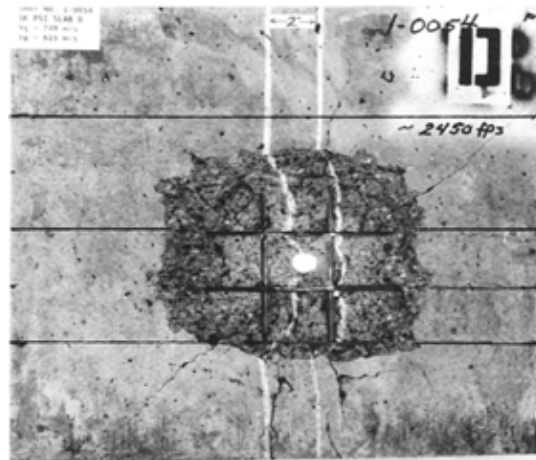


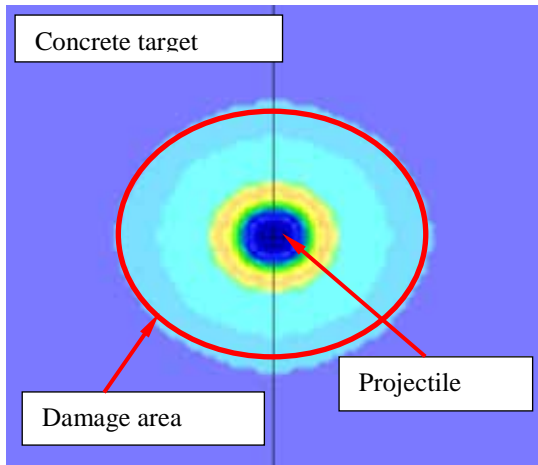
Figure 8.4: Spalling and scabbing happened on the front and rear side of concrete slab during the projectile impact process



(a)



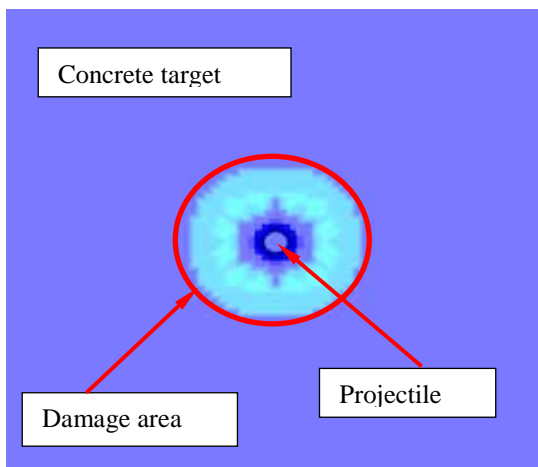
(b)



(c)



(d)



(e)



(f)

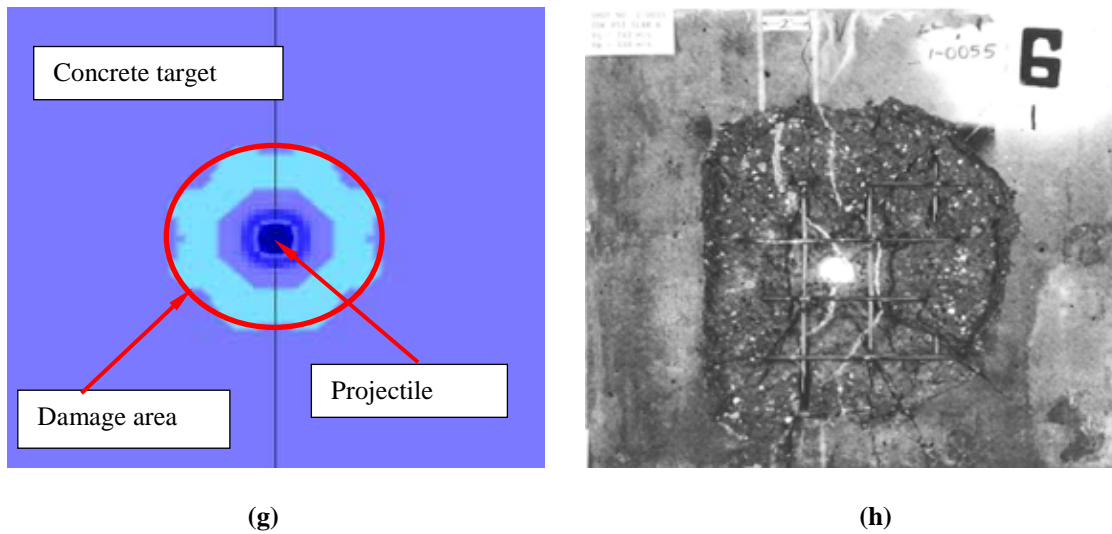


**Figure 8.5: Comparisons between experimental and modeling results of concrete slab after impact loadings, (a) modeling result of front surface of concrete slab (48 MPa), (b) experimental result of front surface of concrete slab (48 MPa), (c) modeling result of rear surface of concrete slab (48 MPa), (d) experimental result of rear surface of concrete slab (48 MPa), (e) modeling result of front surface of concrete slab (140 MPa), (f) experimental result of front surface of concrete slab (140 MPa), (g) modeling result of rear surface of concrete slab (140 MPa), (h) experimental result of rear surface of concrete (140 MPa)**

Additionally, the comparisons of damage degree and appearance between experimental and modeling results of concrete slab after impact loadings are presented in Figure 8.5. The impact velocity of the projectile is around 750 m/s. It can be noticed that the modeling results show that there are always perforation holes and an approximately circular damage area on both front and rear surface of the concrete slab. Moreover, the diameter of the perforation hole is relatively small, which is similar as that of the impact projectile. All of these obtained modeling results are consistent with the experimental results, which imply that the proposed finite elements model is reliable. However, from the experimental results, it can be found that the spalling and scabbing area of NSC and HSC are similar to each other, while the modeling results show that the HSC has relatively smaller damage area. Actually, the spalling and scabbing properties of concrete are very important for the protective structures, since the flying fragments may cause secondary damage to the human staying behind the structures. Hence, it is necessary to clarify the difference of the damage area between experiments and modeling should be attributed to experimental deviation or modeling error. However, in Hanchak et al. (1992), the detailed damage area values of concrete slabs are not presented, which means the obtained modeling results should be validated by other parameters.

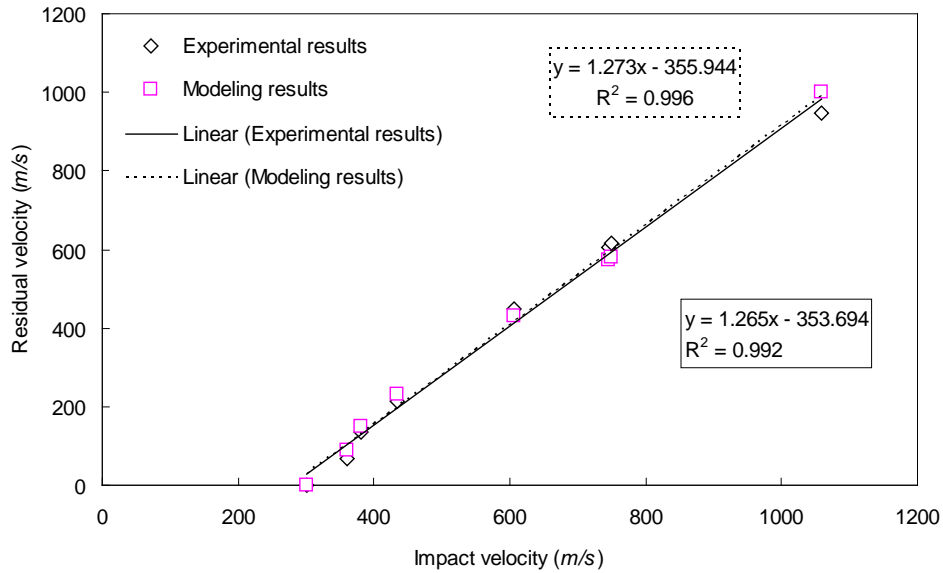


**Figure 8.6:** Comparison of the experimental (Hanchak et al., 1992) and modeling results: residual velocity of the projectile after the impact on the concrete plate (48 MPa)

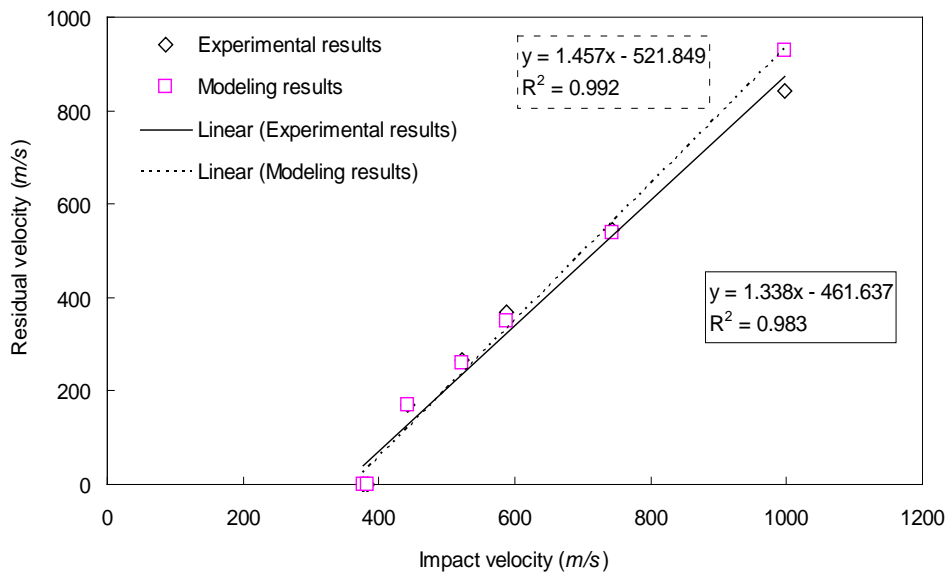


**Figure 8.7:** Comparison of the experimental (Hanchak et al., 1992) and modeling results: residual velocity of the projectile after the impact on the concrete plate (140 MPa)

To further validate whether the proposed model can well represent the impact experiments, the modeling and experimental results of residual velocity for the projectile are compared and illustrated in Figures 8.6 and 8.7. It is clear that the modeling results are in good agreement with the experimental data for both normal strength concrete (NSC) and high strength concrete (HSC). With an increase the of impact velocity, a linearly

increase of the residual velocity for projectile can be observed. In the case for NSC, the lines represent experimental and modeling results are almost coincident, which means the proposed model can well predict the velocity of projectile after impacting on concrete with relatively low strength. In addition, for the results of HSC, the experimental and modeling results are very similar when the impact velocity is relatively low. However, when the impact velocity of projectile is relatively high (e.g. about 1000 m/s), the modeling result can overestimate its residual velocity, as shown in Figure 8.7.

### 8.3.3 Prediction of the sustainable UHPFRC dynamic performance

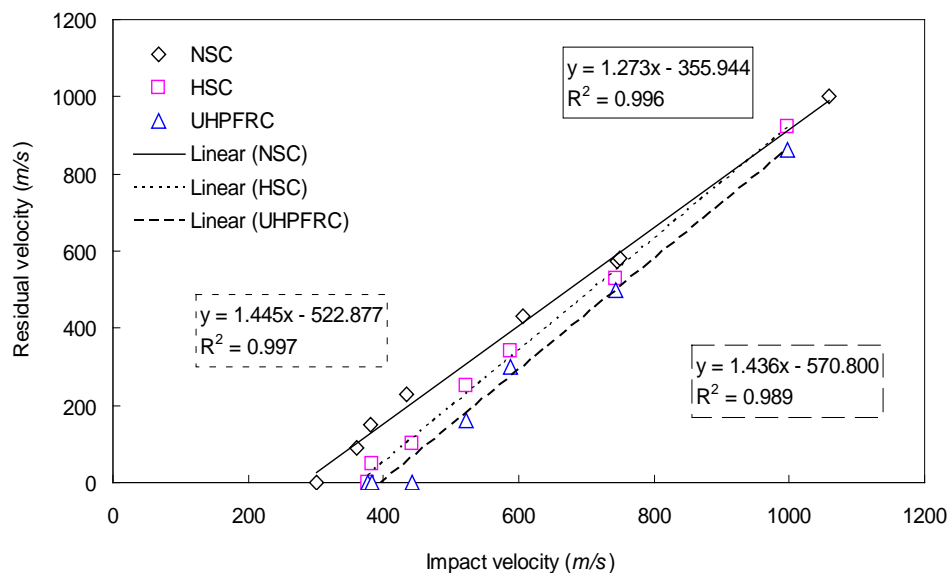
In general, based on the results shown in Figures 8.6 and 8.7, it can be summarized that the proposed model can represent the velocity reduction of the solid projectile after impacting on the normal and high strength concretes. Hence, combing with the experimental results obtained in Chapter 5 (the sustainable UHPFRC with 2% hook ended steel fibres, vol.), the model is utilized to predict the performance of the sustainable UHPFRC under projectile impact. The parameters for UHPFRC material model are shown in Table 8.3, and the projectile is still assumed to be a rigid part. The impact velocities of projectile are 376 m/s, 382 m/s, 443 m/s, 522 m/s, 587 m/s, 743 m/s and 998 m/s.

Table 8.3: Material parameters of the sustainable UHPFRC for impact analysis

<i>Density</i>	<i>Shear modulus</i>	<i>Strength constants</i>						
$\rho$ (kg/m <sup>3</sup> )	G (MPa)	A	B	N	C	$f'_c$ (MPa)	$S_{max}$ (MPa)	$\epsilon'_0$
2540	36400	0.75	1.65	0.76	0.07	135	21.7	1.0
<i>Damage constants</i>								
	$D_1$		$D_2$			$(\epsilon_p^f + \mu_p^f)_{min}$		
	0.05		1.0			0.01		
<i>Equation of state, EOS constants</i>								
$P_{crush}$ (MPa)	$\mu_{crush}$	$K_1$ (GPa)	$K_2$ (GPa)	$K_3$ (GPa)	$P_{lock}$ (GPa)	$\mu_{lock}$		
26.0	0.01	12.5	17.1	20.8	1.05	0.1		

A comparison of the modeling results for rigid projectile impact on normal strength concrete (NSC), high strength concrete (HSC) and developed sustainable UHPFRC is illustrated in Figure 8.8. It can be noticed that, for these three different types of concrete, with the increase of the impact velocity of projectile, linearly development of its residual velocity can be observed. Moreover, it is noteworthy that the projectile residual velocity is always the lowest after impacting on UHPFRC, particularly when the impact velocity is relatively low. For instance, when the projectile impact velocity is about 376 m/s, its residual velocity is about 149 m/s for NSC and 0 for both HSC and UHPFRC. When the project impact velocity increases to around 443 m/s, its residual velocity is about 100 m/s

for HSC and still 0 for UHPFRC. Hence, based on these obtained results, it can be summarized that the sustainable UHPFRC has much better impact resistance capacity under the relatively low velocity projectile impact, compared to HSC or NSC. In addition, with an increase of the projectile impact velocity, it can be found that the difference of impact resistance abilities between NSC and HSC slightly decreases, as shown in Figure 8.8. This may be attributed to the basic characteristics of plain concrete. When the projectile impact velocity is around 1000 m/s, its kinetic energy is very large, which means the increase of the compressive strength is less efficient to absorb so much energy, similarly to that presented in Hanchak et al. (1992 and Zhang et al. (2005). To further improve the energy absorption ability of HSC, one of the promising methods is by adding appropriate type and amount of fibres, particularly the hook ended fibres. As described in Chapter 5, due to the fact that the plastic deformation and pullout process of hook ended steel fibres (HF) can absorb a large amount of energy, the sustainable UHPFRC with 2% HF (vol.) should show better energy dissipation ability than HSC. To demonstrate this prediction, an absorbed energy comparison between these concretes is executed and illustrated in Figure 8.9. The absorbed energy amount is calculated by employing kinetic energy equation ( $E = 1/2 \times mv^2$ ,  $E$  is the energy,  $m$  is the mass and  $v$  is the velocity).



**Figure 8.8: Modeling comparison of the projectile residual velocity after impact on normal strength concrete (NSC), high strength concrete (HSC) and the developed sustainable UHPFRC**

From Figure 8.9, it can be noticed that, under the impact of projectile with different velocities, the absorbed energy amount of the sustainable UHPFRC is always the largest, while the NSC shows the lowest energy absorption capacity. With an increase of projectile impact velocity, the difference of the absorbed energy amount between HSC and UHPFRC gradually increases, which implies that the addition of fibres can effectively enhance the energy dissipation capacity especially at high impact velocity. For

instance, when the projectile impact velocity is around 1000 m/s, the absorbed energy amount of HSC is about 36 kJ (close to that of NSC - 30 kJ), while this value for the developed sustainable UHPFRC is around 63 kJ. Moreover, it is noteworthy that with an increase of the projectile impact velocity, the absorbed energy amount of these three concrete slabs firstly increase then decrease, which is similar as the obtained experimental results shown in Hanchak et al. (1992). This may be attributed to the high kinetic energy of the utilized projectile and the relatively small thickness of the used concrete slab. When the projectile has very high velocity (about 1000 m/s) and kinetic energy (about 250 kJ), it can easily damage and perforate the concrete slab, and relatively less energy is consumed in this perforation process. Therefore, to resist this kind of projectile impact, thicker concrete slab or multiple layers of concrete slabs should be appropriately utilized.

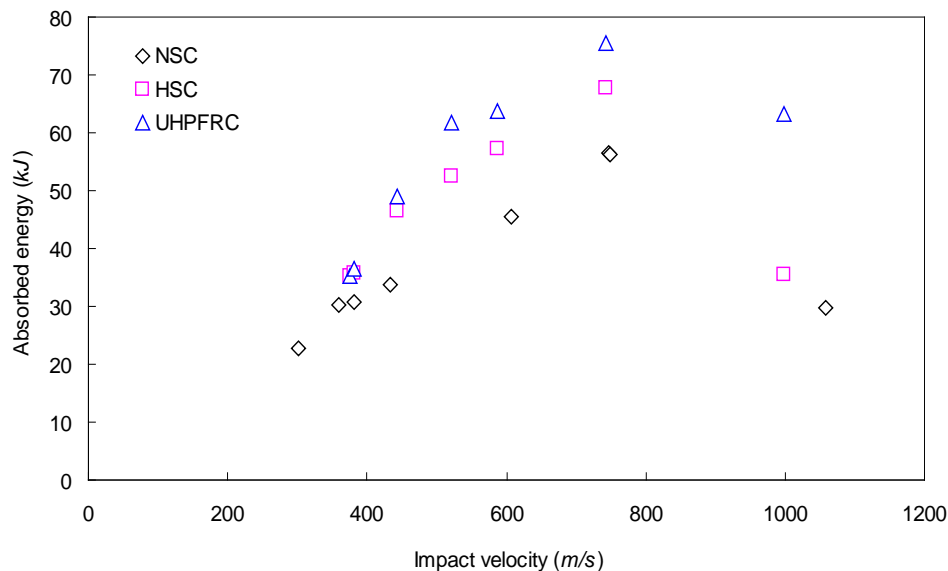


**Figure 8.9: Modeling comparison of the energy dissipation capacity between normal strength concrete (NSC), high strength concrete (HSC) and the developed sustainable UHPFRC under projectile impact loadings**

In summary, in most cases, the energy dissipation capacity of HSC is better than that of NSC. When the impact projectile has a very high velocity and large kinetic energy, the difference of energy dissipation capacity between NSC and HSC is relatively small. To further improve the impact resistance of concrete, the appropriate addition of steel fibres is a promising method. In this study, the modeling results demonstrate that the developed sustainable UHPFRC has much better energy dissipation capacity than HSC, particularly when the impact velocity and kinetic energy of projectile are relatively high. Therefore, the sustainable UHPFRC (with 2% HF, vol.) is more suitable to be utilized in protective structure than NSC and HSC.

### 8.3.4 Summary

In this section, a finite elements model is generated in LS-DYNA to evaluate the energy dissipation capacity of concrete slab under the impact of projectile with different velocities. This model is validated by the experimental results obtained from the literature. It is demonstrated that the proposed model can predict the velocity reduction of the solid projectile after impacting on the normal and high strength concretes. Moreover, the validated model is utilized to predict the performance of the sustainable UHPFRC under the projectile impact. The modeling results show that, when the projectile has very high impact velocity and kinetic energy, the enhancement of compressive strength of concrete slab is less effective to improve its impact resistance. One of the promising methods to further improve the energy dissipation capacity of HSC is adding appropriate type and amount of fibres. Compared to normal strength concrete (NSC) and high strength concrete (HSC), the modeling results reveal that the developed sustainable UHPFRC has much better energy dissipation ability, particularly when the projectile has a very high impact velocity and kinetic energy.

## 8.4 Conclusions

Among all the impact categories (high-rate impact, shock, blast loads and so on), the impact from hard projectile is the most common one. In the past century, large amounts of experimental investigations have been executed to determine the impact resistance of different type of concretes under projectile impact. A series of empirical formulae were proposed, based on experimental studies, to predict the penetration of hard projectiles and to support the design of protective structure. Nevertheless, with the development of concrete industry, a series of advanced concretes (e.g. SCC, HSC, UHPC and UHPFRC) can be produced today, which implies that the proposed empirical formulae (about 70 years ago) are not suitable to be used to predict the impact resistance of the advanced concretes. Hence, there is a strong need to evaluate the energy dissipation capacity of the advanced concretes with relatively low material and labour cost. According to these premises mentioned above, the energy dissipation capacity of the developed sustainable UHPFRC under projectile impact is investigated based on modeling approach in this study. A commercial hydrocode - LS-DYNA is employed to simulate the performance of concrete under projectile impact. In this study, it is demonstrated that the developed sustainable UHPFRC has much better energy dissipation capacity and is more suitable to be utilized in places where a large amount of energy may be released, compared to normal strength concrete (NSC) and high strength concrete (HSC).



## Chapter 9

### Application of the sustainable UHPFRC in protective elements

#### 9.1 Introduction

As a result of increasing concerns regarding public and structure safety in recent decades, the dynamic performance of infrastructures under impact loadings and their energy absorption capacity have become an emerging research focus in the concrete industry (Beppu et al., 2008; Wen and Xian, 2015; Sovják et al., 2015). Among all the impact categories (high-rate impact, shock, blast loads and so on), the impact from hard projectile is the most common one, which can be attributed to the continuous military interest since the beginning of last century (Kennedy, 1976). Due to the fact that the impact projectile in the military field normally has high velocity (about 700-1000 m/s, such as bullet or missile), its kinetic energy is quite high, which may cause serious damage to concrete target or even the collapse of whole construction. Hence, it is important to investigate the impact resistance of concrete under the high velocity hard projectile impact.

The specific characteristics of UHPFRC (high mechanical properties and relatively high steel fibre content) demonstrate that it has much better impact resistance than the other concretes, such as normal strength concrete (NSC), steel fibre reinforced concrete (SFRC) or high strength concrete (HSC), and is suitable to be utilized at the place where a large amount of energy may suddenly be released (Wu et al., 2009; Yu et al., 2015b). Nevertheless, it can be noticed that the investigation of UHPFRC under high velocity projectile impact loadings is scarce. For instance, Sovják et al. (2013, 2015) examined the resistance of slim UHPFRC targets to projectile impact using in-service bullets. The impact velocity of the used bullet was in the range of 691-720 m/s. It was verified experimentally that the optimal fibre content in UHPFRC mixture is 2% by volume. Using less than 2% of fibre volume fraction might be unsafe in the slim UHPFRC targets due to increased volume of secondary fragments generated from the back side of the slab and also due to the higher residual penetration potential of the bullet exiting the back side of the slab. Using more than 2% of fibre volume fraction could be inefficient as well. Máca et al. (2014) described the mix design of UHPFRC and its response to deformable and non-deformable projectile impact. It was verified that UHPFRC has much greater resistance to impact loading compared to traditional FRC. Thus, implementation of UHPFRC may result in highly resistant concrete elements such as cladding panels and walls in modern protective structures while maintaining its standard thicknesses and

appearance. Ren et al. (2013) presented the effect of projectile impact and penetration on the phase composition and microstructure of high performance concretes. The evidence of various phase changes due to impact and penetration was detected by XRD. Compared with the control sample, the tested UHPFRC exhibited the possible presence of coesite, a high-pressure and high-temperature form of silica. Other possible phase changes during impact could include transformations from belite to larnite and from tobermorite to clinotobermorite, dehydroxylation of portlandite and ettringite and formation of new phases such as calcite and spinel.

As shown in the previous chapters, considering the sustainable development of concrete industry, a sustainable UHPFRC can be produced based on the modified A&A model and appropriate fibres hybridization design. It is demonstrated that the developed sustainable UHPFRC has superior workability and mechanical properties. In Chapter 7, the energy absorption capacity of the sustainable UHPFRC under pendulum impact is investigated. However, the velocities of the impact hammers are relatively low, which are about 6.0 m/s for the small “Charpy Impact Device” and 8.6 m/s for the big “Modified Pendulum Impact Device”. Although Chapter 8 presents the numerical modeling results of the sustainable UHPFRC under relatively high velocity projectile impact, the results predicted by the proposed model still need to be further validated. Hence, to widen the application of the developed sustainable UHPFRC, particularly the application in military field, it is important to clarify its impact resistance under high velocity projectile impact loading.

Consequently, the objective of this chapter is to apply the sustainable UHPFRC in protective elements and investigate its dynamic performance under high velocity projectile impact. Two types of projectiles and four different impact velocities are selected. Except for the experimental study, the numerical tool (LS-DYNA) is employed to simulate the impact process.

## **9.2 Materials and methodologies**

### **9.2.1 Materials, mix design and concrete production**

The utilized materials and mix design of the sustainable UHPFRC are similar as that shown in Section 7.3.2. Based on the obtained experimental results shown in Figures 5.14 and 5.19, the sustainable UHPFRC with hook ended steel fibres (HF) or hook ended steel fibres combined with long straight fibres (LSF) have great potential energy absorption capacity. Therefore, mixture recipes of No. 7 and 8, shown in Table 7.1, are selected here.

Following the method presented in Figure 3.2, the concrete matrix is mixed with the steel fibres. The fresh concrete is cast in the mould with the size of 500 mm × 500 mm × 100 mm, as shown in Figure 9.1. Due to the fact that the developed sustainable UHPFRC has good workability, the fresh concrete is poured in the middle of the mould, without

applying vibration (i.e. treated as self-compacting concrete). After 3-4 days, the samples are demoulded and cured in the water. After curing for about 28 days, all the samples are taken from the water and prepared for the shooting test. To avoid the unexpected damage to the samples during the transportation, all the samples are securely packaged, as shown in Figure 9.2.



**Figure 9.1:** Utilized wooden moulds (left) and the cast fresh concrete sample in fresh state (right)



**Figure 9.2:** Samples prepared for the shipment

### 9.2.2 Experimental methodologies

In this study, two types of projectiles are used: one is in-service bullet (7.62 mm, as shown in Figures 9.3a and b), and the other one is fragment simulating projectile (FSP, 20 mm, as shown in Figures 9.3c and d). In general, based on the NATO document AEP-55 (2011), two impact velocities are chosen for each type of projectile: 830 and 930 m/s for the bullet (7.62 mm) and 860 and 960 m/s for the FSP (20 mm). Based on the mass of the used projectiles and the impact velocities, it is possible to calculate the kinetic energy of the projectiles during the impact tests, which are shown in Table 9.1. Additionally, to

achieve these designed velocities, relevant calibrations are executed beforehand. The launching set-ups for these projectiles are illustrated in Figure 9.4. The impact velocity of projectile is measured by radar velocity sensors fixed on the launchers.

**Table 9.1: Mass, velocity and kinetic energy of the impact projectiles**

Type	Mass (g)	Velocity (m/s)	Kinetic energy (J)
Bullet (7.62 mm)	8.35	830	2876
	8.35	930	3611
FSP (20 mm)	53.8	860	19895
	53.8	960	24791



(a)



(b)



(c)



(d)

**Figure 9.3: Utilized bullet (7.62 mm) (a and b) and FSP (20 mm) (c and d)**

According to STANAG 2280 (2009), the distance between target concrete plate and the launch point is 30 m, and witness plates are placed behind the target with a minimum air gap of 100 mm between the target and the witness plate. The used witness plate is hardboard with a thickness of about 2 mm. To clearly understand the performance of the developed sustainable UHPFRC under high velocity projectiles impact, two high speed cameras are used to record the variation of both front and rear sides of the concrete slab. The rates of the utilized high speed cameras are 26143 fps (frames per second) and 21052 fps for the front and rear camera, respectively. The shooting set-up can be easily expressed as the scheme shown in Figure 9.5.

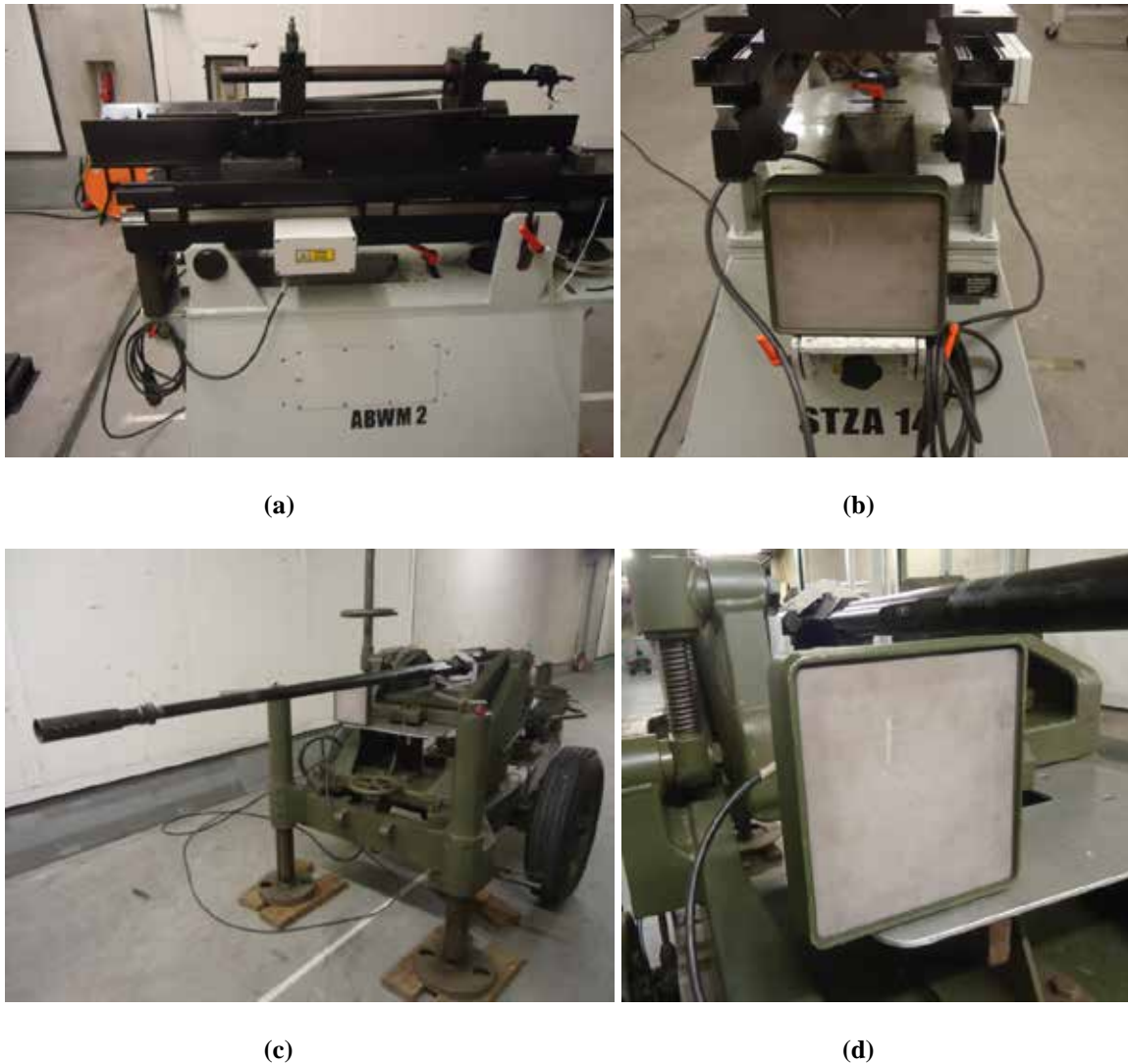


**Figure 9.4: Bullet (7.62 mm) launching device (a) and its radar velocity sensor (b); FSP (20 mm) launching device (c) and its radar velocity sensor (d)**

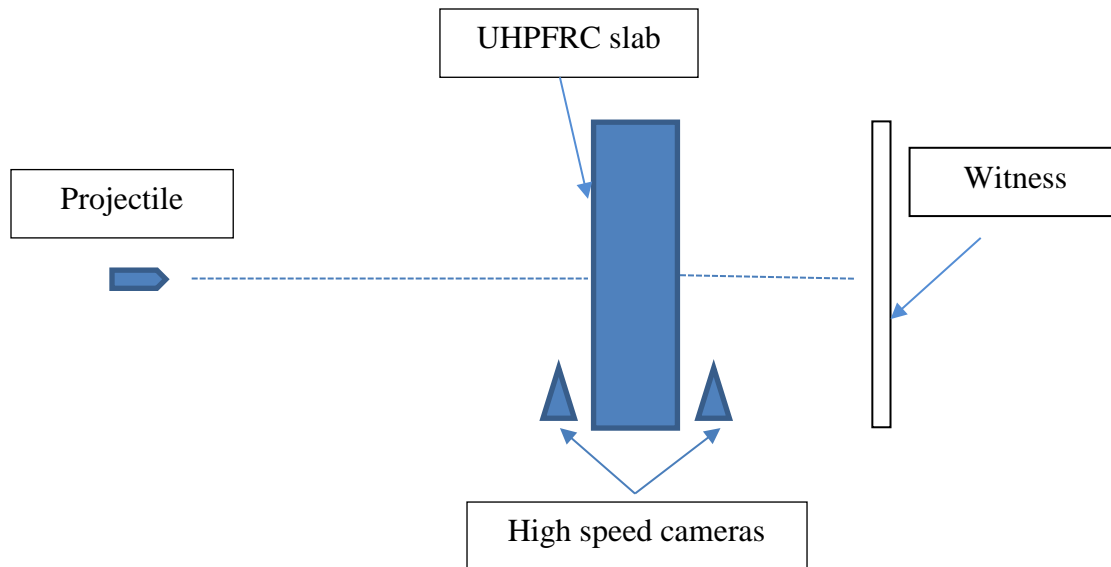


**Figure 9.5: Scheme of the shooting test**

Moreover, based on STANAG 2280 (2009), a group of 3 individual shots is fired at the appropriate range on each concrete plate. As shown in Figure 9.6, the distance between hits should be in the range from 25 mm to 120 mm. After each shot, both the target and witness plates should be examined. Based on the appearance of the witness plate, it is possible to confirm that whether the concrete target has been perforated or not.

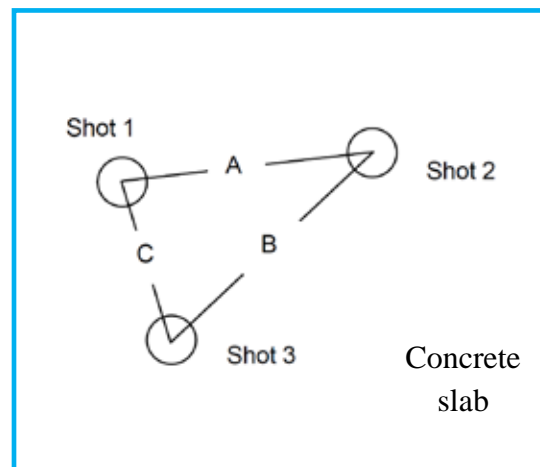


**Figure 9.6: Impact pattern of individual projectile**

During the shooting tests, the concrete slab is fixed on a heavy frame (as shown in Figure 9.7), and the frame is fix on the ground. Hence, the frame and sample position will not be influenced by the projectile impact. Two high speed cameras are installed at the side of the sample, and sufficient light is provided surrounding the concrete slab.



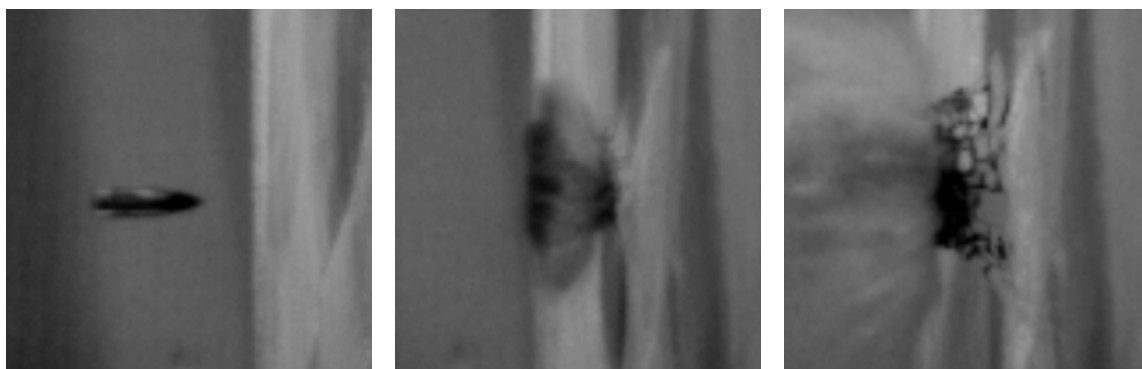
Figure 9.7: Installed sample before the testing

### 9.3 Experimental results and discussions

#### 9.3.1 The sustainable UHPFRC under bullet (7.62 mm) impact

- *Impact velocity  $\approx 830$  m/s*

Figures 9.8 and 9.9 present the variation of front and rear surfaces of the sustainable UHPFRC with hybrid fibres during the first shot. It can be noticed that the moment when the projectile initially contacts with the concrete target (Figure 9.8b), a relatively small crater (similar as the diameter of the used projectile) and a large amount of dust are created. Subsequently, many cracks grow surrounding the crater and the size of the crater increase simultaneously (Figure 9.8c). Then the growth of the crater stops and a large amount of small fragments fly off the concrete target, opposite to the projectile impact direction (Figures 9.8d and e). On the rear surface of the UHPFRC target, it is important to notice that the bullet impact (7.62 mm, velocity  $\approx 830$  m/s) only results in several cracks, without causing serious perforation or scabbing damages (as shown in Figure 9.9).



(a)  $t = 0$  ms

(b)  $t = 0.2$  ms

(c)  $t = 0.4$  ms

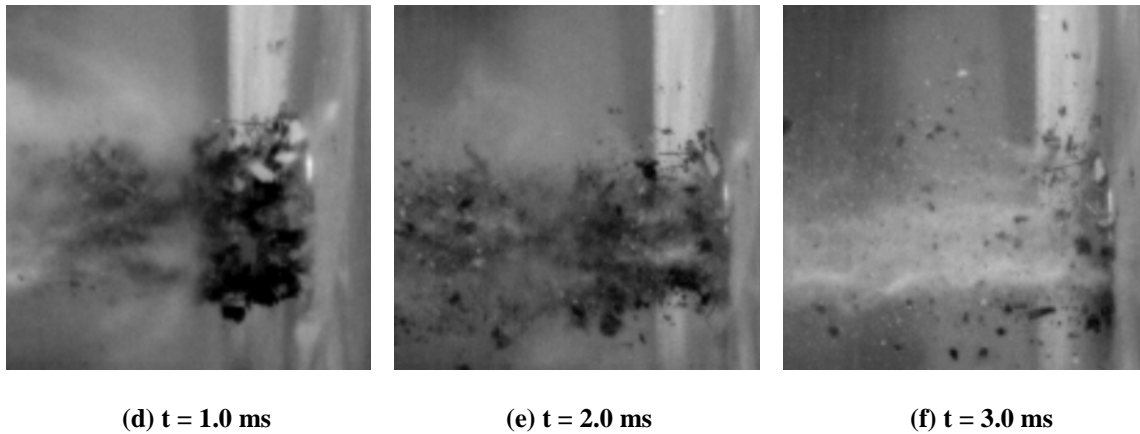


**Figure 9.8:** Dynamic performance of the UHPFRC with hybrid fibres under the bullet (7.62 mm, velocity  $\approx 830$  m/s) impact (front surface, first shot)

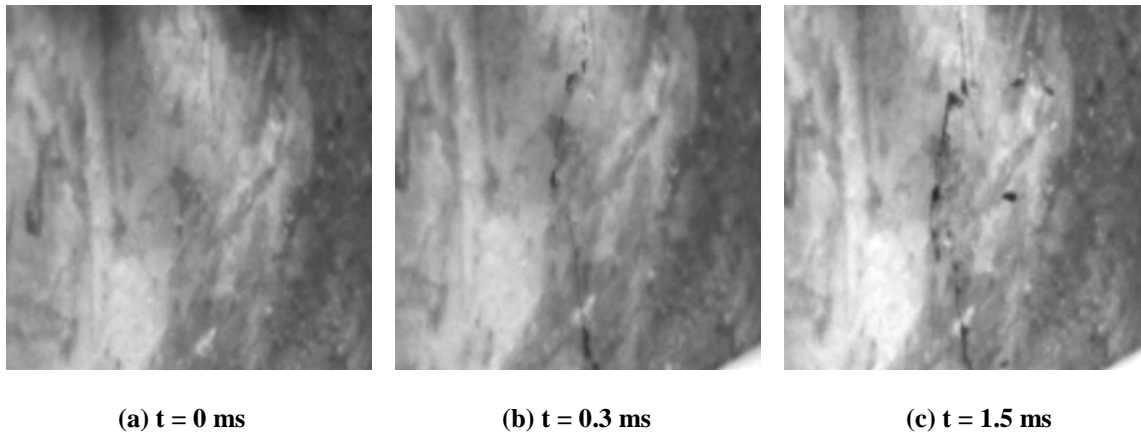


**Figure 9.9:** Dynamic performance of the UHPFRC with hybrid fibres under the bullet (7.62 mm, velocity  $\approx 830$  m/s) impact (rear surface, first shot)

Figure 9.10 illustrates the appearance of both the front and rear surface of the UHPFRC target after the first shot and three shots. Based on the measurement, it can be found that the diameter and volume of these generated craters have similar diameters and volumes, which fluctuate around 6 cm and  $30 \text{ cm}^3$ , respectively. Moreover, all the three impact projectiles are blocked inside of the concrete, and their penetration depths are 5.7 cm, 6.0 cm and 6.8 cm. From Figures 9.10b and d, it can be noticed that some locally distributed cracks appear after each shot. After three shots, the scabbing at the rear surface of the concrete target is very limited. Based on these obtained experimental results, it can be summarized that the bullet (7.62 mm, velocity  $\approx 830$  m/s) can cause very locally damages to the concrete target, and the developed UHPFRC target can well resist this impact.

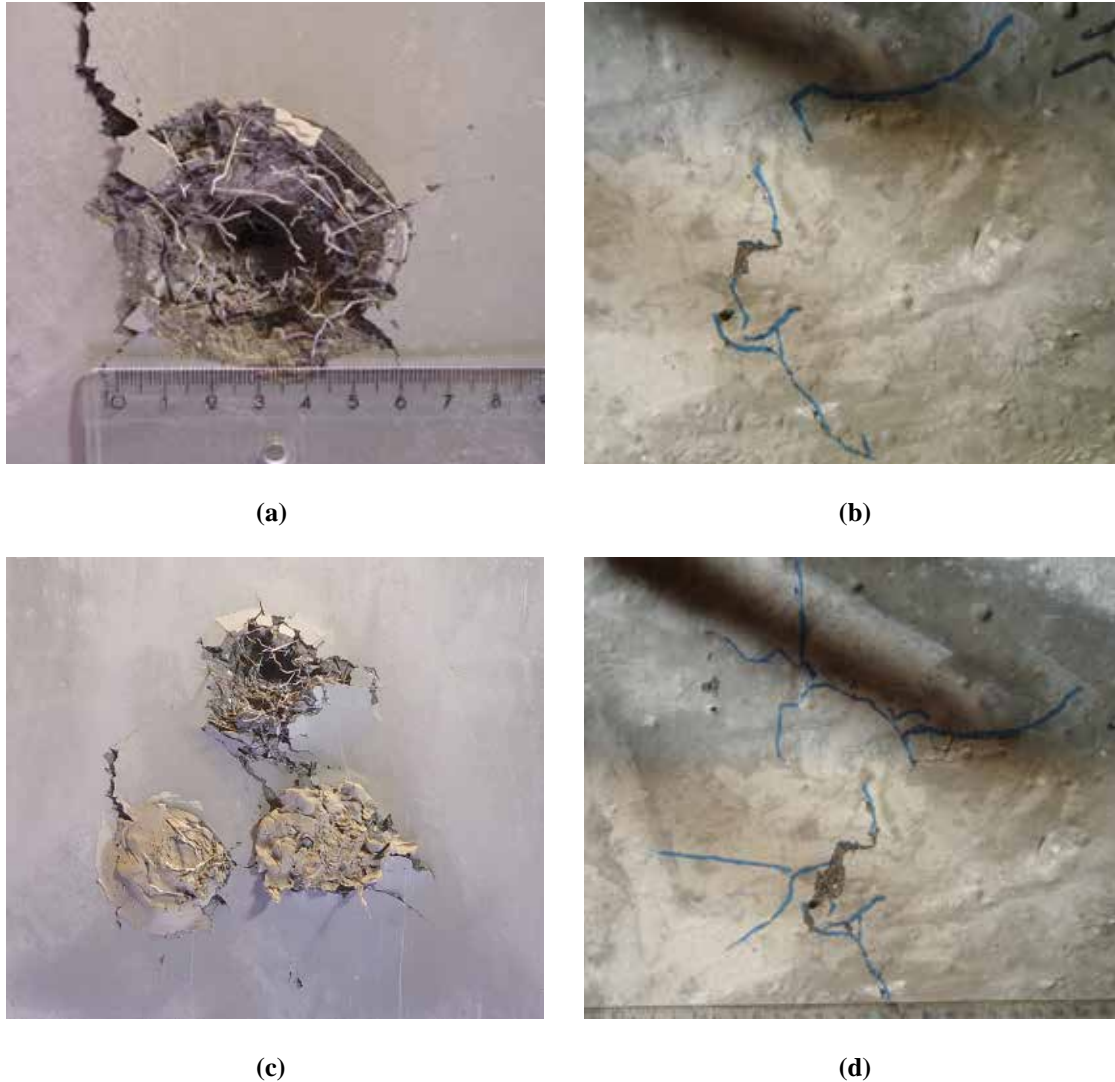


**Figure 9.10: Front and rear appearance of the tested UHPFRC slab with hybrid fibres: (a) front surface after the first shot, (b) rear surface after the first shot, (c) front surface after three shots, (d) rear surface after three shots**

As commonly known, there are several phenomena associated with projectile impact effects on concrete targets, as shown in Figure 8.1 (Kennedy, 1976). When the impact velocities are relatively small, the projectile will strike the concrete target and bounce off without creating any local damage. With an increase of the impact velocity, pieces of concrete are ejected off of the concrete impacted face. This spalling forms a spall crater that extends over a substantially greater area than the cross-sectional area of the striking projectile. As the velocity continues to increase, the projectile will penetrate the target to depths beyond the depth of the spall crater, forming a cylindrical penetration hole with a diameter only slightly greater than the projectile diameter. As the penetration depth increases, the projectile will stick to the concrete target rather than rebounding. Further increases in the initial velocity produce cracking of the concrete on the back surface

followed by scabbing of concrete from this rear surface. The zone of scabbing is normally much wider but not as deep as the front face crater. Once scabbing begins, the depth of penetration will increase rapidly. For low barrier thickness to projectile diameter ratios (less than 5) the pieces of scabbed concrete can be large in size and have substantial velocities. As the projectile velocity increases further, perforation of the target will occur as the penetration hole extends through to the scabbing crater and the projectile may subsequently exit from the rear face of the target with a residual velocity.

In this study, due to the relatively high impact velocity and energy, the bullets penetrate into the concrete target and cause a cylindrical penetration hole beyond the depth of the spall crater. However, the scabbing is difficult to be observed at the concrete rear surface after the impact loadings, which may be attributed to the application of steel fibres in UHPFRC. As be demonstrated by Sovják et al. (2013 and 2015), the added steel fibres in UHPFRC can well grip the concrete matrix and dissipate the impact energy during the impact process. Hence, compared to normal strength concrete, high strength concrete and plain UHPC, UHPFRC show much better impact resistance ability in reducing the spalling, scabbing and penetration depth.

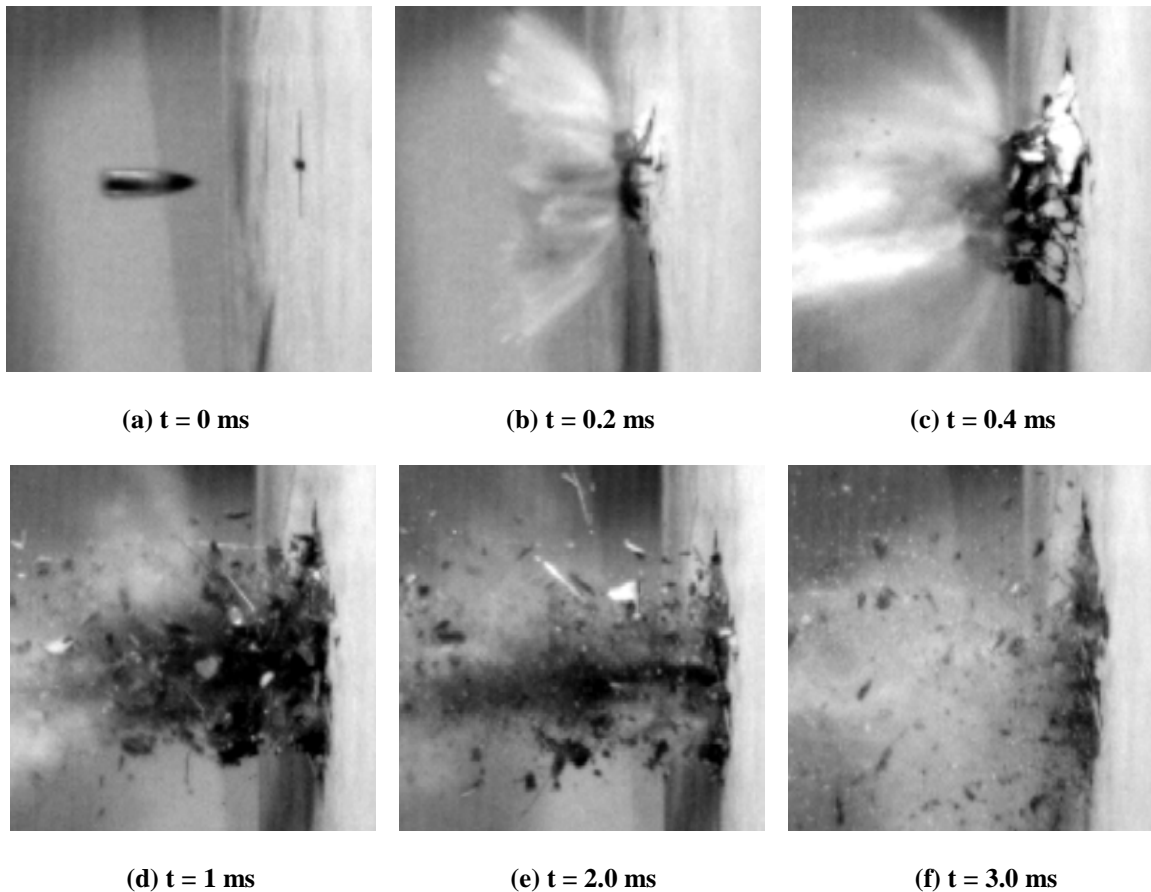


**Figure 9.11: Dynamic performance of the UHPFRC with single sized fibres under the bullet (7.62 mm, velocity  $\approx$  830 m/s) impact (front surface, first shot)**

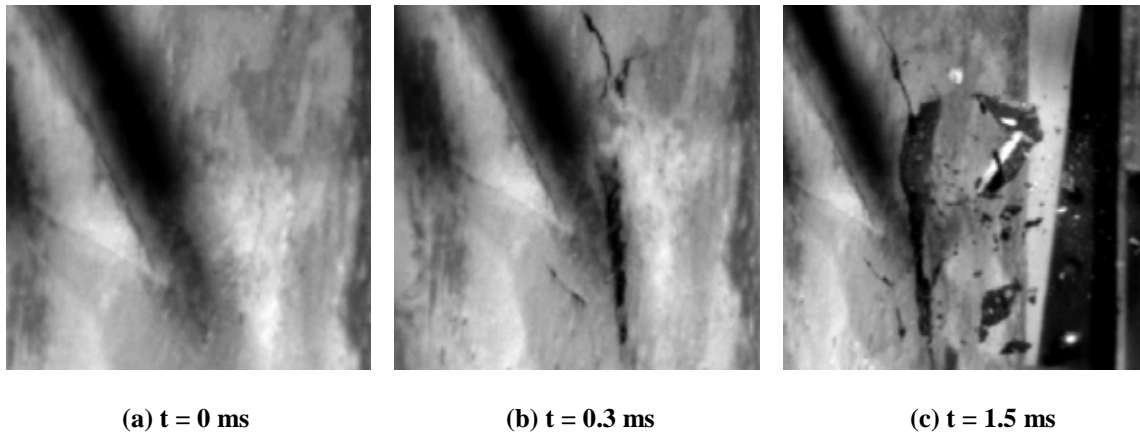


**Figure 9.12: Dynamic performance of the UHPFRC with single sized fibres under the bullet (7.62 mm, velocity  $\approx$  830 m/s) impact (rear surface, first shot)**

To understand the effect of different fibres on the impact resistance capacity of concrete, the dynamic performance of the sustainable UHPFRC with single sized fibres (hook ended steel fibres) under the bullet (7.62 mm, velocity  $\approx$  830 m/s) impact (first shot) is shown in Figures 9.11 and 9.12. In general, the high speed camera photos presented in Figure 9.11 are similar as that shown in Figure 9.8, which implies that these two UHPFRC mixtures (with hybrid or single sized fibres) have similar dynamic behaviour under the bullet (7.62 mm, velocity  $\approx$  830 m/s) impact at the front surface. Nevertheless, some differences can still be observed between Figures 9.8 and 9.11. For instance: 1) some debonded steel fibres can be observed in Figures 9.11d and e; 2) after the impact loading, the generated fragments from the mixture with single sized fibres are larger than those from the concrete target with hybrid fibres.

**Table 9.2 Bullet impact velocity and obtained experimental results of UHPFRC target**

Impact order	Impact velocity (m/s)	UHPFRC with hybrid fibres			UHPFRC with single sized fibres		
		Residual velocity (m/s)	Crater diameter (cm)	Penetration depth (cm)	Residual velocity (m/s)	Crater diameter (cm)	Penetration depth (cm)
1	827.2	0	5.8	5.7	-	-	-
2	832.6	0	5.8	6.0	-	-	-
3	830.0	0	6.5	6.8	-	-	-
1	831.7	-	-	-	0	7.5	6.5
2	827.7	-	-	-	0	8.0	6.8
3	829.8	-	-	-	0	7.5	7.0

From Figure 9.12, it is important to notice that the bullet impact can not only cause cracks but also very obvious scabbing at the rear surface of the sustainable UHPFRC with single sized fibres. Although all of these three projectiles can be blocked inside of concrete, the rear surface of concrete target has been damaged (as shown in Figure 9.13).

As described in the previous section, once scabbing begins, the depth of penetration will increase rapidly (Kennedy, 1976). Here, the penetration depths of these projectiles are 6.5 cm, 6.8 cm and 7 cm, which are larger than that measured in the UHPFRC with hybrid fibres. All the collected experimental data are shown in Table 9.2

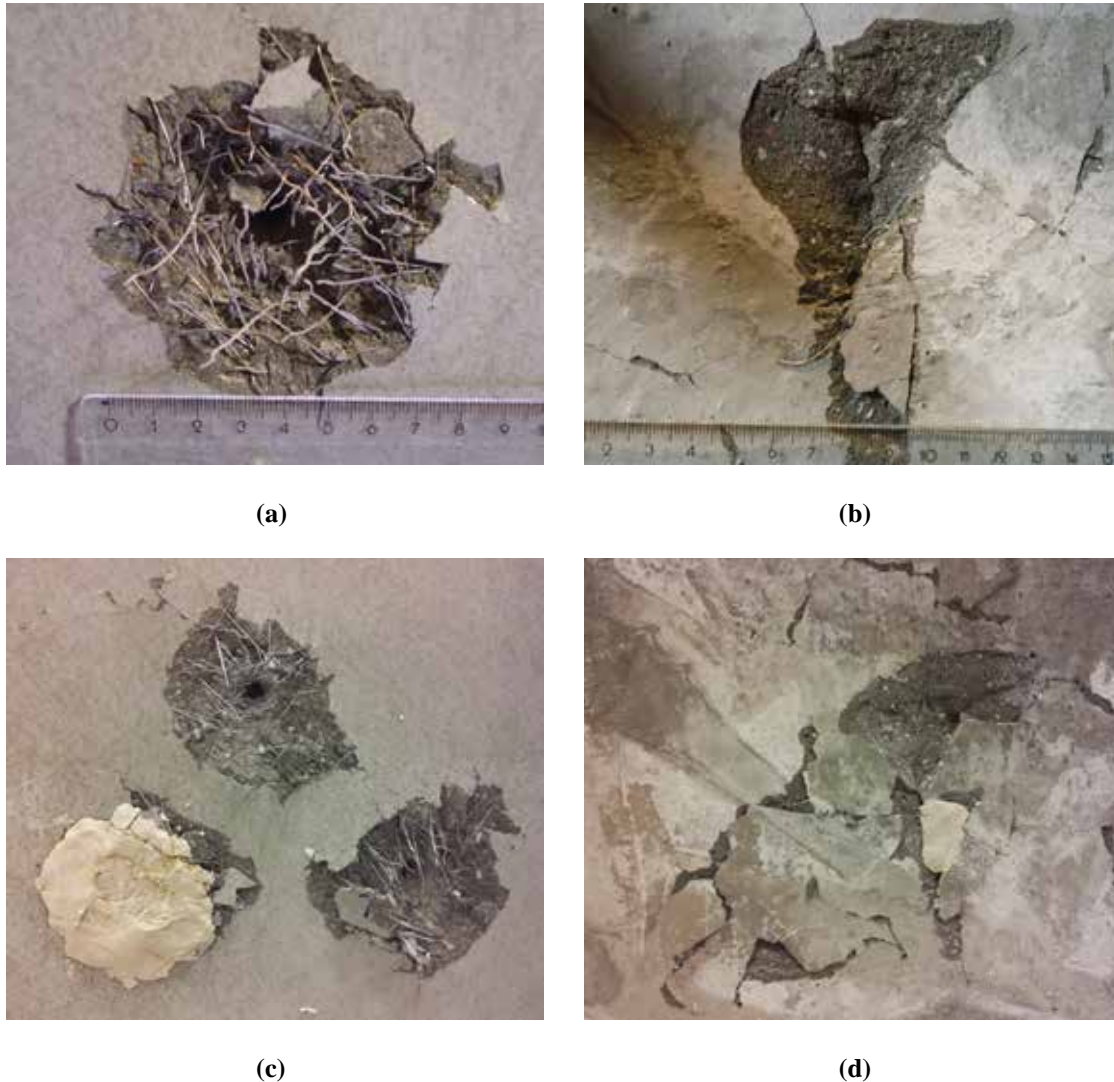


**Figure 9.13: Front and rear appearance of the tested UHPFRC slab with single sized fibres: (a) front surface after the first shot, (b) rear surface after the first shot, (c) front surface after three shots, (d) rear surface after three shots**

In practice, the scabbing at the rear surface of concrete structure is considered very dangerous, since the flying fragments can cause secondary damage to humans and objects standing behind/inside the concrete structure. Hence, to design a safe and reliable concrete structure, the scabbing at the rear surface of concrete under impact should be effectively limited. In this study, under the same impact circumstance (bullet, 7.62 mm, velocity  $\approx 830$  m/s), the UHPFRC with hybrid fibres shows much better scabbing

resistance ability than the one with single sized fibres. This can be attributed to the fact that hybrid fibres can effectively resist the cracks development and dissipate the impact energy. As described in Chapter 5, the short fibres can bridge the micro-cracks while the long fibres are more efficient in preventing the development of macro-cracks, which cause that the stress in the hybrid fibres reinforced concrete can be well distributed and its mechanical properties can be improved (Markovic, 2006). Hence, when impact occurs, the generated stress is relatively homogeneously distributed in the UHPFRC with hybrid fibres, and the growth of micro and macro cracks is simultaneously restricted. However, in the case of UHPFRC with single sized fibres (hook ended steel fibres), the development of micro-cracks is not disturbed, which causes that the many macro-cracks can quickly appear and part of the concrete may debond from the whole concrete structure.

Consequently, based on the obtained experimental results, it can be concluded that the addition of hybrid fibres is beneficial for improving the scabbing resistance capacity of UHPFRC under high velocity bullet impact ( $\approx 830$  m/s) and reduce the projectile penetration depth.

- ***Impact velocity  $\approx 930$  m/s***

Figures 9.14 and 9.15 present the dynamic process of the sustainable UHPFRC with hybrid fibres exposed to high velocity bullet (7.62 mm, velocity  $\approx 930$  m/s) impact (first shot). Here, compared to the impact tests shown in the previous part, the projectile impact velocity has increased by about 100 m/s and its impact energy has been increased by about 26%. As shown in Figure 9.14, it can be found that the front surface reactions of the UHPFRC target under the bullet impact with different velocities (830 m/s and 930 m/s) are similar. A series of phenomena, such as the generation of cracks, crater, fragments, can be clearly observed. However, on the rear surface of the sustainable UHPFRC target with hybrid fibres, a different dynamic performance between two different velocities (830 m/s and 930 m/s) bullet impact can be observed. As shown in Figure 9.15, not only cracks appear during the impact process, but also the scabbing is created. Moreover, the impacting projectile can perforate the used UHPFRC target. These phenomena can be attributed to the relatively high impact energy. Although the added hybrid fibres are beneficial in resisting the growth of cracks and dissipating the energy, the relatively high energy amount and short impact time may cause that its energy dissipation efficiency is not as good as in the low velocity impact situation or quasi-static condition. In this study, two bullets (7.62 mm, velocity  $\approx 930$  m/s) perforate the UHPFRC target and one (the second shot) is blocked inside of concrete. The deviation among the experimental results may be attributed to the heterogeneity of the developed concrete. Therefore, to obtain more reliable results, more tests are needed.

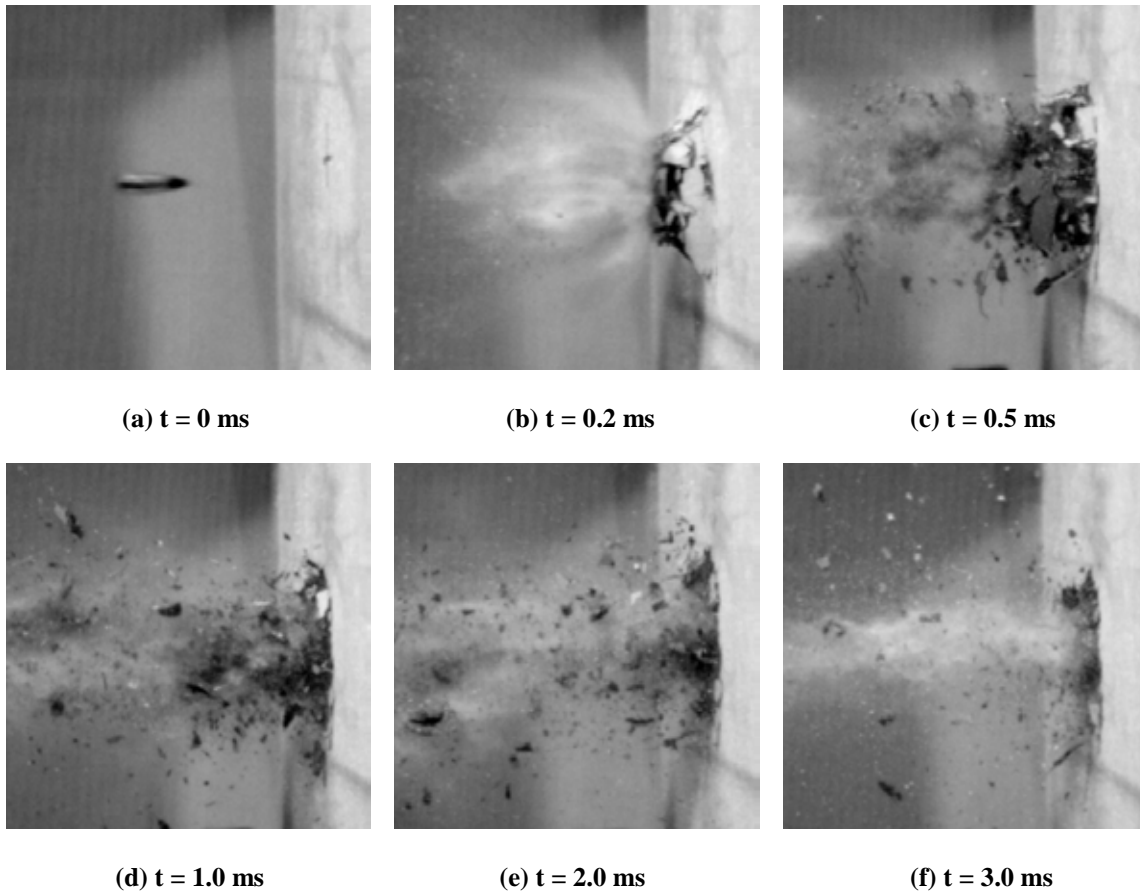


**Figure 9.14: Dynamic performance of the UHPFRC with hybrid fibres under the bullet (7.62 mm, velocity  $\approx 930$  m/s) impact (front surface, first shot)**

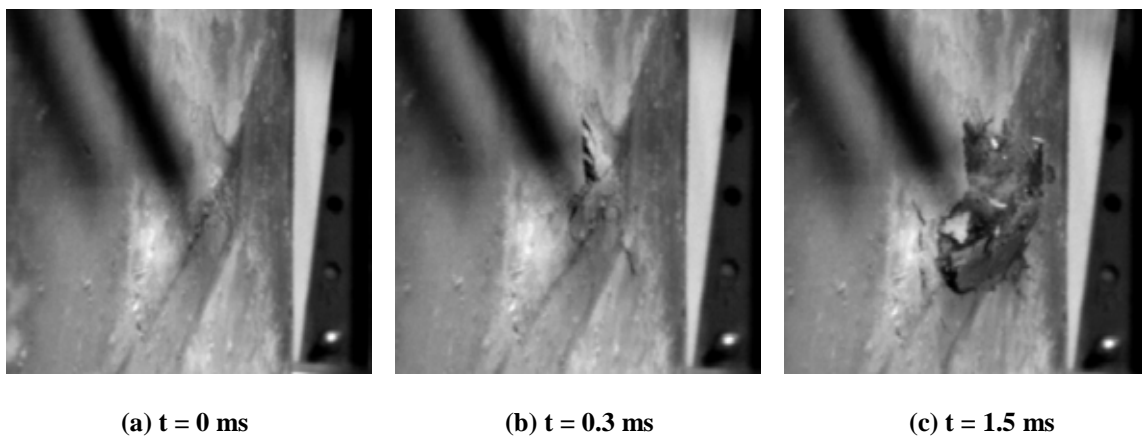


**Figure 9.15: Dynamic performance of the UHPFRC with hybrid fibres under the bullet (7.62 mm, velocity  $\approx 930$  m/s) impact (rear surface, first shot)**

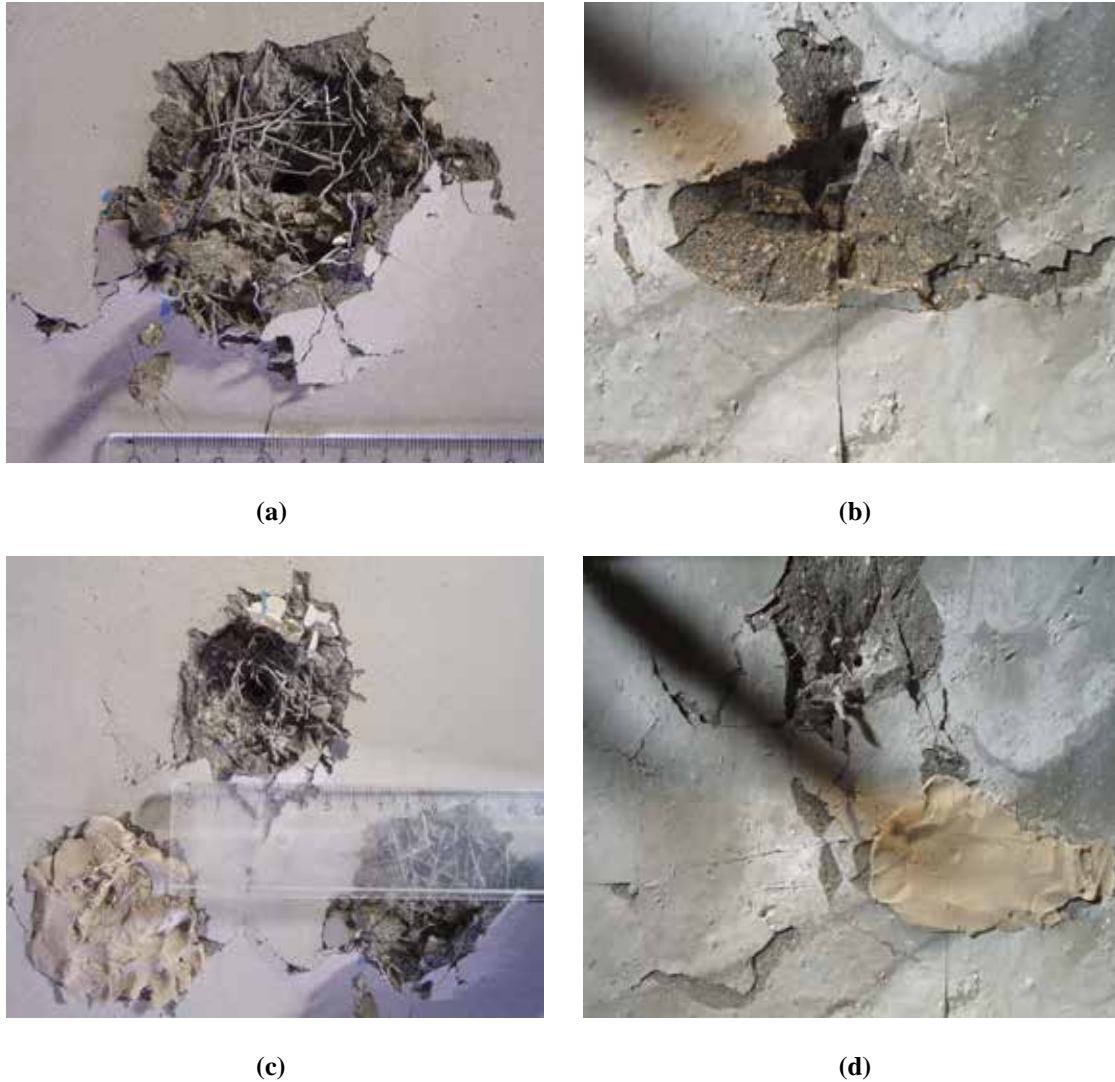


**Figure 9.16: Front and rear appearance of the tested UHPFRC slab with hybrid fibres: (a) front surface after the first shot, (b) rear surface after the first shot, (c) front surface after three shots, (d) rear surface after three shots**

Figures 9.17 and 9.18 illustrate the impact process of the sustainable UHPFRC with single sized fibres under high velocity bullet impact (7.62 mm, velocity  $\approx 930$  m/s). Similarly to the photos shown in Figure 9.11, the impact caused a crater with a diameter of around 8 cm at the concrete front surface, and many fragments and debonded steel fibres can be observed. Nevertheless, at the rear surface of the UHPFRC target, it is obvious that the scabbing area is much larger than that presented in Figures 9.12 and 9.15. Moreover, two projectiles perforated the concrete target and one projectile (the third shot) was blocked inside of the concrete target. The deviation among the experimental results may be also attributed to the heterogeneity of the developed concrete. All the collected experimental data are presented in Table 9.3.

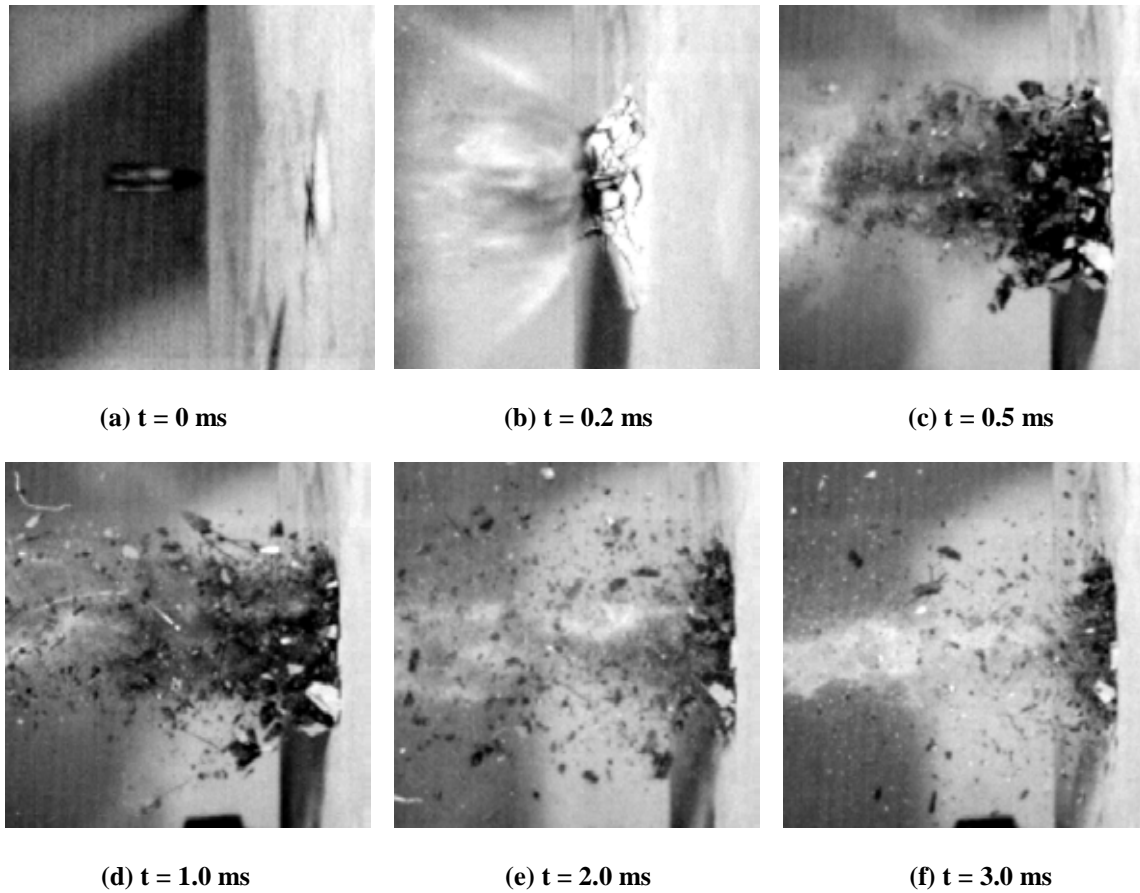


**Figure 9.17: Dynamic performance of the UHPFRC with single sized fibres under the bullet (7.62 mm, velocity  $\approx 930$  m/s) impact (front surface, first shot)**

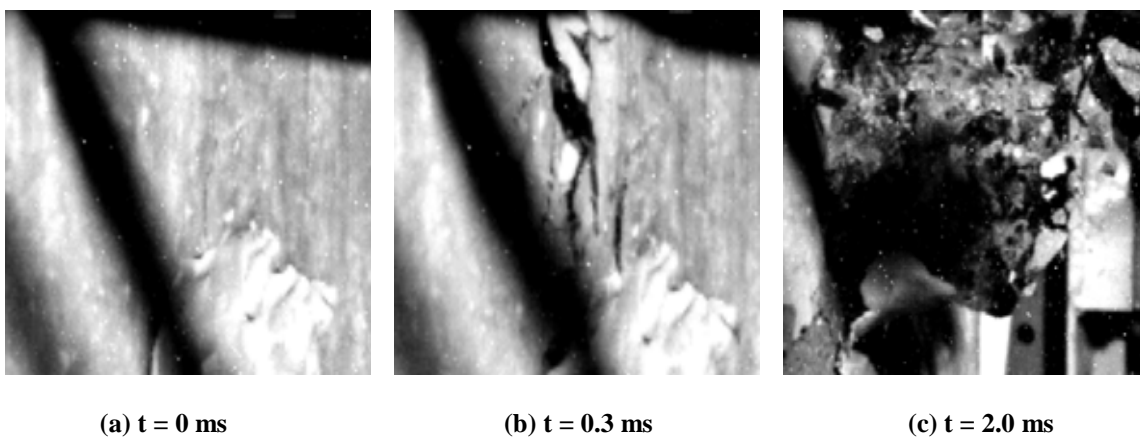


**Figure 9.18: Dynamic performance of the UHPFRC with single sized fibres under the bullet (7.62 mm, velocity  $\approx 930$  m/s) impact (rear surface, first shot)**

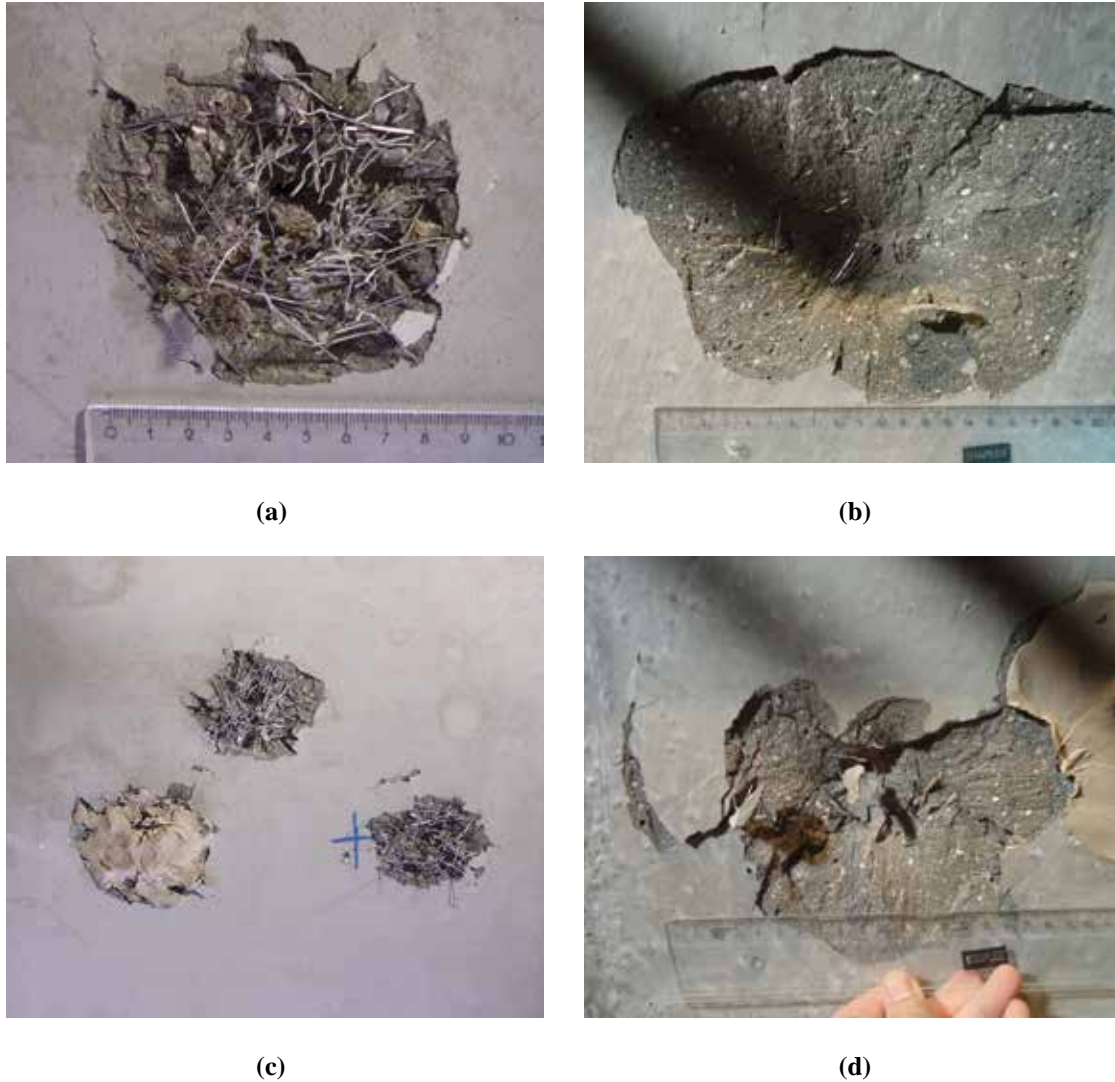


**Figure 9.19: Front and rear appearance of the tested UHPFRC slab with single sized fibres: (a) front surface after the first shot, (b) rear surface after the first shot, (c) front surface after three shots, (d) rear surface after three shots**

**Table 9.3 Bullet impact velocity and obtained experimental results of UHPFRC target**

Impact number	Impact velocity (m/s)	UHPFRC with hybrid fibres			UHPFRC with single sized fibres		
		Residual velocity (m/s)	Crater diameter (cm)	Penetration depth (cm)	Residual velocity (m/s)	Crater diameter (cm)	Penetration depth (cm)
1	922.9	25	7	10.0	-	-	-
2	923.8	0	6.8	8.5	-	-	-
3	914.9	60	6.8	10.0	-	-	-
1	919.4	-	-	-	75	8.0	10.0
2	919.8	-	-	-	85	7.8	10.0
3	921.7	-	-	-	0	7.8	9.0

In general, it can be summarized that the added hybrid fibres are beneficial in improving the impact resistance capacity of the sustainable UHPFRC, particularly in reducing its scabbing area. Yet, to further improve the impact resistance capacity of the sustainable UHPFRC slab (10 cm) under high energy bullet impact, a promising method is to increase the thickness of the concrete slab.

Actually, the conclusion drawn above is not in line with the results shown in Chapter 5, in which it has been experimentally demonstrated that the long hook ended steel fibres are the most efficient one (compared to other straight steel fibres) in improving the flexural toughness or energy absorption capacity of UHPFRC. In the hybrid design of the sustainable UHPFRC, with constant steel fibre content, the addition of straight steel fibres (especially the short straight fibres) can significantly reduce its toughness or energy absorption ability (as shown in Figure 5.19). The differences between the results obtained in Chapter 5 and the results presented here can be attributed to the different experimental evaluation methods, which will be detailed explained in the following content.

As presented in Chapter 5, the energy absorption ability of UHPFRC is evaluated by comparing the area under the load-deflection plot obtained from the 4-point bending test. The test is executed in quasi-static condition, which means the whole tested beam is under the stress and the used fibres have enough time to be pulled out. Compared to the straight steel fibres, the hook ended steel fibres have much larger grip force with the concrete matrix, which causes that more energy will be consumed in the fibres pullout process. Therefore, the energy absorption capacity of UHPFRC with only hook ended steel fibres is larger than that of the mixture with hybrid steel fibres. However, the high velocity bullet impact test is very different from the quasi-static 4-point bending test. Due to the relatively high velocity of projectiles, the impact occurs in a very short time ( $\mu\text{s}$  scale), which causes that only local damages appear in the sustainable UHPFRC target (as shown in Figures 9.8-9.19). As mentioned before, the short fibres can bridge the micro-cracks while the long fibres are more efficient in preventing the development of macro-cracks, which causes that the stress in the hybrid fibres reinforced concrete can be well distributed (Markovic, 2006). Hence, for the sustainable UHPFRC with hybrid fibres under high velocity projectile impact, the crack growth around the local damage area of UHPFRC can be well restricted and the fragment sizes are relatively small (as shown in Figure 9.20). Yet, in the case of the UHPFRC with single sized fibres, it can be noticed that the fragment sizes are relatively large and some embedded hook ended steel fibres can be found in the fragment (as shown in Figure 9.20). This can be attributed to the fact that the applied single sized fibres cannot homogeneously distribute the stress and limit the cracks (especially the micro-cracks) development. Therefore, some macro-cracks are easily created and the debonding of some relatively large fragments (small rupture cross section) from the concrete matrix happens. Hence, for the sustainable UHPFRC with only hook ended steel fibres, its total rupture cross section is relatively small and some

embedded steel fibres did not undergo the fibres pullout process, which can decrease its energy dissipation capacity under the high velocity projectile impact.



**Figure 9.20:** Fragments generated at the rear surface of the UHPFRC with hybrid fibres (A) and single sized fibres (B) after bullet (7.62 mm, velocity  $\approx 930$  m/s) impact

### 9.3.2 The sustainable UHPFRC under FSP (20 mm) impact

- *Impact velocity  $\approx 860$  m/s*

Figure 9.21 illustrates the dynamic behaviour of the sustainable UHPFRC with hybrid fibres under the FSP (20 mm, velocity  $\approx 860$  m/s) impact. It can be noticed that during the impact process, a large amount of dust and fragments are created, which cause that it is difficult to monitor the cracks growth based on the high speed camera photos. Moreover, differently from that shown in Figure 9.8, many debonded steel fibres can be observed in Figures 9.21c and d. These observed phenomena can be attributed to the relatively high impact energy of FSP. In this study, the used FSP mass (about 53.8 g) is almost 6 times of that of utilized bullet (about 8.35 g). Hence, based on the kinetic energy equation, it can be easily calculated that the impact energy of FSP is almost 6 times of that of the bullet with the same velocity. Additionally, in Figure 9.21e, it can be noticed that the FSP rebounds from the concrete target with a relatively low velocity (about 5 m/s), which means the used sustainable UHPFRC slab can resist the FSP impact at the front side. As mentioned before, when the impact velocity of projectile is relatively high, the projectile can penetrate the target to depths beyond the depth of the spall crater, forming a cylindrical penetration hole with a diameter only slightly greater than the missile diameter. As the penetration depth increases, the projectile will stick to the concrete target rather than rebound (Kennedy, 1976). Nevertheless, as shown in Figure 9.23a, it can be noticed that the FSP impact almost generates a cylindrical crater with a diameter (about 60 mm) much larger than that of the FSP diameter (20 mm), and the penetration depth of the FSP is about 4 cm. Due to the relatively large crater diameter and the relatively small penetration depth, it is difficult for the concrete to catch the FSP.

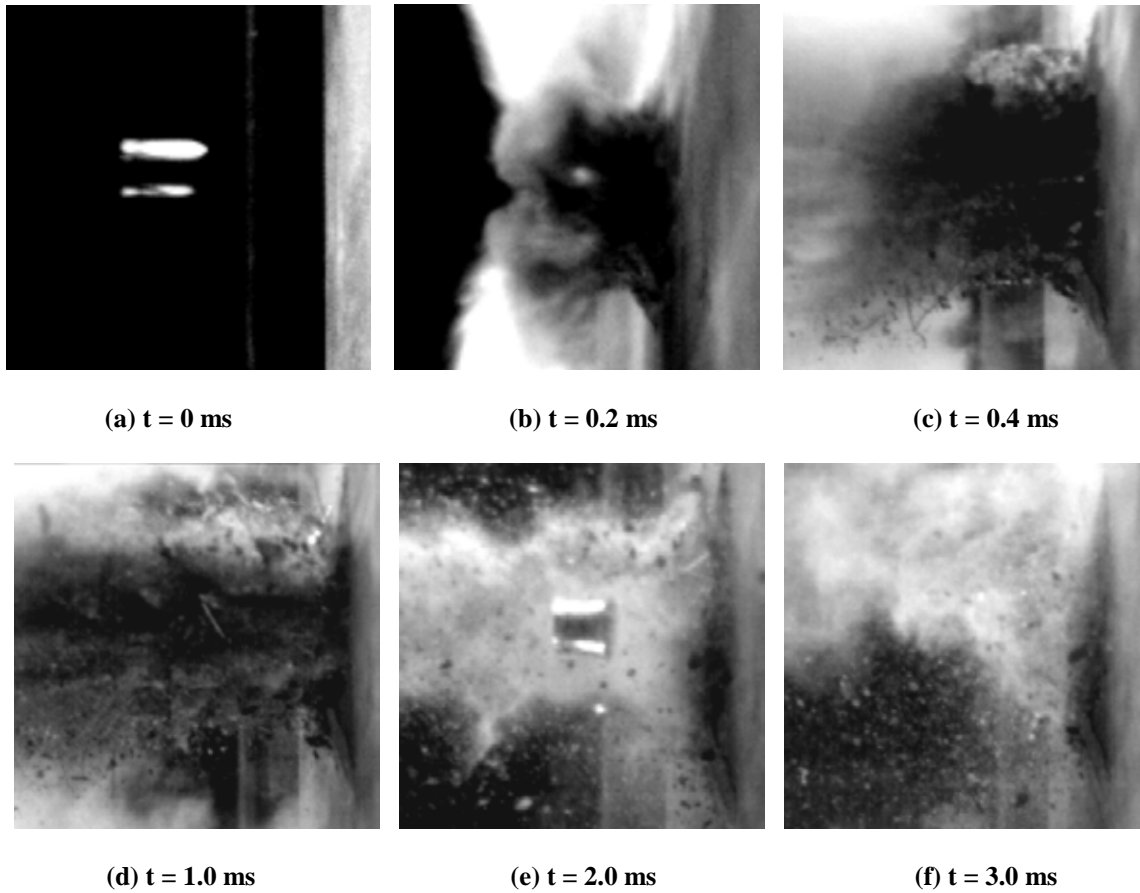


**Figure 9.21: Dynamic performance of the UHPFRC with hybrid fibres under the FSP (20 mm, velocity  $\approx 860$  m/s) impact (front surface, first shot)**

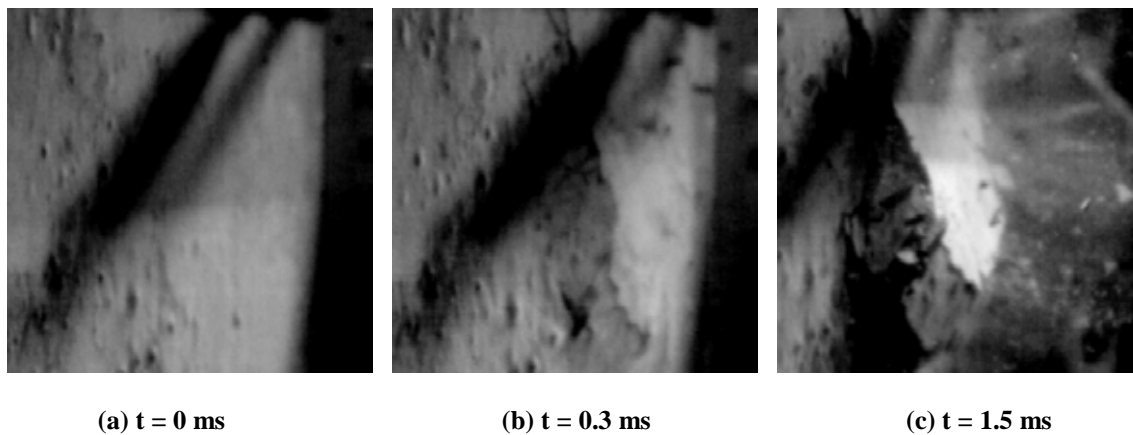


**Figure 9.22: Dynamic performance of the UHPFRC with hybrid fibres under the bullet (7.62 mm, velocity  $\approx 930$  m/s) impact (rear surface, first shot)**

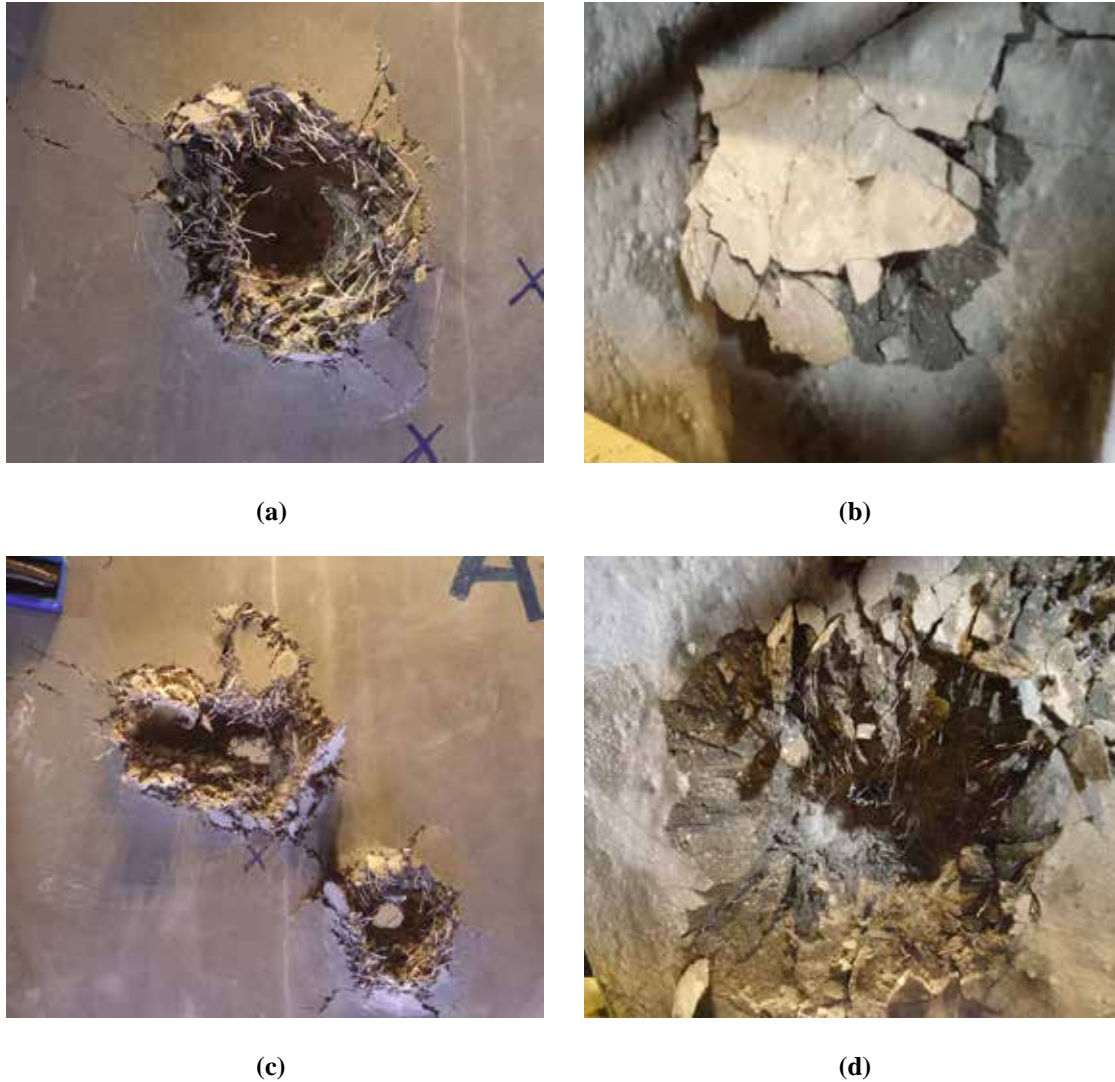


**Figure 9.23: Front and rear appearance of the tested UHPFRC slab with hybrid fibres: (a) front surface after the first shot, (b) rear surface after the first shot, (c) front surface after three shots, (d) rear surface after three shots**

At the rear surface of the sustainable UHPFRC target, the cracks growth and a large amount of fragments can be observed (as shown in Figure 9.22), which can be also attributed to the relatively high impact energy of FSP. However, differently from the normal scabbing damage, it can be noticed that a large part of the damaged concrete at the rear surface of the UHPFRC target still connects with the main body of concrete slab, as shown in Figure 9.23b. This can be attributed to the application of hybrid steel fibres, and the impact energy can be well dissipated. However, after three shots, it can be noticed that the UHPFRC target has been seriously damaged, and clear perforation holes can be observed. Moreover, scabbing with relatively large diameters (about 15 cm) can be found at the rear surface of the concrete target (as shown in Figure 9.23). This can be attributed to the fact that the internal structure of the UHPFRC target has been damaged

during the first shot. Therefore, for the second or third shot, the impact resistance capacity of the sustainable UHPFRC significantly decreases.

In general, due to the relatively large diameters and impact energy of FSP, the obtained experimental results from second or third shots are affected by the first shot. Hence, the recommendation of three times shooting on each sample prescribed in STANAG 2280 (2009) is not suitable to be utilized here to evaluate the dynamic performance of concrete under FSP (20 mm) impact loadings. Although the developed sustainable UHPFRC slab can resist the first impact from FSP (20 mm, velocity  $\approx 860$  m/s) and rebound the projectile, the phenomenon should be further demonstrated by more tests.

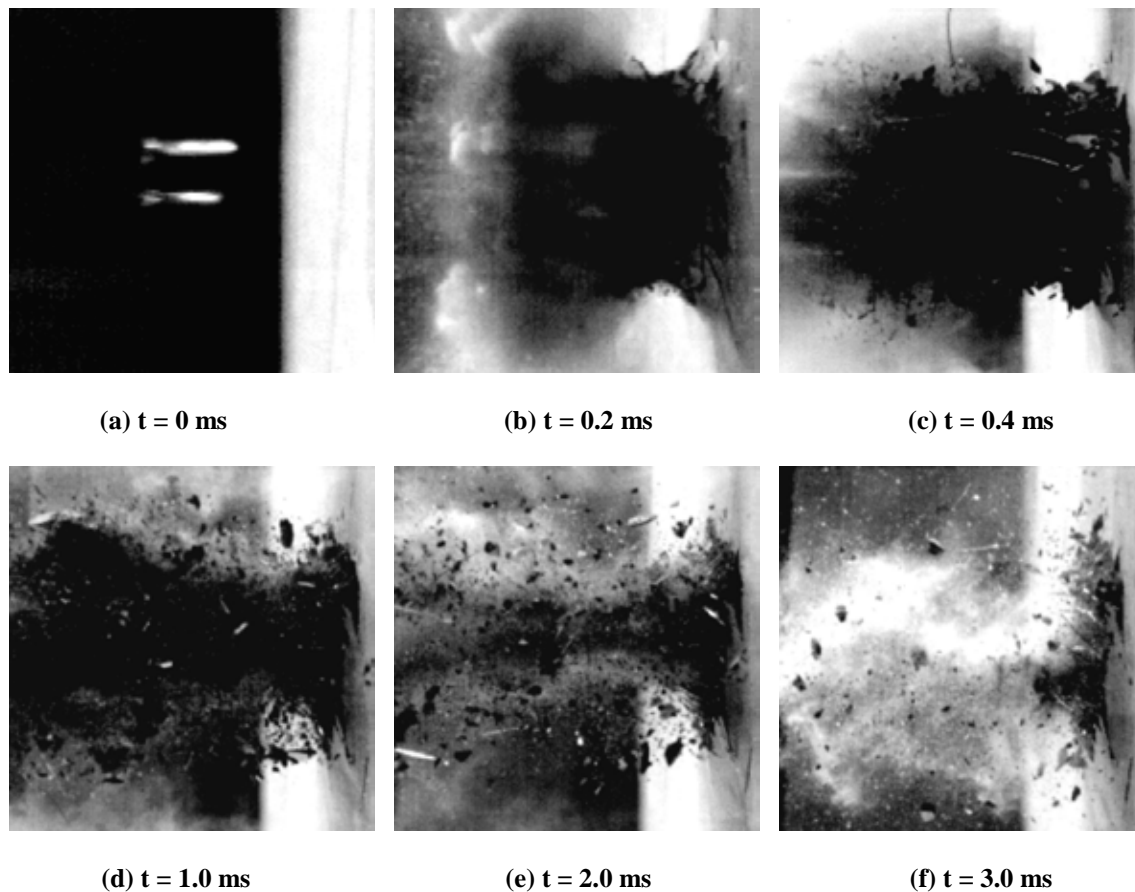


**Figure 9.24:** Dynamic performance of the UHPFRC with single sized fibres under the FSP (20 mm, velocity  $\approx 860$  m/s) impact (front surface, first shot)

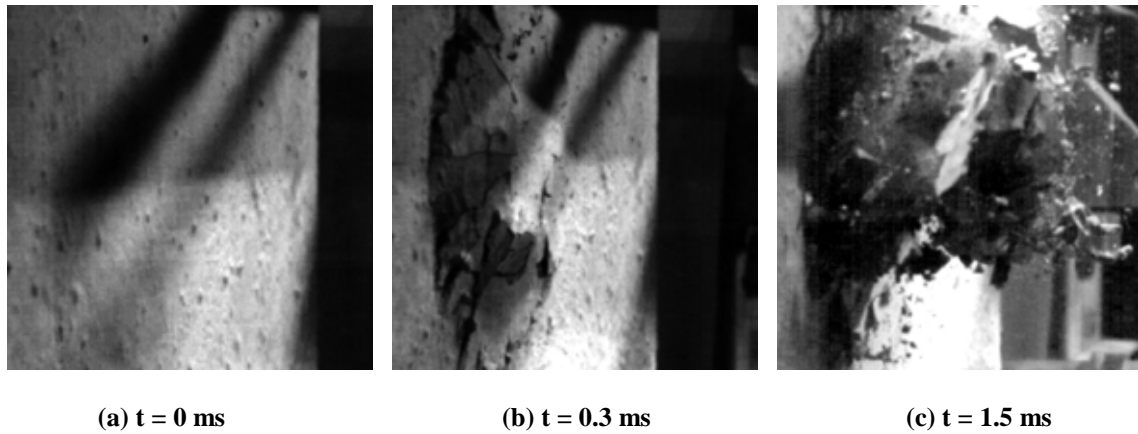


**Figure 9.25: Dynamic performance of the UHPFRC with single sized fibres under the FSP (20 mm, velocity  $\approx 860$  m/s) impact (rear surface, first shot)**

The dynamic performance of the sustainable UHPFRC with single sized fibres (HF) under the FSP (20 mm, velocity  $\approx 860$  m/s) impact (first shot) is shown in Figures 9.24 and 9.25. As can be seen, the front surface reaction of the UHPFRC target under FSP (20 mm, velocity  $\approx 860$  m/s) impact is similar to that shown in Figure 9.21. A large amount of dust and fragments are generated during the impact process, and some debonded steel fibres can be found. Nevertheless, at the rear surface of the UHPFRC target, many fragments with relatively large size and obvious scabbing can be observed, which are different from that presented in Figure 9.22. Moreover, in the first shot, the FSP can perforate the UHPFRC target and the diameter of the scabbing area is about 22 cm at the concrete rear surface, as shown in Figure 9.26. After three shots, it can be noticed that the UHPFRC with single sized fibres has already been seriously damaged and some generated craters are even connected to each other, as shown in Figure 9.26.

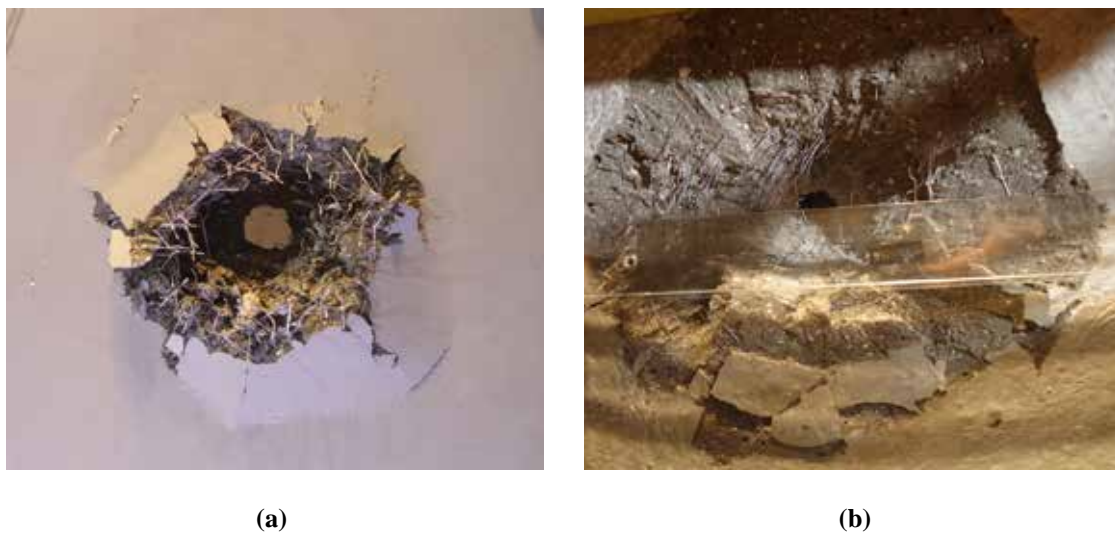




**Figure 9.26: Front and rear appearance of the tested UHPFRC slab with single sized fibres: (a) front surface after the first shot, (b) rear surface after the first shot, (c) front surface after three shots, (d) rear surface after three shots**

These experimental results further demonstrate that the hybrid fibres are more efficient than single sized fibres in improving the impact resistance capacity of the sustainable UHPFRC under high velocity projectile impact. Due to well stress distribution and cracks restriction abilities of hybrid fibres, the generated fragments from the UHPFRC with hybrid fibres are smaller than that from the mixture with single sized fibres, as shown in Figure 9.27. Hence, compared to the UHPFRC with single sized fibres, more rupture cross sections are generated and more fibres are pulled out in the UHPFRC with hybrid fibres during the impact process, which is beneficial for improving the impact resistance capacity of the sustainable UHPFRC target.



**Figure 9.27: Fragments generated at the rear surface of the UHPFRC with hybrid fibres (A) and single sized fibres (B) under the FSP (20 mm, velocity  $\approx$  860 m/s) impact**

• *Impact velocity  $\approx 960$  m/s*

To further evaluate the impact resistance of the sustainable UHPFRC (particularly the one with the hybrid fibres) under the impact of FSP (20 mm) with higher velocity, the test with an impact velocity of about 960 m/s are executed.

Figure 9.28 illustrates the front surface reaction of the sustainable UHPFRC with hybrid fibres under high velocity FSP (20 mm, velocity  $\approx 960$  m/s) impact. It can be noticed that the presented high speed camera photos are similar to those shown in Figure 9.21. A large amount of dust, fragments and some debonded steel fibres are mainly observed. However, there is no rebounded FSP shown in Figure 9.28, which means the FSP may perforate the UHPFRC target. In Figure 9.29, obvious scabbing and fragments can be observed at the rear surface of the concrete target, which are different from that shown in Figure 9.22. From Figure 9.30, it is clear that the concrete target is perforated by the FSP, and the diameters of crater and scabbing are about 10 cm and 21 cm, respectively. After three shots, the UHPFRC target has already been seriously damaged and some craters are connected to each other.

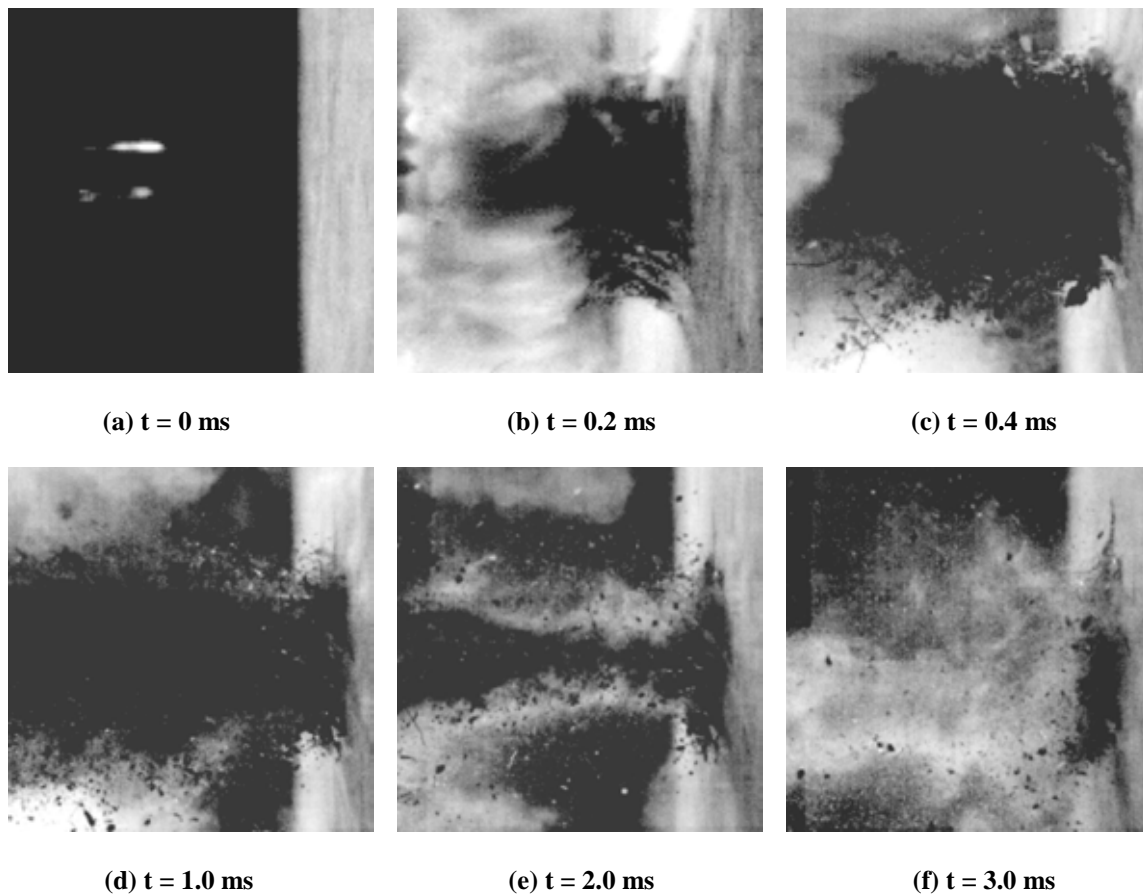


**Figure 9.28: Dynamic performance of the UHPFRC with hybrid fibres under the FSP (20 mm, velocity  $\approx 960$  m/s) impact (front surface, first shot)**

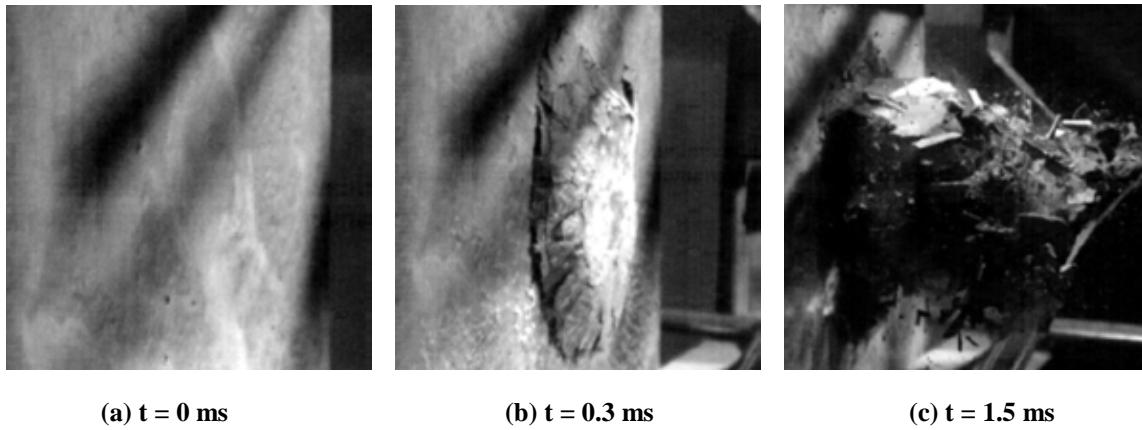


**Figure 9.29: Dynamic performance of the UHPFRC with hybrid fibres under the FSP (20 mm, velocity  $\approx 960$  m/s) impact (rear surface, first shot)**

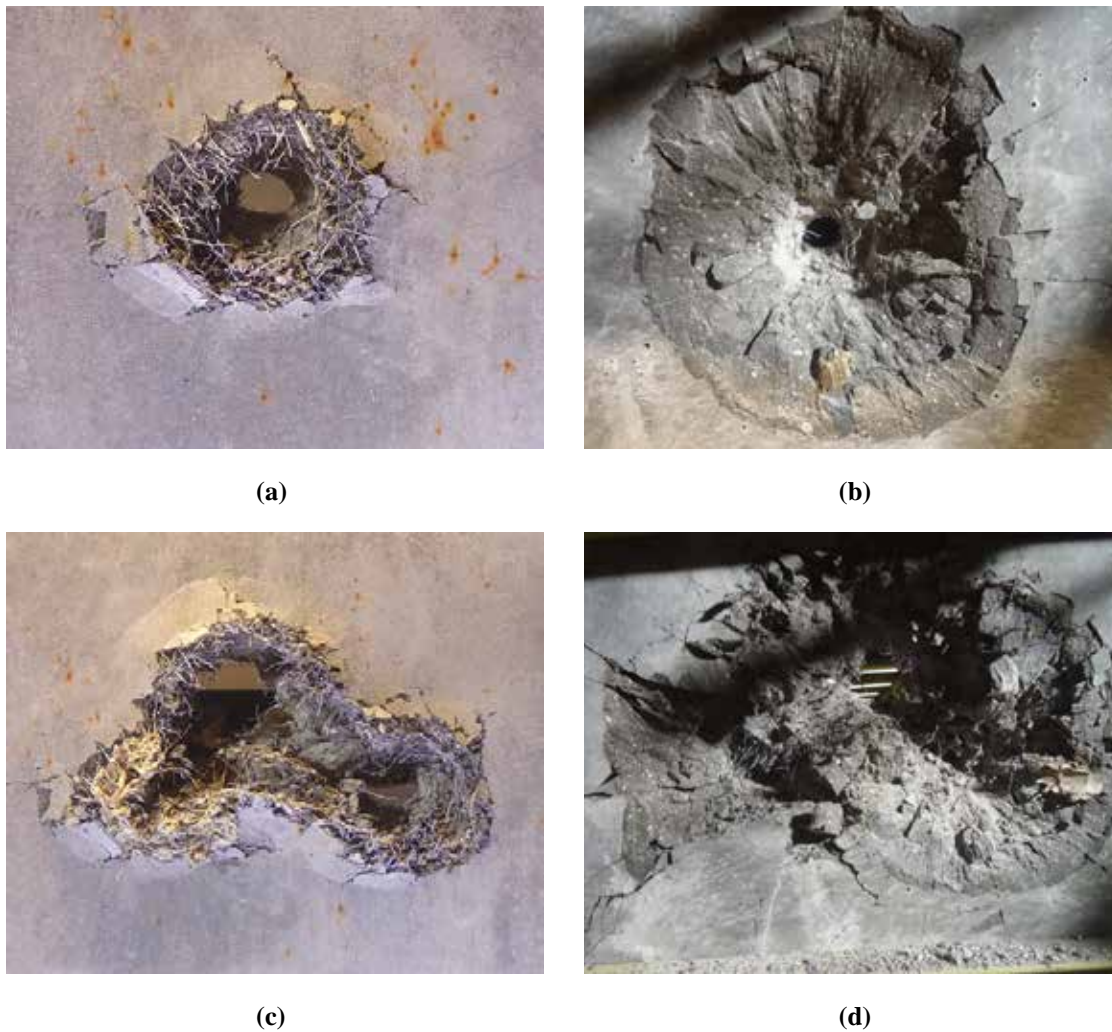


**Figure 9.30: Front and rear appearance of the tested UHPFRC slab with hybrid fibres: (a) front surface after the first shot, (b) rear surface after the first shot, (c) front surface after three shots, (d) rear surface after three shots**

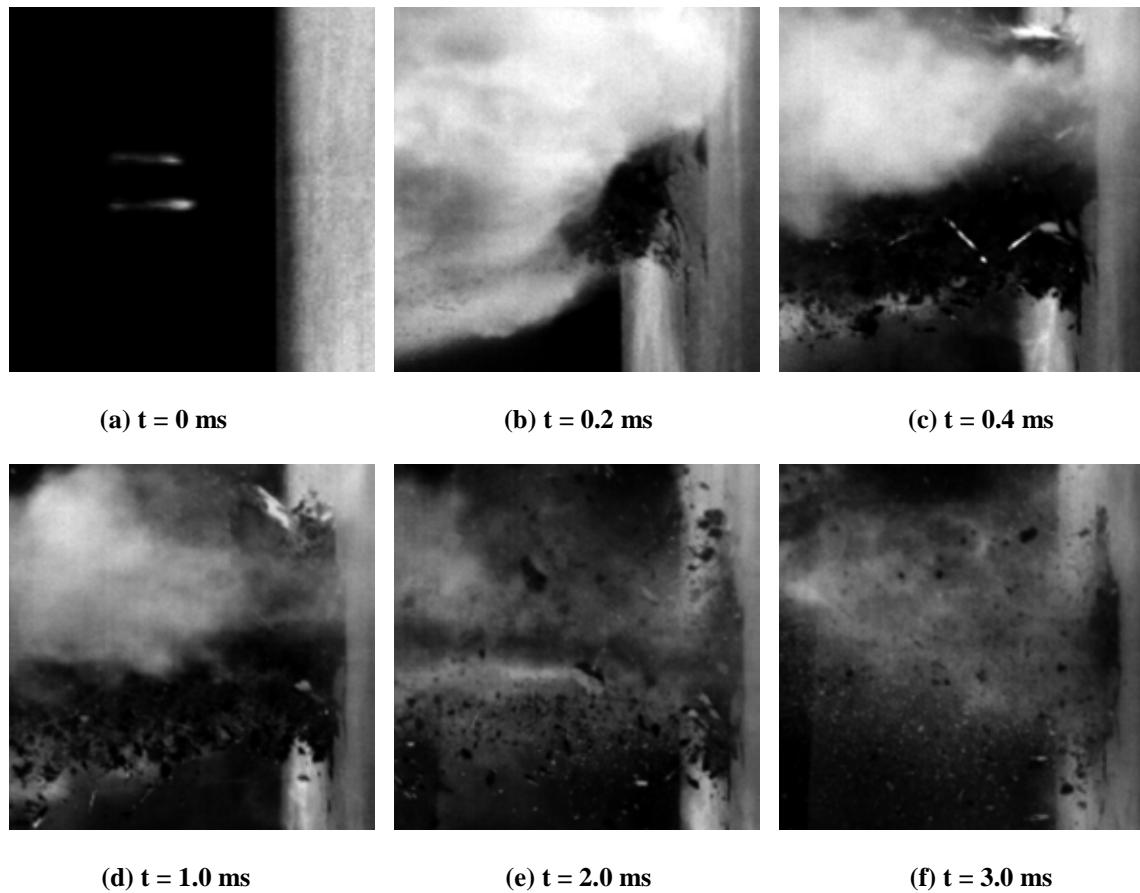


**Figure 9.31: Dynamic performance of the UHPFRC with single sized fibres under the FSP (20 mm, velocity  $\approx 960$  m/s) impact (front surface, first shot)**

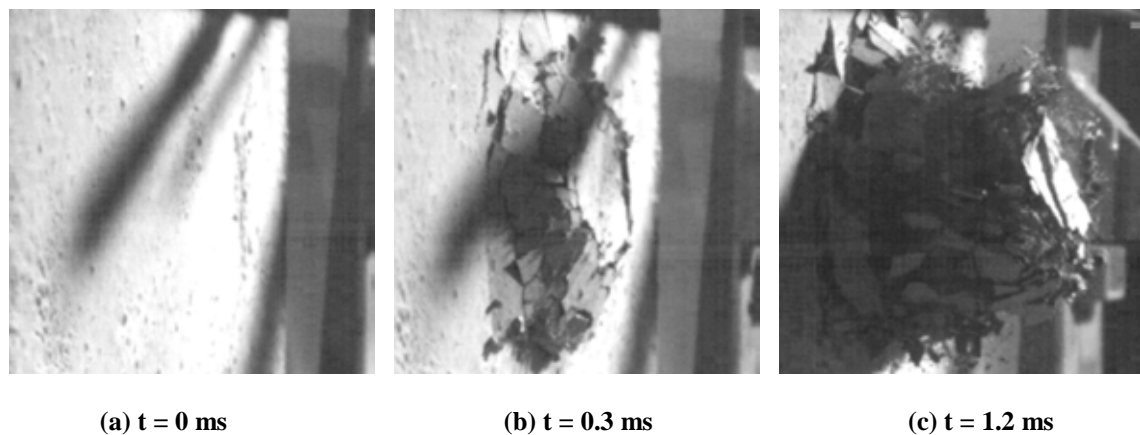


**Figure 9.32: Dynamic performance of the UHPFRC with single sized fibres under the FSP (20 mm, velocity  $\approx 960$  m/s) impact (rear surface, first shot)**

According to the obtained experimental results, it can be summarized that the sustainable UHPFRC with hybrid fibres is ineffective in resisting the impact from FSP (20 mm, velocity  $\approx 960$  m/s), while it can rebound the FSP with an impact velocity of about 860

m/s. This difference can be attributed to the different impact energy. Based on the kinetic energy equation, it can be calculated that the impact energy has increased by 25% when the FSP velocity increases from 860 m/s to 960 m/s. Therefore, the increased impact energy can cause serious scabbing damage at the rear surface of the sustainable UHPFRC target and help the FSP to perforate the concrete slab.

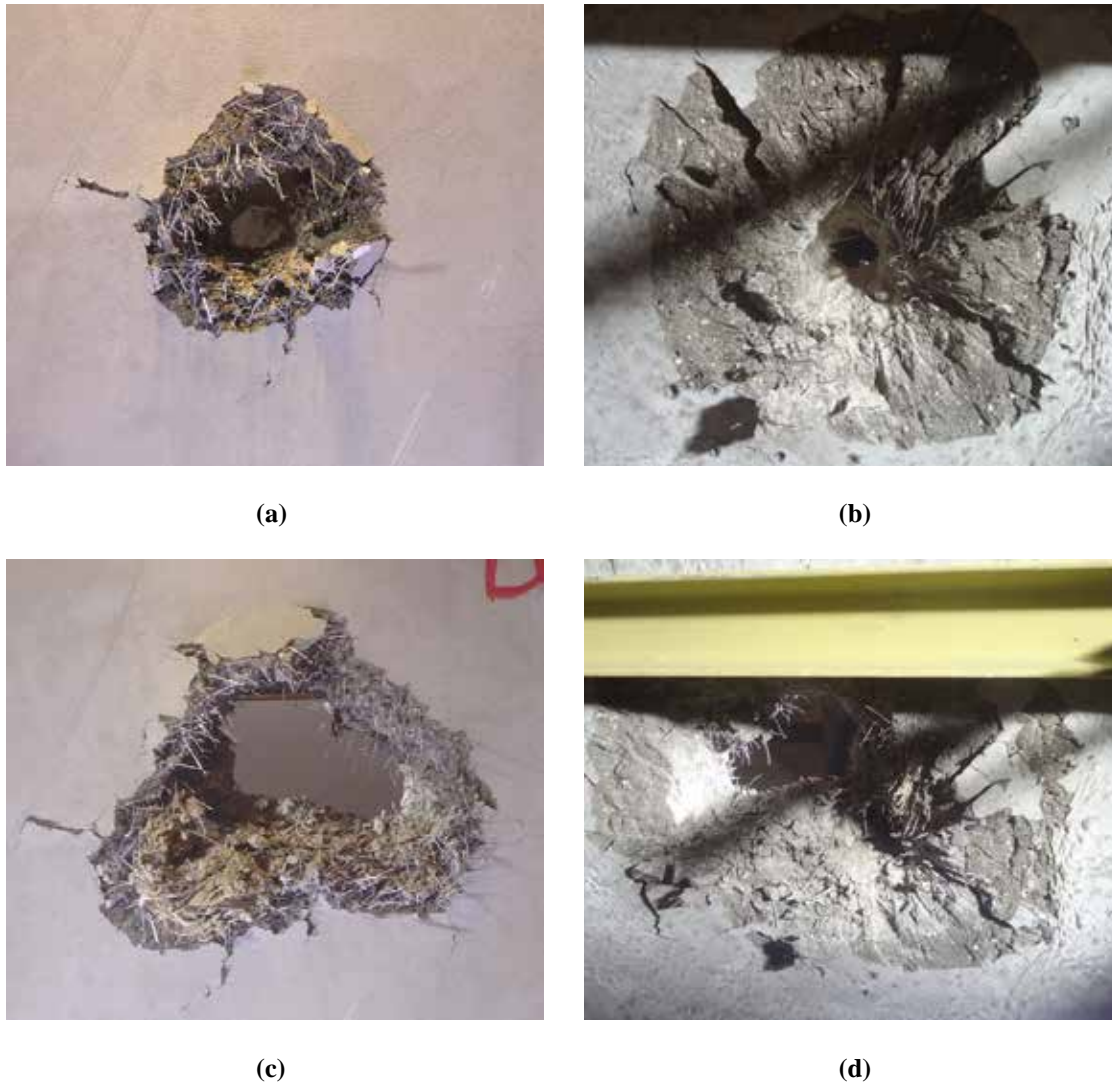


**Figure 9.33: Front and rear appearance of the tested UHPFRC slab with single sized fibres: (a) front surface after the first shot, (b) rear surface after the first shot, (c) front surface after three shots, (d) rear surface after three shots**

Figures 9.31 and 9.32 present the dynamic performance of the sustainable UHPFRC with single sized fibres under the FSP (20 mm, velocity  $\approx$  960 m/s) impact. It can be noticed that both the front and rear surfaces of the concrete target show similar reaction as the UHPFRC target under the FSP (20 mm, velocity  $\approx$  860 m/s) impact. The FSP can perforate the UHPFRC slab and the diameters of crater and scabbing are 11 cm and 25

cm, respectively. After three shots, the concrete slab has been seriously damaged and the generated craters connect to each other, as shown in Figure 9.33. These results further demonstrate the developed UHPFRC slab with single sized fibres cannot resist the impact from high velocity FSP (20 mm).

### 9.3.3 Summary

In this section, the dynamic performance of the sustainable UHPFRC under high velocity bullet (7.62 mm) and FSP (20 mm) impact is presented. In general, it can be concluded that the developed sustainable UHPFRC slab (thickness = 10 cm) with hybrid steel fibres can well resist the impact of bullet (7.62 mm) with a velocity of about 830 m/s, while slight scabbing on the rear surface of the UHPFRC slab with single sized fibres can be created. The obtained crater area on the front surface of the sustainable UHPFRC is similar to that observed by Sovják et al. (2015). When the projectile impact velocity is about 930 m/s, the deviation between the obtained results appears. For the impact from FSP (20 mm) with a velocity of 860 m/s, the developed sustainable UHPFRC slab (thickness = 10 cm) with hybrid fibres can resist the first shot and rebound the projectile, while the UHPFRC target with single sized fibres can be perforated by the projectile. When the impact velocity of FSP increases to about 960 m/s, the developed UHPFRC slabs (thickness = 10 cm) both with hybrid steel fibres and the one with single sized fibres can be perforated by the projectile. Additionally, due to the relatively large dimensions and impact energy of FSP, the results obtained after the second and third shots are affected by the first shot. Hence, to obtain more representative results, more tests should be executed.

## 9.4 Modeling of the sustainable UHPFRC under projectile impact

### 9.4.1 Introduction

Based on the obtained experimental results, the numerical modeling of the sustainable UHPFRC target under high velocity projectile impact loadings is executed and presented in this section.

As mentioned in the previous section, due to the specific shape and high impact velocity of FSP, the experimentally obtained results after the second or third shot are influenced by the first shot, and obvious deformation of FSP can be observed after the impact (as shown in Figure 9.34b). Nevertheless, for the bullet (7.62 mm), it can be noticed that there is almost no deformation can be observed on the collected hard core after impact (as shown in Figure 9.34a), which means it can be treated as a rigid part in the modeling process. Hence, based on the obtained experimental results and in order to simplify the modeling, only the sustainable UHPFRC slab under high velocity bullet impact process is simulated in this section.

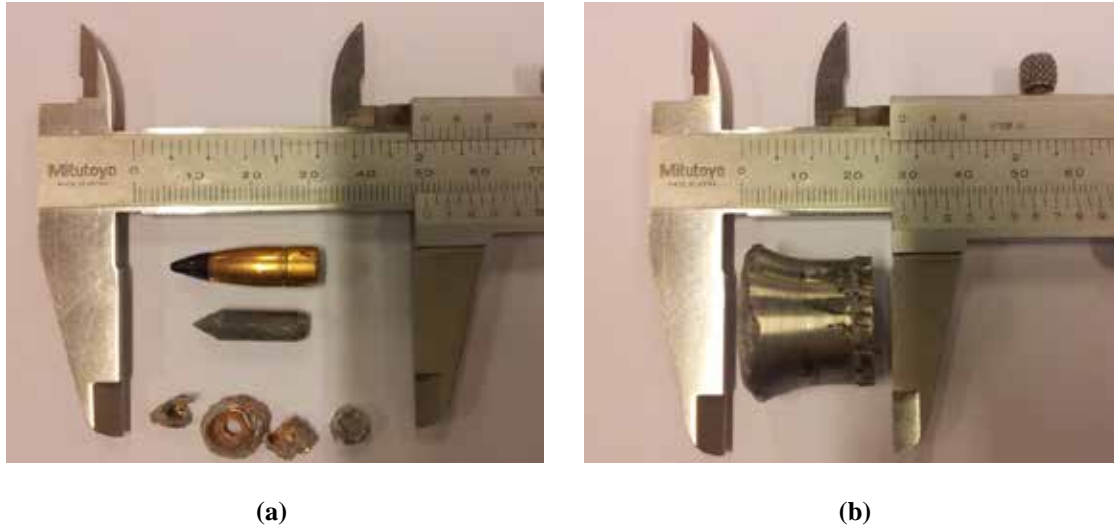
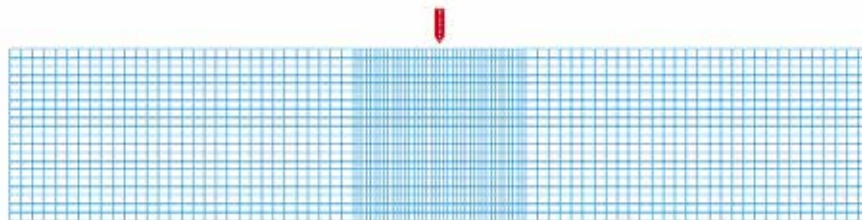


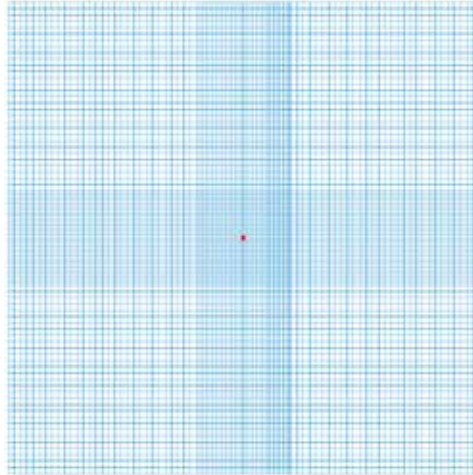
**Figure 9.34:** Collected projectiles after impact tests: (a) projectile from bullet (7.62 mm, including the broken bullet jackets); (b) FSP (20 mm)

#### 9.4.2 Model of UHPFRC slab under high velocity bullet impact

In Figure 9.34a, it can be found that the impact core is covered by a metal jacket, which is destroyed during the impact process subsequently. To simplify the numerical modeling, it is assumed that the hard core directly impacts on the concrete target and the energy consumed in destroying the external jacket is ignored. According to the measured dimensions of the collected hard core and the sustainable UHPFRC slab, a finite element model is created in LS-DYNA and shown in Figure 9.35. As can be seen, compared to the UHPFRC target part, the projectile part is relatively small. Hence, to guarantee the modeling results are reliable and representative, the meshed gridding is relatively dense surrounding the impact area (as shown in Figure 9.35). The mesh used in the computation has 50012 elements and 54656 nodes. The contact types are “surface to surface” and “eroding”. The boundary of the tested sample is fixed. However, the influence of the mesh size, mesh bias and friction effects are not included in this work. These issues will be focused in a future study. Additionally, it is assumed that each impact happens at the centre of the concrete target and no influence exists between every two shots.



(a)



(b)

Figure 9.35: The created models of bullet and UHPFRC target in LS-DYNA and the generated finite element grids: (a) side view; (b) top view

Table 9.4: Material parameters of the sustainable UHPFRC with hybrid fibres

Density $\rho$ (kg/m <sup>3</sup> )	Shear modulus G (MPa)	Strength constants						
		A	B	N	C	$f'_c$	$S_{\max}$	$\epsilon'_0$
2540	36400	0.75	1.65	0.76	0.07	135	21.7	1.0
<b>Damage constants</b>								
	D <sub>1</sub>		D <sub>2</sub>			$(\epsilon'_p + \mu'_p)_{\min}$		
	0.05		1.0			0.01		
<b>Equation of state, EOS constants</b>								
$P_{crush}$ (MPa)	$\mu_{crush}$	K <sub>1</sub> (GPa)	K <sub>2</sub> (GPa)	K <sub>3</sub> (GPa)	$P_{lock}$ (GPa)	$\mu_{lock}$		
26.0	0.01	12.5	17.1	20.8	1.05	0.1		

Table 9.5: Material parameters of the sustainable UHPFRC with single sized fibres

Density $\rho$ (kg/m <sup>3</sup> )	Shear modulus G (MPa)	Strength constants						
		A	B	N	C	$f'_c$	$S_{\max}$	$\epsilon'_0$
2540	35500	0.75	1.65	0.76	0.07	128	18.1	1.0
<b>Damage constants</b>								
	D <sub>1</sub>		D <sub>2</sub>			$(\epsilon'_p + \mu'_p)_{\min}$		
	0.05		1.0			0.01		
<b>Equation of state, EOS constants</b>								
$P_{crush}$ (MPa)	$\mu_{crush}$	K <sub>1</sub> (GPa)	K <sub>2</sub> (GPa)	K <sub>3</sub> (GPa)	$P_{lock}$ (GPa)	$\mu_{lock}$		
22.0	0.008	12.1	16.4	20.0	1.04	0.1		

In the modeling, similarly to the obtained experimental results, two concrete slabs (UHPFRC with hybrid fibres and UHPFRC with single sized fibres) are utilized. To fully describe the concrete's dynamic response within an impact force, the Holmquist Johnson

Cook Concrete model (Holmquist et al., 1993) is again chosen to describe the reaction of concrete under the high velocity impact. A detailed description of this model is shown in Appendix 1. Based on the results obtained in Chapters 5 and 8, the parameters of material model for the used concrete are presented in Tables 9.4 and 9.5. In addition, during the impact process, the projectile is assumed to be non-deformable part (rigid material). A description of rigid material model is shown in Appendix 2.

### 9.4.3 Validation of the model

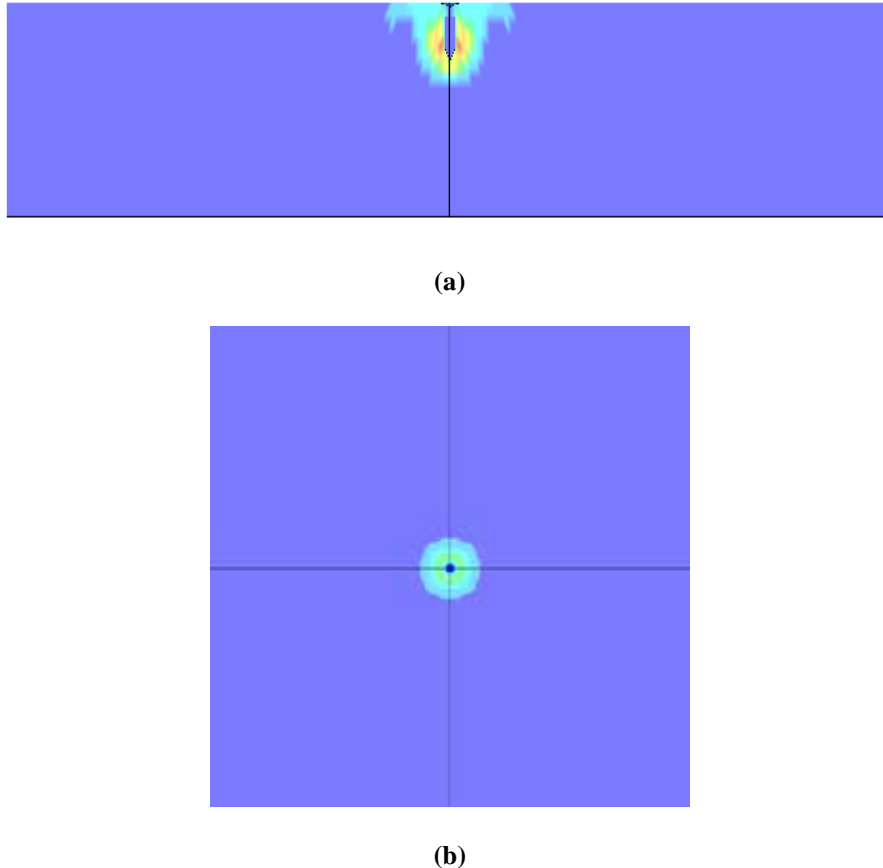
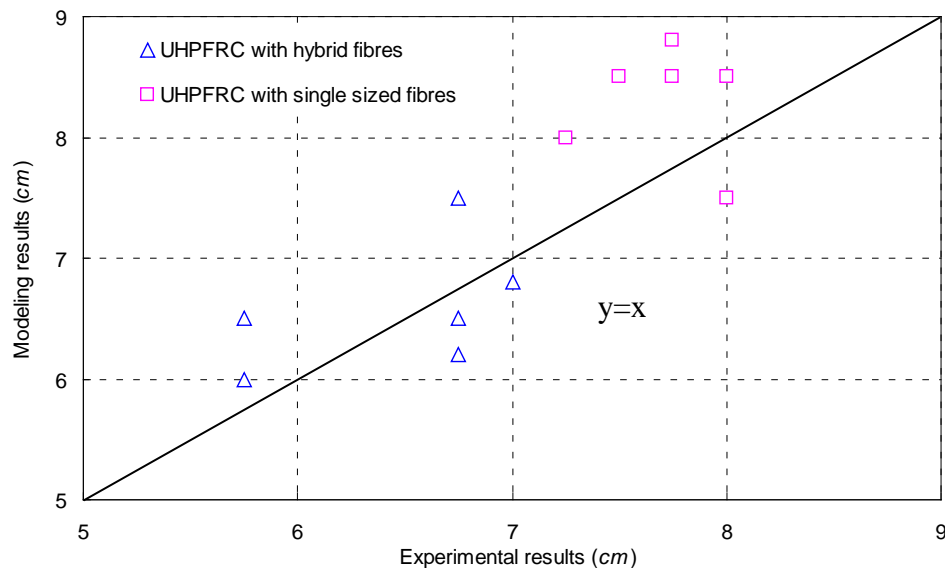


**Figure 9.36: An example of the numerical modeling results of the sustainable UHPFRC under bullet impact (velocity  $\approx 830$  m/s): (a) side view; (b) top view**

Figure 9.36 illustrates an example of the numerical modeling results of the sustainable UHPFRC under high velocity bullet impact. It can be noticed that the concrete area close to the impact projectile is under great stresses. In most cases, the stress can cause brittle tensile fracture firstly in the concrete target, which is then followed by compression-shear failure, since the compressive strength of concrete is much higher than its tensile strength (Katrin and Paul, 2008; Hassan et al., 2012; Park et al., 2012; Rossi, 2013). Moreover, it can be found that the damage area on the front surface of the UHPFRC target is relatively small, which is around 10 times of the projectile diameter. This phenomenon can be attributed to the following two reasons: 1) the used projectile has relatively small

diameter (about 6 mm), while the dimension of concrete target is much larger ( $500 \times 500 \times 100$  mm); 2) the used the steel fibres (especially the hybrid steel fibres) can effectively restrict the growth of cracks and crater area.

To accurately validate the proposed model, three experimental parameters are mainly used here: 1) crater area on the front surface; 2) projectile penetration depth; 3) projectile residual velocity. The detailed experimental information about projectile impact velocity, projectile residual velocity, crater diameter and projectile penetration depth can be found in Tables 9.2 and 9.3.



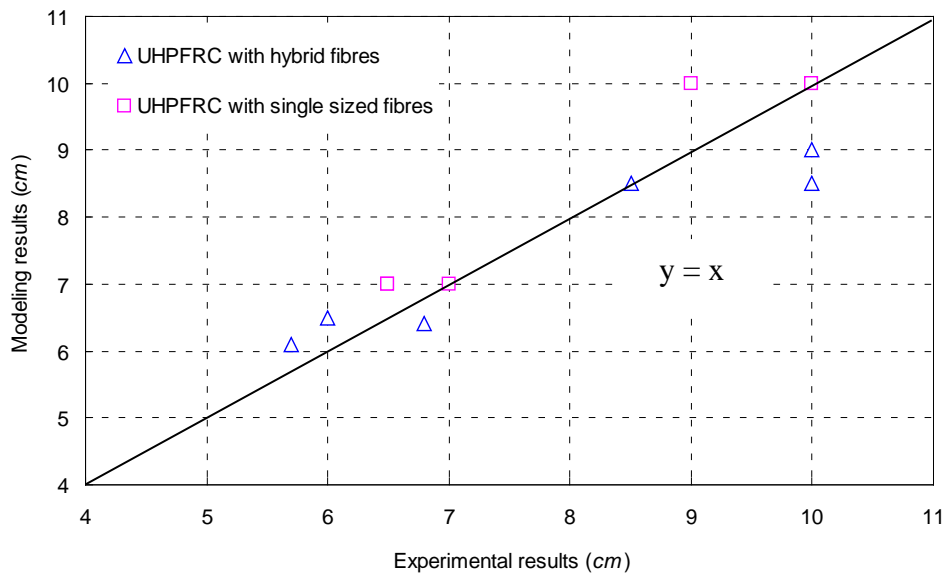
**Figure 9.37: Comparison of the experimental and modeling results of the crater area on the front surface of the sustainable UHPFRC after high velocity bullet impact**

Figure 9.37 presents the comparison of the experimental and modeling results of the crater area on the front surface of the sustainable UHPFRC after the high velocity bullet impact. As can be seen, all the points fluctuate around the line ( $y = x$ ), which means a general agreement exists between the modeling and experimental results. Yet, to further minimize the deviations between the results, more impact experiments should be executed. Moreover, it can also be noticed that all the craters areas can be simply divided into two categories: crater diameter smaller than 7 cm (UHPFRC with hybrid fibres) and crater diameter larger than 7 cm (UHPFRC with single sized fibres). This further demonstrates that the utilized hybrid steel fibres are more efficient than single sized fibres in restricting the development of cracks and crater area.

Figure 9.38 illustrates the comparison of the experimental and modeling results of the projectile penetration depth in the sustainable UHPFRC after the high velocity bullet impact. Similarly to that shown in Figure 9.37, all the points fluctuate around the line ( $y = x$ ), which implies that the modeling results are consistent with the obtained

experimental results. However, when the projectile penetration depth is relatively large, also a relatively higher deviation can be noticed. This can be attributed to the heterogeneity of the used concrete slabs. As can be seen in Section 9.3, when the impact velocity of projectile is about 930 m/s, two projectiles can perforate the UHPFRC slabs (with hybrid fibres and with single sized fibres), while one projectile is blocked inside the concrete. Hence, to more accurately validate the modeling results, more experimental tests should be executed. In addition, it can be found that projectile penetration depth in the UHPFRC with hybrid steel fibres is smaller than that in the UHPFRC with single sized fibres. This phenomenon further demonstrates that the utilized hybrid fibres can not only efficiently minimize the crater area, but also reduce the projectile penetration depth.

Figure 9.39 presents the experimental and modeling results of projectile residual velocity after impact on the sustainable UHPFRC target. It is clear that when the impact velocity of projectile is about 830 m/s, the modeling results agree well with the experimental results. In this case, the projectiles are blocked inside the concrete target, i.e. the projectile residual velocity is zero. However, similarly to that shown in Figure 9.38, when the projectile impact velocity is about 930 m/s, the deviation between experimental and modeling results can be noticed. This can be also attributed to the heterogeneity of the used UHPFRC slabs. Although, to guarantee the homogeneity of the sustainable UHPFRC, large aggregates ( $> 4$  mm) have already been eliminated in the concrete production, the distribution of the added steel fibres (hook ended steel fibres) may strongly affect the heterogeneity of UHPFRC. Therefore, during the shooting tests, two projectiles can perforate the concrete target while one projectile is blocked, which implies that more tests and more representative results are needed.



**Figure 9.38: Comparison of the experimental and modeling results of projectile penetration depth in the sustainable UHPFRC after high velocity bullet impact**

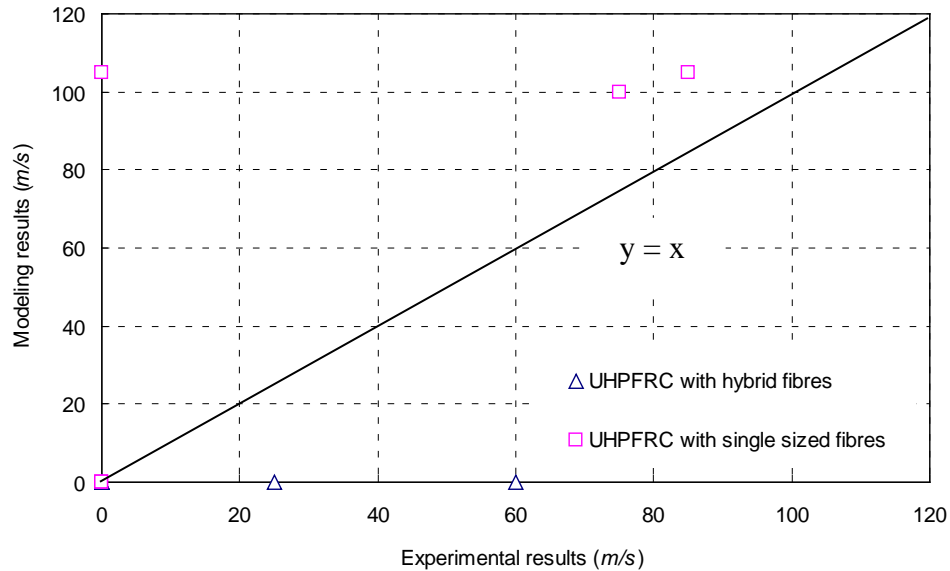


**Figure 9.39: Comparison of the experimental and modeling results of projectile residual velocity after the impact on the sustainable UHPFRC**

#### 9.4.4 Summary

In this section, numerical modeling of the sustainable UHPFRC under high velocity projectile impact loadings is executed, employing LS-DYNA. Based on the experimental design and results, a finite element model is proposed and validated. In general, it can be concluded that when the projectile impact velocity is about 830 m/s, the obtained modeling results coincide with that of the experimental results. Nevertheless, when the projectile impact velocity is about 930 m/s, a deviation between the modeling and experimental results can be observed, which can be attributed to the heterogeneity of used concrete slabs. Consequently, to validate the proposed model better, more experimental tests should be executed.

### 9.5 Conclusions

In this chapter, the developed sustainable UHPFRC is applied in protective elements and its dynamic performance under high velocity projectile impact is investigated, including experiments and numerical modeling. Four types of combinations of projectiles and impact velocities are selected. According to the obtained results, the following conclusions can be drawn:

- 1) The developed sustainable UHPFRC slab (thickness = 10 cm) with hybrid steel fibres can well resist the impact of bullet (7.62 mm) with a velocity of about 830 m/s. The crater diameter is about 6 cm and no scabbing can be observed at the rear surface of the concrete target. For the sustainable UHPFRC slab (thickness = 10 cm) with single sized fibres (HF), it can also resist the impact of bullet (7.62

- mm) with a velocity of about 830 m/s. Nevertheless, at the rear surface of the concrete target, slight scabbing can be created.
- 2) When the bullet (7.62 mm) impact velocity is about 930 m/s, the deviation between the obtained experimental results appears. Two bullets can perforate the UHPFRC targets and one was blocked inside the concrete. The deviation among the experimental results may be also attributed to the heterogeneity of the developed concrete. To obtain more representative results, more tests should be executed.
  - 3) For the impact from FSP (20 mm) with a velocity of 860 m/s, the developed sustainable UHPFRC slab (thickness = 10 cm) with hybrid fibres can resist the first shot and rebound the projectile, while the UHPFRC target (thickness = 10 cm) with single sized fibres can be perforated by FSP with the same velocity. When the impact velocity of FSP increases to about 960 m/s, the developed UHPFRC slabs both with hybrid steel fibres and the one with single sized fibres can be perforated by the projectile. To further improve the impact resistance capacity of the sustainable UHPFRC, a promising method is to increase the thickness of the concrete target.
  - 4) Due to the relatively large dimensions and impact energy of FSP (20 mm), the results obtained after the second and third shots are affected by the first shot. Hence, the recommendation of three times shooting on each sample shown in STANAG 2280 (2009) is not suitable to be utilized here to evaluate the dynamic performance of concrete under high velocity FSP (20 mm) impact loadings. To obtain more representative results, more tests are required.
  - 5) Compared to the UHPFRC with single sized fibres, the one with hybrid steel fibres show much better impact resistance capacity in reducing the crater area, projectile penetration depth and projectile residual velocity. This can be attributed to the fact that the high velocity impact occurs in a very short time ( $\mu\text{s}$  scale), and only local damages appear in the sustainable UHPFRC target. Around the damaged area, the used hybrid fibres can efficiently prevent the cracks growth (micro and macro) and well distribute the external stress, which cause that the fragments sizes are relatively small and a large amount of energy is consumed on fracturing the concrete matrix and pulling the fibres out.
  - 6) A finite element model is created in LS-DYNA to simulate the process of the sustainable UHPFRC under high velocity bullet impact. Then, the obtained experimental results (crater area, projectile penetration depth and projectile residual velocity) are utilized to validate the proposed model. In general, it can be concluded that when the bullet impact velocity is about 830 m/s, the obtained

modeling results coincide with those of the experimental research. Nevertheless, when the bullet impact velocity is about 930 m/s, a deviation between the modeling and experimental results can be observed, which can be attributed to the heterogeneity of the concrete slabs and some experimental error. Consequently, to more accurately validate the proposed model, more experimental tests should be executed.



# Chapter 10

## Conclusions and recommendations

### 10.1 Conclusions

Due to the complicated international circumstances, increasing terrorist attack events and unpredictable accidents, there is a strong demand for impact resistance materials in both the civil and military fields. Based on the previous investigations (Bindiganavile et al., 2002; Parant et al., 2007; Zhang et al., 2007; Habel and Gauvreau, 2008; Lai et al., 2009), it has been proven that a strong concrete matrix combined with a large amount of steel fibres is beneficial for improving the impact resistance capacity of concrete, since debonding of fibres from matrix can absorb a large amount of energy that is released during the impact loading process. Hence, a relatively new type of concrete - Ultra-High Performance Fibre Reinforced Concrete (UHPFRC) is a promising solution for the infrastructure where a large amount of energy may be suddenly released. However, UHPFRC is still a relatively new building material, whose dynamic performance under impact loadings is not fully understood. Moreover, so far, the UHPFRC development commonly ignore the sustainability and environmental impact, as normally a large amount of binders is used and the efficiencies of the utilized powders and fibres are not considered. Consequently, based on these premises, this thesis presents an approach to develop a sustainable UHPFRC and investigate its dynamic performance under impact loadings.

The development of a sustainable UHPFRC can be achieved by employing an optimized particle packing model, efficient application of powders and fibres, and proper use of waste/recycled materials, individually or simultaneously. The properties assessment of the sustainable UHPFRC developed in this study mainly include its workability, air content, water-permeable porosity, mechanical properties, flexural toughness, cement hydration kinetics and thermal properties. Moreover, the impact resistance/energy dissipation capacity of the developed sustainable UHPFRC is thoroughly investigated, employing the “Charpy Impact Device” and a “Modified Pendulum Impact Device”. An equation is proposed to compute the energy dissipated in the sustainable UHPFRC under the Charpy impact test. Additionally, to widen the application of the developed sustainable UHPFRC in the military field, its dynamic performance under high velocity projectile impact is investigated, including experimental tests and numerical modeling. This research is performed based on a combination of theoretical and experimental

investigation. The main conclusions are drawn from the performed experimental and modeling study and elaborated in the following sections.

### **10.1.1 Optimized mix design of UHPFRC**

Mix design is always a hotspot of concrete investigation, particularly for advanced concretes (e.g. self-compacting concrete, high strength concrete, high performance concrete). As commonly known, an optimum packing of the granular ingredients of concrete is the key for a good and durable concrete (Fuller and Thompson, 1907; Andreasen and Andersen, 1930; De Larrard and Sedran, 1994; De Larrard and Sedran, 2002; Fennis et al., 2009). For the design of mortars and concretes, several mix design tools are in use, such as Linear Packing Density Model (LPDM), Solid Suspension Model (SSM) and Compressive Packing Model (CPM). However, all these design methods are based on the packing fraction of individual components (cement, sand etc.) and their combinations, and therefore it is complicated to include very fine particles in these mix design tools, as it is difficult to determine the packing fraction of such very fine materials or their combinations.

As be mentioned before, due to the fact that a large amount of fines are normally utilized in the production of UHPFRC, the design methods listed above are inefficient for the design of UHPC or UHPFRC. Hence, in Chapter 3, the design of the UHPFRC mixtures is based on the aim to achieve a densely compacted cementitious matrix, employing the modified Andreasen & Andersen particle packing model (A&A model) and the approach developed earlier (Brouwers and Radix., 2005; Hüsken and Brouwers, 2008; Hunger and Brouwers, 2009; Hüsken, 2010; Hunger, 2010). According to the obtained experimental results, it is demonstrated that an optimized UHPFRC can be produced with relatively low binder amount (about  $650 \text{ kg/m}^3$ ), without sacrificing its superior mechanical properties (e.g. compressive strength at 28 days is about 140 MPa). Consequently, the modified A&A model is an effective method to develop sustainable UHPFRC, characterized by both low cost and low environmental impact.

### **10.1.2 Sustainable development of UHPFRC focus on ingredients point of view**

For the production of UHPFRC, a number of powders (cement, pozzolanic materials and non-active fillers) and fibres are normally utilized. However, by far, the efficiency of these used powders and fibres is not well considered and optimized. Hence, in this thesis, the development of sustainable UHPFRC is based on an efficient application of powders (Chapter 4), fibres (Chapter 5) and appropriate using waste/recycled materials (Chapter 6).

The effect of nanosilica and mineral admixtures (FA, GGBS and LP) on the properties of UHPC is firstly evaluated. Nanosilica is a relatively new material, which has an extremely fine particle size and higher activity than silica fume. From the obtained

experimental results, it is proven that a relatively small amount of nanosilica can significantly improve the microstructure and mechanical properties of UHPC. Nevertheless, an overdose of nanosilica can increase fresh concrete viscosity and increase its porosity in hardened state, which is negative for improving the mechanical properties of UHPFRC. Hence, the optimal dosage of the utilized nanosilica is about 3.74% by the mass of the binder amount in this study, which is in line with Quercia (2014). In addition, it is found that the hydration process of UHPC mixtures with almost the same amount of FA, GGBS and LP is similar to each other during the initial five days. Afterwards, the hydration rate of the mixture with GGBS is obviously accelerated. Due to the specific cementitious system of UHPC (very small water/binder ratio and relatively high SP amount), it is observed that the pozzolanic reaction of FA is significantly retarded, which means that a very limited amount of FA can react with  $\text{Ca}(\text{OH})_2$  after curing for 91 days. Additionally, it is demonstrated that the developed UHPC with an appropriate amount of mineral admixtures has much lower environmental impact than the other UHPCs shown in the available literature. Hence, based on the different requirements (workability, mechanical properties, or environmental impact) from practice, different mineral admixtures should be appropriately chosen in the UHPC production.

Subsequently, toward the efficient utilization of the steel fibres in UHPFRC, the effect of binary and ternary hybrid fibres on the properties of UHPFRC is investigated. From the obtained experimental results it can be noticed that different fibres can provide different contributions to the properties of UHPFRC. For instance, binary fibres are beneficial in improving its workability (about 90 cm in slump flow, based on EN-12350-8 (2010)) and mechanical properties (about 30 MPa and 140 MPa for 28 days flexural and compressive strengths, respectively). Hook ended steel fibres (HF) can significantly increase the toughness of UHPFRC to about 35 *Nm*, based on JSCE SF-4 (1984). Therefore, according to the different requirements (good workability, high mechanical properties or high toughness) from practice, different fibre types and hybridization designs should be well chosen, which could ensure the efficient use of the fibres and make UHPFRC more sustainable. In this study, to design a protective UHPFRC with relatively high energy absorption capacity, the hook ended fibres (HF) is found to be a good choice.

Finally, a tentative study on the sustainable UHPFRC production incorporating waste bottom ash (WBA) is performed. It is demonstrated that with an appropriate application of nanosilica, steel fibres and polypropylene fibres, about 20% of the fine aggregates can be replaced by WBA in the production of UHPFRC. Due to the negative effect of the metallic aluminium in WBA, the developed UHPFRC has relatively lower compressive strength (about 115 MPa). Nevertheless, the coarse surface of WBA and some threadlike matter on its surface cause the flexural strength of the developed UHPFRC to be comparable to the other UHPFRCs presented in literature. Hence, this developed sustainable UHPFRC with WBA is more suitable to be utilized in applications which

require high flexural properties. In this research, the aim is to develop a sustainable protective UHPFRC, which implies that the produced material should be sustainable and simultaneously have great impact resistance capacity. Due to the fact that the material is under great compressive, flexural and tensile stresses during the impact process, the UHPFRC with WBA is less suitable to be utilized to produce a protective structure. Hence, for the impact resistance evaluation shown in Chapters 7-9, all sustainable UHPFRCs are produced based on the optimized particle packing model, and an efficient application of powders and steel fibres.

### **10.1.3 Energy dissipation capacity of the developed UHPFRC**

In this study, the energy dissipation capacity of the developed sustainable UHPFRC under impact loadings is evaluated by employing “Charpy Impact Device” (Chapter 7), “Modified Pendulum Impact Device” (Chapter 7) and high velocity projectile launchers (Chapter 9).

The dynamic impact test results obtained from “Charpy Impact Device” show that the fibre length plays a dominating role in improving the energy dissipation capacity of the sustainable UHPFRC. With a constant total steel fibre amount, the addition of short fibres can cause a decrease of the energy absorption capacity of the concrete target. However, from the results obtained from the “Modified Pendulum Impact Device”, it is demonstrated that the addition of hybrid steel fibres is more efficient than single sized fibres in increasing the energy dissipation capacity of the sustainable UHPFRC. The difference between the obtained results is mainly attributed to the fibre categories and sample dimensions. During the pendulum impact process, the impact energy absorbed by the sustainable UHPFRC is mainly composed of two parts: the energy consumed to break the concrete matrix and the energy used to pull out the fibres embedded in the broken cross sections. For the Charpy impact test, due to the fact that the used concrete sample is relatively small ( $25.4 \text{ mm} \times 25.4 \text{ mm} \times 50.8 \text{ mm}$ ), all the targets are broken after only single impact (as shown in Figure 7.13). Hence, the cracks can be created immediately, and more energy is consumed in pulling the fibres out, which cause the advantages of hybrid steel fibres (LSF + SSF) in stress distribution and micro-cracks resistance to not be well utilized. Considering the fact that the used SSF is relatively short and easy to be debonded from the concrete matrix, the addition of SSF can cause a decrease in the energy absorption capacity of the concrete target. On the contrary, in the case of the tests executed by the “Modified Pendulum Impact Device”, the used sample dimensions are relatively large ( $500 \text{ mm} \times 500 \text{ mm} \times 100 \text{ mm}$ ), which causes the concrete target not to be broken after the first impact (as shown in Figure 7.21). Therefore, the creation of cracks plays an important role in resisting the impact loadings. Due to the fact the stress in the hybrid fibres reinforced concrete can be better distributed than that in the single sized fibres reinforced concrete, more small cracks are created in the sustainable UHPFRC with hybrid steel fibres, which simultaneously means that more energy is

consumed in the creation of cracks and also growth of these cracks. Hence, the sustainable UHPFRC with hybrid steel fibres is more suitable for the production of protective structures.

Additionally, based on the results obtained from the high velocity projectile impact tests (projectile velocity is about 900 m/s and the sample dimensions are 500 mm × 500 mm × 100 mm), it can also be noticed that the sustainable UHPFRC with hybrid fibres (HF + LSF) shows much better impact resistance capacity than the one with only HF type. This can be attributed to the fact that the high velocity projectile impact occurs in a very short time ( $\mu\text{s}$  scale), which causes only local damages to appear on the surface of the sustainable UHPFRC target. As mentioned before, the short fibres can bridge the micro-cracks while the long fibres are more efficient in preventing the development of macro-cracks, which causes the stress in the hybrid fibres reinforced concrete to be well distributed (Markovic, 2006). Hence, for the sustainable UHPFRC with hybrid fibres under high velocity projectile impact, the crack growth around the local damage area of UHPFRC can be well restricted and fragment sizes are relatively small. Yet, in the case of the UHPFRC with single sized fibres, due to the fact that the impact stress cannot be homogeneously distributed during the impact process, the fragment sizes are relatively large and some embedded hook ended steel fibres can be found in the fragment. Consequently, for the sustainable UHPFRC with only hook ended steel fibres, its total rupture cross section is relatively small and some embedded steel fibres did not undergo the fibres pullout process, which can significantly decrease its energy dissipation capacity under the high velocity projectile impact. In general, to effectively produce a protective structure for civil or military using, the sustainable UHPFRC with hybrid steel fibres (HF+LSF) is a good choice.

#### **10.1.4 Modeling of UHPFRC under impact loadings**

In this thesis, the modeling studies of the sustainable UHPFRC mainly focus on its energy absorption capacity under Charpy impact test and its dynamic performance under high velocity hard projectile impact.

In Chapter 7, a new equation is proposed to compute the energy absorption capacity of the sustainable UHPFRC with hybrid fibres under the Charpy impact test. It is demonstrated that the new model features a good correlation with the experimental results, especially for the samples with a lower energy absorption capacity. When the impact resistance ability of the UHPFRC is relatively high, the modeling results slightly underestimate the experimental results (by about 9%), which could be attributed to the energy dissipated into the test device. Moreover, due to the fact that concrete has a very complicated nonlinear behaviour and is difficult to be fully described for general stress conditions by a simple constitutive model, a commercial hydrocode - LS-DYNA is employed to simulate the performance of concrete under projectile impact, which is

shown in Chapter 8. A finite elements model of concrete under projectile impact loading is firstly created based on literature experiments. Then, the literature experimental results are used to validate the proposed model. Afterwards, the energy dissipation capacity of the developed sustainable UHPFRC under hard projectile impact is assessed and predicted by using the validated model in LS-DYNA. Based on the obtained modeling results, it is demonstrated that the developed sustainable UHPFRC has a much better energy dissipation capacity and is more suitable to be utilized in places where a large amount of energy may be released, compared to normal strength concrete (NSC) and high strength concrete (HSC). However, these obtained modeling results need to be further validated. Therefore, in Chapter 9, performed high velocity projectile impact tests are presented and the obtained experimental results are utilized to validate the created LS-DYNA model. In general, it can be concluded that when the bullet impact velocity is about 830 m/s, the obtained modeling results coincide with experimental research. Nevertheless, when the bullet impact velocity is about 930 m/s, a deviation between modeling and experimental results can be observed, which can be attributed to the heterogeneity of used concrete slabs and some experimental errors. Consequently, to more accurately validate the proposed model, more experimental tests should be executed.

## 10.2 Recommendations for future research

This thesis presents the development of sustainable protective Ultra-High Performance Fibre Reinforced Concrete (UHPFRC), including mix design, properties assessment and modeling studies. Although the obtained experimental and modeling results answer a number of questions, further research is still needed on many issues and remaining open-questions, which are formulated as follows:

- 1) In this thesis, it is demonstrated that the modified A&A model is an effective method to develop sustainable UHPFRC with both low cost and low environmental impact. However, considering the fact that the utilized maximum particle size is relatively small (about 2 mm) and the workability of the developed UHPFRC is very good (about 90 cm of slump flow, based on EN-12350-8 (2010)), the influence of steel fibres on the particle packing skeleton is ignored. To further improve the application of the modified A&A model in UHPFRC or other fibre reinforced concrete, it would be beneficial to include the fibre effect in the particle packing model.
- 2) To develop a sustainable UHPFRC, not only the powders, aggregates and fibres are important, but also the utilized superplasticizer (SP) deserves attention and detailed investigations, since the price of SP is relatively higher compared to the other used ingredients. Hence, clarifying the effect of SP (e.g. dosage, type and so on) on the properties of UHPFRC and producing a UHPFRC with efficient SP application still need further attention.

- 3) The developed “Modified Pendulum Impact Device” (as shown in Chapter 7) still needs to be further improved, since the energy absorbed by the sample during the last impact (breaking the sample) is difficult to be quantified. Moreover, the damping or vibration of the frames, used to hang the hammer and samples during the impacts, should be further minimized.
- 4) In Chapter 9, due to the relatively large dimensions and impact energy of FSP (20 mm), the results obtained from the second and third shots are affected by the first shot. Hence, the advice of three times shooting on each sample shown in STANAG 2280 (2009) is not suitable here to evaluate the dynamic performance of concrete under high velocity FSP (20 mm) impact loadings. Hence, in the next step, the tests of the sustainable UHPFRC under high velocity FSP (20 mm) impact should be only performed one time for each concrete slab. Moreover, when the bullet impact velocity is about 930 m/s, a deviation between modeling and experimental results can be observed, which cause the proposed model in LS-DYNA to not be well validated. Hence, to more accurately validate the proposed model, more experimental tests should be performed.
- 5) Excepting the pendulum and projectile impacts, there are also many other impact categories, such as shock, earth quake and high energy blast loads. Therefore, clarifying the dynamic performance of the developed sustainable UHPFRC under different impact categories is beneficial for understanding the basic characteristics of UHPFRC and pointing out the most suitable application field of UHPFRC.
- 6) In this research, most of the experiments were executed on the laboratory scale. Nevertheless, to fully assess the developed sustainable UHPFRC, some tests of UHPFRC on relatively large scale should be executed, which can further widen the application of the developed sustainable UHPFRC in practice.
- 7) Due to the fact that numerical modeling is an efficient method to investigate the impact resistance of UHPFRC under impact loadings, more fundamental research employing numerical modeling tools is needed to deeply understand the intrinsic mechanism of the sustainable UHPFRC under impact loadings.



## Bibliography

- ABAQUS Analysis User's Manual, (2004). ABAQUS Inc., version 6.4.
- ACI Committee 544, (1993). Guide for specifying, proportioning, mixing, placing, and finishing steel fibre reinforced concrete, *ACI Mater J* 90 (1): 94-101.
- Acker P. and Behloil M., (2004). Ductal technology: a large spectrum of properties a wide range of applications. In proceedings of the 1st international Symposium on UHPC. Heft 3, Kassel University press.
- Afrough S.V., (2008). Experimental study of FRC properties. M.S. thesis: Bu-AliSina University, Hamedan, Iran.
- Agardh L. and Laine L., (1999). 3D FE-simulation of high-velocity fragment perforation of reinforced concrete slabs. *Int J Impact Eng* 22: 911-922.
- Alarcon-Ruiz L., Platret G., Massieu E., Ehrlacher A., (2005). The use of thermal analysis in assessing the effect of temperature on a cement paste. *Cem Concr Res* 35(3): 609-613.
- Aldahdooh M.A.A., Muhamad Bunnori N., Megat Johari M.A., (2013). Development of green ultra-high performance fibre reinforced concrete containing ultrafine palm oil fuel ash. *Constr Build Mater* 48: 379-389.
- Almansa E.M. and Cánovas M.F., (1999). Behaviour of normal and steel fibre-reinforced concrete under impact of small projectiles. *Cem Concr Res* 29: 1807-1814.
- Alonso C. and Fernandez L., (2004). Dehydration and rehydration processes of cement paste exposed to high temperature environments. *J Mater Sci* 39(9): 3015-3024.
- Al-Oraimi S.K. and Seibi A.C., (1995). Mechanical characterization and impact behaviour of concrete reinforced with natural fibres. *Comp Struct* 32: 165-171.
- Alwan J.M., Naaman A.E., Hansen W., (1991). Pull-out work of steel fibres from cementitious composites: Analytical investigation. *Cem Concr Compos* 13 (4): 247-255.
- Amde A.M., Mirmiran A., Walter T.A., (1997). Local damage assessment of turbine missile impact on composite and multiple barriers. *Nucl Eng Des* 178 (1/2): 145-156.
- Amstrong A., (2013). An overview of global cement sector trends. Insights from the Global Cement Report 10th Edition. International Cement Review, XXX Technical Congress FICEM-APCAC, 2 September, 2013 Lima, Peru.
- Andreasen A.H.M. and Andersen J., (1930). Über die Beziehungen zwischen Kornabstufungen und Zwischenraum in Produkten aus losen Körnern (mit einigen Experimenten). *Kolloid-Zeitschrift* 50: 217-228 (In German).
- Anderson W.F., Watson A.J., Kaminskyj A.E., (1992). The resistance of SIFCON to high velocity impact. In: Proceeding of the second international conference on structures under shock and impact, Portsmouth (U.K.): 89-98.

- Artelt C. and Garcia E., (2008). Impact of superplasticizer concentration and of ultra-fine particles on the rheological behaviour of dense mortar suspensions. *Cem Concr Res* 38: 633-642.
- ASTM C1202, (2005). Standard Test Method for Electrical Indication of Concrete's Ability to Resist Chloride Ion Penetration. In *Annual Book of ASTM Standards*, vol. 04.02. American Society for Testing and Materials, Philadelphia, July.
- ASTM C 1018-97, (1998). Standard test methods for flexural toughness and first crack strength of fibre reinforced concrete. American Society for Testing and Materials .
- ASTM E23, (1992) Standard Test Methods for Notched Bar Impact Testing of Metallic Materials. American Society for Testing and Materials.
- AUTODYN user manual, (2001). Century Dynamics, Inc., version 4.2.
- Bache H.H., (1991). Densified cement/ultra-fine particle based materials. In: *Second International Conference on Superplasticizers in Concrete*, Ottawa, Canada, 10–12 June.
- Bangash M.Y.H., (1993). *Impact and explosion: structural analysis and design*. Boca Raton, FL: CRC Press.
- Banthia N., Yan C., Sakai K., (1998). Impact Resistance of Fibre Reinforced Concrete at Subnormal Temperatures. *Cem Concr Comp* 20: 393-404.
- Banthia N. and Nandakumar N., (2003). Crack growth resistance of hybrid fibre reinforced cement composites. *Cem Concr Compos* 25(1): 3-9.
- Banthia N. and Gupta R., (2004). Hybrid fibre reinforced concrete (HyFRC): fibre synergy in high strength matrices. *Mater Struct* 37(10): 707-716.
- Banthia N., Majdzadeh F., Wu J., Bindiganavile V., (2014). Fibre synergy in Hybrid Fibre Reinforced Concrete (HyFRC) in flexure and direct shear. *Cem Concr Comp* 48: 91-97.
- Benson D.J., (2009). *The History of LS-DYNA*. University Of California, San Diego.
- Bentz D., Feng X., Haecker C., Stutzman P., (2000). Analysis of CCRL proficiency cements 135 and 136 using CEMHYD3D, NIST Internal Report 6545.
- Bentz D.P., (2006). Modeling the influence of LP filler on cement hydration using CEMHYD3D. *Cem Concr Comp* 28(2): 124-129.
- Beppu M., Miwa K., Itoh M., Katayama M., Ohno T., (2008). Damage evaluation of concrete plates by high-velocity impact. *Int J Impact Eng* 35: 1419-1426.
- Berra M., Carassiti F., Mangialardi T., Paolini A.E., Sebastiani M., (2012). Effects of nanosilica addition on workability and compressive strength of Portland cement pastes. *Constr Build Mater* 35: 666-675.
- Berriaud C., Sokolovsky A., Gueraud R., Dulac J., Labrot R., (1978). Local behaviour of reinforced concrete walls under missile impact. *Nucl Eng Des* 45: 457-469.
- Berry E.E., Hemmings R.T., Cornelius B.J., (1990). Mechanisms of hydration reactions in high volume FA pastes and mortars. *Cem Concr Comp* 12(4): 253-261.

- Bessey G.E., (1938). Proceedings of the symposium on the chemistry of cements, Stockholm, Ingeniarsveterskapsakademien, Stockholm, 233- 234.
- Bhat G. and Kandagor V., (2014). Synthetic polymer fibres and their processing requirements. *Advances in Filament Yarn Spinning of Textiles and Polymers*, Woodhead Publishing.
- Bindiganavile V., Banthia N., Aarup B., (2002). Impact response of ultra-high-strength fibre-reinforced cement composite. *ACI Mater J* 99: 543-548.
- Birkimer D.L. and Lindemann R., (1971). Dynamic Tensile Strength of Concrete Materials, *ACI J, Proceedings V. 68(1)*: 47-49.
- Birkimer, D.L., (1968). Critical Normal Fracture Strain of Portland Cement Concrete, PhD thesis, University of Cincinnati, Cincinnati.
- Bischoff P.H. and Perry S.H., (1991). Compressive behaviour of concrete at high strain rates. *Mater Struct* 24: 425-450.
- Björnström J., Martinelli A., Matic A., Börjesson L., Panas I., (2004). Accelerating effects of colloidal nanosilica for beneficial calcium-silicate-hydrate formation in cement. *Chem Phys Lett* 392 (1-3): 242-248.
- Bludau C., Keuser M., Kustermann A., (2006). Perforation resistance of high-strength concrete panels. *ACI Struct J* 103(2): 188-195.
- Bornemann R. and Schmidt M., (2002). The role of powders in concrete. In: proceedings 6th international symposium on utilization of high strength/high performance concrete, Leipzig 2: 863-872.
- Booker P.M., Cargile J.D., Kistler B.L., Saponara V.L., (2009). Investigation on the response of segmented concrete targets to projectile impacts. *Int J Impact Eng* 36: 926-939.
- Boulekbatche B., Hamrat M., Chemrouk M., Amziane S., (2010). Flowability of fibre-reinforced concrete and its effect on the mechanical properties of the material. *Constr Build Mater* 24:1664-1671.
- Brouwers H.J.H., (2006). Particle-size distribution and packing fraction of geometric random packings. *Phys. Rev. E* 74: 031309-1-031309-14.
- Brouwers H.J.H. and Radix H.J., (2005). Self-compacting concrete: theoretical and experimental study. *Cem Concr Res* (35): 2116-2136.
- Brühwiler E. and Denarié E., (2008). Rehabilitation of concrete structures using ultra-high performance fibre reinforced concrete. In: Proceedings, UHPC-2008: the second international symposium on ultra-high performance concrete, March 05–07, Kassel, Germany.
- Burlion N., (1997). Compaction des betons: elements de modelisation et caracterisation experimentale. PhD dissertation, LMT, ENS de Cachan, France.
- Camps G., Turatsinze A., Sellier A., Escadeillas G., Bourbon X., (2008). Steel-fibre-reinforcement and hydration coupled effects on concrete tensile behaviour. *Eng Fract Mech* 75: 5207-5216.

- Capros P., Kouvaritakis N., Mantzos L., (2001). Economic evaluation of sectorial emission reduction objectives for climate change top-down analysis of greenhouse gas emission possibilities in the EU. Contribution to a study for DG environment. European commission.
- Carlson E.T. and Berman H.A., (1960). Some observations on the calcium aluminate carbonate hydrates. *J Res Nat Bur Stand*, 64A (4): 333-341.
- Castellote M., Alonso C., Andrade C., Turrillas X., Campo J., (2004). Composition and microstructural changes of cement pastes upon heating, as studied by neutron diffraction. *Cem Concr Res* 34(9): 1633-1644.
- CEB, (2010). Concrete structures under impact and impulsive loading. In: *CEB Bulletin d'information*, vol. 187. Lausanne, France: Committee Euro-International du Beton.
- CEC, (1999). Council Directive 1999/31/ EC of 26 April 1999 on the landfill of waste, *Off. J. Eur. Communities*, 16/7/1999, L182/1-19.
- Chawla K.K., (1997). *Composite materials science and engineering*. Springer-Verlag, New York, Page: 234-236.
- Chen W. and Brouwers H.J.H., (2007a). The hydration of slag, part 1: reaction models for alkali-activated slag. *J Mater Sci* 42: 428-443.
- Chen W. and Brouwers H.J.H., (2007b). The hydration of slag, part 2: reaction models for blended cement. *J Mater Sci* 42: 444-464.
- Chimenos J.M., Segarra M., Fernández M.A., Espiell F., (1999). Characterization of the bottom ash in a municipal solid waste incinerator. *J. Hazard. Mater.* A64: 211-222.
- Clifton J.R., (1982). Penetration resistance of concrete: a review. Special Publication. Washington, DC: National Bureau of Standards: 480-485.
- Constantinides G. and Ulm F.J., (2007). The nanogranular nature of C-S-H. *J Mech Phys Solids* 55: 64-90.
- Corbett G.G., Reid S.R., Johnson W., (1996). Impact loading of plates and shells by free-flying projectiles: a review. *Int J Impact Eng* 18:141-230.
- Corinaldesi V. and Moriconi G., (2012). Mechanical and thermal evaluation of Ultra-High Performance Fibre Reinforced Concretes for engineering applications. *Constr Build Mater* 26: 289-294.
- Cotsovos D.M. and Pavlovic M.N., (2008). Numerical investigation of concrete subjected to compressive impact loading. Part 1: A fundamental explanation for the apparent strength gain at high loading rates. *Comput Struct*, 86: 145-163.
- Dancygier A.N. and Yankelevsky D.Z., (1996). High strength concrete response to hard projectile impact. *Int J Impact Eng* 18(6): 583-99.
- Dancygier A.N. and Yankelevsky D.Z., (1999). Effects of reinforced concrete properties on resistance to hard projectile impact. *ACI Struct J* 96(2): 259-269.
- Dancygier A.N., Yankelevsky D.Z., Jaegermann C., (2007). Response of high performance concrete plates to impact of non-deforming projectiles. *Int J Impact Eng* 34: 1768-1779.

- Dawood E.T. and Ramli M., (2012). Mechanical properties of high strength flowing concrete with hybrid fibres. *Constr Build Mater* 28: 193-200.
- Deeb R., Ghanbari A., Karihaloo B.L., (2012). Development of self-compacting high and ultra high performance concretes with and without steel fibres. *Cem Concr Compos* 34: 185-190.
- Denarié E. and Brühwiler E., (2011). Strain Hardening Ultra-high Performance Fibre Reinforced Concrete: Deformability versus Strength Optimization. *International Journal for Restauration of Buildings and Monuments* 2011 *Aedificatio*, 17 (6): 397-410.
- De Larrard F. and Sedran T., (1994). Optimization of ultra-high-performance concrete by the use of a packing model. *Cem Concr Res* 24: 997-1009.
- De Larrard F., Sedran T., (2002). Mixture-proportioning of high-performance concrete, *Cem Concr Res* 32: 1699-1704.
- Edgington J., Hannant D.J., Williams R.I.T., (1978). Steel fibre reinforced concrete, fibre reinforced materials, the construction press, Lancaster, England, 112-128.
- El-Dieb A.S., (2009). Mechanical, durability and microstructural characteristics of ultra-high-strength self-compacting concrete incorporating steel fibres. *Mater Des* 30: 4286-4292.
- EN-196-1, (2005). Methods of testing cement - Part 1: Determination of strength. British Standards Institution-BSI and CEN European Committee for Standardization.
- EN-933-1 (1997). Tests for geometrical properties of aggregates. Determination of particle size distribution. Sieving method.
- EN-1015-3, (2007). Methods of test for mortar for masonry - Part 3: Determination of consistence of fresh mortar (by flow table). British Standards Institution-BSI and CEN European Committee for Standardization.
- EN-1097-7 (1999). Test for mechanical and physical properties of aggregates - part 6: Determination of particle density of filler-Pycnometer method.
- EN-12350-8, (2010). Testing fresh concrete - Part 8: Self-compacting concrete -Slump-flow test. British Standards Institution-BSI and CEN European Committee for Standardization.
- EN-12390-3, (2009). Testing hardened concrete - Part 3: Compressive strength of test specimens. British Standards Institution-BSI and CEN European Committee for Standardization.
- EN-12390-5, (2009). Testing hardened concrete - Part 5: Flexural strength of test specimens. British Standards Institution-BSI and CEN European Committee for Standardization.
- Erdem S., Dawson A.R., Thom N.H., (2012a). Influence of the micro - and nanoscale local mechanical properties of the interfacial transition zone on impact behaviour of concrete made with different aggregates. *Cem Concr Res* 42: 447-458.

- Erdem S., Dawson A.R., Thom N.H., (2012b). Impact load-induced micro-structural damage and micro-structure associated mechanical response of concrete made with different surface roughness and porosity aggregates. *Cem Concr Res* 42: 291-305.
- Erzar B. and Forquin P., (2011). Experiments and mesoscopic modeling of dynamic testing of concrete. *Mech Mater* 43: 505-527.
- Farnam Y., Mohammadi S., Shekarchi M., (2010). Experimental and numerical investigations of low velocity impact behaviour of high-performance fibre-reinforced cement based composite. *Int J Impact Eng* 37: 220-229.
- Favre J.P., Désarmot G., Sudre O., Vassel A., (1997). Were McGarry or Shiriajeva right to measure glass–fibre adhesion? *Compos Interfaces* 4: 313-326.
- Fehling E., Bunje K., Schmidt M., Schreiber W. (2008) The “Gärtnerplatzbrücke”: Design of First Hybrid UHPC-Steel Bridge across the River Fulda in Kassel, Germany. 2<sup>nd</sup> International Symposium on Ultra High Performance Concrete, March 05-07, Kassel, Germany, 581-588.
- Feldman R.F., Carette G.G., Malhotra V.M., (1990). Studies on mechanics of development of physical and mechanical properties of high-volume FA-cement pastes. *Cem Concr Comp* 12(4): 245-251.
- Fennis S.A.A.M., Walraven J.C., den Uijl J.A., (2009). The use of particle packing models to design ecological concrete, *Heron* 54: 185-204.
- Féret R., (1892). Sur la compacité des mortiers hydrauliques, *Ann. Ponts Chauss* IV: 5 – 164 (in French).
- Forrestal M.J. and Hanchak S.J., (2002). Penetration limit velocity for ogive-nose projectiles and limestone targets. *J Appl Mech ASME* 69: 853-854.
- Forteza R., Far M., Seguí C., Cerdá V., (2004). Characterization of bottom ash in municipal solid waste incinerators for its use in road base. *Waste Manag* 24: 899-909.
- Friedlingstein P., Houghton R.A., Marland G., Hackler J., Boden T.A., Conway T.J., Canadell J.G., Raupach M.R., Ciais P., Le Quere C., (2010). Uptake on CO<sub>2</sub> emissions. *Nat Geosci* 3: 811-812.
- Fröhlich S. and Schmidt M., (2012). Influences on Repeatability and Reproducibility of Testing Methods for Fresh UHPC. The 3<sup>rd</sup> International Symposium on UHPC and Nanotechnology for High Performance Construction Materials and Concrete Construction Series, 19: 225-232.
- Fuller W.B. and Thompson S.E., (1907). The laws of proportioning concrete. *T Am Soc Civ Eng* 33: 222-298.
- Funk J.E. and Dinger D.R., (1994). Predictive Process Control of Crowded Particulate Suspensions, Applied to Ceramic Manufacturing. Kluwer Academic Publishers, Boston, the United States.
- Ganesan N., Indira P.V., Sabeena M.V., (2014). Bond stress slip response of bars embedded in hybrid fibre reinforced high performance concrete. *Constr Build Mater* 50: 108-115.

- Georgin J.F. and Reynouard J.M., (2003). Modeling of structures subjected to impact: concrete behaviour under high strain rate. *Cem Concr Comp* (25): 131-143.
- Ghafari E., Costa H., Júlio, E., Portugal A., Durães L., (2014). The effect of nanosilica addition on flowability, strength and transport properties of ultra high performance concrete. *Mater Design* 59: 1-9.
- Giampaolo C., Mastro S.L., Poletini A., Pomi R., Sirini P., (2002). Acid neutralisation capacity and hydration behaviour of incineration bottom ash-Portland cement mixtures. *Cem Concr Res* 32(5): 769-775.
- Govindjee S., Kay G.J., Simo J.C., (1994). Anisotropic and numerical simulation of brittle damage in concrete. Report Number UCB/SEM M-94/18. Berkeley, CA: University of California at Berkeley, Department of Civil Engineering.
- Govindjee S., Kay G.J., Simo J.C., (1995). Anisotropic and numerical simulation of brittle damage in concrete. *Int J Numer Meth Eng* 38: 3611-3633.
- Grattan-Bellew P.E., (1996). Microstructural investigation of deteriorated Portland cement concretes. *Constr Build Mater* 10(1): 3-16.
- Green B.H. (2006). Development of a high-density cementitious rock-matching grout using nano-particles. Proceedings of ACI Session on Nanotechnology of Concrete: Recent Developments and Future Perspectives, 7 November, Denver, USA, 119-130.
- Grote D.L., Park S.W., Zhou M., (2001). Dynamic behaviour of concrete at high strain rates and pressures: 1. Experimental characterization. *Int J Impact Eng* 25(9): 869-886.
- Grünewald S., (2004). Performance-based design of self-compacting fibre reinforced concrete. Delft University of Technology, Delft, the Netherlands.
- Habel K. and Gauvreau P., (2008). Response of ultra-high performance fibre reinforced concrete (UHPFRC) to impact and static loading. *Cem Concr Comp* 30(10): 938-946.
- Habel K., Viviani M., Denarié E., Brühwiler E., (2006). Development of the mechanical properties of an Ultra-High Performance Fibre Reinforced Concrete (UHPFRC), *Cem Concr Res* 36: 1362-1370.
- Habert G., Denarié E., Šajna A., Rossi P., (2013). Lowering the global warming impact of bridge rehabilitations by using Ultra High Performance Fibre Reinforced Concretes. *Cem Concr Comp* 38: 1-11.
- Hanchak S.J., Forrestal M.J., Young E.R., Ehrgott J.Q., (1992). Perforation of concrete slabs with 48 MPa (7 ksi) and 140 MPa (20 ksi) unconfined compressive strengths. *Int J Impact Eng* 12(1): 1-7.
- Handoo S.K., Agarwal S., Agarwal S.K., (2002). Physicochemical, mineralogical, and morphological characteristics of concrete exposed to elevated temperatures. *Cem Concr Res* 32(7): 1009-1018.
- Hanehara S., Tomosawa F., Kobayakawaa M., Hwang K., (2001). Effects of water/powder ratio, mixing ratio of FA, and curing temperature on pozzolanic reaction of FA in cement paste. *Cem Concr Res* 31: 31-39.

- Hassan A.M.T., Jones S.W., Mahmud G.H., (2012). Experimental test methods to determine the uniaxial tensile and compressive behaviour of ultra-high performance fibre reinforced concrete (UHPFRC). *Constr Build Mater* 37: 874-882.
- He J., Barry E.S., Della M. R., (1984). Hydration of FA-portland cements. *Cem Concr Res* 14(4): 505-512.
- Hewlett P.C., (1988). *Lea's Chemistry of Cement and Concrete*, 3th edition John Wiley & Son Inc., New York, 1-1053.
- Holmquist T.J., Johnson G.R., Cook W.H., (1993). A Computational Constitutive Model For Concrete Subjected To Large Strains, High Strain Rates, and High Pressures. *International Symposium on Ballistics*, 14: 591-600.
- Hou P., Kawashima S., Wang K., Corr D.J., Qian J., Shah S.P., (2013). Effects of colloidal nanosilica on rheological and mechanical properties of fly ash-cement mortar. *Cem Concr Comp* 35 (1): 12-22.
- Houst, Y.F., Bowen, P., Perche, F., Kauppi, A., Borget, P., Galmiche, L., Le Meins, J.F., Lafuma, F., Flatt, R.J., Schober, I., Banfill, P.F.G., Swift, D.S., Myrvold, B.O., Petersen, B.G., Reknès, K. (2008). Design and function of novel superplasticizers for more durable high performance concrete (superplast project). *Cem Concr Res* 38: 1197-1209.
- Huang F.L., Wu H.J., Jin Q.K., Zhang Q.M., (2005). A numerical simulation on the perforation of reinforced concrete slabs. *Int J Impact Eng* 32(1-4): 173-187.
- Hunger M. and Brouwers H.J.H., (2009). Flow analysis of waterpowder mixtures: Application to specific surface area and shape factor. *Cem Concr Comp* 31(1): 39-59.
- Hunger M., (2010). An integral design concept for ecological self-compacting concrete. PhD thesis. Eindhoven University of Technology, Eindhoven, the Netherlands.
- Hüsken G., (2010). A multifunctional design approach for sustainable concrete with application to concrete mass products. PhD thesis. Eindhoven University of Technology, Eindhoven, the Netherlands.
- Hüsken G. and Brouwers H.J.H., (2008). A new mix design concept for each-moist concrete: A theoretical and experimental study. *Cem Concr Res* 38: 1249-1259.
- Hwang C.L. and Shen D.H., (1991). The effects of blast-furnace GGBS and FA on the hydration of portland cement. *Cem Concr Res* 21(4): 410-425.
- Interim Recommendations of Ultra High Performance Fibre Reinforced Concrete (UHPFRC). French association of civil engineering. January, 2002.
- ISO 13320-1. Particle size analysis-Laser diffraction methods - Part 1: General principles. International Organization for Standardization, CH-1211 Geneve 20, Switzerland, 1-42.
- Izquierdo M., Vazquez E., Querol X., Barra M., López A., Plana F., (2001). Use of bottom ash from municipal solid waste incineration as a road material, in: *International Ash Utilization Symposium*, 4th, Lexington, KY, United States, 31-38.

- Jacques R. and Cete L., (2004). First recommendation for ultra-high-performance concrete and example of application, in: M. Schmidt, E. Fehling, C. Geisenhansluke (Eds.), *Ultra High Performance Concrete*, Kassel University Press, Kassel, 79-90.
- Jalal M., Mansouri E., Sharifipour M., Pouladkhan A.R., (2012). Mechanical, rheological, durability and microstructural properties of high performance self-compacting concrete containing SiO<sub>2</sub> micro and nanoparticles. *Mater Des* 34:389-400.
- Jansen D., Neubauer J., Goetz-Neunhoeffler F., Haerzschel R., Hergeth W.D., (2012). Change in reaction kinetics of a Portland cement caused by a superplasticizer – calculation of heat flow curves from XRD data. *Cem Concr Res* 42(2): 327-332.
- Johnson G.R., (2011). Numerical algorithms and material models for high-velocity impact computations. *Int J Impact Eng* 38: 456-472.
- Johnston C.D. (1996). Proportioning, mixing and placement of fibre-reinforced cements and concretes, *Production Methods and Workability of Concrete*, Edited by Bartos, Marrs and Cleland, E&FN Spon, London, 155-179.
- Johnston C.D., (2001). *Fibre-Reinforced Cements and Concretes*, Gordon and Breach Science Publishers, Amsterdam, ISBN: 9056996940.
- JSCE Standard SF-4, (1984). Method of test for flexural strength and flexural toughness of fibre reinforced concrete. Japan Society of Civil Engineers (JSCE).
- Kanavas N., (2014). The Effect of Hybrid-Steel Fibres on the Properties of Ultra High Performance Fibre Reinforced Concrete (UHPFRC) – Towards to the Efficient Utilization of Fibres. Report of master project II, Eindhoven University of Technology, Eindhoven, the Netherlands.
- Kanda T. and Li V.C., (1998). Interface property and apparent strength of high-strength hydrophilic fibre in cement matrix, *J Mater Civil Eng* 10:5-13.
- Kanda T. and Li V.C., (2006). Practical design criteria for saturated pseudo strain hardening behaviour in ECC. *J Adv Concr Technol* 2006, 4(1): 59-72.
- Kang S., Lee Y., Kim J., Kim Y., (2011). The effect of fibre distribution characteristics on the flexural strength of steel fibre-reinforced ultra-high strength concrete. *Constr Build Mater* 25(5): 2450-2457.
- Katrin H. and Paul G., (2008). Response of ultra-high performance fibre reinforced concrete (UHPFRC) to impact and static loading. *Cem Concr Comp* 30: 938-946.
- Kennedy R.P., (1976). A review of procedures for the analysis and design of concrete structures to resist missile impact effects. *Nucl Eng and Des* 37:183-203.
- Kevin D.I. and Kenneth E.D., (1991). A review of LP additions to Portland cement and concrete. *Cem Concr Comp* 13(3): 165-170.
- Kim D.J., Park S.H., Ryu G.S., Koh K.T., (2011a). Comparative flexural behaviour of Hybrid Ultra-High Performance Fibre Reinforced Concrete with different macro fibres. *Constr Build Mater* 25: 4144-4155.
- Kim H.K., Lee H.K., (2011b). Use of power plant bottom ash as fine and coarse aggregates in high-strength concrete. *Constr Build Mater* 25: 1115-1122.

- Kim H.K., Jeon J.H., Lee H.K., (2012). Flow, water absorption, and mechanical characteristics of normal and high-strength mortar incorporating fine bottom ash aggregates. *Constr Build Mater* 26: 249-256.
- Kim S.M., Abu Al-Rub R.K., (2011c). Meso-scale computational of the plastic-damage response of cementitious composites. *Cem Concr Res* 41: 339-358.
- King D., (2012). The effect of silica fume on the properties of concrete as defined in concrete society report 74, cementitious materials, 37th Conference on Our World in Concrete and Structures, Singapore, 29-31.
- Koiter W.T., (1953). Stress-strain relations, uniqueness and variational theorems for elastic-plastic materials with a singular yield surface. *Q Appl Math* 11: 350-354.
- Kojima I., (1991). An experimental study on local behaviour of reinforced concrete slabs to missile impact. *Nucl Eng Des* 130 (2): 121-132.
- Kong D., Du X., Sun W., Zhang H., Yang Y., Shah S.P., (2012). Influence of nanosilica agglomeration on microstructure and properties of the hardened cement-based materials. *Constr Build Mater* 37: 707-715.
- Kooiman A.G., (2000). Modelling steel fibre reinforced concrete for structural design. PhD thesis, Delft University of Technology, Delft, the Netherlands.
- Kovács R., (1975). Effect of the hydration products on the properties of fly-ash cements. *Cem Concr Res* 5(1): 73-82.
- Krieg R.D., (1972). A simple constitutive description for cellular concrete. Report SCDR 72-0883. Albuquerque, NM: Sandia National Laboratories.
- Kumar A., Oey T., Kim S., Thomas D., Badran S., Li J., Fernandes F., Neithalath N., Sant G., (2013). Simple methods to estimate the influence of LP fillers on reaction and property evolution in cementitious materials. *Cem Concr Comp* 42: 20-29.
- Land G. and Stephan D., (2012). The influence of nanosilica on the hydration of ordinary Portland cement. *J Mater Sci* 47: 1011-1017.
- Lai J. and Sun W., (2009). Dynamic behaviour and visco-elastic damage model of ultra-high performance cementitious composite. *Cem Concr Res* 39: 1044-1051.
- Lappa E.S., (2007). High strength fibre reinforced concrete, static and fatigue behaviour in bending. PhD thesis, Delft University of Technology, Delft, the Netherlands.
- Lau A. and Anson M., (2006). Effect of high temperatures on high performance steel fibre reinforced concrete. *Cem Concr Res* 36: 1698-1707.
- Lazaro A., Brouwers H.J.H., Quercia Bianchi, Geus G. J.W., (2012). The properties of amorphous nanosilica synthesized by the dissolution of olivine. *Chem Eng J* 211-212: 112-121.
- Lazaro A., (2014). Nanosilica production at low temperatures from the dissolution of olivine. PhD thesis. Eindhoven University of Technology, Eindhoven, the Netherlands.
- Lea F.M., (1971). The chemistry of cement and concrete. Chemical publishing company, New York, 202-233.

- Lee H.K., Kim H.K., Hwang E.A., (2010). Utilization of power plant bottom ash as aggregates in fibre-reinforced cellular concrete. *Waste Manage* 30: 274-284.
- Leung C.K.Y., and Geng Y., (1995). Effect of lateral stresses on fibre debonding/pull-out. *Compos Eng* 5(10): 1331-1348.
- Li C., Sun H., Li L., (2010). A review: the comparison between alkali-activated GGBS (Si + Ca) and metakaolin (Si + Al) cements. *Cem Concr Res* 40: 1341-1349.
- Li H., Zhang M., Ou J., (2007). Flexural fatigue performance of concrete containing nanoparticles for pavement. *Int J Fatigue* 29: 1292-301.
- Li H., Xiao H., Yuan J., Ou J., (2004). Microstructure of cement mortar with nanoparticles. *Compos Eng* 35 (2): 185-189.
- Li J., Zhang Y.X., (2012). Evaluation of constitutive models of hybrid-fibre engineered cementitious composites under dynamic loadings. *Constr Build Mater* 30: 149-160.
- Li Q.M., Reid S.R., Wen H.M., Telford A.R., (2005). Local impact effects of hard missiles on concrete targets. *Int J Impact Eng* 32: 224-284.
- Li W. and Xu J., (2009). Mechanical properties of basalt fibre reinforced geopolymeric concrete under impact loading. *Mat Sci Eng A* 505: 178-186.
- Li X.G., Lv Y., Ma B.G., Chen Q.B., Yin X.B., Jian S.W., (2012). Utilization of municipal solid waste incineration bottom ash in blended cement. *J Clean Prod* 32: 96-100.
- Lin D.F., Lin K.L., Chang W.C., Luo H.L., Cai M.Q. (2008). Improvements of nano-SiO<sub>2</sub> on sludge/fly ash mortar. *Waste Manage* 28: 1081-1087.
- Lothenbach B., Scrivener K., Hooton R.D., (2011). Supplementary cementitious materials. *Cem Concr Res* 41: 1244-1256.
- LS-DYNA keyword user's manual, version 970, 2003. Livermore Software Technology Corporation, April.
- LSTC, (2009). "LS-DYNA Keyword User's Manual, Volume 1". Livermore Software Technology Corporation (LSTC).
- Ltifi M., Guefrech A., Mounanga P., Khelidj A., (2011). Experimental study of the effect of addition of nanosilica on the behaviour of cement mortars. *Proce Eng* (10): 900-905.
- Lu X. and Hsu C.T.T., (2006). Behaviour of high strength concrete with and without steel fibre reinforcement in triaxial compression. *Cem Concr Res* 36: 1679-1685.
- Lu Y.B. and Li Q.M., (2011). About the dynamic uniaxial tensile strength of concrete-like materials, *Int J Impact Eng* 38: 171-180.
- Luccioni B.M., Ambrosinia R.D., Danesia R.F., (2004). Analysis of building collapse under blast loads. *Eng Struct* 26(1): 63-71.
- Luo X., Sun W., Chan S.Y.N., (2000). Characteristics of high-performance steel fibre-reinforced concrete subject to high velocity impact. *Cem Concr Res* 30(6): 907-914.
- Máca P., Sovják R., Konvalinka P., (2014). Mix design of UHPFRC and its response to projectile impact. *Int J Impact Eng* 63: 158-163.

- Madani B., Zoubir M., Tayeb B., (2011). Effect of Limestone Fillers the Physic-Mechanical Properties of Limestone Concrete. *Phys Proc* 21: 28-34.
- Madani H., Bagheri A., Parhizkar T., (2012). The pozzolanic reactivity of monodispersed nanosilica hydrosols and their influence on the hydration characteristics of Portland cement. *Cem Concr Res* 42 (12): 1563-1570.
- Mahmud G.H., Yang Z., Hassan A.M.T., (2013). Experimental and numerical studies of size effects of Ultra-High Performance Steel Fibre Reinforced Concrete (UHPRFC) beams. *Constr Build Mater* 48: 1027-1034.
- Makita T., Brühwiler E., (2014). Tensile fatigue behaviour of Ultra-High Performance Fibre Reinforced Concrete combined with steel rebars (R-UHPRFC). *Int J Fatigue* 59: 145-152.
- Malvar L.J. and Ross C.A., (1998). Review of Strain Rate Effects for Concrete in Tension, *ACI Mater J* 95(6): 735-739.
- Markovic I., (2006). High-performance hybrid-fibre concrete – development and utilisation. PhD thesis, Delft University of Technology, Delft, the Netherlands.
- Mcvay M.K., (1988). Spall Damage of Concrete Structures, Technical Report SL-88-22, U.S. Army Corps of Engineers, Waterways Experiment Station, Vicksburg, MS.
- Mehmet G., Erhan G., Mustafa E. K., Veysel B., Kasim M., (2012). Fresh and hardened characteristics of self compacting concretes made with combined use of marble powder, limestone filler, and fly ash. *Constr Build Mater* 37: 160-170.
- Mellinger F.M. and Birkimer D.L., (1966). Measurement of Stress and Strain on Cylindrical Test Specimens of Rock and Concrete under Impact Loading, Technical Report 4-46, U.S. Army Corps of Engineers, Ohio River Division Laboratories, Cincinnati, OH, Apr., 71.
- Millard S.G., Molyneaux T.C.K., Barnett S.J., Gao X., (2010). Dynamic enhancement of blast-resistant ultra high performance fibre-reinforced concrete under flexural and shear loading. *Int J Impact Eng* 37(4): 405-413.
- Mindess S., (1988). Properties of concrete reinforced with fibrillated polypropylene fibres under impact loading. *Cem Concr Res* 18: 109-115.
- Mindess S. and Yan C., (1993). Perforation of plain and fibre reinforced concretes subjected to low-velocity impact loading. *Cem Concr Res* 23: 83-92.
- Mindess S., Wang N., Rich D.L., Morgan D.R., (1998). Impact Resistance of polyolefin fibre reinforced precast units. *Cem Concr Res* 20: 387-392.
- Ministerial Order PG-3, (2004). Pliego de prescripciones técnicas generales para obras de carreteras y puentes, Ministry of Development, Order FOM/891/2004.
- Mohamed A.K. and Ahmed F., (2014). Effect of reinforcement on the response of concrete panels to impact of hard projectiles. *Int J Impact Eng* 63: 1-17.
- Mohammadi Y., Carkon-Azad R., Singh S.P., Kaushik S.K., (2009). Impact resistance of steel fibrous concrete containing fibres of mixed aspect ratio. *Constr Build Mater* 23: 183-189.

- Monteiro P.J.M., Kirchheim A.P., Chae S., Fischer P., MacDowell A.A., Schaible E., Wenk H.R., (2009). Characterizing the nano and micro structure of concrete to improve its durability. *Cem Concr Comp* 31(8): 577-584.
- Müller U. and Rübner K., (2006). The microstructure of concrete made with municipal waste incinerator bottom ash as an aggregate component. *Cem Concr Res* 36: 1434-1443.
- Naaman A.E. and Gopalaratnam V.S., (1983). Impact properties of steel fibre reinforced concrete in bending. *Int J Cemt Comp Lightweight Concr* 5: 225-233.
- Naaman A.E. and Homrich J.R., (1989). Tensile stress-strain properties of SIFCON, *ACI Mater J* 86 (3): 244-251.
- Nataraja M.C., Dhang N., Gupta A.P., (2000). Toughness characterization of steel fibre reinforced concrete by JSCE approach. *Cem Concr Res* 30: 593-597.
- Nazari A. and Riahi S., (2011). The effects of SiO<sub>2</sub> nanoparticles on physical and mechanical properties of high strength compacting concrete. *Compos Eng* 42(3): 570-578.
- NDRC, (1946). Effects of impact and explosion. Summary Technical Report of Division 2, vol. 1, National Defence Research Committee, Washington, DC.
- Nelson E.B. and Guillot D., (2006). *Well Cementing*. Second edition, Schlumberger Ltd., Sugar Land, Texas, USA.
- Neville A.M., (1995). *Properties of concrete*. Longman House, Burnt Mill, Harlow, England.
- Nia A. A., Hedayatian M., Nili M., Sabet V.A., (2012). An experimental and numerical study on how steel and polypropylene fibres affect the impact resistance in fibre-reinforced concrete. *Int J Impact Eng* 46: 62-73.
- Nili M. and Afroughsabet V., (2010a). The effects of silica fume and polypropylene fibres on the impact resistance and mechanical properties of concrete. *Constr Build Mater* 24: 927-933.
- Nili M. and Afroughsabet V., (2010b). Combined effect of silica fume and steel fibres on the impact resistance and mechanical properties of concrete. *Int J Impact Eng* 37: 879-886.
- Noumowe A., (2005). Mechanical properties and microstructure of high strength concrete containing polypropylene fibres exposed to temperatures up to 200 °C. *Cem Concr Res* 35: 2192-2198.
- NT Build 492, (1999). *Concrete, mortar and cement-based repair materials: Chloride migration coefficient from non-steady-state migration experiments*. Nordtest method, Finland.
- Oertel T., Hutter F., Tänzer R., Helbig U., Sextl G., (2013). Primary particle size and agglomerate size effects of amorphous silica in ultra-high performance concrete. *Cem Concr Comp* 37: 61-67.

- Ohkubo K., Beppu M., Ohno T., Satoh K., (2008). Experimental study on the effectiveness of fibre sheet reinforcement on the explosive-resistant performance of concrete plates. *Int J Impact Eng* 35: 1702-1708.
- Ogawa K., Uchikawa H., Takemoto K., Yasui I., (1980). The mechanism of the hydration in the system  $C_3S$ -pozzolana. *Cem. Concr. Res* 10: 683-696.
- Okamura H. and Ozawa K., (1995). Mix-design for self-compacting concrete. *Concrete Library JSCE* 25: 107-120.
- Ong K.C.G., Basheerkhan M., Paramasivam P., (1999). Resistance of fibre concrete slabs to low velocity projectile impact. *Cem Concr Comp*, 21: 391-401.
- Pan J.R., Huang C., Kuo J.J., Lin S.H., (2008). Recycling MSWI bottom and fly ash as raw materials for Portland cement. *Waste Manage* 28: 1113-1118.
- Pane I. and Hansen W., (2005). Investigation of blended cement hydration by isothermal calorimetry and thermal analysis. *Cem Concr Res* 35: 1155-1164.
- Papadakis V.G., (1999). Effect of FA on Portland cement systems Part I: low-calcium FA. *Cem Concr Res* 29: 1727-1736.
- Parant E., Rossi P., Jacquelin E., Boulay C., (2007). Strain rate effect on bending behaviour of new ultra-high-performance cement-based composite. *ACI Mater J* 104: 458-463.
- Park S.H., Kim D.J., Ryu G.S., Koh K.T., (2012). Tensile behaviour of Ultra-High Performance Hybrid Fibre Reinforced Concrete. *Cem Concr Comp* 34: 172-184.
- Pera J., Coutaz L., Ambroise J., Chababbet M., (1997). Use of incinerator bottom ash in concrete. *Cem Concr Res* 27(1): 1-5.
- Plank J., Schroefl C.H., Gruber M., Lesti M., Sieber R., (2009). Effectiveness of polycarboxylate superplasticizer in ultra-high strength concrete: The importance of PCE compatibility with silica fume. *J Adv Concr Technol* 7 (1): 5-12.
- Pu X.C., (2004). Super high strength and high performance concrete. Chongqing University press, China (in chinese).
- Puntke W., (2002). Wasseranspruch von feinen Kornhaufwerken, *Beton* 52(5): 242 - 248 (in German).
- Qiao X.C., Tyrer M., Poon C.S., Cheeseman C.R., (2008). Characterization of alkali-activated thermally treated incinerator bottom ash. *Waste Manage* 28: 1955-1962.
- Qin C. and Zhang C., (2011). Numerical study of dynamic behaviour of concrete by meso-scale particle element. *Int J Impact Eng* 38: 1011-1021.
- Qing Y., Zenan Z., Deyu K., Rongshen C., (2007). Influence of nano-SiO<sub>2</sub> addition on properties of hardened cement paste as compared with silica fume. *Constr Build Mater* 21: 539-545.
- Quercia G., Spiesz P., Hüsken G., Brouwers H.J.H., (2014). SCC modification by use of amorphous nano-silica. *Cem Concr Comp* 45: 69-81.
- Quercia G., (2014). Application of nanosilica in concrete. PhD thesis. Eindhoven University of Technology, Eindhoven, the Netherlands.

- Quercia G., Hüsken G., Brouwers H.J.H., (2012). Water demand of amorphous nano silica and its impact on the workability of cement paste, *Cem Concr Res* 42: 344-357.
- Ramachandran V.S., Paroli R.M., Beaudoin J.J., Delgado A.H. (2002). *Handbook of Thermal Analysis of Construction Materials*. William Andrew Publishing, Norwich, New York, USA.
- Rambo D.A.S., Silva F.A., Filho R.D.T., (2014). Mechanical behaviour of hybrid steel-fibre self-consolidating concrete: Materials and structural aspects. *Mater Design* 54: 32-42.
- Ramakrishna G. and Sundararajan T., (2005). Impact strength of a few natural fibre reinforced cement mortar slabs: a comparative study. *Cem Concr Comp* 27: 547-553.
- Ramezani-pour A.A., Esmaeili M., Ghahari S.A., Najafi M.H., (2013). Laboratory study on the effect of polypropylene fibres on durability, and physical and mechanical characteristic of concrete for application in sleepers. *Constr Build Mater* 44: 413-418.
- Randl N., Steiner T., Ofner S., Baumgartner E., Mészöly T., (2014). Development of UHPC mixtures from an ecological point of view. *Constr Build Mater* 67: 373-378.
- Regourd M., (1980). Structure and behaviour of GGBS cement hydrates. *Principal Paper III, 2, VII th Int. Congress Chemistry of Cement. Paris, Vol. I, III.2: 9-26.*
- Regourd M., Thomassin J.H., Baillif P., Touray J.C., (1983). Blast-furnace GGBS hydration surface analysis. *Cem Concr Res* 13: 549-556.
- Richard P. and Cheyrezy M., (1995). Composition of reactive powder concretes, *Cem Concr Res* 25 (7): 1501-1511.
- Romualdi J. and Mandel J., (1964). Tensile Strength of concrete affected by uniformly distributed and closely spaced short lengths of wire reinforcement. *J Amer conc Inst* 61(6): 657-671.
- Ross C.A., Thompson P.Y., Tedesco J.W., (1989). Split-Hopkinson pressure-bar tests on concrete and mortar in tension and compression. *ACI Mate J* 86(5): 475-481.
- Ross C.A., Tedesco J.W., Kuennen S.T., (1995). Effects of strain rate on concrete strength. *ACI Mate J* 92(1): 37-47.
- Ross C.A., Jerome D.M., Tedesco J.W., Hughes M.L., (1996). Moisture and strain rate effects on concrete strength. *ACI Mate J* 93(3): 293-300.
- Rossi, P., Acker, P., Malier, Y., (1987). Effect of steel fibres at two stages: the material and the structure. *Mater Stru* 20: 436-439.
- Rossi P., (2013). Influence of fibre geometry and matrix maturity on the mechanical performance of ultra-high-performance cement-based composites. *Cem Concr Comp* 37: 246-248.
- Saeid K., Hazizan M.A., Morteza J., Jalal R., (2012). The effects of polypropylene fibres on the properties of reinforced concrete structures. *Constr Build Mater* 27: 73-77.
- Safiuddin M.d. and Hearn N., (2005). Comparison of ASTM saturation techniques for measuring the permeable porosity of concrete. *Cem Concr Res* 35: 1008-1013.

- Sandler I.S. and Rubin D., (1979). An algorithm and a modular subroutine for the cap model. *Int J Numer Anal Met* 3: 173-186.
- Sari M., Prat E., Labastire J.F. (1999). High strength self-compacting concrete: Original solutions associating organic and inorganic admixtures. *Cem Concr Res* 29: 813-818.
- Sawamoto Y., Tsubota H., Kasai Y., Koshika N., Morikawa H., (1998). Analytical studies on local damage to reinforced concrete structures under impact loading by discrete element method. *Nucl Eng Des* 179: 157-177.
- Schmidt M., Amrhein K., Braun T., Glotzbach C., Kamaruddin S., Tänzer R., (2013). Nanotechnological improvement of structural materials - Impact on material performance and structural design. *Cem Concr Comp* 36: 3-7.
- Schmidt W., (2014). Design concepts for the robustness improvement of self-compacting concrete. PhD thesis. Eindhoven University of Technology, Eindhoven, the Netherlands.
- Schumacher P., (2006). Rotation capacity of self-compacting steel fibre reinforced concrete. PhD thesis, Delft University of Technology, Delft, the Netherlands.
- Schutter G.D., (1999). Hydration and temperature development of concrete made with blast-furnace GGBS cement. *Cem Concr Res* 29: 143-149.
- Senff, L., Labrincha, J.A., Ferreira, V.M., Hotza, D., Repette, W.L. (2009). Effect of nanosilica on rheology and fresh properties of cement pastes and mortars. *Constr Build Mater* 23: 2487-2491.
- Senff, L., Hotza, D., Repette, W.L., Ferreira, V.M., Labrincha, J.A. (2010). Mortars with nano-SiO<sub>2</sub> and micro-SiO<sub>2</sub> investigated by experimental design. *Constr Build Mater* 24: 1432-1437.
- Senff L., Hotza D., Lucas S., Ferreira V.M., Labrincha J.A., (2012). Effect of nano-SiO<sub>2</sub> and nano-TiO<sub>2</sub> addition on the rheological behaviour and the hardened properties of cement mortars. *Mater Sci Eng: A* 532: 354-361.
- Sharma A., Reddy G.R., Varshney L., Bharath H., Vaze K.K., Ghosh A.K., (2009). Experimental Investigations on Mechanical and Radiation Shielding Properties of Hybrid Lead-Steel Fibre Reinforced Concrete. *Nucl Eng Des* 239:1180-1185.
- Shih J.Y., Chang T.P., Hsiao T.C., (2006). Effect of nanosilica on characterization of Portland cement composite. *Mater Sci Eng: A* 424(1-2): 266-274.
- Shirai T., Kambayashi A., Ohno T., Taniguchi H., Ueda M., Ishikawa N., (1997). Experiment and numerical simulation of double-layered RC plates under impact loadings. *Nucl Eng Des* 176 (3): 195-205.
- Shugar T.A, Holland T.J., Malvar L.J., (1992). Applications of finite element technology to reinforced concrete explosive containment structures. In: *Proceedings of The 25th DoD Explosive Safety Seminar*. Anaheim, CA, 4: 133-159.
- Silva F.A., Butler M., Mechtcherine V., Zhu D., Mobasher B., (2011). Strain rate effect on the tensile behaviour of textile-reinforced concrete under static and dynamic loading. *Mat Sci Eng A* 528:1727-1734.

- Simo J.C., Ju J.W., Pister K.S., Taylor R.L., (1988). An assessment of the cap model: consistent return algorithms and rate-dependent extensions. *J Eng Mech* 114(2): 191-218.
- Snozzi L., Caballero A., Molinari J.F., (2011). Influence of the meso-structure in dynamic fracture simulation of concrete under tensile loading. *Cem Concr Res* 41: 1130-1142.
- Sobolev K. and Ferrara M. (2005a). How nanotechnology can change the concrete world - Part 1. *Am. Ceram. Bull.* 84 (10): 14-17.
- Sobolev K. and Ferrara M. (2005b). How nanotechnology can change the concrete world- Part 2. *Am. Ceram. Bull.* 84 (11): 16-20.
- Sobolev K., Flores I., Hermosillo R., (2006). Nanomaterials and nanotechnology for high performance cement composites. In Proceedings of ACI Session on "Nanotechnology of Concrete: Recent Developments and Future Perspectives". American Concrete Institute, 7 November, Denver, USA, 91-118.
- Soetens T., Gysel A. V., S. Taerwe M. L., (2013). A semi-analytical model to predict the pull-out behaviour of inclined hooked-end steel fibres. *Constr Build Mater* 43: 253-265.
- Song P.S., Hwang S., Sheu B.C., (2005a). Strength properties of nylon- and polypropylene-fibre-reinforced concretes. *Cem Concr Res* 35: 1546-1550.
- Song P.S., Wu J.C., Hwang S., Sheu B.C., (2005b). Assessment of statistical variations in impact resistance of high-strength concrete and high-strength steel fibre-reinforced concrete. *Cem Concr Res* 35: 393-399.
- Soroka I. and Setter N., (1977). The effect of fillers on strength of cement mortars. *Cem Concr Res* 7(4): 449-456.
- Sovják R., Vavříník T., Máca P., Zatloukal J., Konvalinka P., Song Y., (2013). Experimental investigation of Ultra-high Performance Fibre Reinforced Concrete slabs subjected to deformable projectile impact. *Procedia Eng* 65: 120-125.
- Sovják R., Vavříník T., Zatloukal j., Máca P., Mičunek T., Frydrýn M., (2015). Resistance of slim UHPFRC targets to projectile impact using in-service bullets. *Int J Impact Eng* 76: 166-177.
- Spiesz P., (2013). Durability of concrete with emphasis on chloride migration. PhD thesis. Eindhoven University of Technology, Eindhoven, the Netherlands.
- Spiesz P., Yu Q.L., Brouwers H.J.H., (2013). Development of cement-based lightweight composites - Part 2: Durability related properties, *Cem Concr Comp* 44: 30-40.
- STANAG 2280, (2009). Test procedures and classification of the effects of weapons on structures. North Atlantic Treaty Organization (NATO).
- Sukontasukkul P., (2004). Toughness evaluation of steel and polypropylene fibres reinforced concrete beams under bending. *Thammasat Int. J. Sc. Tech.* 9(3): 35-41.
- Sun W., Mandel J.A., Said S., (1986). Study of the interface strength of steel fibre reinforced cement based composites. *ACI Mate J* 83: 597-605.

- Süper W., (1980). Rechnerische Untersuchung stoßartig beanspruchter stahlbetonplatten. Lehrstuhl für Beton-und stahlbetonbau, Forschg. Kolloquim Dortmund.
- Swamy R.N. and Jojagha A.H., (1982). Impact resistance of steel fibre reinforced lightweight concrete. *Int J Cem Comp Lightweight Concr* 4: 209-220.
- Tai Y.S., (2009). Uniaxial compression tests at various loading rates for reactive powder concrete. *Theor Appl Fract Mec* 52: 14-21.
- Tang M.C., (2004). High performance concrete-past, present and future, in: M. Schmidt, E. Fehling, C.Geisenhansluke (Eds.), *Ultra High Performance Concrete*, Kassel University Press, Kassel, 3-9.
- Taylor H.F.W., (1997). *Cement chemistry*. 1st edition, London: Academic Press.
- Tayeh B.A., Abu Bakar B.H., Megat Johari M.A., Voo Y.L., (2012). Mechanical and permeability properties of the interface between normal concrete substrate and ultra-high performance fibre concrete overlay. *Constr Build Mater* 36: 538-548.
- Tazawa E. and Miyazawa S., (1999). Effect of constituents and curing conditions on autogenous shrinkage of concrete, in: E. Tazawa (Ed.), *Autogenous Shrinkage of Concrete*, Taylor & Francis, 269-280.
- Tedesco J.W. and Ross C.A., (1998). Strain rate dependent constitutive equations for concrete. *J Press Vess-T ASME* 120(4): 398-405.
- Teng T.L., Chu Y.A., Chang F.A., Shen B.C., Cheng D.S., (2008). Development and validation of numerical model of steel fibre reinforced concrete for high-velocity impact. *Comp Mater Sci* 42: 90-99.
- Thomas J.J., Jennings H.M., Chen J.J., (2009). Influence of nucleation seeding on the hydration mechanisms of tricalcium silicate and cement. *J Phys Chem C* 113(11): 4327-4334.
- Thomassin J.H., Goni J., Baillif P., Touray J.C., Jaurand N.C., (1977). An XPS study of the dissolution kinetics of chrysotile in 0.1n oxalic acid at different temperatures. *Phys. Chem. Minerals* 1: 385-398.
- Toledo Filho R.D., Koenders E.A.B., Formagini S., Fairbairn E.M.R., (2012). Performance assessment of Ultra-High Performance Fibre Reinforced Cementitious Composites in view of sustainability. *Mater Des* 36: 880-888.
- Tuan N.V., Ye G., Breugel K., Copuroglu O., (2011a). Hydration and microstructure of ultra-high performance concrete incorporating rice husk ash. *Cem Concr Res* 41: 1104-1111.
- Tuan N.V., Ye G., Breugel K., Fraaij A.L.A., Dai B. D., (2011b). The study of using rice husk ash to produce ultra-high performance concrete. *Constr Build Mater* 25: 2030-2035.
- Tu Z. and Lu Y., (2009). Evaluation of typical concrete material models used in hydrocodes for high dynamic response simulations. *Int J Impact Eng* 36: 132-146.
- UNSTATS, (2010). *Greenhouse gas emissions by sector (absolute values)*. United Nation Statistical Division: Springer.

- Valcuende M., Parra C., Marco E., Garrido A., Martínez E., Cánoves J., (2012). Influence of LP filler and viscosity-modifying admixture on the porous structure of self-compacting concrete. *Constr Build Mater* 28(1): 122-128.
- Vandewalle L., (1993). *Vezelversterkt Beton*, Studiedag 'Speciale Betonsoorten en Toepassingen, Katholieke Universiteit Leuven, Departement Burgerlijke Bouwkunde, 77-98.
- Verhagen A.D., (2012-2015). Private communications, discussions and suggestions about this research (including the design of the "Modified Pendulum Impact Device").
- Violeta B.B., (2003). SCC mixes with poorly graded aggregate and high volume of limestone filler, *Cem Concr Res* 2003; 33(9): 1279-1286.
- Vossoughi F., Ostertag C.P., Monteiro P.J.M., Johnson G.C., (2007). Resistance of concrete protected by fabric to projectile impact. *Cem Concr Res* 37: 96-106.
- Voo Y.L., Nematollahi B., Said A.B.B.M., Gopal B.A., Yee T.S., (2012). Application of Ultra-High Performance Fibre Reinforced Concrete – The Malaysia Perspective. *Int J Sustain Constr Eng Tech* 3(1): 2180-3242.
- Wafa F.F., (1990). Properties and Applications of Fibre Reinforced Concrete. *JKAU Eng. Sci.* 2: 49-63.
- Wang C., Yang C., Liu F., Wan C., Pu X., (2012). Preparation of Ultra-High Performance Concrete with common technology and materials. *Cem Concr Comp* 34: 538-544.
- Wang N., Mindess S., Ko K., (1996). Fibre reinforced concrete beams under impact loading. *Cem Concr Res* 26(3): 363-376.
- Wang W., Liu J., Agostini F., Davy C.A., Skoczylas F., Corvez D., (2014). Durability of an Ultra High Performance Fibre Reinforced Concrete (UHPFRC) under progressive aging. *Cem Concr Res* 55: 1-13.
- Wang Z.L., Li Y.C., Shen R.F., Wang J.G., (2007). Numerical study on craters and penetration of concrete slab by ogive-nose steel projectile. *Comput Geotech* 34(1): 1-9.
- Wei F., Michael W. G., Della M. R., (1985). The retarding effects of FA upon the hydration of cement pastes: The first 24 hours. *Cem Concr Res* 15(1): 174-184.
- Wen H.M. and Xian Y.X., (2015). A unified approach for concrete impact. *Int J Impact Eng* 77: 84-96.
- Werner S., Thienel K.C., Kustermann A., (2013). Study of fractured surfaces of concrete caused by projectile impact. *Int J Impact Eng* 52: 23-27.
- Williams M.S., (1994). Modeling of local impact effects on plain and reinforced concrete. *ACI Struct J* 91(2): 178-187.
- Wu C., Oehlers D.J., Rebentrost M., Leach J., Whittaker A.S., (2009). Blast testing of ultra-high performance fibre and FRP-retrofitted concrete slabs. *Eng Struct* 31(9): 2060-2069.
- Wu X., Roy D.M., Langton C.A., (1983). Early stage hydration of GGBS-cement. *Cem Concr Res* 13(2): 277-286.

- Wu X., Jiang W., Roy D.M., (1990). Early activation and properties of GGBS cement. *Cem Concr Res* 20(6): 961-974.
- Wu H., Fang Q., Chen X.W., Gong Z.M., Liu J.Z., (2015). Projectile penetration of ultra-high performance cement based composites at 510–1320 m/s. *Constr Build Mater* 74: 188-200.
- Xu B., Toutanji H.A., Gilbert J., (2010). Impact resistance of poly (vinyl alcohol) fibre reinforced high-performance organic aggregate cementitious material. *Cem Concr Res* 40: 347-351.
- Xu Z., Hao H., Li H.N., (2012a). Mesoscale modeling of fibre reinforced concrete material under compressive impact loading. *Constr Build Mater* 26: 274-288.
- Xu Z., Hao H., Li H.N., (2012b). Mesoscale modeling of dynamic tensile behaviour of fibre reinforced concrete with spiral fibres. *Cem Concr Res* 42: 1475-1493.
- Yan H., Sun W., Chen H., (1999). The effect of silica fume and steel fibre on the dynamic mechanical performance of high-strength concrete. *Cem Concr Res* 29: 423-426.
- Yang I.H., Joh C., Kim B.S., (2010). Structural behaviour of ultra-high performance concrete beams subjected to bending. *Eng Struct* 32: 3478-3487.
- Yang S.L., Millard S.G., Soutsos M.N., Barnett S.J., Le T.T., (2009). Influence of aggregate and curing regime on the mechanical properties of ultra-high performance fibre reinforced concrete (UHPFRC). *Constr Build Mater* 23: 2291-2298.
- Yao W., Li J., Wu K., (2003). Mechanical properties of hybrid fibre-reinforced concrete at low fibre volume fraction. *Cem Concr Res* 33(1):27-30.
- Yap S.P., Bu C.H., Alengaram U.J., Mo K. H., Jumaat M.Z., (2014). Flexural toughness characteristics of steel–polypropylene hybrid fibre-reinforced oil palm shell concrete. *Mater Design* 57: 652-659.
- Yazici H., (2007). The effect of curing conditions on compressive strength of ultra high strength concrete with high volume mineral admixtures. *Build Environ* 42: 2083-2089.
- Yonten K., Majid T.M., Marzougui D., Eskandarian A., (2005). An assessment of constitutive models of concrete in the crashworthiness simulation of roadside safety structures. *Inte J Crashworthines* 10(1): 5-19.
- Yoo D.Y., Kang S.T., Yoon Y.S., (2014). Effect of fiber length and placement method on flexural behaviour, tension-softening curve, and fiber distribution characteristics of UHPFRC. *Constr Build Mater* 64: 67-81.
- Yu Q.L., (2012). Design of environmentally friendly calcium sulfate-based building materials. Towards an improved indoor air quality. PhD thesis. Eindhoven University of Technology, Eindhoven, the Netherlands.
- Yu Q.L., Spiesz P., Brouwers H.J.H., (2013). Development of cement-based lightweight composites - Part 1: Mix design methodology and hardened properties. *Cem Concr Comp* 44: 17-29.

- Yu R., Spiesz P., Brouwers H.J.H., (2012). A method for calculating equivalent diameter of fibre in self-compacting fibre reinforced concrete. Proceedings of the 18th Ibaasil, International Conference on Building Materials. Bauhaus-Universitat Weimar. Weimar, Germany, 2-0546-2-0553.
- Yu R., Spiesz P., Brouwers H.J.H., (2014a). Mix design and properties assessment of Ultra- High Performance Fibre Reinforced Concrete (UHPFRC), *Cem Concr Res* 56: 29-39.
- Yu R., Spiesz P., Brouwers H.J.H., (2014b). Effect of nanosilica on the hydration and microstructure development of Ultra-High Performance Concrete (UHPC) with a low binder amount. *Constr Build Mater* 65: 140-150.
- Yu R., Tang P., Spiesz P., Brouwers H.J.H., (2014c). A study of multiple effects of nanosilica and hybrid fibres on the properties of Ultra-High Performance Fibre Reinforced Concrete (UHPFRC) incorporating waste bottom ash (WBA). *Constr Build Mater* 60: 98-110.
- Yu R., Spiesz P., Brouwers H.J.H., (2014d). Static and impact resistance of a green Ultra-High Performance Hybrid Fibre Reinforced Concrete (UHPFRC): Experiments and modeling. *Constr Build Mater* 68: 158-171.
- Yu R., Spiesz P., Brouwers H.J.H., (2015a). Development of an eco-friendly Ultra-High Performance Concrete (UHPC) with efficient cement and mineral admixtures uses. *Cem Concr Comp* 55: 383-394.
- Yu R., Spiesz P., Brouwers H.J.H., (2015b) Development of Ultra-High Performance Fibre Reinforced Concrete (UHPFRC): towards an efficient application of binders and fibres. *Constr Build Mater* 79: 273-282.
- Zeng Q., Li K., Fen-chong T., Dangla P., (2012). Determination of cement hydration and pozzolanic reaction extents for fly-ash cement pastes. *Constr Build Mater* 27: 560-569.
- Zhang Y., Sun W., Liu S., Jiao C., Lai J., (2008). Preparation of C200 green reactive powder concrete and its static–dynamic behaviours. *Cem Concr Comp* 30: 831-838.
- Zhang M.H., Shim V.P.W., Lu G., Chew C.W., (2005). Resistance of high-strength concrete to projectile impact. *Int J Impact Eng* 31: 825-841.
- Zhang M.H., Sharif M.S.H., Lu G., (2007). Impact resistance of high-strength fibre-reinforced concrete. *Mag Concrete Res* 59(3): 199-210.
- Zhao S., Fan J., Sun W., (2014). Utilization of iron ore tailings as fine aggregate in ultrahigh performance concrete. *Constr Build Mater* 50: 540-548.
- Zhu D.J., Peled A., Mobasher B., (2011). Dynamic tensile testing of fabric-cement composites. *Constr Build Mater* 25(1): 385-395.



## List of abbreviations and symbols

### Abbreviations

A&A	Andreasen & Andersen particle packing model
B	Binder
bwoc	by weight of cement
CPM	Compressive Packing Model
C-S	Compressive strength
DE	Germany
DEF	Delayed Ettringite Formation
DIF	Dynamic increase factor
DP	Dormant period
DSC	Differential Scanning Calorimetry
EU	European Union
FA	Fly ash
fps	Frame per second
FRC	Fibre reinforced concrete
F-S	Flexural strength
GGBS	Ground Granulated Blast furnace Slag
HF	Hook ended steel fibre
HPFRC	High Performance Fibre Reinforced Concrete
HSC	High strength concrete
HT	Heat treatment
ITZ	Interfacial Transition Zone
LLS	Laser light scattering
LOI	Loss-on-ignition
LP	Limestone powder
LPDM	Linear Packing Density Model
LPG	Liquefied petroleum gas
LSF	Long straight steel fibre
LSM	Least Squares Method
MMD	Mass-median-diameter
MMFRC	Multi-modal fibre reinforced concrete
MS	Microsand
mS	Microsilica
nS	Nanosilica
NFRC	Normal fibre reinforced concrete
NSC	Normal strength concrete

OPC	Ordinary Portland cement
P	Powder
PPF	Polypropylene fibre
PSD	Particle size distribution
QP	Quartz powder
Ref.	Reference sample
RGC	Recycled glass cullet
RHA	Rice husk ash
RSS	Sum of the squares of the residuals
RST	Relative setting time
S	Sand (0-2 mm)
SCC	Self-Compacting Concrete
SEM	Scanning Electron Microscope
SF	Silica Fume (microsilica)
SFRC	Steel fibre reinforced concrete
SIFCON	Slurry Infiltrated Fibre Concrete
SP	Superplasticizer
SP/C	Superplasticizer to cement ratio
SSA	Specific Surface Area
SSF	Short straight steel fibre
SSM	Solid Suspension Model
TF	Flexural toughness factor
TG	Thermo-gravimetric
TRMP	Time to reach the maximum peak
UHPC	Ultra-High Performance Concrete
UHPFRC	Ultra-High Performance Fibre Reinforced Concrete
vol.	Volume fraction
W	Water
WBA	Waste bottom ash
W/B	Water to binder ratio
W/C	Water to cement ratio
W/P	Water to powder ratio
XRD	X-ray diffraction
XRF	X-ray Fluorescence

**Symbols***Roman:*

$A$	Material parameter	[-]
$A_{(L/150)}$	Flexural toughness at the deflection ( $L/150$ )	[Nžm]
$b$	Empirical constant	[-]
$B$	Material parameter	[-]
$B'$	Width of specimen	[cm]
$C$	Material parameter	[-]
$d$	Diameter of the projectile	[m]
$d_0$	Base diameter of the used cone	[cm]
$d_1$	Diameter of the spread fresh concrete	[cm]
$d_2$	Diameter of the spread fresh concrete (perpendicular to $d_1$ )	[cm]
$d'$	Diameter of the used straight fibres	[mm]
$d_1'$	Diameter of long straight fibres	[mm]
$d_2'$	Diameter of short straight fibres	[mm]
$D'$	Damage parameter	[-]
$D_1$	Damage constant	[-]
$D_2$	Damage constant	[-]
$e$	Perforation limits	[cm]
$E_{absorbed}$	Absorbed energy by UHPFRC slab	[J]
$E_{total-absorbed}$	Total absorbed energy by UHPFRC slab	[J]
$f_c$	Compressive strength of concrete target	[MPa]
$f_{cd}$	Unconfined uniaxial compressive strength in dynamic loading	[MPa]
$f_{cs}$	Unconfined uniaxial compressive strength in quasi-static loading	[MPa]
$f_t$	Dynamic tensile strength at $\varepsilon'$	[MPa]
$f_{ts}$	Static tensile strength at $\varepsilon_s'$	[MPa]
$f'_c$	Quasi-static uniaxial compressive strength	[MPa]
$g$	Gravity of earth	[m/s <sup>2</sup> ]
$H_1$	Initial height of hammer in Charpy impact test	[cm]
$H_2$	Residual height of hammer after impact in Charpy impact test	[cm]
$h_s$	Scabbing limit	[cm]
$k$	Empirical constant	[-]
$k'$	Fibre embedded length	[cm]
$K_t$	Strength improvement ratio	[%]
$K_1$	Constants	[-]
$K_2$	Constants	[-]
$K_3$	Constants	[-]
$L$	Fibre length	[mm]

$l_1$	Length of long straight fibres	[mm]
$l_2$	Length of short straight fibres	[mm]
$L$	Span in the 4-point bending test	[mm]
$m$	Mass of the materials	[g]
$m_{binder}$	Total mass of the binders per cube meter concrete	[kg/m <sup>3</sup> ]
$m_d$	Mass of oven dried sample	[g]
$m_s$	Mass of the saturated sample in surface-dry condition	[g]
$m_w$	Mass of water-saturated sample in water	[g]
$m_{w-p}$	Water demand from Puntke test	[g]
$M_{CaCO_3}$	Mass change of paste caused by the decomposition of CaCO <sub>3</sub>	[g]
$M$	Mass of the projectile	[kg]
$M_{hammer}$	Mass of impact hammer	[kg]
$M_i$	Mass of the fraction i in solid materials	[g]
$M_j$	Mass of the fraction j in solid materials	[g]
$M_{slab}$	Mass of concrete slab	[kg]
$M_{water}$	Mass of non-evaporable water	[g]
$M_{water-Full}$	Water required for the full hydration of cement	[g]
$M_{105}$	Mass of paste after heat treatment under 105 °C for 2 hours	[g]
$M_{1000}$	Mass of paste after heat treatment under 1000 °C for 2 hours	[g]
$n$	Number of the chosen points between $D_{min}$ and $D_{max}$	[-]
$N^*$	Nose shape factor	[-]
$p$	Porosity of the tested material	[%]
$p_c$	Percolation porosity at failure threshold	[%]
$P$	Pressure	[MPa]
$P_{crush}$	Pressure arising in a uniaxial compression test	[MPa]
$P_{lock}$	Locking pressure	[MPa]
$P_{mix}$	The composed mix	[-]
$P_{tar}$	The target grading calculated from Eq. (3.2)	[-]
$P^*$	Normalized pressure	[MPa]
$r$	Radius of the used fibres	[mm]
$R^2$	Coefficient of determination	[-]
$S_a$	Area of the broken cross section	[mm <sup>2</sup> ]
$S_i$	Compressive strength of concrete with fibres	[MPa]
$S_0$	Compressive strength of concrete without fibres	[MPa]
$T$	Maximum tensile stress	[MPa]
$T^*$	Normalized largest tensile strength	[-]
$U$	Total energy absorbed by the UHPFRC sample	[Nžm]
$U_f$	Energy needed to pull out the fibre	[Nžm]
$U_{f1}$	Energy needed to pull out the long straight fibres	[Nžm]
$U_{f2}$	Energy needed to pull out the short straight fibres	[Nžm]

$U_m$	Crack energy absorbed by the reference sample (without fibres)	[Nžm]
$U_{\Delta}$	Modified total energy absorbed by the UHPFRC samples	[Nžm]
$V_{container}$	Volume of the cylindrical container	[cm <sup>3</sup> ]
$V_f$	Volumetric amount of the fibres in concrete	[%]
$V_{f1}$	Volumetric amount of the long straight fibres	[%]
$V_{f2}$	Volumetric amount of the short straight fibres	[%]
$V_{hammer}$	Initial impact velocity of the hammer	[m/s]
$V_{hammer-residual}$	Residual velocity of hammer after the impact.	[m/s]
$V_l$	Volumetric amount of the long straight fibres	[%]
$V_{liquid}$	Volume of liquid in the container	[cm <sup>3</sup> ]
$V_m$	Volume fraction of the concrete matrix	[%]
$V_p$	Volume of the tested powder material	[cm <sup>3</sup> ]
$V_s$	Volumetric amount of the short straight fibres	[%]
$V_{solid}$	Volume of solid particles in the container	[cm <sup>3</sup> ]
$V_{true}$	True volume of the material	[cm <sup>3</sup> ]
$V_w$	Volumetric water demand of the powder material for saturation	[cm <sup>3</sup> ]
$V_0$	Projectile impacting velocity	[m/s]
$W_{fp}$	Average work needed to pull out the fibre	[Nžm]
$x$	Penetration depth of projectile	[m]
$x'$	Fibre pulled out distance	[mm]
$X_{binder}$	Binder efficiency	[-]
$X_s$	Short fibre volume fraction	[-]

*Greek:*

$\beta_t$	Cement hydration degree at hydration time $t$	[%]
$\rho$	Current density	[g/cm <sup>3</sup> ]
$\rho_0$	Reference density	[g/cm <sup>3</sup> ]
$\rho_i$	Density of the fraction $i$ in solid materials	[g/cm <sup>3</sup> ]
$\rho_j$	Density of the fraction $j$ in solid materials	[g/cm <sup>3</sup> ]
$\rho_{specific}$	Specific density	[g/cm <sup>3</sup> ]
$\psi$	Void faction of the saturated powder material	[-]
$\phi$	Diameter of projectile	[mm]
$\varphi_{air}$	Air content	[%]
$\varphi_{v,water}$	Water-permeable porosity	[%]
$\zeta_{Reschke}$	Particle shape factor	[-]
$\Gamma$	Relative slump	[-]
$\sigma$	Strength	[MPa]
$\sigma_0$	Strength at zero porosity	[MPa]
$\varepsilon'$	Dynamic strain rate	[s <sup>-1</sup> ]

$\varepsilon_s'$	Quasi-static strain rate	[s <sup>-1</sup> ]
$\varepsilon'^*$	Dimensionless strain rate	[-]
$\varepsilon_0'$	Reference strain rate	[s <sup>-1</sup> ]
$\Delta HF$	Change in heat flow	[mW/g <sub>cement</sub> ]
$\Delta Q$	Difference of normalized heat released amount	[J/g <sub>cement</sub> ]
$\Delta \varepsilon_p$	Equivalent plastic strain increment	[-]
$\Delta \mu_p$	Equivalent plastic volumetric strain increment	[-]
$\tau_i$	Interfacial frictional shear stress	[MPa]
$\mu_{crush}$	Volumetric strain arising in a uniaxial compression test	[-]
$\mu_{lock}$	Locking volumetric strain	[-]

## Appendix 1

### Details of Johnson Holmsquist Concrete model

In Johnson Holmsquist Concrete model, the equivalent strength of material is expressed as a function of the pressure, strain rate and damage (Holmsquist et al., 1993):

$$\sigma^* = \frac{A}{\epsilon^*} (1 - D') + B P^{*N} \epsilon^* + C \ln \epsilon^* \quad (\text{A.1.1})$$

where  $P^*$  denotes the normalized pressure, shown as  $P^* = P/f'_c$ ;  $P$  denotes pressure,  $f'_c$  denotes the quasi-static uniaxial compressive strength,  $\epsilon^*$  denotes the dimensionless strain rate, given by  $\epsilon^* = \epsilon' / \epsilon'_0$ ,  $\epsilon'$  represents the actual strain rate,  $\epsilon'_0$  represents the reference strain rate.  $D'$  ( $0 < D' < 1$ ) denotes the damage parameter. Additionally  $A$ ,  $B$ ,  $N$ , and  $C$  denote the material parameters.

The model accumulates the damage from both equivalent plastic strain and plastic volumetric strain, and is expressed as:

$$D' = \dot{a} \frac{\Delta \epsilon_p + \Delta \mu_p}{\epsilon_p^f + \mu_p^f} \quad (\text{A.1.2})$$

Here,  $\Delta \epsilon_p$  and  $\Delta \mu_p$  represent the equivalent plastic strain increment and plastic volumetric strain increment, respectively, during one cycle integral computation.  $(\epsilon_p^f + \mu_p^f)$  represents the plastic strain to fracture under a constant pressure, which can be expressed as follows:

$$\epsilon_p^f + \mu_p^f = D_1 (P^* + T^*)^{D_2} \quad (\text{A.1.3})$$

where  $D_1$  and  $D_2$  represent damage constants, and  $T^* = T / f'_c$  is the normalized largest tensile strength ( $T$  represents the maximum tensile stress).

The equation of state (*EOS*) of this model describes the relationship between hydrostatic pressure and volume. The loading and unloading process of concrete can be divided into three response regions (as shown in Figure A.1-1). The first zone is the linear elastic zone, where the material is elastic state. The elastic bulk modulus is given by  $k = P_{crush} / \mu_{crush}$ , where  $P_{crush}$  and  $\mu_{crush}$  represent the pressure and volumetric strain arising in a uniaxial compression test. Within the elastic zone, the loading and unloading equation of state is given by:

$$P = Km \quad (\text{A.1.4})$$

where  $\mu = \rho/\rho_0 - 1$ ,  $\rho$  denotes the current density, and  $\rho_0$  denotes the reference density.

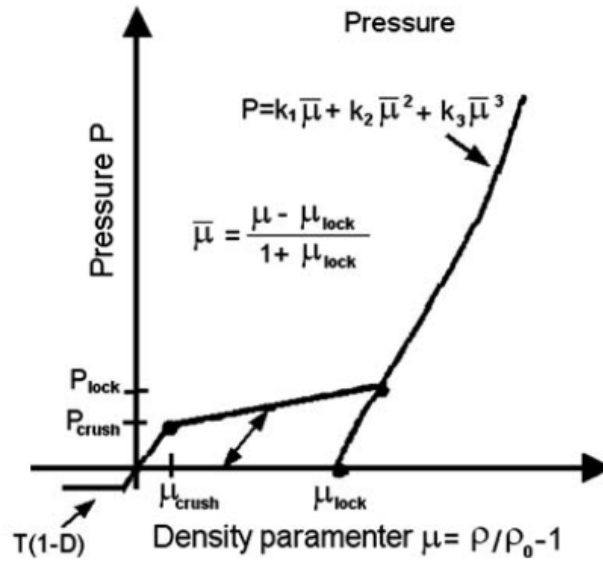


**Figure A.1-1: The relationship between hydrostatic pressure and material volumetric strain (Holmsquist et al., 1993)**

The second zone arises at  $P_{crush} < P < P_{lock}$ , where the material is in the plastic transition state. In this area, the concrete interior voids gradually reduce in size as the pressure and plastic volumetric strain increase. The unloading curve is solved by the difference from the adjacent regions.

The third area defines the relationship for fully dense material (concrete has no air voids). The relationship between pressure and the volumetric strain is given by:

$$P = K_1 \bar{m} + K_2 \bar{m}^2 + K_3 \bar{m}^3 \quad (\text{A.1.5})$$

where  $K_1, K_2, K_3$  are constants and modified volumetric strain is defined as:

$$\bar{m} = \frac{\mu - \mu_{lock}}{1 + \mu_{lock}} \quad (\text{A.1.6})$$

where  $\mu_{lock}$  is the locking volumetric strain.

**Appendix 2****Description of rigid material model**

In the rigid material model, parts made from this material are considered to belong to a rigid body (for each part ID). Also, the coupling of a rigid body with MADYMO and CAL3D can be defined via this material. The rigid material model provides a convenient way of turning one or more parts comprised of beams, shells or solid elements into a rigid body. Approximating a deformable body as rigid is a preferred modeling technique in many real world applications. For example, in sheet metal forming problems the tooling can properly and accurately be treated as rigid. In the design of restraint systems the occupant can, for the purposes of early design studies, also be treated as rigid. Elements which are rigid are bypassed in the element processing and no storage is allocated for storing history variables; consequently, the rigid material type is very cost efficient (LS-DYNA keyword user's manual, 2003).

## Summary

### **Development of sustainable protective Ultra-High Performance Fibre Reinforced Concrete (UHPFRC) ---Design, assessment and modeling**

To obtain a new product that contributes to a better and safer life for human beings, this thesis aims at the development of sustainable protective Ultra-High Performance Fibre Reinforced Concrete (UHPFRC). Firstly, a series of methods and strategies are utilized to design a sustainable UHPFRC, which can be briefly summarized as follows: 1) optimized design of UHPFRC matrix based on particle packing model; 2) efficient application of the powders in UHPFRC production; 3) efficient utilization of fibres in UHPFRC production; 4) appropriate application of waste/recycled materials in UHPFRC production. Here, the design of the UHPFRC is based on the aim to achieve a densely compacted cementitious matrix, employing the modified Andreasen & Andersen particle packing model. Moreover, industry by-products (fly ash, ground granulated blast-furnace slag) and waste/recycled material (waste bottom ash) are appropriately utilized to replace cement and aggregates, respectively. Additionally, hybridization design of utilized fibres is employed to improve the efficiency of fibres. Next, the properties of the developed sustainable UHPFRC are evaluated. A series of standards and approaches are employed to assess its workability, air content, water-permeable porosity, mechanical properties, flexural toughness, microstructure development, hydration kinetics, thermal properties and impact resistance capacity. For the impact resistance capacity of the developed sustainable UHPFRC, two types of pendulum impact set-ups and a high velocity projectile launcher are employed. Afterwards, based on the obtained experimental results, the modeling of dynamic behaviour of the sustainable UHPFRC under different impact loadings is performed. The modeling can be mainly divided into two sections: 1) energy absorption of UHPFRC under Charpy impact loading; 2) numerical simulation of UHPFRC under projectile impacts. This research is performed based on a combination of theoretical and experimental investigation. The final outcome is a methodology to design a sustainable UHPFRC and the dynamic performance of this developed UHPFRC under different impact loadings, which are beneficial for widening the application of UHPFRC and further understanding some intrinsic characteristics of UHPFRC under impact.

## List of publications

Publications written within this PhD project are listed below:

### Peer-reviewed journals

- 1) **Yu R.**, Spiesz P., Brouwers H.J.H., Sustainable Ultra- High Performance Fibre Reinforced Concrete (UHPFRC) under high velocity projectile impact, Part 2: Modeling study (In preparation).
- 2) **Yu R.**, Spiesz P., Brouwers H.J.H., Sustainable Ultra- High Performance Fibre Reinforced Concrete (UHPFRC) under high velocity projectile impact, Part 1: Experimental investigation (To be sbmitted).
- 3) **Yu R.**, Beers L.J.P. van, Spiesz P., Brouwers H.J.H., Dynamic performance of a sustainable Ultra- High Performance Fibre Reinforced Concrete (UHPFRC) under pendulum impact loadings. *Constr Build Mater* (Under review).
- 4) **Yu R.**, Spiesz P., Brouwers H.J.H., Energy absorption capacity of a sustainable Ultra-High Performance Fibre Reinforced Concrete (UHPFRC) in quasi-static mode and under high velocity projectile impact. *Cem Concr Compos* (Under review).
- 5) **Yu R.**, Onna D.V. van, Spiesz P., Yu Q.L., Brouwers H.J.H., (2015). Development of Ultra-Lightweight Fibre Reinforced Concrete applying expanded waste glass. *J Clean Prod*, In press, doi:10.1016/j.jclepro.2015.07.082.
- 6) **Yu R.**, Spiesz P., Brouwers H.J.H., (2015) Development of Ultra-High Performance Fibre Reinforced Concrete (UHPFRC): towards an efficient application of binders and fibres. *Constr Build Mater* 79: 273-282. (**most downloaded articles list: 24**)
- 7) **Yu R.**, Spiesz P., Brouwers H.J.H., (2015). Development of an eco-friendly Ultra-High Performance Concrete (UHPC) with efficient cement and mineral admixtures uses. *Cem Concr Compos* 55: 383-394. (**most downloaded articles list: 2**)
- 8) **Yu R.**, Spiesz P., Brouwers H.J.H., (2014). Static and impact resistance of a green Ultra-High Performance Hybrid Fibre Reinforced Concrete (UHPHFRC): Experiments and modeling. *Constr Build Mater* 68: 158-171.
- 9) **Yu R.**, Spiesz P., Brouwers H.J.H., (2014). Effect of nanosilica on the hydration and microstructure development of Ultra-High Performance Concrete (UHPC) with a low binder amount. *Constr Build Mater* 65: 140-150.

- 10) **Yu R.**, Spiesz P., Brouwers H.J.H., (2014). Impact resistance capacity of a green Ultra-High Performance Hybrid Fibre Reinforced Concrete (UHPFRC): Experimental and modeling study. *Int J Eng Res Tech* 03(13): 158-164.
- 11) **Yu R.**, Tang P., Spiesz P., Brouwers H.J.H., (2014). A study of multiple effects of nanosilica and hybrid fibres on the properties of Ultra-High Performance Fibre Reinforced Concrete (UHPFRC) incorporating waste bottom ash (WBA). *Constr Build Mater* 60: 98-110.
- 12) **Yu R.**, Spiesz P., Brouwers H.J.H., (2014). Mix design and properties assessment of Ultra- High Performance Fibre Reinforced Concrete (UHPFRC), *Cem Concr Res* 56: 29-39. (*most downloaded articles list: 18*)
- 13) Gao X., Yu Q.L., **Yu R.**, Brouwers H.J.H., Shui Z.H., (2014). Investigation of the effect of slag and limestone powder addition in alkalia activated metakaolin. *Int J Eng Res Tech* 03(13): 123-128.

#### Conference proceedings

- 14) **Yu R.**, Spiesz P., Brouwers H.J.H. (2015). Energy absorption ability of a sustainable Ultra-High Performance Fibre Reinforced Concrete (UHPFRC): Experiments and numerical simulation. Proceedings of the 19<sup>th</sup> Ibausil, International Conference on Building Materials. Bauhaus-Universitat Weimar. Weimar, Germany.
- 15) **Yu R.**, Spiesz P., Brouwers H.J.H. (2015). Effect of mineral admixtures on the properties of a sustainable Ultra-High Performance Concrete (UHRC). Proceedings of the 7<sup>th</sup> High Performance Fibre Reinforced Cement Composites. Stuttgart, Germany.
- 16) **Yu R.**, Spiesz P., Brouwers H.J.H. (2015). Sustainable development of an Ultra-High Performance Hybrid Fibres Reinforced Concrete (UHPHFRC): towards an efficient utilization of fibres. Proceedings of the 7<sup>th</sup> High Performance Fibre Reinforced Cement Composites. Stuttgart, Germany.
- 17) **Yu R.**, Spiesz P., Brouwers H.J.H. (2014). Impact resistance capacity of a green Ultra-High Performance Hybrid Fibre Reinforced Concrete (UHPFRC) : experimental and modeling study. Proceedings of the 5<sup>th</sup> International Conference of Non-Traditional Cement and Concrete (NTCC2014). In V. Bilek & Z. Kersner (Eds.). Brno, Czech Republic, 275-278.
- 18) Gao X., Yu Q.L., **Yu R.**, Brouwers H.J.H., Shui Z.H., (2014). Investigation on the effect of slag and limestone powder addition in alkali activated metakaolin. Proceedings of the 5<sup>th</sup> International Conference of Non-Traditional Cement and

- Concrete (NTCC2014). In V. Bilek & Z. Kersner (Eds.). Brno, Czech Republic, 21-26.
- 19) **Yu R.**, Spiesz P., Brouwers H.J.H. (2013). Effect of colloidal nanosilica on the hydration of Ultra-High Performance Concrete (UHPC). Proceedings of the 1<sup>st</sup> International Conference on the Chemistry of Construction Materials. GDCh-Division of Chemistry of Construction Chemicals. Berlin, Germany, 269-272.
- 20) **Yu R.**, Spiesz P., Brouwers H.J.H. (2013). Mix design and properties evaluation of Ultra-High Performance Fibre Reinforced Concrete (UHPFRC). Proceedings of the 15<sup>th</sup> International Symposium on Interaction of the Effects of Munitions with Structure (ISIEMS2013). Federal Office of Bundeswehr Infrastructure, Germany; Defense Threat Reduction Agency, USA. Potsdam, Germany, No. 172.
- 21) **Yu R.**, Spiesz P., Brouwers H.J.H. (2013). Numerical simulation of Ultra-High Performance Fibre Reinforced Concrete (UHPFRC) under high velocity impact of deformable projectile. Proceedings of the 15<sup>th</sup> International Symposium on Interaction of the Effects of Munitions with Structure (ISIEMS2013). Federal Office of Bundeswehr Infrastructure, Germany; Defense Threat Reduction Agency, USA. Potsdam, Germany, No. 173.
- 22) Tang P., Yu Q.L., **Yu R.**, Brouwers H.J.H., (2013). The application of MSWI bottom ash fines in high performance concrete. Proceedings of the 1<sup>st</sup> International Conference on the Chemistry of Construction Materials. GDCh-Division of Chemistry of Construction Chemicals. Berlin, Germany, 435-438.
- 23) **Yu R.**, Spiesz P., Brouwers H.J.H., (2012). A method for calculating equivalent diameter of fibre in self-compacting fibre reinforced concrete. Proceedings of the 18<sup>th</sup> Ibausil, International Conference on Building Materials. Bauhaus-Universitat Weimar. Weimar, Germany, 2-0546-2-0553.



**Curriculum vitae**

Rui Yu was born on 9<sup>th</sup> July 1986 in Hubei, China. In June 2008, he graduated with a Bachelor of Material Science and Engineering from Wuhan University of Technology (WHUT) in Wuhan, China. He was awarded scholarships for achievement in studying (2005, 2006, 2007 and 2008) and his graduation thesis was awarded as the first price in Hubei province in 2008. As the same year, he obtained an exemption qualification to continuously study as a master student in Wuhan University of Technology (WHUT), and his research topics were recycled building materials and efficient application of dehydrated cement paste. In December 2010, he received his Master degree in Materials Science. From October 2011, he moved to the Netherlands and started a PhD project under the supervision of Prof. dr. ir. H.J.H. Brouwers in Eindhoven University of Technology. His research interests include sustainable building materials, Ultra High Performance Fibre Reinforced Concrete and dynamic performance of concrete under impact loadings. He has published 12 SCI journal articles since 2010, and the summation of the journal impact factors is about 31. Additionally, he is the reviewer of more than 10 Journals, including Journal of Hazardous Materials, Journal of Cleaner Production, Cement and Concrete Composites, Construction and Building Materials. In 2014, he was awarded as the outstanding reviewer of Construction and Building Materials.



**Bouwstenen** is een publikatiereeks van de Faculteit Bouwkunde, Technische Universiteit Eindhoven. Zij presenteert resultaten van onderzoek en andere activiteiten op het vakgebied der Bouwkunde, uitgevoerd in het kader van deze Faculteit.

**Bouwstenen** zijn telefonisch te bestellen op nummer  
040 - 2472383

Kernredactie  
MTOZ

Reeds verschenen in de serie

## **Bouwstenen**

nr 1

### **Elan: A Computer Model for Building Energy Design: Theory and Validation**

Martin H. de Wit

H.H. Driessen

R.M.M. van der Velden

nr 2

### **Kwaliteit, Keuzevrijheid en Kosten: Evaluatie van Experiment Klarendal, Arnhem**

J. Smeets

C. le Nobel

M. Broos

J. Frenken

A. v.d. Sanden

nr 3

### **Crooswijk: Van 'Bijzonder' naar 'Gewoon'**

Vincent Smit

Kees Noort

nr 4

### **Staal in de Woningbouw**

Edwin J.F. Delsing

nr 5

### **Mathematical Theory of Stressed Skin Action in Profiled Sheeting with Various Edge Conditions**

Andre W.A.M.J. van den Bogaard

nr 6

### **Hoe Berekenbaar en Betrouwbaar is de Coëfficiënt $k$ in $x$ -ksigma en $x$ -ks?**

K.B. Lub

A.J. Bosch

nr 7

### **Het Typologisch Gereedschap: Een Verkennende Studie Omtrent Typologie en Omtrent de Aanpak van Typologisch Onderzoek**

J.H. Luiten

nr 8

### **Informatievoorziening en Beheerprocessen**

A. Nauta

Jos Smeets (red.)

Helga Fassbinder (projectleider)

Adrie Proveniers

J. v.d. Moosdijk

nr 9

### **Strukturering en Verwerking van Tijdgegevens voor de Uitvoering van Bouwwerken**

ir. W.F. Schaefer

P.A. Erkelens

nr 10

### **Stedebouw en de Vorming van een Speciale Wetenschap**

K. Doevendans

nr 11

### **Informatica en Ondersteuning van Ruimtelijke Besluitvorming**

G.G. van der Meulen

nr 12

### **Staal in de Woningbouw, Korrosie-Bescherming van de Begane Grondvloer**

Edwin J.F. Delsing

nr 13

### **Een Thermisch Model voor de Berekening van Staalplaatbetonvloeren onder Brandomstandigheden**

A.F. Hamerlinck

nr 14

### **De Wijkgedachte in Nederland: Gemeenschapsstreven in een Stedebouwkundige Context**

K. Doevendans

R. Stolzenburg

nr 15

### **Diaphragm Effect of Trapezoidally Profiled Steel Sheets:**

### **Experimental Research into the Influence of Force Application**

Andre W.A.M.J. van den Bogaard

nr 16

### **Versterken met Spuit-Ferrocement: Het Mechanische Gedrag van met Spuit-Ferrocement Versterkte Gewapend Betonbalken**

K.B. Lubir

M.C.G. van Wanroy

nr 17

**De Tractaten van  
Jean Nicolas Louis Durand**  
G. van Zeyl

nr 18

**Wonen onder een Plat Dak:  
Drie Opstellen over Enkele  
Vooronderstellingen van de  
Stedebouw**  
K. Doevendans

nr 19

**Supporting Decision Making Processes:  
A Graphical and Interactive Analysis of  
Multivariate Data**  
W. Adams

nr 20

**Self-Help Building Productivity:  
A Method for Improving House Building  
by Low-Income Groups Applied to Kenya  
1990-2000**  
P. A. Erkelens

nr 21

**De Verdeling van Woningen:  
Een Kwestie van Onderhandelen**  
Vincent Smit

nr 22

**Flexibiliteit en Kosten in het Ontwerpproces:  
Een Besluitvormingondersteunend Model**  
M. Prins

nr 23

**Spontane Nederzettingen Begeleid:  
Voorwaarden en Criteria in Sri Lanka**  
Po Hin Thung

nr 24

**Fundamentals of the Design of  
Bamboo Structures**  
Oscar Arce-Villalobos

nr 25

**Concepten van de Bouwkunde**  
M.F.Th. Bax (red.)  
H.M.G.J. Trum (red.)

nr 26

**Meaning of the Site**  
Xiaodong Li

nr 27

**Het Woonmilieu op Begrip Gebracht:  
Een Speurtocht naar de Betekenis van het  
Begrip 'Woonmilieu'**  
Jaap Ketelaar

nr 28

**Urban Environment in Developing Countries**  
editors: Peter A. Erkelens  
George G. van der Meulen (red.)

nr 29

**Stategische Plannen voor de Stad:  
Onderzoek en Planning in Drie Steden**  
prof.dr. H. Fassbinder (red.)  
H. Rikhof (red.)

nr 30

**Stedebouwkunde en Stadsbestuur**  
Piet Beekman

nr 31

**De Architectuur van Djenné:  
Een Onderzoek naar de Historische Stad**  
P.C.M. Maas

nr 32

**Conjoint Experiments and Retail Planning**  
Harmen Oppewal

nr 33

**Strukturformen Indonesischer Bautechnik:  
Entwicklung Methodischer Grundlagen  
für eine 'Konstruktive Pattern Language'  
in Indonesien**  
Heinz Frick arch. SIA

nr 34

**Styles of Architectural Designing:  
Empirical Research on Working Styles  
and Personality Dispositions**  
Anton P.M. van Bakel

nr 35

**Conjoint Choice Models for Urban  
Tourism Planning and Marketing**  
Benedict Dellaert

nr 36

**Stedelijke Planvorming als Co-Productie**  
Helga Fassbinder (red.)

nr 37

**Design Research in the Netherlands**

editors: R.M. Oxman  
M.F.Th. Bax  
H.H. Achten

nr 38

**Communication in the Building Industry**

Bauke de Vries

nr 39

**Optimaal Dimensioneren van  
Gelaste Plaatliggers**

J.B.W. Stark  
F. van Pelt  
L.F.M. van Gorp  
B.W.E.M. van Hove

nr 40

**Huisvesting en Overwinning van Armoede**

P.H. Thung  
P. Beekman (red.)

nr 41

**Urban Habitat:  
The Environment of Tomorrow**

George G. van der Meulen  
Peter A. Erkelens

nr 42

**A Typology of Joints**

John C.M. Olie

nr 43

**Modeling Constraints-Based Choices  
for Leisure Mobility Planning**

Marcus P. Stemerding

nr 44

**Activity-Based Travel Demand Modeling**

Dick Ettema

nr 45

**Wind-Induced Pressure Fluctuations  
on Building Facades**

Chris Geurts

nr 46

**Generic Representations**

Henri Achten

nr 47

**Johann Santini Aichel:  
Architectuur en Ambiguiteit**

Dirk De Meyer

nr 48

**Concrete Behaviour in Multiaxial  
Compression**

Erik van Geel

nr 49

**Modelling Site Selection**

Frank Witlox

nr 50

**Ecolemma Model**

Ferdinand Beetstra

nr 51

**Conjoint Approaches to Developing  
Activity-Based Models**

Donggen Wang

nr 52

**On the Effectiveness of Ventilation**

Ad Roos

nr 53

**Conjoint Modeling Approaches for  
Residential Group preferences**

Eric Molin

nr 54

**Modelling Architectural Design  
Information by Features**

Jos van Leeuwen

nr 55

**A Spatial Decision Support System for  
the Planning of Retail and Service Facilities**

Theo Arentze

nr 56

**Integrated Lighting System Assistant**

Ellie de Groot

nr 57

**Ontwerpend Leren, Leren Ontwerpen**

J.T. Boekholt

nr 58

**Temporal Aspects of Theme Park Choice  
Behavior**

Astrid Kemperman

nr 59

**Ontwerp van een Geïndustrialiseerde  
Funderingswijze**

Faas Moonen

nr 60

**Merlin: A Decision Support System for Outdoor Leisure Planning**

Manon van Middelkoop

nr 61

**The Aura of Modernity**

Jos Bosman

nr 62

**Urban Form and Activity-Travel Patterns**

Daniëlle Snellen

nr 63

**Design Research in the Netherlands 2000**

Henri Achten

nr 64

**Computer Aided Dimensional Control in Building Construction**

Rui Wu

nr 65

**Beyond Sustainable Building**

editors: Peter A. Erkelens  
Sander de Jonge  
August A.M. van Vliet

co-editor: Ruth J.G. Verhagen

nr 66

**Das Globalrecyclingfähige Haus**

Hans Löfflad

nr 67

**Cool Schools for Hot Suburbs**

René J. Dierkx

nr 68

**A Bamboo Building Design Decision Support Tool**

Fitri Mardjono

nr 69

**Driving Rain on Building Envelopes**

Fabien van Mook

nr 70

**Heating Monumental Churches**

Henk Schellen

nr 71

**Van Woningverhuurder naar Aanbieder van Woongenot**

Patrick Dogge

nr 72

**Moisture Transfer Properties of Coated Gypsum**

Emile Goossens

nr 73

**Plybamboo Wall-Panels for Housing**

Guillermo E. González-Beltrán

nr 74

**The Future Site-Proceedings**

Ger Maas

Frans van Gassel

nr 75

**Radon transport in Autoclaved Aerated Concrete**

Michel van der Pal

nr 76

**The Reliability and Validity of Interactive Virtual Reality Computer Experiments**

Amy Tan

nr 77

**Measuring Housing Preferences Using Virtual Reality and Belief Networks**

Maciej A. Orzechowski

nr 78

**Computational Representations of Words and Associations in Architectural Design**

Nicole Segers

nr 79

**Measuring and Predicting Adaptation in Multidimensional Activity-Travel Patterns**

Chang-Hyeon Joh

nr 80

**Strategic Briefing**

Fayez Al Hassan

nr 81

**Well Being in Hospitals**

Simona Di Cicco

nr 82

**Solares Bauen: Implementierungs- und Umsetzungs-Aspekte in der Hochschulausbildung in Österreich**

Gerhard Schuster

nr 83

**Supporting Strategic Design of Workplace Environments with Case-Based Reasoning**

Shauna Mallory-Hill

nr 84

**ACCEL: A Tool for Supporting Concept Generation in the Early Design Phase**

Maxim Ivashkov

nr 85

**Brick-Mortar Interaction in Masonry under Compression**

Ad Vermeltfoort

nr 86

**Zelfredzaam Wonen**

Guus van Vliet

nr 87

**Een Ensemble met Grootstedelijke Allure**

Jos Bosman

Hans Schippers

nr 88

**On the Computation of Well-Structured Graphic Representations in Architectural Design**

Henri Achten

nr 89

**De Evolutie van een West-Afrikaanse Vernaculaire Architectuur**

Wolf Schijns

nr 90

**ROMBO Tactiek**

Christoph Maria Ravesloot

nr 91

**External Coupling between Building Energy Simulation and Computational Fluid Dynamics**

Ery Djunaedy

nr 92

**Design Research in the Netherlands 2005**

editors: Henri Achten

Kees Dorst

Pieter Jan Stappers

Bauke de Vries

nr 93

**Ein Modell zur Baulichen Transformation**

Jalil H. Saber Zaimian

nr 94

**Human Lighting Demands: Healthy Lighting in an Office Environment**

Myriam Aries

nr 95

**A Spatial Decision Support System for the Provision and Monitoring of Urban Greenspace**

Claudia Pelizaro

nr 96

**Leren Creëren**

Adri Proveniers

nr 97

**Simlandscape**

Rob de Waard

nr 98

**Design Team Communication**

Ad den Otter

nr 99

**Humaan-Ecologisch Georiënteerde Woningbouw**

Juri Czabanowski

nr 100

**Hambase**

Martin de Wit

nr 101

**Sound Transmission through Pipe Systems and into Building Structures**

Susanne Bron-van der Jagt

nr 102

**Het Bouwkundig Contrapunt**

Jan Francis Boelen

nr 103

**A Framework for a Multi-Agent Planning Support System**

Dick Saarloos

nr 104

**Bracing Steel Frames with Calcium Silicate Element Walls**

Bright Mweene Ng'andu

nr 105

**Naar een Nieuwe Houtskeletbouw**

F.N.G. De Medts

nr 108

**Geborgenheid**

T.E.L. van Pinxteren

nr 109

**Modelling Strategic Behaviour in Anticipation of Congestion**

Qi Han

nr 110

**Reflecties op het Woondomein**

Fred Sanders

nr 111

**On Assessment of Wind Comfort by Sand Erosion**

Gábor Dezső

nr 112

**Bench Heating in Monumental Churches**

Dionne Limpens-Neilen

nr 113

**RE. Architecture**

Ana Pereira Roders

nr 114

**Toward Applicable Green Architecture**

Usama El Fiky

nr 115

**Knowledge Representation under Inherent Uncertainty in a Multi-Agent System for Land Use Planning**

Liyang Ma

nr 116

**Integrated Heat Air and Moisture Modeling and Simulation**

Jos van Schijndel

nr 117

**Concrete Behaviour in Multiaxial Compression**

J.P.W. Bongers

nr 118

**The Image of the Urban Landscape**

Ana Moya Pellitero

nr 119

**The Self-Organizing City in Vietnam**

Stephanie Geertman

nr 120

**A Multi-Agent Planning Support System for Assessing Externalities of Urban Form Scenarios**

Rachel Katoshevski-Cavari

nr 121

**Den Schulbau Neu Denken, Fühlen und Wollen**

Urs Christian Maurer-Dietrich

nr 122

**Peter Eisenman Theories and Practices**

Bernhard Kormoss

nr 123

**User Simulation of Space Utilisation**

Vincent Tabak

nr 125

**In Search of a Complex System Model**

Oswald Devisch

nr 126

**Lighting at Work: Environmental Study of Direct Effects of Lighting Level and Spectrum on Psycho-Physiological Variables**

Grazyna Górnicka

nr 127

**Flanking Sound Transmission through Lightweight Framed Double Leaf Walls**

Stefan Schoenwald

nr 128

**Bounded Rationality and Spatio-Temporal Pedestrian Shopping Behavior**

Wei Zhu

nr 129

**Travel Information: Impact on Activity Travel Pattern**

Zhongwei Sun

nr 130

**Co-Simulation for Performance Prediction of Innovative Integrated Mechanical Energy Systems in Buildings**

Marija Trčka

nr 131

**Allemaal Winnen**

M.J. Bakker

nr 132

**Architectural Cue Model in Evacuation Simulation for Underground Space Design**

Chengyu Sun

nr 133

**Uncertainty and Sensitivity Analysis in Building Performance Simulation for Decision Support and Design Optimization**

Christina Hopfe

nr 134

**Facilitating Distributed Collaboration in the AEC/FM Sector Using Semantic Web Technologies**

Jacob Beetz

nr 135

**Circumferentially Adhesive Bonded Glass Panes for Bracing Steel Frame in Façades**

Edwin Huveners

nr 136

**Influence of Temperature on Concrete Beams Strengthened in Flexure with CFRP**

Ernst-Lucas Klamer

nr 137

**Sturen op Klantwaarde**

Jos Smeets

nr 139

**Lateral Behavior of Steel Frames with Discretely Connected Precast Concrete Infill Panels**

Paul Teewen

nr 140

**Integral Design Method in the Context of Sustainable Building Design**

Perica Savanović

nr 141

**Household Activity-Travel Behavior: Implementation of Within-Household Interactions**

Renni Anggraini

nr 142

**Design Research in the Netherlands 2010**

Henri Achten

nr 143

**Modelling Life Trajectories and Transport Mode Choice Using Bayesian Belief Networks**

Marloes Verhoeven

nr 144

**Assessing Construction Project Performance in Ghana**

William Gyadu-Asiedu

nr 145

**Empowering Seniors through Domotic Homes**

Masi Mohammadi

nr 146

**An Integral Design Concept for Ecological Self-Compacting Concrete**

Martin Hunger

nr 147

**Governing Multi-Actor Decision Processes in Dutch Industrial Area Redevelopment**

Erik Blokhuis

nr 148

**A Multifunctional Design Approach for Sustainable Concrete**

Götz Hüsken

nr 149

**Quality Monitoring in Infrastructural Design-Build Projects**

Ruben Favié

nr 150

**Assessment Matrix for Conservation of Valuable Timber Structures**

Michael Abels

nr 151

**Co-simulation of Building Energy Simulation and Computational Fluid Dynamics for Whole-Building Heat, Air and Moisture Engineering**

Mohammad Mirsadeghi

nr 152

**External Coupling of Building Energy Simulation and Building Element Heat, Air and Moisture Simulation**

Daniel Cóstola

nr 153

**Adaptive Decision Making In  
Multi-Stakeholder Retail Planning**

Ingrid Janssen

nr 154

**Landscape Generator**

Kymo Slager

nr 155

**Constraint Specification in Architecture**

Remco Niemeijer

nr 156

**A Need-Based Approach to  
Dynamic Activity Generation**

Linda Nijland

nr 157

**Modeling Office Firm Dynamics in an  
Agent-Based Micro Simulation Framework**

Gustavo Garcia Manzato

nr 158

**Lightweight Floor System for  
Vibration Comfort**

Sander Zegers

nr 159

**Aanpasbaarheid van de Draagstructuur**

Roel Gijsbers

nr 160

**'Village in the City' in Guangzhou, China**

Yanliu Lin

nr 161

**Climate Risk Assessment in Museums**

Marco Martens

nr 162

**Social Activity-Travel Patterns**

Pauline van den Berg

nr 163

**Sound Concentration Caused by  
Curved Surfaces**

Martijn Vercammen

nr 164

**Design of Environmentally Friendly  
Calcium Sulfate-Based Building Materials:  
Towards an Improved Indoor Air Quality**

Qingliang Yu

nr 165

**Beyond Uniform Thermal Comfort  
on the Effects of Non-Uniformity and  
Individual Physiology**

Lisje Schellen

nr 166

**Sustainable Residential Districts**

Gaby Abdalla

nr 167

**Towards a Performance Assessment  
Methodology using Computational  
Simulation for Air Distribution System  
Designs in Operating Rooms**

Mônica do Amaral Melhado

nr 168

**Strategic Decision Modeling in  
Brownfield Redevelopment**

Brano Glumac

nr 169

**Pamela: A Parking Analysis Model  
for Predicting Effects in Local Areas**

Peter van der Waerden

nr 170

**A Vision Driven Wayfinding Simulation-System  
Based on the Architectural Features Perceived  
in the Office Environment**

Qunli Chen

nr 171

**Measuring Mental Representations  
Underlying Activity-Travel Choices**

Oliver Horeni

nr 172

**Modelling the Effects of Social Networks  
on Activity and Travel Behaviour**

Nicole Ronald

nr 173

**Uncertainty Propagation and Sensitivity  
Analysis Techniques in Building Performance  
Simulation to Support Conceptual Building  
and System Design**

Christian Struck

nr 174

**Numerical Modeling of Micro-Scale  
Wind-Induced Pollutant Dispersion  
in the Built Environment**

Pierre Gousseau

nr 175

**Modeling Recreation Choices  
over the Family Lifecycle**

Anna Beatriz Grigolon

nr 176

**Experimental and Numerical Analysis of  
Mixing Ventilation at Laminar, Transitional  
and Turbulent Slot Reynolds Numbers**

Twan van Hooff

nr 177

**Collaborative Design Support:  
Workshops to Stimulate Interaction and  
Knowledge Exchange Between Practitioners**

Emile M.C.J. Quanjel

nr 178

**Future-Proof Platforms for Aging-in-Place**

Michiel Brink

nr 179

**Motivate:  
A Context-Aware Mobile Application for  
Physical Activity Promotion**

Yuzhong Lin

nr 180

**Experience the City:  
Analysis of Space-Time Behaviour and  
Spatial Learning**

Anastasia Moiseeva

nr 181

**Unbonded Post-Tensioned Shear Walls of  
Calcium Silicate Element Masonry**

Lex van der Meer

nr 182

**Construction and Demolition Waste  
Recycling into Innovative Building Materials  
for Sustainable Construction in Tanzania**

Mwita M. Sabai

nr 183

**Durability of Concrete  
with Emphasis on Chloride Migration**

Przemysław Spiesz

nr 184

**Computational Modeling of Urban  
Wind Flow and Natural Ventilation Potential  
of Buildings**

Rubina Ramponi

nr 185

**A Distributed Dynamic Simulation  
Mechanism for Buildings Automation  
and Control Systems**

Azzedine Yahiaoui

nr 186

**Modeling Cognitive Learning of Urban  
Networks in Daily Activity-Travel Behavior**

Şehnaz Cenani Durmazoğlu

nr 187

**Functionality and Adaptability of Design  
Solutions for Public Apartment Buildings  
in Ghana**

Stephen Agyefi-Mensah

nr 188

**A Construction Waste Generation Model  
for Developing Countries**

Lilliana Abarca-Guerrero

nr 189

**Synchronizing Networks:  
The Modeling of Supernetworks for  
Activity-Travel Behavior**

Feixiong Liao

nr 190

**Time and Money Allocation Decisions  
in Out-of-Home Leisure Activity Choices**

Gamze Zeynep Dane

nr 191

**How to Measure Added Value of CRE and  
Building Design**

Rianne Appel-Meulenbroek

nr 192

**Secondary Materials in Cement-Based  
Products:  
Treatment, Modeling and Environmental  
Interaction**

Miruna Florea

nr 193

**Concepts for the Robustness Improvement  
of Self-Compacting Concrete:**

**Effects of Admixtures and Mixture  
Components on the Rheology and Early  
Hydration at Varying Temperatures**

Wolfram Schmidt

nr 194

**Modelling and Simulation of Virtual Natural Lighting Solutions in Buildings**

Rizki A. Mangkuto

nr 195

**Nano-Silica Production at Low Temperatures from the Dissolution of Olivine - Synthesis, Tailoring and Modelling**

Alberto Lazaro Garcia

nr 196

**Building Energy Simulation Based Assessment of Industrial Halls for Design Support**

Bruno Lee

nr 197

**Computational Performance Prediction of the Potential of Hybrid Adaptable Thermal Storage Concepts for Lightweight Low-Energy Houses**

Pieter-Jan Hoes

nr 198

**Application of Nano-Silica in Concrete**

George Quercia Bianchi

nr 199

**Dynamics of Social Networks and Activity Travel Behaviour**

Fariya Sharmeen

nr 200

**Building Structural Design Generation and Optimisation including Spatial Modification**

Juan Manuel Davila Delgado

nr 201

**Hydration and Thermal Decomposition of Cement/Calcium-Sulphate Based Materials**

Ariën de Korte

nr 202

**Republiek van Beelden: De Politieke Werkingen van het Ontwerp in Regionale Planvorming**

Bart de Zwart

nr 203

**Effects of Energy Price Increases on Individual Activity-Travel Repertoires and Energy Consumption**

Dujuan Yang

nr 204

**Geometry and Ventilation: Evaluation of the Leeward Sawtooth Roof Potential in the Natural Ventilation of Buildings**

Jorge Isaac Perén Montero

nr 205

**Computational Modelling of Evaporative Cooling as a Climate Change Adaptation Measure at the Spatial Scale of Buildings and Streets**

Hamid Montazeri

nr 206

**Local Buckling of Aluminium Beams in Fire Conditions**

Ronald van der Meulen

nr 207

**Historic Urban Landscapes: Framing the Integration of Urban and Heritage Planning in Multilevel Governance**

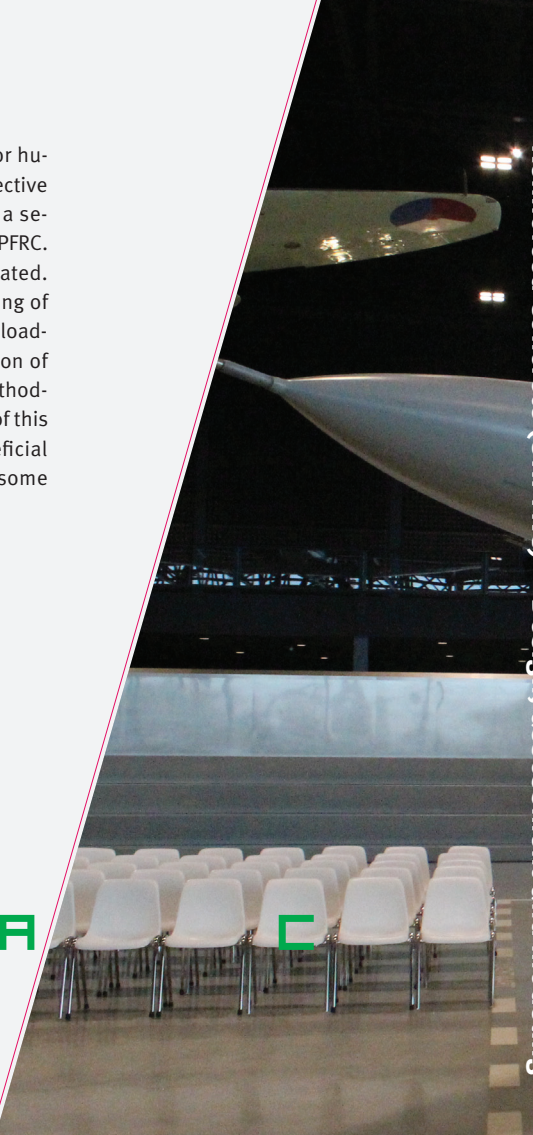
Loes Veldpaus

nr 208

**Sustainable Transformation of the Cities: Urban Design Pragmatics to Achieve a Sustainable City**

Ernesto Antonio Zumelzu Scheel

To obtain a new product that contributes to a better and safer life for human beings, this thesis aims at the development of sustainable protective Ultra-High Performance Fibre Reinforced Concrete (UHPFRC). Firstly, a series of methods and strategies are utilized to design a sustainable UHPFRC. Next, the properties of the developed sustainable UHPFRC are evaluated. Afterwards, based on the obtained experimental results, the modeling of dynamic behaviour of the sustainable UHPFRC under different impact loadings is performed. This research is performed based on a combination of theoretical and experimental investigation. The final outcome is a methodology to design a sustainable UHPFRC and the dynamic performance of this developed UHPFRC under different impact loadings, which are beneficial for widening the application of UHPFRC and further understanding some intrinsic characteristics of UHPFRC under impact.



F

A

C

B

W

K

E

H

L

/ Department of the Built Environment

**TU** / **e**

Technische Universiteit  
**Eindhoven**  
University of Technology